72-57

AAR CARGO SYSTEMS
a division of AAR Manufacturing Group, Inc.

October 28, 2004

Mr. William Brach, SFPO
US NRC
Document Control Office
11555 Rockville Pike
Rockville, MD 20852

Dear Mr. Brach:

Enclosed herewith is a Topical Report submitted on behalf of AAR Corporation. The report subject is "Credit for 90% of the 10B in BORAL." BORAL is a neutron shielding product manufactured by AAR Corporation at it Cargo Systems Division in Livonia, Michigan.

We have been coordinating its release with Mr. Stewart Brown, Project Manager in the Spent Fuel Program Office of the USNRC. It is in support of two current licensing requests by spent fuel storage cask design firms in the US. Please accept the report into your system as soon as practical. If you have any questions about the report, its form or submission, please do not hesitate to call me at 734-466-8210 or email at dallas.mayfield@aarcorp.com.

Thank you in advance for your cooperation in this process.

Sincerely,

Dallas D. Mayfield
Vice President, Business Development

Encl: Topical Report-Credit for 90% of the 10B in BORAL

NMSS01

TOPICAL REPORT

Credit for 90% of the ^{10}B in BORAL

Submitted by:
AAR Manufacturing
12633 Inkster Road
Livonia, Michigan 48150
Tel: 734-522-2000
Fax: 734-522-2240

AAR Report 1829, Revision 0

October 27, 2004

Table of Contents

List of Figures

Abstract

This Topical Report was prepared to provide manufacturing information and test data to support applications from dry spent fuel cask/canister designers for 90% credit for the ^{10}B specified for BORAL neutron absorber sheets. BORAL has been approved by the Nuclear Regulatory Commission (NRC) for use in most of the dual-purpose fuel casks and canisters certified under 10CFR72 (storage) and 10CFR71 (transport), with credit for 75% of the specified ^{10}B areal density.

BORAL is a laminated composite material composed of a solid aluminum cladding enclosing an inner core of compacted aluminum and boron carbide (B_4C) powders. BORAL is made by hot rolling an aluminum box filled with the blended aluminum and B_4C powders (ingot). The hot rolling process compresses the Al/B_4C powders into a cermet with a density about 93-96% of the theoretical density of fully compacted powders. BORAL sheets are typically 0.075 – 0.300 inch thick and contain between 40- 65% B_4C in the core.

NRC regulatory guides (NUREG's 1536[1], 1567[2], 1609[3], 1617[4], 5661[5]) instruct applicants to limit the credit for the ^{10}B in the neutron absorber to 75% for criticality calculations for dry fuel storage and transport packages, unless comprehensive tests are performed to demonstrate the presence, uniformity, effectiveness, and durability of the absorber material. If the applicant can demonstrate that these criteria are met, the NRC will consider approving credit for up to 90% of the poison in the absorber.

In accordance with NRC guides, AAR has performed comprehensive tests that conclusively confirm that the ^{10}B in BORAL is uniformly distributed and is highly effective for absorbing thermal neutrons and assuring criticality safety. BORAL has been used in spent fuel storage pools for decades and has shown no significant degradation or loss of functionality from long term exposure to high levels of gamma, fast neutron, and thermal neutron radiation.

In recent years, BORAL has been widely used in dry fuel storage casks and canisters. Cask designers have tested BORAL and confirmed the safety and durability of BORAL in their specific dry spent fuel storage systems. AAR has implemented a BORAL Improvement Program to further improve the material properties for dry storage applications. Credit for 90% of the ^{10}B in BORAL is the next step in the improvement program. Increasing the ^{10}B credit from 75% to 90% will reduce the amount of B_4C required, which will provide AAR more flexibility in the design and continued improvement of BORAL, while maintaining a conservative margin for criticality safety.

1.0 Background

BORAL is a laminated composite material composed of solid aluminum cladding enclosing an inner core of compacted aluminum and boron carbide (B_4C) powders. BORAL is made by hot rolling an aluminum box filled with the blended aluminum and B_4C powders (ingot). The hot rolling process compresses the Al/B_4C powders into a cermet with a density about 93-96% of the theoretical density of fully compacted powders. BORAL sheets are typically 0.075 – 0.300 inch thick and contain between 40- 65% B_4C in the core. BORAL is highly effective at absorbing thermal neutrons and assuring criticality safety at any time water is inside the package (i.e., during fuel loading operations / lid closure and hypothetical accident which results in water intrusion).

BORAL is a proprietary product of AAR Corporation. It is produced by AAR Manufacturing in Livonia, Michigan. BORAL has been in continuous production since 1956, initially by Brooks & Perkins as shown in Figure 1-1[6]. AAR acquired Brooks & Perkins in 1981 and has continued production at the same facility. All production activities – manufacturing, inspection, and acceptance testing – are performed at the Livonia facility.

In accordance with NRC guidance, designers of dry fuel storage systems currently take credit for only 75% of the ^{10}B specified in BORAL. This limit is based on the effects of "neutron channeling" or "streaming" between the boron carbide (B_4C) particles observed in early generation boron carbide / aluminum (boral) neutron absorbers.

Boral was developed in the 1950's by the Atomic Energy Commission (AEC). The early boral products - were manufactured by several organizations, including the AEC. (Please note that "boral" was a generic term at that time; "boral" in lower case letters is used in this report to differentiate generic boral materials from AAR's patented, trademarked product, BORAL, which will be capitalized.)

The process developed by the AEC was to mix the B_4C particles into molten aluminum, cast the mixture into blocks, and roll the blocks into plates or sheets. The molten aluminum process was difficult and could use only small quantities of B_4C (up to 35% in commercial production)[6,7,8]. As shown in Figure 1-1, the B_4C particles were relatively large compared to modern BORAL, which contributed to the channeling effect. The large particles also had a self-shielding effect which reduced the effectiveness of the ^{10}B in the B_4C.

B&P becomes the first industry producer of BORAL

Brooks & Perkins has just become the first commercial supplier of Boral. This is a new material. It is used as a neutron shield in atomic energy installations and atomic power plants.

Boral is said to offer as much neutron shielding protection as 26 inches of concrete where the neutrons are of thermal energies. It does not shield against the passing of gamma rays.

The Atomic Energy Commission developed Boral at their Oak Ridge Plant, where it has been produced by the Government in limited amounts only. The product consists of a core of boron carbide uniformly dispersed in aluminum, clad on both sides with commercially pure aluminum. Boral can be produced with the core material having various concentrations of boron carbide.

Now that atomic power plants are operating in submarines and in an experimental airplane, and several industrial power plants are in the development stage, it has become advisable to have a commercial supplier of Boral. B&P is highly qualified, primarily because of its successful pioneering of methods for working some of the newer metals, including zirconium; also the fact that it operates a rolling mill at nearby Livonia. Here B&P has just installed a new 3000 cycle ultra high frequency induction furnace, now used for the production of the Boral core material.

The grade of Boral offered by B&P has a 35% concentration of boron carbide. The Boral plate is rolled ⅛" and ¼" thick. Standard sizes offered are 30" x 96", 30" x 48", 15" x 96", and 15" x 48". The approximate weight per square foot of ¼" thick 35% Boral plate is 3.4 pounds.

Boral and zirconium are, in a sense, companion products. Both are used in atomic applications. B&P has been deep-drawing zirconium for the past two years. Unlike Boral, zirconium is transparent to the passage of neutrons while acting as the container of the atomic fuel.

Microphoto of cross section of ¼" thick Boral plate, 10 X magnification. Shows crystalline structure of boron carbide in center, with aluminum cladding on top and bottom.

Rolling mill superintendent J. C. Merritt is looking at a formed Boral cylinder. The three-inch-thick rolling slab, ready for break-down, is a cast Boral core surrounded by pure aluminum cladding.

Figure 1-1
Boral Produced by Brooks & Perkins in 1956

A reference cited in several NRC guides is a paper by W. Burrus, published in 1958, titled "How Channeling between Chunks Raises Neutron Transmission through Boral"[9]. Burrus developed a mathematical model to calculate neutron transmission through heterogeneous absorbers, such as boral. Although Burrus did not perform any neutron transmission experiments, he referenced experimental measurements performed by other researchers, including measurements through ⅛ inch and ¼ inch thick boral made by Brooks & Perkins ("Boral Radiation Attenuation Characteristics"[10]). The measured neutron transmission through the ⅛ inch thick boral sample was 7.0×10^{-3}; transmission through the ¼ inch thick sample was 5.6×10^{-4}.

Since Transmission = (1 - Neutron Absorption), the ⅛ inch thick boral sheet absorbed 99.3% of the neutrons and the ¼ inch thick plate absorbed 99.94% of the neutrons. Burrus compared the absorption by boral to the calculated value of a theoretical homogeneous B_4C absorber to determine the amount of neutron channeling.

The experimental measurements referenced in Burrus' paper compared to his calculated values and the amount of channeling are shown below:

B&P Sample Thickness	**Experimental Absorption**	**Calculated Absorption for Homogeneous Absorber**	**Channeling**
⅛ inch	99.30%	99.80%	0.50%
¼ inch	99.94%	99.99%	0.05%

This test data shows that the channeling and self-shielding effects in boral were small, and that boral was very effective in absorbing thermal neutrons. Burrus' mathematical model for a heterogeneous absorber can be used to calculate the amount of channeling as a function of the size(s) of the B_4C particles and the volume percent of B_4C. In his paper (which summarized a report prepared under contract with the AEC, "Radiation Transmission Through Boral and Similar Heterogeneous Materials Consisting of Randomly Distributed Absorbing Chunks"[11]), Burrus used his model to calculate the neutron transmission through a boral sheet with the following assumptions:

Thickness of the sheet = 0.125 inch
Thickness of the mixed B_4C-Al core = .085 inch
Volume % B_4C = 40%

Particle diameters and volume %:

Particle Diameter (inch)	Particle Diameter (microns)	Volume %
0.038	965	42.5
0.024	610	27.5
0.016	406	15.0
0.009	228	15.0

Figure 1-2 is a representation of the relative size of the B_4C chunks in Burrus' heterogeneous absorber calculation.

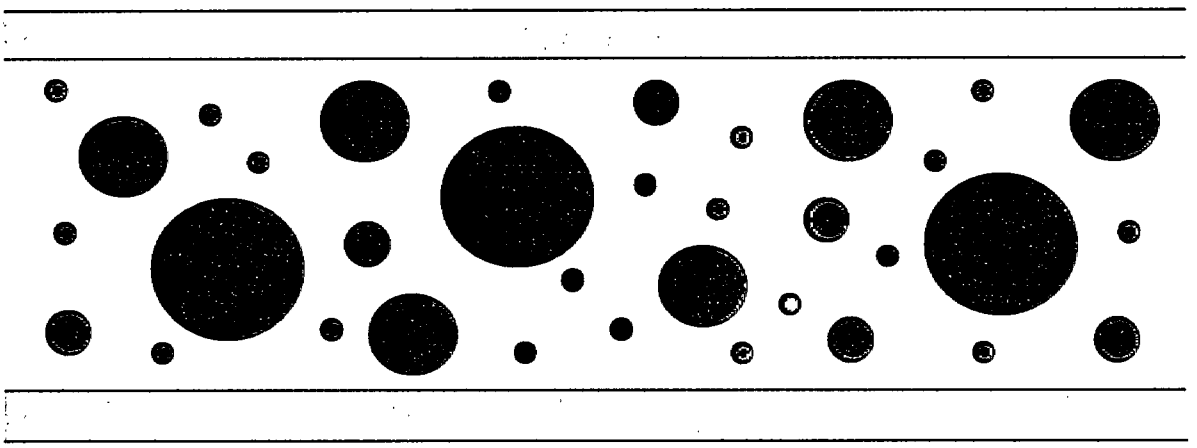

Figure 1-2
Burrus Model of a Heterogeneous Al-B_4C Absorber

Based on these assumptions, Burrus calculated the transmission of normally incident neutrons to be 7.6% (92.4% of the neutrons would be absorbed). This is more than 10 times the measured transmission through boral that Burrus reported in his paper. The model shows that to have significant channeling, the ^{10}B areal density has to be low and the B_4C particles have to be very large relative to the absorber thickness (the largest particles in his example have a diameter that is 45% of the thickness of the core). Although the model developed by Burrus is valid and provides a reasonable approximation of neutron transmission through a heterogeneous B_4C absorber, the example that he used greatly exaggerated the channeling/streaming effect.

Soon after the AEC transferred its boral technology to Brooks & Perkins for commercialization, Brooks & Perkins recognized the manufacturing difficulties and limitations of the molten aluminum process. Brooks & Perkins conducted a development program during the 1960's to improve the process and was successful in making boral using a powder process, which is still used today. Brooks & Perkins applied for a patent for the powder process in 1975 and the patent was granted in 1977. The powder process allows the use of much smaller B_4C powder and higher B_4C concentrations.

Figure 1-3 shows the small B_4C particle size and uniform distribution of B_4C in modern BORAL. For comparison, this example is the same thickness and the same magnification as the Brooks & Perkins boral plate shown in Figure 1-1.

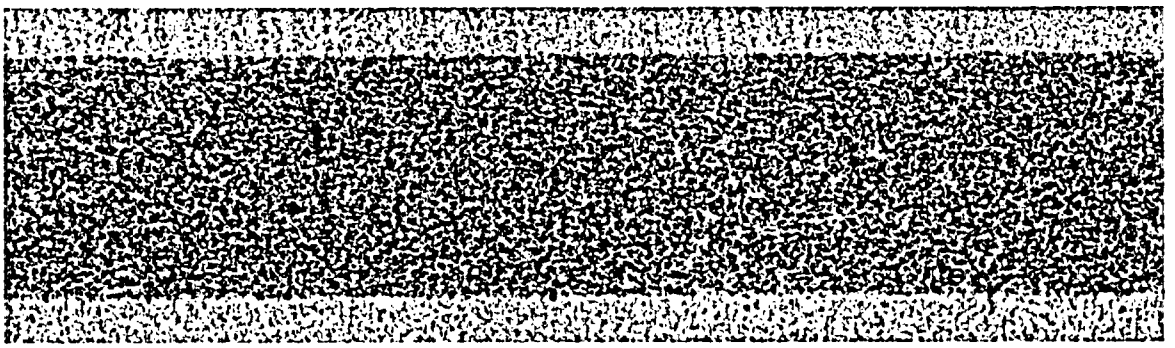

Figure 1-3
BORAL Made by the AAR Powder Process

Extensive qualification testing was performed on BORAL produced with the new powder process, including the following studies:

- "Experimental Observation of BORAL Plates Encased in Stainless Steel Under the Influence of Gamma and Neutron Fluxes"[12]
- "Quantitative Analysis of Boral Panels"[13]
- Neutron transmission measurements vs. B_4C mesh size and neutron energy[14]
- "Neutron Transmission Through Boral Shielding Material"[15]
- "Neutron Transmission Through Boral Shielding Material; Theoretical Model and Experimental Comparison"[16]
- "Boral Neutron Absorbing/Shielding Material, Product Performance Report"[17]
- "Effects of Gamma Radiation on the Neutron Attenuation Properties of Boral"[18]
- "Corrosion Resistance of BORAL to One Year of Exposure to BWR Storage Pool Water"[19]
- "Spent Fuel Storage Module Corrosion Report"[20]
- "Storage Module Corrosion Testing"[21]
- "The Suitability of Brooks & Perkins Spent Fuel Storage Module for Use in PWR Storage Pool"[22]

Another reference cited in the NRC guides is "Criticality Effect of Neutron Channeling Between Boron Carbide Granules in Boral for a Spent-Fuel Shipping Cask"[23] by Wells, Marnon, and Karam. Following is Table 1 from Wells' paper, which compared his transmission measurement through BORAL and calculation for a homogeneous absorber to Burrus' data:

Experimental and Calculated Transmission Coefficients for Boral (Wells, Marnon, and Karem)

Areal Density (g/cm^2 ^{10}B)	W.R. Burrus		Wells, Marnon, Karam	
	Exp.	Calc. (Homogeneous)	Exp.	Calc. (Homogeneous)
0.030	7.0×10^{-3}	2.0×10^{-3}	---	---
0.040	---	---	4.8×10^{-4}	9.1×10^{-5}
0.060	5.6×10^{-4}	5.5×10^{-5}	---	---

The experimental neutron transmission measurement was 0.00048, i.e., the BORAL absorbed 99.952% of the neutrons, confirming that BORAL is highly effective in absorbing thermal neutrons. Wells' data shows the calculated channeling effect (the difference between the measured transmission through BORAL and the calculated value for a homogeneous absorber) is extremely small (0.00048 - 0.000091 = 0.000389).

Wells' measurement was made using a collimated neutron beam with perpendicular incidence to the BORAL sample. In a moderated spent fuel package, the neutrons will strike the BORAL sheet with isotropic incidence, so most of the neutrons will have a longer path through the absorber material. As shown by Burrus in Figure 3 of his paper[9], with isotropic incidence, the channeling effect essentially disappears.

AAR includes a large amount of additional B_4C to compensate for any nonuniformities, including the small channeling effect. Consequently, BORAL designed and manufactured to a customer specified ^{10}B areal density is at least as effective as a homogeneous absorber with that ^{10}B areal density. This report will document the design, manufacturing processes, and testing which assure that BORAL is safe, effective, and durable under all operating conditions for dry fuel storage casks and canisters.

2.0 Topical Report Requirements (LIC-500)

The NRC instruction LIC-500, "Processing Request for Reviews of Topical Reports", states: "To be accepted for the Topical Report Program the report should meet all four of the following criteria:

(1) The report deals with a specific safety-related subject regarding a nuclear power plant that requires a safety assessment by the NRC staff, for example, component design, analytical models or techniques, or performance testing of components and/or systems that can be evaluated independently of a specific license application. Technical reports submitted in support of plant-specific license amendment applications are not defined as topical reports under this program.

(2) The report is, or is expected to be, referenced in a number of license amendment requests.

(3) The report contains complete and detailed information on the specific subject presented. Conceptual or incomplete preliminary information will not be reviewed.

(4) NRC approval of the report will increase the efficiency of the review process for applications that reference the report."

This report meets all four criteria:

(1) This report deals with the performance of a neutron absorber, a Safety Category A material (per NUREG/CR-6407[24]), that can be evaluated independently of a specific license application.

(2) It is expected that all of the dry fuel storage system suppliers that currently use BORAL will request 90% credit in a future license amendment and will reference this report.

(3) This report contains complete and detailed information, including the results of comprehensive testing to support an applicant's request for 90% credit for the ^{10}B in BORAL.

(4) NRC approval of this report will increase the efficiency of the review process for applications that reference this report.

3.0 BORAL Manufacturing Process

BORAL is manufactured by the following process:

- Ingot design – calculating the ingot size and the weight percent of aluminum and B_4C powders required to meet the customer specified BORAL sheet dimensions (length, width, and thickness) and minimum ^{10}B areal density.

  AAR uses a proprietary formula to calculate the amount of B_4C required in the powder mix to assure that there is 95% probability and 95% confidence that the ^{10}B content in BORAL exceeds the minimum ^{10}B required for the customer design. The formula is conservatively based on the minimum B_4C purity in the boron carbide powder per ASTM C750, the minimum amount of boron present in B_4C per the AAR specification, a conservative value of the ^{10}B isotope in naturally occurring boron, the minimum sheet thickness, the maximum cladding thickness, and the low side of statistical variations in powder mix as established in AAR's powder blending qualification process. In addition, the formula includes a large additional margin of B_4C to offset any nonuniformities, including effects of particle size (channeling, streaming, or self-shielding).

  The general formula for calculating the ^{10}B areal density in an aluminum/B_4C matrix is:

  $$A = \rho WBEt$$

  where:

  A = ^{10}B areal density (g/cm^2)
  ρ = composite density of the Al/B_4C matrix (g/cm^3)
  W = wt % B_4C in the matrix
  B = wt % boron in B_4C
  E = wt % ^{10}B content (or enrichment)
  t = thickness of the sheet (cm)

  The minimum ^{10}B areal density, A, is specified by the customer. AAR calculates the amount of B_4C (W) required in BORAL by the following formula:

  $$W = A/(\rho BEt)$$

  with the following values and assumptions:

  ρ = (theoretical density of compacted Al/B_4C) x (average core density, % of TD)
  B = 76 wt %, the minimum percentage of boron in B_4C per the AAR specification
  E = 18.3 wt % ^{10}B in natural boron
  t = (nominal thickness of the BORAL core) – (maximum tolerance)

  In addition to the conservative assumptions used to calculate the quantity of B_4C for the powder mixture, AAR adds a large margin of additional B_4C (greater than 10%) to compensate for any nonuniformities and assure that the effective ^{10}B content exceeds the customer specified minimum requirement.

- Powder blending – measuring and blending the appropriate amount of B_4C and aluminum powders.

  Each powder is measured by weight and placed into a separate container. The B_4C powder content in BORAL varies from 40% to 65% depending on the customer's requirements. The powders are poured into the powder blender as shown in Figure 3-1, and mixed in accordance with AAR procedures. A random sample is taken from every blended powder batch and is chemically tested to verify the correct ratio of aluminum and B_4C powders and to confirm proper mixing.

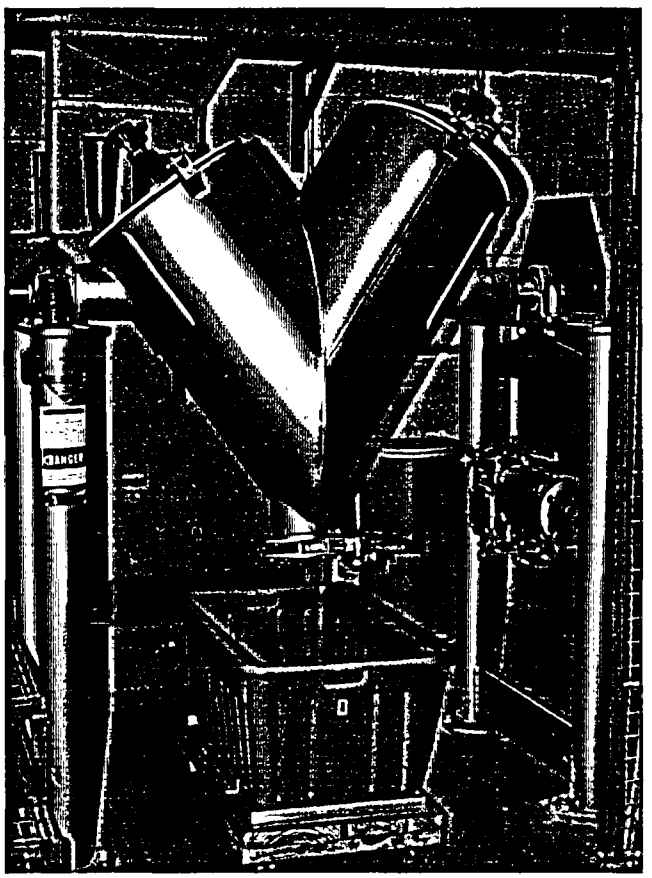

Figure 3-1
Powder Blender

- Ingot preparation – making, filling and closing an aluminum ingot in preparation for rolling.

  The ingot shell is made from an extruded aluminum tube. The tube is filled with the calculated amount of powder, measured by weight. The powder mix is hand compacted to the cold design density. A closure bar is placed in the open end of the filled ingot; the ingot is closed by welding the closure bar in place. Figure 3-2 shows ingots prepared for heating.

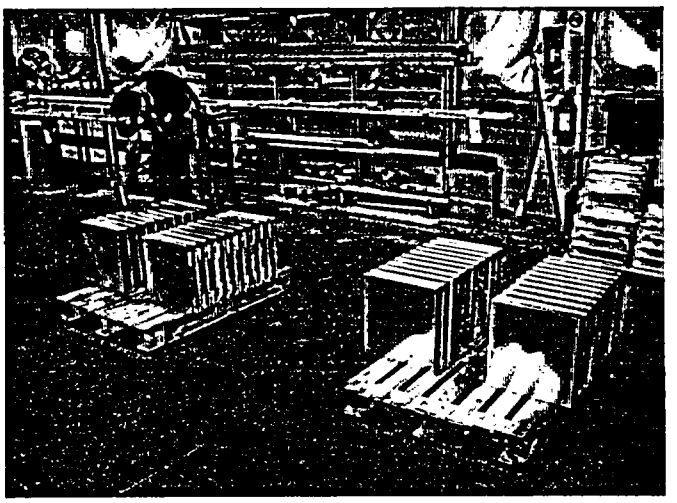

Figure 3-2
BORAL Ingots

- Heating – heating the ingots to the AAR proprietary heating profile.

  See Section 4.0 "BORAL Improvement Program", Phase 1, for a general explanation.

- Rolling – hot rolling the ingots to the customer specified thickness according to the AAR proprietary rolling schedule. Figure 3-3 shows the final rolling pass of a BORAL ingot into a rolled BORAL sheet.

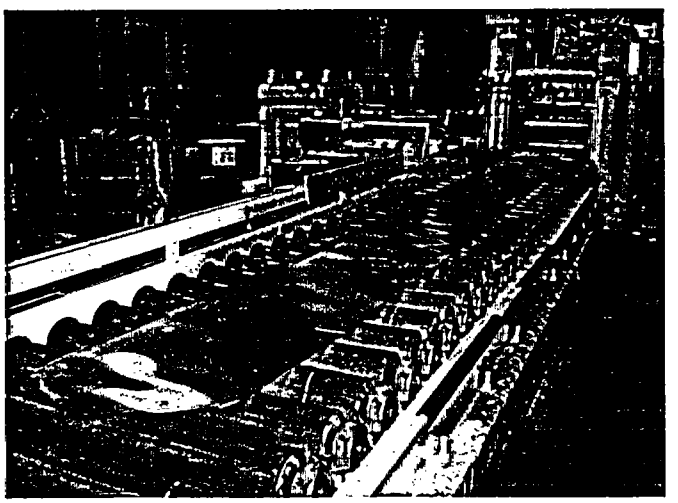

Figure 3-3
Rolled BORAL Sheet

- Finishing – annealing the rolled sheet to improve flatness, shearing to final sheet dimensions, deburring the edges, and cleaning the surfaces. Figure 3-4 shows BORAL sheets stacked after finishing processes.

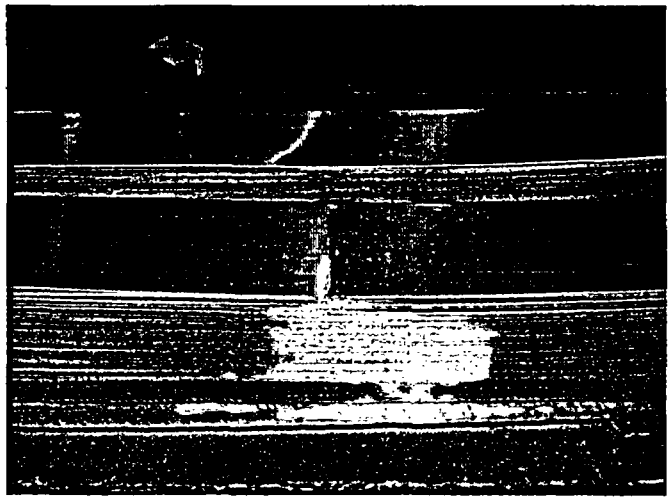

Figure 3-4
Finished BORAL Sheets

- Inspection and testing – performing visual and dimensional inspection.

  This step includes verifications of size dimensions, visual inspection for surface anomalies, and testing of sample coupons for ^{10}B areal density by chemical testing or neutron attenuation testing. Figure 3-5 shows coupons to be chemical tested to verify areal density.

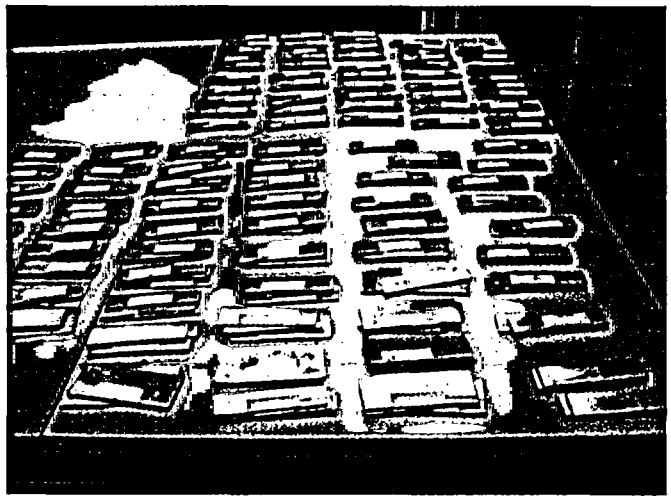

Figure 3-5
BORAL Samples

Figure 3-6 shows BORAL coupons being dissolved as part of the chemical testing process.

Figure 3-6
Chemical Testing

4.0 BORAL Improvement Program

Hundreds of thousands of BORAL sheets are in service in spent fuel pools worldwide, many in service for more than 30 years. The only significant problem that has been experienced with BORAL in spent fuel pools is occasional occurrences of "blisters" in the cladding of the BORAL sheets. A blister is a small, localized separation of the cladding from core.

Blisters are caused by the penetration of water into the BORAL core through the open edges or a pinhole leak in the cladding and the subsequent oxidation of compacted aluminum powder in the core. The general oxidation reaction is:

$$2\ Al + 3\ H_2O = Al_2O_3 + 3\ H_2$$

The hydrogen released by the oxidation reaction generally escapes through the core porosity and out through the open edges, but on rare occasions the aluminum oxide builds up and closes the pathways (aluminum oxide molecules are 1.5 times larger than the volume of elemental aluminum) and trap water within the BORAL core. The trapped water continues to react with the aluminum and generate hydrogen. The accumulated hydrogen then builds up enough pressure to separate the cladding from the core and create blisters. Hydrogen blisters are typically 0.25 to 1.25 inch in diameter and 1/16 to 1/8 inch high. Extensive testing on blisters has shown that the Al/B_4C core stays intact and there is no loss of BORAL's ability to absorb thermal neutrons. Blisters have been identified in only a small fraction of a percent of BORAL sheets.

For dry fuel storage applications, a canister or cask is usually in the pool water no more than one or two days - not enough time for the aluminum oxidation process to progress to the point that it traps water in the BORAL core. Some cask suppliers have tested BORAL for their systems under normal and off-normal conditions, based on maximum design basis fuel parameters, and/or worst case conditions. AAR has been advised by the cask suppliers that no blisters have occurred under test conditions representing the most demanding design and operating conditions (however, blisters can be induced at heat-up rates much greater than that which can occur in actual operations or by repeated cycles of tests). Nevertheless, in mid-2003, AAR initiated a BORAL Improvement Program specifically to reduce the potential for blisters to occur in dry fuel storage applications. The improvement program has three phases:

Phase 1. – Review of Manufacturing Processes

Phase 1 was a review of all BORAL manufacturing processes to determine if any process improvements could be made that would increase the integrity of BORAL. An AAR technical team reviewed the BORAL processing experience, researched aluminum processing and new powder metallurgy technologies, and performed experimental research. All of the processes were considered satisfactory; however, research indicated there were potential benefits for higher temperature ingot pre-heat. Based on this research, AAR tested a higher temperature ingot heating profile.

The objective was to use the heating process not only for preparation for hot rolling, but also to increase the oxide layer on the aluminum powder (dry passivation). The thicker the protective oxide layer before BORAL goes into fuel storage pool water, the less oxidation and consequently, less hydrogen generation when the BORAL is placed in the pool. (AAR has used a

customer specified wet passivation process on some BORAL in the past, which had generally good results, but was not as consistent as it needed to be).

Following is a description of the aluminum oxidation process from the ASM reference book, "The Surface Treatment and Finishing of Aluminum and its Alloys"[25] which reflects the importance of the oxide layer in inhibiting corrosion:

> "When a freshly formed aluminum metal surface is exposed to the atmosphere, it is immediately covered with a thin film of oxide, and this oxide film quickly re-forms when damaged. An important and beneficial feature of this oxide film is that its molecular volume is stoichiometrically 1.5 times that of the metal film used up in oxidation. This then means that the oxide film is under compressive stress, and will not only cover the metal continuously, but can cope with a certain amount of substrate deformation without rupturing. It is to this protective surface layer that the aluminum industry owes its existence.
>
> "Reports of the structure of this low temperature, air-formed film have varied widely although, in general, it is assumed to be amorphous, with the outer surface being a hydrated aluminum oxide. At higher temperatures (above 450°C), crystalline γ-Al_2O_3 is formed, and then, in the molten state, α-Al_2O_3 can occur.
>
> "The kinetics of oxide growth on pure aluminum are complex. The currently accepted mechanism has been described recently by Wefers ("Aluminium", 1981). At ambient temperatures a limiting oxide film thickness of 2-3 nm will be produced within one day; thermal oxidation is controlled by diffusion of aluminum and oxygen ions at temperatures up to ~ 400°C and, in this temperature range, asymptotically decaying rate laws are observed. However, when the temperature is raised towards and above 450°C, the exponential oxidation rate changes to a linear relationship between weight gain and time. This change in mechanism represents crystallization to γ-Al_2O_3, which will disrupt the continuity of the film. At temperatures above 500°C, it has been reported that the preparation of the sheet, i.e., both metallurgical and surface roughness features, can alter the oxidation kinetics."

Table 1 of the same reference shows the thickness of the oxide coating on aluminum as a function of temperature:

Natural oxide on pure Al (formed at below 300°C)	1-3 nm
Natural oxide on pure Al (formed at temperatures above 300°C)	up to 30 nm

Thus, the aluminum oxide transitions from a hydrated form [$2\ Al + (3+x)\ H_2O = Al_2O_3 \cdot x(H_2O) + 3H_2$] at ambient temperature, to the crystalline, anhydrous γ phase at high temperature. The γ oxide thickness continues to grow as a function of both increased temperature (up to the melting point of aluminum) and time. The thicker oxide layer reduces the oxidation rate in the water environment and consequently mitigates the primary mechanism for the formation of blisters.

AAR contracted with its aluminum powder supplier, The Aluminum Powder Company, Limited (Alpoco), and the University of Nottingham to conduct thermal tests on the specific aluminum powder used by AAR to measure the aluminum oxide film growth as a function of temperature and time.

The results of this proprietary study, titled "Oxidation of Al Powder"[26], were important to understanding the temperature/time effects on the aluminum oxide layer thickness and provided the basis for establishing the proprietary BORAL ingot heating process parameters. The aluminum oxide thermal growth curve is represented in Figure 4-1.

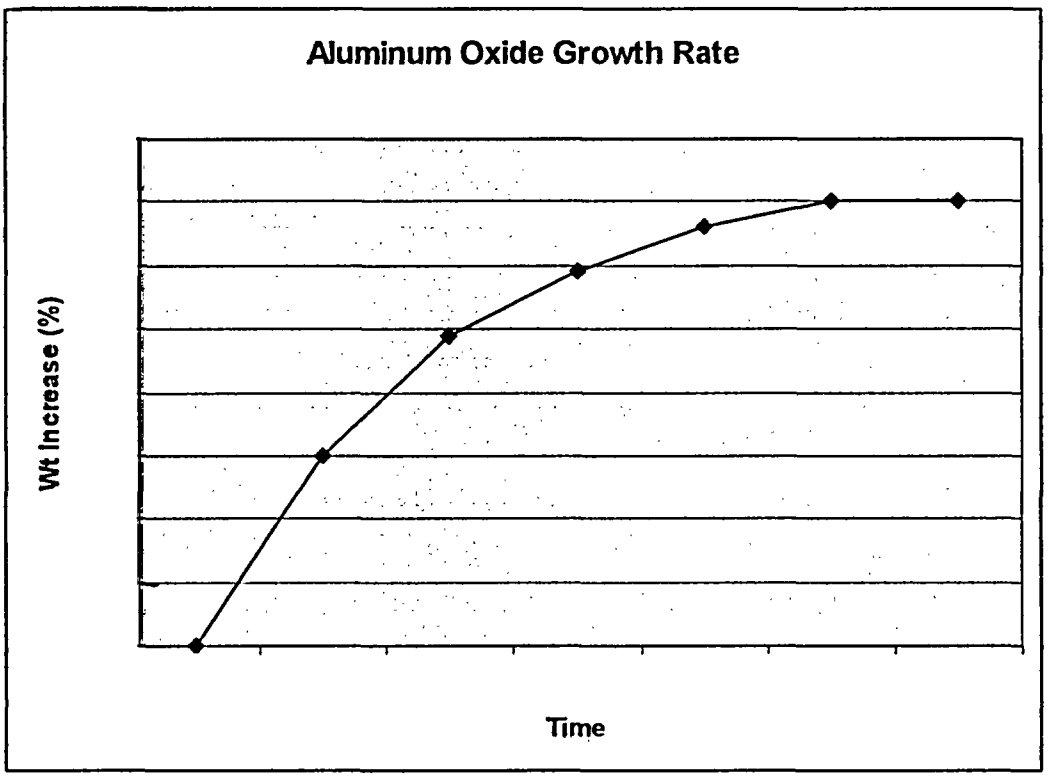

Figure 4-1
Oxide Film Growth on AAR Aluminum Powder

Since the pre-roll density of the B_4C and aluminum powders in the ingot is approximately 56%, the rest of the volume in the powder is air, which provides sufficient oxygen for the thermal oxidation process. For its test program, AAR heated ingots to the optimum oxidation temperature (above the rolling temperature), held that temperature for the duration needed for effective thermal growth of the aluminum oxide layer, and then allowed the ingots to cool to the lower rolling temperature. The old and new heating profiles are illustrated in Figure 4-2.

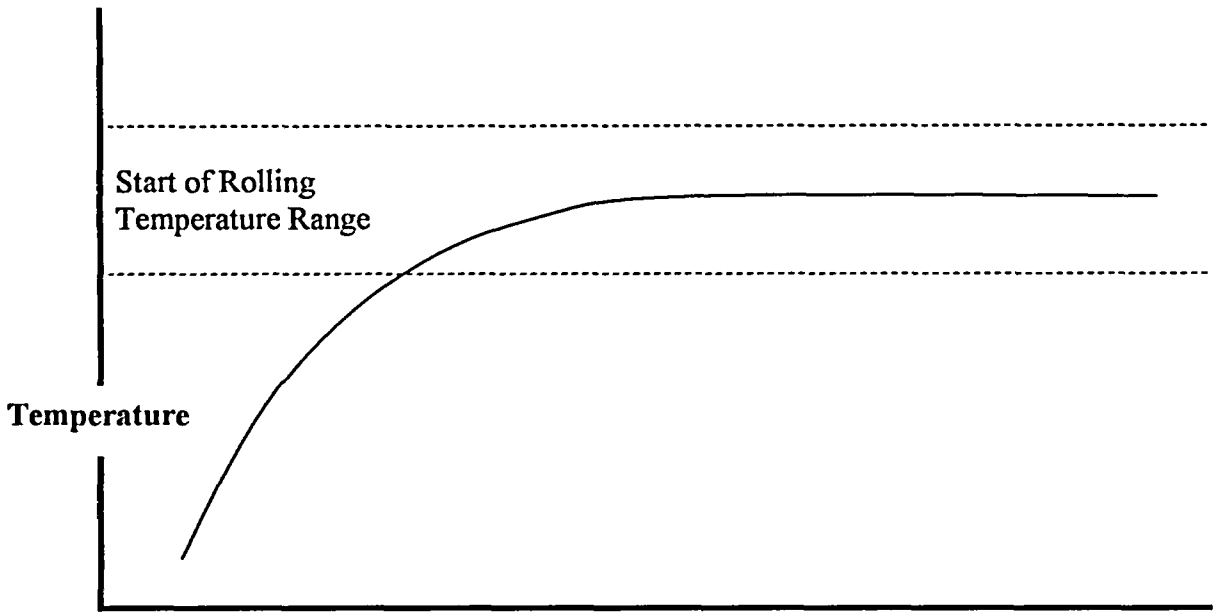

Old Heat-up Profile

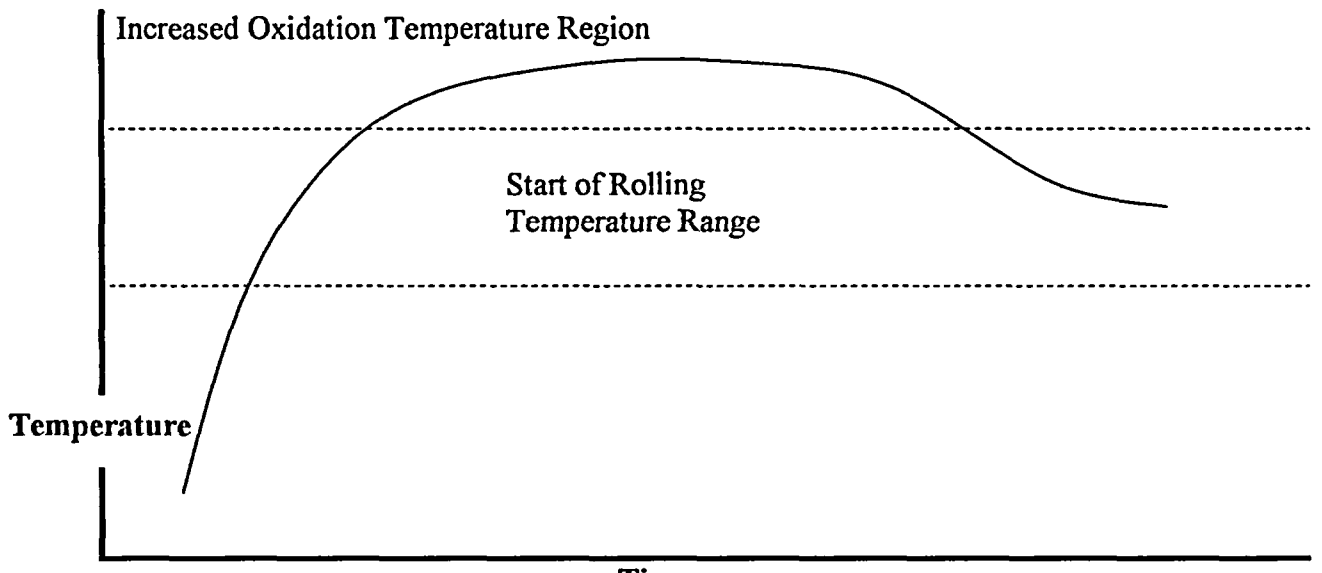

New Heat-up Profile

Figure 4-2
Ingot Heat-up Profiles

The Electric Power Research Institute (EPRI) and AAR co-sponsored a test program to evaluate BORAL made using the new heating profile ("Improved BORAL"). The test program was performed by Northeast Technologies Corporation (NETCO). NETCO tested the durability of BORAL by subjecting coupons to repeated cycles of simulated fuel loading conditions (pressurization in heated water for both BWR and PWR water chemistries) followed by vacuum drying / heat-up tests, until a blister formed. BORAL produced with the new heating profile showed significantly greater resistance to blister formation compared to BORAL tested in earlier NETCO test programs. Further discussion of the test program and results is included in Section 5.5. The new heating profile has been incorporated into the BORAL manufacturing process.

Phase 2 – Alternative Materials and Process Evaluation

Phase 2 was an evaluation and test program to compare alternative materials and new processes for manufacturing BORAL. One series of tests used different aluminum alloy powders in the core. Two alloys showed significantly greater resistance to blisters than 1100 series powder in test-to-failure tests. One of the powders evaluated was high strength 6061 aluminum alloy. BORAL made with 6061 alloy powder has been designated as BORAL-6000. AAR has also made BORAL with 6061 alloy cladding. The type of aluminum alloy powder used in the core does not change the effectiveness of ^{10}B in BORAL, therefore the request for 90% credit also applies to BORAL-6000.

Phase 3 – 90% Credit for ^{10}B

Phase 3 in the improvement program is 90% credit for the ^{10}B in BORAL. The increase in credit from 75% to 90% gives AAR more flexibility in the BORAL design. The increased credit reduces the ^{10}B areal density required in the BORAL by 16.7%. One design improvement is to reduce the core thickness and increase the cladding thickness. For example, a 0.100 inch thick sheet of BORAL has a core thickness of approximately 0.072 inch, with 0.014 inch thick cladding on both sides of the core. Reducing the ^{10}B areal density by 16.7% allows the core thickness to be reduced to 0.060 inch. The difference of 0.012 inch can be added to the cladding thickness, increasing the cladding thickness from 0.014 to 0.020 inch, an increase of more than 40%. This increases the cladding bending strength (i.e., resistance to blisters) by a factor of approximately two. Increasing the cladding thickness also increases the corrosion margin, another safeguard against blister formation.

Summary

BORAL is conservatively designed for criticality control in dry fuel storage/transport applications. The design and manufacturing processes assure that the ^{10}B in BORAL is uniformly distributed and effective. The BORAL Improvement program has already improved the material properties of BORAL for dry fuel storage conditions. Approval of 90% credit for the ^{10}B present in BORAL will allow AAR to further improve the material properties of BORAL, specifically the resistance to cladding deformation, with no compromise to criticality safety.

5.0 Evaluation of BORAL for 90% Credit for ^{10}B

To qualify for 90% credit for the ^{10}B present in BORAL, NRC guides state that comprehensive testing must be performed to demonstrate the presence, uniformity, effectiveness, and durability of the neutron absorber material. This section will discuss the design, manufacturing controls, and confirmatory testing that assures BORAL meets all of these criteria.

5.1 Presence of ^{10}B in BORAL

The presence of ^{10}B in BORAL is confirmed by redundant material and process verifications, including: B_4C material certification from the supplier specifying the total boron content, all significant impurities, and the isotopic content of ^{10}B in the boron; an independent over-check of the B_4C powder composition by a qualified metallurgical laboratory; an in-house chemical test of a sample from each batch of blended powder; in-house chemical testing of samples from finished sheets to verify that the B_4C in the sample meets or exceeds the minimum requirement, and periodic neutron attenuation tests to verify chemical tests results.

Statistical analyses of the B_4C powder purity, the boron content in the B_4C, and the percentage of ^{10}B in the boron are included in Attachment A.

5.2 Uniformity of ^{10}B in BORAL

The uniformity of the ^{10}B in BORAL can be demonstrated by at least four methods: (1) evaluation of the effectiveness of the manufacturing process and process controls to assure that the B_4C and aluminum powders are properly mixed, which, in turn, assures that the B_4C will be evenly distributed in the core matrix, (2) visual and/or metallographic examination of the BORAL core, (3) neutron attenuation testing of a statistically significant number of random samples to determine the mean and variance of the ^{10}B isotope in BORAL sheets, and (4) chemical testing of a statistically significant number of random samples to determine the mean and variance of the B_4C in the core, combined with verification of ^{10}B isotopic concentration in the boron.

1. **Effectiveness of the manufacturing process** – AAR (and Brooks & Perkins before 1981) has used the same manufacturing process for making BORAL for more than 30 years resulting in a manufacturing process that is well established. Process controls including AAR's procedures, employee training and experience, in-process inspections, and QA oversight assures that the B_4C will be evenly distributed in the core matrix with consistency and repeatability.
2. **Visual and metallographic examination of the B_4C particle distribution in the BORAL core** – Since the BORAL core is exposed around the edges of the sheet, any significant nonuniformity along the edges are visually apparent. There are numerous metallographic examinations and photomicrographs available of BORAL cores (such as Figure 1-3). All show that the B_4C particles are uniformly distributed in the aluminum matrix.

3. **Neutron attenuation testing of a statistically significant number of random samples to determine the mean and variance of the ^{10}B isotope in BORAL sheets** – AAR contracted NETCO to perform neutron attenuation measurements on a statistically large number of random samples to establish the confidence level for uniformity of ^{10}B in BORAL in a typical production lot, specifically to support this Topical Report. The production quantity was 3236 sheets, made from 114 powder batches (each powder batch yielded 30 sheets). One sheet made from each powder batch was selected at random and two coupons were cut from random locations on the sheet, making a total of 228 BORAL test coupons. The coupons were approximately 5.5 x 11.0 inches. The minimum required ^{10}B areal density was 0.020 g/cm^2. Neutron attenuation measurements were made at each corner of each test coupon, for a total of 912 measurements. The measurements and analyses are compiled in the NETCO report titled, "Review and Evaluation of ^{10}B Areal Density Measurements of BORAL Coupons"[27]. The ^{10}B areal density distribution (Figure 4-1 from the NETCO report) is shown in Figure 5-1. The complete NETCO report is included in Attachment B.

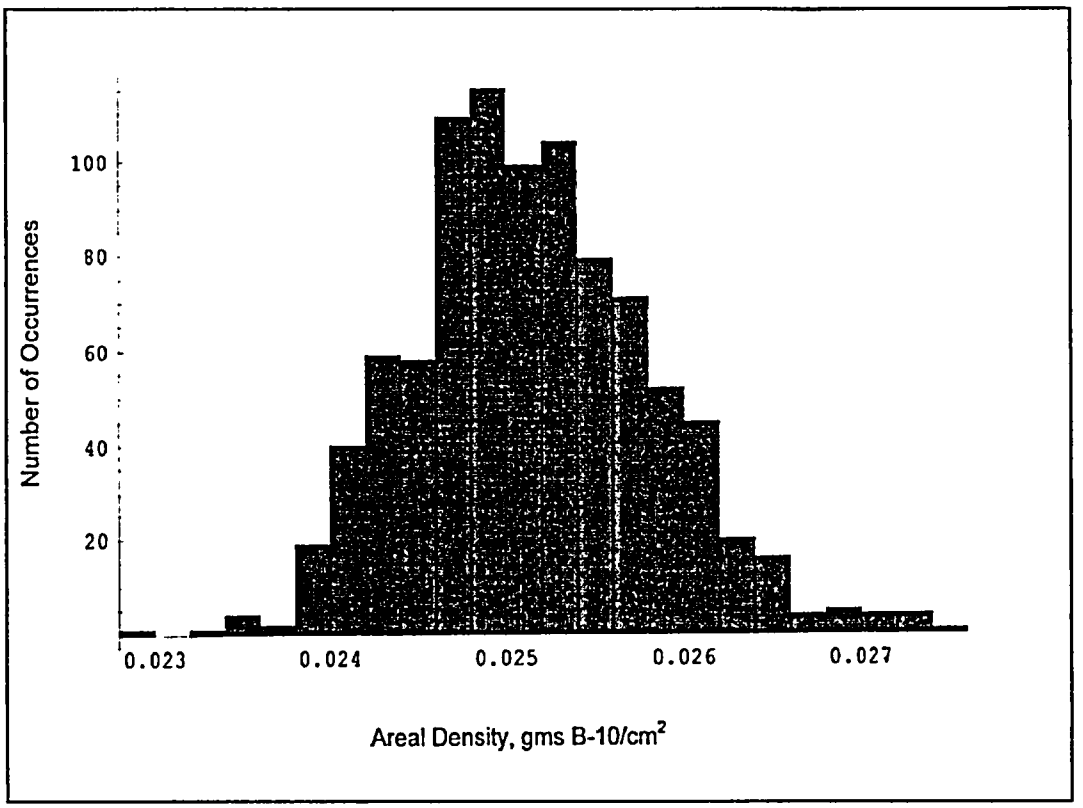

Figure 5-1

NETCO Neutron Attenuation Measurements of

0.020 g ^{10}B /cm^2 Areal Density BORAL

The Summary and Conclusions of the NETCO report state:

> "Areal density measurements obtained via neutron attenuation testing at 4 locations each on 228 BORAL coupons have been evaluated. The data have been demonstrated to be normally distributed. Accordingly, a one sided tolerance factor for normally distributed data can be applied. This has been computed following the method of Natrella and is 3.226 at 99% probability and 95% confidence level.
>
> "The proposed method of Reference 1* has been applied to the data set. The minimum certified areal density for this BORAL is 0.020 gms $^{10}B/cm^2$. The mean of the measured data is 0.02514 gms $^{10}B/cm2$. At a 99.9% probability and a 95% confidence level the one sided tolerance limit is 0.0229 gms $^{10}B/cm^2$ which exceeds the 111% of the minimum certified areal density. Accordingly 90% credit for B-10 is demonstrated."
>
> *Standard Guide for Thermal Neutron Absorber (Poisons) for Criticality Control in Dry Cask Storage Systems (DCSS) or Transportation Packages Containing Fissile Materials, proposed by ASTM Subcommittee c26.03, 5/8/2003

The data in Appendix A of the NETCO report demonstrates that the ^{10}B in BORAL is uniform throughout a sheet and is consistent for a large production lot. The data also shows that the ^{10}B loading in BORAL is very conservative. In this case, the specified ^{10}B areal density is 0.020 g $^{10}B/cm^2$ and the as-manufactured BORAL has an average greater than 0.025 g $^{10}B/cm^2$, with no measurement less than 0.0225 g $^{10}B/cm^2$. Since the cask designer takes credit for 75% of the specified areal density, the design requirement is for 0.015 g $^{10}B/cm^2$. Approval of 90% credit for the ^{10}B would allow the cask designer to take credit for 0.018 g $^{10}B/cm^2$, so there is still a very large margin of conservatism for criticality safety.

4. **Chemical testing of a statistically significant number of random samples to determine the mean and variance of the B_4C in the core, combined with verification of ^{10}B isotopic concentration in the boron** – AAR's standard $B_4C/^{10}B$ verification method is a chemical test. Chemical testing is an accurate, reliable method for determining the ^{10}B areal density. The chemical analysis is performed using hydrochloric acid to dissolve the aluminum in the BORAL leaving only the B_4C. Once the B_4C is recovered and weighed, the ^{10}B areal density is determined by calculation. From time to time, AAR benchmarks the results of the chemical testing with neutron attenuation tests. AAR tested the coupons from the 114 sheets used in the NETCO evaluation using AAR's standard chemical test. The results from the chemical tests were consistent with the neutron attenuation tests - the average ^{10}B measured by neutron attenuation was 0.0252 g/cm^2 compared to 0.0249 g/cm^2 from the chemical measurement and calculation. The AAR chemical test procedure is designed to be conservative, which was confirmed by the attenuation measurements. These test results are included in Attachment C.

   During production of BORAL, a sample from each ingot included in the production's sampling plan is tested. A test sample is cut from one end of each BORAL sheet made from the ingot (2 PWR sheets or 3 BWR sheets per ingot). The edges of all the samples are measured for thickness and a 1 cm^2 test specimen is cut from the thinnest location. This procedure assures that all the sheets made from that ingot will have a ^{10}B areal density at least that of the test specimen.

5.3 Neutron Channeling Through BORAL

NUREG/CR-5661 states:

> "Limiting added poison material credit to 75% without comprehensive testing is based on concerns for potential 'streaming' of neutrons due to nonuniformities. It has been shown that boron carbide granules embedded in aluminum permit channeling of a beam of neutrons between the grains and reduce the effectiveness for neutron absorption."

The NRC Spent Fuel Project Office's Interim Staff Guidance 15 (ISG-15) entitled, "Materials Evaluation"[28], states:

> "In heterogeneous absorber materials, the neutron poisons may take the form of particles dispersed or precipitated in a matrix material. Materials with large poison particles (e.g., 80 micrometer particles of unenriched boron carbide) have been shown to absorb significantly fewer neutrons than homogeneous materials with the same poison loading (Burrus, Wells). The reduced neutron absorption in heterogeneous materials results from particle self-shielding effects, streaming or channeling of neutrons between poison particles."

After rolling, the average B_4C particle size in BORAL is about 50 microns, which is smaller than the particle size that cause significant channeling between particles. The amount of neutron channeling through BORAL can be approximated by the methodology referenced in ISG-15 (Burrus).

In the study, "Radiation Transmission Through Boral and Similar Heterogeneous Materials Consisting of Randomly Distributed Absorbing Chunks"[11], Burrus developed four methods for calculating neutron transmission through boral:

- Formulas for Materials with Single-Sized Right Cylindrical Chunks;
- Formulas for Materials with Right Cylindrical Chunks of Multiple Sizes;
- Formulas for Materials with Arbitrary Chunk Sizes;
- Formulas Including Energy and Angular Distributions.

For simplicity, the first method is used herein (this method is conservative, since only normally incident neutrons are considered).

Following are excerpts from Burrus' report:

> "If scattering is neglected, the transmission through a slab of material consisting of a distribution of chunk sizes is given by:

$$T = \int_0^t P(x,t)\tau(x)dx$$

where:

P(x,t)dx = fraction of rays which encounter a thickness of absorbing material between x and x+dx in traversing a total thickness t of material

$\tau(x)$ = fraction of radiation transmitted through a chunk of material of thickness x"

"It is assumed that the chunks are right circular cylinders with their generators normal to the surface of the slab. Right cylindrical chunks are chosen because a ray that passes through a normally oriented right cylinder always passes through a chunk thickness equal to the cylinder height."

"The slab is considered to be divided into an integral number (N) of layers of thickness (Δ) equal to the height of a cylinder of absorbing material. This division is made by translating the cylinders vertically so that the center of a cylinder is moved to the center of the layer in which it falls." The model is illustrated in Figure 5-2.

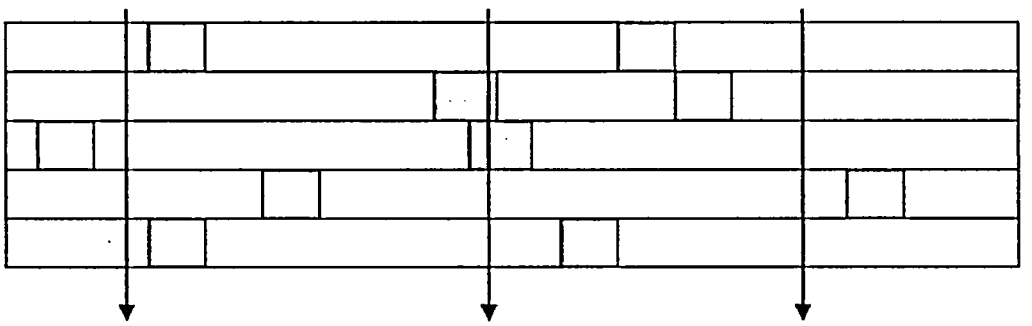

Figure 5-2
Burrus Model of Layers in Absorber

"The transmission through a slab divided in this manner is the same as the transmission through the undivided slab since every normally incident ray sees the same thickness of chunk material in either case. The probability that a given ray will encounter exactly n chunks is given by Bernoulli's binomial distribution:

$$P_n = V^n(1-V)^{N-n}\, C(N,n)$$

where:

V = probability that a ray will encounter a chunk in passing through a layer (the volume fraction of chunks)

V^n = probability that n chunks will be encountered in n specified layers

$(1-V)^{N-n}$ = probability that the rest of the layers are not occupied by other chunks

C(N,n) = number of combinations of N things taken n at a time and is equal to the number of ways in which the n specified layers could be selected from N layers = N!/[(N-n)!n!]"

"If exponential attenuation in the chunk material is assumed, then the probability that a given ray penetrates the slab is:

$$\tau(n) = e^{-\Sigma n\Delta}$$

where:

Σ = linear attenuation coefficient for the chunk material
n = the number of chunks encountered
Δ = height of chunks encountered
$n\Delta$ = total chunk material thickness along this ray"

"Summing the overall average transmission of the slab and combining the result with the binomial theorem gives:

$$T = (Ve^{-\Sigma\Delta} + 1\text{-}V)^N \quad \text{(equation 6 in Burrus' report)}$$

"Equation 6 has a simple physical interpretation which could have given Equation 6 at once. Since V is the probability that a ray will encounter a chunk at a given layer, (1-V) is the probability that a ray will miss the chunks in the layer. $Ve^{-\Sigma\Delta}$ is the probability that those rays that hit a chunk will penetrate the layer. Thus the quantity in brackets is just the average transmission through one layer. Since the chunks are randomly distributed, each layer acts independently and the overall average transmission T is the product of the transmission of all N sublayers."

Applying the formula to BORAL:

$Ve^{-\Sigma\Delta}$ in the Burrus equation is the formula for transmission, T, through a homogeneous absorber, usually expressed as:

$$T = e^{-\Sigma t}$$

where:

Σ = macroscopic cross section = $N_B\sigma_a$
t = the absorber thickness
N_B = atom density of ^{10}B
σ_a = absorption cross section for ^{10}B = 3836 barns (for thermal neutrons)

A typical BORAL design for dry storage applications has the following parameters:

- Sheet thickness = 0.100 inch
- Core thickness = 0.072 inch
- B_4C wt% in the core = 60%

For an average particle (right circular cylinder) height of 50 microns (0.00197 inch), the transmission through a single B_4C particle can be calculated.

The atom density of ^{10}B, N_B, in B_4C =

$$N_B = (\rho_{BC} B N_A)/M_B$$

where:

ρ_{BC} = density of B_4C in BORAL = (95% TD) (2.52 g/cm^3) = 2.394 g/cm^3
B = ^{10}B in B_4C = (.76 B/B_4C) (.183 ^{10}B/B) = .139
N_A = Avogadro's number = 6.022 x 10^{23} atoms/mole
M_B = g/mole for ^{10}B = 10.0129 g/mole

N_B = 2.00 x 10^{22} atoms/cm^3
and
$\Sigma = N_B \sigma_a$ = (2.00 x 10^{22} atoms/cm^3) (3836 x 10^{-24} cm^2) = 76.7/cm

and

$$T = e^{-(76.7/cm)(0.005\ cm)} = 0.68$$

Conservatively ignoring the scattering and absorption cross sections for carbon and ^{11}B, the neutron transmission through the 50 micron (0.00197 inch) thick B_4C particle is calculated as 0.68. The transmission through a 50 micron layer of absorber containing 60% B_4C using Burrus' equation 6 is:

$$T = (0.60 \times 0.68) + (1 - 0.60) = 0.808$$

The integer number of layers in a layered model with a core thickness of 0.072 inch is 0.072/0.00197 = 36. The normally incident thermal neutron transmission through the total sheet thickness is $T = (0.808)^{36} = 0.0004$ (the scattering and absorption cross sections for aluminum are conservatively ignored).

Since neutron absorption is 1 – T, the calculation shows that BORAL absorbs 99.96% of the neutrons. Burrus also shows that for isotropic incidence, transmission is reduced by a factor of approximately four (absorption = 99.99%).

If the average B_4C particle size is twice the thickness, 100 microns, T through a single layer is 0.49, the integer number of layers is 0.072/0.00394 = 18, and T through 18 layers is $(0.49)^{18}$ = 0.0008. Thus, a heterogeneous absorber with 100 micron B_4C particles absorbs 99.92% of the neutrons. The increase in the channeling effect for the increase in average particle size from 50 microns to 100 microns is about 0.04%. Reducing the particle size from 50 microns to 10 microns reduces channeling by 0.02%. These calculated values are consistent with the guidance in ISG-15, i.e., there is not much effect of the particle size on neutron attenuation for average B_4C particle sizes less than 80 microns, but as the average particle size increases above 100 microns (constant ^{10}B areal density), the channeling effect becomes more significant. The calculated channeling effect as a function of particle size is shown in Figure 5-3.

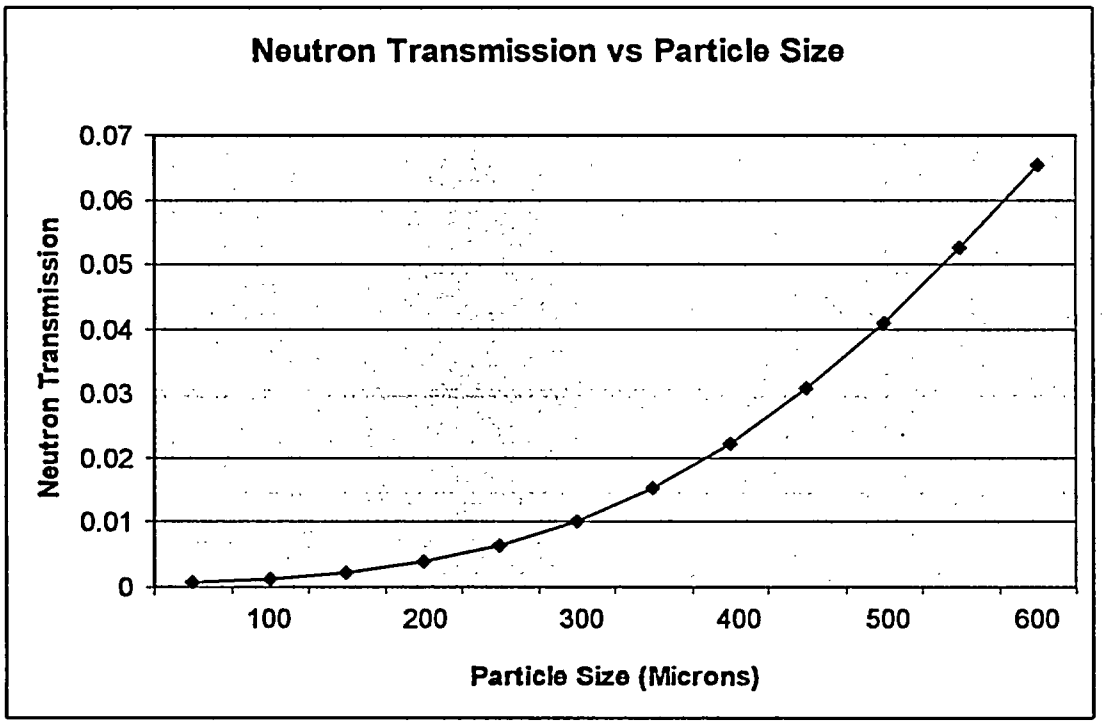

Figure 5-3
Calculated Neutron Channeling Effect

Neutron transmission through BORAL with different B_4C particle sizes has been measured by the University of Michigan[14,20]. The effect of particle size, as measured by transmission testing, is consistent with the calculated values shown in Figure 5-3. The transmission measurements confirm that the effect of further reductions in B_4C particle size below 80 microns is very small.

The formula for neutron transmission, $T = e^{-\Sigma t}$, can be used to calculate transmission as a function of ^{10}B areal density [(^{10}B density in the absorber) x (thickness of the absorber)]. Neutron absorption (1-T) for a homogeneous ^{10}B absorber is shown in Figure 5-4. The curve shows that absorption asymptotically approaches unity with increasing ^{10}B areal density.

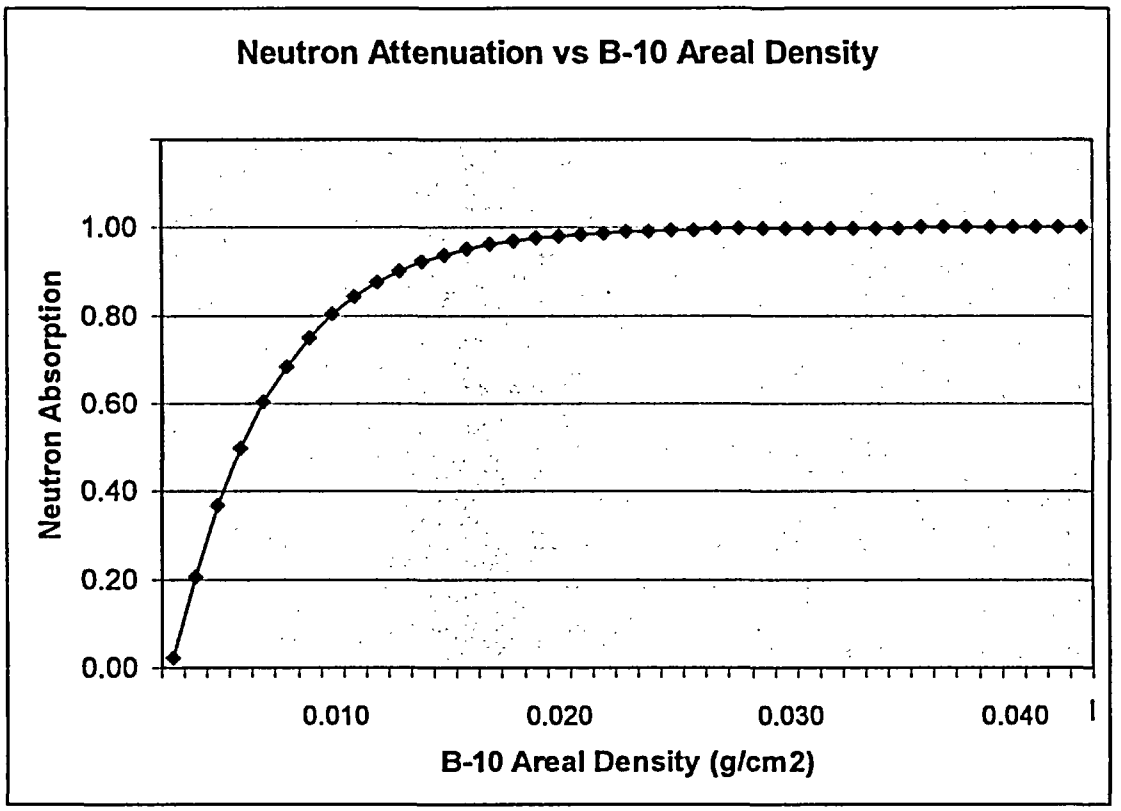

Figure 5-4
Neutron Attenuation vs ^{10}B Areal Density

Using Burrus' method to approximate the neutron transmission through a heterogeneous absorber with large B_4C particles, Figure 5-5 shows a comparison of the calculated values for transmission through a homogeneous and a heterogeneous absorber.

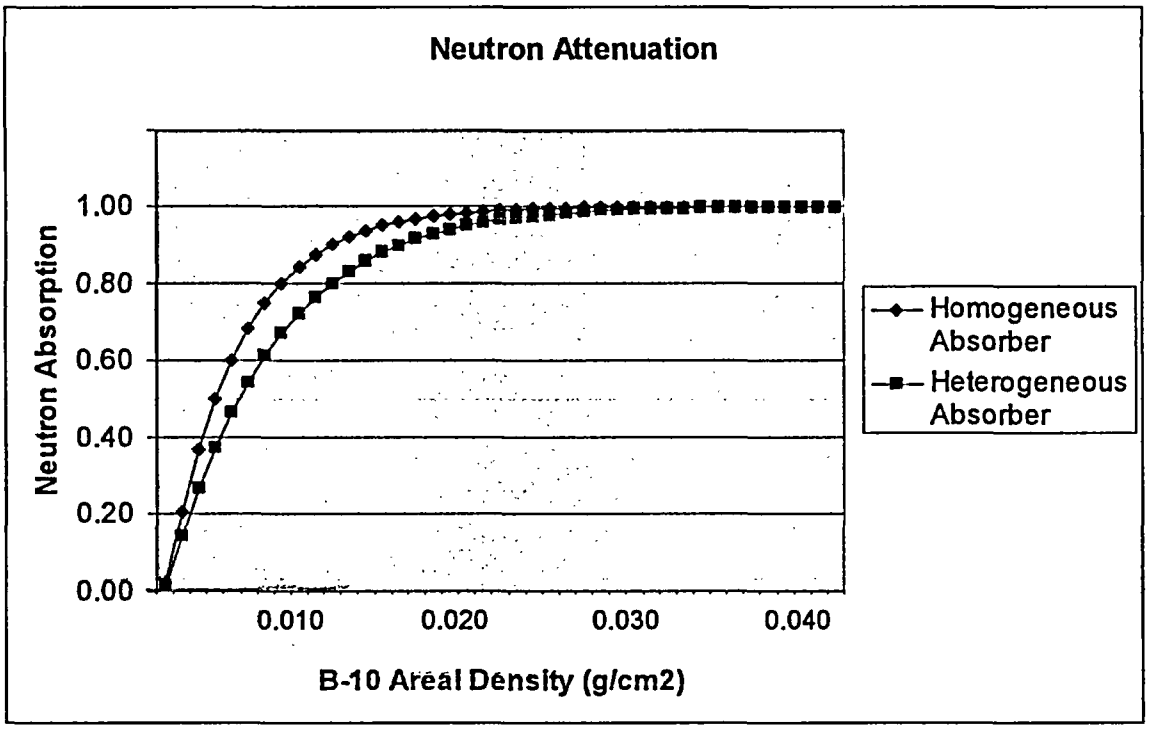

Figure 5-5
Comparison of Neutron Absorption by Homogeneous and Heterogeneous Absorbers

The effectiveness of the heterogeneous absorber is determined from the difference between the curves. At low ^{10}B areal densities, as the areal density increases, the curves diverge, indicating a decrease in effectiveness. At higher areal densities, the curves converge with increasing areal density, indicating that at higher ^{10}B areal densities, the heterogeneous absorber becomes more effective (more like a homogeneous absorber). In the limit, increasing the B_4C / decreasing the aluminum in the matrix, the heterogeneous material becomes homogeneous B_4C.

Figure 5-6 is a plot of the difference between the curves in Figure 5-5 (transmission difference = neutron absorption by the homogeneous absorber - neutron absorption by the heterogeneous absorber). Figure 5-6 illustrates the decrease in the channeling effect at higher ^{10}B areal densities.

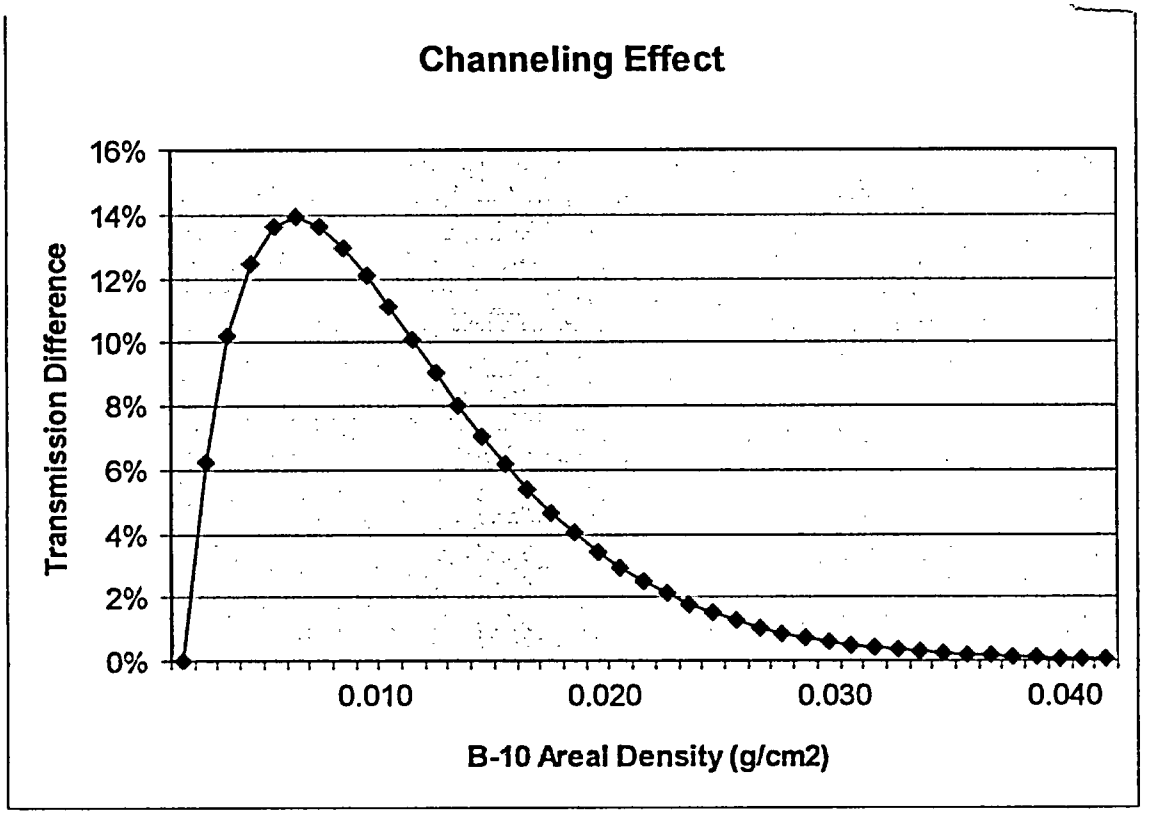

Figure 5-6
Channeling Effect as a Function of ^{10}B Areal Density

Most criticality codes model the neutron absorber as a uniform, homogeneous arrangement of the constituent atoms in the absorber material. No real absorber is completely uniform and homogeneous. For a given ^{10}B areal density, a real absorber has nonuniformities that will result in variations in ^{10}B from the homogeneous assumption. Therefore, all neutron absorbers are manufactured with an additional margin of ^{10}B to assure that there is a high degree of confidence that at any location in the absorber sheet, the ^{10}B present will exceed the minimum specified requirement.

5.4 Effectiveness of ^{10}B in BORAL

The effectiveness of the ^{10}B in a neutron absorber can be measured directly by neutron transmission tests. Transmission measurements show the net effectiveness of the absorber and can be used as the basis for establishing the amount of credit for the ^{10}B in the absorber. This Section will show that the absorption by BORAL manufactured to a specified ^{10}B areal density exceeds the absorption by a homogeneous absorber with that ^{10}B areal density.

ISG-15 states:

> "The effects of material heterogeneity on poison effectiveness should be tested by performing neutron attenuation and/or reactivity worth measurements on material samples or coupons. The test measurements should be calibrated against identical measurements performed on known homogeneous materials of similar composition (e.g., zirconium diboride with a known thickness of aluminum for calibrating measurements of Boral or borated aluminum) [Gao]."

The reference cited in the above paragraph is a dissertation by Jun Gao entitled, "Modeling of Neutron Attenuation Properties of Boron-Aluminum Shielding Materials."[29] Gao tested BORAL using neutron transmission measurements and compared the results to measurements through zirconium diboride standards with known ^{10}B areal densities. Figure 5-6 is reproduced from Gao's dissertation. Following is Gao's discussion of the tests results:

> "The good match of the transmission coefficient curves of ZrB2 and BORAL implied that when having the same 10B areal density, these two materials have the same neutron attenuation effect." And "in the above experiments, the streaming effect was not observed."

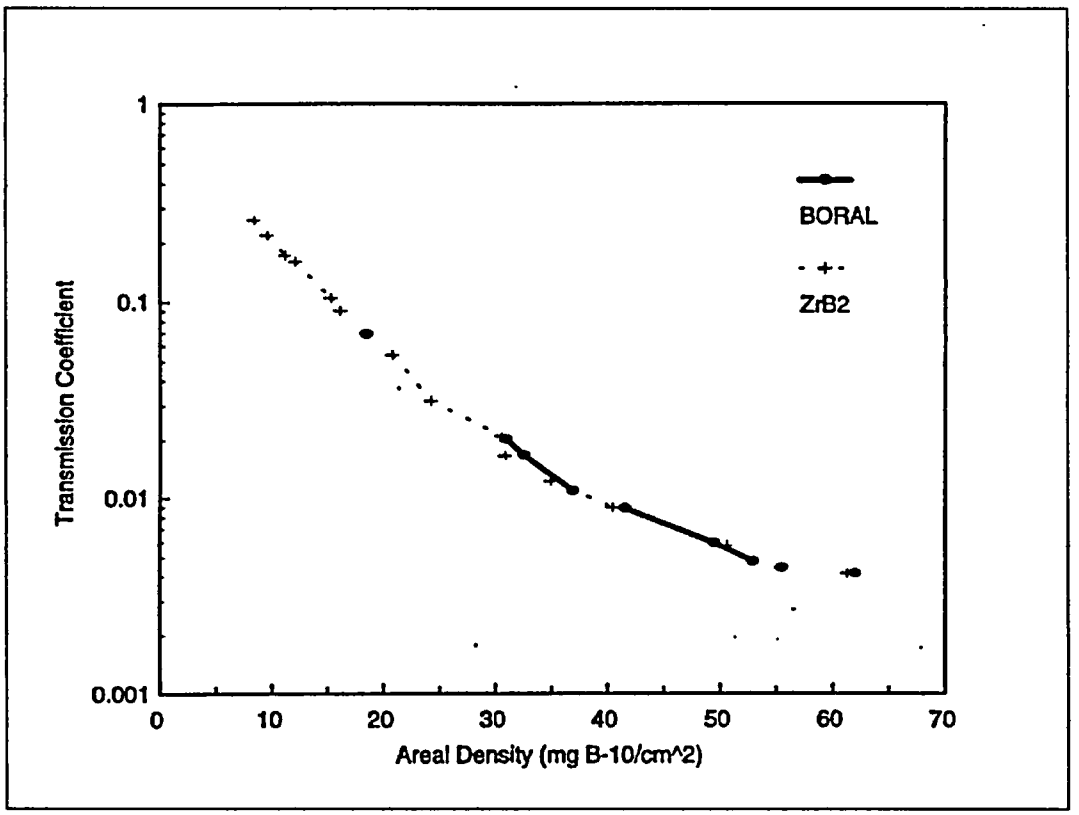

Figure 5-7
Comparison of Neutron Transmission Through BORAL and ZrB_2 (Gao)

Gao's measurements show that there are no significant channeling/streaming effects through BORAL. Nevertheless, the BORAL design formula includes a large margin of additional B_4C to assure that the effective ^{10}B content in BORAL exceeds the customer specified minimum.

To demonstrate the net effectiveness of BORAL, NETCO tested as-manufactured BORAL using neutron attenuation measurements. To benchmark the tests, NETCO used standards made from an aluminum/B_4C metal matrix composite (MMC) material, which is essentially a homogeneous absorber, with known ^{10}B areal densities, over the range of areal densities of interest. BORAL samples with low (0.015 g $^{10}B/cm^2$), medium (0.028 g $^{10}B/cm^2$), and high (0.037 g $^{10}B/cm^2$) areal densities were tested and the values were fitted to the BORAL curve shown in Figure 5-7[30]. The measurements confirm that the neutron absorption by as-manufactured BORAL has a significant margin above the specified minimum ^{10}B areal density.

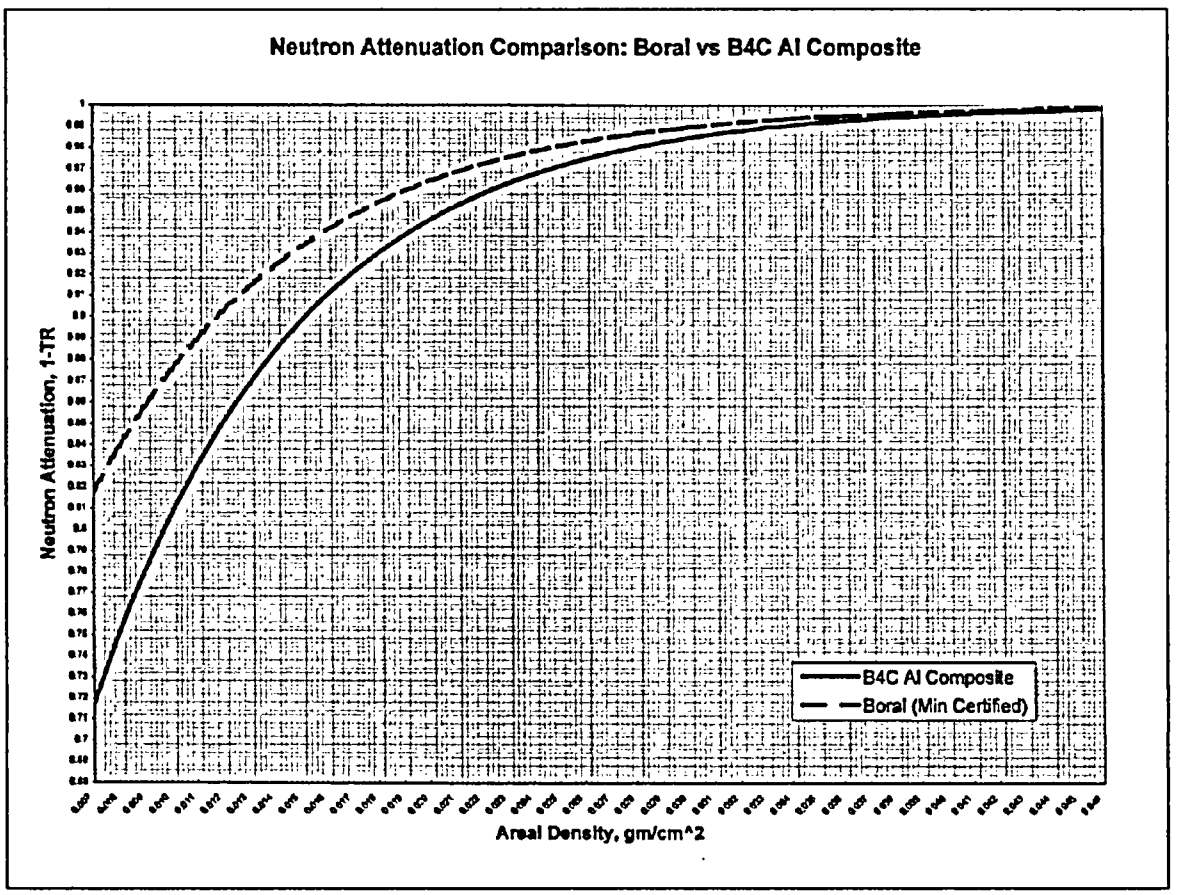

Figure 5-8
Effectiveness of ^{10}B in BORAL

In summary, the ^{10}B in BORAL is uniformly distributed and thermal neutron channeling through BORAL is not significant. BORAL designs for dry storage applications generally have a high B_4C content (50% and higher) and high ^{10}B areal density (0.025 g/cm^2 and greater), and therefore, the effectiveness of the ^{10}B in BORAL is very high. Any nonuniformities are compensated by the conservative BORAL design, so that the effective ^{10}B contained in BORAL is greater than the customer specified minimum value.

If any changes are made in the BORAL design (such as a change in the powder formula, change in B_4C powder size/distribution, etc.) or the manufacturing process that could adversely affect the effectiveness of BORAL, new qualification testing and/or acceptance tests will be performed on the as-manufactured BORAL. The effectiveness of the ^{10}B in BORAL for a new design or manufacturing process will be confirmed by neutron attenuation measurements. The ^{10}B content determined by neutron attenuation testing will be used to benchmark the standard AAR chemical tests for subsequent acceptance tests of BORAL of the new design.

5.5 Durability of BORAL

The durability of BORAL in high radiation environments has been proven by testing and decades of in-service exposure in spent fuel pools. The durability of BORAL in the environments it will experience in dry fuel storage has been confirmed by several test programs performed by cask suppliers for their specific designs and operating conditions, and by NETCO.

Following are excerpts from a test report prepared by NAC International entitled, "Evaluation of the Structural Fitness of BORAL for Use in NAC Spent Fuel Canisters"[31]:

> "NAC International (NAC) has recently completed a comprehensive testing program to evaluate the structural fitness of BORAL for use in NAC's PWR spent fuel storage and transportation canisters. The testing program included nine separate tests that represented, or exceeded, the maximum design basis conditions that the BORAL will experience during actual canister operations. Based on the test results, NAC has concluded that BORAL is structurally stable and will perform its function as a neutron absorber under all canister operating conditions."
>
> "The NAC testing program was designed to determine if BORAL is structurally capable of withstanding the environmental conditions inside an NAC PWR spent fuel canister. The most severe conditions occur while the fuel is being loaded in the canister in the spent fuel pool and during canister closure, draining, and drying operations. These conditions include: water pressure during fuel loading (for a 40-foot deep pool, the water pressure at the bottom is 17.3 psig); the hydrostatic pressure test of the shield lid weld of 21 psig; and the heat-up of the BORAL after the water is drained from the canister and the canister is vacuum dried (maximum of 30°F/hr for design basis fuel of 23 kW/canister). The tests were designed to simulate the design basis limits as described in the applicable NAC-MPC and NAC-UMS® Final Safety Analysis Reports (FSARs). Significant margins were added to the test values to assure conservatism. The conditions that occur during fuel loading and canister closure

operations were evaluated and were found to bound any other conditions during normal interim storage at the ISFSI or during normal transport conditions."

"The results of the extensive testing program performed by NAC International demonstrate that BORAL is structurally stable under the conditions that the BORAL will experience during NAC canister operations. Tests at values well above the maximum operating values confirmed that adequate material performance margins exist."

EPRI/NETCO recently completed an extensive study of the performance of Improved BORAL (made using the high temperature heating profile) under dry cask operating conditions. The test results will be published in the near future in an EPRI report titled "BORAL Behavior Under Simulated Cask Vacuum Drying Conditions, Part 2"[32]. The following summary is included with permission from EPRI.

The test parameters were:

Test Parameter	Value
Water Immersion	
Water chemistry BWR	Demineralized
Water chemistry PWR	Boric acid (2500 ppm B)
Temperature, °F	100° ± 2°
Time at temperature, hours	96
Pressure, psig	16 ± 1
Time at pressure, hours	96
Hydro Testing	
Temperature, °F	200° ± 2°
Time at temperature, hours	17 (ramp from 100° to 200°)
Pressure, psig	21 ± 1
Time at pressure, minutes	10 ± 2
Vacuum Drying Test	
Initial heatup, °F	250°
Pressure during initial heatup	1 atm
Time to initial temperature, hours	4
Temperature for start of vacuum drying, °F	250°
Final Temperature, °F	550°
Ramp to final temperature, hours	10
Time at final temperature, hours	4
Pressure for vacuum drying, inches H2O	3.3 ± 0.2

A total of 16 coupons were used in the tests. The test coupons were prepared from 4 panels of BORAL. Two coupons from each panel were "dry passivated" and two coupons were non-passivated. The dry passivation process was heating the coupons at 1000°F for 4 hours to increase the thickness of the aluminum oxide layer. Of each pair of coupons from each panel, one coupon was tested in demineralized water and one was tested in 2500 ppm boric acid.

The coupons were originally scheduled for testing through five wetting/drying cycles. Due to the start of a small blister on one coupon in Cycle 5, two additional cycles were added. The blister formed on a coupon that was non-passivated and tested in the PWR water (boric acid) group. The single blister grew and cracked during the 6th cycle and was removed after that cycle for examination. No new blisters formed on any of the other coupons during the 6th and 7th cycles.

There were several significant conclusions from this study, including:

- The new ingot heating profile makes BORAL more resistant to blister formation.
- The NETCO results agree with other studies that indicate that BORAL with low B_4C content generally has lower porosity, and lower porosity BORAL is more susceptible to blister formation.
- BORAL made with 50% or greater B_4C in the core absorbs more water, but the water escapes easily during vacuum drying and heat-up. BORAL with high B_4C loadings (50-65%) is more blister resistant, since there is less aluminum to fill in the irregular volume around the B_4C particles, which results in greater porosity. Greater porosity allows water to escape and prevents blisters.
- None of the BORAL coupons that were "dry passivated" by NETCO (heated to 1000°F for 4 hours prior to testing) had any sign of blisters or other deformation after 7 test cycles.

An important finding was a corrosion mechanism for blister formation. Following is an excerpt from the draft report:

> "The data from the Series 1 tests clearly show that the current AAR manufacturing process produces a BORAL which is resistant to the formation of blisters during MPC wetting and vacuum drying conditions. Destructive examination of one blister which formed in cycle 5 and grew into two large coincident blisters in cycle 6 provide clear evidence as to the mechanism of blister formation. Corrosion pits, likely due to chemical contamination on the clad surface, grew in depth in the first four wetting cycles, penetrating the clad during wetting cycle 5 and providing a pathway for boric acid into the core."

Following the identification of pitting corrosion as the mechanism for the formation of the blister, NETCO destructively examined blisters formed on coupons in previous tests. NETCO found through-cladding penetrations at the site of all blisters. Most of the penetrations appeared to be corrosion pits.

5.6 Conclusion

In conclusion, the design, manufacturing, and performance of BORAL satisfy all of the criteria for 90% credit for the minimum amount of ^{10}B specified. With 90% credit for the specified ^{10}B in BORAL, AAR will be able to further enhance the integrity of BORAL by increasing the cladding thickness. The thicker cladding will provide greater resistance to deformation and additional corrosion protection. These improvements, combined with the new heat process used in manufacturing to increase the protective aluminum oxidation layer and reduce hydrogen generation, will minimize or eliminate the occurrence of blisters in BORAL.

6.0 References:

1. NUREG-1536, "Standard Review Plan for Dry Cask Storage Systems"
2. NUREG-1567, "Standard Review Plan for Spent Fuel Dry Storage Facilities"
3. NUREG-1609, "Standard Review Plan for Transportation Packages for Radioactive Material"
4. NUREG-1617, "Standard Review Plan for Transportation Packages for Spent Nuclear Fuel"
5. NUREG/CR-5661, "Recommendations for Preparing the Criticality Safety Evaluation of Transportation Packages"
6. "Magnesium", quarterly magazine published by Brooks & Perkins, August 1956
7. "BORAL: A NEW THERMAL NEUTRON SHIELD", ORNL-242, by V.L. McKinney and Theodore Rockwell, 1949; and Supplement I, ORNL-981, May 1954
8. "Results of a Survey on the Use of Boral in Shielding", paper presented at the Atomic Energy Commission Conference on Radiation Shielding, May, 1954
9. "How Channeling between Chunks Raises Neutron Transmission through Boral", Walter R. Burrus, Nucleonics, January 1958
10. "Boral Radiation Attenuation Characteristics", KT-251, Massachusetts Institute of Technology, November 27, 1956
11. "Radiation Transmission Through Boral and Similar Heterogeneous Materials Consisting of Randomly Distributed Absorbing Chunks", ORNL-2528, Walter R. Burrus, January 18, 1960
12. "Experimental Observation of BORAL Plates Encased in Stainless Steel Under the Influence of Gamma and Neutron Fluxes", University of Michigan, February 1976
13. "Quantitative Analysis of Boral Panels", Brooks & Perkins Report No. 540, July 30, 1976
14. Neutron transmission measurements vs. B_4C mesh size and neutron energy (data and graphs) sent with cover letter to L. Mollon, Brooks & Perkins, from R. Burn, University of Michigan, December 2, 1976
15. "Neutron Transmission Through Boral Shielding Material", University of Michigan, January 1978
16. "Neutron Transmission Through Boral Shielding Material; Theoretical Model and Experimental Comparison", University of Michigan, April 1978
17. "Boral Neutron Absorbing/Shielding Material, Product Performance Report", Brooks & Perkins Report No. 624, July 20, 1982
18. "Effects of Gamma Radiation on the Neutron Attenuation Properties of Boral", Brooks & Perkins Report No. 637, February 1985
19. "Corrosion Resistance of BORAL to One Year of Exposure to BWR Storage Pool Water", Brooks & Perkins Report No. 551, February 1977
20. "Spent Fuel Storage Module Corrosion Report", Brooks & Perkins Report No. 554, June 1, 1977

21. "Storage Module Corrosion Testing", Brooks & Perkins Report No. 561, not dated
22. "The Suitability of Brooks & Perkins Spent Fuel Storage Module for Use in PWR Storage Pool", Brooks & Perkins Report No. 578, July 7, 1977
23. "Criticality Effect of Neutron Channeling Between Boron Carbide Granules in Boral for a Spent-Fuel Shipping Cask", A. H. Wells, D. R. Marnon, and R. A. Karam, 1987
24. NUREG/CR-6407, "Classification of Transportation Packaging and Dry Spent Fuel Storage System Components According to Importance to Safety"
25. "The Surface Treatment and Finishing of Aluminum and its Alloys", S. Wernick, R. Pinner, and P.G. Sheasby, ASM International, Fifth Edition, 1987
26. "Oxidation of Al Powder," Study prepared by Nottingham University for AAR Manufacturing, September 2004
27. "Review and Evaluation of ^{10}B Areal Density Measurements of BORAL Coupons", Prepared for AAR Cargo Systems by Northeast Technology Corp., February 2004
28. Interim Staff Guidance 15, "Materials Evaluation", NRC Spent Fuel Project Office
29. "Modeling of Neutron Attenuation Properties of Boron-Aluminum Shielding Materials", Jun Gao, Dissertation to the School of Engineering and Applied Science, University of Virginia, August 1997
30. "Neutron Attenuation Comparison: Boral vs B_4C Al Composite," transmittal from S. Leuenroth, NETCO, to J. Hobbs, AAR, September 13, 2004
31. "Evaluation of the Structural Fitness of BORAL for Use in NAC Spent Fuel Canisters", NAC International, March 2002
32. "BORAL Behavior Under Simulated Cask Vacuum Drying Conditions, Part 2", EPRI, soon to be published

ATTACHMENT A

Statistical Analyses of B_4C Powder Purity, Boron Content in B_4C, and Percentage of ^{10}B in Boron

Attachment A
Page 1 of 3

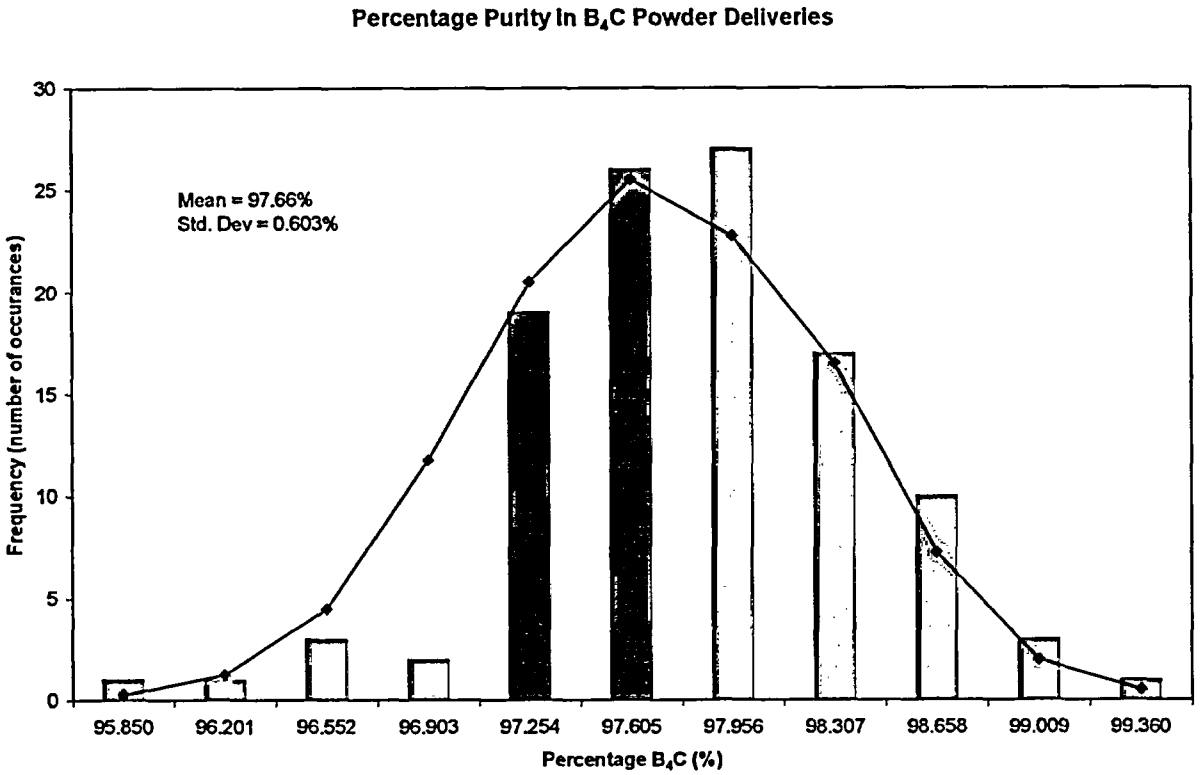

Figure A-1
Statistical Analyses of the B_4C Powder Purity

Attachment A
Page 2 of 3

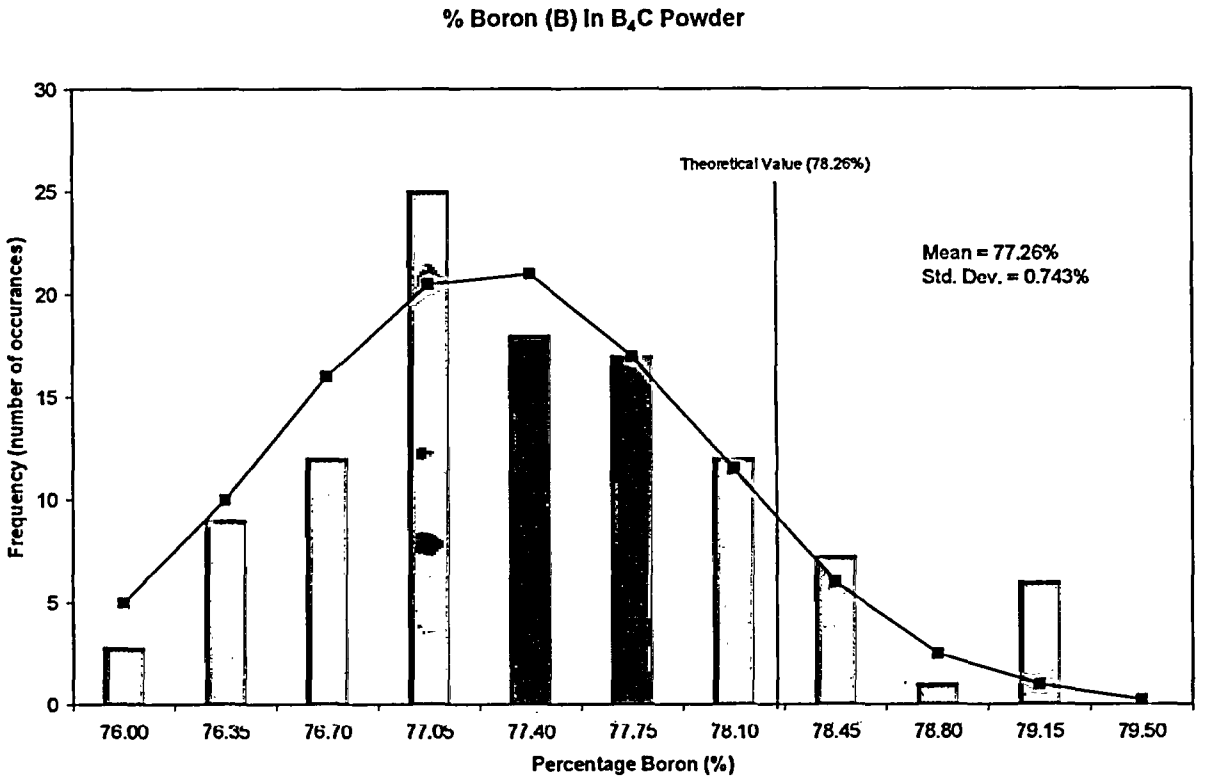

Figure A-2
Statistical Analyses of Boron Content in B_4C

Attachment A
Page 3 of 3

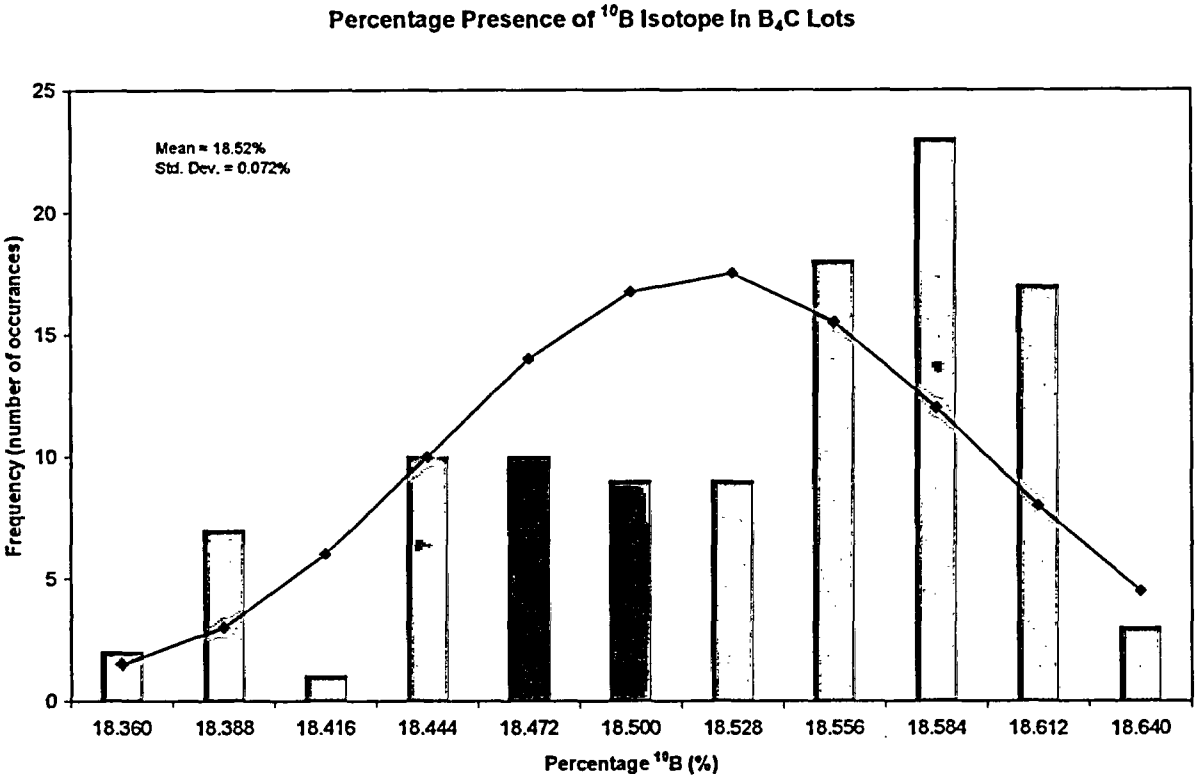

Figure A-3
Statistical Analyses of Percentage of ^{10}B in Boron

ATTACHMENT B

NETCO report titled "Review and Evaluation of ^{10}B Areal Density Measurements of BORAL Coupons"

Attachment B
Page 1 of 21

Report No. : NET 230-01

Review and Evaluation of B_{10} Areal Density Measurements of BORAL Coupons

February 2004

Prepared
for
AAR Cargo Systems, Inc.
under
Purchase Order No.: 219535

Prepared
by
Northeast Technology Corp.
108 North Front Street
UPO Box 4178
Kingston, NY 12402

Rev.	Date	Prepared by:	Reviewed by:	Approved (QA):
-0-	3/25/04			

NET-230-01

Table of Contents

NET-230-01

Review and Evaluation of ^{10}B Areal Density Measurements of BORAL Coupons

1.0 Introduction

BORAL is the trade name for a neutron absorber manufactured by AAR Corporation of Livonia, Michigan. BORAL is a laminated panel with solid aluminum cladding and a core of blended boron carbide (B_4C) and aluminum powders, compressed by hot rolling. Boral is manufactured according to established processes and procedures.

The purpose of this test program is to provide applicants for dry fuel storage systems supporting data to request NRC approval for credit for 90% of the ^{10}B contained in BORAL used in the system. NRC Standard Review Plans limit the credit for ^{10}B contained in fixed neutron absorbers for dry fuel storage systems to 75%, unless comprehensive tests are performed to verify that the fabrication process for the neutron absorber assures the presence and uniformity of the neutron poison (^{10}B) in the absorber material.

A method has been proposed (Reference 1) for the computation of percent credit for boron-based neutron absorbers. This method specifies that "material for which data is presented to show the measured attenuation for thermal neutrons to be at or above the acceptance attenuation (A_e), is given the full credit of 90 percent." This test program was developed to meet the test requirement for 90% credit. The neutron attenuation tests, combined with the established BORAL manufacturing procedures, provide verification of the presence and uniformity of the ^{10}B in BORAL panels.

The coupons tested used in this program were provided by AAR. AAR selected the coupons from a commercial production run of 3236 BORAL panels. Production required 114 powder batches; each powder batch yields 30 panels. One panel was randomly selected from each group of 30 panels made from each unique powder batch. Two coupons were cut from random locations from each of the 114 BORAL panels selected for the test, for a total of 228 BORAL test coupons.

The coupons were rectangular and approximately 5.5 inches wide by 11.0 inches long. The minimum certified areal density for these coupons is 0.020 gms B-10/cm^2. The areal densities were measured at 4 locations on each coupon providing a total of 912 measurements. The measurements were made via neutron attenuation testing using known calibration standards to determine the areal densities.

This report documents a statistical analysis of the 912 areal density measurements which demonstrates compliance with requirements for 90% boron credit in dry storage casks. The analysis described subsequently serves to demonstrate that this criteria is satisfied for the 912 areal density measurements on BORAL coupons.

NET-230-01

2.0 Methodology

The proposed method specifies that it "is to be used to compute the level of credit to be allowed for 1/v neutron absorber materials, such as boron or lithium. The computation of the allowed level of credit uses the results of neutron attenuation measurements performed on samples of the absorber material placed in a beam of thermal neutrons."

The standard specifies the following variables among its definitions:

A = neutron attenuation, a measured value taken on a given absorber material in a beam of thermal neutrons with fixed energy spectrum. A is assumed to be normally distributed with mean μ and standard deviation σ.

A_a = acceptance value of neutron attenuation, based on a qualified homogeneous absorber standard such as ZrB_2, evaluated at 111% (i.e.1/0.90) of the poison density assumed in the criticality computational model.

A_d = attenuation tolerance limit, a statistic of the data

n = number of coupon measures of attenuation A

P = probability

μ = true mean of A

$\bar{x}$ = estimate of μ

σ = true standard deviation of A

S = estimate of σ

C_p = exact number of standard deviations required at probability P

K_p = tolerance coefficient that is substituted for C_p when μ and σ are estimated by $\bar{x}$ and S, respectively

γ = confidence level

The method specifies that, "data taken under the above rules are used to bound the probability P that the value of neutron attenuation A at an arbitrary location on the material is greater than the acceptance attenuation A_a. This is done by computing an attenuation tolerance limit, A_d, such that, with 95 percent confidence, the probability is less than 0.001 that $A < A_d$."

NET-230-01

In the current analysis, the areal density has been computed instead of the neutron attenuation. The areal density is directly proportional to the neutron attenuation. The analysis described subsequently demonstrates that with 95 percent confidence the probability is less than 0.001 that the measured areal density will be less than 111% of the minimum certified areal density.

Implicit in the proposed method is the assumption that the data is normally distributed. To satisfy that this requirement has been met, two tests for normality, Kolmogorov-Smirnov and Anderson-Darling, have been applied to the test data. In addition, the cumulative probability versus areal density has been examined as a further test of normality.

3

NET-230-01

3.0 Test Data

3.1 Test Method

Tests have been performed by NETCO in the Beam Hole Laboratory of the Breazeale Reactor Facility at Penn State University. In these tests a collimated thermal beam of neutrons from the reactor is passed through the Boral coupons placed perpendicular to the incident beam. The intensity of the incident and attenuated beams are measured with BF_3 detectors. These attenuation values were then converted to areal density measurements using a curve fit based on attenuation measurements on coupons of known areal density.

Four locations on each coupon were tested in this manner and the resulting data has been compiled into a single data file that was utilized for this analysis.

3.2 Raw Data

The coupon test results are contained in Appendix A. A subset of the data containing only the areal density measurements is constructed for use in the subsequent statistical analyses. The data is structured in four columns with each column representing a different measurement location on each coupon. All of the data points are plotted here to illustrate the distribution of measured areal density values.

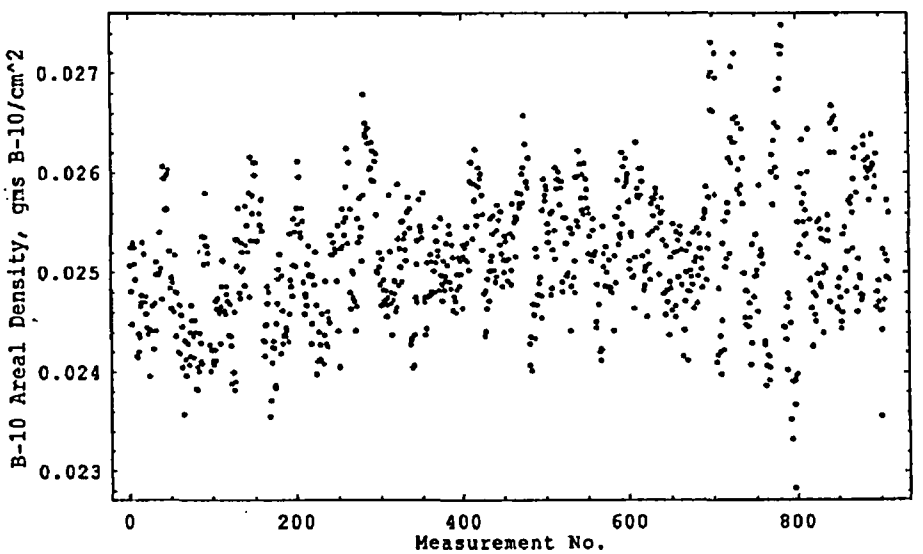

Figure 3-1: Measured Areal Density versus Measurement Number

NET-230-01

3.3 One-Sided Tolerance Factor Calculation

The proposed method specifies that a one-sided tolerance factor be calculated to determine, with 95% confidence, the value above which 99.9% of the areal density measurements lie. The tolerance factor itself varies with the degree of confidence, fraction of data in question, and number of samples being tested. Factors have been calculated in tables for several different parameters, however, none of the available tables contain the parameters specified for this test. As such, an approximate formula for the tolerance factor is utilized to provide the necessary value given the parameters of this analysis.

The approximate calculation of a one-sided tolerance factor κ, comes from the following formulas (Reference 2):

$$K = \frac{Z_{1-P} + \sqrt{Z_{1-P}^2 - ab}}{a} \qquad \text{Equation 1}$$

$$a = 1 - \frac{Z_{1-P}^2}{2(N-1)}; b = Z_{1-P}^2 - \frac{Z_{1-\gamma}^2}{N} \qquad \text{Equation 2}$$

where:

Z_{1-P} = Standard Normal Score at 1 - P level of significance

N = Number of Samples (912)

These equations are an approximation, however and deviate conservatively from the tabular values in Reference 2 for smaller samples sizes. The difference between the two methods quickly approaches zero after as few as 40 samples. Given that we are working with a sample size of 912, the approximation formula will produce an adequately precise value.

The one-Sided Tolerance factor for P=0.999, α=0.05 & n=912 is calculated to be 3.22572

NET-230-01

4.0 Analysis of Areal Density Measurements

4.1 Distributed Properties of the Areal Density Measurements

In order to apply the one sided tolerance factors described in Section 4.1, it must be demonstrated that the areal density data are normally distributed. Figure 4-1 shows the areal density measurements distribution. Table 4-1 contains a summary of the properties of the distributed data. The tests show what appears to be a normally distributed data set with a mean coupon areal density of 0.025 gms B-10/cm^2. There is a slight skewing of the data towards higher areal density values and the kurtosis shows that there is more concentration of data near the mean than in a completely normal distribution. However, these values represent a small deviation from a normal distribution and are conservative with respect to a minimum areal density evaluation.

Figure 4-1: Areal Density Measurements: Distributed Data

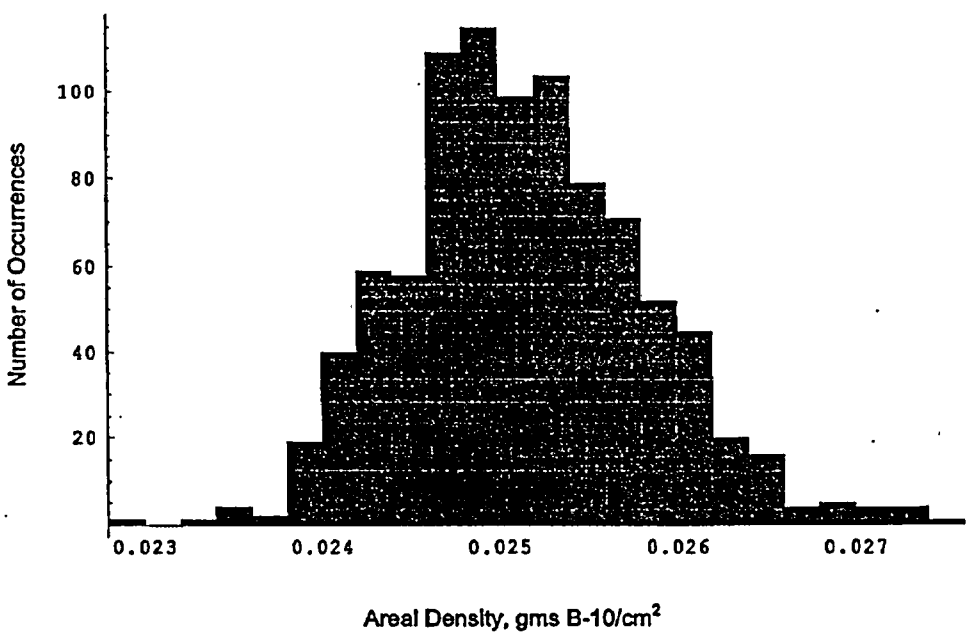

NET-230-01

Table 4-1

Properties of the Distributed Data

Location Statistics		Dispersion Statistics		Shape Statistics	
Mean	0.0251432	Variance	4.587×10^{-7}	Skewness	0.309405
Harmonic Mean	0.0251251	Standard Deviation	0.000677	Quartile Skewness	0.056328
Median	0.0251133	Mean Deviation	0.0005399	Kurtosis Excess	0.177064
		Median Deviation	0.000447		

4.2 Test for Normality

The first step in testing for normality is to construct a cumulative probability plot from the data set. This is accomplished by arranging the data set in order of ascending areal density and computing the cumulative frequency for each data point as:

$$\frac{(j-0.05)}{10} \qquad \text{Equation 3}$$

For j = 1...912

Figure 4-2 is plot of the cumulative probability versus areal density. It is noted that the data appears to be clustered toward the center of the distribution. This is expected based on the Kurtosis excess shown in Table 4-1. It is also noted that with the exception of a few data points at the upper and lower tails of the distribution, the cumulative probability is well approximated by a straight line. This confirms that a normal distribution is an appropriate model.

The Anderson-Darling and Kolmogorov/Smimoff test statistics are calculated subsequently as further tests of normality.

NET-230-01

Figure 4-2: Cumulative Probability versus Areal Density

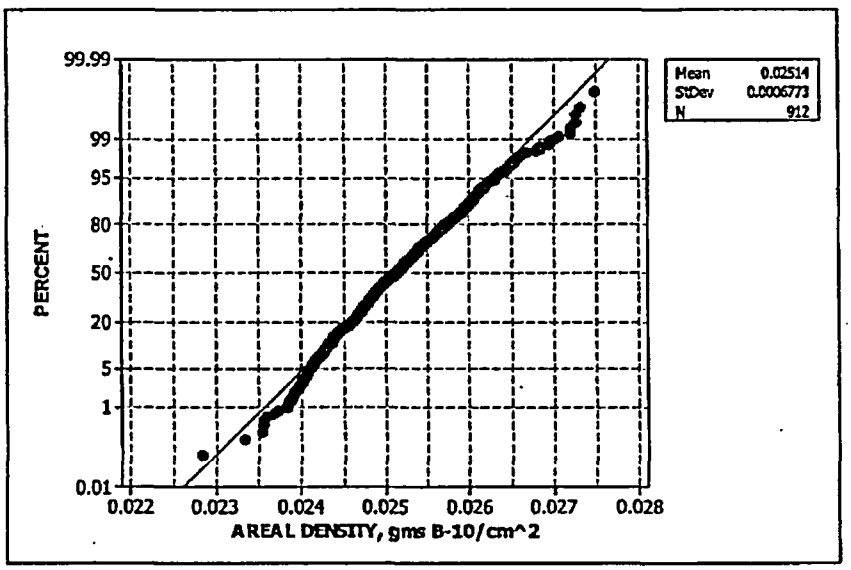

4.2.1 Kolmogorov-Smirnov Test for Normality

In applying the Kolmogorov/Smirnoff test for normality, a test statistic D is calculated for the data distribution. D is the difference between the ordered areal density values and their predicted cumulative probability under the assumption of a normal distribution. The calculated value for the BORAL areal density data is 0.0329.

Under the Kolmogorov/Smirnoff test, D must be less than a certain critical value. The large sample critical value at a 95% confidence is 0.24. Accordingly, we cannot reject the hypothesis that the density are normal distributed.

4.2.2 Anderson-Darling Test for Normality

The Anderson-Darling test is based on the test statistic, A^2, which examines the differences between the tails of the normal distribution and the tails of the test data. The null hypothesis (that the data is normally distributed) is rejected for measures of the test statistic that exceeds a certain critical value.

The test statistic can be calculated numerically from:

$$A^2 = -\left[\sum_{i=1}^{n}(2i-1)(\ln(u_i)+\ln(1-u_{n+1-i}))\right]/n - n \qquad \text{Equation 4}$$

where u_i is the value of the theoretical cumulative distribution at the i^{th} largest observation. The test statistic calculated for the Boral areal density values is 1.3018.

The large sample critical value for the Anderson-Darling test is 2.492 at 95% confidence and 3.857 at 99% confidence. Thus we cannot reject the null hypothesis that the data are normally distributed. It is noted that there is some significant deviation in the tails of the data, a situation to which the Anderson-Darling test is very sensitive. This is reflected in the relatively high test statistic value (1.3018) for the test data.

4.3 One-Sided Tolerance Limit and Assessment of 90% Boron Credit

The following equation provides the one sided tolerance limit to the observed coupon areal density:

$$A_d = \bar{x} - K_{.912}S \qquad \text{Equation 5}$$

where the variable definitions are identical to those outlined previously. Given that the data passes the test for normality, the calculation for the above one-sided tolerance limit is applicable.

Thus the lower tolerance areal density limit is 0.0229 gms B-10/cm^2. The minimum certified areal density is 0.020 gms B-10/cm^2 for the Boral samples tested. The areal density at 111% of the minimum certified value of 0.020 is 0.0222 gms B-10/cm^2. Thus 0.0229 gms B-10/cm^2 > 0.0222 gms B-10/cm^2 and $A_d \geq A_s$ and 90% boron credit is demonstrated.

NET-230-01

5.0 Summary and Conclusions

Areal density measurement obtained via neutron attenuation testing at 4 locations each on 228 Boral coupons have been evaluated. The data have been demonstrated to be normally distributed. Accordingly, a one sided tolerance factor for normally distributed data can be applied. This has been computed following the method of Natrella and is 3.226 at 99.9% probability and 95% confidence level.

The proposed method of Reference 1 has been applied to the data set. The minimum certified areal density for this Boral is 0.020 gms B-10/cm^2. The mean of the measured data is 0.02514 gms B-10/cm^2. At a 99.9% probability and a 95% confidence level the one sided lower tolerance limit is 0.0229 gms B-10/cm^2 which exceeds 111% of the minimum certified areal density. Accordingly 90% credit for boron-10 is demonstrated.

6.0 References

1) Standard Guide for Thermal Neutron Absorber (Poisons) for Criticality Control in Dry Cask Storage Systems (DCSS) or Transportation Packages Containing Fissile Materials, Proposed by ASTM Subcommittee c26.03, 5/8/2003.

2) Natrella, M.G., Experimental Statistics, National Bureau of Standards Handbook 91, 8/1/63.

NET-230-01

Appendix A

BORAL Coupon B-10 Areal Density Test Data

(For each coupon B-10 areal density $\left(\frac{gm}{cm^2}\right)$ is provided for locations A, B, C and D)

NET-230-01

Appendix A

Test Data

Coupon ID	A	B	C	D
WN310009-1-1	0.025062784	0.024806101	0.025250876	0.024480108
WN310009-1-2	0.025295658	0.025086125	0.025252807	0.024921785
WN310010-1-1	0.024152418	0.024151064	0.024378336	0.024202582
WN310010-1-2	0.024352811	0.024659791	0.024761737	0.024701446
WN310025-1-1	0.025310048	0.02518946	0.024700361	0.024747781
WN310025-1-2	0.024580798	0.024444167	0.024380079	0.02440745
WN310039-1-1	0.023953087	0.024438754	0.024408661	0.02465363
WN310039-1-2	0.024672659	0.024228369	0.024687562	0.024413707
WN310048-1-1	0.025107024	0.024973144	0.0249895	0.02497466
WN310048-1-2	0.025397755	0.025000009	0.025044618	0.024732663
WN310057-3-1	0.026060044	0.025943994	0.02593695	0.025635984
WN310057-3-2	0.02597623	0.025634738	0.025991252	0.026032276
WN310061-1-1	0.025224999	0.024849114	0.024948213	0.024638632
WN310061-1-2	0.024898957	0.024600053	0.025178941	0.02480407
WN310075-3-1	0.024364684	0.024797911	0.024201101	0.024193524
WN310075-3-2	0.024664107	0.024569897	0.024569525	0.024457774
WN310089-2-1	0.024046765	0.023573319	0.024314851	0.023963183
WN310089-2-2	0.02412745	0.02396863	0.024289791	0.024072452
WN310092-1-1	0.024400776	0.024162693	0.02467133	0.024521085
WN310092-1-2	0.02436154	0.024143137	0.024520822	0.024401198
WN310104-1-1	0.023831937	0.024049098	0.023821381	0.02400616
WN310104-1-2	0.024390186	0.024299037	0.024099889	0.024080493
WN310110-1-1	0.025373166	0.025079003	0.025794203	0.025359912
WN310110-1-2	0.025280417	0.025269293	0.025199859	0.025094384
WN310121-1-1	0.024272875	0.024006694	0.024225933	0.024220253
WN310121-1-2	0.024102052	0.024075745	0.02421622	0.024114638
WN310139-2-1	0.024712177	0.024640813	0.024742599	0.024591163
WN310139-2-2	0.02461095	0.024280069	0.024661688	0.024862879
WN310146-2-1	0.025119246	0.025126485	0.024612966	0.024587419
WN310146-2-2	0.02486097	0.024785377	0.02470586	0.024366957
WN310159-1-1	0.024683577	0.024266206	0.024359331	0.023880987
WN310159-1-2	0.023998171	0.023817214	0.024607315	0.023905208

Attachment B
Page 16 of 21

NET-230-01

WN310160-3-1	0.025342119	0.025062351	0.025643139	0.025336303
WN310160-3-2	0.024797053	0.02473757	0.025010589	0.025302956
WN310178-3-1	0.025207332	0.025038543	0.025669036	0.024866697
WN310178-3-2	0.025284033	0.025471761	0.025206727	0.024754864
WN310189-3-1	0.025791584	0.02616027	0.025330142	0.025774087
WN310189-3-2	0.025591125	0.026108237	0.025977552	0.026101363
WN310191-1-1	0.025329923	0.025311747	0.025331261	0.025591665
WN310191-1-2	0.025491384	0.025480582	0.02572866	0.025418951
WN310203-3-1	0.024319779	0.024152398	0.024305606	0.024461341
WN310203-3-2	0.024471521	0.024689251	0.024861995	0.024804559
WN310219-3-1	0.023548182	0.023711944	0.024098474	0.024253562
WN310219-3-2	0.024307312	0.024244783	0.02386301	0.023837085
WN310229-3-1	0.024489568	0.024689865	0.025025203	0.024938471
WN310229-3-2	0.025186076	0.024188899	0.024962587	0.024289017
WN310231-3-1	0.024612605	0.024355676	0.024385391	0.024363196
WN310231-3-2	0.024447336	0.024428654	0.02430794	0.0245779
WN310248-2-1	0.025387475	0.024924922	0.024860293	0.024765164
WN310248-2-2	0.025536062	0.025070611	0.025410071	0.025061323
WN310253-3-1	0.025646942	0.025484394	0.026117152	0.025959746
WN310253-3-2	0.025397081	0.025362524	0.025650442	0.025515734
WN310269-1-1	0.024897995	0.024583602	0.02478124	0.024753167
WN310269-1-2	0.024664961	0.025079898	0.025277477	0.024967961
WN310270-2-1	0.024975498	0.024282817	0.024952272	0.024487692
WN310270-2-2	0.024964347	0.024884132	0.025208686	0.024663578
WN310284-3-1	0.023974464	0.024105729	0.024405032	0.024127656
WN310284-3-2	0.024273225	0.024117766	0.024584294	0.02408033
WN310295-3-1	0.024372285	0.02436898	0.024914282	0.024282916
WN310295-3-2	0.024605536	0.024256535	0.024545289	0.024495201
WN310309-3-1	0.025377409	0.025378078	0.025188766	0.025179848
WN310309-3-2	0.025307682	0.025199705	0.02524281	0.025231378
WN310312-3-1	0.024912399	0.024416244	0.025476981	0.024053059
WN310312-3-2	0.025239974	0.025239084	0.025265478	0.025639317
WN310327-1-1	0.025504648	0.025385105	0.025855037	0.02555185
WN310327-1-2	0.026239722	0.025292016	0.026102825	0.025639398
WN310331-1-1	0.024798475	0.024638805	0.025009472	0.024991368
WN310331-1-2	0.024741325	0.02471565	0.024410207	0.024655964
WN310343-1-1	0.025540763	0.025536554	0.025310426	0.025738992

NET-230-01

WN310343-1-2	0.025364315	0.025453822	0.025116241	0.025771357
WN310359-2-1	0.026783062	0.026392283	0.026498241	0.026358498
WN310359-2-2	0.026428689	0.026293496	0.026444899	0.026025109
WN310367-2-1	0.026053634	0.026302659	0.025920976	0.0262237
WN310367-2-2	0.025909552	0.02610902	0.025577502	0.02618893
WN310371-1-1	0.025011299	0.024982683	0.02520151	0.025050198
WN310371-1-2	0.024884052	0.024664818	0.025132229	0.024827907
WN310388-3-1	0.024923048	0.024715196	0.024817084	0.024668895
WN310388-3-2	0.024546168	0.024745426	0.025770323	0.025209445
WN310390-3-1	0.02479099	0.02469223	0.024367891	0.024716781
WN310390-3-2	0.024784283	0.024908228	0.024600173	0.024642192
WN310401-2-1	0.025878628	0.025339147	0.024874567	0.025243269
WN310401-2-2	0.025052215	0.02550945	0.024901818	0.025521616
WN310418-3-1	0.025339326	0.025232267	0.025390233	0.025117152
WN310418-3-2	0.02560807	0.025748131	0.025442231	0.025637384
WN310428-3-1	0.024271066	0.024319813	0.02435357	0.024035317
WN310428-3-2	0.024063883	0.024367709	0.024739131	0.024698693
WN310433-3-1	0.025082176	0.025327353	0.025729351	0.025461976
WN310433-3-2	0.025456227	0.025409627	0.025349646	0.025793764
WN310443-1-1	0.024743934	0.024702981	0.024372821	0.024436573
WN310443-1-2	0.024754107	0.025098629	0.02473717	0.024766014
WN310452-3-1	0.02518011	0.024802825	0.025108593	0.024785904
WN310452-3-2	0.025004612	0.024793911	0.025460044	0.025097562
WN310464-3-1	0.025312942	0.025217135	0.02516141	0.024815393
WN310464-3-2	0.025541755	0.024962146	0.024711228	0.02487988
WN310471-1-1	0.025109669	0.02482858	0.02495189	0.024909421
WN310471-1-2	0.025300498	0.025069008	0.025478954	0.025385999
WN310486-3-1	0.024901833	0.024838183	0.025281738	0.024611482
WN310486-3-2	0.025148373	0.024755141	0.024710614	0.024588301
WN310493-3-1	0.024829724	0.024976731	0.025151142	0.024861691
WN310493-3-2	0.024975819	0.025118687	0.024972047	0.02463536
WN310501-1-1	0.025157272	0.025279835	0.025253202	0.025126509
WN310501-1-2	0.025462926	0.025298829	0.025104468	0.025019828
WN310510-2-1	0.025908263	0.026099029	0.026107352	0.025887887
WN310510-2-2	0.025336303	0.02572533	0.026233009	0.025884894
WN310527-1-1	0.025481268	0.025568707	0.026055574	0.025854099
WN310527-1-2	0.025931636	0.025983497	0.025776582	0.025578602

NET-230-01

WN310532-2-1	0.025230941	0.02478146	0.02436056	0.024817718
WN310532-2-2	0.024401762	0.024631024	0.024934355	0.024711376
WN310545-2-1	0.0255409	0.025012667	0.025112927	0.025171974
WN310545-2-2	0.025388614	0.025577035	0.025018442	0.024898188
WN310550-2-1	0.02542234	0.024949884	0.025673425	0.025528334
WN310550-2-2	0.025609758	0.02561872	0.02528044	0.025184991
WN310564-1-1	0.024860678	0.025124858	0.0249959	0.025364587
WN310564-1-2	0.025321788	0.025116591	0.025140268	0.024912686
WN310570-3-1	0.025132215	0.025390106	0.024876752	0.02502303
WN310570-3-2	0.025690245	0.025363542	0.025505345	0.02515642
WN310588-2-1	0.025560333	0.025525504	0.025797359	0.025692725
WN310588-2-2	0.025650119	0.025653986	0.025779399	0.025985878
WN310597-2-1	0.026055311	0.025695887	0.026571999	0.026289661
WN310597-2-2	0.025902261	0.025907078	0.025846972	0.026147002
WN310606-2-1	0.024062615	0.024282215	0.024343733	0.024010414
WN310606-2-2	0.024683882	0.024569179	0.024676478	0.024333554
WN310614-1-1	0.025242764	0.025152711	0.024665262	0.024779327
WN310614-1-2	0.024891686	0.024948751	0.024760994	0.024545099
WN310622-1-1	0.02562412	0.025937174	0.025725776	0.025771429
WN310622-1-2	0.025867963	0.025825565	0.025490722	0.025401633
WN310636-2-1	0.025303872	0.025593779	0.024771754	0.024836724
WN310636-2-2	0.025618324	0.025231276	0.025427714	0.02514052
WN310641-1-1	0.026045256	0.025834679	0.025928522	0.026006486
WN310641-1-2	0.02591236	0.025681345	0.025849059	0.025909118
WN310659-3-1	0.024810211	0.024904006	0.025549148	0.025552879
WN310659-3-2	0.025290864	0.024956939	0.025295604	0.024990644
WN310661-3-1	0.02544206	0.024415477	0.025443774	0.024864616
WN310661-3-2	0.025389151	0.024943107	0.025113668	0.024795219
WN310673-1-1	0.02595298	0.025514257	0.025964729	0.025461431
WN310673-1-2	0.026222721	0.026083706	0.025741865	0.025626861
WN310681-3-1	0.025977647	0.025577403	0.026092906	0.025741408
WN310681-3-2	0.025933166	0.02582296	0.025644319	0.025185094
WN310693-3-1	0.025591089	0.02537274	0.025175017	0.02511485
WN310693-3-2	0.02542702	0.025543833	0.025167034	0.025210573
WN310701-1-1	0.024501274	0.024448863	0.024885668	0.02468246
WN310701-1-2	0.024198248	0.024231005	0.024119184	0.024216958
WN310710-1-1	0.025467378	0.025051779	0.025193495	0.024864528

NET-230-01

WN310710-1-2	0.025260051	0.024998043	0.024850422	0.024861822
WN310728-3-1	0.025127696	0.024810021	0.024846345	0.024802291
WN310728-3-2	0.024799985	0.024407892	0.025170221	0.02489289
WN310733-3-1	0.025559264	0.025559608	0.025921588	0.025649635
WN310733-3-2	0.025288257	0.025378526	0.025346304	0.025489753
WN310745-1-1	0.026202934	0.026056797	0.02586212	0.026145506
WN310745-1-2	0.025902687	0.025943795	0.025983518	0.025710089
WN310759-1-1	0.025112095	0.025030996	0.025404133	0.025366216
WN310759-1-2	0.0249411	0.024964823	0.024631391	0.025148673
WN310763-1-1	0.026301315	0.025773783	0.025842904	0.025742988
WN310763-1-2	0.026041929	0.025777342	0.026038304	0.025915963
WN310776-1-1	0.025165627	0.024825168	0.02500519	0.024872873
WN310776-1-2	0.025053279	0.024550734	0.025212468	0.025086737
WN310786-3-1	0.025378184	0.024921798	0.025683668	0.025412133
WN310786-3-2	0.025737209	0.025573234	0.025733904	0.025787788
WN310791-3-1	0.02584014	0.025442477	0.025660619	0.024975916
WN310791-3-2	0.025592207	0.025497983	0.025744519	0.025609594
WN310807-3-1	0.025322167	0.024785026	0.024785919	0.024568568
WN310807-3-2	0.025278884	0.024695299	0.024828751	0.024367554
WN310813-3-1	0.02490395	0.024836401	0.02514519	0.024618467
WN310813-3-2	0.025491691	0.025197242	0.024552158	0.024657685
WN310825-2-1	0.02541107	0.025205095	0.025328842	0.0249446
WN310825-2-2	0.025466841	0.025385065	0.025232287	0.024883781
WN310836-3-1	0.024162393	0.02442615	0.024711995	0.024999296
WN310836-3-2	0.025221841	0.024116583	0.024815298	0.024801459
WN310846-3-1	0.025279596	0.025021011	0.024959364	0.024881907
WN310846-3-2	0.025405526	0.024636274	0.025104153	0.025145653
WN310851-1-1	0.025443351	0.024686542	0.024967928	0.02539637
WN310851-1-2	0.025241852	0.025135294	0.025028236	0.024853993
WN310866-3-1	0.025539447	0.025625909	0.025589767	0.025862206
WN310866-3-2	0.02492544	0.025240426	0.025382668	0.025750327
WN310871-3-1	0.026961002	0.026626005	0.027308424	0.027002474
WN310871-3-2	0.026609806	0.02577504	0.026958406	0.02720173
WN310885-3-1	0.024095254	0.024168342	0.024839255	0.024363037
WN310885-3-2	0.02420533	0.023981384	0.024518909	0.024221127
WN310897-3-1	0.025290828	0.02552143	0.025045637	0.025141162
WN310897-3-2	0.025697439	0.025605473	0.026143261	0.025188571

NET-230-01

WN310907-3-1	0.026344906	0.026100927	0.027060588	0.026301247
WN310907-3-2	0.02653737	0.026309943	0.027197811	0.026561292
WN310912-3-1	0.025829769	0.026024011	0.026502411	0.025788299
WN310912-3-2	0.025870462	0.026447015	0.026145357	0.025692452
WN310928-3-1	0.024981785	0.024540925	0.02481346	0.024472949
WN310928-3-2	0.024807789	0.02445237	0.024691669	0.024543779
WN310931-3-1	0.024069098	0.024284694	0.025289389	0.024737283
WN310931-3-2	0.024748683	0.024955737	0.025378319	0.024968369
WN310946-3-1	0.025020172	0.024603974	0.025869272	0.025167781
WN310946-3-2	0.025156528	0.025233171	0.025188455	0.025083087
WN310952-1-1	0.024304976	0.024271267	0.023861064	0.024061947
WN310952-1-2	0.02417239	0.023912524	0.024154305	0.024041451
WN310966-3-1	0.026009042	0.026009858	0.026173751	0.025679621
WN310966-3-2	0.026311714	0.026050909	0.026495584	0.025950786
WN310971-2-1	0.026828762	0.026454073	0.0272698	0.026834928
WN310971-2-2	0.026942264	0.027188124	0.027260417	0.027476265
WN310986-2-1	0.02446054	0.024442969	0.02432269	0.024020344
WN310986-2-2	0.024649469	0.024779945	0.024734018	0.024488035
WN310997-3-1	0.023521666	0.023314106	0.023897216	0.022831721
WN310997-3-2	0.023666809	0.023909867	0.023957032	0.023974017
WN311002-3-1	0.025506813	0.025195715	0.025845998	0.025278931
WN311002-3-2	0.025990362	0.025691342	0.026321948	0.025512048
WN311016-3-1	0.025784427	0.025366324	0.025628456	0.02538139
WN311016-3-2	0.026009691	0.025147917	0.026432893	0.02552978
WN311027-1-1	0.024918312	0.024638023	0.024260028	0.024254805
WN311027-1-2	0.024792061	0.024573407	0.02476535	0.02450682
WN311034-2-1	0.02550881	0.024981448	0.025525401	0.024877124
WN311034-2-2	0.025429175	0.024848053	0.025333782	0.024388988
WN311047-1-1	0.02498632	0.025059344	0.025316043	0.025031688
WN311047-1-2	0.025573643	0.025424281	0.025317077	0.024701745
WN311053-1-1	0.026495456	0.026194857	0.026672636	0.026519733
WN311053-1-2	0.026551271	0.026199289	0.026565494	0.026434853
WN311065-1-1	0.024642446	0.024621218	0.024849719	0.024933374
WN311065-1-2	0.024746579	0.024435316	0.024497935	0.024591602
WN311077-2-1	0.025384107	0.025458075	0.025031535	0.025015043
WN311077-2-2	0.024801187	0.02520689	0.025708875	0.025212974
WN311081-1-1	0.025690483	0.025756339	0.025601634	0.025241545

Attachment B
Page 21 of 21

NET-230-01

WN311081-1-2	0.025938463	0.026148243	0.026236717	0.025799113
WN311099-2-1	0.024842107	0.024606005	0.025133383	0.024965113
WN311099-2-2	0.02477038	0.024938619	0.024725744	0.024760487
WN311109-2-1	0.026271628	0.026359608	0.026117825	0.026050723
WN311109-2-2	0.025940697	0.026141315	0.02600297	0.025718767
WN311111-2-1	0.026021941	0.02605259	0.026378062	0.026090108
WN311111-2-2	0.026068011	0.025967582	0.025846989	0.026184472
WN311120-1-1	0.024642737	0.024805468	0.024916453	0.024702933
WN311120-1-2	0.024617647	0.023551083	0.024418997	0.024628727
WN311139-3-1	0.025230235	0.024722828	0.025182761	0.024944969
WN311139-3-2	0.02571714	0.025109932	0.025598794	0.02492805

Converted by *Mathematica* February 4, 2004

ATTACHMENT C

AAR BORAL
Chemical Analysis
vs.
Neutron Attenuation

Attachment C
Page 1 of 3

Chemical Analysis versus Neutron Attenuation

Chemical Analysis Method	
Serial Number	gms/cm2
WN310009	0.0246
WN310010	0.0233
WN310025	0.0236
WN310039	0.0239
WN310048	0.0243
WN310057	0.0251
WN310061	0.0239
WN310075	0.0231
WN310089	0.0228
WN310092	0.0233
WN310104	0.0236
WN310110	0.0249
WN310121	0.0237
WN310139	0.0246
WN310146	0.024
WN310159	0.0232
WN310160	0.025
WN310178	0.0249
WN310189	0.0261
WN310191	0.0251
WN310203	0.0243
WN310219	0.0233
WN310229	0.0246
WN310231	0.0244
WN310248	0.025
WN310253	0.0257
WN310269	0.0233
WN310270	0.0247
WN310284	0.0238
WN310295	0.0242
WN310309	0.0256
WN310312	0.0259
WN310327	0.0254
WN310331	0.0239
WN310343	0.0256
WN310359	0.0258
WN310367	0.026
WN310371	0.0245
WN310388	0.0242
WN310390	0.0239
WN310401	0.0265
WN310418	0.025
WN310428	0.0241
WN310433	0.0257
WN310443	0.0242
WN310452	0.025

Neutron Attenuation Method	
Serial Number	gms/cm2
WN310009	0.0251
WN310010	0.0242
WN310025	0.0253
WN310039	0.024
WN310048	0.0251
WN310057	0.0259
WN310061	0.0252
WN310075	0.0244
WN310089	0.024
WN310092	0.0244
WN310104	0.0238
WN310110	0.0254
WN310121	0.0243
WN310139	0.0247
WN310146	0.0251
WN310159	0.0247
WN310160	0.0253
WN310178	0.0252
WN310189	0.0258
WN310191	0.0253
WN310203	0.0243
WN310219	0.0235
WN310229	0.0245
WN310231	0.0246
WN310248	0.0254
WN310253	0.0256
WN310269	0.0249
WN310270	0.025
WN310284	0.024
WN310295	0.0244
WN310309	0.0254
WN310312	0.0249
WN310327	0.0255
WN310331	0.0248
WN310343	0.0255
WN310359	0.0268
WN310367	0.0261
WN310371	0.025
WN310388	0.0249
WN310390	0.0248
WN310401	0.0259
WN310418	0.0253
WN310428	0.0243
WN310433	0.0251
WN310443	0.0247
WN310452	0.0252

Attachment C
Page 2 of 3

Chemical Analysis versus Neutron Attenuation

Chemical Analysis Method	
Serial Number	gms/cm2
WN310464	0.0246
WN310471	0.0251
WN310486	0.0248
WN310493	0.0252
WN310501	0.0254
WN310510	0.0265
WN310527	0.0256
WN310532	0.0258
WN310545	0.0251
WN310550	0.0256
WN310564	0.0244
WN310570	0.025
WN310588	0.0227
WN310597	0.0262
WN310606	0.0247
WN310614	0.0242
WN310622	0.0254
WN310636	0.025
WN310641	0.0254
WN310659	0.0244
WN310661	0.0253
WN310673	0.0255
WN310681	0.0254
WN310693	0.0252
WN310701	0.024
WN310710	0.0245
WN310728	0.0248
WN310733	0.0257
WN310745	0.0257
WN310759	0.0252
WN310763	0.0252
WN310776	0.0251
WN310786	0.0259
WN310791	0.025
WN310807	0.0246
WN310813	0.0247
WN310825	0.025
WN310836	0.0248
WN310846	0.0249
WN310851	0.0253
WN310866	0.025
WN310871	0.027
WN310885	0.0239
WN310897	0.025
WN310907	0.0263
WN310912	0.0261

Neutron Attenuation Method	
Serial Number	gms/cm2
WN310464	0.0253
WN310471	0.0251
WN310486	0.0249
WN310493	0.0248
WN310501	0.0252
WN310510	0.0259
WN310527	0.0255
WN310532	0.0252
WN310545	0.0255
WN310550	0.0254
WN310564	0.0249
WN310570	0.0251
WN310588	0.0256
WN310597	0.0261
WN310606	0.0241
WN310614	0.0252
WN310622	0.0256
WN310636	0.0253
WN310641	0.026
WN310659	0.0248
WN310661	0.0254
WN310673	0.026
WN310681	0.026
WN310693	0.0256
WN310701	0.0245
WN310710	0.0255
WN310728	0.0251
WN310733	0.0256
WN310745	0.0262
WN310759	0.0251
WN310763	0.0263
WN310776	0.0252
WN310786	0.0254
WN310791	0.0258
WN310807	0.0253
WN310813	0.0249
WN310825	0.0254
WN310836	0.0242
WN310846	0.0253
WN310851	0.0254
WN310866	0.0255
WN310871	0.027
WN310885	0.0241
WN310897	0.0253
WN310907	0.0263
WN310912	0.0258

Attachment C
Page 3 of 3

Chemical Analysis versus Neutron Attenuation

Chemical Analysis Method	
Serial Number	gms/cm2
WN310928	0.0249
WN310931	0.0244
WN310946	0.0248
WN310952	0.0242
WN310966	0.0261
WN310971	0.0269
WN310986	0.024
WN310997	0.0231
WN311002	0.0256
WN311016	0.0256
WN311027	0.0242
WN311034	0.0253
WN311047	0.0247
WN311053	0.0261
WN311065	0.0245
WN311077	0.0253
WN311081	0.027
WN311099	0.0251
WN311109	0.0257
WN311111	0.0255
WN311120	0.025
WN311139	0.0248

Neutron Attenuation Method	
Serial Number	gms/cm2
WN310928	0.025
WN310931	0.0241
WN310946	0.025
WN310952	0.0243
WN310966	0.026
WN310971	0.0268
WN310986	0.0245
WN310997	0.0235
WN311002	0.0255
WN311016	0.0258
WN311027	0.0249
WN311034	0.0255
WN311047	0.025
WN311053	0.0265
WN311065	0.0246
WN311077	0.0254
WN311081	0.0262
WN311099	0.0251
WN311109	0.0259
WN311111	0.0258
WN311120	0.0249
WN311139	0.0252

Chemical Analysis stats	
MINIMUM 10B	.02 gms/cm2
AVG 10B	0.0249
STD DEVIATION	0.000894613

Neutron Attenuation stats	
MINIMUM 10B	.02 gms/cm2
AVG 10B	0.0252
STD DEVIATION	0.000676959

Note (1): Samples are a minimum 10B of .02 gms/cm2 and a nominal thickness of .075"

Note (2): Differences in Average 10B between chemical analysis and Neutron attenuation arises from the conservatism in Chemical Analysis testing methods

Report by: Phill Pusilo (3-9-2004)

TOPICAL REPORT
REFERENCE DOCUMENTS
BOOK 1 of 2

Credit for 90% of the ^{10}B in BORAL

Submitted by:
AAR Manufacturing
12633 Inkster Road
Livonia, Michigan 48150
Tel: 734-522-2000
Fax: 734-522-2240

AAR Report 1829, Revision 0

October 27, 2004

Please Note

Complete text contained on CD enclosed in Book 1

NUREG–1536

Standard Review Plan
for Dry Cask Storage Systems

Final Report

Manuscript Completed: January 1997
Date Published: January 1997

Spent Fuel Project Office
Office of Nuclear Material Safety and Safeguards
U.S. Nuclear Regulatory Commission
Washington, DC 20555–0001

6.0 CRITICALITY EVALUATION

I. Review Objective

The criticality review ensures that spent fuel remains subcritical under normal, off-normal, and accident conditions involving handling, packaging, transfer, and storage.

II. Areas of Review

This portion of the dry cask storage system (DCSS) review evaluates the criticality design and analysis related to spent fuel handling, packaging, transfer, and storage procedures for normal, off-normal, and accident conditions. Consequently, this chapter of the DCSS Standard Review Plan (SRP) provides guidance for use in conducting a comprehensive criticality evaluation that *may* encompass any or all of the following areas of review:

1. criticality design criteria and features
2. fuel specification
3. model specification
   a. configuration
   b. material properties
4. criticality analysis
   a. computer programs
   b. multiplication factor
   c. benchmark comparisons
5. supplemental information

III. Regulatory Requirements

Spent fuel storage systems must be designed to remain subcritical unless at least two unlikely independent events occur. Moreover, the spent fuel cask must be designed to remain subcritical under all credible conditions. Regulations specific to nuclear criticality safety of the cask system are specified in 10 CFR 72.124 and 72.236(c). Other pertinent regulations include 10 CFR 72.24(c)(3), 72.24(d), and 72.236(g). Normal and accident conditions to be considered are also identified in 10 CFR Part 72.

IV. Acceptance Criteria

In general, the DCSS criticality evaluation seeks to ensure that the given design fulfills the following acceptance criteria:

1. The multiplication factor (k_{eff}), including all biases and uncertainties at a 95-percent confidence level, should not exceed 0.95 under all credible normal, off-normal, and accident conditions.

2. At least two unlikely, independent, and concurrent or sequential changes to the conditions essential to criticality safety, under normal, off-normal, and accident conditions, should occur before an accidental criticality is deemed to be possible.

3. When practicable, criticality safety of the design should be established on the basis of favorable geometry, permanent fixed neutron-absorbing materials (poisons), or both. Where solid neutron-absorbing materials are used, the design should provide for a positive means to verify their continued efficacy during the storage period.

4. Criticality safety of the cask system should not rely on use of the following credits:

   a. burnup of the fuel
   b. fuel-related burnable neutron absorbers

c. more than 75 percent for fixed neutron absorbers[a] when subject to standard acceptance tests.

V. Review Procedures

Review the criticality design features and criteria in SAR Chapters 1 and 2. Also review SAR Chapter 6 for any additional details concerning criticality design features and criteria. Assess the bounding specifications for the spent fuel. Examine the models used by the applicant in the criticality analyses. Verify that the applicant has addressed criticality safety considerations under normal, off-normal, and accident conditions. Verify that the cask system design complies with 10 CFR Part 72. In addition, verify that the criticality calculations determine the highest k_{eff} that might occur under all loading states under normal, off-normal, and accident conditions involving handling, packaging, transfer, or storage. To the extent practicable, use independent methods to perform any k_{eff} calculations to evaluate the applicant's design.

1. Criticality Design Criteria and Features

Review the principal criticality design criteria presented in SAR Chapter 2, as well as any related detail provided in SAR Chapter 6. Also review the general cask description presented in SAR Chapter 1 and any related information provided in Chapter 6. Verify that the information in Chapter 6 is consistent with the information in Chapters 1 and 2. Also, verify that all drawings, figures, and tables are sufficiently detailed to support in-depth staff evaluation.

In addition to the general dimensions of the cask components and spacing of fuel assemblies in the basket, the criticality design often relies on neutron poisons. These may be in the form of fixed poisons in the basket structure and/or soluble poisons in the water of the spent fuel pool. The NRC staff accepts the use of borated water as a means of criticality control if the applicant specifies a minimum boron content, and strict controls are established to ensure that the minimum required boron concentration is maintained, which in turn becomes an operating control and limit in SAR Chapter 12. These operating controls should also be discussed in the SER. If borated water is used for criticality control, administrative controls and/or design features should be implemented to ensure that accidental flooding with unborated water cannot occur, or the criticality evaluation should consider accidental flooding with unborated water. If the cask is also intended for transport, borated water cannot be relied upon for criticality control.

2. Fuel Specification

Review the specifications for the ranges or types of spent fuel that will be stored in the cask as presented in SAR Sections 1 and 2, as well as any related information provided in SAR Sections 6. Verify that the spent fuel specifications given in Section 6 are consistent with, or bounded by, the specifications given in Section 1 and 2.

Of primary interest is the type of fuel assemblies and maximum fuel enrichment, which should be specified and used in the criticality calculations. Some boiling water reactors (BWR) use multiple fuel pin enrichments, in which case, the criticality calculations should use the maximum fuel pin enrichment present. Depending upon the fuel design, an applicant may propose use of assembly averaged, or lattice averaged enrichments. This may be acceptable if the applicant can demonstrate that any averaging techniques are technically defensible and, for the criticality calculation, produce conservative results. Because of the natural uranium blankets present in many BWR designs, use of an assembly-averaged enrichment is not normally considered appropriate or conservative for BWR fuel.

Although the burnup of the fuel affects its reactivity, the NRC staff does not currently allow credit for burnup, either in depleting the quantity of fissile nuclides or in producing fission product poisons for spent fuel storage or transport casks. Specifications for the fuel that will be stored in the cask should be included in Section 12 of both the SAR and SER and should also be explicitly listed in the Certificate of Compliance.

The fresh fuel assumption should be used in the criticality analyses; therefore, inadvertent loading of the cask with unirradiated fuel is not a major concern. Nonetheless, detailed loading procedures may need to

[a] For greater credit allowance, special, comprehensive fabrication tests capable of verifying the presence and uniformity of the neutron absorber are needed.

Please Note

Complete text contained on CD enclosed in Book 1

NUREG-1567

Standard Review Plan
for Spent Fuel Dry Storage Facilities

Final Report

Manuscript Completed: February 2000
Date Published: March 2000

Spent Fuel Project Office
Office of Nuclear Material Safety and Safeguards
U.S. Nuclear Regulatory Commission
Washington, D.C. 20555-0001

even grow by a chain reaction, which can produce as many or more neutrons than are absorbed. In criticality terminology, the term, k-effective or k_{eff} is the net ratio of neutrons produced per neutron absorbed in a mass of fissionable material. A k_{eff} of 1.0 indicates a critical mass whereas a k_{eff} of less than 1.0 is an indication of a subcritical condition.

8.4.1 Criticality Design Criteria and Features

8.4.1.1 Criteria

The regulatory requirements given in 10 CFR 72.40 and 10 CFR 72.124 identify acceptable design criteria. The NRC generally considers the design criteria identified below to be acceptable to meet the criticality requirements of 10 CFR 72 for storage confinement casks:

- The multiplication factor, k_{eff}, including all biases and uncertainties at a 95 percent confidence level, must not exceed 0.95 under all credible normal, off-normal, and accident conditions and events.

- Conditions for criticality safety (satisfaction of the limit on multiplication factor, k_{eff}) of subject radioactive material while at the Independent Spent Fuel Storage Installations (ISFSI) or Monitored Retrievable Storage (MRS) must include:

  - no burnup credit. (The conservative assumption of fresh unburned fuel provides a worst case criticality analysis; however, 10 CFR 72.3 requires that spent fuel have been irradiated and cooled at least one year as a condition for storage.) Alternately, burnup credit may be taken using the guidelines described in section 8.4.5 of this SRP.

  - no credit taken for flammable neutron absorbers or for any solid poisons that may melt or lose any significant mass from the original solid form by melting or vaporization at any of the temperature and pressure conditions that may be experienced while in use

  - no credit taken for liquid neutron shielding material (except that k_{eff} for the situation of a loaded confinement cask with liquid that serves as both shielding and absorber and is used in the confinement cask during loading operations or in the pool shall be based on presence of the water and bounding level(s) of poison)

  - no more than 75 percent credit for fixed neutron absorbers, unless comprehensive fabrication acceptance tests capable of verifying the presence and uniformity of the neutron absorber are implemented

  - determination and use of optimum (i.e., most reactive) moderator density

Please Note

Complete text contained on CD enclosed in Book 1

NUREG-1609

Standard Review Plan
for Transportation Packages for Radioactive Material

Manuscript Completed: March 31, 1999

Spent Fuel Project Office
Office of Nuclear Material Safety and Safeguards
U.S. Nuclear Regulatory Commission
Washington, DC 20555-0001

6.5.3.2 Material Properties

Verify that the appropriate mass densities and atom densities are provided for materials used in the models of the packaging and contents. Material properties should be consistent with the condition of the package under the tests of §71.71 and §71.73, and any differences between normal conditions of transport and hypothetical accident conditions should be addressed.

Ensure that materials relevant to the criticality design (e.g., poisons, foams, plastics, and other hydrocarbons) are properly specified. No more than 75% of the specified minimum neutron poison concentration should generally be considered in the criticality evaluation. Verify that materials will not degrade during the service life of the packaging.

6.5.3.3 Computer Codes and Cross-Section Libraries

Verify that the application uses an appropriate computer code (or other acceptable method) for the criticality evaluation. Standard codes should be clearly referenced. Other codes or methods should be described in the application, and appropriate supplemental information should be provided.

Ensure that the criticality evaluations use an appropriate cross-section library. If multigroup cross sections are used, confirm that the neutron spectrum of the package has been appropriately considered and that the cross sections are properly processed to account for resonance absorption and self-shielding. Additional information regarding cross-sections is provided in NMSS Information Notice No. 91-26 and NUREG/CR-6328.

Verify that the code has been properly used in the criticality evaluation. Key input data for the criticality calculations should be identified. These include number of neutrons per generation, number of generations, convergence criteria, mesh selection, etc., depending on the code used. The application should include at least one representative input file for a single package, undamaged array, and damaged array evaluation. Verify, as appropriate, that the information from the criticality model, material properties, and cross sections is properly input into the code.

At least one representative output file (or key sections) should be included in the application. Ensure that the calculation has properly converged and that the calculated multiplication factors from the output files agree with those reported in the evaluation.

6.5.3.4 Demonstration of Maximum Reactivity

Verify that the analyses demonstrate the most reactive configuration of each case listed in Section 6.5.1.2 (single package, array of undamaged packages, and array of damaged packages). Assumptions and approximations should be clearly identified and justified.

Ensure that the analysis determines the optimum combination of internal moderation (within the package) and interspersed moderation (between packages), as applicable. Confirm that preferential flooding of different regions within the package is considered as appropriate. As noted in Section 6.5.2, the maximum allowable fissile material is not necessarily the most reactive contents.

Please Note

Complete text contained on CD enclosed in Book 1

NUREG-1617

Standard Review Plan
for Transportation Packages for Spent Nuclear Fuel

Final Report

Manuscript Completed: January 2000
Date Published: March 2000

Spent Fuel Project Office
Office of Nuclear Material Safety and Safeguards
U.S. Nuclear Regulatory Commission
Washington, D.C. 20555-0001

6.3.5 Evaluation of Package Arrays under Normal Conditions of Transport

The SAR must evaluate arrays of packages under normal conditions of transport to determine the maximum number of packages that may be transported in a single shipment. [10 CFR 71.35 and 10 CFR 71.59]

6.3.6 Evaluation of Package Arrays under Hypothetical Accident Conditions

The SAR must evaluate arrays of packages under hypothetical accident conditions to determine the maximum number of packages that may be transported in a single shipment. [10 CFR 71.35 and 10 CFR 71.59]

6.3.7 Benchmark Evaluations

The package must be evaluated to demonstrate that it satisfies the criticality safety requirements of 10 CFR Part 71. [10 CFR 71.31(a)(2) and 10 CFR 71.35]

6.3.8 Burnup Credit

There are no regulatory requirements that are specific to burnup credit. The general criticality requirements apply. However, based on experience, the staff has developed guidelines to facilitate the review of burnup credit, when it is included in the analysis. Burnup credit evaluations are performed in accordance with Sections 6.4.8.1 through 6.4.8.6.

6.4 ACCEPTANCE CRITERIA

6.4.1 Description of Criticality Design

The regulatory requirements in Section 6.3.1 identify the acceptance criteria.

6.4.2 Spent Nuclear Fuel Contents

The regulatory requirements in Section 6.3.2 identify the acceptance criteria.

6.4.3 General Considerations for Criticality Evaluations

In addition to the regulatory requirements identified in Section 6.3.3, the packaging model for the criticality evaluation should generally consider no more than 75% of the specified minimum neutron poison concentrations. The model for the SNF should include no burnable poisons. Methods for including fuel burnup in the criticality calculations need to have prior approval by NRC.

The sum of the effective multiplication factor (k_{eff}), two standard deviations (95% confidence), and the bias adjustment should not exceed 0.95 to demonstrate subcriticality by calculation. A bias that reduces the calculated value of k_{eff} should not be applied.

Examine the Structural Evaluation and Thermal Evaluation sections of the SAR to determine the effects of the normal conditions of transport and hypothetical accident conditions on the packaging and its contents. Verify that the models used in the criticality calculation are consistent with these effects.

Examine the sketches or figures of the model used for the criticality calculations. Verify that the dimensions and materials are consistent with those in the drawings of the actual package. Differences should be identified and justified. Within the specified tolerance range, dimensions should be selected to result in the highest reactivity.

Verify that the SAR considers deviations from nominal design configurations. For example, the fuel assemblies might not always be centered in each basket compartment, and the basket might not be exactly centered in the package. In addition to a fully flooded package, the SAR should address preferential flooding as appropriate. This includes flooding of the fuel-cladding gap and other regions (e.g., flux traps) for which water density might not be uniform in a flooded package.

Determine whether the SAR includes a heterogeneous model of each fuel rod or homogenizes the entire assembly. With current computational capability, homogenization should generally be avoided. If such homogenization is used, the SAR must demonstrate that it is applied correctly or conservatively. As a minimum, this demonstration should include calculation of the multiplication factor of one assembly and several benchmark experiments (see Section 6.5.7) using both homogeneous and heterogeneous models.

6.5.3.2 Material Properties

Verify that the appropriate mass densities and atom densities are provided for all materials used in the models of the packaging and contents. Material properties should be consistent with the condition of the package under the tests of 10 CFR 71.71 and 10 CFR 71.73, and any differences between normal conditions of transport and hypothetical accident conditions should be addressed. The sources of the data on material properties should be referenced.

No more than 75% of the specified minimum neutron poison concentration of the packaging should generally be considered in the criticality evaluation. In addition, because of differences in net reactivity due to depletion of fissile material and burnable poisons, no credit should be taken for burnable poisons in the fuel. Ensure that neutron absorbers and moderators (e.g., poisons and neutron shielding) are properly controlled during fabrication to meet their specified properties. Such information should be discussed in more detail in the Acceptance Tests and Maintenance Program section of the SAR. Additional guidance on neutron poisons is provided in NUREG-1647.

Review materials to identify any criticality properties that could degrade during the service life of the packaging. If appropriate, ensure that specific controls are in place to assure the effectiveness of the packaging during its service life. Such information should also be discussed in more detail in the Acceptance Tests and Maintenance Program or Operating Procedures sections of the SAR.

6.5.3.3 Computer Codes and Cross Section Libraries

NUREG/CR-5661

RECOMMENDATIONS FOR PREPARING THE CRITICALITY SAFETY EVALUATION OF TRANSPORTATION PACKAGES

OAK RIDGE NATIONAL LAB., TN

APR 97

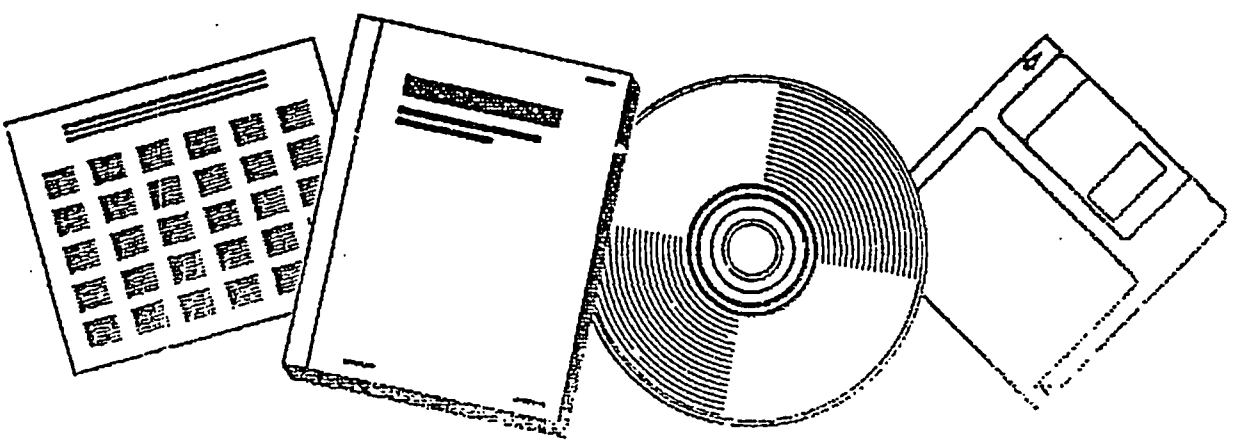

U.S. DEPARTMENT OF COMMERCE
National Technical Information Service

NUREG/CR-5661
ORNL/TM-11936

Recommendations for Preparing the Criticality Safety Evaluation of Transportation Packages

Prepared by
H. R. Dyer, C. V. Parks

Oak Ridge National Laboratory

Prepared for
U.S. Nuclear Regulatory Commission

AVAILABILITY NOTICE

Availability of Reference Materials Cited in NRC Publications

Most documents cited in NRC publications will be available from one of the following sources:

1. The NRC Public Document Room, 2120 L Street, NW., Lower Level, Washington, DC 20555-0001

2. The Superintendent of Documents, U.S. Government Printing Office, P. O. Box 37082, Washington, DC 20402-9328

3. The National Technical Information Service, Springfield, VA 22161-0002.

Although the listing that follows represents the majority of documents cited in NRC publications, it is not intended to be exhaustive.

Referenced documents available for inspection and copying for a fee from the NRC Public Document Room include NRC correspondence and internal NRC memoranda; NRC bulletins, circulars, information notices, inspection and investigation notices; licensee event reports; vendor reports and correspondence; Commission papers; and applicant and licensee documents and correspondence.

The following documents in the NUREG series are available for purchase from the Government Printing Office: formal NRC staff and contractor reports, NRC-sponsored conference proceedings, international agreement reports, grantee reports, and NRC booklets and brochures. Also available are regulatory guides, NRC regulations in the *Code of Federal Regulations*, and *Nuclear Regulatory Commission Issuances*.

Documents available from the National Technical Information Service include NUREG-series reports and technical reports prepared by other Federal agencies and reports prepared by the Atomic Energy Commission, forerunner agency to the Nuclear Regulatory Commission.

Documents available from public and special technical libraries include all open literature items, such as books, journal articles, and transactions. *Federal Register* notices, Federal and State legislation, and congressional reports can usually be obtained from these libraries.

Documents such as theses, dissertations, foreign reports and translations, and non-NRC conference proceedings are available for purchase from the organization sponsoring the publication cited.

Single copies of NRC draft reports are available free, to the extent of supply, upon written request to the Office of Administration, Distribution and Mail Services Section, U.S. Nuclear Regulatory Commission, Washington, DC 20555-0001.

Copies of industry codes and standards used in a substantive manner in the NRC regulatory process are maintained at the NRC Library, Two White Flint North, 11545 Rockville Pike, Rockville, MD 20852-2738, for use by the public. Codes and standards are usually copyrighted and may be purchased from the originating organization or, if they are American National Standards, from the American National Standards Institute, 1430 Broadway, New York, NY 10018-3308.

DISCLAIMER NOTICE

NUREG/CR-5661

NRC FORM 335 (2-89) NRCM 1102, 3201, 3202 — U.S. NUCLEAR REGULATORY COMMISSION

BIBLIOGRAPHIC DATA SHEET

(See instructions on the reverse)

NUREG/CR-5661
ORNL/TM-11936

2. TITLE AND SUBTITLE

Recommendations for Preparing the Criticality Safety Evaluation of Transportation Packages

3. DATE REPORT PUBLISHED

MONTH	YEAR
April	1997

4. FIN OR GRANT NUMBER

B0009

5. AUTHOR(S)

H.R. Dyer, C.V. Parks

6. TYPE OF REPORT

7. PERIOD COVERED (Inclusive Dates)

8. PERFORMING ORGANIZATION - NAME AND ADDRESS (If NRC, provide Division, Office or Region, U.S. Nuclear Regulatory Commission, and mailing address; if contractor, provide name and mailing address.)

Oak Ridge National Laboratory
Oak Ridge, TN 37831-6370

9. SPONSORING ORGANIZATION - NAME AND ADDRESS (If NRC, type "Same as above"; if contractor, provide NRC Division, Office or Region, U.S. Nuclear Regulatory Commission, and mailing address.)

Spent Fuel Project Office
Office of Nuclear Material Safety and Safeguards
U.S. Nuclear Regulatory Commission
Washington, DC 20555-0001

10. SUPPLEMENTARY NOTES

11. ABSTRACT (200 words or less)

This report provides recommendations on preparing the criticality safety section of an application for approval of a transportation package containing fissile material. The analytical approach to the evaluation is emphasized rather than the performance standards that the package must meet. Where performance standards are addressed, this report incorporates the requirements of 10 CFR Part 71.

12. KEY WORDS/DESCRIPTORS (List words or phrases that will assist researchers in locating the report.)

transportation, criticality safety, safety analysis, fissile material

13. AVAILABILITY STATEMENT

unlimited

14. SECURITY CLASSIFICATION

(This Page)

unclassified

(This Report)

unclassified

15. NUMBER OF PAGES

16. PRICE

NUREG/CR-5661

NUREG/CR-5661
ORNL/TM-11936

Recommendations for Preparing the Criticality Safety Evaluation of Transportation Packages

Manuscript Completed: March 1997
Date Published: April 1997

Prepared by
H. R. Dyer, C. V. Parks

Oak Ridge National Laboratory
Managed by Lockheed Martin Energy Research Corp.
Oak Ridge, TN 37831-6370

M. G. Bailey, NRC Project Manager

Prepared for
Spent Fuel Project Office
Office of Nuclear Material Safety and Safeguards
U.S. Nuclear Regulatory Commission
Washington, DC 20555-0001
NRC Job Code B0009

ABSTRACT

This report provides recommendations on preparing the criticality safety section of an application for approval of a transportation package containing fissile material. The analytical approach to the evaluation is emphasized rather than the performance standards that the package must meet. Where performance standards are addressed, this report incorporates the requirements of 10 CFR Part 71.

CONTENTS

LIST OF FIGURES

LIST OF TABLES

ACKNOWLEDGMENTS

The authors gratefully acknowledge the overall direction and specific contributions provided during the preparation of this report by staff of the U.S. Nuclear Regulatory Commission's Spent Fuel Project Office. In particular, the efforts of the Technical Monitor, M. G. Bailey, in consolidating and communicating the NRC comments was an invaluable asset to the completion of this report. R. H. Odegaarden, private consultant, contributed valuable ideas and initial text for this document, and J. J. Lichtenwalter used the final draft to prepare Appendix A. Lichtenwalter's contributions were partially supported by his role as a participant in the post-graduate research program administered by the Oak Ridge Institute for Science and Education. The technical review comments provided by Lichtenwalter and C. M. Hopper were helpful in preparing the document for publication. The timely and carefully prepared manuscript and many drafts by Lindy Norris are also greatly appreciated.

1 INTRODUCTION

1.1 BACKGROUND

This report provides recommendations on preparing the criticality safety section of an application for approval of a transportation package containing fissile material. This report was prepared in consultation with the staff of the Spent Fuel Project Office of the U.S. Nuclear Regulatory Commission (NRC).

Packages used to transport fissile and Type B quantities of radioactive material are designed and constructed to meet the performance criteria specified in Title 10 of the Code of Federal Regulations, *Part 71–Packaging and Transportation of Radioactive Material* (10 CFR Part 71).[1] To assist an applicant in preparing an application for approval of such packaging, the NRC issued Regulatory Guide 7.9, *Standard Format and Content of Part 71 Applications for Approval of Packaging for Radioactive Material* (Standard Format Guide).[2] The Standard Format Guide indicates the information to be provided in the application and establishes a uniform format for presenting that information. This report (NUREG/CR-5661) supplements Chapter 6, *Criticality*, of the Standard Format Guide. This report should not be considered a substitute for referring to the Standard Format Guide or to 10 CFR Part 71.

1.2 PURPOSE AND SCOPE

The purpose of this report is to clarify the design information and analysis information that should be included in the criticality safety section of an application for approval of a package. This report also recommends an acceptable analytical approach for performing the criticality safety evaluation. The criticality calculations performed herein use the SCALE code system[3] to illustrate the analysis approach. However, the report does not endorse any particular computational tool and stresses that any computational tools (SCALE system or any other code) used in the evaluation must be demonstrated as valid for the criticality safety analysis of the specific package design.

In this report, the performance requirements of 10 CFR Part 71 or the Standard Format Guide have not been emphasized; it is assumed that the reader is familiar with these documents. The completed criticality evaluation should address and demonstrate compliance with all applicable performance requirements, and the application should follow the Standard Format Guide. Sections 2 through 6 of this report have been compiled assuming that the recommendations in this report will be implemented in an application that has been prepared to demonstrate compliance with the requirements of 10 CFR Part 71 and in accordance with the Standard Format Guide.

1.3 SUMMARY RECOMMENDATIONS

This report recommends information and assumptions to be considered in the criticality section of an application for approval of a transportation package. A summary of these recommendations is listed below. The list provides the information and assumptions that should be considered; additional information and/or assumptions may need to be considered depending on the package design and the approach used in the safety evaluation.

1. Provide a complete description of the contents and the packaging (including maximum and minimum mass of all materials, maximum ^{235}U enrichment, physical parameters, type, form, and composition). See Sect 2 for more details.

2. Provide a description (including sketches with dimensions and materials) of the calculational models, point out the differences between the models and actual package design, and discuss how these differences affect the calculations. See Sect. 3 for more details.

3. For packages equipped with fixed neutron absorbers, assume no more than 75% of the minimum neutron absorber content, unless comprehensive acceptance tests are implemented that are capable of verifying the presence and uniformity of the neutron absorber. See Sect. 3.1.3.

4. Demonstrate and consider the most reactive content loading and the most reactive configuration of the contents, the packaging, and the package array in the criticality evaluation. For spent fuel packages, assume unburned (fresh) fuel isotopic concentrations; however, do not take credit for any fixed burnable absorbers in the fuel. See Sects. 3.2–3.4 for more details.

5. Provide a description of the code(s) and cross-section data used in the safety analysis, together with references that provide complete information. Discuss software capabilities and limitations of importance to the criticality safety evaluations. See Sect. 4 for details.

6. Use appropriate validation procedures to justify the bias and uncertainties associated with the calculational method. In addition to the bias and uncertainties, the NRC position is that transportation packages should have a minimum administrative subcritical margin of 0.05 Δk. See Sect. 5 for more details.

7. For the following cases, demonstrate that the effective neutron multiplication factor (k_{eff}) calculated in the safety analysis is limited to 0.95 after consideration of appropriate bias and uncertainties (see Sect. 5.4).

   a. **a single package** with optimum moderation within the containment system, close water reflection, and the most reactive packaging and content configuration (consistent with the effects of normal conditions of transport or hypothetical accident conditions, whichever is more reactive);

   b. **an array of 5N undamaged packages** (packages subject to normal conditions of transport) with nothing between the packages and close water reflection of the array; and

   c. **an array of 2N damaged packages** (packages subject to hypothetical accident conditions) if each package were subjected to the tests specified in §71.73, with optimum interspersed moderation and close water reflection of the array.

   See Sects. 3.4 and 6.1–6.2 for more details.

8. Calculate and report the transport index (TI) for criticality control based on the value of N determined in the array analyses. See Sect. 6.3 for more details.

9. Provide sufficient information in the application to support independent analyses without reference to external documents.

2 PACKAGE DESCRIPTION

The criticality section of the application for approval of a transportation package should include a description of the packaging and its contents. Descriptions of the packaging and contents should be consistent with the engineering drawings and with other figures and text provided in other sections of the application. Other sections of the application may be referenced to ensure consistency and to limit duplication. However, a description of the package sufficient for understanding the criticality evaluation should be provided without reference to other sections. This description should focus on the package dimensions and material components that can influence k_{eff} (e.g., fissile material inventory and placement, neutron absorber material and placement, reflector materials), rather than structural information such as bolt placement and trunnions. This section of the report clarifies the information that is expected in the criticality safety section of the application.

2.1 CONTENTS

The criticality safety section of the application should have a complete and detailed description of the contents of the packaging. This should include content quantities, dimensions, and configurations that are most limiting in terms of criticality safety. The application should clearly state the full range of contents for which approval is requested. Thus parameter values (e.g., maximum ^{235}U enrichment, multiple fuel assembly types, fuel pellet diameter, fuel masses) needed to bound the packaging contents within prescribed limits should be provided. For packages with multiple loading configurations, each configuration should also be specifically described, including all possible partial-load configurations. The description of the contents should include

1. the type of materials (e.g., fissile and nonfissile isotopes, reactor fuel assemblies, packing materials, and neutron absorbers),

2. the form and composition of materials (e.g., gases, liquids, and solids as metals, alloys, or compounds),

3. the quantity of materials (e.g., masses, densities, ^{235}U enrichment, isotopic distribution, H/X, and C/X), including tolerances for any nominal values given, and

4. other physical parameters (e.g., geometric shapes, configurations, dimensions, orientation, spacing, and gaps), including tolerances for any nominal values given.

The criticality safety section of the application should also describe the configuration of the contents after the package has been subjected to the hypothetical accident conditions. Appropriate references to the structural and thermal sections of the application should be made. Any changes from the normal conditions content configurations should be described.

2.2 PACKAGING

The criticality section of the application should include a description of the packaging with emphasis on the design features pertinent to the criticality safety evaluation. The features that should be emphasized are

1. the materials of construction and their relevance to criticality safety.

2. pertinent dimensions and volumes, including tolerances and allowable deviations.

3. the limits on design features relied on for criticality safety (e.g., minimum dimensions for fixed neutron absorbers, minimum loading of neutron absorber material, minimum separation distances), and

4. other design features that contribute to criticality safety.

The application should also describe the configuration of the packaging after the package has been subjected to the hypothetical accident conditions. Appropriate references to the structural and thermal sections of the application should be made. Any changes from the normal condition packaging configuration which may affect the criticality evaluation should be described.

2.3 SPECIFICATION OF TRANSPORT INDEX

The application should specify the TI for criticality control. The TI is the dimensionless number (rounded up to the next tenth) that designates the degree of control (e.g., limits package accumulation) to be provided by the carrier. The TI is defined by 10 CFR Part 71 to address concerns for radiation protection (TI value is maximum dose in millirem per hour at 1 m from the package surface) and criticality control. The TI for criticality control is calculated by dividing 50 by the number "N." The number "N" used to determine the TI for criticality control is derived from separate consideration (see Sects. 6.2 and 6.3) of the number of damaged and undamaged packages that can be adequately subcritical in an array subject to the conditions of 10 CFR § 71.59(a).

3 CRITICALITY SAFETY ANALYSIS MODELS

The application for approval of transportation packages should provide specific information on all calculational models used to perform the criticality safety evaluation. This section provides recommendations on the information that should be provided for each calculational model.

3.1 GENERAL

The applicant should perform criticality safety analysis for single packages and arrays of packages. In each case, the package conditions under normal conditions of transport (i.e., an undamaged package) and the package conditions under hypothetical accident conditions (i.e., damaged package) should be considered. For each evaluation, a calculational model should be developed. An exact model of the package may not be necessary. However, the calculational models should explicitly include the physical features important to criticality safety. Also, any modeling approximations should be shown to be conservative or essentially neutral relative to a more exact model.

The applicant should provide three types of calculational models: contents models, the single-package models, and package array models. The contents models should include all geometric and material regions out to the containment boundary (or to a convenient boundary, such as the strongback of a fresh fuel assembly package). Each contents model should dimensionally fit inside the undamaged and damaged package models used in the single-package and package array evaluations. Additional calculational models may be needed to describe the range of contents or the various array configurations or damage configurations that should be analyzed.

The criticality section of the application should contain a detailed description of the calculational models. Sections 3.1.1 through 3.1.4 discuss the items that should be included with the description of the calculational models.

3.1.1 Sketches

The criticality section of the application should include simplified, dimensioned sketches of the calculational models. Sketches drawn specifically for the various portions of the model are preferable to engineering drawings. However, the sketches should be consistent with the engineering drawings. Any differences with the engineering drawings, or with other figures in the application, should be noted and explained.

The sketches should be simplified by limiting the dimensional features on each sketch and by providing multiple sketches, with each sketch building on the previous one. Multiple sketches for each calculational model may be necessary to show sufficient detail. Also, multiple sketches may be necessary to show different undamaged and damaged package configurations.

3.1.2 Dimensions

The sketches discussed in Sect. 3.1.1 should show the dimensions that are used in the calculations (see examples in Appendix A). Any difference between dimensions used in the sketches and those in the engineering drawings, or other figures of the application, should be noted and explained. The dimensions on the sketches should be specified in both SI and English units.

The criticality section should address dimensional tolerances of the packaging, including components containing neutron absorbers. When developing the calculational models, adjustments should be made for tolerances that tend to add conservatism (i.e., produce higher k_{eff} values). For example, subtraction of the

negative tolerance from the nominal wall thickness of steel should be conservative for array calculations and may have no significant effect on the single-package calculation.

3.1.3 Materials

The range of material specifications (including tolerances and uncertainties) for the packaging and contents should be addressed in the criticality section of the application. Specifications and tolerances for all fissile materials, neutron-absorbing materials, materials of construction, and moderating materials should be confirmed with the engineering drawings of the packaging or the specified design criteria. The range of material specifications should be used to select parameters that produce the highest k_{eff} value consistent with normal and hypothetical accident conditions. For example, the ^{235}U enrichment of the fuel should be maximized, while the ^{10}B enrichment of a neutron poison component should be minimized. In practice, the effect of small variations in dimensions or material specifications may also be considered by determination of a reactivity allowance that covers the k_{eff} change due to the parameter changes under consideration. This additional reactivity allowance should be positive and included as an additional element of the calculational uncertainty (see Sect. 5.4).

For each calculational model, the atom density of any neutron absorber (e.g., boron, cadmium, or gadolinium) added to the packaging for criticality control should be limited to 75% of the minimum neutron absorber content specified in the application. This minimum neutron absorber content should be verified by chemical analysis, neutron transmission measurements, or other acceptable methods. A percentage of neutron absorber material greater than 75% may be considered in the analysis only if comprehensive acceptance tests, capable of verifying the presence and uniformity of the neutron absorber, are implemented. The adequacy of these tests will be considered on a case-by-case basis. Use of independent tests that verify the presence of the absorber material and adequate demonstration that the tests have appropriate sensitivity to the quantities of concern (presence and uniformity of absorber constituents) are issues that should be considered.

Limiting added absorber material credit to 75% without comprehensive tests is based on concerns for potential "streaming" of neutrons due to nonuniformities. It has been shown that boron carbide granules embedded in aluminum permit channeling of a beam of neutrons between the grains and reduce the effectiveness for neutron absorption. The experimental work of Refs. 4 and 5 shows that for a monoenergetic neutron beam, the granulated boron carbide areal density of 0.040 g/cm^2 of ^{10}B is equivalent to a homogeneous areal density of 0.033 g/cm^2 of ^{10}B. The efficiency of boron as a neutron absorber allows credit for only 75% of the poison to be a manageable value for most transportation package designs. The 75% value demonstrated by this work is conservative for several reasons: (1) many neutron poisons tend to be distributed homogeneously through a component of the packaging and are not distributed in a granular fashion, and (2) the experimental work is based on the use of a monodirectional beam of neutrons, while in most package designs an isotropic source of neutrons will be impinging on the wall (thus reducing the potential for intragranular transmission). Nevertheless, the 75% value is a prudent value consistent with demonstrated percentages found in experimental work.

A table should be provided in the application that identifies all of the different material regions in the criticality safety calculational models. This table should list the following for each region: the material in each region, the density of the material, the constituents of the material, the weight percent and atom density of each constituent, the region mass represented by the model, and the actual mass of the region (consistent with the contents and packaging description discussed in Sect. 2). The materials, densities, and masses provided in the sketches should be consistent with the corresponding items in the engineering drawings and should have the

same numerical values used in the input of the calculational method. For each sketch representing a portion of the calculation model, there should be a corresponding subsection discussing the material compositions and densities of each region shown in the sketch. All density values that are used, whether input by the analyst or retrieved by the code from a software database, should be reported in the application.

The source of all material density values should be reported. If a density value other than that found in standard references (e.g., materials or engineering handbook) is used in the calculation, the applicant should explain why the density is different, how the value was determined, and how the value affects the k_{eff}. Compositional differences should also be discussed.

3.1.4 Differences Between the Models and the Actual Package Configuration

The calculational models described in the criticality safety section of the application should be consistent with the undamaged and damaged package configurations as described in other sections (general, structural, thermal) of the application. Any differences (e.g., in dimensions, material, geometry) between the calculational models and the package configurations should be identified. The applicant should show how these different values (in dimensions, densities, etc.) were determined and justify the values used in the calculational models. Also, the applicant should discuss and explain how the differences impact the calculated k_{eff} values.

3.2 CONTENTS MODELS

The contents model should provide a detailed description of the packaging contents as they are assumed to be configured in the single-package and package array calculations. Models that show the contents under normal conditions of transport and under hypothetical accident conditions should be included in the application. A contents model representing each of the different loading configurations (full- and partial-load configurations) should also be provided. A single-contents model that will encompass different loading configurations should be considered only if the justification is clear and straightforward.

Each contents model should provide a description of the fissile contents of a package in its most reactive configuration, consistent with its physical and chemical form within the containment vessel under the normal or hypothetical accident conditions considered by the model. If the contents can vary over some parameter range (e.g., mass, enrichment, spacing), the criticality safety analysis should demonstrate that the model describes and uses the parameter specification that provides the maximum k_{eff} value under normal and hypothetical accident conditions. In designing the calculational models, tolerances that tend to add conservatism (i.e., produce higher k_{eff} values) should be included. Any assumed fissile material distribution that limits the maximum k_{eff} of the package contents should be justified.

The contents models for packages that transport loose pellets should ensure that variations in pellet size and spacing are considered in determining the configuration that produces the maximum k_{eff} value. The maximum pellet enrichment should be considered in the criticality safety evaluation. Fuel elements should consider the actual fuel pin spacing provided by the element.

At this time, the NRC does not accept burnup credit for spent fuel transportation packages. Therefore, unburned (fresh) fuel isotopics should be considered in the evaluation of packages containing spent fuel; however, no credit should be taken for any fixed burnable absorbers in the fuel when the fuel has been irradiated.

Other fissile materials should assume a particle spacing that results in maximum reactivity. Packages that transport isotopic waste containing fissile material should ensure that the limiting concentration and/or mix of fissile material is used in the safety analysis. Contents that are unknown or uncertain must be assumed to have a value that maximizes k_{eff}.

3.3 SINGLE-PACKAGE MODELS

The single-package models, together with the contents model(s), should depict the configuration of the packaging and contents under normal conditions of transport and under hypothetical accident conditions. These models should be those used to demonstrate that a single package remains adequately subcritical (see Sect. 5.4) per the requirements of 10 CFR § 71.55. The calculational model (single-package and contents model) for the single-package evaluation should consider the following items:

1. The undamaged single-package model should represent the physical condition of a package subjected to the test specified in 10 CFR § 71.71 (normal conditions of transport).

2. The damaged single-package model should represent the physical condition of a package subjected to the tests specified in 10 CFR § 71.73 (hypothetical accident conditions).

3. The packaging and contents should be in the most reactive configuration consistent with the chemical and physical form of the material. Determination of the most reactive configuration should account for the effects of both the normal and hypothetical accident conditions. In development of the damaged package models, the applicant should consider (a) the change in internal and external dimensions due to impact; (b) loss of material, such as neutron shield or wooden overpack, due to the fire test; (c) rearrangement of fissile material or neutron absorber material within the containment system due to impact, fire, or immersion; and (d) the effects of temperature changes on the package material and/or the neutron interaction properties.

4. Water moderation should be considered to occur to the most reactive extent possible. Partial flooding or preferential flooding (i.e., uneven flooding among the regions of a package to the most reactive extent), if possible, should be considered. If the contents are cladded fuel rods, flooding of the pellet-to-clad-gap regions should be considered. If fuel rods or pellets are annular, flooding of the annulus should also be considered, even if the rods or pellets are cladded. Moderation by other packaging materials should also be considered.

5. The containment system should be reflected closely on all sides by at least 30 cm of water. Package materials that are present and are better reflectors than water should be considered. For example, a lead shield around the containment system may provide more effective reflection than water.

In many cases, one model can be used to envelop both the undamaged and the damaged single-package models If only one model is used in the single-package analysis, the applicant should justify that this model bounds the most reactive undamaged and damaged configuration of the package.

3.4 PACKAGE ARRAY MODELS

The package array models should depict the arrangements of packages that are used in the calculations necessary to fulfill the requirements of 10 CFR § 71.59. At least two array models are needed: an array of

5N undamaged packages (normal conditions of transport) and an array of 2N damaged packages (hypothetical accident conditions). The configuration of the individual packages (undamaged and damaged) used in the respective array models should be the worst case for the array of packages, which may not be the same as the worst case for a single package. The dimensions of the array that provides the limiting subcritical k_{eff} value should be determined as described in Sect. 6.2. The calculational models for the array analysis should consider the following items:

1. The applicant should demonstrate that the most reactive array configuration has been considered in the criticality safety evaluation. The exact lattice arrangement may be represented by a simplified arrangement if justification is provided.

2. The applicant should consider all types of array arrangements. Often an array model that provides the lowest surface-to-volume ratio (typically one with equal dimensions on each side of the array) is a good initial arrangement because this model should minimize neutron leakage from the array (see Sect. 6.2).

3. The array of packages should be reflected on all sides by a close-fitting water reflector at least 30 cm thick.

4. The following criteria for moderation in the containment system should be assessed and separately applied for normal conditions of transport and hypothetical accident conditions. Optimum moderation is the condition that produces the highest k_{eff} value over the range of moderation conditions. Sources of moderation in the containment system are water leaking into the containment system, and the packaging materials and contents inside the containment system.

   Typically, the analysis for the array of undamaged packages can assume that the packages are dry internally, provided that there is no water leakage into the package, including the containment system, when the package is subjected to the tests specified in 10 CFR § 71.71.

   The analysis for the array of damaged packages should assume water leakage into the containment system to the most reactive degree. For those cases where water inleakage is not assumed, the application must adequately demonstrate that water inleakage would not occur under hypothetical accident conditions. The adequacy of such demonstrations will be assessed on a case-by-case basis. The acceptance criteria for these demonstrations are beyond the scope of this report.

   Regardless of whether water inleakage is assumed, internal moderation provided by the materials and contents (e.g., plastics, foam, impurities, or residual moisture in the fuel) in the package should be considered when determining optimum moderation. If the moderation provided by the packaging materials or contents overmoderates the package contents, and by its physical and chemical form cannot leak from the containment vessel, then its overmoderating properties can be considered in the model. For example, a solid moderator which is shown to overmoderate the fissile material can be considered in the calculational model if its continued presence is demonstrated under normal conditions of transport and hypothetical accident conditions.

5. If there can be leakage of water into the package, then partial and preferential flooding should be considered in determining optimum moderation. For fuel with pellet-to-clad gaps, flooding of the gap region should be considered.

6. Optimum interspersed hydrogenous moderation should be determined in the evaluation of arrays of damaged packages. Optimum interspersed moderation is the degree of hydrogenous moderation between packages that results in the highest k_{eff} value. In addition to interspersed moderation, moderation in regions of the package outside the containment system should also be considered if these regions consist of voids, hydrogenous or other moderating materials, or water-absorbing materials (e.g., foam, wood). The overmoderating or "isolating" effect of a packaging material may be considered, provided that the material remains in place and maintains its overmoderating or "isolating" properties under hypothetical accident conditions. Note that moderation between packages, moderation in regions of the package outside the containment system, and moderation within the containment system need to be considered concurrently to the most reactive extent.

4 METHOD OF ANALYSIS

This section of the report discusses the information that should be supplied on the computer code, nuclear cross-section data, and technique used to complete the criticality safety evaluation.

4.1 COMPUTER CODE SYSTEM

The computer codes used in the safety evaluation should be identified and described in the application or adequate references should be included. Verification that the software is performing as expected is important. The applicant should identify all hardware and software (titles, versions, etc.) used in the calculations as well as pertinent configuration control information. Correct installation and operation of the computer code should be demonstrated by performing and reporting (in the application or by reference) the results of the sample problems or general validation problems provided with the software package. Capabilities and limitations of the software that are pertinent to the calculational models should be discussed with particular attention to limitations that may affect the calculated k_{eff} value.

Computational methods that fully consider the anisotropic angular terms of the Boltzmann radiation transport equation are preferred for use in criticality safety analysis. The deterministic discrete-ordinates technique and the Monte Carlo statistical technique are the most rigorous and flexible techniques available to consider the anisotropic scattering terms. These techniques solve, respectively, the differential and integral eigenvalue (e.g., the k_{eff} value) form of the Boltzmann equation. Monte Carlo analyses are prevalent because these codes can better model the geometry detail needed for most criticality safety analyses. Well-documented and well-validated computational methods, such as those provided in the SCALE code system,[3] may require less description than a limited-use and/or unique computational method. The use of computational methods that limit or eliminate the angular terms in the Boltzmann equation (e.g., diffusion theory) or use simpler methods to estimate k_{eff} should be thoroughly justified.

When using a Monte Carlo code, the applicant should consider the imprecise nature of the k_{eff} value provided by the statistical technique. Every k_{eff} value should be reported with a standard deviation, σ. Typical Monte Carlo codes provide an estimate of the standard deviation of the calculated k_{eff}. The applicant may wish to obtain a better estimate for the standard deviation (Monte Carlo code estimates typically underpredict σ) by repeating the calculation with different valid random numbers and using this set of k_{eff} values to estimate σ_o. If fewer than 20 to 25 k_{eff} values are provided in the set, the estimation of σ should be calculated using the student-t distribution formula. Also, because of the statistical nature of Monte Carlo methods, this method should not be used to determine changes in k_{eff} due to small problem parameter variations. The change in k_{eff} due to a parameter change should be statistically significant (greater than at least 3σ) to indicate a trend in k_{eff}.

The geometry model limitations of deterministic discrete-ordinates methods typically restrict their applicability to calculation of bounding, simplified models and investigation of the sensitivity of k_{eff} to changes in system parameters. These sensitivity analyses can use a model of a specific region of the full problem (e.g., a fuel pin or homogenized fissile material unit surrounded by a detailed basket model) to demonstrate changes in reactivity with small changes in model dimensions or material specification. Applicants should consider such analyses when necessary to ensure or demonstrate that the full package model has utilized conservative assumptions relative to calculation of the system k_{eff} value. For example, a one-dimensional fuel pin model may be used to demonstrate the reactivity effect of tolerances in the clad thickness.

4.2 CROSS SECTIONS AND CROSS-SECTION PROCESSING

The calculational method consists of both the computer code and the neutron cross-section data used by the code. The criticality safety evaluation should be performed using cross-section data that are derived from measured data involving the various neutron interactions (e.g., capture, fission, and scatter). Although not infallible, unmodified data processed from compendiums of evaluated nuclear data (e.g., the various versions of the Evaluated Nuclear Data Files in the United States or the Joint European Files) should be considered as the major sources of such data.

The neutron cross-section data and any codes used to process the data for the criticality safety analyses should be identified, described, and referenced in the application. The codes used to process the data are subject to the same recommendations provided in the initial paragraph of Sect. 4.1. The application should identify the source of the neutron cross-section data (e.g., specific version of an evaluated nuclear data file) and supply pertinent references that document the content of the cross-section library, the procedure used to generate the cross-section library, and its range of applicability. Verification that the data library consists of the cross-section data described and referenced in the application is important. The applicant should demonstrate correct installation and operation of the data library by performing and reporting the results of any sample problems or general validation problems provided with the software package. Capabilities and limitations of the data library that are pertinent to the calculational models should be discussed with particular attention to discussing limitations that may affect the calculations. For example, the 123-group library once provided in the SCALE code package did not have resonance data for ^{235}U. Although not an issue for low-enriched, well-moderated systems that the library was generated to analyze, this lack of data made the library inappropriate for high-enriched, low-moderation systems.[6]

Continuous energy and multienergy-group (multigroup) cross-section libraries are acceptable. The number of energy groups and the energy boundaries of each group should be specified for a multigroup library. Known limitations (e.g., omission or limited range of resonance data, limited order of scattering) that may affect the analysis should be provided. The temperature range over which the cross-section data are applicable needs to be considered in the analyses and specified in the application. For multigroup cross sections, the order of scatter available on the library and applied in the calculation should be indicated. For continuous energy data, the number of points in the nuclide set should be specified. Computer programs and methods used to perform functions such as cross-section mixing for problem materials, problem-dependent resonance self-shielding, or cell-weighting of mixtures to represent heterogeneous configurations should be identified and discussed consistent with the recommendations of Sect. 4.1.

Any special techniques used in the analysis to improve the adequacy or use of the cross-section data should be discussed. For example, the SCALE system sequences automatically perform a problem-dependent resonance calculation for only one type of unit cell within a lattice. If deemed important, resonance-corrected data for materials outside the lattice, or for other types of unit cells within the lattice, can be calculated separately and provided via an optional input field.

4.3 CODE INPUT

All major code input parameters or options used in the criticality safety analysis should be identified and discussed in the application. This identification and discussion of code input should be provided in addition to the actual case inputs (or at least a sampling of the inputs for the various types of calculational models). For a Monte Carlo analysis, the applicant should indicate, among other things, the neutron starting distribution, the

number of histories tracked (number of generations and particles per generation), boundary conditions selected, order of scatter selected (for multigroup codes), any special reflector treatment, and any special biasing option. For a discrete-ordinates analysis, the applicant should specify the spatial mesh used in each region, the angular quadrature used, the order of scatter selected, the boundary conditions selected, and the flux convergence criteria. Any of these input parameters can influence the accuracy of the results; therefore, the selection of the input values should be carefully considered and, to the extent possible, be consistent with the data used in the validation analyses.

4.4 ADEQUACY OF CALCULATION

The criticality safety section of the application should review and discuss calculational issues that are important in ensuring an accurate k_{eff} value is obtained, Adequate problem-dependent treatment of multigroup cross sections, use of sufficient cross-section energy groups (multigroup) or data points (continuous energy), and proper convergence of the numerical results are examples of issues the applicant may need to review and discuss in the criticality section of the application. To the degree allowed by the code, the applicant should demonstrate or discuss any checks made to confirm that the calculational model prepared for the criticality safety analysis is consistent with the code input. For example, code-generated plots of the geometry models and outputs of material masses by region may be beneficial in this confirmation process. The statistical nature of Monte Carlo calculations is such that there are no fixed rules, criteria, or tests for judging when calculational convergence has occurred. Thus the applicant should discuss the code output or other measures used to confirm the adequacy of convergence. For example, many Monte Carlo codes provide output edits that should be reviewed to determine adequate convergence, including:

1. the k_{eff} by generation run,
2. plot of average k_{eff} by generation run,
3. final k_{eff} edit table by generation skipped,
4. plot of k_{eff} by generation skipped, and
5. frequency distribution bar graph.

Other conditions in the output that may indicate a convergence problem should be reviewed, for example,[7]

1. upward or downward trends in k_{eff} by generation run over the last half of the total generations,
2. upward or downward trends in k_{eff} by generation for the first half of generations skipped,
3. sudden changes of greater than one standard deviation in either k_{eff} plot,
4. abnormally high or low generation k_{eff} ($\pm 20\%$ of calculated mean), and
5. a calculated result that is not consistent with expected results based on previous experience (may be indicative of other problems).

It is also advisable to check for adequate sampling of isolated fissile regions by examining the printed regionwise fission event data and associated statistics.

If necessary, the applicant should review the code documentation as well as literature (such as Refs. 7 and 8) to obtain practical discussions on the uncertainties associated with Monte Carlo codes used to calculate k_{eff} and advice on output features and trends that should be observed. If convergence problems were encountered by the applicant, a discussion of the problem and the steps taken to obtain an adequate k_{eff} value should be provided. For example, calculational convergence may be achieved by selecting a different neutron starting distribution or running additional neutron histories. Modern personal computers and workstations allow a significant number of particle histories to be tracked: a minimum of 200,000 histories is now typical

As a minimum, portions of output (such as the plots of k_{eff} by generation run and k_{eff} by generation skipped) from selected cases should be included in the application. In selecting the output to provide, the applicant should consider that the goal is to demonstrate that the calculations have been performed as described and run to successful completion.

5 VALIDATION OF CALCULATIONAL METHOD

The application should demonstrate that the calculational method (codes and cross-section data) used to establish criticality safety has been validated against measured data that can be shown to be applicable to the package design characteristics. The validation process should provide a basis for the reliability of the calculational method and should justify that the calculated k_{eff}, plus bias and uncertainties, for the necessary package conditions will ensure an actual package $k_{eff} \leq 0.95$.

The applicant should comply with the following guidelines[9] in performing and documenting the validation process:

1. bias and uncertainties should be established through comparison with critical experiments that are applicable to the package design;

2. the range of applicability for the bias and uncertainty should be based on the range of parameter variation in the experiments;

3. any extension of the range of applicability beyond the experimental parameter field should be based on trends in the bias and uncertainty as a function of the parameters and use of independent calculational methods; and

4. a margin of subcriticality should be included. The NRC currently regards 0.05 Δk as the minimum administrative margin of subcriticality that should be considered for transportation packages.

Although significant reference material is available to demonstrate the performance of many different criticality safety codes and cross-section data combinations, the application needs to demonstrate that the specific calculational method used by the applicant (e.g., code version, cross-section library, and computer platform) is validated in accordance with the above process. The remainder of this section of the report provides recommendations on the assumptions that should be made and the information that should be provided in performing and documenting the validation process.

5.1 SELECTION OF CRITICAL EXPERIMENTS

The first phase in the validation process should be to establish an appropriate bias and uncertainty for the calculational method by using well-defined critical experiments that have parameters (e.g., materials, geometry, etc.) that are characteristic of the package design. The single-package configuration, the array of packages, and the normal and hypothetical accident conditions should be considered in selecting the critical experiments for the validation process. Ideally, the set of experiments should match the package characteristics that most influence the neutron energy spectrum and reactivity. These characteristics include:

1. the fissile isotope (^{233}U, ^{235}U, ^{238}Pu, ^{239}Pu, and ^{241}Pu according to the definition of 10 CFR 71), form (e.g., homogeneous, heterogeneous, metal, oxide, fluoride), and isotopic composition of the fissile material;

2. hydrogenous moderation, consistent with the normal conditions of transport and hypothetical accident conditions, in and between packages that results in maximum k_{eff} (if substantial amounts of other moderators such as carbon or beryllium are in the package, these should also be considered);

3. the type (e.g., boron, cadmium), placement (between, within, or outside the contents), and distribution of absorber material and materials of construction;

4. the single-package contents configuration (e.g., homogeneous or heterogeneous) and packaging reflector material (e.g., lead, steel); and

5. the array configuration including spacing, interstitial material, and number of packages.

Unfortunately, it is unlikely that the complete combination of package characteristics will be found from available critical experiments, and critical experiments for large arrays of packages do not currently exist. Thus the applicant should model a sufficient variety of critical experiments to demonstrate the capability of the calculational method in predicting k_{eff} for each individual experiment that has characteristics that are also judged to be important to the k_{eff} of the package (or array of packages) under normal conditions of transport and hypothetical accident conditions.

Reference 10 provides general guidance on selecting critical experiments and provides descriptions of a significant number of critical experiments appropriate for low-enriched lattice systems. The critical experiments that are selected by the applicant should be briefly described in the application with references provided for detailed descriptions. The applicant should indicate any deviation from the reference experiment description including the basis for the deviation (e.g., discussions with experimenter, experiment log books). Since validation and supporting documentation may result in a voluminous report, it is acceptable to summarize the results in the application and reference the validation report for specific information.

5.2 ESTABLISHMENT OF BIAS AND UNCERTAINTY

For validation using critical experiments, the bias in the calculational method is the difference between the calculated k_{eff} value of the critical experiment and unity (1.0). Typically, a calculational method is termed to have a positive bias if it overpredicts the critical condition (i.e., calculated $k_{eff} > 1.0$) and a negative bias if it underpredicts the critical condition (i.e., calculated $k_{eff} < 1.0$). A calculational methodology should have a bias that either has no dependence on a characteristic parameter or is a smooth, well-behaved function of characteristic parameters. The applicant should analyze a sufficient number of critical experiments to determine if trends may exist with parameters important in the validation process [e.g., hydrogen-to-fissile ratio (H/X), ^{235}U enrichment, neutron absorber material]. As indicated in Sect. 4.1, the k_{eff} values should change by at least 3σ to indicate any type of parametric trend. The bias for a set of criticals should be taken as the difference between the best fit of the calculated k_{eff} data and 1.0. Where trends exist, the bias will not be constant over the parameter range. If no trends exist, the bias will be constant over the range of applicability. For trends to be recognized, they must be statistically significant.

The applicant should consider three general sources of uncertainty: the experimental data or technique, the calculational method, and the particular analyst and calculational models. Examples of uncertainties in experimental data are uncertainties reported in material or fabrication data or uncertainties due to an inadequate description of the experimental layout. Examples of uncertainties in the calculational method are uncertainties in the approximations used to solve the mathematical equations, uncertainties due to solution convergence, and uncertainties due to cross-section data or data processing. Interpretation of the calculated results, individual modeling techniques, and selection of code input options are possible sources of uncertainty due to the analyst or calculational model.

In general, all of these sources of uncertainty should be cumulatively observed in the variability of the calculated k_{eff} results obtained for the critical experiments. The variability should include the Monte Carlo standard deviation in each calculated critical experiment k_{eff} value as well as any change in the calculated value

caused by the consideration of experimental uncertainties. Thus these uncertainties will be included in the bias and uncertainty in the bias. This variation or uncertainty in the bias should be established by a valid statistical treatment of the calculated k_{eff} values for the critical experiments. Methods exist (see Ref. 10) that allow the bias and uncertainty in the bias to be evaluated as a function of changes in a selected characteristic parameter.

Calculational models used to analyze the critical experiments should be provided or adequate references to such discussions should be provided. Input data sets used for the analysis should be provided along with an indication of whether these data sets were developed by the applicant or obtained from other identified sources (e.g., published references, data bases). Known uncertainties in the experimental data should be identified, along with a discussion of how (or if) they were included in the establishment of the overall bias and uncertainty for the calculational method. The statistical treatment used to establish the bias and uncertainty should be thoroughly discussed in the application with suitable references where appropriate. Relative to experimental uncertainties, the applicant should provide a discussion on the approach used to model the experiments (i.e., with nominal dimensions and material compositions or with conservative tolerances, with simplifications in the geometry and material specifications, etc.).

5.3 ESTABLISHMENT OF RANGE OF APPLICABILITY

As an integral part of the code validation effort, the applicant should define the range of applicability for the established bias and uncertainty. The applicant should demonstrate that, considering both normal and hypothetical accident conditions, the package is within this range of applicability and/or the applicant should define the extension of the range necessary to include the package. The range of applicability should be defined by identifying the range of important parameters (see Ref. 10 for guidance on identifying important parameters) and/or characteristics for which the code was (or was not) validated. The procedure or method used to define the range of applicability should be discussed and justified in the application for approval. For example, the method of Ref. 10 indicates the range of applicability to be the limits (upper and lower) of the characteristic parameter used to correlate the bias and uncertainties. The characteristic parameter may be defined in terms of, for example, the hydrogen-to-fissile ratio (e.g., H/X = 10 to 500), the average energy causing fission, the ratio of total fissions to thermal fissions (e.g., F/F_{th} = 1.0 to 5.0), or the ^{235}U enrichment.

Use of the bias and uncertainty for the evaluation of a package with characteristics beyond the defined range of applicability is endorsed by consensus guidance.[9] This guidance indicates the extension should be based on trends in the bias as a function of system parameters and, if the extension is large, confirmed by independent calculational methods. However, the applicant should consider that extrapolation can lead to a poor prediction of actual behavior. Even interpolation over large ranges with no experimental data can be misleading (see Ref. 6 for an example). The applicant should also consider the fact that comparisons with other calculational methods can illuminate a deficiency or provide concurrence; however, given discrepant results from independent methods, it is not always a simple matter to determine which result is "correct" in the absence of experimental data (see Ref. 11 for an illustration).

The applicant should recognize that there is no available guidance on what constitutes a "large" extension, nor any guidance on how to extend trends in the bias. In fact, it is not just the trend in the bias that the applicant should consider, but the trend in the uncertainties and bias. The paucity of experimental data near one end of a parameter range may cause the uncertainty to be larger in that region. (Note: Any extension of the uncertainty using the method of Ref. 10 should consider the behavior of the uncertainty as a function of the parameter, not just the maximum value of the uncertainty.) Proper extension of the bias and uncertainty means the applicant should determine and understand the trends in the bias and uncertainty. The applicant should exercise extreme

care in extending the range of applicability and provide in the application a detailed justification for the need for an extension, along with a thorough description of the method and procedure used to estimate the bias and uncertainty in this extended range.

5.4 ESTABLISHMENT OF ACCEPTANCE CRITERIA

The criticality safety section of the application should demonstrate how the bias and uncertainty determined from the comparison of the calculational method with critical experiments are used to establish a minimum k_{eff} value [i.e., upper subcritical limit (USL)] so that similar systems with a higher calculated k_{eff} are considered to be critical. The USL should be established with an additional margin of subcriticality (often termed a safety margin) included.[9] The following general relationship (see Ref. 10) for establishing the acceptance criteria should be used in the application for approval:

$$k_c - \Delta k_u \geq k_{eff} + 2\sigma + \Delta k_m ,$$

where

k_c = mean value of k_{eff} resulting from the calculation of benchmark critical experiments using a specific calculational method and data;
Δk_u = an allowance for the calculational uncertainty;
Δk_m = a required margin of subcriticality (minimum of 0.05 for applications of approval for packaging);
k_{eff} = the calculated value obtained for the package or array of packages;
σ = is the standard deviation of the k_{eff} value obtained with Monte Carlo analysis.

If the calculational bias β is defined as $\beta = k_c - 1$, then the bias is negative if $k_c < 1$ and positive if $k_c > 1$. Thus the acceptance criteria may be rewritten as

$$1.00 + \beta - \Delta k_u \geq k_{eff} + 2\sigma + 0.05,$$

or

$$k_{eff} + 2\sigma \leq 0.95 - \Delta k_u + \beta .$$

The maximum USL that should be used for a package evaluation is

$$USL = 0.95 - \Delta k_u + \beta .$$

The uncertainty, Δk_u, will always be greater than or equal to zero, whereas the bias, β, can be positive or negative. However, a positive bias is not recommended; therefore, the equation should be revised to

$$USL = 0.95 - \Delta k_u + \bar{\beta}$$

where $\bar{\beta} = \begin{cases} \beta \text{ if } \beta \leq 0 \\ 0, \text{ if } \beta > 0 . \end{cases}$

The applicant should consider that the value for Δk_m (=0.05) may need to be increased by an arbitrary amount if there is a lack of sufficient critical data to adequately determine the calculational bias and uncertainty. The statistical method of Ref. 10 provides a technique to estimate Δk_u and Δk_m based on available data. This estimate for Δk_m can be used to demonstrate that the value of 0.05 for the margin of subcriticality is adequate

for the given set of critical experiments used in the validation. A paucity of critical experiment data or the need to extend beyond the range of applicability may indicate the applicant should consider the adequacy of the 0.05 value. Also, for high-reactivity worth systems where the value of k_{eff} is particularly sensitive to parameter changes in the package, a margin of subcriticality greater than 0.05 Δk should be considered by the applicant.

6 CRITICALITY CALCULATIONS AND RESULTS

This section of the report describes the criticality calculations that should be performed and documented in the criticality safety section of the application for approval of a package. The criticality safety evaluation should demonstrate the subcriticality of a single package and an array of packages during normal conditions of transport and hypothetical accident conditions, and determine the TI for criticality control of a shipment. For the purposes of this evaluation, the applicant should consider the term "subcriticality" to mean that the calculated k_{eff} value (including any Monte Carlo standard deviation) is less than the USL defined by Sect. 5.4.

The calculations that the applicant should include in the criticality safety section will depend on the various parameter changes and conditions that should be considered, the packaging design and features, the contents, and the damaged condition of the package. The calculated results should be presented in a tabular form with a case identifier, a brief description of the conditions for each case, and the case results. Values of k_{eff} obtained from Monte Carlo codes should always indicate the estimated standard deviation. Additional information should be included in the table if it supports and simplifies the description in the text. The case description should be clearly presented in the tables to permit easy cross-reference between the table and the text. Tables 1 and 2 show an example of the format desired to summarize the results of single-package and package array calculations.

The following subsections present a logical, generic approach to the calculational effort that should be described in the application for approval. Two series of calculational cases should be performed: (1) a series of single-package cases and (2) a series of array cases. Both series should consider normal and hypothetical accident conditions. Subsets of the array series for different size arrays or different package arrangements may also be necessary. Each array series should include calculations to determine the number of undamaged packages that will ensure subcriticality of an array under normal conditions of transport, as well as calculations to determine the number of damaged packages that ensure subcriticality of an array under hypothetical accident conditions. A TI for criticality control should be derived (see Sect. 6.3) from these array sizes based on the prescription of 10 CFR § 71.59.

6.1 SINGLE PACKAGE

The applicant should perform a series of calculations to demonstrate that the single package remains subcritical under normal conditions of transport and hypothetical accident conditions (per the requirements of 10 CFR § 71.55).

The single-package calculations also provide useful points of reference for subsequent calculations involving variations of certain parameters.

The single-package series of calculations must consider a model of the single containment vessel fully reflected by water (a 30-cm-thick region of full-density water is recommended). The containment vessel should be optimally moderated with the fissile content in its most reactive credible configuration. This water-reflected, optimally moderated containment vessel analysis should be compared with one where the water reflector is replaced by the package material (including water flooding in voids) that surrounds the containment system. Package materials such as lead may provide better reflection of the containment system than water. Demonstration that these two single, undamaged cases are adequately subcritical satisfies the requirements of 10 CFR § 71.55(b).

Table 1 Example format of table for single-package calculations

Case	Water reflected[a]	Internal moderation[b]	$k_{eff} \pm \sigma$[c]
SU1	No	0.0	
SU2	Yes	0.0	
SU3	Yes	0.001	
SU4	Yes	0.003	
.	.	.	
.	.	.	
SUx	Yes	1.0	
SUy	No	1.0	

[a]When fully reflected, water should be at least 30-cm thick on all faces.
[b]Internal moderation is the specific gravity water equivalent of hydrogenous content within all void spaces inside the package, including the containment vessel.
[c]σ is one standard deviation of the calculated Monte Carlo result.

Table 2 Example format of table for array calculations

Case[a]	Array size	Internal moderation[b]	Interspersed moderation[c]	$k_{eff} \pm \sigma$[d]
IA1	Infinite	0.0	0.0	
IA2	Infinite	0.0	0.001	
IA3	Infinite	0.0	0.003	
.				
.				
IAx	Infinite	0.0	1.0	
FA1	7 × 7 × 7			
FA2	7 × 7 × 7			
FA3	7 × 7 × 7			
.				
.				
FA10	5 × 5 × 5			
FA11	5 × 5 × 5			
.				
.				

[a]Case identifier IA represents infinite arrays and FA represents finite arrays; all finite arrays should be reflected by at least 30 cm of water on all faces.
[b]Internal moderation is the specific gravity water equivalent of hydrogenous content within all void spaces inside the package, including the containment vessel.
[c]Interspersed moderation is the specific gravity water equivalent of hydrogenous content between packages.
[d]σ is one standard deviation of the calculated Monte Carlo result.

The remaining single-package cases provided in the application should systematically investigate progressive states of water flooding and package reflection representative of the normal and hypothetical accident conditions. If the hypothetical accident conditions cause damage to the contents or packaging, the damaged configuration of the package should be considered. If a package has multiple void regions, including regions within the containment system, flooding each region independently and consecutively should be considered. Variations in the flooding sequence should be considered by the applicant [e.g., partial flooding, variations caused by the package lying in horizontal or vertical orientations, flooding (moderation) at less than full-density water, progressively flooding regions from the inside out]. Water flooding of cladded fuel rod gap regions should be considered. The final case of this single-package series should represent a package completely water-flooded and water-reflected. The primary objectives of the single-package cases should be

1. to demonstrate that a single package is subcritical when subjected to the normal conditions of transport and hypothetical accident conditions as specified by 10 CFR § 71.55, and

2. to identify the specific conditions that produce the highest k_{eff} value.

For packages with different fissile material loading configurations (including partial-load configurations), the applicant should use a similar approach for each different loading, unless a limiting-contents model is developed and demonstrated in the application to provide a bounding reactivity for the different loadings. The results of the single-package calculations can influence the approach and the number of calculations required for the array series calculations, particularly if there are different content loading configurations.

6.2 EVALUATION OF PACKAGE ARRAYS

The applicant should perform the package array calculations to obtain the information needed to determine the TI for criticality control as prescribed by 10 CFR § 71.59. The applicant may consider beginning the array calculations with an infinite array model because, if the infinite array is adequately subcritical under normal and hypothetical accident conditions, no additional array calculations should be necessary. If the infinite array under normal and hypothetical accident conditions is shown to be above the USL, a large (number of packages) finite array should be selected and all cases recalculated. Successively smaller finite arrays may be required until the array sizes for normal and hypothetical accident conditions are found to be below the USL. As an alternative, an applicant may initiate the analyses using any array size–for example, one that is based upon the number of packages planned to be shipped on a vehicle.

Care should be taken so that the most reactive array configuration of packages has been considered in the criticality safety assessment. In investigating different array arrangements, the competing effects of leakage from the array system and of interaction between packages in the array should be considered. Array arrangements that minimize the surface-to-volume ratio decrease leakage and should, in simplistic terms, maximize k_{eff}. Preferential geometric arrangement of the packages in the array should be considered. For example, consider packages where the fissile material is loaded off-center. In this case, the need to optimize the interaction may mean that an array is more reactive when packages are grouped in a single or double layer The effect of the external water reflector also needs to be considered. For some array cases there may be little moderator present within the array, so increasing the surface area may lead to more moderation and possibly higher reactivity. The exact package arrangement may be represented by a simplified arrangement if adequate justification is provided. For example, Appendix A demonstrates a case where a triangular-pitch arrangement of packages can, in simple cases, be represented by using an appropriately modified package model within a square-pitch lattice arrangement. In more compl cases, the effect of having a triangular pitch may be

important, since interaction between three triangularly pitched packages could be a dominating factor. Because there are so many competing effects, any simplifications made in the assessment need to be justified; something that is obvious from the point of view of array leakage may not be as obvious from the point of view of package interaction. All finite arrays of packages should be reflected on all sides by a close-fitting, full-density water reflector at least 30 cm thick.

Each array model for undamaged packages is not required to include interspersed moderation; however, moderation built into the packaging (e.g., due to hydrogenous packaging materials) or added to the packaging due to normal conditions of transport (e.g., the spray test) should be included to the most reactive extent possible under normal conditions. For damaged packages, varying amounts of hydrogenous moderation should be added in all regions that can be flooded within (see discussion of Sect. 6.1 for single package) and between the packages (i.e., interspersed moderation) by varying the density of water in these regions. If water in-leakage is considered (see Sect. 3.4), then the water density should be varied from zero to full density in increments such that the optimum moderator density is determined. The applicant should provide a plot of the k_{eff} value as a function of the moderator density to demonstrate the trend and the location of the highest k_{eff} value.

As an interspersed moderator is added to the region between packages, the spacing of the packages may become important because of the amount of moderator that may be present. For this reason, it is sometimes convenient to model an infinite array of packages using an array unit cell consisting of the individual package and a tight-fitting repeating boundary. If the k_{eff} response to increasing interspersed moderator density for this array with the units in contact has an upward trend (positive slope) at full-density moderation, the applicant should consider increasing the size of the unit cell and recalculating k_{eff} as a function of moderation density. Increasing the size of the unit cell provides an increased edge-to-edge spacing between packages and makes more volume available for the interspersed moderator. The applicant should stop this procedure only after confirming that the packages are isolated and that added interstitial space is only providing additional water reflection.

To illustrate this recommended procedure, consider a cylindrical shipping package with a diameter of one unit and a height (or length) of two units. With a tight-fitting cuboid around the cylinder, 21.5% of the cuboid's volume is outside the package and is available for an interspersed moderator. By increasing the cuboid's dimensions so that the edge-to-edge spacing between the packages in all directions is 10% of the package diameter, then 38.2% of the cuboid's volume is outside the package and is available for an interspersed moderator. This small increase in edge-to-edge spacing corresponds to a 126% increase in volume available for the interspersed moderator. Therefore, if the k_{eff} value is increasing at full water density with the packages in contact, then increasing the packaging spacing to permit additional interspersed moderation may be necessary.

The applicant should consider combinations of density and spacing variation (consistent with normal and hypothetical accident conditions) that may cause a higher k_{eff} value to be calculated and should provide a discussion in the application that demonstrates the maximum k_{eff} value has been determined. Figure 1 depicts some typical plots of k_{eff} versus interspersed water moderator density illustrating the moderation, absorption, and reflection characteristics that may be encountered in packaging safety evaluations. These curves represent changes in array moderation for a fixed package spacing. Curves A, B, and C represent arrays for which an array of packages at the selected spacing is overmoderated and increasing water moderation only lowers (curves B and C) or has no effect (curve A) on the k_{eff} value. Curves D, E, and F represent arrays for which the array is undermoderated at zero water density, and increasing the moderator density causes the k_{eff} value to ...

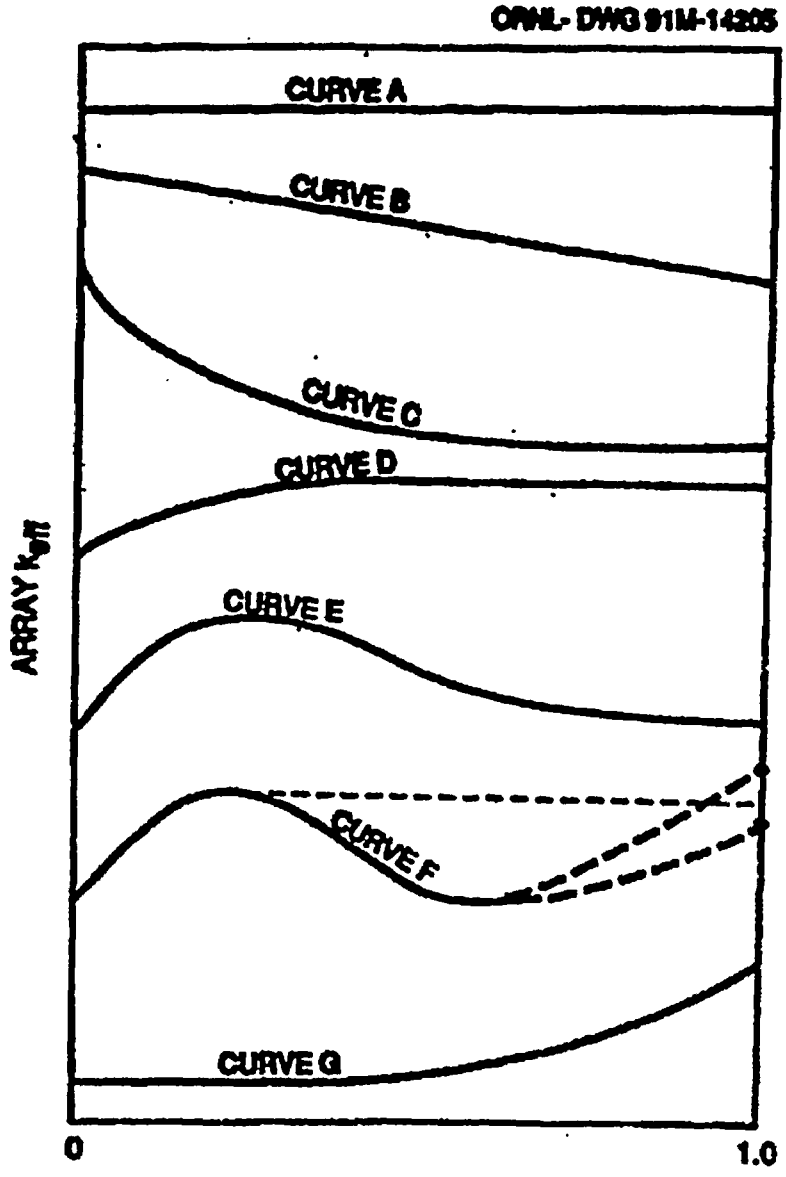

Figure 1 Typical plots of array k_{eff} vs interspersed water moderator density

increase. Then as the water density increases further, neutron absorption comes into effect, neutron interaction between packages decreases, and the k_{eff} value levels out (curve D) or decreases (curves E and F). The applicant should consider that peaking effects such as seen in curves E and F frequently occur at very low moderator density (e.g., 0.001 to 0.1 fraction of full density). Therefore, the applicant should exercise care when selecting the values of interspersed moderator density to calculate in the search for the maximum k_{eff} value.

As indicated above, optimum moderation conditions for the array of packages represented by curves D, E, and F have been obtained; and the only mechanism that could make the k_{eff} value of curve D, E, or F rise above the value at full-density water is increased reactivity due to increased reflection provided by more interspersed water (i.e., additional spacing between packages). If the array k_{eff} at full-density moderation is less than the k_{eff} of the flooded and reflected single unit, the edge-to-edge spacing of the packages is not sufficient to permit full reflection.

However, for responses such as those illustrated in curves D, E, and F, there is no need to increase spacing and recalculate the array k_{eff} because the maximum k_{eff} of the array will be that of the reflected single unit, or the k_{eff} of the optimally moderated array (i.e., the first local maxima of curves D, E, and F), whichever is larger. For curves A through F, the packages in the array are essentially isolated at full-density moderation and the corresponding k_{eff} will typically be the same (within statistical limits) as the flooded and reflected single-unit case.

Curve G represents an array where the optimum array moderator density has not been achieved even with full-density water, and the maximum k_{eff} has not been determined. For this situation, the applicant should increase the center-to-center spacing of the packages in the array and all cases should be recalculated. The center-to-center spacing must be sufficiently large for the curve to reach a plateau (like curve D) or to peak and then decrease (like curves E and F).

The treatment of array moderation can be easy or complex, depending on the placement of the materials of construction and their susceptibility to damage from hypothetical accident conditions. For all of these conditions and combinations of conditions, the applicant should carefully investigate the optimum degree of internal and interspersed moderation consistent with the chemical and physical form of the material and the packaging, and should demonstrate that subcriticality is maintained. The applicant should consider the numerous conditions for which the effects of moderation must be investigated, such as

1. moderation from packing materials that are inside the primary containment system,
2. moderation due to preferential flooding of different regions in the packages,
3. moderation from hydrogenous materials of construction (e.g., thermal insulation and neutron shielding), and
4. interspersed moderation in the region between the packages in an array.

In determining the TI of an array of packages under normal conditions of transport, the applicant should consider only the possible ranges of hydrogenous (or other) moderators present in the package [items (1) and (3) above and, if applicable, item (2) above]; interspersed moderation between packages [item (4) above] from conditions such as mist, rain, snow, or flooding need not be considered (per the specifications of 10 CFR § 71.59). In determining the TI of an array of damaged packages, the applicant should carefully consider all four of the above conditions, including how each form of moderation can change under hypothetical accident conditions. As an example, consider a package with thermally degradable insulation. The applicant should evaluate the array with the insulation for the normal conditions of transport. For the hypothetical accident

conditions, the applicant should investigate moderation effects caused by changes in the insulation due to the thermal tests. The applicant should carefully evaluate the varying degrees of internal moderation in the containment.

6.3 RELATING ANALYSES TO TRANSPORT INDEX

The TI for criticality control should be determined by the applicant using the information from the array analyses on the number of packages that will remain subcritical (below the USL) under normal and hypothetical accident conditions. The USL should be determined using the criteria discussed in Sect. 5.4. Table 3 illustrates the tabular form that the applicant should use to summarize the results on the limiting number of packages shown to be subcritical in the analysis of the package arrays. The value N in the table can be defined so that

N = maximum number of packages per shipment for a nonexclusive use shipment, where $5 \leq N \leq \infty$.
2N = maximum number of packages per shipment for an exclusive use shipment, where $0.5 \leq N \leq \infty$.

Table 3 Requirements of 10 CFR § 71.59

Case	No. of fissile packages that must be subcritical
Undamaged	5N with nothing between packages
Damaged	2N with optimum interspersed moderation

With the information provided in Table 3, the applicant can determine the TI for criticality control using the expression

$$TI = 50 \div N .$$

7 SUMMARY

This report provides recommendations on the information that should be included in the criticality safety section of an application for approval of a transportation package. The emphasis has been on the design information, analysis models, and computational results and discussion that should be in the application. However, the applicant should recognize that the recommendations may not be exhaustive and that additional information or analyses may be needed for selected applications.

Section 2 of the report discusses the design information that the applicant should include in the criticality safety section of the application. Specification of the contents (e.g., form, type, mass, composition) considered in the application should be provided, including any anticipated variations and uncertainties.

Section 3 of the report reviews the description and figures that should be included in the application to adequately explain the calculational models. In preparing these models, the applicant should limit the use of fixed neutron absorbers to 75% of the composition, unless adequate (see Sect. 3.1.3) consideration is made for testing the presence and uniformity of the absorber. Fixed, burnable poisons should not be considered in spent fuel packages. And, until the NRC provides direction on use of spent fuel isotopics, it is recommended that unburned (fresh) fuel isotopics be assumed in applications for spent fuel packages. Water moderation and reflection specifications based on the normal and accident conditions of 10 CFR Part 71 must be considered in the development of the analysis models.

Sections 4-5 of the report recommend the information that should be considered by the applicant in selecting and using an appropriate analysis method (code and nuclear data) for determination of the neutron multiplication factor. Codes that adequately model the kinematics of neutron transport, including angular scattering, are needed to provide the best estimate of k_{eff}. The codes and data used in the application should be validated against critical experiments appropriate for the package conditions and contents. This validation provides a basis for development of a USL that considers bias and uncertainties (determined from the validation), the statistical nature of the analysis method, and a margin of subcriticality. The minimum margin of subcriticality accepted by the NRC for transportation packages is 0.05 Δk.

Section 6 of the report discusses the analyses that should be considered to demonstrate that the requirements of 10 CFR § 71.55 and 71.59 are met. This section provides practical information on how to proceed with the analyses, the single-package and array conditions that should be considered, and a process for determination of the TI for criticality control. Development and analysis of the array models should carefully consider the various conditions that could lead to an increased k_{eff} value. Optimum moderation of the packages according to the normal and accident conditions, package arrangement and spacing for optimum interaction between packages, and proper water reflection of the array should be considered.

8 REFERENCES

1. "Compatibility with the International Atomic Energy Agency (IAEA); Final Rule," Part II, 10 CFR Part 71 of *Federal Register* 60(188), 50248-50289 (September 28, 1995).

2. *Standard Format and Content of Part 71, Applications for Approval of Packaging for Radioactive Material*, Regulatory Guide 7.9 (Proposed Revision 2), U.S. Nuclear Regulatory Commission, Washington, DC (May 1986).

3. *SCALE: A Modular Code System for Performing Standardized Computer Analyses for Licensing Evaluation*, Vols. I-III, NUREG/CR-0200, Rev. 4 (ORNL/NUREG/CSD-2/R4) (April 1995).

4. A. H. Wells, D. R. Marnon, and R. A. Karam, "Criticality Effect of Neutron Channeling Between Boron Carbide Granules in Boral for a Spent Fuel Shipping Cask," *Trans. Am. Nucl. Soc.* 54, 205-206 (1987).

5. W. R. Burrus, "How Channeling Between Chunks Raises Neutron Transmission Through Boral," *Nucleonics* 16, 1, 91 (January 1958).

6. C. V. Parks, R. Q. Wright, and W. C. Jordan, *... ...y of the 123-Group Cross-Section Library for Criticality Analyses of Water-Moderated Uranium Systems*, NUREG/CR-6328 (ORNL/TM-12970), U.S. Nuclear Regulatory Commission, August 1995.

7. N. F. Landers and L. M. Petrie, "Uncertainties Associated with the Use of the KENO Monte Carlo Criticality Codes," p. 289 in *Proc. International Topical Meeting on Safety Margins in Criticality Safety*, San Francisco, California, November 26-30, 1989.

8. R. A. Forster, T. E. Booth, T. J. Urbatsch, K. A. Van Riper, and L. S. Waters, "Analyses and Visualization of MCNP Criticality Results," *Trans. Am. Nucl. Soc.* 1, Albuquerque, New Mexico, September 17-21, 1995.

9. *American National Standard for Nuclear Criticality Safety in Operations with Fissionable Materials Outside Reactors*, ANSI/ANS-8.1-1983 (Revision of ANSI N16.1-1975), American Nuclear Society, 1983.

10. J. J. Lichtenwalter and S. M. Bowman, *Criticality Benchmark Guide for Light-Water-Reactor Fuel in Transportation and Storage Packages*, NUREG/CR-6361 (ORNL/TM-13211), U.S. Nuclear Regulatory Commission, 1997.

11. C. V. Parks, W. C. Jordan, L. M. Petrie, and R. Q. Wright, "Use of Metal/Uranium Mixtures to Explore Data Uncertainties," *Trans. Am. Nucl. Soc.* 73, 217 (1995).

12. M. D. DeHart and S. M. Bowman, *Validation of the SCALE Broad Structure 44-Group ENDF/B-V Cross-Section Library for Use in Criticality Safety Analyses*, ORNL/TM-12460, Oak Ridge Natl. Lab., September 1994.

Preceding page blank

APPENDIX A

EXAMPLE OF CALCULATIONAL MODELS AND RESULTS

This appendix uses a simple example of a fictitious transport package to illustrate many of the recommendations provided in this report regarding the content of the criticality safety section of the application for a transport package. This example package and analysis have not been approved by the NRC, and there has been no assessment as to whether the package would meet all of the requirements for approval. The descriptions provided herein do not include all the information that would be necessary for an actual package evaluation; rather they provide an illustrative sampling of the type of information discussed in this report.

The following sections provide information as if it were imbedded as the criticality section of the application. However, since this is intended to be an illustrative example, only that information pertinent to developing the calculational models is included. The dimensional and material specifications provided are the minimum to support the calc lations in this appendix and do not represent certified container loadings or configurations. Also, the descriptions, calculations, and justifications presented here may not be complete or acceptable to the NRC.

A.1 GENERAL DESCRIPTION (Example)

The transport package uses a 55-gal steel drum overpack [22.5-in.(57.15-cm) inside diam by 40.5-in. (102.87-cm) inside height]. The drum body and bottom are fabricated from a 16-gauge [0.064-in. (0.16-cm)] low carbon steel sheet. The drum lid (head) is fabricated from a 14-gauge [0.080-in. (0.20-cm)] low-carbon steel sheet. Two approximately equally spaced, rolling hoops are swaged into the drum body. The removable head is closed by means of a bolt-locking ring.

The inner container (containment vessel) is the containment boundary. The inner container is fabricated from a 0.25-in. (0.64-cm)-thick carbon steel plate. The inner container [12.0-in. (30.48-cm) inside diam by 28.0-in. (71.12-cm) inside height] has a welded bottom plate and welded cover plate.

The 55-gal drum is filled between the drum wall and inner container with insulating fiber board that provides thermal insulation and vibration and shock isolation, and centers the inner container within the drum. The insulating fiber board provides a thickness between the inner container and drum of 5.0 in. (12.7 cm) radially and 5.0 in. (12.7 cm) axially (top and bottom).

The package shall be used to transport unirradiated uranium dioxide (UO_2) pellets of 0.325-in. (0.83-cm) nominal outside diameter. The contents are not to exceed 116.16 kg of UO_2 pellets at an enrichment in the ^{235}U isotope of 4.01%.

A.2 PACKAGE DESCRIPTION

Sections A.2.1 and A.2.2 describe the package contents and packaging, specifically the dimensions and material components that influence k_{eff}.

Preceding page blank

A.2.1 CONTENTS

The package shall be used to transport right cylindrical UO_2 pellets of 10.40 g/cm^3 oxide density. The pellets have a 0.325-in. (0.83-cm) nominal outside diameter and height and a maximum enrichment of 4.01 wt % ^{235}U. The uranium isotopic distribution is given in Table A.1.

Table A.1 Uranium isotopic distribution

Isotope	wt %
^{234}U	0.02
^{235}U	4.01
^{236}U	0.02
^{238}U	95.95

A.2.2 PACKAGING

The packaging consists of the inner container assembly (DWG-X12G64) comprising 316 stainless steel tubes that accommodate the fuel pellets, the inner container or containment vessel (DWG-D184K), plywood board, insulating fiber board, and the 55-gal drum (DWG-4201V).

A.2.2.1 Inner Container Assembly

Pellets and end plugs are contained in 27.75-in. (70.49-cm)-long stainless steel tubes of 0.350-in. (0.89-cm) inside and 0.366-in. (0.93-cm) outside diam. Each of the 316 tubes is filled with 80 pellets. The composition and atom densities of the 304-stainless steel tubes and other package materials are given in Table A.2. The tube ends are sealed with 0.350-in. (0.89-cm)-diam, 1.0-in. (2.54-cm)-long top and 0.75-in. (1.91-cm)-long bottom stainless steel plugs that are welded in place. The tube bottoms are welded into 0.75-in. (1.91-cm)-deep recesses on a 0.528-in. (1.34-cm)-square pitch of a 1.0-in. (2.54-cm)-thick, 12.0-in. (30.48-cm)-diam stainless steel bottom plate. The tube tops extend through 0.375-in. (0.95-cm)-diam holes to the top of a 1.0-in. (2.54-cm)-thick, 12.0-in. (30.48-cm)-diam stainless steel top plate. Rubber o-rings between the tubes and plate holes provide a tight tube-to-top-plate fit. The top plate is connected by four 26.0-in. (66.04-cm)-long, 0.667-in. (1.69-cm)-diam stainless steel support rods to the bottom plate. The structural evaluation has shown that the inner container assembly remains intact, and the pellets remain inside the tubes, under normal conditions of transport and hypothetical accident conditions.

A.2.2.2 Inner Container

The inner container is fabricated from 0.25-in. (0.635-cm)-thick carbon steel plate. The inner container [12.0-in. (30.48-cm)-inside diameter by 28.0-in. (71.12-cm) inside height] has a welded 0.25-in. (0.635-cm)-thick bottom plate with a welded 0.25-in. (0.635-cm)-thick cover plate.

Table A.2 Material specifications

Material	Density (g/cm^3)	Constituent	Atomic density (atoms/b-cm)
304 stainless steel	7.92	Fe	5.935e-2
		Cr	1.7428e-2
		Nu	7.7188e-3
		Mn	1.7363e-3
Insulating fiber board	0.24	H	8.914e-3
		C	5.348e-3
		O	4.457e-3
Plywood	0.45	H	1.671e-2
		C	1.003e-2
		O	8.357e-3
Water	0.9982	H	6.675e-2
		O	3.338e-2
Carbon steel	7.821	C	3.9250e-3
		Fe	8.3498e-2
Rubber	1.321	C	3.8414e-2
		H	5.1298e-2
		Ca	2.2627e-3
		S	4.2182e-4
		O	1.0988e-2
		Si	8.4972e-5

A.2.2.3 Drum

The transport package uses a 55-gal steel drum overpack [22.5-in. (57.15-cm) inside diameter by 40.5-in. (102.87-cm) inside height]. The drum body and bottom are fabricated from a 16-gauge [0.064-in. (0.163-cm)] low-carbon steel sheet. The drum lid (head) is fabricated from a 14-gauge [0.080-in. (0.20-cm)] low-carbon steel sheet. Two approximately equally spaced, rolling hoops are swaged into the drum body. The removable head is closed by means of a bolt-locking ring.

The 55-gal drum is filled between the drum wall and inner container with insulating fiber board that provides thermal insulation and vibration and shock isolation, and centers the inner container within the drum. The drum is loaded top-to-bottom with (1) a 5.0-in. (12.7-cm)-thick, 22.5-in. (57.15-cm)-diam insulating fiber board block, (2) a 1.0-in. (2.54-cm)-thick, 22.5-in. (57.15-cm)-diam plywood load bearing plate, (3) the inner container assembly, centered, and surrounded by a 22.5-in. (57.15-cm)-outer-diam, 12.5-in. (31.75-cm)-inner-diam, 13.75-in. (34.93-cm)-thick insulating fiber board ring, followed by a 1.0-in. (2.54-cm)-thick, 22.5-in. (57.15-cm)-outer-diam, 12.5-in. (31.75-cm)-inner-diam plywood support ring, followed by a 22.5-in. (57.15-cm)-outer-diam, 12.5-in. (31.75-cm)-inner-diam, 13.75-in. (34.93-cm)-thick insulating fiber board ring, (4) a 1.0-in. (2.54-cm)-thick, 22.5-in. (57.15-cm)-diam plywood load-bearing plate, and (5) a 5.0-in. (12.7-cm)-thick, 22.5-in. (57.15-cm)-diam insulating fiber board block.

A.3 CRITICALITY SAFETY ANALYSIS MODELS

Section A.3.1.1 provides dimensioned sketches of a modeled package. The material specifications for regions of the sketches in Sect. A.3.1.1 are given in Sect. A.3.1.2. Section A.3.1 identifies differences between the models and actual package configurations. Section A.3.2 describes the contents models representing each of the different loading configurations. Models depicting the configuration of packaging and contents of a single package under normal and accident conditions are discussed in Sect. A.3.3. Section A.3.4 contains a discussion on the package array models.

A.3.1 GENERAL MODEL

A.3.1.1 Dimensions

Figure A.1 represents the vertical elevations of the package seen along the vertical centerline of the package. A cross section of the package along A-A of Fig. A.1 is displayed in Fig. A.2. The figures' dimensions were used in the calculations.

Note: Although not included in this example, a real application should not *a priori* use nominal dimensions, but instead should address dimensional tolerances of the package that tend to add conservatism to the models.

A.3.1.2 Materials

Figures A 1 and A.2 show cross sections of the single-package calculational model. Table A.3 identifies the regions, materials, material densities, and masses as used in the calculations, and the actual masses.

Note: Although not included in this example, a real application should not *a priori* use nominal material specifications, but instead should address maximum and minimum fissile, neutron-absorbing, moderating, and structural materials parameter values that produce conservative k_{eff} results within the allowable tolerances

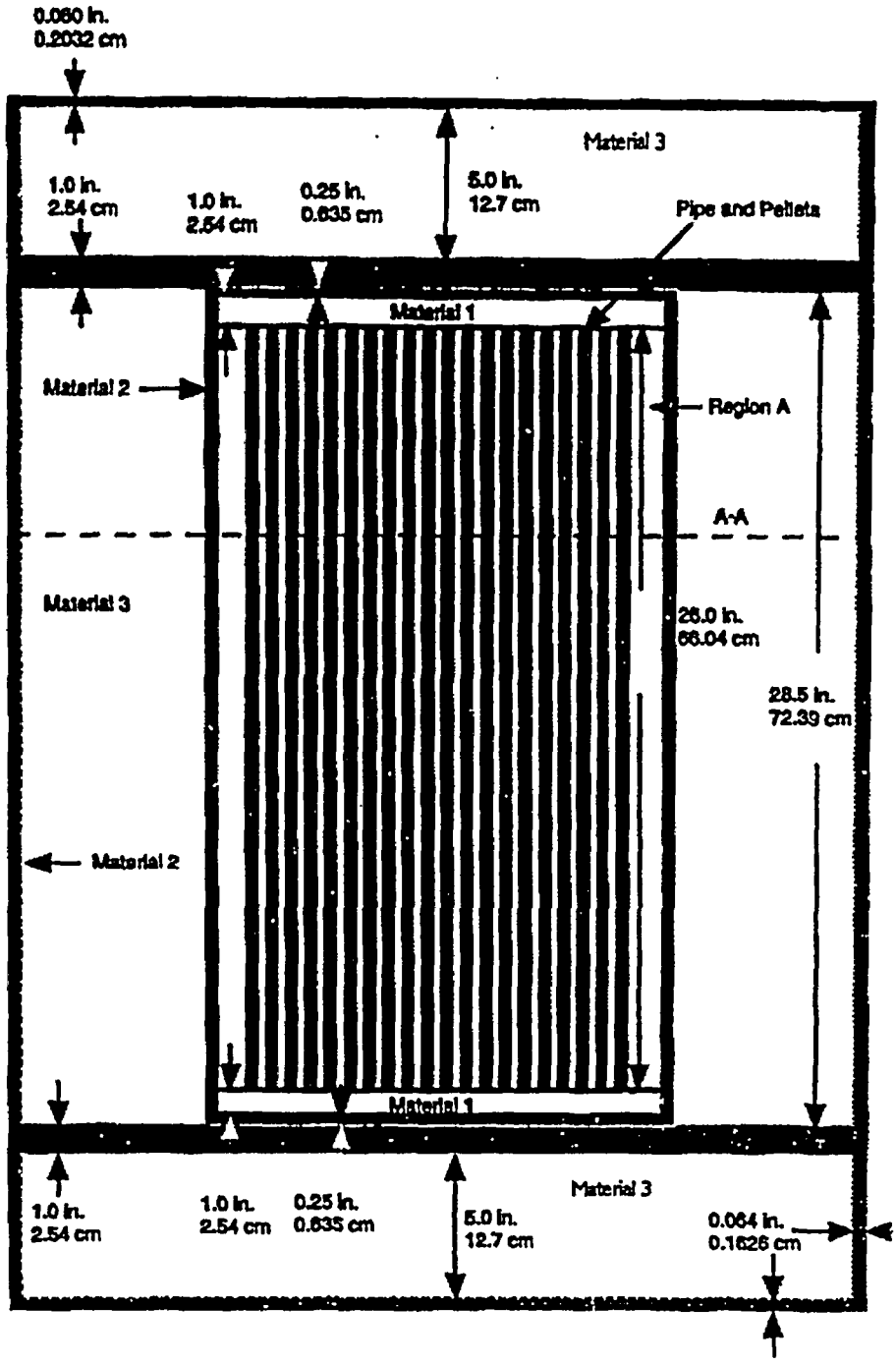

Figure A.1 Axial cross section of the single-package model

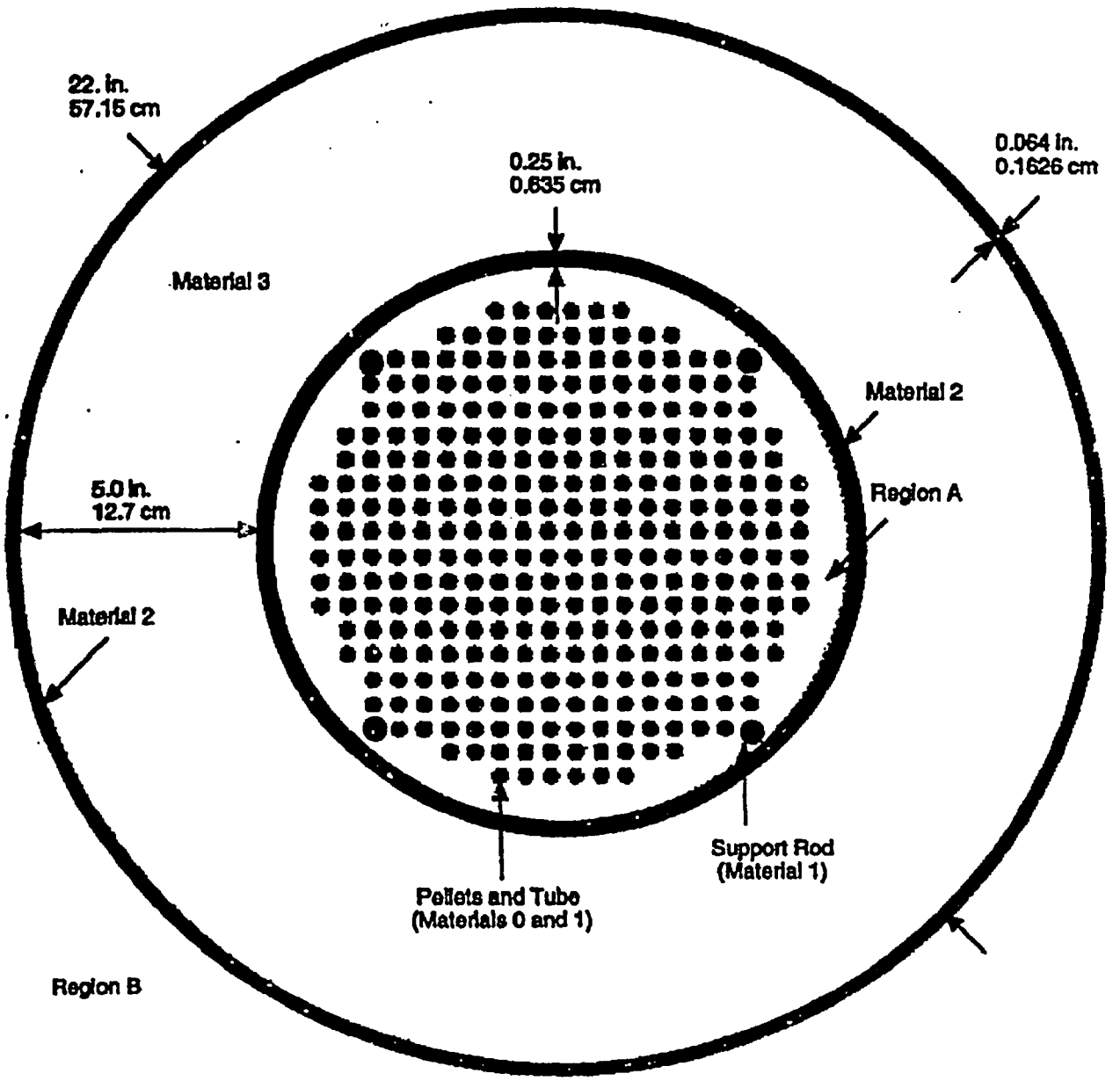

Figure A.2 Radial cross section of single-package model

Table A.3 Material specifications for Figs. A.1 and A.2

Material No.	Material	Density (g/cm³)	Model mass (kg)	Actual mass (kg)
0	UO_2	10.40	116.19	116.16
1	SS-304	7.92[a]	41.87	42.12
2	Carbon steel	7.8212[a]	73.37	77.23
3	Insulating fiber board	0.24	46.42	44.29
4	Plywood	0.45	5.860	8.796

[a]SCALE Standard Composition Library values.

A.3.1.3 Models—Actual Package Differences

The single-package calculational model of the 55-gal drum differs from the actual drum in the treatment of the drum wall. In the model, the drum wall is a straight wall cylinder without the rolling hoops. The drum model does not have the top and bottom inset into the drum wall, bolts, locking rings, etc.

The rubber o-ring fittings around the tubes in the top plate of the inner container assembly were treated as stainless steel, the surrounding material. The change constitutes such a small change in stainless steel mass in the positive axial direction relative to the fuel region that the impact on k_{eff} would be negligible. To simplify the modeling, the center plywood support ring was modeled as insulating fiber board, the surrounding material. The exchange of materials would have a negligible effect on k_{eff} because the constituents of the two materials are identical and the thickness of the region is small relative to the radial surface of the containment vessel (i.e., ~4% of the surface available for radial neutron leakage).

A.3.2 CONTENTS MODEL

Figure A.2 shows the package contents (pellets in tubes) configured for both the single-package and package-array calculations. Each tube is physically restricted to a maximum loading of 80 pellets. Partial-loading (variable-mass) configurations are allowed, as are variations in pellet enrichment (up to 4.01 wt % ^{235}U). However, partial loadings must be from the inner tubes outward with only the last loaded tube containing less than 80 pellets (see Chapter 1). Because of this restriction and the fixed tube spacing, partial loadings do not require further analysis because they are bounded by the more reactive configuration of full loading. Chapter 2 of the application for approval has shown that the tube spacing remains at 1.34 cm (0.528 in.), and that the pellets remain inside the tubes, under normal conditions of transport and hypothetical accident conditions.

A.3.3 SINGLE PACKAGES

To meet the general requirements for fissile material packages, 10 CFR § 71.55, a package must be designed and its contents so limited that it would be subcritical under the most reactive configuration of the material, optimum moderation, and close reflection of the containment system by water on all sides or surrounding materials of the packaging. Models of both reflective conditions have been considered. The package was subjected to the tests specified in 10 CFR § 71.71. Normal Conditions of Transport, and, as reported in

Chapters 2 and 3, the geometric form of the package was not substantially altered, no water leakage into the containment occurred, and no substantial reduction in the effectiveness of the packaging was observed. In short, the damage incurred will not affect the technical evaluation, and the package contents under normal conditions of transport will be less reactive than the contents under the aforementioned general requirements, requiring no further analysis.

To address the requirement of 10 CFR § 71.55(e), a single package was analyzed with optimum internal moderation and a 30-cm water reflector on all sides. The damaged package experienced a 4.7% reduction in diameter due to impact testing (see Chapter 2, Structural Evaluation). The packaging diameter reduction is to be analyzed as a reduction in insulating fiber board and plywood thicknesses while conserving the carbon steel drum, insulating fiber board, and plywood masses. Limited material loss occurred as a result of fire testing (see Chapter 3, Thermal Evaluation). The outer 0.8 in. (2.03 cm) of insulating fiber board (axially and radially) and plywood (radially) exhibited charring and off-gassing during the fire test. The regions were modeled as residual carbon and water (immersion test). The water from the immersion test optimally moderates the inner containment. The minimal damage resulting from crush and puncture tests (see Chapter 2, Structural Evaluation) will not influence the reactivity of the packages.

A.3.4 PACKAGE ARRAYS

Cylindrical transport packages such as this example package may be shipped in a tightly packed triangular-pitch configuration (or may be shifted to that configuration because of hypothetical accident conditions). This arrangement may provide a more reactive configuration than a square-pitch arrangement because the triangular pitch provides absolute minimum center-to-center spacing of the fissile contents, the maximum density of fissile units, and thus the greatest potential for increased neutron interaction between fissile contents. To avoid the complex modeling required to analyze triangular-pitch arrays with the computational method used in this application, a square-pitch array model with a modified single-package model was developed to emulate the effects of a triangular-pitch package array. The single-package modification involved a reduction of the drum diameter by 7% to produce an array density in a square-pitch lattice equal to the array density of a triangular-pitch lattice of packages with the full-diameter package. If the mass of steel of the drum and the mass of the insulating fiber board are conserved, the neutron reaction rates within the array are essentially identical. To conserve the mass of steel in this example, the drum wall density was increased; and to conserve the mass of the insulating fiber board in this example, the insulating fiber board density was increased. The diameter reduction was applied only to regions of the "array package model," not the "contents model."

The justification for the 7% diameter reduction is seen in the following derivation. Consider three full-diameter packages in contact on triangular pitch and four reduced-diameter packages in contact on square pitch. The equivalent array density of each configuration is

$$\rho_t = \frac{3(m/6)}{\left(\frac{1}{2}\right)(d_t)\left(\frac{\sqrt{3}}{2}\right) \times (d_t)(h)} = \frac{m}{(d_t^2)(\sqrt{3}/2)\,(h)},$$

and

$$\rho_s = \frac{4(m/4)}{(d_s^2)(h)} = \frac{m}{(d_s^2)(h)}.$$

where

the subscripts *t* and *s* indicate triangular and square pitch, respectively,
d is the package diameter,
h is the package height (same for both packages), and
m is the fissile material mass (same for both packages).

If ρ_t is set equal to ρ_s and d_s is calculated in terms of d_t, the diameter of a square pitch is 0.9306 that of the triangular pitch, to produce the equivalent array density. If a constant mass of materials is maintained outside the fissile unit (i.e., the thermal insulation and steel outer drum), the neutron reaction rates between fissile units remain constant. Because the drum is smaller in diameter, the mass of thermal insulation is conserved by increasing the density, and the mass of steel in the outer drum is conserved by increasing the steel density.

Two array model types are included in the evaluation. The first model type consists of an infinite array of close-packed, triangular-pitch, undamaged packages consistent with the normal conditions of transport. From 10 CFR § 71.59, standards for arrays of fissile material packages, undamaged package arrays are evaluated with void between the packages. The second model type consists of various size finite arrays of close-packed triangular-pitch, damaged packages. As required by 10 CFR § 71.59, the damaged packages are evaluated as if each package was subjected to the tests specified in 10 CFR § 71.73, Hypothetical Accident Conditions. with optimum interspersed hydrogenous moderation. Further, the finite array of packages must be reflected by 30 cm of water on all sides.

Various finite array sizes had to be investigated in order to ascertain the number of subcritical packages under hypothetical accident conditions The condition of each damaged package in the array is that described in Sect. A.3.3 for the single package.

A.4 METHOD OF ANALYSIS

Sections A.4.1 and A.4.2 describe the sequences and modules of the SCALE-4.3 system used in the analysis of these computational models. Section A.4.3 identifies all major code input parameters. Section A.4.4 discusses the adequacy of the calculations.

All calculations were performed on CA02 and CA29, IBM RS/6000 workstations in the Computational Physics and Engineering Division at ORNL with SCALE version 4.3 (1/6/97 production date) and the 44-group ENDF/B-V cross-section library.

A.4.1 COMPUTER CODE SYSTEM

SCALE is a computational system consisting of a set of well-established codes and data libraries suitable for analyses of nuclear fuel facility and package designs in the areas of criticality safety, radiation shielding, source-term characterization, and heat transfer. The codes are compiled in a modular fashion and are called by control modules that provide automated sequences for standard system analyses in each area. The CSAS control module contains automated sequences that perform problem-dependent cross-section processing and three-dimensional (3-D) Monte Carlo calculations of neutron multiplication.

KENO V.a, a 3-D multigroup Monte Carlo criticality code, determines the effective multiplication factor (k_{eff}) from the problem-dependent cross-section data and the user-specified geometry data. Other calculated

KENO V.a quantities include average neutron lifetime and generation time, energy-dependent leakages, energy- and region-dependent absorptions, fissions, fluxes, and fission densities.

A.4.2 CROSS SECTIONS AND CROSS-SECTION PROCESSING

All neutronic control sequences use the SCALE Material Information Processor to calculate material number densities, prepare geometry data for resonance self-shielding and optional flux-weighting cell calculations, and create data input files for the cross-section processing codes. The BONAMI and NITAWL-II codes are then used to perform problem-specific (resonance- and temperature-corrected) cross-section processing. BONAMI applies the Bondarenko method of resonance self-shielding for nuclides that have Bondarenko data included in the cross-section library. NITAWL-II uses the Nordheim integral treatment to perform resonance self-shielding corrections for nuclides that have resonance parameters included with their cross-section data.

The analyses discussed in this evaluation were performed using the broad-structure, 44-group neutron cross-section library. The 44-group library was chosen because the evaluated package contents have many similarities (e.g., form, enrichment) to light-water-reactor (LWR) fuel, and the 44-group library has demonstrated markedly improved performance in LWR-type fuel analyses over the ENDF/B-IV 27-group library. The reason: the 44-group neutron cross-section library was collapsed from the 238-group AMPX master-format neutron cross-section library contains data for all the nuclides available in ENDF/B-V, and the 44-group library was collapsed using a fuel cell spectrum based on a 17 × 17 Westinghouse pressurized-water-reactor (PWR) fuel assembly.

Additionally, the broad-group structure was designed to accommodate two windows in the oxygen cross-section spectrum, a window in the iron cross-section spectrum, the Maxwellian peak in the thermal range, and the 0.3-eV resonance in ^{239}Pu (which, because of low energy and lack of resonance data, cannot be modeled by the Nordheim integral treatment in NITAWL-II).

A.4.3 CODE INPUT

All problems were started with a flat initial neutron distribution over the system, in fissile material only. All problems were run for 305 generations of 400 neutrons per generation, skipping the first five generations, for a total of 120,000 histories. Mirror image reflection was applied to the orthogonal-plane boundaries of the single-package model to simulate infinite array-package models. A 12-in. (30.48-cm) water differential albedo with four incident angles was applied to the outer boundary of the single-package models and finite-array models to simulate tight, full-density water reflection. Biasing options were not applied.

Figures A.3(a) and A.3(b) are sample input files. The files correspond to cases f-2_4 and f-2_4a, a 4 × 4 × 1 array of optimally moderated, damaged packages in square, with diameter correction factor of Sect. A.3.4, and triangular-pitch arrays.

A.4.4 CONVERGENCE OF CALCULATIONS

UO_2 mass data for each problem were checked against KENO V.a output. The input geometries were checked by examining the 2-D plots generated by KENO V.a. Problem convergence was determined by examining plots of k_{eff} by generation run and skipped, as well as the final k_{eff} edit tables. No trends were observed either in k_{eff} by generation run over the last half of total generations or, correspondingly, in k_{eff} by generation skipped over the first half of total generations. No sudden changes of greater than one standard deviation in k_{eff} by

```
=csas25
KENO-V.a, 4x4x1 array, optimally moderated damaged
'packages, square pitch, 4.7% and 7% diameter reduction
44g      latt
uo2 1 0.9489 293 92235 4.01 92234 0.02 92236 0.02 92238
                95.95 end
h2o   2 1.0       end
ss304 3 1.0       end
c  4 0 3.9250e-3 end
fe 4 0 8.3498e-2 end
h  5 0 1.029e-2  end
c  5 0 7.727e-3  end
o  5 0 6.464e-3  end
h  6 0 2.128e-2  end
c  6 0 1.277e-2  end
o  6 0 1.064e-2  end
c  7 0 4.550e-3  end
fe 7 0 9.679e-2  end
h  8 0 1.135e-2  end
c  8 0 6.809e-3  end
o  8 0 5.674e-3  end
c  9 0 7.757e-3  end
h2o   9 0.001     end
c 10 0 6.809e-3  end
h2o  10 0.001     end
h2o  12 1.0       end
end comp
squarepitch 1.34 0.8255 1 2 0.9296 3 0.889  12 end
read parm run=yes plt=no gen=305 npg=400 nsk=5 end parm
read geom
unit 1
cylinder 1 1 0.4128  2p33.02
cylinder 2 1 0.4445  2p33.02
cylinder 3 1 0.4648  2p33.02
cuboid   2 1 4p0.670 2p33.02
unit 2
cylinder 3 1 0.667   2p33.02
cuboid   2 1 4p     0 2p33.02
unit 3
array 2 -4.02 0 -33.02
unit 4
array 3 -6.7  0 -33.02
unit 5
array 4 0 -4.02 -33.02
unit 6
array 5 0 -6.7  -33.02
unit 7
array 1 -10.72  -10.72   -33.02
cylinder 2 1 15.24   2p33.02
hole 6 10.72   0  0
hole 6 -12.06  0  0
hole 5 12.06   0  0
hole 5 -13.41  0  0
hole 4 0 10.72    0
hole 4 0 -12.06   0
hole 3 0 12.06    0
hole 3 0 -13.41   0
reflector 3  1 0 2r2.54   1
reflector 4  1 3r0.635    1
reflector 5  1 7.4165 2r0 1
reflector 9  1 2.032  2r0 1
reflector 6  1 0 2r2.54   1
reflector 8  1 0 2r10.668 1
reflector 10 1 0 2r2.032  1
reflector 7 1 0.1626 0.2032 0.1626 1
cuboid    0 1 4p25.4862 51.6383 -51.5977
global unit 8
array 6 3*0.0
end geom
read array
ara=1 nux=16 nuy=16 nuz=1 fill 2 14r1 2 224r1 2 14r1 2
end fill
ara=2 nux=6  nuy=1  nuz=1 fill 6r1  end fill
ara=3 nux=10 nuy=1  nuz=1 fill 10r1 end fill
ara=4 nux=1  nuy=6  nuz=1 fill 6r1  end fill
ara=5 nux=1  nuy=10 nuz=1 fill 10r1 end fill
ara=6 nux=4  nuy=4  nuz=1 fill 16r7 end fill
end array
read bnds all=h2o end bnds
end data
end
```

Figure A.3a Sample input file f-2_4

```
=csas26
KENO-VI, 4x4x1 array, optimally moderated damaged
'packages, triangular pitch, 4.7% diam. reduction
44g      latt
uo2 1 0.9489 293 92235 4.01 92234 0.02 92236 0.02 92238
95.95 end
h2o 2 1.0 end
ss304 3 1.0 end
c  4 0 3.9250e-3 end
fe 4 0 8.3498e-2 end
h  5 0 1.029e-2  end
c  5 0 6.173e-3  end
o  5 0 5.144e-3  end
h  6 0 1.841e-2  end
c  6 0 1.105e-2  end
o  6 0 9.207e-3  end
c  7 0 4.167e-3  end
fe 7 0 8.864e-2  end
h  8 0 9.821e-3  end
c  8 0 5.892e-3  end
o  8 0 4.910e-3  end
c  9 0 6.173e-3  end
h2o 9  0.001     end
c 10 0 5.892e-3  end
h2o 10 0.001     end
h2o 11 1.0       end
end comp
squarepitch 1.34 0.8255 1 2 0.9296 3 0.889  11 end
read parm run=yes plt=no gen=305 npg=400 nsk=5 end parm
read geom
unit 1
cylinder 10 0.4128  2p33.02
cylinder 20 0.4445  2p33.02
cylinder 30 0.4648  2p33.02
cuboid   40 4p0.670 2p33.02
media 1 1 10
media 2 1 20 -10
media 3 1 30 -20 -10
media 2 1 40 -30 -20 -10
boundary 40
unit 2
cylinder 10 0.667   2p33.02
cuboid   20 4p0.670 2p33.02
media 3 1 10
media 2 1 20 -10
boundary 20
unit 3
cuboid   10 4p0.670 2p33.02
media 2 1 10
boundary 10
unit 4
cylinder 10 15.24 2p33.02
array 1 10 place 12 12 1 -0.67 -0.67 0
cylinder 20  15.24   2p35.56
cylinder 30  15.875  2p36.195
cylinder 40  25.1922 2p36.195
cylinder 50  27.2242 2p36.195
cylinder 60  27.2242 2p38.735
cylinder 70  27.2242 2p49.403
cylinder 80  27.2242 2p51.435
cylinder 90  27.3868 51.6382 -51.5976
hexprism 100 27.3869 51.6383 -51.5977
media 3  1 20  -10
media 4  1 30  -20
media 5  1 40  -30
media 9  1 50  -40
media 6  1 60  -50
media 8  1 70  -60
media 10 1 80  -70
media 7  1 90  -80
media 0  1 100 -90
boundary 100
unit 5
hexprism 10 27.3869 51.6383 -51.5977
media 2 1 10
boundary 10
global unit 6
cylinder 10 189.74  51.6383 -51.5977
array 2 10 place 5 5 1 -27.3869 -27.3869 0
cylinder 20 225. 2p82.
media 2 1 20 -10
boundary 20
end geom
read array
ara=1 nux=24 nuy=24 nuz=1 fill 48r3 9r3 6r1 9r3 7r3 10r1
7r3 4r3 2 14r1 2 4r3 4r3 16r1 4r3 1q24 3r3 10r1 3r3 1q24
2r3 20r1 2r3 5q24 3r3 10r1 3r3 1q24 4r3 16r1 4r3 1q24 4r3
2 14r1 2 4r3 7r3 10r1 7r3 9r3 6r1 9r3 48r3 end fill
ara=2 typ=cyl nux=10 nuy=10 nuz=1 fill 30r5 4r5 3r4 4r5
3r5 4r4 3r5 3r5 4r4 3r5 2r5 4r4 4r5 30r5 end fill
end array
end data
end
```

Figure A.3b Sample input file f-2_4a

generation run or skipped, resulting from an abnormal k_{eff} generation, were found. Frequency distribution bar graphs appear to approximate normal distribution with single peaks and no significant outlying values.

A.5 VALIDATION OF CALCULATION METHOD

For the purpose of this example, a negative value of 0.01 will be assumed for the bias and uncertainty ($\Delta k_u - \beta$) associated with using SCALE-4.3 and the 44-group cross-section library. This is consistent with published information on validation of this computational method using low-enriched lattice criticals.[10,12] Note: The applicant should demonstrate the justification for the bias and uncertainty in the application for approval.

Using the general equation for the USL from Sect. 5.4 and the requirements of 10 CFR 71, it can be found that for the calculations to be considered subcritical, the following condition should be satisfied:

$$k_{eff} + 2\sigma \leq 0.95 - \Delta k_u + \bar{\beta} ,$$
$$k_{eff} + 2\sigma \leq 0.94 .$$

A.6 CRITICALITY CALCULATIONS AND RESULTS

This evaluation demonstrates the subcriticality of a single package (Sect. A.6.1) and an array of packages (Sect. A.6.2) during normal conditions of transport and hypothetical accident conditions. The determined TI for criticality control of a damaged and undamaged shipment is given in Sect. A.6.3.

A.6.1 SINGLE PACKAGE

Calculations show that a single package remains subcritical under general requirements for fissile material packages under normal conditions of transport and under hypothetical accident conditions. To meet the general requirements for fissile material packages, 10 CFR § 71.55, a package must be designed and its contents so limited that it would be subcritical under the most reactive configuration of the material, optimum moderation, and close reflection of the containment system by water on all sides or surrounding materials of the packaging. Case s-0 of Table A.4 represents the optimally moderated inner containment reflected on all sides by 30 cm of water. For case s-1, the container reflection is provided by the surrounding materials of the packaging and 30 cm of water. In both cases, the gap region between the tubes and pellets are completely flooded with full-density water, as is the void region in the inner container (Region A of Fig. A.2). Full-density water is optimum in both regions because the fissile content of the package is slightly undermoderated at a tube pitch of 1.34 cm (see Fig. A.4). The highest single-package k_{eff} of 0.8942 ± 0.0019 is considered subcritical (i.e., $0.8942 + 2 \cdot 0.0019 = 0.8980 < 0.94$).

Case s-2 in Table A.4 is the result for a single damaged package with internal water flooding and 30 cm of water reflection on all sides. As with the undamaged cases, the reported k_{eff} is less than the established USL of 0.94. The results for a reflected, damaged containment system would have been identical to the undamaged case (case s-0) because the configurations of the containment system or contents did not change under hypothetical accident conditions.

All calculations (damaged and undamaged) were performed at the maximum allowable ^{235}U enrichment (4.0 wt %) to ensure maximum reactivity and eliminate the need for calculations at lower possible enrichments.

Table A.4 Single-package calculations

Case	Description	$k_{eff} \pm \sigma$
s-0	Optimally moderated, reflected undamaged containment	0.8942 ± 0.0019
s-1	Optimally moderated, reflected undamaged package	0.8798 ± 0.0019
s-2	Optimally moderated, reflected damaged package	0.8820 ± 0.0018

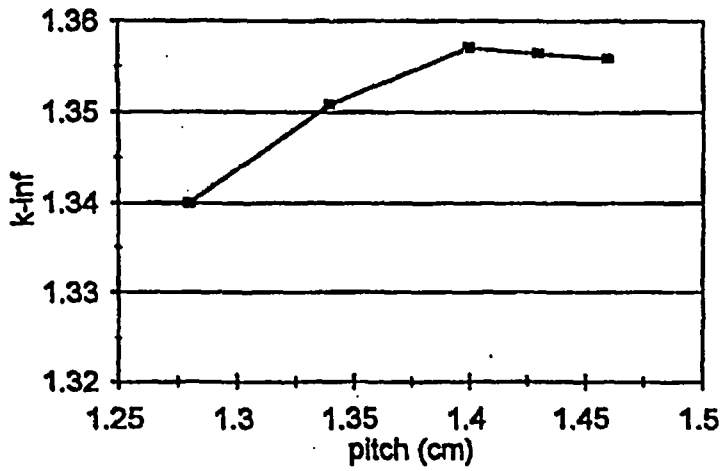

Figure A.4 k_∞ vs pitch for 4.01 wt % ^{235}U UO_2 pellets

A.6.2 PACKAGE ARRAYS

The calculational results of Table A.5 show that an infinite array of packages is adequately subcritical under normal conditions of transport. Case i-1, an infinite, triangular-pitch array of dry packages under normal conditions, calculates at a k_{eff} of 0.5343 ± 0.0012. An infinite array of packages under hypothetical accident conditions, however, is not subcritical. Case i-2_7 represents an infinite array of close-packed, triangular-pitch (diameter reduction factor), flooded packages with optimum moderated contents, a 4.7% reduction in diameter, effects due to charring and off-gassing, and optimum interspersed moderation. The k_{eff} for case i-2_7 is 0.9755 ± 0.0021, which exceeds the subcritical limit (i.e., 0.9755 + 2·0.0021 = 0.9797 > 0.94). Since the infinite array under hypothetical accident conditions calculates above the USL, finite array calculations are necessary.

Cases i-3_1 through i-3_3 are variants of i-2_7 that investigate flooding of the insulating fiber board charred region. The optimally moderated package array i-3_2 has full-density water inside the package containment, has 0.001 g H_2O/cm^3 in the charred region of the packaging, and has void between packages.

Table A.5 Results for triangular-pitch array calculations

Case	Interspersed H_2O density (g/cm^3)	Description	$k_{eff} \pm \sigma$
i-1	0	Infinite array, normal conditions of transport	0.5343 ± 0.0012
f-1	-	1×1×1 array, hypothetical accident conditions	0.8820 ± 0.0018
i-2_1	0.9982	Infinite, hypothetical accident conditions	0.9238 ± 0.0021
i-2_2	0.95	Infinite, hypothetical accident conditions	0.9237 ± 0.0021
i-2_3	0.5	Infinite, hypothetical accident conditions	0.9297 ± 0.0023
i-2_4	0.1	Infinite, hypothetical accident conditions	0.9618 ± 0.0025
i-2_5	0.01	Infinite, hypothetical accident conditions	0.9716 ± 0.0024
i-2_6	0.001	Infinite, hypothetical accident conditions	0.9718 ± 0.0024
i-2_7	0[a]	Infinite, hypothetical accident conditions	0.9755 ± 0.0021
i-3_1	0	Infinite, hypothetical accident conditions, 0 g H_2O/cm^3 charred region	0.9755 ± 0.0021
i-3_2	0	Infinite, hypothetical accident conditions, 0.01[b] H_2O/cm^3 charred region	0.9772 ± 0.0027
i-3_3	0	Infinite, hypothetical accident conditions, 0.01 g H_2O/cm^3 charred region	0.9759 ± 0.0022
f-2_1	0	2×2×1 array, hypothetical accident conditions	0.9103 ± 0.0018
f-2_2	0	2×2×2 array, hypothetical accident conditions	0.9158 ± 0.0018
f-2_3	0	3×3×1 array, hypothetical accident conditions	0.9270 ± 0.0017
f-2_4	0	4×4×1 array, hypothetical accident conditions	0.9369 ± 0.0019
f-2_4a	0	4×4×1 array, hypothetical accident conditions	0.9335 ± 0.0028[c]
f-2_5	0	3×3×2 array, hypothetical accident conditions	0.9306 ± 0.0017
f-2_6	0	5×5×1 array, hypothetical accident conditions	0.9284 ± 0.0019
f-2_7	0	3×3×3 array, hypothetical accident conditions	0.9405 ± 0.0023
f-2_8	0	4×4×2 array, hypothetical accident conditions	0.9359 ± 0.0017

[a]Determined to be near optimum interstitial moderation via CSAS4 search.
[b]Determined to be new optimum moderation via CSAS4 search
[c]KENO-VI calculation.

Cases f-2_1 through f-2_8 are variants of case i-3_2 and represent finite arrays of close-packed, triangular-pitch packages (diameter reduction factor) that have optimally moderated contents, a reduced diameter by 4.7%, charred insulating fiber board, varying interstitial moderation, and 30 cm of full-density water reflection tightly fit on the array boundary. The finite array of 4 × 4 × 2 (case f-2_8) packages is considered just subcritical because 0.9359 + 2·0.0017 = 0.9393 falls below the USL of 0.94.

Case f-2_4a is equivalent to case f-2_4a except that f-2_4a was modeled with KENO-VI, which allows explicit modeling of triangular-pitch arrays and does not require the use of the drum diameter reduction factor of Sect. A.3.4. The calculational results of f-2_4 and f-2_4a are statistically the same, attesting to the correctness of the diameter reduction factor.

A.6.3 TRANSPORTATION INDEX

The TI for criticality control is determined by the number of packages that remain below the USL. For normal conditions of transport, an infinite array of packages is subcritical. However, under hypothetical accident conditions, only up to 32 damaged packages would remain subcritical. Thus a maximum of 16 packages may be shipped for a nonexclusive shipment, and the TI = 3.

Note: The example presented in this appendix is for illustrative purposes only. The fictitious transport package used in this example has not been approved by the NRC, and no assessment has been made as to whether the package would meet the requirements for NRC approval. Also, the descriptions, calculations, and justifications presented in this example have not been fully reviewed by the NRC, and may not be complete or acceptable to the NRC.

THE MAGAZINE OF TITANIUM • • • BORAL

Magnesium

Published Quarterly By BROOKS & PERKINS, INC. August 1956

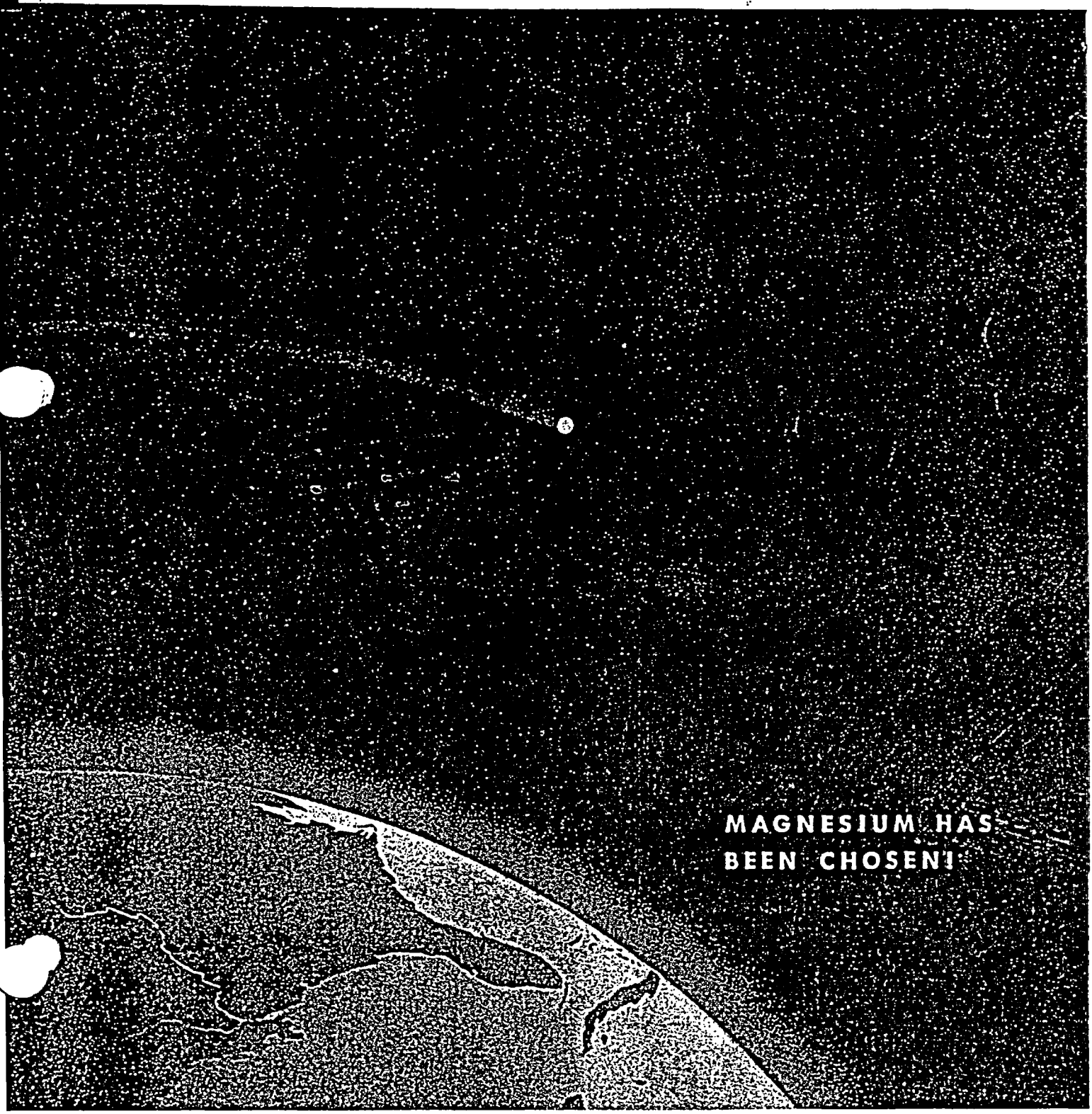

B&P becomes the first industry producer of BORAL

Brooks & Perkins has just become the first commercial supplier of Boral. This is a new material. It is used as a neutron shield in atomic energy installations and atomic power plants.

Boral is said to offer as much neutron shielding protection as 26 inches of concrete where the neutrons are of thermal energies. It does not shield against the passing of gamma rays.

The Atomic Energy Commission developed Boral at their Oak Ridge Plant, where it has been produced by the Government in limited amounts only. The product consists of a core of boron carbide uniformly dispersed in aluminum, clad on both sides with commercially pure aluminum. Boral can be produced with the core material having various concentrations of boron carbide.

Now that atomic power plants are operating in submarines and in an experimental airplane, and several industrial power plants are in the development stage, it has become advisable to have a commercial supplier of Boral. B&P is highly qualified, primarily because of its successful pioneering of methods for working some of the newer metals, including zirconium; also the fact that it operates a rolling mill at nearby Livonia. Here B&P has just installed a new 3000 cycle ultra high frequency induction furnace, now used for the production of the Boral core material.

The grade of Boral offered by B&P has a 35% concentration of boron carbide. The Boral plate is rolled 1/8" and 1/4" thick. Standard sizes offered are 30" x 96", 30" x 48", 15" x 96", and 15" x 48". The approximate weight per square foot of 1/4" thick 35% Boral plate is 3.4 pounds.

Boral and zirconium are, in a sense, companion products. Both are used in atomic applications. B&P has been deep-drawing zirconium for the past two years. Unlike Boral, zirconium is transparent to the passage of neutrons while acting as the container of the atomic fuel.

Microphoto of cross section of 1/4" thick Boral plate, 10 X magnification. Shows crystalline structure of boron carbide in center, with aluminum cladding on top and bottom.

Rolling mill superintendent J. G. Merritt is looking at a formed Boral cylinder. The three-inch-thick rolling slab, ready for break-down, is a cast Boral core surrounded by pure aluminum cladding.

U. S. DEPARTMENT OF COMMERCE
Office of Technical Services

distributes this and thousands of similar reports in the interest of science, industry, and the public—for which research and new products mean better health, better living, and a stronger economy.

A GOVERNMENT RESEARCH REPORT

HOW TO GET OTHER REPORTS

The Office of Technical Services is the Nation's clearinghouse for reports of research supported by the Army, Navy, Air Force, Atomic Energy Commission, and other Government agencies.

Abstracts of new reports available are published semimonthly in U. S. GOVERNMENT RESEARCH REPORTS ($15 a year domestic).

Selected Reports of particular interest to small business are described monthly in TECHNICAL REPORTS NEWSLETTER ($1 a year domestic).

Translations of foreign technical material are also available from the Office of Technical Services and other sources. These are listed or abstracted semimonthly in TECHNICAL TRANSLATIONS ($12 a year domestic).

The above periodicals may be ordered from Superintendent of Documents, U. S. Government Printing Office, Washington 25, D. C., or through a U. S. Department of Commerce Field Office.

Inquiries about the availability of reports and translations on any particular subject may be directed to Office of Technical Services, U. S. Department of Commerce, Washington 25, D. C., or to any Commerce field office.

Microfilm.—Any reports available from the Office of Technical Services will be provided in microfilm (35 mm) on request. The following prices are charged for microfilm: 1 through 20 pages, 80 cents minimum; and three cents per page for every page in excess of 20 pages.

UNITED STATES ATOMIC ENERGY COMMISSION

AECD-3625

BORAL: A NEW THERMAL NEUTRON SHIELD

By
V. L. McKinney
Theodore Rockwell, III

SUPPLEMENT I

By
A. S. Kitzes
W. Q. Hullings

May 1954
[TIS Issuance Date]

Technical Division and Reactor Experimental
Engineering Division
Oak Ridge National Laboratory
Oak Ridge, Tennessee

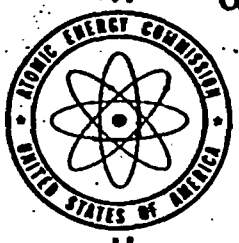

Technical Information Service, Oak Ridge, Tennessee

Subject Category, PHYSICS

Operated by Carbide and Carbon Chemicals Company for the U. S. Atomic Energy Commission under Contract No. W-7405-eng-26.

BORAL: A NEW THERMAL NEUTRON SHIELD, was issued as ORNL-242 in 1949, and was declassified June 16, 1953.

SUPPLEMENT I, was issued as ORNL-981 on July 3, 1951, and was declassified December 4, 1952. (AECD-3476).

This combined report replaces both of the above reports and is complete without omission.

Printed in USA. [redacted] Available from the Office of Technical Services, Department of Commerce, Washington 25, D. C.

BORAL: A NEW THERMAL NEUTRON SHIELD

By

V. L. McKinney and Theodore Rockwell, III

May 1954
[TIS Issuance Date]

1.0 Abstract

A technique has been developed for making large sheets or castings of B_4C and aluminum complex for absorption of thermal neutrons without production of hard gamma radiation. The $\frac{1}{4}$" sheet has the following properties:

Boron Content: 50% B_4C (or 40% B) by volume
0.91 g B/cm3 or 0.58 g B/cm^2 of $\frac{1}{4}$" sheet.

Thermal Neutron Attenuation of 10^{10} in $\frac{1}{4}$" (based on $\Sigma^B_{rth} = 100$ cm^{-1}).

Density: 2.53 g/cm3 or $2\frac{1}{2}$ #/ft^2

Cost: 15-20 \$/ft^2

Tensile Strength: 5500 psi (10 times concrete, 1/10 mild steel, about equal best plastics).

Thermal Conductivity: Somewhat better than steel (more precise measurements in progress).

Can be sheared, sawed, welded, punched, drilled, tapped, rolled, and hot-pressed. Sheets 7' by 33' by $\frac{1}{4}$" are in preparation for shearing to 5' x 6' test sheets.

It is felt that this material will have many uses where a large thermal neutron flux must be absorbed without production of hard gammas, e.g. inner section of reactor shields, shutters for thermal columns, instrumentation.

2.0 Introduction

The absorption of thermal neutrons without production of hard gamma radiation can be a very important function. For example, if the radiation impinging upon a shield is such that the thermal neutrons outnumber the quanta of hard gammas by a factor of 100, and these thermal neutrons are absorbed in the shield to produce hard gammas (the usual result), then the incident gamma flux which must be shielded has been effectively increased by this factor, i.e., an additional 26" of concrete (or equivalent) must be added to the shield. If instead, these incident thermal neutrons were absorbed without hard gamma production (e.g. in a thin film of boron), the 26" of hypothetical concrete could be removed. E. Creutz of Carnegie Institute of Technology estimates that a comparable thickness of concrete added to the CIT cyclotron shield would have cost over $20,000 in materials and floor space. In a stationary reactor shield it might cost ten times this amount. It might tip the balance of feasibility in a mobile reactor shield.

The $B^{10}(n,\alpha)Li^{7}$ reaction is uniquely suited for such a function. Natural boron, containing 18.8% B^{10}, has a cross-section of 703 barns for this reaction at thermal energy, falling off as 1/v to about 0.1 barn at 1 MeV where the function becomes irregular. The residual activity is negligible and the 0.42 MeV gamma, which is emitted after 93% of the captures, is soft enough to be easily absorbed. Cadmium, by contrast, emits a 6 MeV gamma and leaves four unstable isotopes after irradiation.

Boron can be bought in many forms: Nearly pure crystalline boron at $200 - 300 per pound, amorphous boron at $15 per pound, and B_4C in various grades and prices starting near $7 per pound. The crystalline B is quite pure, the amorphous B 60-80%, the B_4C 75-80% B. B_4C is not only the cheapest form of highly concentrated boron, it is also exceedingly refractory, chemically inert, mechanically hard, and atomically dense; in each of these properties it exceeds almost all other known materials. For $8 to 10 per pound, it can be obtained quite pure.

Being difficult to work, it seems desirable to bind the B_4C with a more docile material for handling. Aluminum appears to be the most promising cementing agent: it has a low cross-section for the production of hard capture gammas, it is ductile and easily fabricated, has high thermal conductivity, is inexpensive, light weight, and corrosion resistant.

The question of radiation damage naturally arise. Since aluminum is the continuous phase, it should not suffer from destruction of the embedded B_4C particles. Radiation damage studies on aluminum show that, with the possible exception of warpage, no deleterious effects should be expected. The diffusion of helium (from the n,α reaction) through the aluminum is expected to take place without damage. Irradiation tests will be made.

3.0 Early Experiments

The objective was to achieve as high a fraction as possible of B_4C. In addition it was felt that no B_4C should be exposed at the surface and no loose B_4C should exist within the sheet. In this way

it was hoped to minimize the possibility of escape of B_4C from the sheet due to blistering during operation or machining during fabrication. Arbitrarily a 1:1 ratio by volume of B_4C to aluminum was chosen. For a $\frac{1}{4}$" sheet, this is sufficient to give a 10^{10} attenuation of thermal neutrons, assuming a macroscopic cross-section for boron of 100 cm^{-1}, or for boral, 40 cm^{-1}. Actually a 1:1 weight ratio was used for the unclad material, giving a volume ration of 2.7 B_4C : 2.45 Al, but this is compensated for by the cladding on both sides which occupies a total of 16% of the thickness. It was found that a significantly larger fraction of B_4C could not be obtained without seriously impairing the mechanical and thermal properties of the material. In the rare cases where greater quantities of boron are needed, a thicker sheet can more easily be used.

Experimental work was started in December 1948 under Frank Kerze of the Engineering Materials Section and was shortly thereafter moved to the new Y-12 facilities of the Shielding Group.

3.1 Foil and Powder Method (See Figure 1)

B_4C powder was sprinkled in thin layers between ten .005" aluminum foils, around which was a wrapper of .064" 2S aluminum sheet. This was hot-rolled at 1130°F, reducing the laminated assembly .050" each pass through the rolls until the laminate had been reduced to $\frac{1}{4}$". The results of this experiment were unsatisfactory because only a small amount of the B_4C embedded itself in the aluminum foil, leaving most of the powder loose between the laminations. The loose B_4C prevented the bonding of the layers of foil and a considerable amount of powder blew out during rolling, preventing bonding of the outside wrapper. Figure 1 shows a sheared section of the finished sheet. Note that the laminations are not bonded to each other.

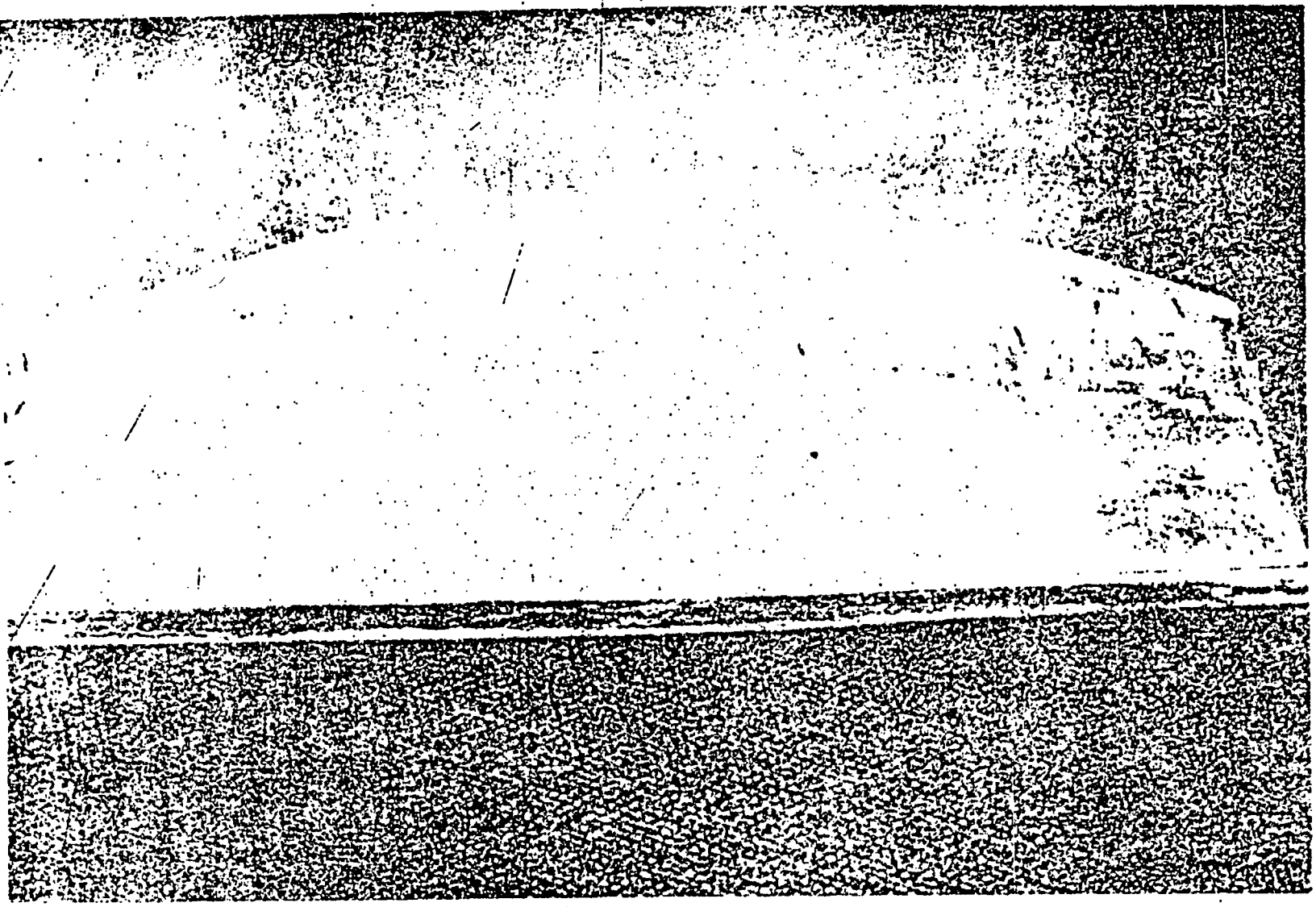

Fig. 1—Al foil and B_4C powder, hot rolled.

3.2 Two-Powder Method (See Figures 2 and 3)

A mixture of B_4C and Al powder was placed in an envelope of Al foil (to prevent dusting during rolling) and this mixture was fitted carefully into an aluminum "picture frame". The frame was covered top and bottom with a single 1/8" wrapper sheet, and the assembly was then soaked at 1130°F for one hour. It was rolled at this temperature, being heated 10 minutes between passes, and reduced to $\frac{1}{4}$".

The first attempts (see Figure 2) were fairly satisfactory, but several serious difficulties arose. The picture frame generally bonded to the wrapper on the first pass, trapping air in the powder mix inside. To minimize this, the envelope containing the powder was pressed within the picture frame on a 100 psi Studebaker pneumatic press, before heating and rolling. In spite of this, a large blister was formed and a vent hole had to be drilled through the wrapper. When the finished sheet was examined, it was found that the wrapper was not bonded to the inner material and there was considerable loose B_4C apparent. In an attempt to improve upon this, several sheets were made, varying the aluminum particle size from approximately 20 mesh to $\frac{1}{4}$" chips, and the B_4C from 100 mesh to 18 mesh. These gave no significant improvement.

A larger sheet was tried by this method, starting with a $9\frac{1}{2}$" x $9\frac{1}{2}$" x 1" (inside dimensions) picture frame (see Figure 3). In addition to the above difficulties, the wrapper became quite soft at the soaking temperature, and handling the large assembly proved quite difficult. It was decided at that time that large satisfactory

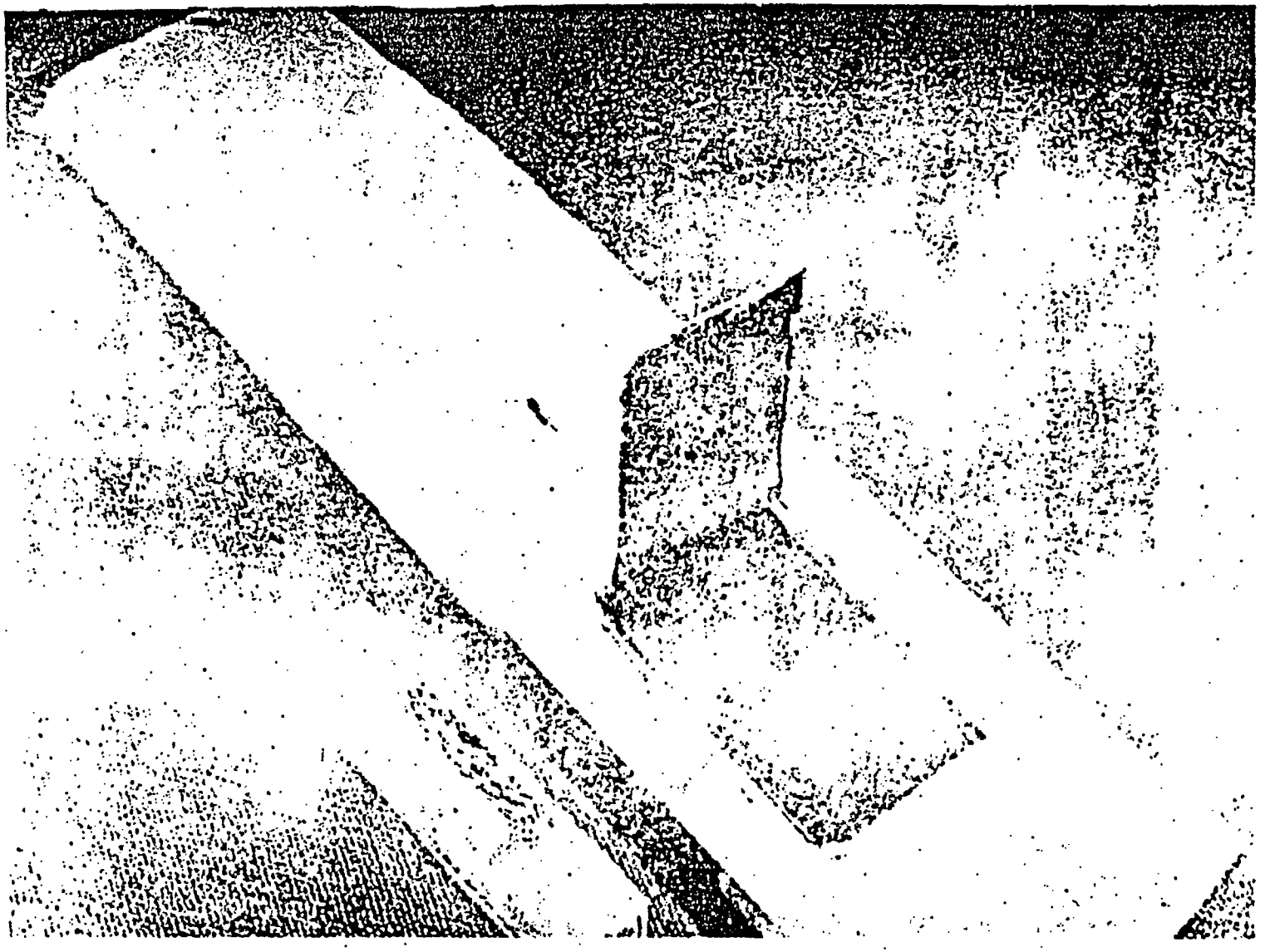

Fig. 2—Al and B_4C powders in picture frame.

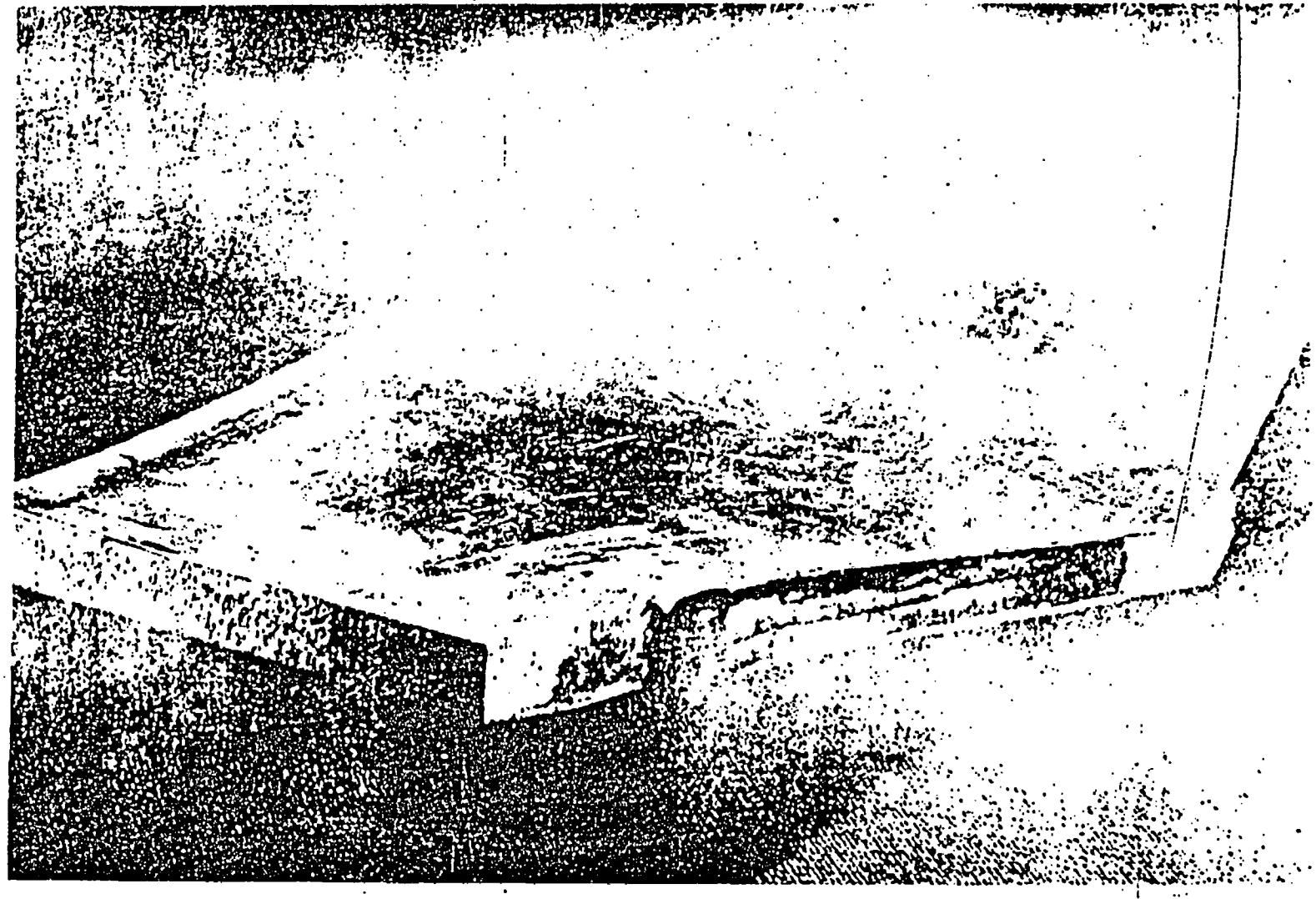

Fig. 3—Large two-powder attempt.

sheets could not be rolled unless the B_4C and aluminum were in the form of a rigid structure during rolling.

3.3 Cast Ingot Method (Figure 4)

Several small-scale attempts were made to mix B_4C powder with molten aluminum. The aluminum did not wet the B_4C and the resultant mix when cooled was crumbly and incohesive. Preheating the B_4C, precipitating B_2O_3 or Al_2O_3 on the B_4C surface, and varying the temperature range, had little effect. Attempts to make an ingot from B_4C and aluminum powder were equally unsuccessful. A non-oxidizing atmosphere seemed to make little difference.

Finally a successful ingot was made as follows: (Figure 4) Half of the aluminum, as powder, and all of the B_4C, were mixed cold and added slowly with stirring to the remaining aluminum which was molten. The temperature, which seemed critical, was kept at 1230°F ± 20. The resultant ingot was somewhat porous (density 2.25 g/cc), but very strong and homogeneous. The porosity was nearly eliminated during rolling, resulting in a sheet with a density of 2.53 g/cc. This method was refined and was the basis of the present fabrication technique.

4.0 Present Fabrication Technique (Figures 5 and 6)

The capacity of the rolling mill at ORNL limits the sheet width to 27" and the billet thickness (including wrapper) to 1½". Therefore it has been decided to roll a billet 1¼" x 7" x 12", with an 1/8" wrapper on each side, which produces a trimmed sheet 20" x 20" x $\frac{1}{4}$". Since the B_4C powder alone stacks to nearly 50% voids, the boral ingot holds B_4C particles which are nearly touching, resulting in a very rigid mass which cannot be poured, even at high temperature. Therefore

Fig. 4—Sections of first ingot and shunt

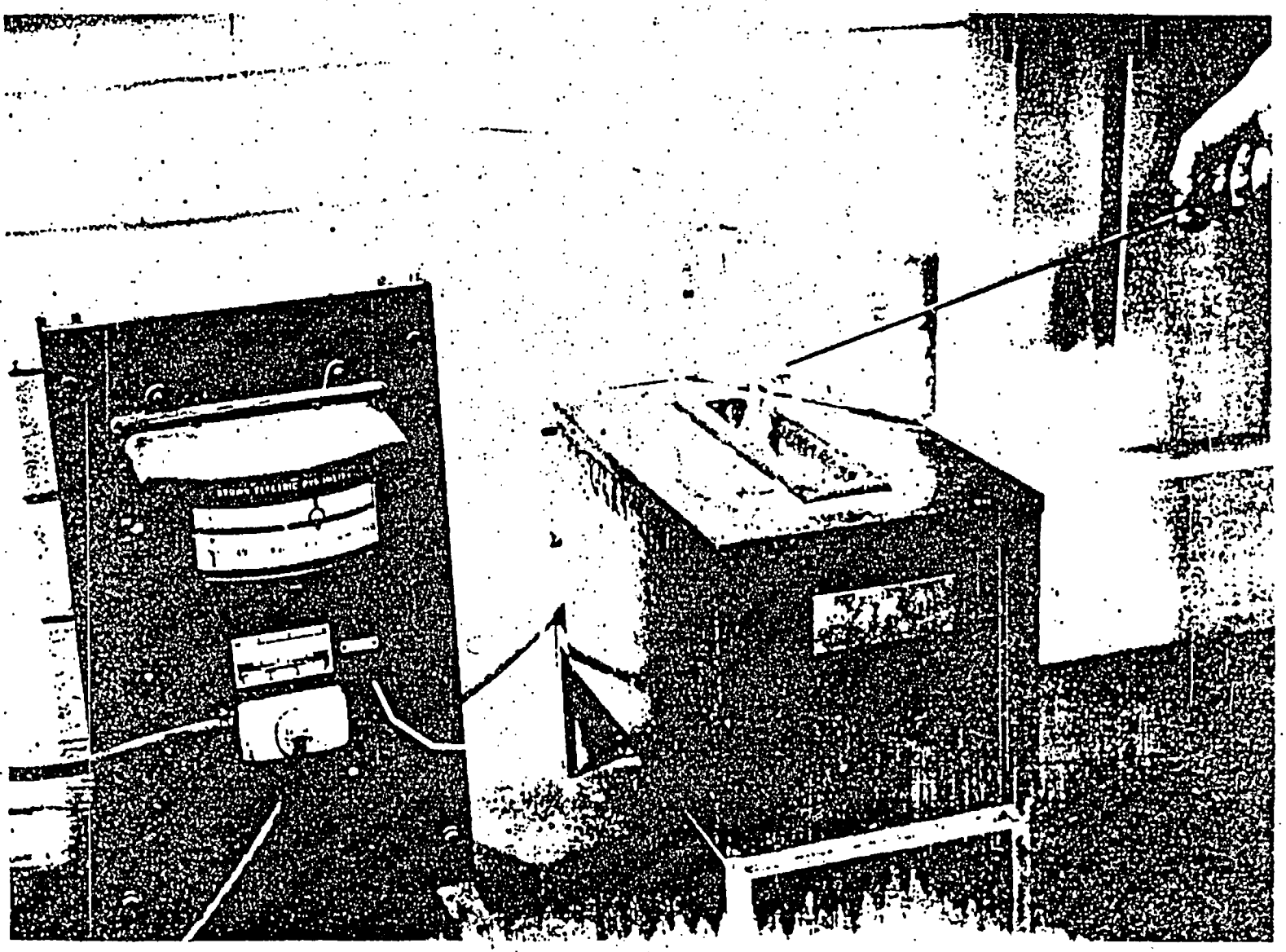

Fig. 5—Casting boral ingot.

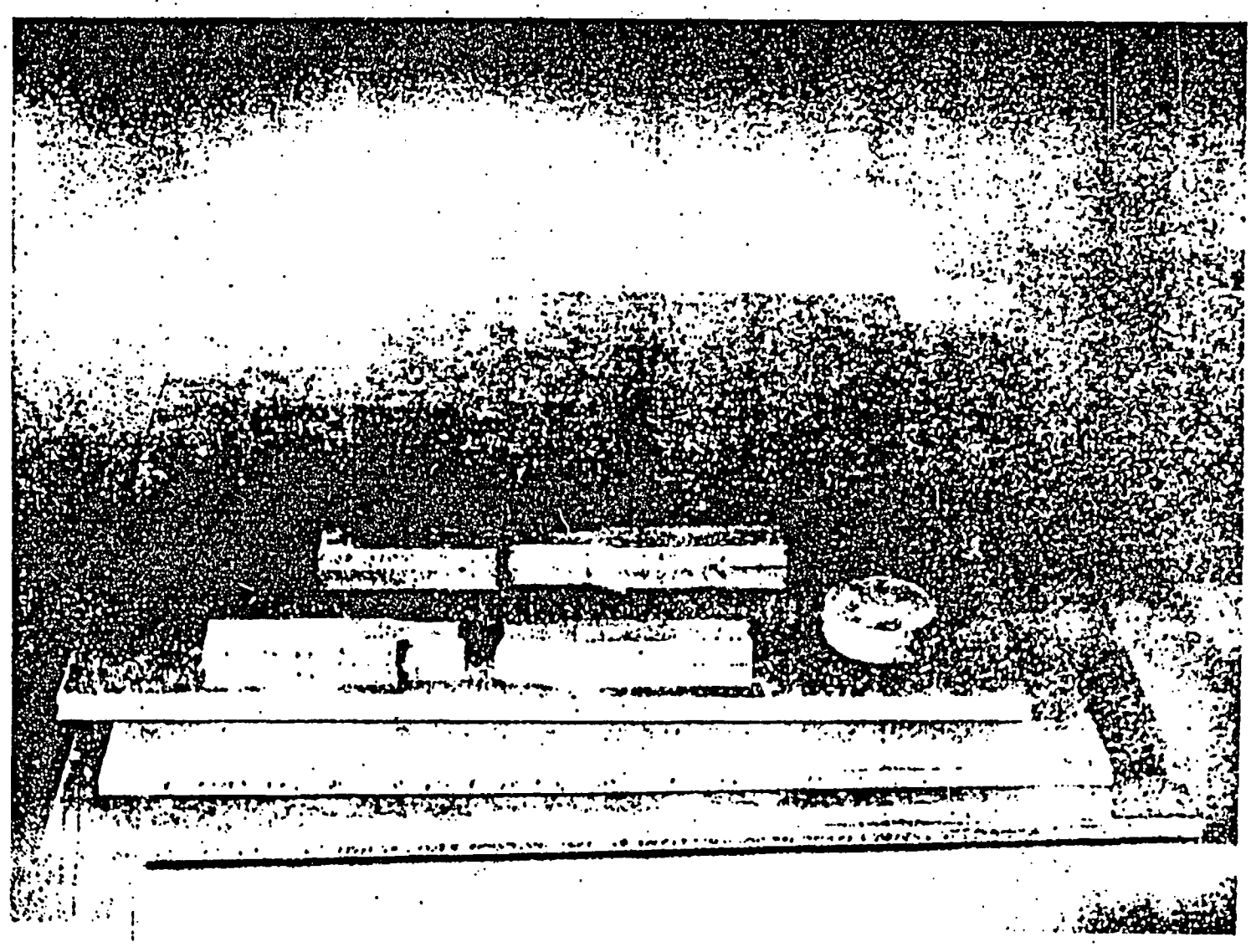

Fig. 6—Finished boral sheets and pieces

it is desirable that the rolling billet be the original casting, and not recast from a larger pig. For this purpose, a special furnace has been built from two standard 6" x 12" muffle furnace elements, which heats a graphite crucible with inside dimensions 7" x 12" x 1¼" with 1/16" taper. The temperature is controlled by a Brown electric pyrometer from a thermocouple set in the graphite, and the mixed powders are stirred into the molten aluminum with a 3/8" steel rod, as shown in Figure 5. A typical ingot is shown on the furnace. To produce an ingot this size requires 825 grams of 2S aluminum pig. To this a cold mixture of 1650 grams B_4C (through 20 on 100 mesh) and 825 grams of aluminum powder (approximately 20 mesh), is added gradually while stirring in order to wet and suspend the B_4C particles in the molten aluminum.

After removing the ingot from the crucible mold, it is then metal-sprayed with a thin coat of aluminum to cover completely any exposed particles of B_4C. A wrapper of 1/8" 2S aluminum sheet, which has been wire-brushed to remove excess oxide and dirt to facilitate bonding, is placed around the ingot to form a cladding of approximately .020" on the 1/4" finished sheet. The assembly is then placed in a Lindberg forced-circulation electric furnace and heated to 1130°F for approximately one hour and rolled. The billet is reduced approximately 10% each pass through the rolls. The material retains considerable ductility at low temperatures and work-heats appreciably during rolling, so that reheating between passes is not necessary if the rolling is carried out at a reasonable pace.

The first heats were run with only the ingot and a wrapper sheet. Since there was nothing to confine the edges of the ingot during rolling, excessive crumbling, edge-cracking, and unevenness resulted. Present runs employ a welded aluminum picture frame to confine the ingot, and this technique yields straight edges, free from cracks. The edges of the wrapper sheet are bent over and tack-welded to the outside of the picture frame, which has several vent holes drilled through it.

5.0 The 250 ft^2 Sheets (Figures 7 and 8)

As indicated above, the maximum width which could be rolled at ORNL was 27". There is a need for several 40" x 43" shutters for the ORNL attenuation facility and several 56" x 66" sheets for experimental work. Arrangements have been made with the Lukens Steel Company of Coatesville, Pennsylvania, to roll two sheets 84" x 396" x $\frac{1}{4}$", from which ten 56" x 66" sheets and four 40" x 33" shutters can be cut. Two ingots, 6" x 36" x 32", weighing 450 pounds each, will be cast and wrapped at Y-12, then shipped to Lukens for rolling. The expenses for this job are being partly borne by NEPA, and the sheets will be used for the joint ORNL-NEPA shield tests in the ORNL attenuation facility.

The method of wrapping is essentially that described in paragraph 4.0 and is shown in detail in Figure 7. The special furnace for casting the ingots (Figure 8) is scaled up from that shown in Figure 5, except that a non-tapered steel crucible is being used. A separate report, ORNL-243, covering this project, will be written as soon as the sheets are rolled.

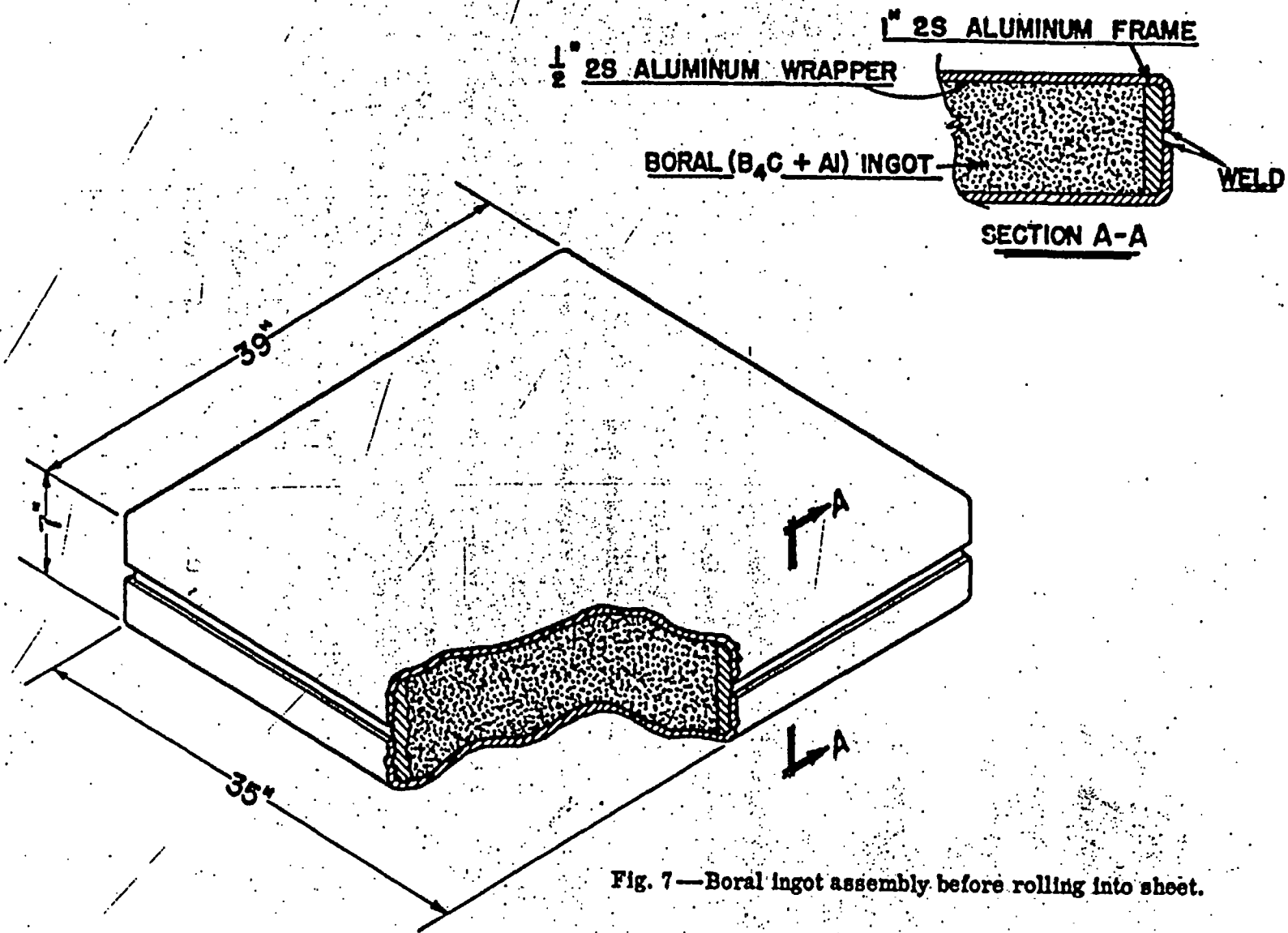

Fig. 7—Boral ingot assembly before rolling into sheet.

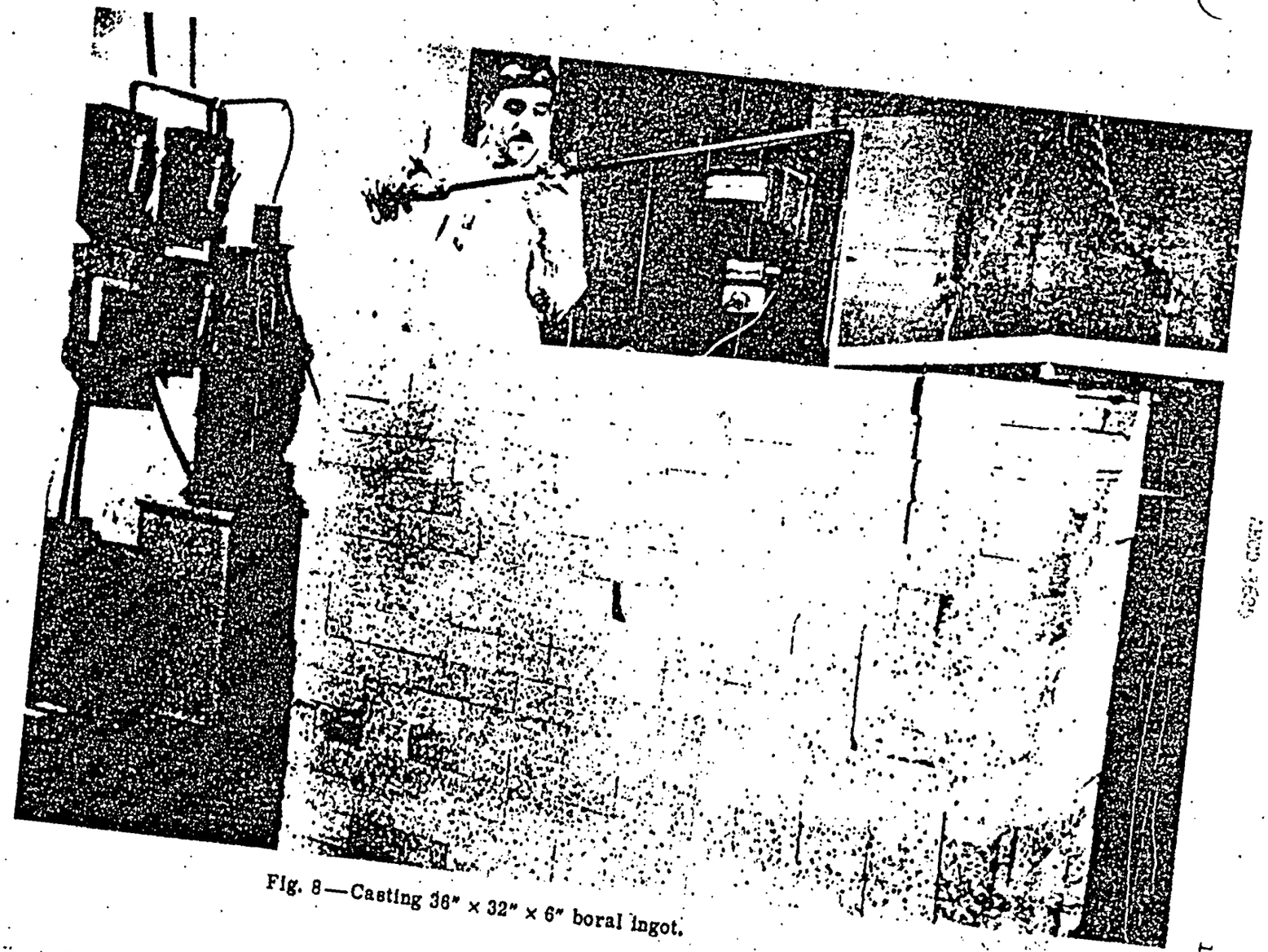

Fig. 8—Casting 36" × 32" × 6" boral ingot.

6.0 Physical Properties

6.1 Data

1. Composition (for ¼" sheet, including .020" Al cladding on each side).
   50% (vol.) B_4C, 50% Al.

	% (wt)	mg-mol/cm3	g/cm3	g/cm2
B	36.0	84.2	0.911	0.578*
Al	55.1	51.7	1.394	0.886
C	8.9	18.7	.225	0.143

* This is sufficient to give 10^{10} attenuation of thermal neutrons

2. Density: 2.53 g/cc
   0.09 lb/in3
   3¼ lb/ft2 for ¼" sheet

3. Strength

   a) Tensile 5,500 psi
   b) Elongation 0.4 %
   c) Shear 8,237 psi
   d) Welded tensile specimens did not fail at weld

4. Thermal Properties

   a) Conductivity: somewhat better than steel (more precise measurements in progress).

   b) Specific Heat: 0.175 Btu/lb x °F or g-cal/g x °C

   c) Melting Point: Maintains mechanical strength up to 1500°F (800°C), above which oxidation is excessive.

   d) Heat Generation from n,α Reaction: 7.4×10^{-10} watts/ft2 x unit thermal neutron flux.

5. Cost: 15-20 $/ft2 for ¼" sheet.

6. Workability: Can be sheared, sawed, welded, punched, drilled, tapped, rolled, hot-formed, and experimentally die-cast.

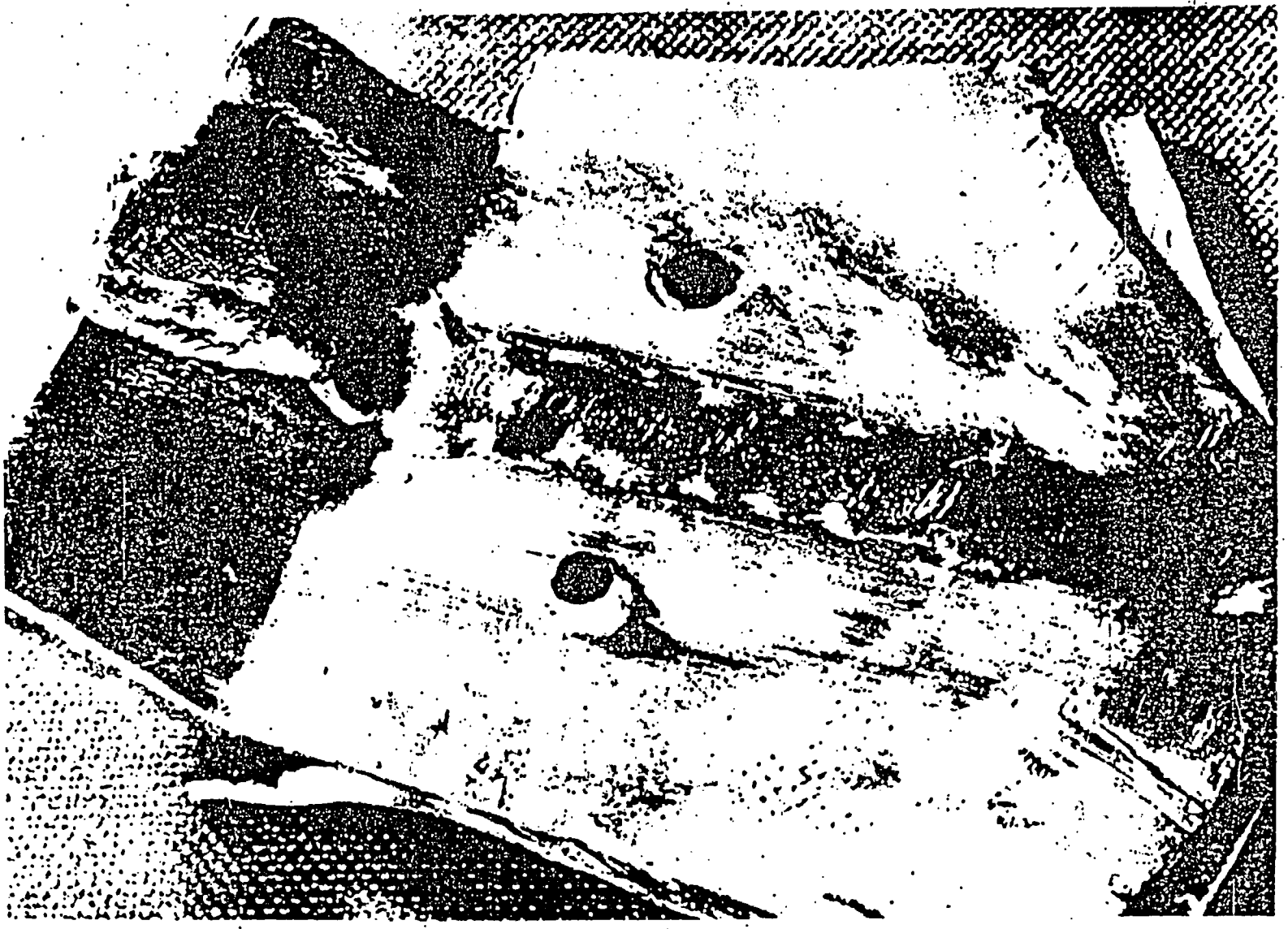

Fig. 9—Boral sawed, welded, punched, and drilled.

6.2 Testing and Calculation Methods

1. Composition

   Calculations are based on 1:1 (vol) B_4C : Al composition. Densities assumed are 2.45 and 2.70 g/cc respectively.

2. Density is based on gross volume measurement and also water displacement, with no significant difference.

3. Tensile strength on 8 normal and 3 welded specimens, as per ASTM (e.g. B209-46T, 1946 ed, Part IB, p 572, fig. 1).

   Shear strength on three $\frac{1}{4}$" x 2" x 8" strips, in modified Johnson Shear Tool (ASTM C102-36, 1946 ed, Part II, p 228, fig. 1)

4. Thermal Conductivity was made by comparing temperature drops through Al rod, Al discs, and boral discs, through which a constant heat flux flows axially (see Figure 9). Comparison of the Al rod and discs gives an approximation of the temperature drop through the brazed interfaces of discs, and this correction, applied to the boral discs, gives the drop through boral compared to drop through Al for same heat flux. Precision was poor and precise tests are being made on new equipment.

   Heat Generation = 5 Mevα/n capture x 929 nv $\frac{\text{captures}}{\text{ft}^2 \times \text{sec}}$ x 1.6×10^{-13} $\frac{\text{watts}}{\text{MeV}}$

5. Cost: \$12/ft^2 for B_4C, \$0.40 for Al, \$1 for rolling.

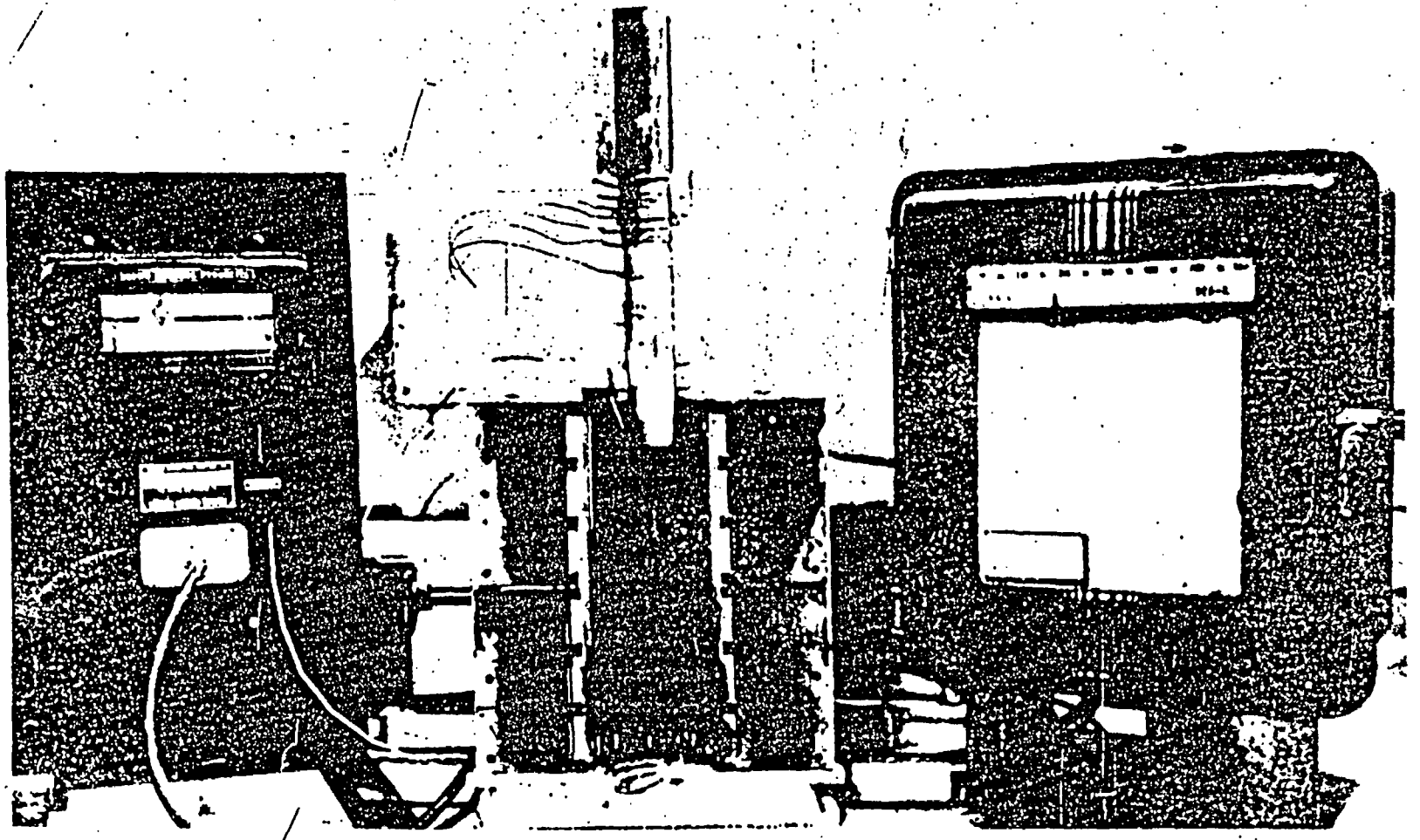

Fig. 10—Sectional view of thermal conductivity apparatus.

7.0 Analyses of Raw Materials for Boral

	Al Powder	Large Al Pig	Small Al Pig	Boral
Ag	<.04%	T	--	T
Al	>.10	VS	VS	VS
B	<.015	--	--	VS
Be	<.004	--	--	--
Ca	<.08	--	--	--
Cd	<.15	--	--	--
Co	<.08	--	--	--
Cr	<.15	--	--	T
Cu	.08	W	W	S*
Fe	.15	W	W	M*
In	<.08	--	--	--
Mg	.04	M	W	S*
Mn	.04	T	T	W
Mo	<.15	T	--	--
Ni	<.08	--	--	T
Pb	.08	--	--	--
Pt	.08	--	--	--
Si	.20	W	T	W
Sn	<.08	--	--	--
Ti	<.04	--	--	--
V	<.08	--	--	--
Zn	<.31	--	--	--
Zr	<.15	--	--	--

*Chemical analyses being made

Symbols for spectrographic analyses: VS very strong
S strong
M medium
W weak
T trace
-- not detected

Analyses were made for all elements listed

Wrapper sheet and spray-metal being analyzed

SUPPLEMENT I

By

A. S. Kitzes and W. Q. Rullings

ABSTRACT

The technique for making large sheets of boral described in ORNL-242, which consists of mixing B_4C with aluminum has been modified and simplified. Recommendations are given for casting and rolling ingots into sheets.

Additional physical property data are included. Tensile strength measurements of boral indicate no serious damage upon irradiation with a total of 2.6×10^{19} nvt in the ORNL reactor. Thermal conductivity for the 50-50 mixture was found to be 25.0 Btu/hr-ft^2-°F/ft at 200 °F and 19.0 Btu/hr-ft^2-°F/ft at 500 °F.

A method for measuring thermal conductivities is described.

In order to make boral available to other sites, ORNL has agreed to accept urgent requests for small amounts of boral as sheets not larger than 24" x 96" x 1/4" or 1/8", other program commitments permitting. Requests or purchase orders for sheet stock or simple fabrication parts may be submitted directly to ORNL, giving detailed requirements.

INTRODUCTION

Boral, as described in ORNL-242, is an engineering material for the absorption of thermal neutrons.

Boral is a mixture of boron carbide (B_4C) and aluminum in which the boron carbide is suspended in molten aluminum and the resultant product allowed to solidify into a form suitable for rolling. It is useful because of its light weight, its high boron content for the absorption of thermal neutrons without production of hard gammas, its good heat conductivity and its thermal stability up to the melting point of aluminum.

In ORNL-242, "Boral: A New Thermal Neutron Shield", McKinney and Rockwell adequately discuss the history, development, and fabrication of boral and establish a procedure for producing large quantities of this material. However, they were unable to conclude their program for the production of large sheets of boral. This report summarizes the work done in concluding the program initiated by McKinney and Rockwell. Additional physical property data and information relative to the availability and fabrication of large quantities of boral are included.

In ORNL-242, McKinney and Rockwell reported that small scale attempts to mix B_4C powder with molten aluminum were unsuccessful. The aluminum did not

wet the B_4C and the resultant mix when cooled was crumbly and incohesive. Preheating the B_4C, coating the B_4C with B_2O_3 or Al_2O_3 and varying the temperature had little effect. A successful ingot was finally made by stirring a mixture of aluminum powder and B_4C into molten aluminum, keeping the temperature at 1230 $^{o}F \pm 20^{o}$. This method was therefore established as the standard procedure for casting ingots.

EXPERIMENTAL DEVELOPMENT PROGRAM

Additions to make Aluminum wet B_4C

In the McKinney-Rockwell procedure, it is difficult to understand and interpret the action of the aluminum powder in causing the molten aluminum to wet the B_4C. In an effort to understand the mechanisms involved, a series of experiments was performed in which varying percentages of Al_2O_3 were substituted for part of the aluminum powder and added to the molten aluminum with the B_4C. The results were negative; the B_4C floated on top of the molten metal.

In a second series of tests, varying percentages of B_2O_3 were mixed with the B_4C and added to the molten aluminum, omitting the use of aluminum powder. Good workable mixes were obtained resulting in strong homogeneous ingots. The B_2O_3 content varied from 5-50% of the weight of the B_4C. During the addition of the B_2O_3-B_4C mixture to the molten metal, a black smoke was given off and green flames popped on the surface of the melt. This same reaction was observed in the McKinney-Rockwell process.

Since the addition of B_2O_3 caused the aluminum to wet the B_4C, a B_2O_3 coating was placed on the carbide by oxidizing it for one hour in a muffle furnace. The oxidized carbide was then added to the molten aluminum. Good workable mixes and perfect ingots were obtained. No black smoke or green flames were evident. This method is now the basis of the present fabrication technique.

The mechanism of how the B_2O_3 influences the wetting of B_4C by the aluminum is still not known. The B_2O_3 probably acts as a fluxing agent and as such helps to minimize the absorption of gases and the oxidation of the aluminum. Since inert atmospheres above the melts made no difference, their use was discontinued. Although either the oxidized carbide or B_2O_3 and carbide can be added freely to the molten aluminum, the oxidized carbide is preferred.

Effect of Temperature During Mixing of B_4C into Aluminum

The temperature at which the oxidized B_4C was added to the molten aluminum was not critical as long as it was below that at which the oxidation of aluminum became severe. No apparent difficulty was observed when oxidized B_4C was added to molten aluminum at 1400°-1450°F; however, the temperature was usually kept at 1300°-1350°F and the B_4C was added at a rate which did not reduce the temperature of the molten aluminum by more than 25°-35°F. Adding big slugs of carbide to the melt caused the mix to cool as much as 400°F and resulted in a loss of time required to reheat the mixture. When the required temperature was again reached, more B_4C was added, and only occasionally when the mix was cooled too much through the addition of larger doses of carbide it was impossible to remelt the mixture without excessive oxidation of the aluminum.

TECHNIQUE FOR CASTING INGOTS

The capacity of the ORNL rolling mill limited the sheet width to 24" and the billet thickness to 1 1/2" including covers. For this reason it was decided to roll ingots, 1" x 20" x 24" with 1/4" cover plates on each side, which produced a trimmed sheet, 24" x 108" x 1/4". A 150 KW Ohio Crankshaft Company "Tocco" tilting type induction furnace was used to heat a graphite crucible 9" in diameter with 1" wall thickness. The temperature was controlled by a Micromax electric pyrometer from a thermocouple set in the graphite. The pre-oxidized B_4C (oxidized at 1000 °F for one hour) was stirred into the molten aluminum by hand with stainless steel paddles, and the mix was then allowed to stand for 10-15 minutes in order to attain a uniform temperature.

While the carbide was stirred into the molten aluminum, a graphite mold, 20" x 24" x 1" was heated electrically to between 800°-900°F. One continuous pour was then made into the heated mold; the residual mix in the crucible was incorporated into the next pour.

During cooling, the ingot shrunk sufficiently for easy removal from the mold. It was then prepared for rolling according to the procedure outlined in ORNL-242 except that the operation of metal spraying with aluminum was eliminated.

To produce an ingot, 20" x 24" x 1" containing 35% B_4C by weight, 13.5 lbs B_4C and 24.5 lbs 2S aluminum pig were required. The B_4C content was decreased from 50%, the percentage used by McKinney and Rockwell, to 35% to facilitate rolling and fabrication of the sheet stock. This phase of the work is more fully discussed in the section entitled, "Rolling at Lukens Steel Company."

Proposed Changes for Casting Ingots

Minor changes which will lower costs and simplify the operation are being incorporated in the aforementioned ingot-casting procedure. Instead of pouring the boron carbide into the mixture by hand, it will flow, at a controlled rate, by gravity from an electrically heated hopper. After oxidation in a muffle furnace, the carbide will be transferred to the hopper and kept at a temperature, probably between 800° - 1000 °F, permitting it to flow freely. This will minimize the temperature drop of the melt during the addition of the carbide and reduce the temperature gradient between the top and bottom of the crucible.

It is also planned that mechanical stirring will replace the manual operation, and the casting mold will be cooled from the bottom by forced air circulation, allowing the entrapped gases to escape from the top.

Advantages of the New Casting Technique over McKinney-Rockwell Method

1) Ten to twelve ingots can be mixed before replacing the crucible and mold. In the McKinney-Rockwell procedure, one crucible per ingot was expended.

2) Elimination of the aluminum powder minimizes the oxidation of the molten aluminum.

3) Elimination of the metal spraying operation prior to cladding the ingots and the use of nitrogen during mixing lowers the cost of the finished sheet.

ROLLING BORAL INGOTS INTO LARGE SHEETS

Rolling at Lukens Steel Company

Unsuccessful attempts at large-scale experimental rolling were made by Lukens Steel Company, Coatesville, Pennsylvania. Two ingots, 27" x 36" x 6", containing 50% B_4C by weight and prepared according to the procedure outlined in ORNL-242, were scheduled for rolling into sheets, 56 1/2" x 66 1/2" x 3/16". Failure of the rolling attempt was attributed to rough handling of the ingots during rolling. Greater care could not be used because the mill designed primarily for steel ingots could not be slowed down to the desired speed and the rolls could not be lubricated with kerosene.

Upon examination of the damaged sheets there was evidence of insufficient aluminum to coat all the B_4C in the 50-50 mixture. It is possible that this defect, which apparently was not too important when rolling small ingots, became more prominent in rolling the larger ones and contributed to the unsuccessful rolling attempt. It was therefore decided to lower the B_4C content in an effort to improve the rolling characteristics.

Even at the lower B_4C concentration, sufficient attenuation of thermal neutrons can be obtained for more applications without using excessively thick sheets.

Rolling at Republic Steel Company

A successful rolling was accomplished at the South Division Plant of the Republic Steel Company in Canton, Ohio. Republic was chosen for this experiment because it had hand-fed or jobber rolling mills which were more suited for the rolling of boral. Two ingots, 23" x 14" x 2", containing 35% B_4C by weight, were prepared, placed in 2" aluminum frames and covered with 1/2"-sheet 2S aluminum. These ingots where than heated to 1100 °F, reduced 50%, reheated to 1000 °F, and rolled into sheets 52" wide, 92" long, and 3/16" thick, the minimum attainable thickness on the rolls. Cold rolls, frequently lubricated with kerosene were used. After a few more large scale experimental rollings, boral could be supplied commercially in sheets, 5' x 10' x 3/16" if this is warranted.

Rolling at ORNL

Because of the small quantities required to meet present commitments, boral was rolled in the ORNL rolling mill. Since the capacity of this mill limited the maximum width of the finished sheet to 24", sheets 24" x 84"-96" x 1/4" or 1/8" were rolled, and wider sheets were fabricated by joining several smaller ones. Ingots were prepared according to the procedure outlined in the section entitled, "Technique for Casting Ingots", placed in 1" frames and clad with 1/4" aluminum. The rolling procedure was essentially the same as the one used at Republic.

PHYSICAL PROPERTIES

Data

1) Composition (for 1/4" sheet including Al cladding on each side)

	Sandwich Material 35% B_4C by Weight		Sandwich Material 50% B_4C by Weight	
	%(wt)	mg/cm^2	%(wt)	mg/cm^2
B	15.7	254	22.4	342
C	4.3	71.6	6.2	100.1
Al	80.0	1303.0	71.4	1103.5

Borals with B_4C contents varying from 10 - 50% in the core can be supplied.

2) Strength

a) Tensile

Tensile specimens containing 50% B_4C by weight were exposed to radiations in the X-10 pile for 14 months with no serious damage.

Weeks of Exposure	Total nvt	Average Tensile Strength (psi)
0	0	5000
6	3.1×10^{18}	6335
8	4.8×10^{18}	7500
30	1.2×10^{19}	5650
60	2.6×10^{19}	5500

Additional samples are now being exposed in the Hanford piles -- no results are available at this time.

b) Elongation - 0.4% (ORNL-242)

c) Shear - 8,237 psi (ORNL-242)

3) Thermal Properties - 50% B_4C by weight

a) Thermal Conductivity (Btu/hr-ft-^oF)

Temp. (^oF)	200	450	500
k	25	19.2	19.0

The above values are being rechecked and additional values for pure B_4C and for boral with varying B_4C content are being obtained.

b) Heat Content: .175 Btu/lb-^oF (ORNL-242)

4) Density: 2.5 g/cc

5) Cost: \$15-\$17/ft^2 for material containing 35% B_4C in the core

6) Workability:

Recommended methods for working boral are shearing and punching. Boral with 35% B_4C can be sawed at low speeds with Do-All saws. All welding must be done with heliarc. Boral tubes can be hot turned or pressed.

7) Availability:

In order to make boral available to other sites, ORNL has agreed to accept urgent requests for small amounts of boral as sheets not larger than 24" x 96" x 1/4" or 1/8", other program commitments permitting. Requests or purchase orders for sheet stock or simple fabricated parts may be submitted directly to ORNL, giving detailed requirements.

8) Other Applications:

Boral can be sprayed onto mild steels. However, the bond between the sprayed material and the base needs improvement.

ACKNOWLEDGEMENTS

The authors wish to acknowledge the assistance of V. L. McKinney and the Y-12 Shops in setting up the casting procedure for producing ingots and of C. D. Smith and his group at ORNL in rolling the boral.

APPENDIX

Principle of Proposed Method for Determining Thermal Conductivities

Longitudinal heat flow through a specimen was measured by the temperature rise of a metered amount of water passing through a heat exchanger located at the base of the sample. The temperature drop across the specimen was measured with thermocouples embedded in the sample a known distance apart. Radiation, conduction and convection losses were minimized by employing an electrically heated guard ring system in which the cavity between the sample and the walls of the guard ring was filled with a powdered thermal insulation, Sil-O-Cel. Under these conditions, the thermal conductivity was computed by means of the relationship

$$k = \frac{Wc_p (\Delta T)_w L}{A (\Delta T)_s}$$

k = thermal conductivity, Btu/hr-ft-^{o}F

cp = specific heat of water, Btu/hr-lb

$(\Delta T)_w$ = temperature rise in water, ^{o}F

L = distance between thermocouples embedded in sample, ft

A = cross-sectional area of sample, ft^2

$(\Delta T)_s$ = temperature drop in sample, ^{o}F

Application of Proposed Method for Determining Thermal Conductivity

In an effort to simulate experimentally the method set forth in the section entitled, "Principle of Proposed Method for Determining Thermal Conductivity," the apparatus diagrammatically shown in Figure 1 was set-up. The Specimen (D), 2 cm in diameter and 5 cm in length was sandwiched between a heat source (A) and a heat exchanger (C) and the complete assembly was held tightly together by a spring loaded clamp (3)(4) to assure thermal contact between the various metal faces. The temperature of the heat source, a solid cylinder of copper wound with high resistance nichrome wire was controlled by a variac. The heat exchanger was also made of copper with water flowing in a baffled path as the heat exchange medium. Knowing the water flow rates, the quantity of heat being conducted was computed from the temperature rise in the water. A thermopile made of fluorothene, containing six iron-constantin thermocouples was used to measure the temperature rise of the water.

The temperature drops of the specimen and simulator (B) were measured with chromel-alumel thermocouples sealed into small holes with saureisen. The simulator or guard assembly (F), a brass tube wound with high resistance nichrome wire was cooled by water (5) as shown in order to effect the same temperature drop in the simulator and specimen. The cavity between the sample and simulator walls was filled with powdered Sil-O-Cel to minimize heat losses. Data were taken when the system reached steady state.

Other Testing and Calculation Methods

1) Density - gross volume measurements

2) Tensile Strength - ASTM B209-46T, 1946 Ed., Part 1B, p 572

3) Shear - ASTM C102-36, 1946 Ed., Part II, p 228

DRAWING NO. 10574

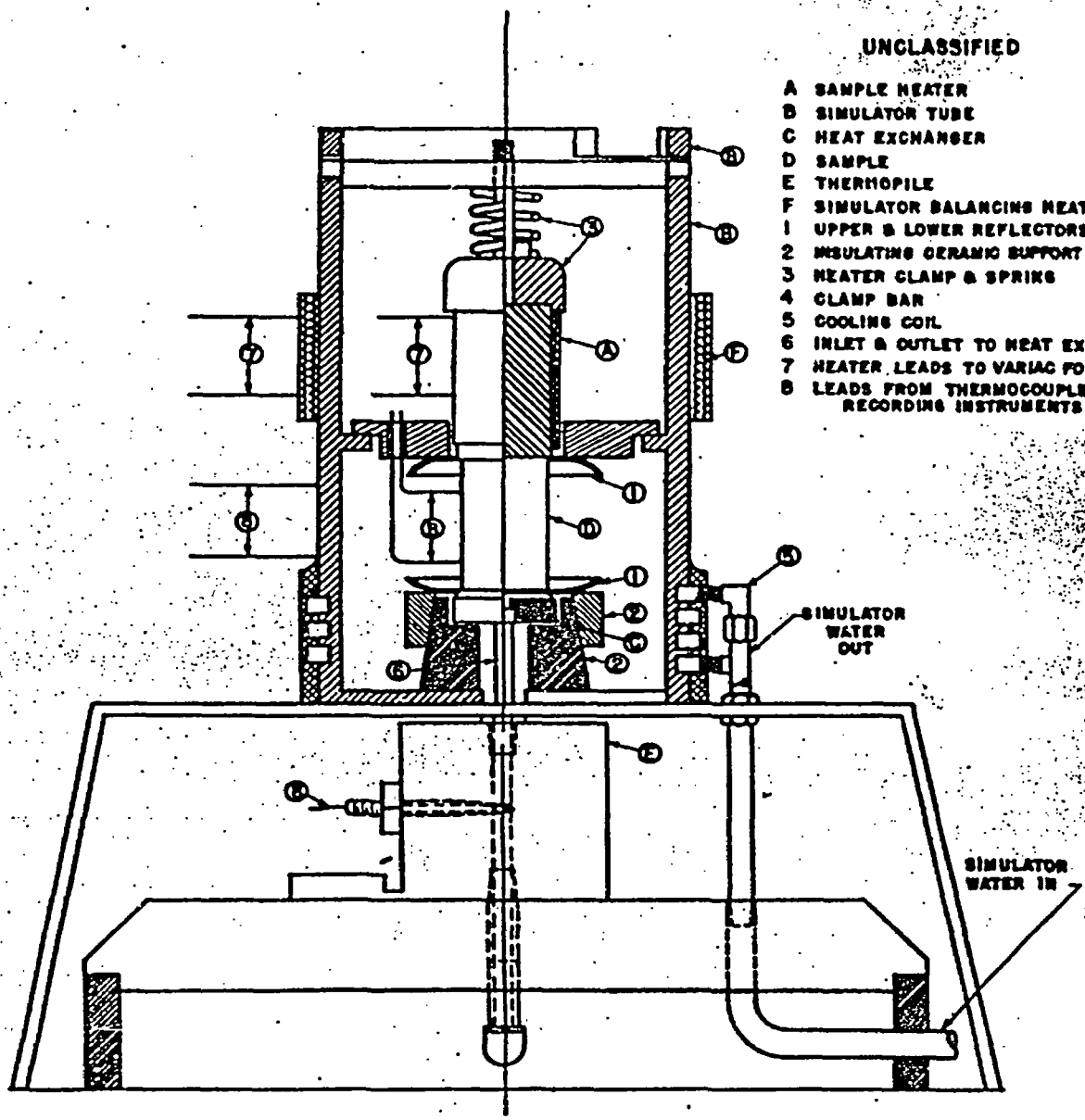

Fig. 1—Thermal conductivity apparatus.

GPO 916427

Howard Pinkham
9/14/55

RESULTS OF A SURVEY ON THE USE OF BORAL IN SHIELDING

A Paper Presented at
The Atomic Energy Commission Conference
on
Radiation Shielding
May 13 and 14, 1954
Knolls Atomic Power Laboratory
Schenectady, New York
by

Neil F. Ritchey
Atomic Energy Advisor
Reynolds Metals Company
Louisville, Kentucky

RESULTS OF A SURVEY ON THE USE OF BORAL IN SHIELDING

Before discussing the results of the Boral survey, I want to make sure that everyone knows what Boral is. For the benefit of new members and guests here today who may not be familiar with Boral, I want to describe very briefly what it is.

Boral is an engineering shielding material that is used to absorb thermal neutrons. Essentially it is a mixture of boron carbide (B_4C) and aluminum, rolled into sheet. The mixture is not used bare in this form, however. It is clad with commercially pure aluminum.

Figure No. 1 shows schematically how ORNL produces Boral. There are no technical details in this sketch, because I only want to show the principle of Boral construction. To make this sketch correct, I would have to show the picture frame cladding around the edges.

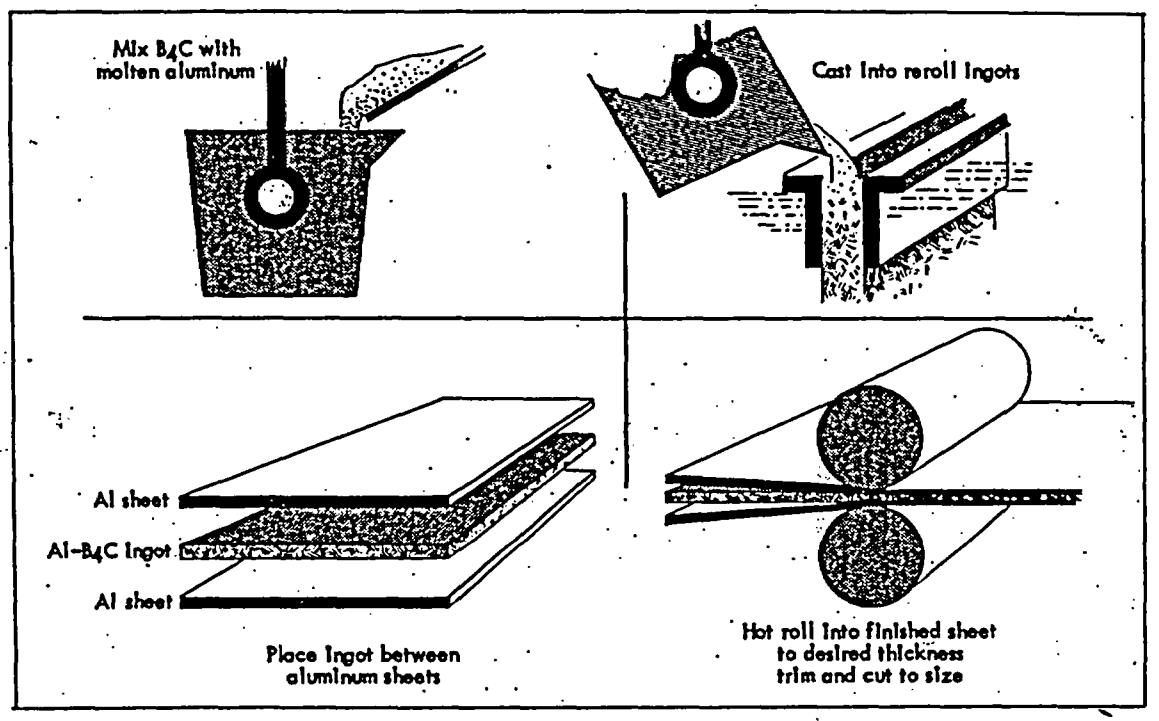

Figure 1

FLOW CHART FOR MAKING BORAL AT ORNL
(SEE ORNL 981 AND ORNL 242)
MAY 1954

You may not be interested in the detailed engineering properties of Boral. I do think you would like to know how Boral compares with other familiar metals. Figure No. 2 shows relative properties of Boral, Aluminum, Copper, Iron and Stainless Steel.

PROPERTY	BORAL	ALUMINUM (ANNEALED)	COPPER (ANNEALED)	IRON (ANNEALED)	STAINLESS STEEL (ANNEALED)
TENSILE STRENGTH (PSI)	5,000	13,000	32,500	38,500	80,000
ELONGATION (PERCENT)	0.4	45	37	45	55
THERMAL CONDUCTIVITY (BTU/IN/FT^2/LB/°F) (AT 200°F)	25	1,509	2,700	743	200
SPECIFIC HEAT BTU/LB/°F	.175	.226	.09	.126	.150
DENSITY (GMS/CM^3)	2.5	2.7	8.9	7.8	8.0

Figure 2

PROPERTIES OF BORAL COMPARED TO
SEVERAL COMMON METALS
MAY 1954

You can see that Boral has low strength; it is brittle; the thermal conductivity is very low - in fact you might say it has high insulating value (k for concrete is about 12; wood is in the range 0.5 to 1.5).

Specific heat or heat capacity of Boral is in between the values for Iron and Aluminum. Its low density has advantages that may have more significance in aircraft shielding than land based reactors.

Figure No. 3 summarizes the results of our survey. The questions we asked are across the top of the chart. The replies received are listed under each column heading.

Most people visualize the use of Boral for stationary reactors component to the concrete shield. Mounting Boral against a flat concrete wall greatly minimizes the manufacturing problems. I have some design ideas to show you in the illustration to follow.

Several aircraft companies indicate that if Boral could be formed into contour shapes, considerable quantities might be used over the long range future. Specific suggested uses include the use of Boral in the form of fabricated boxes to enclose electronic equipment and other radiation sensitive devices. Aside from the reactor shield, some people believe ultimate use of Boral will be made to shield easily activated components of aircraft, particularly the engine.

COMPANIES AND ORGANIZATIONS QUERIED	APPLICATION AGAINST WALL	APPLICATION FABRICATED INTO VESSELS	MINIMUM BORON CONCENTRATION GMS/CM²	MINIMUM TENSILE STRENGTH PSI.	PREFERRED WIDTH AND LENGTH	PREFERRED THICKNESS	COMMENTS ON QUANTITY, PRICE, ETC.
1	X		.18	5,000	4'X8'	1/4"	SMALL QUANTITIES
2	X		.04	SELF SUPPORTING	2-4'X8'	1/8"-1/4"	3-4,000 SQ. FT. PER REACTOR
3	X		.10	—	—	1/4"	SHOULD BE COMPETITIVE TO LEAD EQUIVALENT
4	X		—	SELF SUPPORTING	4'X6'	1/2"	~$5 PER SQ. FT. - SMALL DEMAND
5	X	X	.10	STRONGER THE BETTER	NOT IMPORTANT	THIN AS POSSIBLE	—
6	X		.25	~ 3,000	4'X8'	1/8"	$2-$5 PER SQ. FT. - SMALL DEMAND
7	X		.25	NOT IMPORTANT	4'X8'	1/4"	SMALL DEMAND
8	X		.25	NOT IMPORTANT	SMALL WIDTHS O.K. SMALL SEAMS PERMISSIBLE	1/4"	500 SQ. FT. PER REACTOR NOT LARGE MARKET
9	X		.11 MINIMUM .5 NOT EFFICIENT	—	4'X8'	THIN AS POSSIBLE	SMALL DEMAND
10	X	X	.11	TO PERMIT NORMAL HANDLING	3'X8'	1/8"=100 ATTEN. 1/4"=10,000 ATTEN.	IN AVIATION SHIELD FOR ACCESSORIES AND ENGINE

Figure 3

RESULT OF MAY 1954 BORAL SURVEY

The minimum concentration of Boron believed necessary was quite well agreed upon. Most values were in the range 0.10 to 0.25 grams/cc. As a means of comparison, Boral containing 35% of B_4C by weight of 1/4" total thickness will contain approximately 0.254 gms/cc.

The survey showed that as long as Boral will support itself against a wall, and not fall apart during normal handling, potential users are satisfied.

The dimensions of the sheet are more important to the manufacturer than to you. I will only say that most survey replies stated that panels should be about 4' x 8' and 1/4" thick.

The conclusion I draw from the survey is that the physical and mechanical properties of Boral are satisfactory for stationary land base reactor shielding. For aircraft reactors your indications were that it would be desirable to improve the mechanical properties so that Boral could be formed into simple and semi-complex shapes. For use in shipboard reactors, Boral would not only have to be formed into complex shapes, but it would have to possess high shock resistance.

The most overwhelming agreement from replies to the survey was on the prediction of Boral's future. All except one company could not see a very bright future for Boral. The basis for prediction was the number of reactors that might be built in the future. I will agree that reactors are not going to be mass produced in the next 5 or 10 yrs. But after that it is anyone's guess. It is my opinion that Boral has not been fully considered in the light of new fabrication techniques common to aluminum technology today.

I want to show you several illustrations of recent developments in the aluminum industry. I don't have shield designs incorporating these new aluminum developments with Boral. My only reason for bringing them up at this meeting is to stir up ideas that someday you may recall.

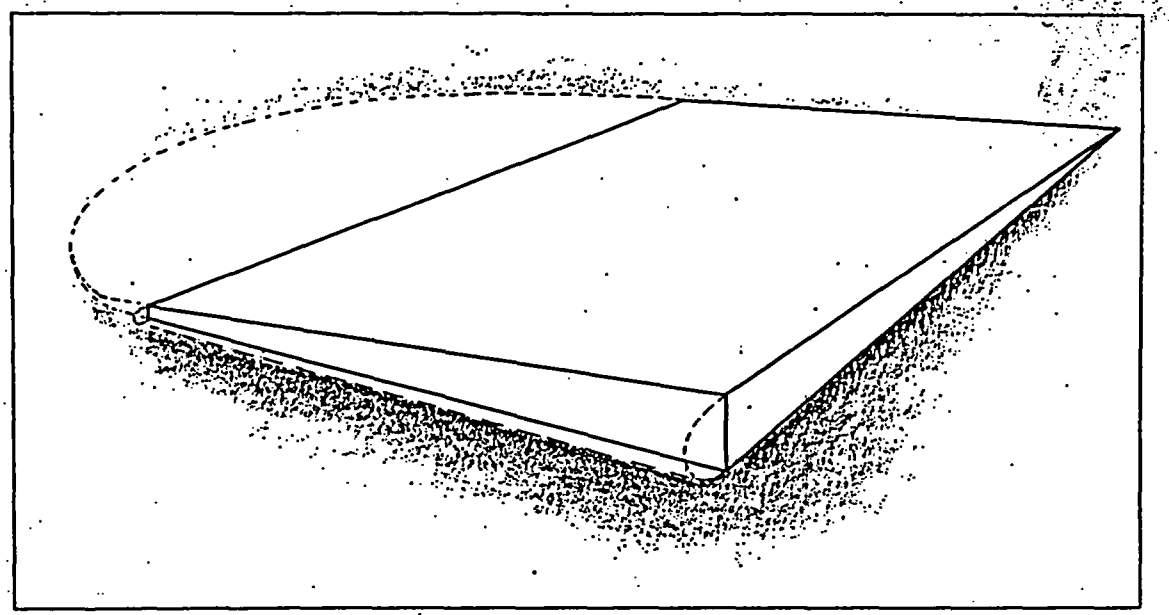

Figure 4

TAPERED ALUMINUM SHEET
MAY 1954

Figure No. 4 shows tapered sheet that the aluminum industry has been called to produce for high speed jets. Notice we outlined in the wing of a plane to give you an idea of how the sheet tapers in two directions. This product will be manufactured on a high production basis using a taper rolling technique.

Why do I bring it up here? Because here is a possibility for obtaining variable Boron concentration to meet cosine flux distribution. If Boral can be hot rolled, we ought to be able to convert it into tapered sheet. The cladding problem might be tough but not insurmmountable. Perhaps you may have a problem someday that will make tapered Boral sheet look promising.

Figure No. 5 was made from a sketch presented by Helmer Enlund of the Detroit Edison Company. Mr. Enlund cautions against the use of Boral in flat contact with the bulk shield if heat removal is a problem.

I hope Mr. Enlund will correct me if I have incorrectly interpreted his reason for not wanting direct contact. Due to the irregularity of the concrete and possible inefficient bonding of the Boral to the concrete, cooling of the shield would be difficult.

At any rate, these two designs are good ideas for getting around the cooling problem.

I don't know myself how the heat developed in the bulk shield, due to primary gammas, compares to the heat resulting from secondary neutron capture gammas. I would think the answer to that question is important, because it tells us whether Boral is effective in suppressing a portion of shield heat.

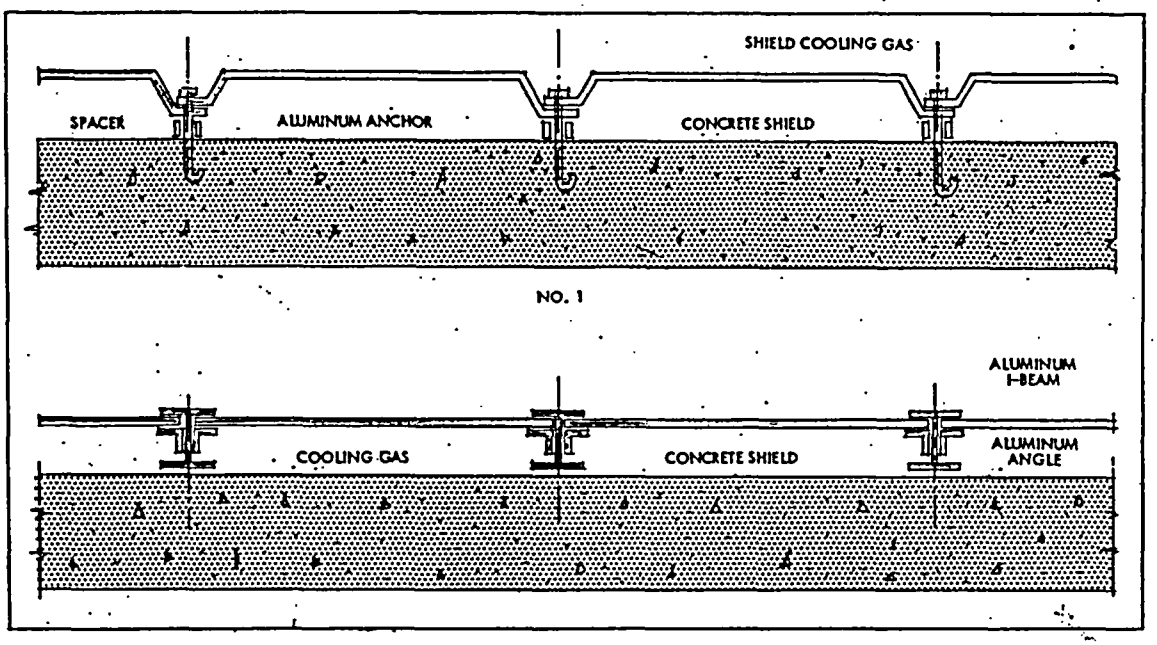

Figure 5

SUGGESTED BORAL SHIELD DESIGNS
FOR DEPRESSION OF HEAT INDUCED BY n-γ HEATING
SUBMITTED BY H.L.F. ENLUND, DETROIT EDISON CO.
MAY 1954

Figure 6 is a schematic chart depicting the principle of a new product called heat transfer sheet. The principle ought to lend itself very nicely to Boral.

What we do here is print a circuit on one sheet of aluminum using an anti-weld or non-bonding agent. Our newest facility now under construction will use the silk screen printing process for higher production.

Next, we lay another sheet over the first. Tack it around the edges - spot welding is satisfactory. Then we hot roll the two sheets to the finished size.

Where the circuit is printed the two sheets do not bond. The last step is to insert an air nozzle in one end of the circuit and expand.

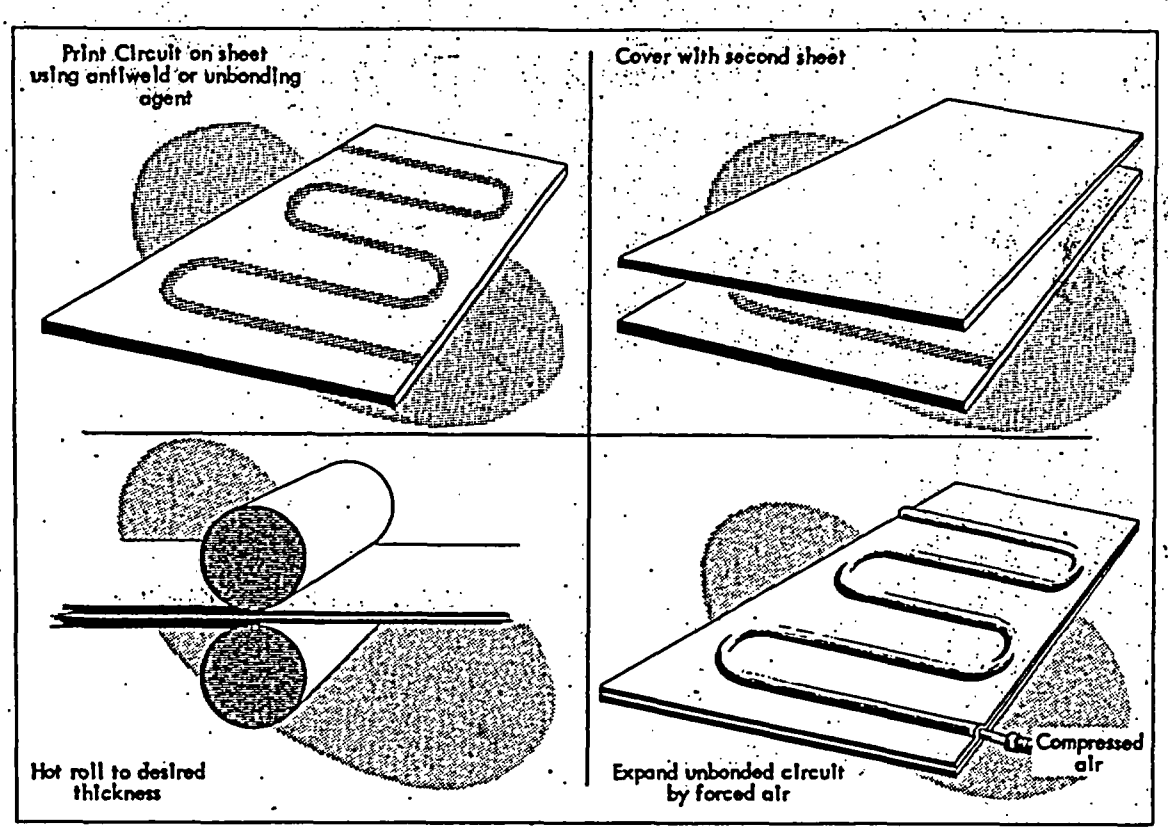

Figure 6

METHOD OF MANUFACTURING HEAT TRANSFER PLATES

(ROLL BONDED AND EXPANDED)

MAY 1954

The net result is sheet with built in cooling coils ready for use.

Figures 7 and 8 show what can be done for stiffened sheet. Figure No. 7 is called integrally stiffened sheet. As you can see, it is first extruded into a tube. The tube is then slit longitudinally and straightened. The flattened section is about 30" wide. We have to extrude in the tube form first, because the largest extrusion presses today will only take shape within a 12" circumscribed circle.

Figure No. 8 illustrates the various roll passes necessary to produce rolled ribbed sheet. Both applications are stiffened aircraft skin.

To sum up, I think our survey shows that there is a definite place for Boral as an engineering material for shielding. It serves as a protector against high energy capture gamma ray generation. It will at the same time provide protection against induced activation.

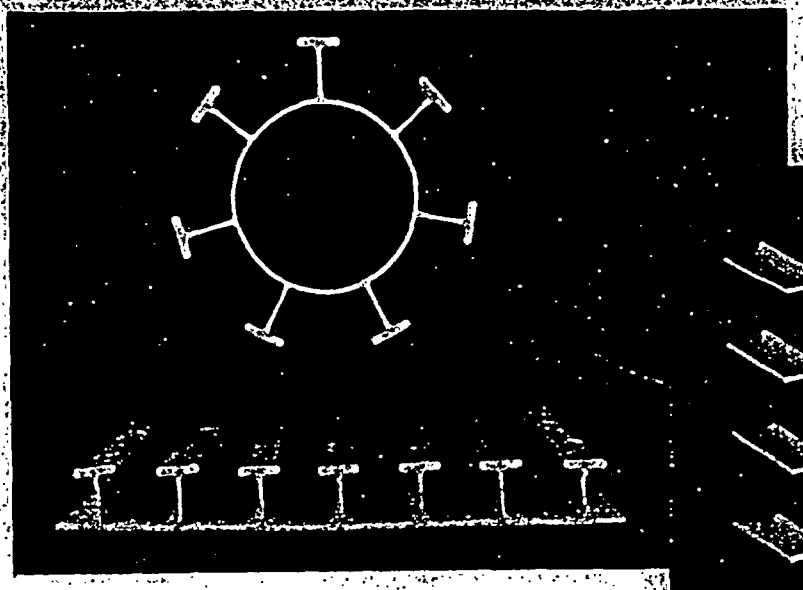

Figure 7

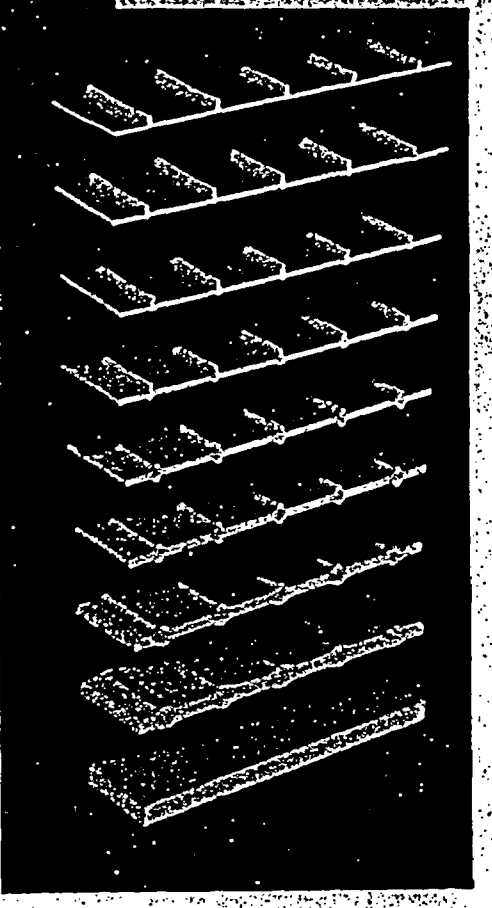

Figure 8

I believe more might be done with Boral if its fabricating and forming properties are evaluated more fully. More familiarity with new techniques in aluminum technology might lend impetus to design usefulness of Boral.

The relatively high cost of Boral can be brought down in proportion to the extent that its need grows. The future of reactor production and, therefore, the demand for neutron shields is bright. Just how bright and how far away that future is, we don't know.

I want to thank everyone who kindly took the time to answer our survey. To those interested people who I didn't contact, I sincerely hope you will report any comments or experience you have had with Boral, either in the discussion today or by letter at a later date.

reprinted from NUCLEONICS | Jan. 1958, Volume 16, No. 1, Pages 91-94

How Channeling between Chunks Raises Neutron Transmission through Boral

By WALTER R. BURRUS*
Lockheed Aircraft Corp.
Marietta, Georgia

Boral is a mixture of boron carbide and aluminum encased between two thin layers of aluminum. Since boron carbide has a large $B^{10}(n,\alpha)Li^7$ cross section at thermal-neutron energies and the accompanying gamma ray is only 0.42 Mev, boral is valuable for use in nuclear shields where a large thermal flux must be absorbed without the production of hard gammas.

However, conventional calculations of the absorption of boral do not consider the channeling of neutrons through the spaces between the boron-carbide chunks. The results of a calculation for the transmission of ⅛-in. and ¼-in. boral that considers the channeling effect are in much better agreement with experimental data than earlier calculations neglecting channeling.

Calculation

The transmission of a slab consisting of randomly distributed chunks of average chord l (normally incident monoenergetic radiation) is given by

$$T = (1 - VF)^{t/l}$$

where T is fractional transmission, V is the volume fraction of the slab occupied by chunks, F is the average absorption of a single chunk, t is the thickness of the slab, and l is the average chord of a chunk.

The average transmission of one layer of the slab of thickness l is $1 - VF$. Since the chunks are assumed to be randomly placed, adjacent layers are statistically independent, and the overall transmission is the product of the transmission of t/l sublayers.

If the chunks are nearly spherical (1)

$$F = \frac{2}{(2r\Sigma)^2}\left[\tfrac{1}{2}(2r\Sigma)^2 - 1 + (1 + 2r\Sigma)e^{-2r\Sigma}\right]$$

where Σ is the linear attenuation coefficient of chunk material and r is the radius of a sphere (or equivalent radius on the basis of volume).

For a chunk of any shape without cavities a theorem due to Gauss states that the average chord l is given by $l = 4v/s$, where v is the volume of the chunk and s is its total surface area. For a sphere this gives $l = \frac{4}{3}r$.

If $VF \ll 1$, the transmission is approximately $T \approx e^{-VtF/l} \approx e^{-Vt\Sigma_{eff}}$. From the equations for F and l we can verify that for the limits of opaque and almost transparent chunks $\Sigma_{eff} = F/l \approx 1/l$ if $l\Sigma \gg 1$ and $\Sigma_{eff} = F/l \approx \Sigma$ if $l\Sigma \ll 1$. It should be noted that the effective linear attenuation coefficient for opaque chunks is $1/l$ and does not depend on Σ since all the trans-

TABLE 1—Size Distribution for B_4C Chunks

Mesh	Average particle diameter (in.)	l (= ⅔r) (in.)	Volume fraction
20–30	0.038	0.0253	17%
36–46	0.024	0.0160	11%
60–70	0.016	0.0107	6%
80–120	0.009	0.0060	6%

TABLE 2—Theoretical and Experimental Neutron Transmission through Boral*

Sample	Neutron source	Detector	Experimental transmission	Channeling calculation	Conventional calculation	Ref.
⅛-in. Alcoa (two samples)	Collimated beam from ORNL graphite reactor	Current detector (LiI xtal Cd difference)	7.0×10^{-2} ±40% (preliminary value)	9.6×10^{-2}	1.3×10^{-2}	6
¼-in. Alcoa	"	"	5.0×10^{-3} (preliminary value)	7.7×10^{-3}	4.8×10^{-4}	9
⅛-in. Brooks and Perkins	Water thermal column of ORNL graphite reactor	Thin indium foil	7.0×10^{-2}	2.7×10^{-2}	2.0×10^{-3}	4
⅛-in. ORNL	"	"	9.4×10^{-2}	2.7×10^{-2}	2.0×10^{-3}	4
¼-in. Brooks and Perkins	"	"	5.6×10^{-4}	1.7×10^{-3}	4.5×10^{-5}	4
¼-in. ORNL	—"—	"	7.6×10^{-4}	1.7×10^{-3}	4.5×10^{-5}	4

* Since the first two samples were measured with a different neutron source and detector, there is no direct comparison with the others.

** There may be some more errors in this Table, but the figures 1, 2, and 3 appear to be correct.

* PRESENT ADDRESS: Physics Department, Ohio State University, Columbus, Ohio.

mitted radiation channels around the chunks.

If the chunks consist of several groups with average chords $l_1, l_2, \ldots$ (and corresponding $V_1, V_2, \ldots, \Sigma_1, \Sigma_2, \ldots$), the transmission can be generalized to give $T \approx \exp - t\,(V_1^*\Sigma_{tr1} + V_2^*\Sigma_{tr2} + \ldots)$, where $V_i^* = V_i/(1 -$ volume fraction of all larger chunks). It is necessary to multiply V_i by $1/(1 -$ volume fraction of all larger chunks) to account for the crowding together of the smaller chunks by the larger ones.

This equation treats the distribution of chunks as if the chunks of various sizes were in separate layers. The result is always too small since it ignores voids that would be present in a layer if the larger chunks were separated out. Nevertheless, the result is correct for limiting cases of opaque and transparent chunks and is qualitatively correct in any case.

To calculate the transmission of ⅛-in. boral, it was assumed that the chunks of boron carbide were spherical. The size distribution shown in Table 1 is typical (*2*) of 20–100-mesh boron carbide usually used in boral. Other parameters used for the calculation are $\Sigma = 190.5$ in.$^{-1}$ at 2,200 m/sec (*3*) (neglecting attenuation in aluminum), $t = 0.085$ in. (not including aluminum cladding), $V = 40\%$ (not including aluminum cladding) $\approx 25\%$ over all.

The resulting transmission from the last equation is plotted against energy in Fig. 1. (It is assumed that Σ is proportional to 1/velocity.) The conventional calculation, assuming no channeling, is shown for comparison. Note that the transmission approaches the opaque-chunk limit at the low-energy end of the scale.

Since the chunks were assumed to be randomly distributed, there is no preferred direction for transmission. The transmission for neutrons incident at an angle θ with the normal can be found by replacing t by $t/\cos\theta$, the slant penetration. Figure 2 shows the transmission averaged over incident angles for an isotropic incident flux. ~~Since transmitted neutron current in the forward direction is relatively greater than the isotropic flux, the average is carried out for both types of detectors.~~ Figure 3 shows the results for ¼-in. boral.

A more extensive description of the method is given in an ORNL report now being published (*6*).

For an isotropic angular distribution of neutrons upon Boral, the transmission for neutron current is different from the transmission for neutron flux; thus the transmission is calculated for both current and flux detectors, (e.g. think foils and thin foils).

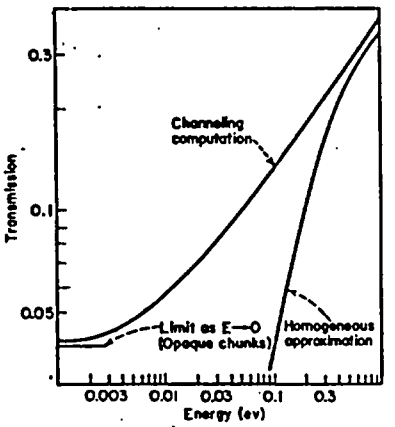

FIG. 1. Channeling computation departs from homogeneous approximation at low energies. Computations are for ⅛-in. boral with typical 20–100-mesh B_4C distribution

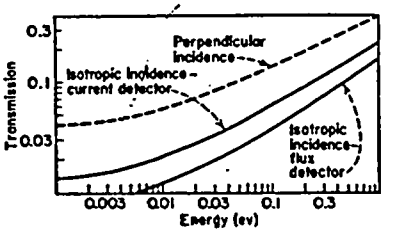

FIG. 2. Transmission of ⅛-in. boral with perpendicular incidence compared with current and flux from isotropic incidence

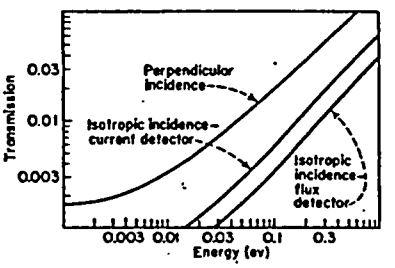

FIG. 3. Computations of Fig. 2 produce these results for ¼-in. boral

Experimental Verification

Experiments performed to test boral have been gross-transmission measurements using various neutron detectors. It is possible to compare the results with calculations only if the angle and energy distribution of incident neutrons and the angle and energy sensitivity of the detector are known. The table on page 91 attempts to compare the calculations with several experiments performed at ORNL.

For the calculations it was assumed that the thermal-neutron spectrum was Maxwellian and that the angular distribution from the thermal column was of the Fermi type (*7*). Effective temperature of the neutrons was taken as room temperature, 293.6° K. The channeling calculations are an average of the results of Figs. 2 and 3 over the Maxwellian spectrum for the appropriate detector. The conventional calculations are based on the thermal-neutron absorption coefficients discussed by Zahn and Laporte (*8*). These coefficients take into account both spectrum hardening and angular distribution.

In the table the channeling calculation is too great in most cases by a factor of 2 or 3. The result of the conventional calculation is too small by more than a factor of 10 for ¼-in. samples.

A considerable difficulty in accurately comparing experiment and calculation is the lack of standardization of boral. After initial development, fabrication was standardized, but the ingot size, cladding thickness, fraction of boron carbide, and particle-size distribution have not been rigorously fixed. In comparing experiments and calculations one must determine or guess the fractional weight of boron carbide, cladding thickness, and the size distribution.

* * *

This work was initiated at the Lid Tank Shielding Facility of the Oak Ridge National Laboratory while the author was on loan from the Wright Air Development Center Materials Laboratory. The author would like to acknowledge the assistance of R. W. Peelle and J. R. Smolen at ORNL and the cooperation of Alan Liebschutz at Lockheed and Stanley Szawlewicz at Wright Air Development Center. The basic method employed makes use of suggestions proposed by R. R. Coveyou and N. M. Smith at ORNL in 1947.

BIBLIOGRAPHY

1. K. M. Case, F. de Hoffmann, G. Placzek, "Introduction to the Theory of Neutron Diffusion," vol. 1, section 10 (U. S. Government Printing Office, 1954)
2. Norton Co., Worcester, Mass., "A Handbook on Boron Carbide, Elemental Boron and Other Stable, Boron-Rich Materials" (1955)
3. D. J. Hughes, J. A. Harvey, Neutron cross sections, BNL-325 (1955)
4. R. O. Maak, B. E. Prince, P. C. Rekemeyer, Boral attenuation characteristics, MIT Engineering Practice School Memo EPS-X-282 (1957)
5. J. Krisan, Thermal cross section and homogeneity test of boral and other shielding materials, ORNL BSF Monthly Report (Aug. 23, 1956)
6. W. R. Burrus, Transmission through boral, ORNL (to be published)
7. E. Fermi, *Ricrca sci.* **7**, 3 (1936); H. A. Bethe, *Rev. Mod. Phys.* **9**, 133 (1937)
8. C. T. Zahn, O. Laporte, *Phys. Rev.* **52**, 67 (1935)
9. G. de Saussure, A nuclear test for thermal neutron absorbing material (Information Meeting on Thermal Neutron Shielding Materials, Oak Ridge National Laboratory, Sept. 20, 1956)

Printed in U.S.A.

MASSACHUSETTS INSTITUTE OF TECHNOLOGY
ENGINEERING PRACTICE SCHOOL

UNION CARBIDE NUCLEAR COMPANY
A DIVISION OF UNION CARBIDE AND CARBON CORPORATION

MEMORANDUM

EPS-X-282

KT-251

November 27, 1956

TO: E.P. Blizard

FROM: R.O. Maak, B.E. Prince, and P.C. Rekemeyer

SUBJECT: Boral Radiation Attenuation Characteristics

DISTRIBUTION:

E.P. Blizard (10)	J.E. Vivian
T.V. Blosser	T.F. Wagner
J.A. Cox	C.D. Zerby
F.O. Lewis	ORGDP Plant Records (2)
F.C. Maienschein	ORNL Laboratory Records (4)
R.C. Reid	M.I.T. Practice School Files (10)

INTRODUCTION

Boral, a mixture of boron carbide and aluminum encased between two thin layers of aluminum, has many uses as a thermal neutron shielding material. Since the $B^{10}(n,\alpha)$ Li^7 reaction has such a large cross section of 735 barns at thermal energies and the accompanying gamma ray is only 0.42 Mev, boral is uniquely suitable for shields where a large thermal neutron flux must be absorbed without production of hard gammas, e.g., inner section of reactor shields, shutters for thermal columns, and instrumentation.

Figures 1 and 2 are dark field illuminated magnified photographs of a cross section of sample boral manufactured by the Oak Ridge National Laboratory. Figures 3 and 4 are photographs of a sample manufactured by Brooks and Perkins in an attempt to improve on the quality of this material. Since the boron carbide is heterogeneously dispersed throughout the aluminum, the gamma ray linear attenuation coefficient and the thermal neutron absorption cross section are a function of the amount of boron carbide content, its particle size, and the degree of dispersion. This investigation is concerned with the experimental determination of the attenuation characteristics of these two samples, and an attempt to theoretically predict, using a Monte Carlo type calculation, the effective macroscopic thermal neutron cross section.

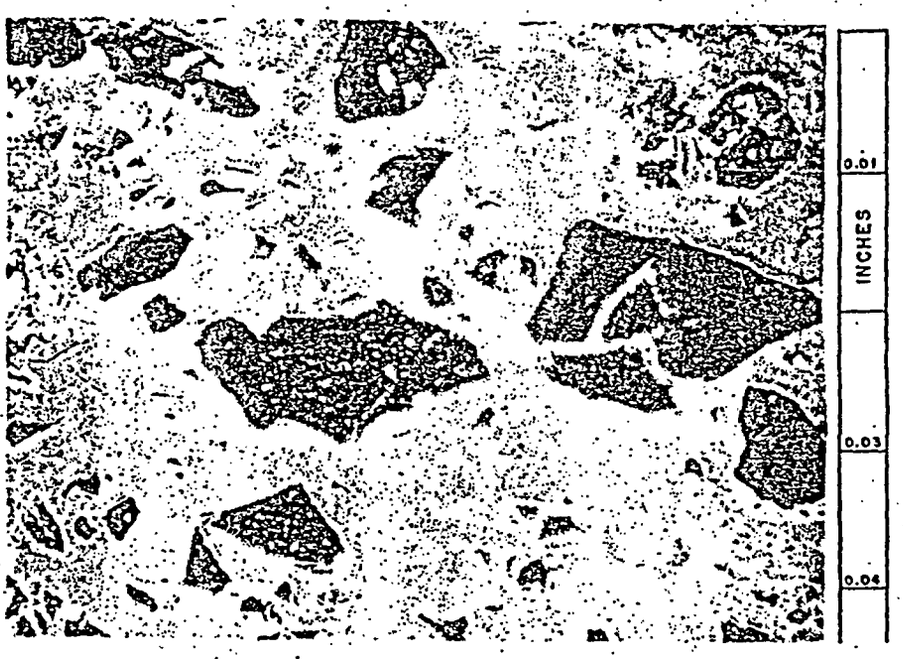

MASSACHUSETTS INSTITUTE OF TECHNOLOGY
ENGINEERING PRACTICE SCHOOL
UNION CARBIDE NUCLEAR COMPANY
A Division of Union Carbide and Carbon Corporation

Dark Field Illuminated Microphotographs of unetched 1/8 inch ORNL samples

DATE	DRAWN BY	FILE NO.	FIG.
11/27/56		EPS-X-282	1

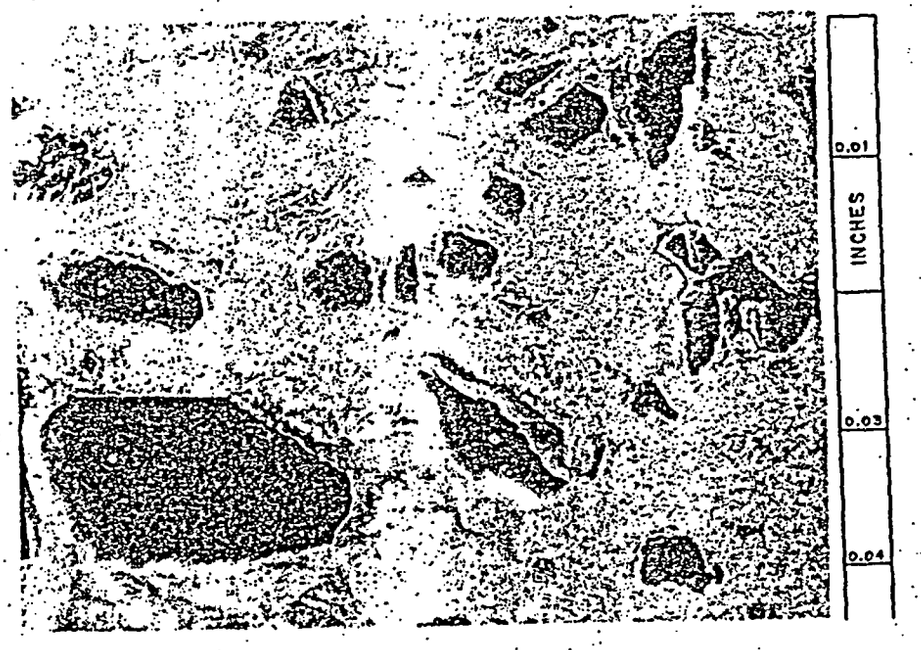

MASSACHUSETTS INSTITUTE OF TECHNOLOGY
ENGINEERING PRACTICE SCHOOL
UNION CARBIDE NUCLEAR COMPANY
A Division of Union Carbide and Carbon Corporation

Dark Field Illuminated Microphotographs of Unotched 1/4 inch ORNL samples

DATE	DRAWN BY	FILE NO.	FIG.
11/27/56		EPS-X-282	2

MASSACHUSETTS INSTITUTE OF TECHNOLOGY
ENGINEERING PRACTICE SCHOOL
UNION CARBIDE NUCLEAR COMPANY
A Division of Union Carbide and Carbon Corporation

Dark Field Illuminated Microphotographs of Unetched 1/8 inch Brooks and Perkins samples

DATE	DRAWN BY	FILE NO.	FIG.
11/27/56		EPS-X-282	3

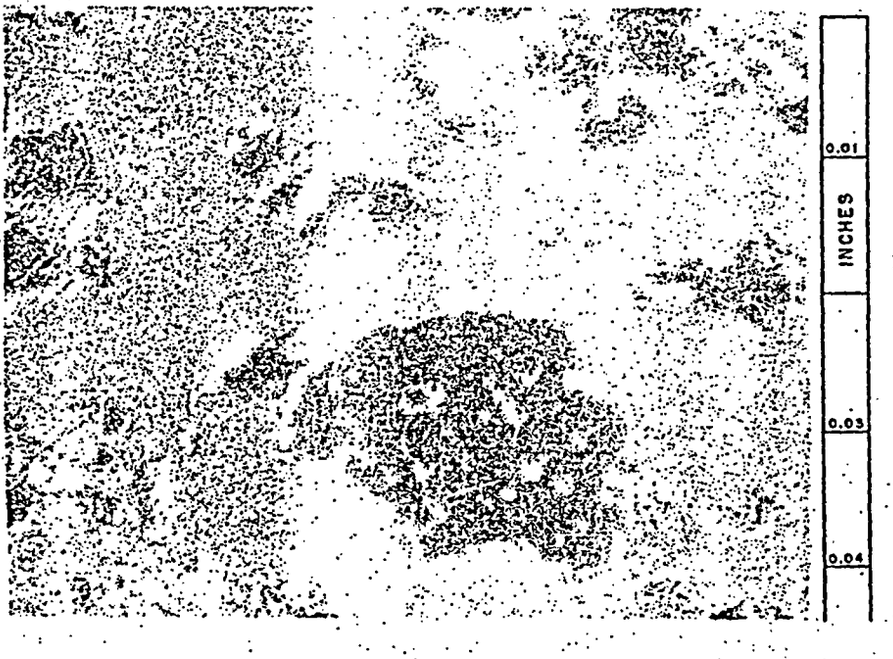

MASSACHUSETTS INSTITUTE OF TECHNOLOGY
ENGINEERING PRACTICE SCHOOL
UNION CARBIDE NUCLEAR COMPANY
A Division of Union Carbide and Carbon Corporation

Dark Field Illuminated Microphotographs of Unetched 1/4 inch Brooks and Perkins samples

DATE	DRAWN BY	FILE NO.	FIG.
11/27/56		EPS-X-282	4

PROCEDURE

Gamma Ray Attenuation

The gamma ray linear attenuation coefficient, μ, was determined by measuring the attenuation of the 0.661 Mev gamma rays from a ten curie cesium-137 source for various thicknesses of the two samples. Readings were taken on an ion chamber at distances of 10, 15, and 20 cm from the top of the source container, and μ determined as the slope of a plot of the log of the counter reading versus plate thickness.

An indication of the effect of non-homogenity of the boral on γ ray attenuation was obtained by taking x-rays of the two samples.

Neutron Attenuation

Experimental:

The attenuation of thermal neutrons was experimentally determined by activating indium foils secured to both sides of a boral sample placed in the water thermal column of the ORNL graphite reactor. A removal cross section, Σ, was defined by the equation $I = I_o e^{-\Sigma x}$, where I and I_o are the upward neutron currents measured by the indium foils. Only upward moving neutrons were detected since the foils were backed with a cadmium cover to remove any thermal neutrons diffusing downward.

Theoretical:

The activation of an indium foil placed in back of an irradiated sample may be determined by solving the integral,

$$Z = \frac{\int_{\Omega}\int_{A} F(\underline{\Omega})\, e^{-\Sigma_b x_p^b(\underline{\Omega},A) - \Sigma_a \left(\frac{t_p}{\cos\theta} - x_p^b(\underline{\Omega},A)\right)} \left(1 - e^{-\frac{\Sigma_f t_f}{\cos\theta}}\right) d\underline{\Omega}\, dA}{\int dA}$$

where Z = neutrons/sec-cm^2 absorbed by foil.

$F(\underline{\Omega})$ = thermal neutrons/unit solid angle, sec.

x_p^b = thickness of B_4C seen by a neutron.

Σ_b = macroscopic total thermal cross section for boron carbide.

Σ_a = macroscopic total thermal cross section for aluminum.

Σ_f = macroscopic total thermal cross section for indium.

$\underline{\Omega}$ = unit vector in direction of neutron velocity.

t_p = thickness of boral plate.

t_f = thickness of indium foil.

θ = angle the neutron path makes with the normal to the plate.

A = area of the plate.

This integral was solved by random sampling of the variables θ and A, and actually measuring x_p^b (θ, A) using a magnified picture of an 1/8" ORNL sample cross section.

The activation of the foil without the plate was analytically calculated from the expression.

$$Z = \int_{\underline{\Omega}} F(\underline{\Omega})(1 - e^{-\Sigma_f t_f/\cos\theta}) \, d\underline{\Omega}$$

The ratio of $Z/Z_o = R$ should be the ratio of the foil readings and an effective cross section may be determined by $R = e^{-\Sigma x}$.

A complete description of the method followed in using this procedure along with the derivation of an expression for $F(\underline{\Omega})$ is given in the Appendix.

RESULTS

The results of the experimental determination of the gamma ray linear attenuation coefficient gave a μ of 0.183 cm^{-1} for the Brooks and Perkins sample and a μ of 0.193 cm^{-1} for the ORNL sample. For pure 2S aluminum, a coefficient of 0.202 cm^{-1} was obtained.

X-ray pictures of the two samples are shown in Figures 5 through 8, where B_4C particles are shown white.

The results of the experimental determination of an effective neutron removal cross section are shown in Table I.

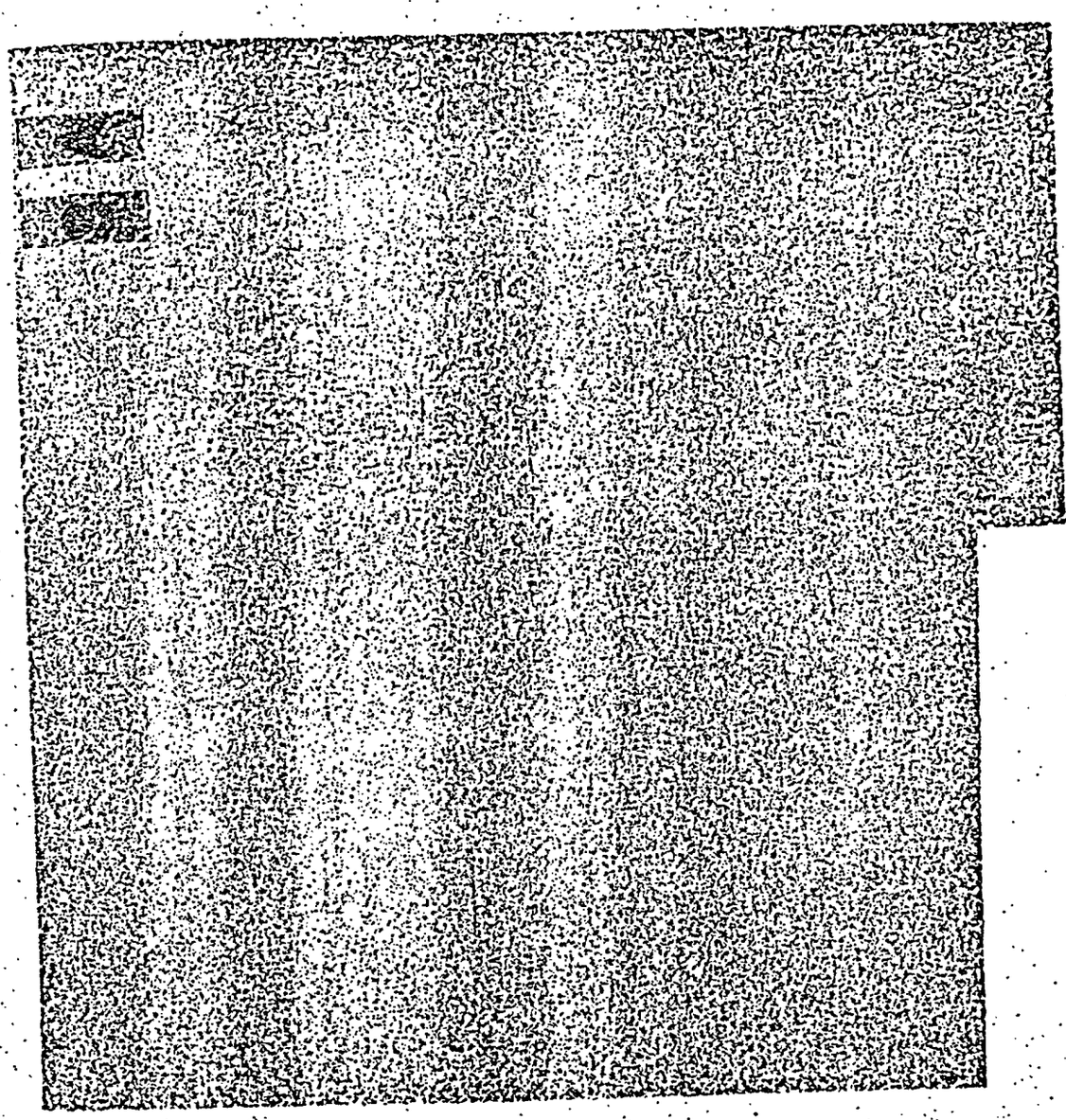

MASSACHUSETTS INSTITUTE OF TECHNOLOGY ENGINEERING PRACTICE SCHOOL UNION CARBIDE NUCLEAR COMPANY A Division of Union Carbide and Carbon Corporation			
X-Ray Photograph of 1/8 inch ORNL Sample			
DATE 11/27/56	DRAWN BY	FILE NO. EPS-X-282	FIG. 5

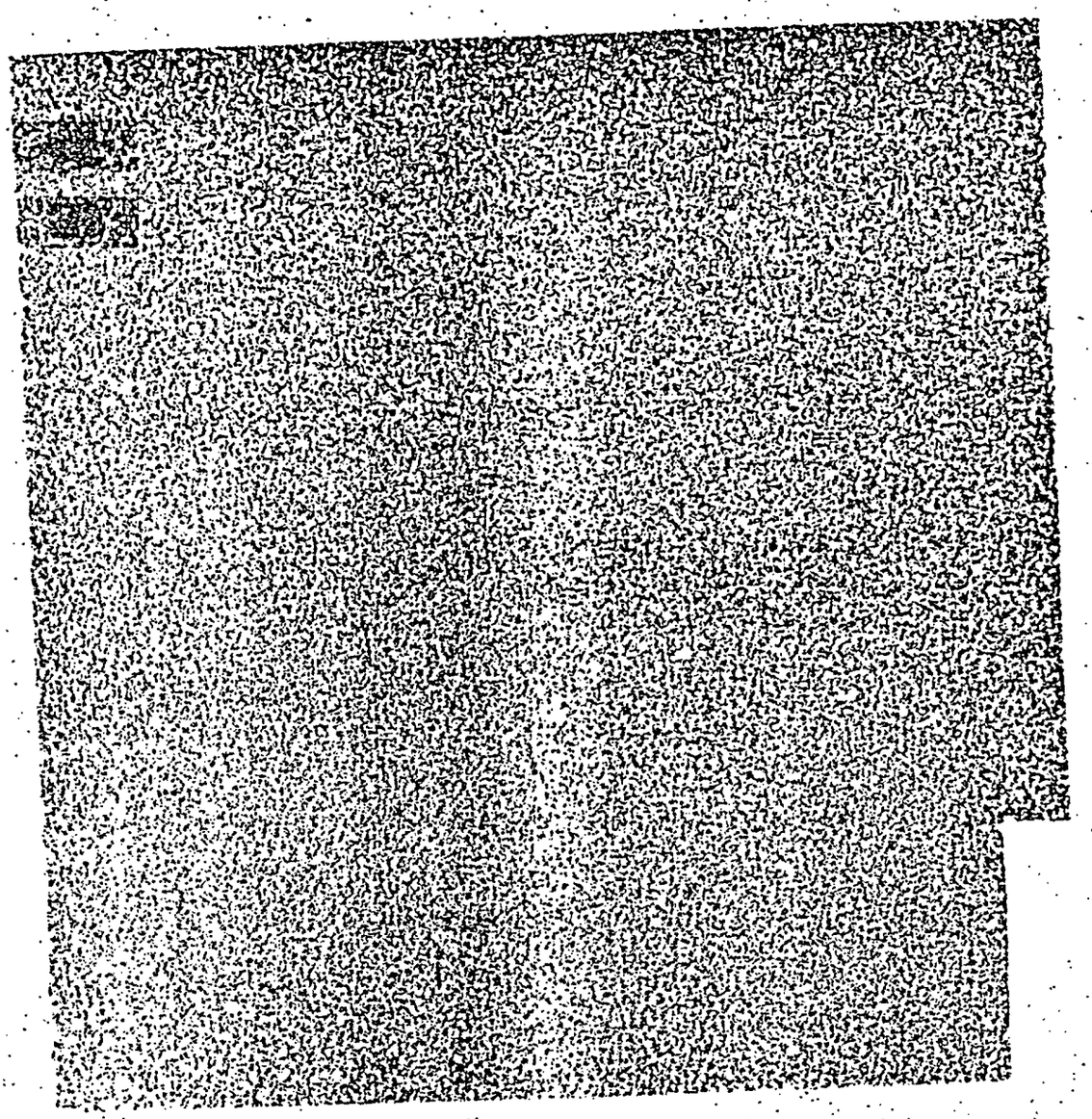

MASSACHUSETTS INSTITUTE OF TECHNOLOGY ENGINEERING PRACTICE SCHOOL UNION CARBIDE NUCLEAR COMPANY A Division of Union Carbide and Carbon Corporation			
X-Ray Photograph of 1/4 inch ORNL Sample			
DATE 11/27/56	DRAWN BY	FILE NO. EPS-X-282	FIG. 6

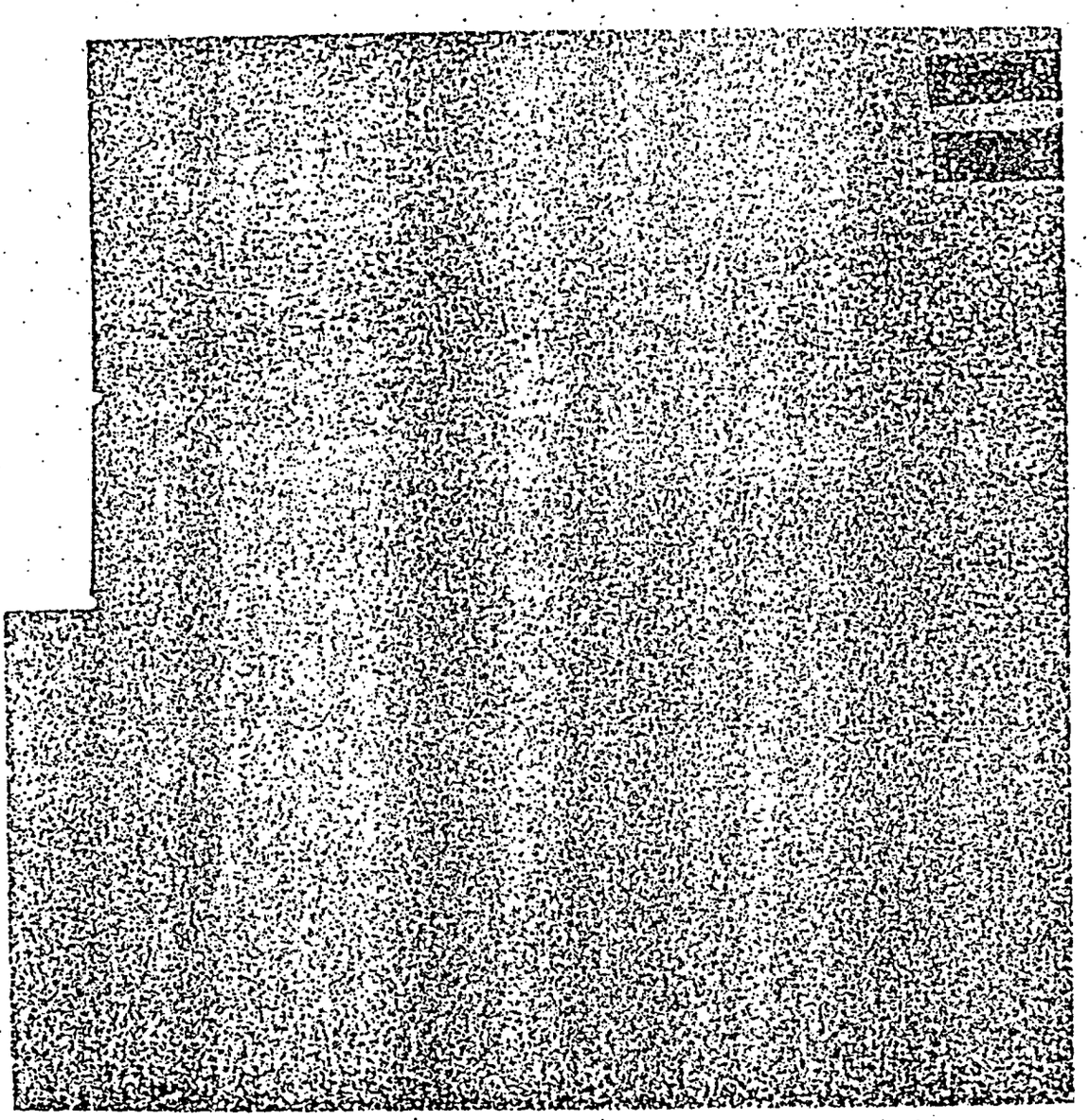

MASSACHUSETTS INSTITUTE OF TECHNOLOGY ENGINEERING PRACTICE SCHOOL UNION CARBIDE NUCLEAR COMPANY A Division of Union Carbide and Carbon Corporation			
X-Ray Photograph of 1/8 inch Brooks and Perkins Sample			
DATE 11/27/56	DRAWN BY	FILE NO. EPS-X-282	FIG. 7

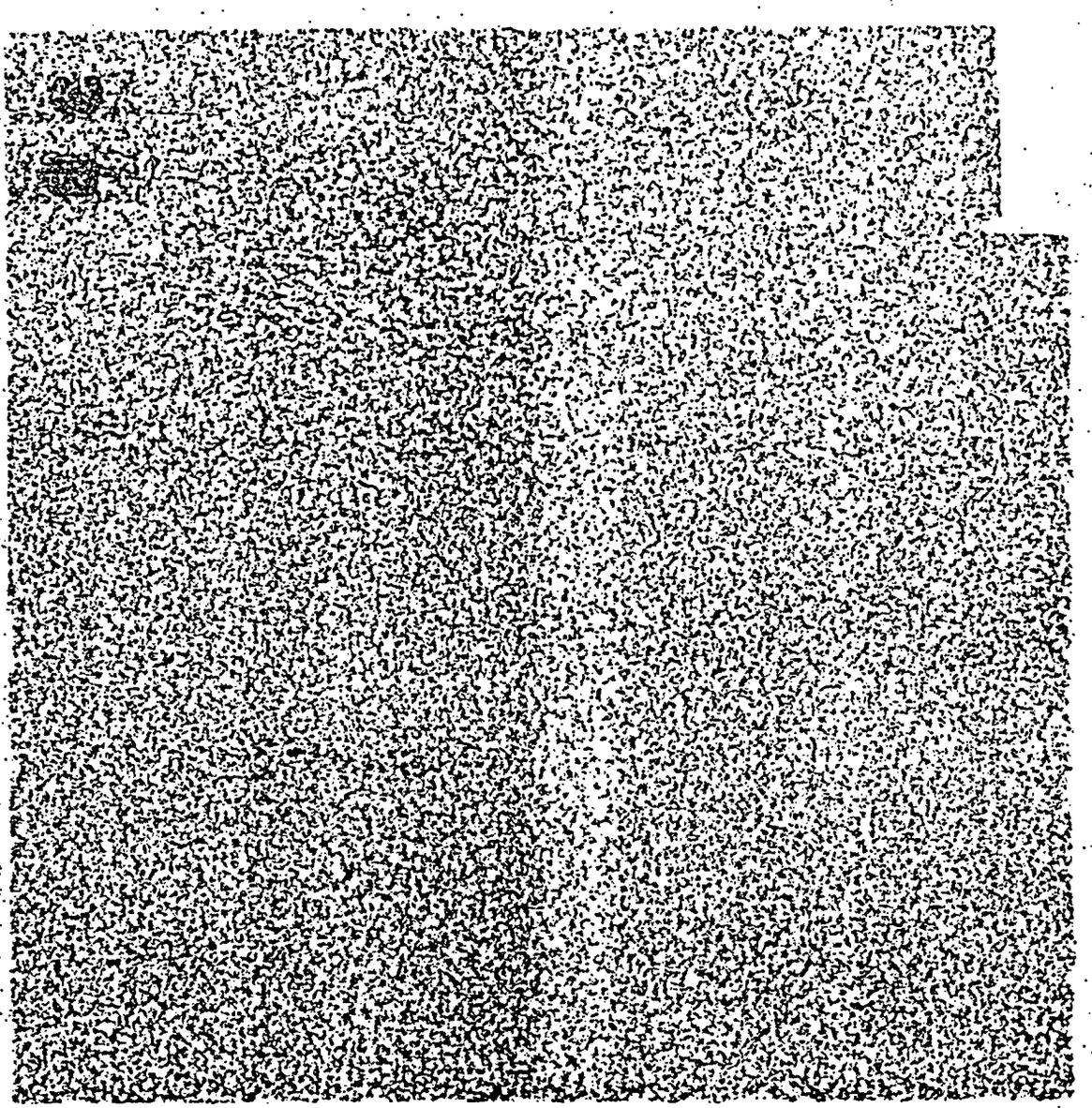

MASSACHUSETTS INSTITUTE OF TECHNOLOGY ENGINEERING PRACTICE SCHOOL UNION CARBIDE NUCLEAR COMPANY A Division of Union Carbide and Carbon Corporation			
X-Ray Photograph of 1/4 inch Brooks and Perkins Sample			
DATE 11/27/56	DRAWN BY	FILE NO. EPS-X-282	FIG. 8

TABLE I

Sample	$\Sigma_{removal}$ cm^{-1}
1/8" Brooks and Perkins	15.6
1/8" ORNL	14.7
1/4" Brooks and Perkins	11.8
1/4" ORNL	11.3

The calculated removal cross section for the 1/8" ORNL sample using the Monte Carlo technique gave $\Sigma_{removal}$ of 13.4 cm^{-1}.

$\Sigma_{removal}$ for a homogeneous mixture of boron carbide and aluminum containing 55% B_4C by volume is 18.9 cm^{-1}.

DISCUSSION OF RESULTS AND CONCLUSIONS

Since the neutron attenuation experiments were not conducted in "good metry", the current does not fall off at an exponential rate given by $I_0e^{-\Sigma x}$. This is due to the neutrons entering the boral at all different angles; thus the average neutron will pass through an amount of boral greater than just the thickness, x. This is indicated in the results by a $\Sigma_{removal}$ for the 1/8" sample larger than that for a 1/4" sample. The first 1/8" of a boral sheet is clearly more effective in removing neutrons than the next 1/8". This effective removal cross section, although it does not have a precise physical significance may be used, however, to obtain an indication of neutron attenuation. A good estimate of the true thermal neutron cross may be obtained by linear extrapolation of the results of the 1/8" and 1/4" thick samples to zero thickness. This gives a value of $\Sigma_a = 18.1$ cm^{-1} for the ORNL boral and $\Sigma_a = 19.4$ cm^{-1} for the Brooks and Perkins sample, both in good agreement with the Σ_a obtained by homogenization.

The good agreement between the experimental $\Sigma_{removal}$ of 14.7 and Monte Carlo calculated value of 13.4 cm^{-1} for the 1/8" ORNL sample demonstrates that these removal cross sections may be predicted fairly accurately by this procedure. The Monte Carlo type calculation has its disadvantages, however, in that it is tedious and time consuming, and electronic computers are of little help. The measurement of x_p^b, the distance a neutrons "sees", must be determined visually.

Robert O. Maak
Robert O. Maak

Blynn E. Prince
Blynn E. Prince

Peter C. Rekemeyer
Peter C. Rekemeyer

APPENDIX

A. Angular Distribution of Neutrons from Thermal Column (6)

An expression is derived below for $F(\underline{\Omega})$, the angular distribution of neutrons from the top of the graphite thermal column. The derived distribution should closely approximate the physical case, and can be readily applied in a hand Monte Carlo calculation (Appendix B).

The graphite thermal column is shown schematically in Figure 9. The boral sample is placed in close proximity to the top of the column and will be assumed to be at w = 0. The thermal neutron flux in the column is well represented by an exponential decrease in the vertical direction and a cosine variation in the horizontal x, y plane (2). Since the center of the column is several diffusion lengths from the x, y boundaries, leakage in these directions will be neglected, i.e., the column is assumed infinite in the x, y plane. Then,

$$\phi = \phi_o e^{-k w} \tag{1}$$

where k is determined experimentally and ϕ_o is the flux at the top of the fuel region.

The scattering collision density in the graphite is,

$$H(w) = \Sigma_s \phi_o e^{-k w} \text{ collisions/cm}^3\text{-sec} \tag{2}$$

Then the number of scattering collisions per sec in the volume element, dV, is H(w) dV. If the scattering is assumed isotropic, the scattered neutrons will leave dV equally in all directions. The number crossing unit area of a sphere of radius r about dV is:

$$\frac{H(w)\, dV\, e^{-\Sigma r}}{4\pi r^2} \text{ neutrons/cm}^2\text{-sec} \tag{3}$$

The corresponding number crossing unit area in the x, y plane about the origin and moving in the direction $\underline{\Omega}$ is given by multiplying (3) by cos θ. Integration over the volume of the graphite results in the total outward neutron current S_o.

$$S_o = \int_V \frac{dV\, H(w)\, e^{-\Sigma r} \cos\theta}{4\pi r^2} \text{ neutrons/cm}^2\text{-sec} \tag{4}$$

If the neutron current were isotropic, the angular distribution would be given by:

$$F_{\text{isotropic}}(\underline{\Omega}') = \frac{S_o}{2} = \text{(neutrons per cm}^2\text{-sec, moving in the direction } \underline{\Omega}' \text{ per unit solid angle)} \tag{5}$$

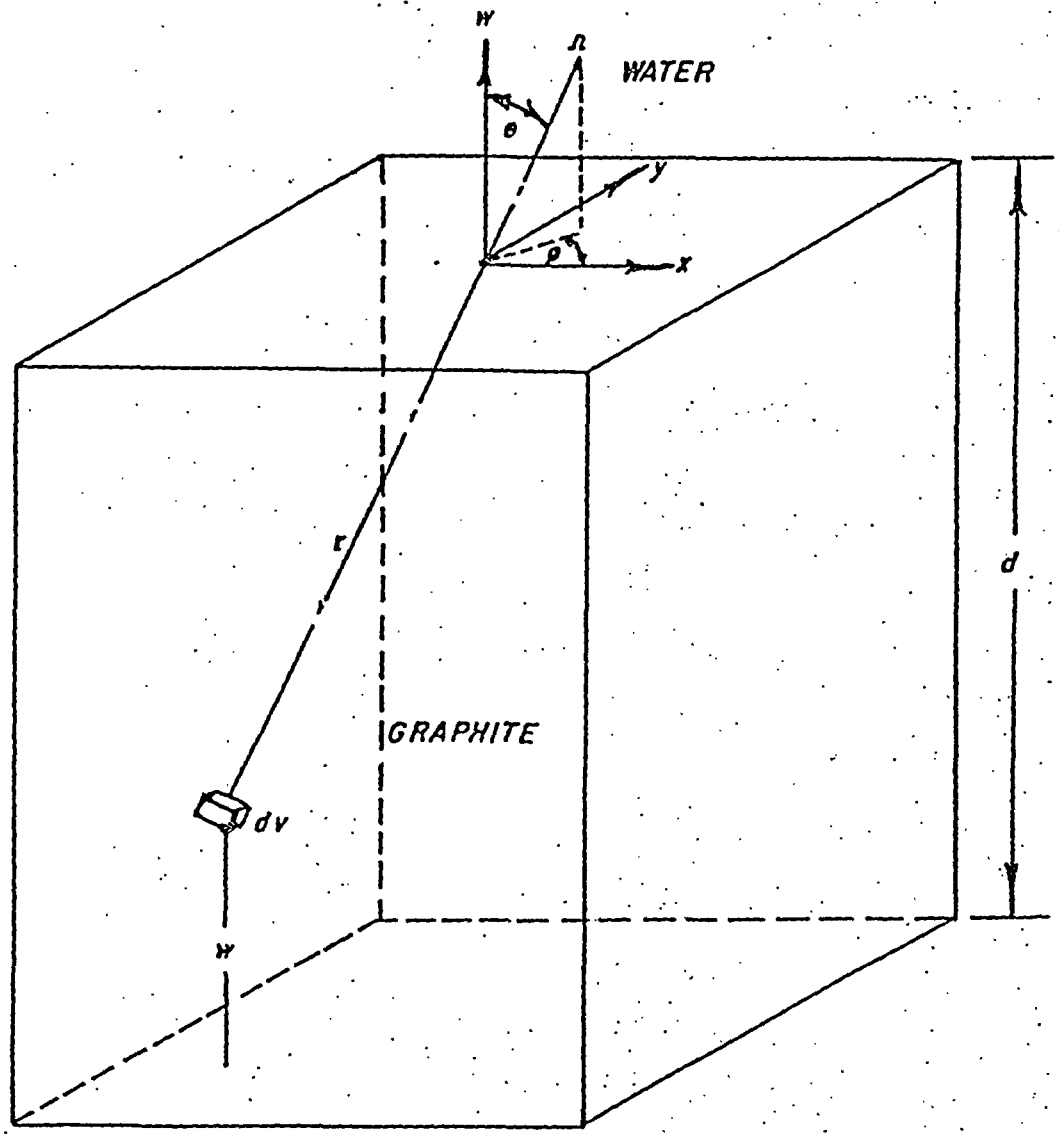

FUEL REGION

MASSACHUSETTS INSTITUTE OF TECHNOLOGY
ENGINEERING PRACTICE SCHOOL
UNION CARBIDE NUCLEAR COMPANY
A Division of Union Carbide and Carbon Corporation

SCHEMATIC DIAGRAM OF THERMAL COLUMN

DATE	DRAWN BY	FILE NO.	FIG.
11-27-56	R.O.M.	EPS-X-282	9

The actual distribution from the column follows by writing the contribution to $F(\underline{\Omega}')$ from dV:

$$dF(\underline{\Omega}') = \frac{H(w)\, e^{-\Sigma r} \cos\theta}{4\pi r^2} \cdot \frac{\delta(\underline{\Omega} - \underline{\Omega}')\, dV}{2\pi} \qquad (6)$$

= (neutrons per cm^2-sec from dV going in the direction $\underline{\Omega}'$ per unit solid angle)

In spherical coordinates $dV = r^2 \sin\theta\, d\theta\, d\phi\, dr = r^2\, dr\, d\underline{\Omega}$. Thus,

$$F(\underline{\Omega}') = \int_r dr \int_{\underline{\Omega}} d\underline{\Omega}\, H(w)\, e^{-\Sigma r} \cos\theta\, \delta(\underline{\Omega} - \underline{\Omega}') \qquad (7)$$

The Dirac delta function has the property (1),

$$\delta(\underline{\Omega} - \underline{\Omega}') = 0, \quad \underline{\Omega} \neq \underline{\Omega}' \qquad (8)$$

and

$$\int_{4\pi} \delta(\underline{\Omega} - \underline{\Omega}')\, d\underline{\Omega} = 1 \qquad (9)$$

where the integration variable $\underline{\Omega}$ ranges over $\underline{\Omega}'$.

In spherical coordinates (9) becomes,

$$\int_{\phi=0}^{2\pi} \int_{\theta=0}^{\frac{\pi}{2}} \delta(\cos\theta - \cos\theta')\, \delta(\phi - \phi') \sin\theta\, d\theta\, d\phi = 1 \qquad (10)$$

Rewriting (7) explicitly, noting $w = d - r\cos\theta$,

$$F(\underline{\Omega}') = \int_0^{2\pi} d\phi \int_0^{\pi/2} d\theta \int_0^{d/\cos\theta} dr\, \frac{\Sigma_s \phi_o}{8\pi^2} e^{-k(d - r\cos\theta) - \Sigma r} \cos\theta \sin\theta\, \delta(\cos\theta - \cos\theta')\, \delta(\phi - \phi') \qquad (11)$$

$$0 \leq \theta' \leq \pi/2 \qquad 0 \leq \phi' \leq 2\pi$$

or,

$$F(\underline{\Omega}') = \int_0^{2\pi} d\phi \int_0^1 d\mu \int_0^{d/\mu} dr\, \frac{\Sigma_s \phi_o}{8\pi^2} e^{-k(d - r\mu) - \Sigma r} \mu\, \delta(\mu - \mu')\, \delta(\phi - \phi') \qquad (12)$$

where $\mu = \cos\theta$

performing the integration over r,

$$F(\underline{\Omega}') = \int_{\phi=0}^{2\pi} d\phi \int_{\mu=0}^{1} d\mu \, \frac{\Sigma_s \phi_o}{8\pi^2} \left(\frac{e^{-\Sigma d/\mu} - e^{-kd}}{k\mu - \Sigma}\right) \mu \, \delta(\mu - \mu') \delta(\phi - \phi') \qquad (13)$$

The integral over μ and ϕ follows from the definition of the delta function (1),

$$F(\underline{\Omega}') = \frac{\Sigma_s \phi_o}{8\pi^2} \left(\frac{e^{-\Sigma d/\mu'} - e^{-kd}}{k\mu' - \Sigma}\right) \mu' \qquad (14)$$

Equation (14) can be further simplified by noting the relative magnitudes of the parameters Σ, k, and d (Appendix D).

$$\Sigma = 0.533 \text{ cm}^{-1} \qquad k = 0.0312 \text{ cm}^{-1} \qquad d = 308 \text{ cm}$$

Thus, $F(\underline{\Omega})$* will be closely approximated by neglecting the first term in comparison to the second.

$$F(\underline{\Omega}) = F(\theta) \cong \frac{\Sigma_s \phi_o}{8\pi^2} \left(\frac{e^{-kd \cos\theta}}{\Sigma - k \cos\theta}\right) \qquad (15)$$

Note that $F(\underline{\Omega})$ is independent of azimuth, as expected from symmetry considerations.

Consider next the neutron distribution in polar angle $f(\theta)$. In the subsequent application of the Monte Carlo method (Appendix B), interpretation of the following will be simplified if use is made of probability density functions (5). Define $f(x)dx$ as the probability that x lies in the interval dx at x. Then $f(x)$ is the probability density function for x. Let the interval of x be $(-\infty, +\infty)$. Since the point x must lie within the interval,

$$\int_{-\infty}^{\infty} f(x) \, dx = 1$$

The probability that x is between $-\infty$ and x_o is,

$$P(x_o) = \int_{-\infty}^{x_o} f(x) \, dx$$

*The primed symbol on the angular coordinates is dropped in the remainder of this section.

It is next shown that the neutron angular distributions can be interpreted as probability density functions.

$$\int_{2\pi} F(\underline{\Omega})\, d\underline{\Omega} = S_o \tag{16}$$

Define the normalized distribution $F'(\underline{\Omega})$ by:

$$\int_{2\pi} F'(\underline{\Omega})\, d\underline{\Omega} = 1 \tag{17}$$

thus,

$$F'(\underline{\Omega}) = \frac{1}{S_o} F(\underline{\Omega}) = \frac{F(\underline{\Omega})}{\int_{2\pi} F(\underline{\Omega}) d\underline{\Omega}} \tag{18}$$

The denominator of Equation (18) is evaluated as follows. From the aximuthal symmetry, $d\underline{\Omega} = 2\pi \sin\theta\, d\theta$. Thus,

$$\int_{2\pi} F(\underline{\Omega})\, d\underline{\Omega} = \int_0^{\pi/2} \frac{\Sigma_s \phi_o}{8\pi^2} e^{-kd} \frac{\cos\theta}{\Sigma - k\cos\theta} 2\pi \sin\theta\, d\theta$$

$$= \frac{\Sigma_s \phi_o}{4\pi} \int_0^1 \frac{\mu\, d\mu}{\Sigma - k\mu}$$

$$= \frac{\Sigma_s \phi_o}{4\pi} e^{-kd} \left(\frac{\Sigma}{k^2} \ln\left(\frac{\Sigma}{\Sigma - k}\right) - \frac{1}{k}\right) \tag{19}$$

Equation (18) becomes,

$$F'(\underline{\Omega}) = F'(\theta) = \left(\frac{1}{2\pi\left(\frac{\Sigma}{k^2} \ln\left(\frac{\Sigma}{\Sigma - k}\right) - \frac{1}{k}\right)}\right) \frac{\cos\theta}{\Sigma - k\cos\theta} \tag{20}$$

From the form of (17), $F'(\underline{\Omega})$ can be interpreted as the probability density function (p.d.f.) for $\underline{\Omega}$. The corresponding p.d.f. in polar angle θ follows from (17) by noting,

$$\int_0^{\pi/2} f(\theta)\, d\theta = 1 \tag{21}$$

Rewriting Equation (17),

$$\int_{2\pi} F'(\underline{\Omega})\, d\underline{\Omega} = \int_0^{\pi/2} F'(\theta)\, 2\pi \sin\theta\, d\theta$$

Thus,

$$f(\theta) = 2\pi F'(\theta) \sin\theta \tag{22}$$

or,

$$f(\theta) = \frac{1}{N} \frac{\cos\theta \sin\theta}{\Sigma - k\cos\theta} \tag{23}$$

$$\text{where } N = \left(\frac{\Sigma}{k^2} \ln\left(\frac{\Sigma}{\Sigma - k}\right) - \frac{1}{k}\right) \tag{24}$$

In the application of the Monte Carlo method, the integrated probability curve, P(θ), is necessary.

$$P(\theta) = \int_0^{\theta} f(\theta')\, d\theta' = \frac{1}{N} \int_0^{\theta} \frac{\cos\theta' \sin\theta'\, d\theta'}{\Sigma - k\cos\theta'}$$

$$= \frac{1}{N} \left[\frac{\Sigma}{k^2} \ln\left(\frac{\Sigma - k\cos\theta}{\Sigma - k}\right) + \frac{(\cos\theta - 1)}{k}\right] \tag{25}$$

where the normalization factor, N, is given by Equation (24)

This curve is plotted in Figure 10 for the parameters of the graphite column listed in Appendix D.

B. Monte Carlo Procedure for Theoretical Determination of Neutron Attenuation by Boral (6)

A mathematical model is given below expressing the attenuation of thermal neutrons by a boral plate. It is then shown how the Monte Carlo procedure can be applied to this model to obtain numerically the attenuation and effective absorption cross section of Boral.

In Figure 11a a thin absorbing foil is shown representing the indium exposed to the thermal neutrons from the column. The saturated activity of the foil per unit area, Z_o, is derived from first principles. The differential activity, dZ_o, from absorption of $F(\underline{\Omega})\, dA\, d\underline{\Omega}$ neutrons, which cross dA at A, in the direction range $d\underline{\Omega}$ about $\underline{\Omega}$ is,

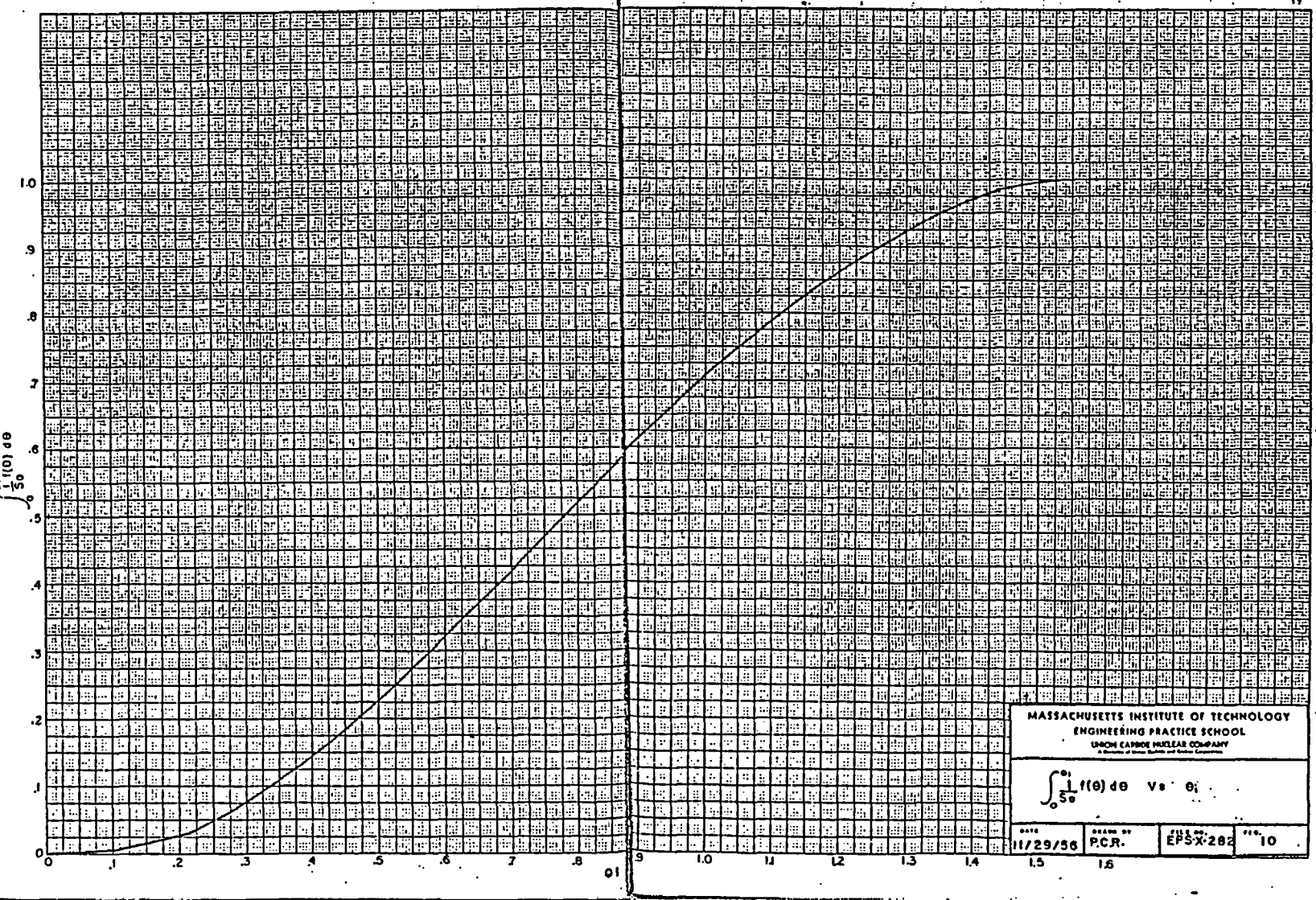
$\int_0^{\theta_i} \frac{1}{5\theta} f(\theta)\, d\theta$
0
.1
.2
.3
.4
.5
.6
.7
.8
.9
1.0
θ_i
1.1
1.2
1.3
1.4
1.5
1.6
MASSACHUSETTS INSTITUTE OF TECHNOLOGY
ENGINEERING PRACTICE SCHOOL
UNION CARBIDE NUCLEAR COMPANY
$\int_0^{\theta_i} \frac{L}{5\theta} f(\theta)\, d\theta$ Vs θ_i
DATE 11/29/56
DRAWN BY P.C.R.
FILE NO. EPS-X-282
FIG. 10

(A)

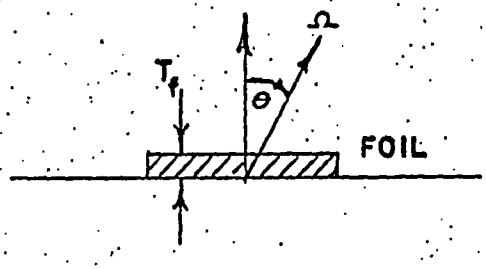

THERMAL COLUMN

(B)

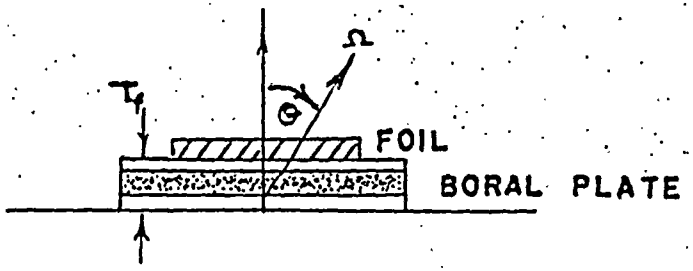

THERMAL COLUMN

MASSACHUSETTS INSTITUTE OF TECHNOLOGY
ENGINEERING PRACTICE SCHOOL
UNION CARBIDE NUCLEAR COMPANY
A Division of Union Carbide and Carbon Corporation

SCHEMATIC DIAGRAM OF INDIUM FOIL
(A). BARE
(B). BACKED BY BORAL PLATE

DATE	DRAWN BY	FILE NO.	FIG.
11-27-56	ROM	EPS-X-282	11

$$dZ_o = F(\underline{\Omega})\,(1 - e^{-\Sigma_f t_f/\cos\theta})\,d\underline{\Omega}\,dA$$

$$Z_o = \frac{\int_{\underline{\Omega}}\int_A F(\underline{\Omega})(1 - e^{-\Sigma_f t_f/\cos\theta})\,d\underline{\Omega}\,dA}{\int_A dA} \qquad (26)$$

Since the foil is homogeneous, the integral over A will not affect the result. This will not be true, however, for the case of a foil backed by the heterogeneous boral plate (Figure 11b). The differential foil activity, dZ, is now given by,

$$dZ = \begin{pmatrix}\text{neutrons crossing dA at}\\ \text{A in the direction range}\\ d\underline{\Omega}\text{ about }\underline{\Omega}\end{pmatrix}\begin{pmatrix}\text{probability of}\\ \text{penetrating}\\ \text{plate}\end{pmatrix}\begin{pmatrix}\text{probability}\\ \text{of absorption}\\ \text{by foil}\end{pmatrix}$$

Since the boron carbide has a large absorption cross section (Σ_a = 72.2 cm^{-1}) (Appendix D), the assumption is made that any neutrons scattering in the plate are changed in direction and effectively absorbed by the boron. Let $x_p^b(\underline{\Omega},A)$ and $x_p^a(\underline{\Omega},A)$ be the respective thicknesses "seen" by a neutron crossing dA at A in the direction range $d\underline{\Omega}$ at $\underline{\Omega}$. The probability or fraction of neutrons penetrating the plate is,

$$e^{-(\Sigma_b x_p^b + \Sigma_a x_p^a)}$$

$x_p^a(\underline{\Omega},A)$ is related to $x_p^b(\underline{\Omega},A)$ by:

$$x_p^a(\underline{\Omega},A) = t_p/\cos\theta - x_p^b(\underline{\Omega},A) \qquad (27)$$

then,

$$dZ = F(\underline{\Omega})e^{-\Sigma_b x_p^b(\underline{\Omega},A)-\Sigma_a(t_p/\cos\theta - x_p^b(\underline{\Omega},A))}(1-e^{-\Sigma_f t_f/\cos\theta})d\underline{\Omega}dA$$

and the average activity per unit area induced in the foil is,

$$\bar{Z} = \frac{\int_{\underline{\Omega}} d\underline{\Omega}\int_A dA\, F(\underline{\Omega})e^{-\Sigma_b x_p^b(\underline{\Omega},A)-\Sigma_a(t_p/\cos\theta - x_p^b(\underline{\Omega},A)}(1-e^{-\Sigma_f t_f/\cos\theta})}{\int dA} \qquad (28)$$

Since the boron carbide particles are distributed in random sizes and positions within the aluminum matrix, analytical solution of this integral is not possible. Instead, it is proposed to apply the Monte Carlo procedure to obtain an approximate solution. Interpretation of the remainder of this section will be simplified if Equation (28) is rewritten in terms of probability density functions (Appendix A). Define:

$$g(A) = \frac{1}{\int dA} = \frac{1}{A_o} \tag{29}$$

where A_o is the total area of the plate exposed to the neutron beam. Then,

$$\int_{A_o} g(A)\, dA = 1 \tag{30}$$

Thus g(A) is the probability density function in position A. Physically Equation (29) states that the neutrons are randomly incident over the plate area, A_o, i.e., for one incident neutron the probability g(A)dA of striking dA is the fraction of the total area A_o, represented by dA.

From Appendix A, $F(\underline{\Omega})$ is related to the probability distribution, f(θ) by,

$$f(\theta)d\theta = \frac{F(\underline{\Omega})d\underline{\Omega}}{S_o} = \frac{2\pi F(\theta)\sin\theta}{S_o} \tag{31}$$

where $F(\underline{\Omega}) = F(\theta)$

Assuming that, on the average, $x_p^b(\underline{\Omega},A)$ is independent of azimuth, the integral (28) can now be rewritten:

$$\bar{Z} = \int_\theta d\theta \int_A dA\, Z(\theta,A)\, f(\theta) g(A)\, dA \tag{32}$$

where;

$$Z(\theta,A) = S_o\, e^{-\Sigma_b x_p^b(\theta,A) - \Sigma_a (t_p/\cos\theta - x_p^b(\theta,A))} \left(1 - e^{-\Sigma_f t_f/\cos\theta}\right) \tag{33}$$

In Equation (33), Z(θ,A) can be interpreted as the foil activity per unit area induced by S_o neutrons per cm^2 incident on the boral plate at A in the direction θ. The weighted average with respect to the probability distributions in θ and A, of the neutrons from the column gives the average foil activity per unit area.

The Monte Carlo method consists in solving Equation (32) by sampling of the

variables θ and A, and studying the individual histories of the neutrons traversing the plate. Let N be the total number of histories studied, and i be the index for the i^{th} sample neutron. If $\hat{Z}$ is the estimate of $\bar{Z}$ obtained from this procedure:

$$\hat{Z} = \frac{1}{N} \sum_{i=1}^{N} Z(\theta_i, A_i) \tag{34}$$

In the method of random selection of the variables θ_i and A_i, decisions are made by means of random numbers. In this problem, random selection of A_i and an alternative method of systematic sampling of θ_i was used. It is shown in Appendix C that use of the latter method reduces the statistical variance of $\hat{Z}$. A description of the sampling procedure is given below.

A random number, y, lying in the interval (0,L) is a number equally probable to lie at any point in that interval. It is convenient to restrict y to the particular interval (0,1). Thus y is defined by the rectangular distribution function:

$$g(y) = \begin{cases} 0 & y > 1 \\ 1 & 0 \leq y \leq 1 \\ 0 & y < 0 \end{cases} \tag{35}$$

$$\int_{-\infty}^{\infty} g(y)\, dy = 1 \tag{36}$$

In the method of random sampling, the decision for the random number y results from comparing the probability that θ lies between θ and $\theta + d\theta$ to the probability that y lies between y and y + dy;

$$f(\theta)d\theta = g(y)\, dy \tag{37}$$

$$g(A)dA = g(y)dy \tag{38}$$

Then,

$$\int_0^{\theta_2} f(\theta)\, d\theta = \int_{-\infty}^{y_i} g(y)\, dy = \int_0^{y_i} 1\, dy = y_i \tag{39}$$

$$\int_0^{A_i} g(A)\, dA = \int_{-\infty}^{y_i} g(y)\, dy = y_i \tag{40}$$

If the plate area, A_o, is normalized to unity, from Equation (29),

$$g(A) = g(y) \tag{41}$$

$$A_i = y_i \tag{42}$$

Alternatively, if the total area is A_o,

$$A_i = y_i A_o \tag{43}$$

If random selection is also used for θ_i,

$$\int_0^{\theta_i} f(\theta)\, d\theta = P_i(\theta_i) = y_i \tag{44}$$

The alternative procedure of systematic selection of θ_i is described next. The physical interpretation is that the θ_i's are chosen at the midpoints of small finite intervals which represent equal probability ranges for θ from zero to $\pi/2$. The neutron history studied at θ_i is assumed to be the average history over the corresponding angular interval.

Mathimatically, θ_i is selected according to the formula;

$$P(\theta_i) = \int_0^{\theta_i} f(\theta)\, d\theta = \frac{i - 1/2}{N} \qquad i = 1, 2 \ldots\ldots N \tag{45}$$

In Figure 10, where the integrated probability curve $P(\theta)$ is shown, Equation 45 is interpreted graphically by dividing the total probability interval,

$$P(\pi/2) = 1 = \int_0^{\pi/2} f(\theta)\, d\theta \tag{46}$$

into N equal parts. θ_i is read from the curve, corresponding to the midpoint of the i^{th} interval on the $P(\theta)$ axis. Letting θ_i^L and θ_i^U represent the lower and upper limits of the i^{th} angular interval;

$$P(\theta_i^L \leq \theta \leq \theta_i^U) = \int_{\theta_i^L}^{\theta_i^U} f(\theta)\, d\theta = \frac{1}{N} \tag{47}$$

= probability that θ is between θ_i^L and θ_i^U.

θ_i, determined from Equation (45) has the property $\theta_i^L < \theta_i < \theta_i^U$. Thus,

$$\int_{\theta_i^L}^{\theta_i^U} f(\theta)\, d\theta = \frac{1}{N} \simeq f(\theta_i)\, \Delta\theta_i \simeq f(\theta)\, d\theta \qquad (48)$$

where it is assumed that N is large.

The procedure for the Monte Carlo calculation of $\hat{Z}$ is now complete. Rewriting Equation (26) in terms of $f(\theta)$,

$$Z_o = \int_{\theta=0}^{\pi/2} S_o\left(1 - e^{-\Sigma_f t_f/\cos\theta}\right) f(\theta)\, d\theta \qquad (49)$$

The thermal neutron attenuation by the boral plate is the ratio of the foil activities,

$$R = \frac{\hat{Z}}{Z_o} \qquad (50)$$

where it is noted that the magnitude of the total neutron current S_o will cancel from the result. The effect thermal absorption cross section Σ_B is given by,

$$R = e^{-\Sigma_B t_p} \qquad (51)$$

C) Analysis of Variance (6)

In this section a discussion is given of the accuracy of the Monte Carlo calculation of $\hat{Z}$. The reason for the use of systematic sampling of θ is shown by proving that the procedure will reduce the variance of $\hat{Z}$.

The variance of a single estimate of $\bar{Z}$, obtained from N neutron histories, is given by;

$$V = \frac{\overline{(Z - \bar{Z})^2}}{N} = \frac{\overline{Z^2} - 2\bar{Z}\bar{Z} + \bar{Z}^2}{N}$$

$$= \frac{\overline{Z^2} - \bar{Z}^2}{N} \qquad (52)$$

Since the true value of Z cannot be known accurately, the best estimate of the variance is given by,

$$V \approx \frac{\hat{Z^2} - \hat{Z}^2}{N-1} *$$

$$\approx \frac{\sum_{i=1}^{N} \frac{Z_i^2}{N} - \left(\sum_{i=1}^{N} \frac{Z_i}{N}\right)^2}{N-1} \approx \sigma^2 \qquad (53)$$

where σ is the standard deviation of the calculated value $\hat{Z}$.

Suppose the variables Θ and A are selected randomly. Let $\hat{Z}_1$ be the estimate of Z obtained from this procedure.

$$\hat{Z}_1 = \frac{1}{N} \sum_{i=1}^{N} Z_1 (\Theta_i, A_i) \qquad (54)$$

and,
$$V_1 = \frac{1}{N} \overline{(Z_1 - \bar{Z})^2} \qquad (55)$$

$$= \frac{1}{N} \iint \left[Z(\Theta,A) - \bar{Z}\right]^2 f(\Theta)\, g(A)\, d\Theta\, dA \qquad (56)$$

Define the conditional average,

$$\bar{Z}(j\Theta) = \int Z(\Theta,A)\, g(A)\, dA \qquad (57)$$

Verbally, $\bar{Z}(j\Theta)$ is the average value of Z given Θ. Add and subtract this quantity to the bracketed term under the integral of Equation (56).

$$V_1 = \frac{1}{N} \iint \left[(Z - \bar{Z}(j\Theta) + \bar{Z}(j\Theta) - \bar{Z})\right]^2 f(\Theta)\, g(A)\, d\Theta\, dA \qquad (58)$$

Algebracially expanding the bracketed term,

$$\left[Z(\Theta,A) - \bar{Z}\right]^2 = \left[(Z - \bar{Z}(j\Theta)^2 + 2(Z - \bar{Z}(j\Theta))(\bar{Z}(j\Theta) - \bar{Z}) + (\bar{Z}(j\Theta) - \bar{Z})^2\right] \qquad (59)$$

$$(Z - \bar{Z}(j\Theta))(\bar{Z}(j\Theta) - \bar{Z}) = Z\,\bar{Z}(j\Theta) - Z\bar{Z} - \bar{Z}(j\Theta)^2 + \bar{Z}(j\Theta)\bar{Z} \qquad (60)$$

Upon integration over A, noting the definition of $\bar{Z}(j\Theta)$, Equation (59) becomes,

$$\bar{Z}(j\Theta)^2 - \bar{Z}(j\Theta)\bar{Z} - \bar{Z}(j\Theta)^2 + \bar{Z}(j\Theta)\bar{Z} = 0 \qquad (61)$$

*The factor N - 1 eliminates small sample bias.

Hence,

$$V_1 = \frac{1}{N} \iiint \left\{ \left[Z - \bar{Z}(j\theta) \right]^2 + \left[\bar{Z}(j\theta) - \bar{\bar{Z}} \right]^2 \right\} f(\theta)\, g(A)\, d\theta\, dA \qquad (62)$$

$$= \frac{1}{N} \overline{\left[Z_1 - \bar{Z}(j\theta) \right]^2} + \frac{1}{N} \left[\bar{Z}(j\theta) - \bar{\bar{Z}} \right]^2$$

$$= \frac{\overline{V(j\theta)}}{N} + \frac{\left[\bar{Z}(j\theta) - \bar{\bar{Z}} \right]^2}{N} \qquad (63)$$

Consider next the case where θ_i is sampled systematically and A_i is randomly selected. Let the estimate of $\bar{Z}$ obtained by this procedure be $\hat{Z}_2$;

$$\hat{Z}_2 = \frac{1}{N} \sum_{i=1}^{N} Z_2(\theta_i, A_i)$$

The average value of Z_2 is given as;

$$\overline{\hat{Z}_2} = \frac{1}{N} \sum_{i=1}^{N} \int Z(\theta_i, A)\, g(A)\, dA$$

$$= \frac{1}{N} \sum_{i=1}^{N} \bar{Z}(j\theta_i) \qquad (64)$$

where the averaging is only done over the variable A, since the θ_i values are fixed. The variance is given by:

$$V_2 \approx \overline{(\hat{Z}_2 - \bar{\bar{Z}}_2)^2} \qquad (65)$$

$$\approx \overline{\left\{ \frac{1}{N} \sum_{i=1}^{N} \left[Z_2(\theta_i A_i) - \bar{Z}(j\theta_i) \right] \right\}^2}$$

$$\approx \frac{1}{N^2} \overline{\left\{ \sum_{i=1}^{N} \left[Z_2(\theta_i, A_i) - \bar{Z}(j\theta_i) \right] \right\}^2}$$

$$\approx \frac{1}{N^2} \sum_{i=1}^{N} \overline{\left[Z_2(\theta_i, A_i) - \bar{Z}(j\theta_i) \right]^2}$$

The summation sign can be taken outside the average, since all the cross terms will cancel when averaged. Thus:

$$V_2 = \frac{1}{N^2} \sum_{i=1}^{N} V(j\theta_i) \qquad (66)$$

From Appendix B;

$$\frac{1}{N} \cong f(\theta)\, d\theta \tag{67}$$

Hence,

$$V_2 \cong \frac{1}{N} \int V(j\theta)\, f(\theta)\, d\theta = \overline{\frac{1}{N} V(j\theta)} \tag{68}$$

By comparing Equation (68) to (63), it is seen that the variance will be reduced if θ_i is selected systematically.

D) Nuclear Constants

TABLE I

CROSS SECTIONS

Element	Absorption Cross Section at 2200 m/sec (3) ($cm^2 \times 10^{+24}$)	Average Thermal Scattering Cross Section ($cm^2 \times 10^{+24}$)	Density (7) (gms/cm^3)	Macroscopic Total Thermal Cross Section[a] (cm^{-1})
Aluminum	0.230	1.4	2.70	0.096
Boron	775	4	-	-
Carbon	0.0032	4.8	2.22	0.533
Boron Carbide	-	-	2.45 (4)	72.2
Indium	145[b]	-	7.31	4.93[b]

Thermal column characteristics:

$$k = 0.0312 \text{ cm}^{-1}$$

$$d = 308.6 \text{ cm}$$

Foil thickness:

$$t_f = 0.0127 \text{ cm}$$

[a] All thermal absorption cross sections are Maxwell-Boltzmann averaged.

[b] Activation cross section for 54.1 minute Indium-116.

E) Sample Calculations

(1) Procedure

Photomicrographs were taken of the polished cross section of a 1/8" ORNL boral plate. A single frame from the total field scanned is shown in Figure 1. The magnification used was 75X. To obtain a field of the total cross sectional area, including the aluminum cladding, single frames were taken of overlapping sections, trimmed, and joined together. This resulted in a large photograph, representing a total field of 1/8" x 1/4". A 0.01 mm scale was then photographed at the same magnification and superimposed across the top of the picture, i.e., the top surface of the aluminum cladding. In this way, length measurements could be made directly in terms of the actual dimensions of the plate and the boron carbide particles. The total length of the top surface was 0.60 cm, scaled in units of 0.01 mm.

The neutron histories were studied individually by laying a straightedge across the picture, with origin at A_i, measured from one end of the top scale, and inclined at the angle θ_i from the normal to the top surface. In selecting A_i, use was made of a table of random numbers, generated on Oracle. The sampling of A_i and θ_i is illustrated in the calculation of Z_1 below. The thickness $x_p^b(\theta_i, A_i)$ of boron carbide, "seen" by the neutron, was measured along the straightedge using the magnified scale.

For each angle θ_i, paths clockwise and counterclockwise from the normal were taken and the corresponding distances in B_4C were averaged. Whenever edge effects were encountered, the point where the neutron path left the side of the film was extrapolated to the opposite side and the path was continued at the same angle.

(2) Calculations

Z_1:

The first random number used was 0.508600678.

$$A_1 = 0.6 \times 0.508600678 = 0.3051604068 \sim 0.305 \text{ cm}$$

θ_1 is obtained from Figure 10.

$$P(\theta_1) = \frac{0.01}{2} = 0.005$$

$$\theta_1 = 0.105 \text{ radians} = 6.0^\circ$$

The values of x_p^b obtained from the photograph were:

$$x_p^b(+\theta_1,A_1) = 0.027 \text{ cm}$$

$$x_p^b(-\theta_1,A_1) = 0.034 \text{ cm}$$

$$x_p^b(\bar{\theta}_1,A_1) = 0.0305 \text{ cm}$$

The plate thickness measured from the microphotograph was,

$$t_p = 0.326 \text{ cm}$$

Substituting the cross sections and foil thickness given in Appendix D,

$$Z_1 = 0.006561$$

$\hat{Z}$:

Similar sampling of 100 neutron histories gave the following results:

$$\sum_{i=1}^{100} Z_i(\theta_i,A_i) = 0.1636$$

$$\sum_{i=1}^{100} Z_i^2(\theta_i,A_i) = 8.34 \times 10^{-4}$$

$$\hat{Z} = \sum_{i=1}^{100} \frac{Z_i}{100} = 0.001636$$

V:

$$V = \frac{\frac{\sum_i Z_i^2}{N} - \left(\frac{\sum_i Z_i}{N}\right)^2}{N-1}$$

$$= 5.73 \times 10^{-8}$$

$$\sigma = \sqrt{V} = 2.39 \times 10^{-4}$$

$$\hat{Z} = 0.00164 \pm 0.00024$$

Z_o:

The activation of the foil without the boral plate was obtained by numerical integration of Equation (26), using the parameters listed in Appendix D.

$$Z_o = 0.1085$$

R:

$$R = \frac{(0.164 \pm 0.024) \times 10^{-2}}{0.1085}$$

$$= (1.51 \pm 0.22) \times 10^{-2}$$

Σ_B:

$$R = e^{-\Sigma_B t_B} = 1.51 \pm 0.22$$

$$\Sigma_B = 13.4 \text{ cm}^{-1}$$

F) Nomenclature

A_o = Total area of plate exposed to neutron flux.

dA = Differential area element.

dV = Differential volume element.

d = Height of thermal column.

F = Neutron angular distribution function $JF(\underline{\Omega})$ is the number of neutrons from the thermal column, per unit surface area, moving in the direction $\underline{\Omega}$ per unit solid angle.

$f(\theta), F'(\underline{\Omega})$ = Probability density function in neutron direction.

$g(A), f(x)$ = Probability density function in neutron incident position.

H = Scattering collision density.

k = Experimentally determined neutron attenuation coefficient in thermal column.

N = Total number of histories studied.

$P(\theta)$ = Integrated probability distribution.

S_o = Total outward neutron current from thermal column.

t_p = Thickness of boral plate.

t_f = Thickness of indium foil.

$x_p^b(\underline{\Omega}, A)$ = Thickness of boron carbide "seen" by a neutron going in the direction $\underline{\Omega}$ from the thermal column and incident at position A on the surface of the boral plate.

V = Variance.

Z_o = Activity of indium foil per unit surface area with foil exposed to direct flux from column.

$\bar{Z}$ = Average activity of indium foil per unit surface area with foil shielded by boral plate.

$\hat{Z}$ = Monte Carlo estimate of $\bar{Z}$.

θ = Angle between neutron velocity and w-axis.

$\underline{\Omega}$ = Unit vector in direction of the neutron velocity.

Σ = Macroscopic total thermal cross section for graphite.

Σ_s = Macroscopic scattering cross section for graphite.

Σ_b = Macroscopic total thermal cross section for boron carbide.

Σ_a = Macroscopic total thermal cross section for aluminum.

Σ_f = Macroscopic total thermal cross section for indium.

σ = Standard deviation of calculated value of Z.

ϕ = Thermal neutron flux at any point x, y, w.

ϕ_o = Thermal neutron flux at base of thermal column.

μ = cos θ.

μ = Linear gamma ray attenuation coefficient.

$\delta(\underline{\Omega} - \underline{\Omega}')$, $\delta(\theta - \theta')$ = Dirac delta function.

ORNL-2528

Copy ____

Contract No. W-7405-eng-26

Neutron Physics Division

RADIATION TRANSMISSION THROUGH BORAL AND SIMILAR HETEROGENEOUS MATERIALS CONSISTING OF RANDOMLY DISTRIBUTED ABSORBING CHUNKS

W. R. Burrus*

Date Issued

JAN 18 1960

OAK RIDGE NATIONAL LABORATORY
Oak Ridge, Tennessee
operated by
UNION CARBIDE CORPORATION
for the
U.S. ATOMIC ENERGY COMMISSION

*Now at Ohio State University, Department of Physics, Columbus, Ohio.

ABSTRACT

Shields that consist of randomly distributed absorbing chunks in a relatively transparent matrix must contain a greater mass of absorber than homogeneous shields which provide the same attenuation. This is the result of radiation "channeling" between the absorbing chunks. Channeling is particularly important for heterogeneous materials when the mean free path for absorption is comparable to the chunk size. A newly developed method for calculating the transmission of radiation through such heterogeneous shields is described. The numerical results of a calculation of the transmission of thermal neutrons by boral (a B_4C-Al mixture) are given, including the effects of energy and angular distributions on the predicted attenuation. The calculated results are in reasonable agreement with available experimental results.

ACKNOWLEDGEMENTS

This work was initiated in April, 1956 while the author was on assignment from the Wright Air Development Center to the ORNL Lid Tank Shielding Facility. At that time two other members of the LTSF staff, Dr. R. W. Peelle and Mr. J. R. Smolen, the latter on assignment from Pratt and Whitney Aircraft, were considering elementary aspects of the same approach, and many of their ideas are included in this report. Simultaneously, Mr. S. Auslender, also on assignment to ORNL from Pratt and Whitney Aircraft, was interested in the method, and he, too, assisted in the work reported here. The author later discovered that Mr. R. R. Coveyou and Dr. N. M. Smith, Jr. had proposed essentially the same approach at ORNL as early as 1947; in fact, the method of calculation proposed here is based on the Coveyou model.

This work was completed while the author was a consultant to the Nuclear Products Branch of the Lockheed Aircraft Corporation, and appreciation is expressed to that organization, especially to Mr. Alan Liebschutz, for granting this opportunity. The author is also grateful to Mr. Stanley Szawlewicz of WADC for his encouragement.

Mr. R. W. Peelle and Mrs. L. S. Abbott have kindly made extensive editorial contributions to the final manuscript.

TABLE OF CONTENTS

INTRODUCTION

One material commonly used as a thermal-neutron shield is boral,[1-3] a heterogeneous mixture of commercial-grade boron carbide and aluminum sandwiched between aluminum plates. The total sandwich is usually rolled to a thickness of 1/8 or 1/4 in. Since the mixture is not uniform, aluminum-filled regions exist between the chunks of B_4C in the B_4C-Al melt. This is apparent in the Dark Field Illuminated Photomicrograph[4] of a sample of the melt in Fig. 1. The dark chunks are B_4C and the light background is aluminum. The B_4C is, of course, the attenuating material, and, in order to use boral to an optimum advantage, it is necessary to have a qualitative understanding of the effects of the B_4C size and distribution on the thermal-neutron transmission. The same is true of any other heterogeneous shield material which consists of "randomly distributed" chunks.

A first approximation of the transmission of a heterogeneous material may be obtained by assuming that the absorbing material is uniformly distributed instead of heterogeneously distributed and using the conventional theory for homogeneous materials, providing the density of the material used in the calculation is reduced to account for the voids. This "reduced density" is simply

$$(\text{reduced density}) = (\text{true absorbing material density}) \times V \qquad (1)$$

where V is the volume fraction occupied by the absorbing material. This approximation will lead to a lower limit for the actual transmission since nonuniformity in the material will tend to augment the transmission. The importance of this effect has been demonstrated by experiments which have

---

1. V. L. McKinney and T. Rockwell, III, Boral: A New Thermal Neutron Shield, ORNL-242 (1949).
2. A. S. Kitzes and W. O. Hullings, Boral: A New Thermal Neutron Shield, Supplement 1, ORNL-981 (1951).
3. J. R. Smolen, ORNL-CF-56-6-163 (1956) (Classified).
4. R. O. Maak, B. E. Prince, and P. C. Rekemeyer, Boral Radiation Attenuation Characteristics, MIT Engineering Practice School, KT-251 (1956).

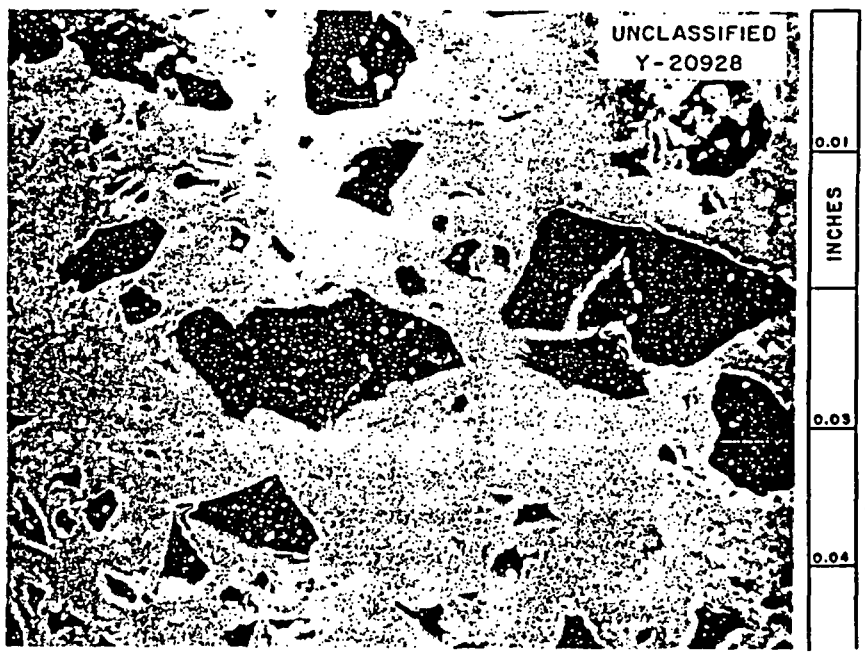

Fig. 1. Typical Samples of ORNL-Fabricated 1/8-in.-thick "Boral". As-polished. 75X

shown that the transmission of thermal neutrons through 1/8-in.-thick boral is much greater (as much as a factor of 40) than the transmission indicated by a homogeneous calculation. Therefore, some other method must be used for computing the transmission through materials such as boral.*

In principle, the transmission of radiation through nonuniform heterogeneous materials may be calculated if the location of the absorbing parts of the material is known. If scattering is neglected, the transmission through a slab of material consisting of a distribution of chunk sizes is given by:

$$T = \int_0^t P(x,t)\tau(x)dx \qquad (2)$$

where

$P(x,t)dx$ = fraction of rays which encounter a thickness of absorbing material between x and x + dx in traversing a total thickness t of material,

$\tau(x)$ = fraction of radiation transmitted through a chunk of material of thickness x.

P(x,t) has been calculated for simple geometric shapes with various orientations (including random) by F. H. Murray,[5] J. A. McLennan,[6] and P. A. M. Dirac.[7] Dirac also developed a general theory for nonuniform media consisting of arbitrarily shaped chunks. $\tau(x)$ may be calculated from the existing theory for the transmission of radiation through homogeneous materials.

*The absorption of dilute mixtures of strongly absorbing chunks was treated by H. Hurwitz and P. F. Zweifel, Nuclear Sci. Eng. 1, 438 (1956), but their formulation would not apply for a mixture as concentrated as boral.

5. F. H. Murray, Fast Effects, Self-Absorption, Fluctuation of Ion Chamber Reading, and the Statistical Distribution of Chord Lengths in Finite Bodies, CP-G-2922 (1945).
6. J. A. McLennan, APEX-197 (1955) (classified).
7. P. A. M. Dirac, Approximate Rate of Neutron Multiplication for a Solid Arbitrary Shape and Uniform Density, British Report MS-D-5 (n.d.).

N. M. Smith[8] considered the case of randomly distributed chunks from another viewpoint. He assumed a hypothetical chunk which is physically similar to actual chunks but mathematically simpler to deal with. The statistical distribution of the thickness of his hypothetical chunk material is shown in Fig. 2 for a 20-cm-thick slab having two-thirds of its volume occupied by chunks which have an average diameter of about 3 cm. $\tau(x)$ is also shown in Fig. 2 for exponential attenuation with an attenuation length of 2 cm. It is obvious that the over-all transmission is much greater than it would be in the homogeneous case, in which all the rays pass through (2/3) x 20 cm of material. In other words, the rays which statistically penetrate less than the average material thickness control the over-all transmission when the transmission $\tau(x)$ of a chunk is much less than unity. This geometrical channeling of rays between chunks is known as the "channeling effect."

R. R. Coveyou[9] has suggested a model to calculate the approximate transmission of radiation through materials in which the channeling effect is important. The material is considered to be divided into layers that have a thickness characteristic of the size of the chunks. Each layer is analogous to a sieve made from attenuating material. Part of the radiation may pass unattenuated through the holes between the chunk material in a given layer, and the rest must pass attenuated through the chunk material. The holes in the layers are assumed to be located statistically independent of holes in adjacent layers so that the over-all transmission is the product of the transmission of each layer. As the chunks are made more attenuating, the radiation passing through the holes between the chunks becomes more important.

In the discussion that follows a method of calculation based on the Coveyou model is presented. The model itself is first discussed and then

---

8. N. M. Smith, Transmission and Scattering of Radiation in Random Aggregates of Pebbles, CNL-21, Revised (n.d.).
9. R. R. Coveyou, Oak Ridge National Laboratory, private communication.

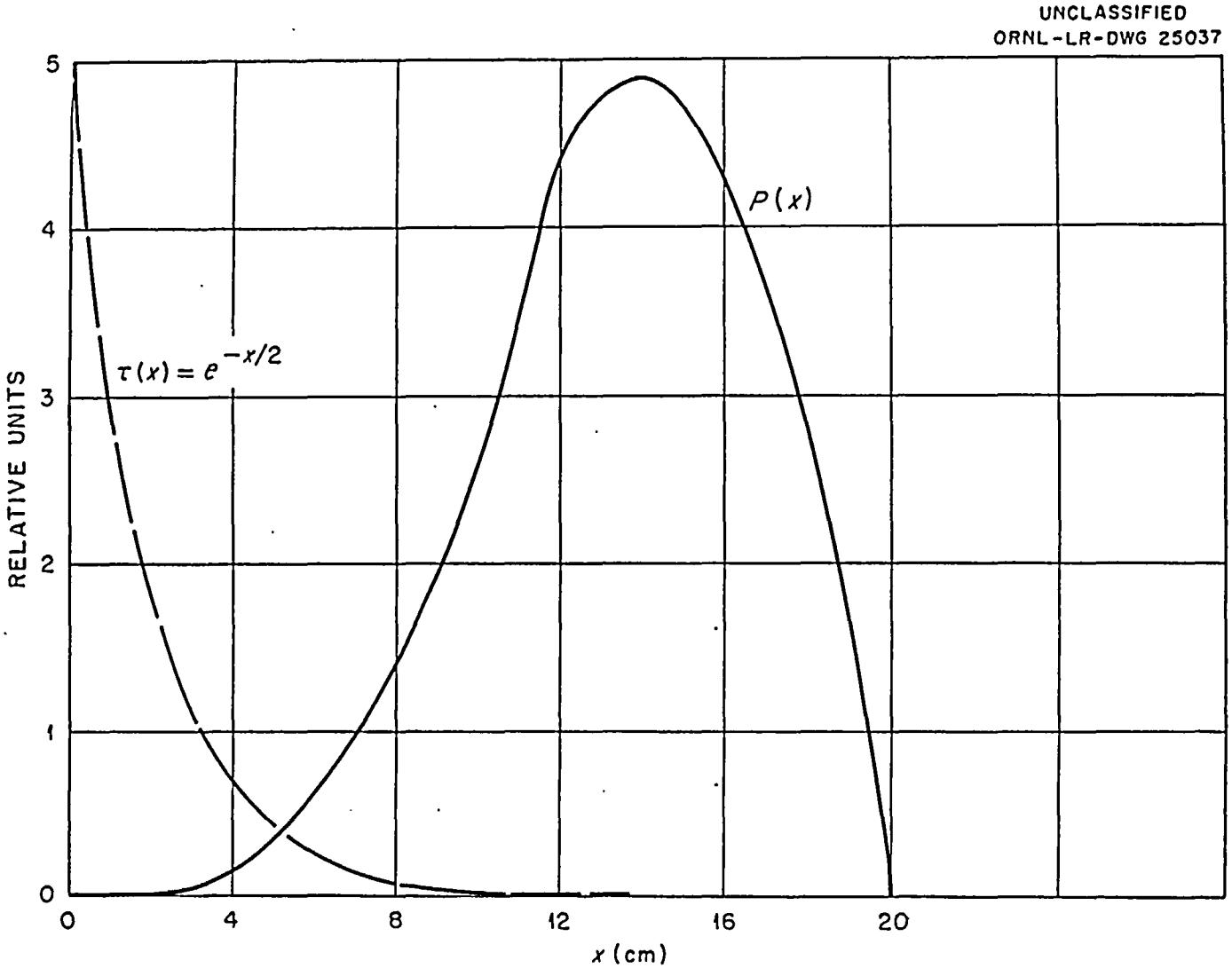

Fig. 2. The Probability $P(x)$ of Penetrating x cm of Chunk Material in Traversing a 20-cm Slab.

extended to include a distribution of various chunk sizes and materials. For simplicity, it is first assumed that the neutron radiation is monoenergetic and normally incident on the face of a plane slab. Exponential attenuation in the chunk material is assumed. The results are then extended to remove these restrictions. An attempt is made at all stages of the development to provide an insight into the relations between transmission and the physical parameters of the chunks involved, and approximations that clarify these relations are emphasized. Scattering is not considered in the calculation.

The applicability of the proposed method is demonstrated in the last two sections of the report in which the transmission of thermal neutrons through a 1/8-in. thickness of boral is calculated, and the results are compared with the transmission indicated by experiments.

I. METHOD OF CALCULATION

Formulas for Materials with Single-Sized Right Cylindrical Chunks

The transmission through a slab consisting of a "random distribution" of single-sized chunks is computed first because of its simplicity. It is assumed that the chunks are right cylinders (cubes, circular cylinders, etc.) with their generators normal to the surface of the slab. Right cylindrical chunks are chosen because it makes the division into layers easy and because a ray that passes through a normally oriented right cylinder always passes through a chunk thickness equal to the cylinder height.

The concept of "random distribution" may be clarified by describing an artificial procedure which yields such a distribution. Randomly selected coordinates (in the desired region) are picked for each chunk in the distribution. If this selection causes two or more chunks to overlap, the selection is rejected and another random assignment is made. Eventually, a selection will be found which is physically realizable. In the simple case of identical cubic chunks, any volume fraction up to unity may be obtained in this manner, although it will require a large number of trials to achieve a realizable distribution as the volume fraction approaches unity.

Chunks which are dumped into a container with no preference as to order or arrangement can be thought of as "randomly packed" chunks as opposed to "randomly distributed" chunks. Randomly packed chunks are usually in intimate contact with at least two neighboring chunks, whereas randomly distributed chunks are not likely to be in contact. If spheres are distributed within a container in the most compact manner, it is possible to obtain volume fractions of 0.74. If the spheres are dumped into the container so that they are "randomly packed," experimental volume fractions of about 0.5 to 0.6 are obtained, depending on the speed and uniformity of pouring, the conditions of the surface of the spheres, etc.

As the actual volume fraction of a distribution of chunks increases, the packing tends to make the material thickness distribution (Fig. 2) less skewed, i.e., with smaller variation in material thickness penetrations. Packing thus causes the over-all transmission to be smaller than that calculated by assuming a random distribution. However, the true transmission will always be bracketed between the random distribution value and the reduced density value. Materials which consist of discrete chunks which are separated by a vehicular medium so that the chunks are not in intimate contact with neighboring chunks are well represented by a "random distribution." Packing becomes a consideration when the volume fraction begins to approach the maximum experimental volume fraction which is about 0.5 for single-sized chunks that are not too different from spheres or cubes. Even when the chunks are closely packed, the randomly distributed transmission is expected to be closer to the true over-all average transmission than the reduced density transmission.

With a randomly distributed mixture of chunks, the transmission may vary statistically over the surface of a material, being unity over a small area (where there is an alignment of voids) and being much smaller than average (where there is an alignment of chunks). The variations are usually on a scale comparable with the attenuation of a single chunk, so that this effect is seldom noticed in practical experiments. If a slab were very thick, however, this effect would become more noticeable.

The slab is considered to be divided into an integral number (N) of layers of thickness (Δ) equal to the height of a cylinder of absorbing material. This division is made by translating the cylinders vertically (see Fig. 3) so that the center of a cylinder is moved to the center of the layer in which it falls. Allowing chunks to protrude beyond the surface is a fairly good approximation to chunks mixed in a binder if no effort is made to level off the surfaces after curing. If the chunks are mixed in a die under pressure, then no chunks will penetrate the surface. This distinction can be taken into account by noting that those chunks which protrude from the surface have their centers located within $\Delta/2$ of the surface. Thus, the apparent boundary of the slab is located a distance $\Delta/2$ inside the real boundary. The method is developed for chunks which may protrude but is applicable for chunks which do not protrude if the "reduced thickness" is used, thus accounting for the apparent boundary at such a surface being $\Delta/2$ inside the slab.

The transmission through a slab divided in this manner is the same as the transmission through the undivided slab since every normally incident ray sees the same thickness of chunk material in either case (as may be seen in Fig. 3). The probability that a given ray will encounter exactly n chunks is given by Bernoulli's binomial distribution:

$$P_n = V^n(1 - V)^{N-n} C_n^N ; \quad C_n^N = \frac{N!}{(N - n)!\, n!} \tag{3}$$

where

V = probability that a ray will encounter a chunk in passing through a layer (the volume fraction of chunks),

V^n = probability that n chunks will be encountered in n specified layers,

$(1 - V)^{N-n}$ = probability that the rest of the layers are not occupied by other chunks,

C_n^N = number of combinations of N things taken n at a time and is equal to the number of ways in which the n specified layers could be selected from N layers.

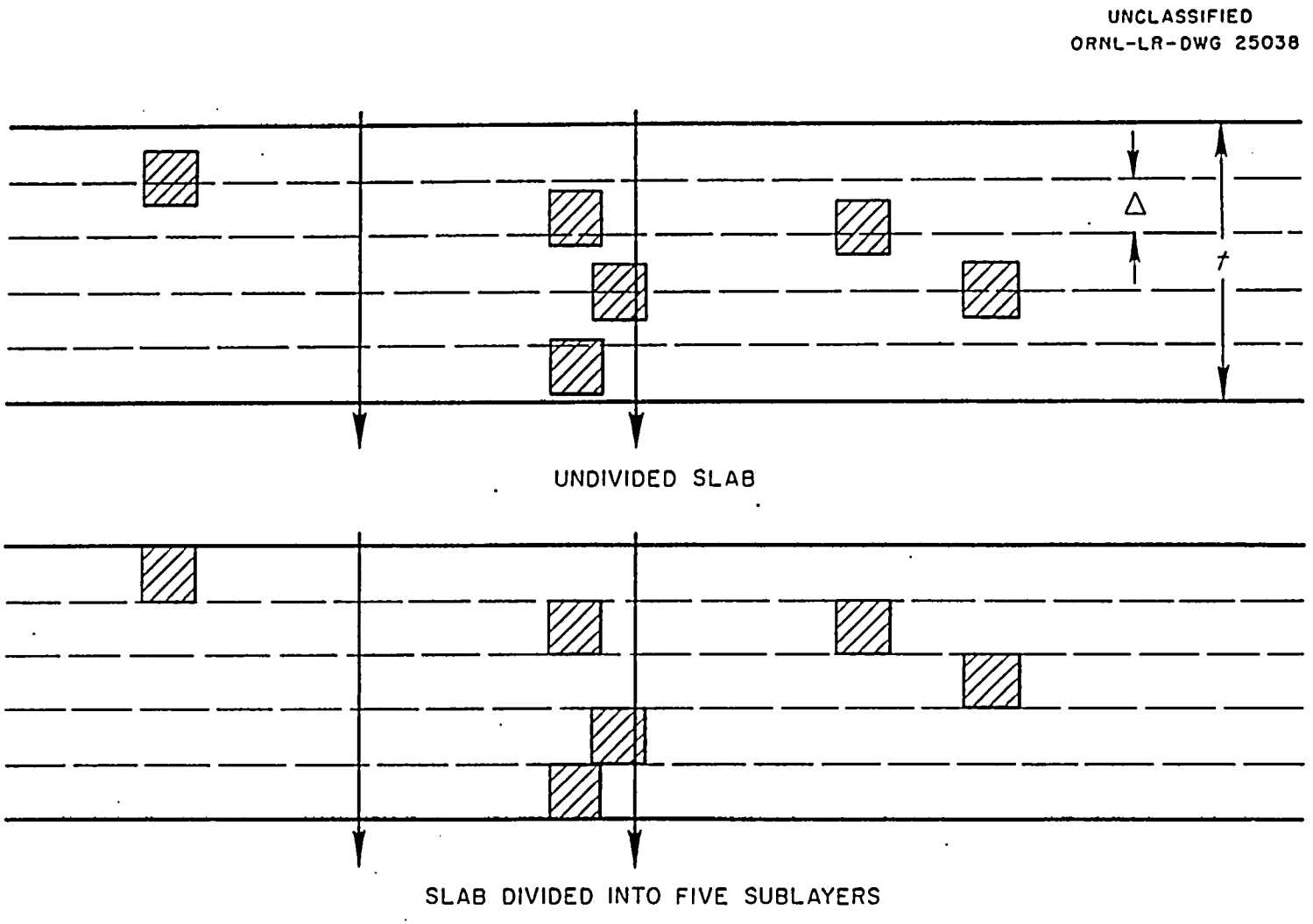

Fig. 3. Illustrating the Division of a Slab into Sublayers.

If exponential attenuation in the chunk material is assumed, then the probability that a given ray penetrates the slab is:

$$\tau(n) = e^{-\Sigma n\Delta} \tag{4}$$

where

Σ = linear attenuation coefficient for the chunk material,

n = number of chunks encountered,

Δ = height of a chunk,

$n\Delta$ = total chunk material thickness along this ray.

The over-all average transmission for the slab is:

$$T = \sum_{n=o}^{N} P_n \tau(n) \tag{5}$$

$$= \sum_{n=o}^{N} V^n (1 - V)^{N-n} C_n^N e^{-\Sigma n\Delta}$$

By the binomial theorem, this may be written as:

$$T = \sum_{n=o}^{N} C_n^N (Ve^{-\Sigma\Delta})^n (1 - V)^{N-n} \tag{6}$$

$$= \left[Ve^{-\Sigma\Delta} + 1 - V\right]^{N=t/\Delta}$$

Equation 6 has a simple physical interpretation which could have given Eq. 6 at once. Since V is the probability that a ray will encounter a chunk at a given layer, (1 - V) is the probability that a ray will miss the chunks in a layer. $Ve^{-\Sigma\Delta}$ is the probability that those rays that hit a chunk will penetrate the layer. Thus the quantity in brackets is just the average transmission through one layer. Since the chunks are randomly distributed,

each layer acts independently and the over-all average transmission T is the product of the transmission of all N sublayers. Equation 6 was derived with the assumption that there was an integral number of layers in the slab. When there is a fractional number of layers, Eq. 6 is still approximately correct since the transmission of such a slab will uniformly decrease as its thickness increases (if the volume fraction of chunks is kept constant), in agreement with the behavior of the equation.

Equation 6 may be written as:

$$T = e^{\frac{t}{\Delta} \ln \left[Ve^{-\Sigma\Delta} + 1 - V\right]} \tag{7}$$

This suggests the concept of an effective linear attenuation coefficient defined by:

$$T = e^{-V\Sigma_{eff}t} \tag{8}$$

Comparing Eq. 7 with Eq. 8 shows that:

$$\Sigma_{eff} = \frac{-\ln \left[Ve^{-\Sigma\Delta} + 1 - V\right]}{V\Delta} = \frac{-\ln \left[1 - V(1 - e^{-\Sigma\Delta})\right]}{V\Delta} \tag{9}$$

Equation 9 may be expanded in a series:

$$\Sigma_{eff} = \frac{V(1 - e^{-\Sigma\Delta})}{V\Delta} + \frac{1}{2} \frac{V^2(1 - e^{-\Sigma\Delta})^2}{V\Delta} + \ldots \tag{10}$$

For small values of $V(1 - e^{-\Sigma\Delta})$, Eq. 10 reduces to

$$\Sigma_{eff} = \frac{1 - e^{-\Sigma\Delta}}{\Delta} \approx \Sigma \quad \text{if } \Sigma\Delta << 1$$

$$\approx \frac{1}{\Delta} \quad \text{if } \Sigma\Delta >> 1 \tag{11}$$

Equation 11 provides a valuable insight into the variation of the efficiency of a chunk with its size. The transmission approaches the reduced density value as the chunks become small or less opaque. The transmission of opaque chunks depends only on Δ since the radiation that penetrates the slab channels around the chunks instead of penetrating them.

The case of opaque chunks is of special interest since it represents the extreme case where all the transmitted radiation channels through the slab. An opportunity to penetrate the slab exists only when the void spaces between chunks are lined up so that there is a direct path through the slab. In this case Eq. 6 becomes:

$$T = (1 - V)^{t/\Delta} \tag{12}$$

If V is small, this can be approximated by:

$$T \approx e^{-tV/\Delta} \tag{13}$$

It is interesting to note that the Poisson distribution function for the probability of straight paths through the slab encountering no chunks, which is only strictly valid when $V << 1$ and $N >> n >> 1$, gives the same answer for this approximation.

Formulas for Materials with Right Cylindrical Chunks of Multiple Sizes

The above treatment of a single chunk size is now extended to include more than one chunk size or material. For two different sized chunks, a division is made into layers and sublayers characteristic of the larger chunks and smaller chunks, respectively. The transmission of a layer is

then found as before except that Eq. 6 is used to determine the transmission of the area between the large chunks. It is shown that the large chunks crowd the smaller ones together and hence the effectiveness of small chunks depends on the volume occupied by larger ones. The effective attenuation cannot be expressed simply as was the case for single-sized chunks, but it is possible to approximate the effective volume fraction in certain limiting cases.

It is assumed first that the chunk distribution is made up of two different sized cylinders (see Fig. 4) with heights Δ_1 and Δ_2 with $\Delta_1 \geqq \Delta_2$. In deriving the approximate result it is assumed that Δ_1 is a multiple of Δ_2. The volume fraction of the Δ_1 chunk is V_1, and the volume fraction of the Δ_2 chunk is V_2. The corresponding attenuation coefficients are Σ_1 and Σ_2. The division of the chunks into sublayers is carried out by further dividing the layers into sublayers as shown in Fig. 4.

Each large (Δ_1) chunk is translated vertically so that it lies in the layer in which its center was formerly located, just as in the division of the single chunk size illustrated in Fig. 3. The small chunks are then translated so that each one lies in the sublayer in which its center was formerly located. Occasionally a small chunk should go into a sublayer which is occupied by a large chunk (see the cross-hatched small chunks in Fig. 4). In this case, the small chunk is translated vertically and inserted at random in some vacant spot. Thus, the original random distribution is divided into layers which are statistically independent of one another and the over-all slab transmission T can be found if the average transmission of one layer is known.

The transmission T_s of a single layer is given by an extension of Eq. 4.

$$T_s = V_1 e^{-\Sigma_1 \Delta_1} + (1 - V_1) \left[\frac{V_2 e^{-\Sigma_2 \Delta_2}}{1 - V_1} + 1 - \frac{V_2}{1 - V_1} \right]^{\Delta_1/\Delta_2} \qquad (14)$$

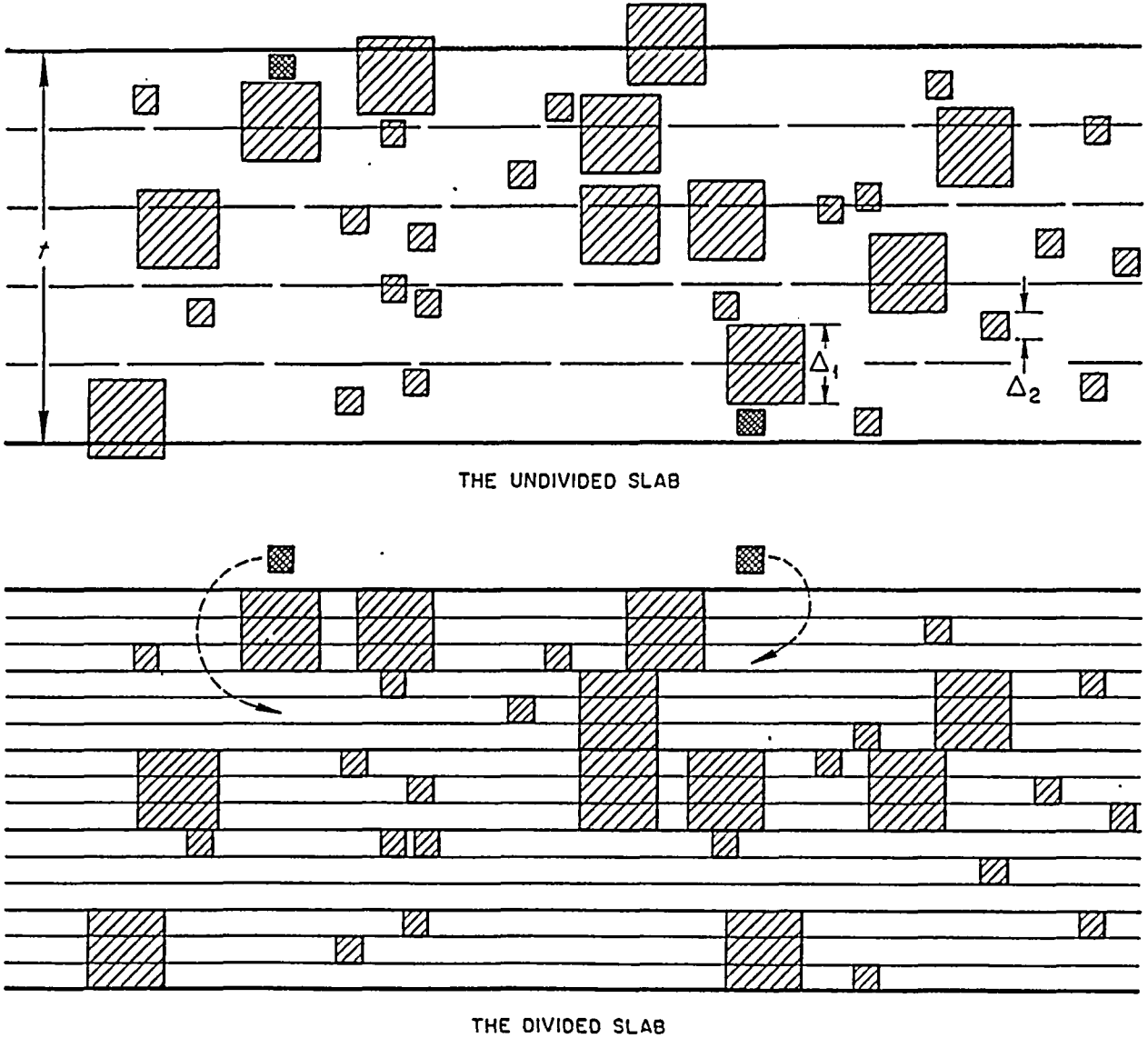

Fig. 4. The Division of a Slab Containing Two Chunk Sizes into Layers and Sublayers.

The first term is the transmission through the larger chunks. The second term is the transmission through the rest of the layer. This second term is identical in Eq. 6 except that the volume fraction of smaller chunks is adjusted to account for the space occupied by the larger chunks. For a given volume fraction of small chunks, the density is larger if there are large chunks present, since the total volume available for the small chunks is less. The volume available to the smaller chunks is $1 - V_1$ so that V_2 must be multiplied by $1/(1 - V_1)$ to account for the effect of the larger chunks. The over-all transmission of the slab is then:

$$T = \left\{ V_1 e^{-\Sigma_1 \Delta_1} + (1 - V_1) \left[\frac{V_2 e^{-\Sigma_2 \Delta_2}}{1 - V_1} + 1 - \frac{V_2}{1 - V_1} \right]^{\Delta_1/\Delta_2} \right\}^{t/\Delta_1} \qquad (15)$$

This formula is applicable to chunks of different materials.

For more than two chunk sizes or materials, the above argument is extended to consider that sub-sublayers contain the next smaller Δ_3 chunks, etc. For three chunk sizes (with $\Delta_1 \geq \Delta_2 \geq \Delta_3$):

$$T = \left\{ V_1 e^{-\Sigma_1 \Delta_1} + (1 - V_1) \left(\frac{V_2 e^{-\Sigma_2 \Delta_2}}{1 - V_1} + \left[1 - \frac{V_2}{1 - V_1} \right] \left[\frac{V_3 e^{-\Sigma_3 \Delta_3}}{1 - V_1 - V_2} + 1 - \frac{V_3}{1 - V_1 - V_2} \right]^{\Delta_2/\Delta_3} \right)^{\Delta_1/\Delta_2} \right\}^{t/\Delta_1} \qquad (16)$$

The extension to an arbitrary number of chunk sizes is evident. The general formula (with $\Delta_1 \geq \Delta_2 \ldots \geq \Delta_n$) is:

Fig. 4. The Division of a Slab Containing Chunk Sizes into Layers and Sublayers.

$$T = \left\{ V_1' e^{-\Sigma_1 \Delta_1} + (1 - V_1') \left(V_2' e^{-\Sigma_2 \Delta_2} + \left[1 - V_2'\right] \left[\cdots\cdots (1 - V_{n-1}') \right.\right.\right.$$

$$\left.\left.\left. \times \left\{ V_n' e^{-\Sigma_n \Delta_n} + 1 - V_n' \right\}^{\Delta_{n-1}/\Delta_n} \cdots\cdots \right]^{\Delta_2/\Delta_3} \right)^{\Delta_1/\Delta_2} \right\}^{t/\Delta_1} \qquad (17)$$

V' is the volume fraction adjusted for the displacement of all larger chunks. The volume occupied by the chunks larger than the ith chunk is $(1 - V_1 - V_2 - \cdots - V_{i-1})$ hence:

$$V_i' = \frac{V_i}{1 - V_1 - V_2 - \cdots V_{i-1}} \qquad (18)$$

V_1 is the same as V_1' since there are no chunks with $\Delta_i > \Delta_1$. Equation 17 may be used to approximate a continuous distribution by choosing a sufficient number of discrete sizes in accord with the distribution. The smallest chunk size may be allowed to go to zero, so that in the limit, the equation is applicable to chunks distributed in a uniformly absorbing medium. In this case, the last bracket in Eq. 11 becomes:

$$\lim_{\Delta_n \to 0} \left\{ V_n' e^{-\Sigma_n \Delta_n} + 1 - V_n' \right\}^{\Delta_{n-1}/\Delta_n} = e^{-V_n' \Sigma_n \Delta_{n-1}} \qquad (19)$$

It is desirable to find an effective value of the attenuation coefficient which indicates the effect of the chunk size distribution on the effectiveness of a particle of a given size. In general, the effectiveness of a chunk of a given size depends on the parameters of all the other chunk sizes, but for certain limiting cases, the effective attenuation can be simply obtained as follows:

I. For all chunks opaque $\left(\Delta_i \Sigma_i >> 1 \text{ for all } i \right)$,

$$T = e^{-\left[\frac{1}{\Delta_1}\ln(1 - V_1') + \frac{1}{\Delta_2}\ln(1 - V_2') + \ldots\right] t} \tag{20a}$$

II. For all chunks almost transparent $\left(\Sigma_i \Delta_i << 1 \text{ for all } i\right)$

$$T = e^{-(V_1\Sigma_1 + V_2\Sigma_2 + \ldots)t} \tag{20b}$$

III. For first m chunks opaque and all others almost transparent,

$$T = e^{-\left[\frac{1}{\Delta_1}\ln(1 - V_1^*) + \ldots + \frac{1}{\Delta_m}\ln(1 - V_m^*) - V_{m+1}^*\Sigma_{m+1} - \ldots\right] t} \tag{20c}$$

where

$$V_i^* = V_i / \left[1 - (\text{volume fraction of all opaque chunks with } \Delta > \Delta_i)\right]$$

IV. For total volume fraction of all chunk sizes << 1,

$$T = e^{-\left[V_i \frac{1 - e^{-\Sigma_1\Delta_1}}{\Delta_1} + V_2 \frac{1 - e^{-\Sigma_2\Delta_2}}{\Delta_2} + \ldots\right] t} \tag{20d}$$

All the above limiting cases can be collectively expressed by:

$$T = e^{-\left[V_1^*\Sigma_1^* + V_2^*\Sigma_2^* + \ldots\right] t} \tag{21}$$

where

$$\Sigma_i^* = -\frac{\ln\left[V_i^* e^{-\Sigma_i\Delta_i} + 1 - V_i^*\right]}{\Delta_i V_i^*}$$

and $V_i^* = V_i / \left[1 - (\text{volume fraction of all opaque chunks with } \Delta > \Delta_i)\right]$.

Note that Σ_i^* is the same as Σ_{eff} for the single chunk size distribution as given by Eq. 9. The physical significance of this result is that the transmission may be approximated in the limiting cases above by the product of the transmissions of separate layers containing a single chunk size if the volume fraction of the chunk in the layer is corrected for the volume occupied by larger opaque chunks in the slab. Each term of the exponent in Eq. 21 gives the transmission of one layer. When none of the approximations are valid, Eq. 21 gives a transmission which is too small since it ignores the voids which should be present in a layer when the larger chunks are separated out. In these cases, Eq. 17 must be used but the approximate Eq. 21 still is useful in qualitatively interpreting the effect of changing the chunk size distribution.

Formulas for Materials with Arbitrary Chunk Shapes

The discussion has thus far been restricted to aligned cylinders because of the simple formulas that resulted. The results can be extended in an approximate way to arbitrarily shaped chunks with random orientation by replacing $(1 - e^{-\Sigma\Delta})$ in the simple formula by F, which represents the absorption of a single chunk averaged over all orientations, and replacing the layer thickness Δ by $\bar{\Delta}$, the average chunk thickness. A theorem due to Gauss[10] shows that for chunks with no concavities,

$$\bar{\Delta} = \frac{4v}{S} \tag{22}$$

where v is the volume of chunk and S is the total surface area of chunk. F is related to the collision probability P_c which is tabulated in Ref. 10 for many shapes of chunks, i.e.,

$$F = \bar{\Delta}\Sigma(1 - P_c) \tag{23}$$

---

10. K. M. Case, F. de Hoffmann, and G. Placzek, Introduction to the Theory of Neutron Diffusion, Vol. I, Section 10, Los Alamos Scientific Laboratory Report, Superintendent of Documents (1953).

For large chunks ($\Sigma\bar{\Delta} >> 1$) with smooth edges (Ref. 10),

$$F = \left[1 - 0\left(\frac{1}{\Sigma\,\bar{\Delta}}\right)^2\right] \tag{24}$$

where $0\left(\frac{1}{\Sigma\,\bar{\Delta}}\right)^2$ means terms of the order of magnitude of $\left(\frac{1}{\Sigma\,\bar{\Delta}}\right)^2$.

For large chunks with irregular edges,

$$F = \left[1 - 0\left(\frac{1}{\Sigma\,\bar{\Delta}}\right)\right] \tag{25}$$

For small chunks ($\Sigma\bar{\Delta} << 1$),

$$F = \Sigma\,\bar{\Delta}\,(1 - v^{1/3}\,\alpha\Sigma) \tag{26}$$

where α is a parameter ≈ 0.5 for spheres. For spheres (Ref. 10)

$$F = \frac{2}{(2r\Sigma)^2}\left[\frac{1}{2}(2r\Sigma)^2 - 1 + (1 + 2r\Sigma)e^{-2r\Sigma}\right] \tag{27}$$

In terms of F, Eq. 6 for single-sized aligned chunks becomes:

$$T = \left[1 - VF\right]^{t/\Delta} \tag{28}$$

The extension to several different types of chunks is straightforward and

$$T = \Bigg\{ V_1'(1 - F_1) + (1 - V_1') \Bigg(V_2'(1 - F_2) + \Big[1 - V_2' \Big] \Big[\cdots \Big[\cdots (1 - V_{n-1}') \Big\{ V_n'(1 - F_n) + 1 - V_n' \Big\}^{\bar{\Delta}_{n-1}/\bar{\Delta}_n} \cdots \Big]^{\bar{\Delta}_2/\bar{\Delta}_3} \Bigg)^{\bar{\Delta}_1/\bar{\Delta}_2} \Bigg]^{t/\bar{\Delta}_1} \Bigg\} \qquad (29)$$

in analogy with Eq. 17 for aligned cylinders. The generalized form of Eq. 21 remains:

$$T = e^{-\left[V_1^* \Sigma_1^* + V_2^* \Sigma_2^* + \cdots \right] t} \qquad (30)$$

where now $V_i^* = V_i \Big/ \Big[1 - (\text{volume fraction of all opaque chunks with } \bar{\Delta} > \bar{\Delta}_i) \Big]$,

$$\Sigma_i^* = - \frac{\ln \left[1 - V_i^* F_i \right]}{\bar{\Delta}_i V_i^*} \qquad (31)$$

Formulas Including Energy and Angular Distributions

All the above discussion assumes a constant linear attenuation coefficient. This assumption is not valid in those cases for which the angular distribution is not collimated and spectrum hardening effects occur. If the chunks are randomly oriented, there will be no preferred direction of transmission in the slab. The transmission for incidence at the angle θ may therefore be calculated by replacing the thickness t by the slant penetration $t/\cos\theta$ in the previous formulas. Then the above formulas may be used to compute the transmission for a single entrance angle and energy and the result integrated in accordance with the prescribed neutron distributions. In general, the transmission including the effects of energy spectra and angular distribution is given by:

$$T(t) = \int_0^{\infty} \int_0^{\pi/2} T(t/\cos\theta, E)\phi(E)\psi(\theta)d\theta dE \qquad (32)$$

where

$T(t/\cos\theta, E)$ = transmission for a given angle and energy,

$\phi(E)$ = effective neutron spectral function,

$\psi(\theta)$ = angular distribution function.

For normal incidence, Eq. 32 simplifies to:

$$T(t) = \int_0^{\infty} T(t,E)\phi(E)dE \qquad (33)$$

For isotropic incidence, Eq. 32 becomes

$$T(t) = \int_0^{\infty} E_2\Big(-\ln T(t,E)\Big)\,\phi(E)dE \quad \text{(flux detector)} \qquad (34a)$$

$$= 2\int_0^{\infty} E_3\Big(-\ln T(t,E)\Big)\,\phi(E)dE \quad \text{(current detector)} \qquad (34b)$$

where the neutron spectral function is (for a Maxwell-Boltzmann distribution):

$$\phi(E) = \sqrt{\frac{4}{\pi}}\,\frac{E^{1/2}}{(KT)^{3/2}}\,e^{-E/KT} \quad \text{(for 1/v detector)} \qquad (35a)$$

$$\phi(E) = \frac{E}{(KT)^2}\,e^{-E/KT} \quad \text{(for constant efficiency detector)} \qquad (35b)$$

The functions E_2 and E_3 are the standard exponential integrals.[11]

II. CALCULATION OF NEUTRON TRANSMISSION THROUGH BORAL

The foregoing method has been used to compute the transmission of neutrons through boral. For the calculation it was assumed that the boral sandwich was rolled to a thickness of 1/8 in. and that the thickness of the B_4C-Al mixture was 0.085 in. with 40 vol% boron carbide. This resulted in an over-all volume fraction of approximately 25% for the absorbing chunks, which were assumed to be spherical in shape. The chunks were first considered to be of 11 different sizes between 20 and 100 mesh (this size distribution was taken from Ref. 12); however, it was found that assuming only four sizes gave approximately the same results, and only four groups were used thereafter. The four groups were as follows:

Size Mesh	Avg. Particle Diameter (in.)	$\bar{\Delta} = (4/3)r$ (in.)	Vol%
20-30	0.038	0.0253	17.0
36-46	0.024	0.0160	11.0
60-70	0.016	0.0107	6.0
80-120	0.009	0.0060	6.0
			40.0

The transmission calculated by this method for normally incident 2200-m/sec (0.0253-ev) neutrons through 1/8-in.-thick boral was 0.076. This is to be compared with a transmission of 0.0015 calculated for normally incident 2200-m/sec neutrons by the homogeneous approximation.

The transmission of normally incident neutrons through a 1/8-in.-thick boral shield as a function of energy is shown in Fig. 5, along with the

---

11. Case, de Hoffman, and Placzek, op. cit., Appendix A.
12. A Handbook on Boron Carbide, Elemental Boron, and Other Stable, Boron-Rich Materials, Norton Company 1417-3PCMX-10-56 CP (1955).

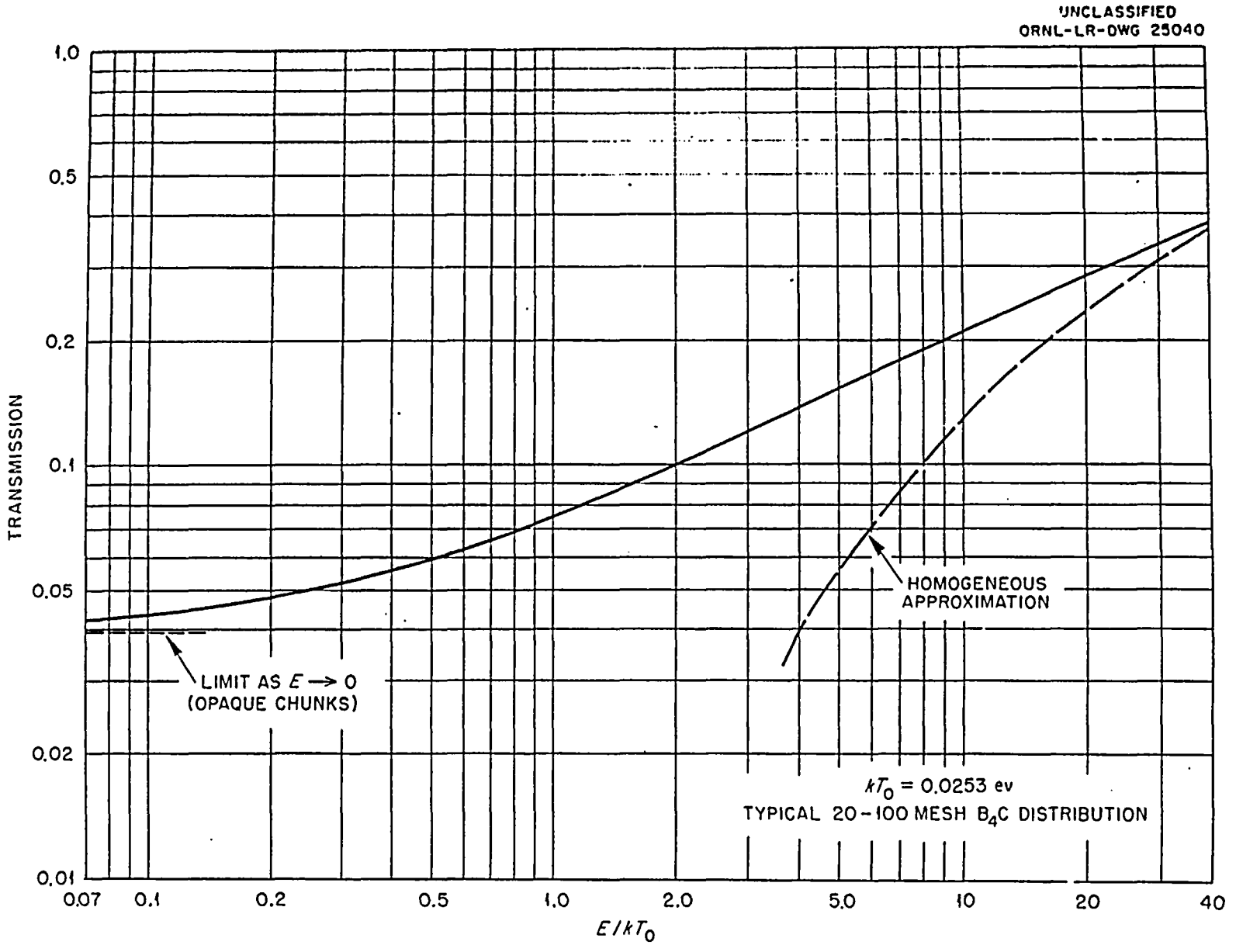
UNCLASSIFIED
ORNL-LR-DWG 25040
TRANSMISSION
1.0
0.5
0.2
0.1
0.05
0.02
0.01
0.07
0.1
0.2
0.5
1.0
2.0
5.0
10
20
40
E/kT0
LIMIT AS E → 0
(OPAQUE CHUNKS)
HOMOGENEOUS
APPROXIMATION
kT0 = 0.0253 ev
TYPICAL 20-100 MESH B4C DISTRIBUTION

limit as the chunks become opaque (low energies). The average transmission over the neutron distribution shown (Maxwell-Boltzmann distribution at room temperature) is 0.096 for a constant efficiency detector and 0.084 for a 1/v detector.

The transmission of isotropically incident neutrons through 1/8-in.-thick boral as a function of energy is shown in Fig. 6. For this case the average transmissions are 0.024 for a constant efficiency flux detector, 0.021 for a 1/v flux detector, 0.041 for a constant efficiency current detector, and 0.034 for a 1/v current detector.

III. COMPARISON OF CALCULATED AND EXPERIMENTAL RESULTS

The calculated results reported above can be compared with the results of two experiments which have been performed at ORNL to determine the transmission through 1/8-in. thicknesses of boral as measured by 1/v detectors. In the first experiment[4] the radiation consisted of thermal neutrons escaping from a thermal column on top of the ORNL Graphite Reactor with an angular distribution of the $(1 + \sqrt{3}\cos\theta)$ type,[13] which is more forwardly peaked than an isotropic flux. Consequently, the experimental values should be between the computed values for normal incidence and those for isotropic incidence. The transmission obtained for a Brooks and Perkins boral sample was 0.070, while the transmission for an ORNL sample was 0.094.

In the second experiment[14] the radiation was a collimated beam of normally incident neutrons from a beam hole at the ORNL Graphite Reactor. The transmissions obtained for two different Alcoa samples were 0.065 and 0.070, respectively.

---

13. R. F. Christy et al., Lecture Series in Nuclear Physics, MDDC-1175 (1943; decl. 1945).
14. G. deSaussure, Oak Ridge National Laboratory, private communication.

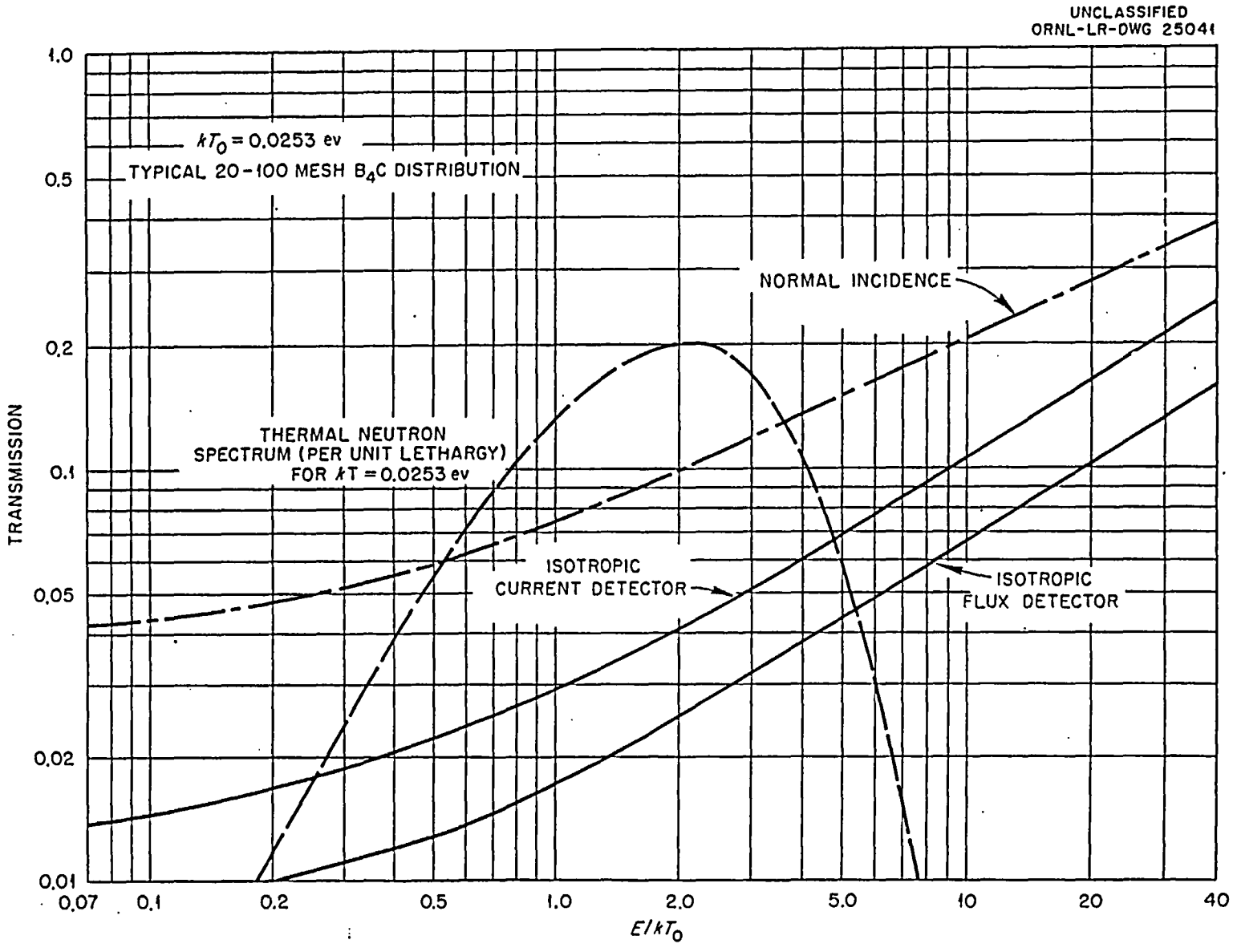

Fig. 6. Neutron Transmission Through 1/8-in.-thick Boral as a Function of Energy; Isotropically Incident Flux.

IV. CONCLUSION

The method proposed in this paper is less elegant than other methods proposed previously, for example, Smith's method,[8] but it is more easily visualized. Furthermore, the degree of agreement between experimental and calculated results seems reasonably good since experimental details of particle size, energy, and angular distribution are incompletely known in each case. It may be concluded that the methods described in this paper can be used to provide useful estimates of the attenuation of radiation in heterogeneous media for which channeling between absorbing chunks is an important process.

MICHIGAN MEMORIAL PHOENIX PROJECT

THE UNIVERSITY OF MICHIGAN

FNR - PML REPORT 1-76

Experimental Observation of BORAL Plates Encased in Stainless Steel Under the Influence of Gamma and Neutron Fluxes

February, 1976

Prepared For

Brooks and Perkins, Incorporated
12633 Inkster Road
Livonia, Michigan 48150

ANN ARBOR, MICHIGAN

Brooks & Perkins, Incorporated

Report No. 572

Prepared by

Brooks & Perkins, Inc.
Advanced Structures Division
12633 Inkster Road
Livonia, Michigan 48150

EXPERIMENTAL OBSERVATION OF BORAL PLATES ENCASED IN STAINLESS STEEL UNDER THE INFLUENCE OF GAMMA AND NEUTRON FLUXES

(See FNR-PML Report 1-76)

FNR-PML REPORT 1-76

Experimental Observation of BORAL Plates Encased in Stainless Steel Under the Influence of Gamma and Neutron Fluxes

FORD NUCLEAR REACTOR
MICHIGAN MEMORIAL - PHOENIX PROJECT
THE UNIVERSITY OF MICHIGAN
Ann Arbor, Michigan

February, 1976

Prepared For

Brooks and Perkins, Incorporated
12633 Inkster Road
Livonia, Michigan 48150

ABSTRACT

Experimental observations were made of BORAL plates encased in stainless steel jackets. Samples were tested dry and with 25 ml distilled water, 70 ml 2000 PPM boron solution, and 20 ml 2000 PPM boron solution injected within the stainless jacket. Samples were subjected to gamma and neutron fluxes in the Ford Nuclear Reactor.

Under irradiation fluxes and water conditions expected in a power reactor spent fuel pool, the BORAL samples exhibited no detectable gas evolution, pressure buildup, or damage due to temperature or other effects.

In the presence of a neutron flux, hydrogen and oxygen gas were evolved from the BORAL samples injected with 2000 PPM boron solution.

TABLE OF CONTENTS

1. INTRODUCTION

1.1 Purpose

The purpose of this report is to provide the results of experimental observations of BORAL plates encased in stainless steel jackets under gamma and neutron flux irradiations.

1.2 Description

Each BORAL sample was a 9 inch x 9 inch plate of 0.26 inch thickness. Each plate was encased in a thin, watertight jacket of stainless steel welded around the edges. A threaded connection was welded in the upper right corner of the face on one side of the stainless steel jacket. Irradiations were conducted in the Ford Nuclear Reactor pool at depths of 12 and 20 feet. An aluminum tube was run from the connection to the surface of the reactor pool for pressure measurements and gas collection.

Prior to testing, each sample plate was baked at 200°C for seven hours in a vacuum oven to remove moisture.

Each sample was tested to 10 P SIG internal pressure. Experimental pressures were limited to 5 P SIG as a reactor safety precaution.

Experimental measurements were made of pressure within each sample. Gas evolved during the tests was collected and analyzed. It was decided that temperature would not be measured. Each sample was observed after irradiation for damage due to pressure, temperature, or other effects.

Each sample was pressurized momentarily to 10 P SIG as it was inserted into the reactor pool to verify watertightness. Once each sample was placed in its experimental position, a 30 inch Hg vacuum was drawn to evacuate as much air as possible. The starting pressure for each test was the 30 inch Hg vacuum.

1.3 Experimental Conditions

The experimental sequence consisted of twelve steps derived from a combination of four different sample plates being subjected to three different irradiation conditions.

Sample 1 was a sealed, dry sample vented only through the gas collection line to the surface of the reactor pool. Sample 2 was identical to Sample 1 except that 25 ml of distilled water was injected within the stainless steel jacket. Sample 3 and Sample 4 were identical to Sample 1 except that 70 ml and 20 ml, respectively, of 2000 PPM boron solution were injected within the stainless steel jacket. The 2000 PPM boron solution was obtained by dissolving 1.23 grams of boric acid, H_3BO_3, in 100 ml of distilled water.

Initially, in Condition 1, each sample was irradiated adjacent to spent reactor fuel in a gamma flux of 2×10^5 rad/hr. In Condition 2 each sample was placed in a holder adjacent to the reactor operating at a power level of 2 MW. The Condition 2 gamma flux was 4×10^7 rad/hr and thermal neutron flux was approximately 1×10^{12} N/cm^2/sec, or 1×10^7 rad/hr. Finally, in Condition 3, each sample was left adjacent to the reactor core immediately after shutdown. Neutron flux was quite low, approximately five orders of magnitude below operating levels, while gamma flux was measured as 1.2×10^6 rad/hr.

The objective in these observations was to simulate conditions in a power reactor spent fuel pool:

Description	Units	PWR	BWR
Gamma Flux	rad/hr	1×10^6	1×10^6
Neutron Flux	rad/hr	Negligible	Negligible
Boron Concentration in Pool Water	PPM	1800	0

Combinations of Samples 2, 3, and 4 under Condition 3 closely simulate actual spent fuel pool conditions.

The 70 ml of boron solution placed in Sample 3 virtually filled the sample with liquid. It was decided to place a smaller liquid volume in Sample 4, 20 ml, and to thoroughly wet all surfaces with liquid prior to irradiation under the assumption that radiolysis, the breakdown of water into hydrogen and oxygen gas under the influence of radiation, would be enhanced by wetting all surfaces and providing a larger liquid to gas surface area within the sample.

2. RESULTS

Table 1 summarizes the observed effects of irradiation conditions on the BORAL samples. The total hours of irradiation per sample are noted in the array.

No pressure increase or gas evolution was observed under any condition for Sample 1, the dry sample, or Sample 2, the sample containing 25 ml of distilled water.

Sample 3 and Sample 4, the samples containing boron solutions, both generated gas when subjected to Condition 2, reactor at power and an irradiation flux of gamma rays and neutrons. Figure 1 is a plot of sample pressure increase as a function of time and dose. Gas was drawn from each sample and analyzed with a gas chromatograph. The results were:

	Sample Gas Constituents (%)		
Sample	Hydrogen	Oxygen	Nitrogen
3	6.5	20.4	73.1
4	41.1	21.6	37.3
4	41.0	21.8	37.2

The hydrogen percentage of Sample 3 was lower than might be expected, an approximate 2:1 hydrogen - oxygen ratio, because Sample 3 was not purged extensively prior to sampling. The chromatograph analysis results are included as Tables 2 - 4.

When Sample 3 and Sample 4 were subjected to gamma flux alone, gas was not evolved and no pressure increase was detected with irradiation time.

	SAMPLE 1 9" x 9" BORAL Plate Stainless Steel Jacket Dry	SAMPLE 2 9" x 9" BORAL Plate Stainless Steel Jacket 25 ml Distilled Water	SAMPLE 3 9" x 9" BORAL Plate Stainless Steel Jacket 70 ml - 2000 PPM Boron	SAMPLE 4 9" x 9" BORAL Plate Stainless Steel Jacket 20 ml - 2000 PPM Boron
CONDITION 1 Spent Fuel γ - 2×10^5 Rad/hr N - Negligible	42 Hours No Detectable Effect	25 Hours No Detectable Effect	19 Hours No Detectable Effect	4 Hours No Detectable Effect
CONDITION 2 Reactor at 2 MW γ - 4×10^7 Rad/hr N - 1×10^7 Rad/hr	24 Hours No Detectable Effect	6 Hours No Detectable Effect	48 Hours Linear pressure increase with irradiation time. Gas Analysis: 6.5% Hydrogen 20.4% Oxygen	152 Hours Linear pressure increase with irradiation time. Gas Analysis: 41.1% Hydrogen 21.6% Oxygen
CONDITION 3 Reactor Shutdown γ - 1.2×10^6 Rad/hr N - Negligible	4 Hours No Detectable Effect	4 Hours No Detectable Effect	12 Hours No Detectable Effect	96 Hours No Detectable Effect

Table 1

Observed Effects of Irradiation Conditions on BORAL Samples

Figure 1

Sample Pressure Profile

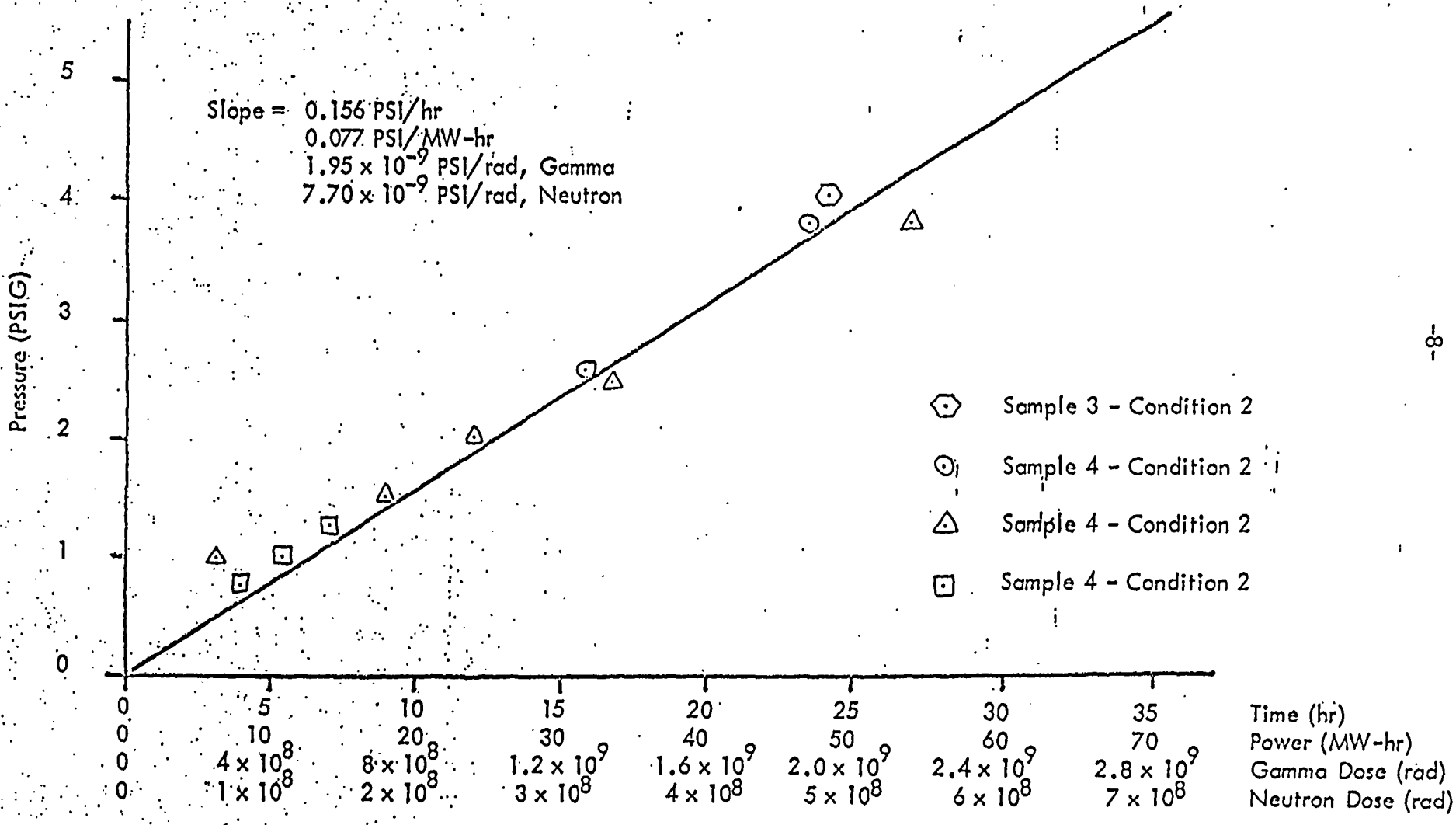

Page 1 of _____

G.C.# 1 8 V.S.# 1

TABLE 2

ANALYSIS SHEET
Van Slyke Apparatus

Rad No. _____

Run No. 1 Vessel No. NO I.D.

Original Sample SAMPLE 2 - BORAL PLATE IN STAINLESS JACKET

Sample, as measured _____

Radiation Source/Location CUP 2 - REACTOR Date 1-19-76

Dose Rate γ - 4×10^7 $\alpha N'$ - 1×10^7 rads/hr

Irradiation Time _____ Total Dose _____ rads

Flow Rate 30.3 cc/MIN. Col.#1 10 cc/19.8 sec Col.#2 10 cc/20.0 sec

Baragraph 30.15 Humid. 21 % Temp. 74°F

V.S. Temp. 22.3°C Vol. 0.823 cc

	P_i	P_o
	474.0 mm	138.6 mm
	473.0 mm	135.8 mm
	472.7 mm	138.7 mm
	3) 1419.7	3) —
P_i ave	473.23 mm	P_o ave 138.7 mm
P_o ave	138.7 mm	
P_T	334.53 mm	

TF2 Closed 2:32 time

Loop Loaded _____ time

Run Start 2:33 time

Total Time 1 MIN.

Integrator Data

* 1 FILE 3
1196 ID

40	20	10	PW
30	30	30	SS
3	3	3	FP
5	5	5	BL
400	200	1	T1
		2	T4
		70	T5
		100	HA
		50	PL
		50000	HL
			SP

900 SEC RUN

TIME		AREA	
124	N_2	151011	
249	O_2	46972	3
415	NOISE	370	2
587	N_2	139299	3
		337652	

TIME	CONC	
124	44.724	
249	13.911	3
415	.110	2
587	41.255	3
	100.000	

Sensitivity Factors Used

1	H_2 1.40×10^{-4}	H_2 1-6	5-2-75
2	O_2 1.408×10^{-3}	O_2 1-2	9-8-75
3	N_2 1.704×10^{-3}	N_2 1-2	4-10-75
4			
5			
6			
7			

Summary Sheet

Date CALC. PRESS.

21.14 = 6.5%
66.14 = 20.4%
237.37 = 73.1%
324.65 mm

WITHIN 3% OF MEASURED.

COMMENTS:

Attst: Rad R Burn
2/12/76

Page 1 of 2

TABLE 3

G.C.# 18 V.S.# 16

ANALYSIS SHEET
Van Slyke Apparatus

Rad No. _____

Run No. 1 Vessel No. 2

Original Sample SAMPLE 5 - BORAL PLATE IN STAINLESS JACKET

Sample, as measured _____

Radiation Source/Location CUP 2 - REACTOR Date 1-29-76

Dose Rate γ - 4×10^7 oN' - 1×10^7 rads/hr

Irradiation Time _____ Total Dose _____ rads

Flow Rate 300cc/MIN Col.#1 10 cc/20.0 sec Col.#2 10 cc/20.0 sec

Baragraph 2995 Humid. 25 % Temp. 73°F

V.S. Temp. 22.4 Vol. 0.823 cc

1ST SAMPLE, AFTER 1 PURGE

	P_i	P_o
	522.1 mm	138.4 mm
	522.4 mm	138.6 mm
	522.0 mm	138.5 mm
	3)1566.5	3)
P_i ave	522.17 mm	138.5 mm
P_o ave	138.5 mm	
P_T	355.67 mm	

TF2 Closed 2:30 time

Loop Loaded _____ time

Run Start 2131 time

Total Time 1 MIN

Integrator Data

1 FILE 3
1296 ID

40	20	10	PW
30	30	30	SS
3	3	3	FP
5	5	5	BL
400	200	1	T1
		2	T4
		70	T5
830 SEC RUN		100	MA
		50	PL
		50000	ML
			SP

Sensitivity Factors Used		Summary Sheet	Date CALC. PRESS	
1 H_2	1.400×10^{-4}	H_2/1-6	5-2-75	146.20mm = 41.1%
2 O_2	1.408×10^{-3}	O_2/1-2	9-8-75	76.77 = 21.6%
3 N_2	1.704×10^{-3}	N_2/1-2	9-10-75	132.59 = 37.3
4	WITHIN 7.3% OF MEASURED = 355.56 mm			100.0%
5				
6				
7				

TIME		AREA
127	H_2	1044272
250	O_2	54527
587	N_2	77813
		1176612

TIME	CONC
127	88.752
250	4.634
587	6.613
	99.999

COMMENTS:

attest: Reid R Dunn
2/12/76

G.C.# 16 V.S.# 16

TABLE 4

ANALYSIS SHEET
Van Slyke Apparatus

Rad No. _____

Run No. 2 Vessel No. 2

Original Sample SAMPLE 3 - BARIL PLATE IN STAINLESS JACKET

Sample, as measured _____

Radiation Source/Location COP 2 - REACTOR Date 1-27-76

Dose Rate γ - 4×10^7 $\alpha N'$ - 1×10^7 rads/hr

Irradiation Time _____ Total Dose _____ rads

Flow Rate 30.0 cc/min Col.#1 ____ cc/ ____ sec Col.#2 ____ cc/ ____ sec

Baragraph _____ Humid. ____ % Temp. _____

V.S. Temp. 22.7°C Vol. 0.823 cc

	P_i	P_o
	357.1 mm	138.1 mm
	356.6 mm	138.1 mm
	356.6 mm	138.3 mm
	3) 1070.3	3) 414.5
P_i ave	356.77 mm	
P_o ave	138.17 mm	138.17 mm
P_T	218.6 mm	

TF2 Closed 3:00 PM time

Loop Loaded _____ time

Run Start 3:01 time

Total Time 1 MIN.

Integrator Data

2 FILE 3

1295 ID

40	20	10	PW
30	30	30	SS
3	3	3	FP
5	5	5	BL
400	200	1	T1
		2	T4
		70	T5
		100	MA
		50	PL
		50000	ML
			SP

84.0 SEC. RUN

Sensitivity Factors Used — Summary Sheet — Date CALC. PRESS

1	H_2	1.400×10^{-4}	H_2 1-6	5-7-75	83.55 mm = 41.0%
2	O_2	1.408×10^{-3}	O_2 1-2	9-8-75	44.52 = 21.8
3	N_2	1.704×10^{-3}	N_2 1-2	9-10-75	75.81 = 37.2
4		WITHIN 0.7% OF MEAS. PRESS.			203.88 100.0%
5					
6					
7					

TIME		AREA
126	H_2	596793
251	O_2	31622
587	N_2	44487
		672902

TIME	CONC
126	88.689
251	4.699
587	6.611
	99.999

COMMENTS:

Attest: Reed D Dunn
2/12/76

3. CONCLUSIONS:

Under irradiation fluxes and water conditions expected in a power reactor spent fuel pool, the BORAL samples tested exhibited no detectable gas evolution, pressure build-up, or damage due to temperature or other effects.

In the presence of a neutron flux, hydrogen and oxygen gases were generated from the samples containing the 2000 PPM boron solution. Pressure built up in the samples as a linear function of irradiation time and neutron dose. Appendix I has been included because it is a report on a similar phenomenon observed in Ford Nuclear Reactor boron carbide (B_4C) powder filled control rods. A similar linear pressure increase with neutron dose was observed. The tests were terminated at a pressure of 60 PSIG out of concern for rupturing the test device. Radiolysis was attributed to ionization from lithium and helium released by the boron-neutron reaction:

$$ {}_0N^1 + {}_5B^{10} \longrightarrow {}_3Li^7 + {}_2He^4 \qquad (3.1) $$

A review of Table 1 shows that radiolysis occurred fairly rapidly in a neutron flux, Condition 2, with 2000 PPM boron solution filled samples, Sample 3 and Sample 4. Sample 2, under the same conditions, exhibited no detectable radiolysis or pressure buildup during the time period of observation. However, in Sample 2, the only boron exposed to water was around the edges of the BORAL plate. Ionizing lithium and helium released within the meat of the plate was stopped by aluminum cladding before reaching the distilled water in the sample.

It is not reasonable to conclude that gas was not generated in the Sample 2 - Condition 2 experiment just because detectable quantities were not observed during the short period of the experiment. It is possible that over an extended period pressure within the jacketed BORAL plate could build up due to radiolysis taking place at a much slower rate.

APPENDIX 1

DEFORMATION OF THE FORD NUCLEAR REACTOR SHIM-SAFETY RODS

Report by:

C. W. Ricker
W. R. Dunbar
J. B. Bullock

Investigations by:

J. B. Bullock
W. R. Dunbar
V. C. Serment
R. H. White

Phoenix Memorial Laboratory

Michigan Memorial Phoenix Project

The University of Michigan

December 1960

Table of Contents

DEFORMATION OF THE FNR SHIM-SAFETY RODS

I. INTRODUCTION

The Ford Nuclear Reactor (FNR), located in the Phoenix Memorial Laboratory on the North Campus of The University of Michigan, is a one megawatt pool type reactor fueled with MTR type fuel elements. Control of the reactor is accomplished by the use of three shim-safety rods and one control rod. These rods move vertically inside special fuel elements in which guide tubes have been inserted in place of the center fuel plates. The shim-safety rods for the FNR, as their name implies, serve the dual function of shim control and safety protection. These rods, worth approximately 3 per cent negative reactivity each, drop into the reactor under the influence of gravity when potentially dangerous conditions exist in the reactor. This results from an interruption of the currents to electromagnets which normally couple the rods to their respective drive mechanisms. A shim-safety rod is constructed from an extruded aluminum tube welded to appropriate endpieces and filled with boron carbide powder (see Sketch I page 2). The powder is loaded through an aperture at the bottom end of the rod. This hole is plugged and welded after the rod is filled.

The FNR was put into operation in September of 1957 and, after initial calibrations, was raised to a power level of 100 kilowatts in February of 1958. Full power operation at one megawatt began in September 1958.

In August of 1960 a potentially hazardous condition arose when one of the shim-safety rods jammed in its special fuel element during a routine start-up of the reactor. There were no operational

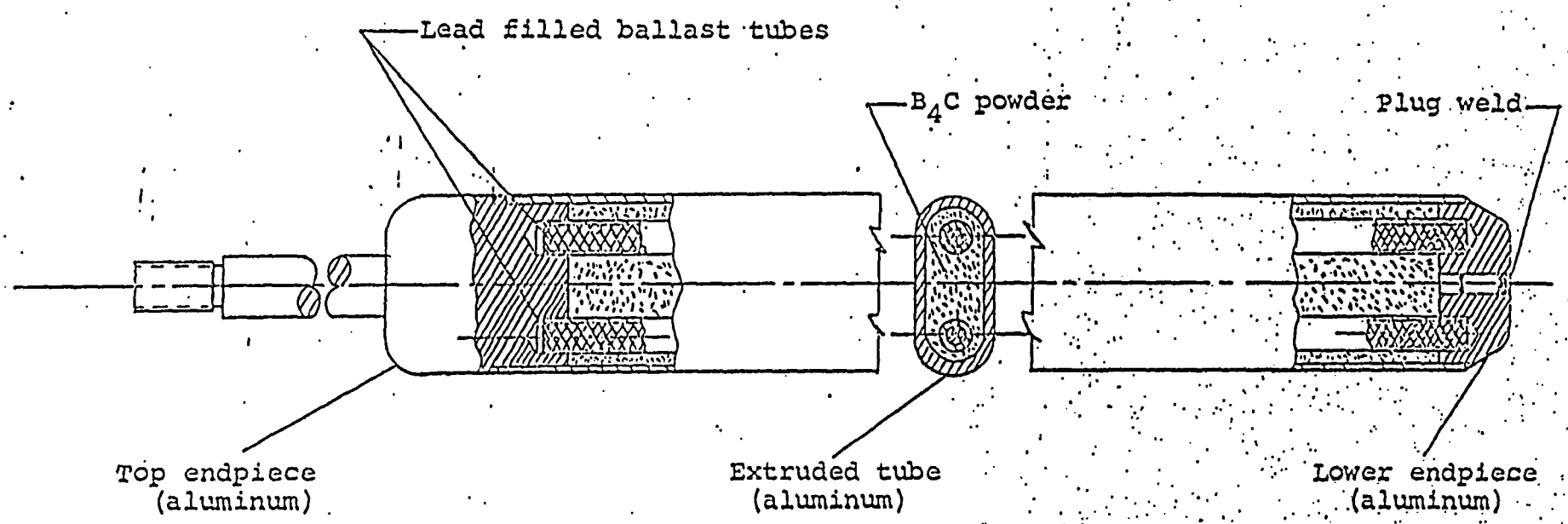

SKETCH I - FNR SHIM-SAFETY ROD

consequences in that the condition was immediately detected and no further attempt was made to start the reactor. All three shim-safety rods were removed and examined. The jammed rod appeared to be deformed. To keep the reactor in operation, three new shim-safety rods were procured, installed and calibrated. The new rods were identical to the original set except for the addition of cadmium liners. The original shim-safety rods are designated as 1-A, 1-B and 1-C, and the new rods as 2-A, 2-B and 2-C. The original set of rods had been in the reactor for 2200 megawatt hours before the jamming incident occurred.

In view of the potentially serious consequences of jammed shim-safety rods, the new rods were removed from the reactor after 320 megawatt hours for an accurate dimensional check. All three rods showed evidence of swelling, and rod 2-C was off-gassing through the bottom plug weld. One of the original rods (1-C) which was in good condition, was substituted for rod 2-C. The shim-safety rods presently installed in the FNR are 2-A, 2-B and 1-C, all of which undergo daily rod-drop tests and are removed from the reactor on a regular schedule and measured dimensionally.

The following sections of this report describe the jamming incident and rod deformations in greater detail, discuss our initial exploratory investigations, and suggest a program of investigation which might establish conclusively the cause of these difficulties. A final report will be distributed after the completion of the program of investigation suggested herein.

II. DESCRIPTION OF SHIM-SAFETY ROD INCIDENTS

A. Incident Involving Rods 1-A, 1-B and 1-C

During reactor start-up on August 11, 1960, the magnet-contact light for shim-safety rod 1-A indicated loss of contact when the rods had been raised about ten inches from their lower limits. This indicated that rod 1-A had become disengaged from the electromagnet which had been pulling the rod out of the reactor core. Withdrawal of the rods was immediately stopped. The staff observer at pool side reported that rod 1-A was still in the raised position even though magnet current was automatically cut off when the magnet-contact light on the operating console indicated the loss of the rod. The special fuel element for rod 1-A was not dislodged from its position in the reactor core.

At this point the currents to the other two electro-magnets were manually cut off. The pool side observer reported that rods 1-B and 1-C dropped normally into the core, but rod 1-A remained suspended. The electromagnets were lowered and 1-A magnet-contact light indicated contact as soon as the electromagnet struck the suspended rod. The rod was then successfully driven to its lower limit of travel by its electromagnet and drive mechanism.

The reactor was further secured and fuel was removed from the lattice along with the special control element containing safety rod 1-A. The rod-element assembly was moved to a holder in the center of the reactor pool. A grappling tool pulled the rod about ten inches out of the control element before the rod jammed again. Inspection showed noticeable swelling of the rod.

A special tool was built to remove the rod from the element. Plate No. 1, page 5, is a photograph of this removal device.

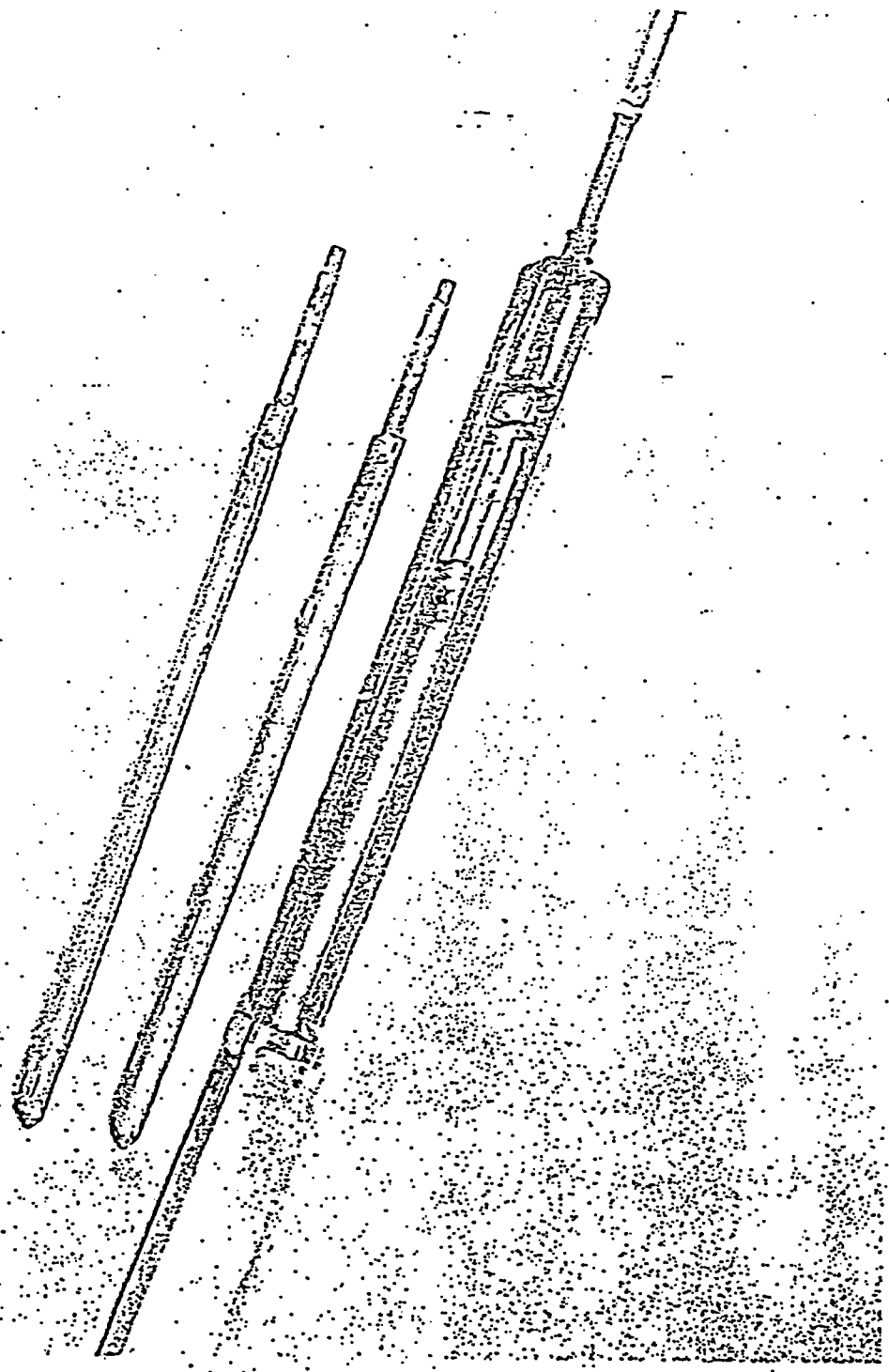

PLATE I - REMOVAL DEVICE

This device attached to the special fuel element was used to remove shim-safety rod 1-A. Rods 1-B and 1-C are also shown.

During the extraction procedure the fuel element was kept submerged in four feet of water for radiation shielding purposes. There was no serious galling of the rod during the removal procedure, nor was there any off-gassing from the rod. There was no evidence of corrosion or damage to the external surface of the rod. Also, there was no apparent damage to the special fuel element.

The three shim-safety rods had been in the reactor since the beginning of operation in September 1957. The reactor had operated at power levels up to one megawatt for a total of 2200 megawatt-hours. There were no indications prior to the incident that safety rod 1-A was sticking within the guide tube of the special fuel element. The rods on the FNR were inspected on several occasions since 1957 by removing them from the reactor and visually inspecting them under about six feet of water. Also, during that time, frequent rod-magnet release time measurements were made. Further, prior to every start-up rod drop tests are performed. None of these indicated potential jamming.

B. Incident Involving Rods 2-A, 2-B and 2-C

After the above incident a new special fuel element was installed in the lattice and three new replacement shim-safety rods 2-A, 2-B and 2-C were installed and calibrated. On November 25, 1960, these rods were removed from the reactor for observation and dimensional checks. Micrometer measurements showed that all three rods had increased in thickness after only 320 hours at one megawatt. Furthermore, rod 2-C was off-gassing at the bottom plug weld. A water-filled Erlenmeyer flask was held over the submerged rod to collect a sample of the gas for analysis.

The cadmium liners in the new set of rods hindered operations because of the induced radioactivity which gave a 6 roentgens per hour reading at the center of the rods. The bottom ends of the rods read greater than 25 roentgens per hour. In contrast, rods 1-A, 1-B and 1-C, without cadmium liners, read one-third of a roentgen per hour at the lower end.

III. INVESTIGATIONS

A. Dimensional Inspection

After removal from the reactor a complete dimensional inspection was made of rods 1-A, 1-B and 1-C. The thickness and width dimensions are shown in Tables I and II respectively (see pages 8 and 9). The dimensions of the replacement rods 2-A, 2-B and 2-C before installation in the reactor are also shown in these tables. Although no records of the initial dimensions are available for rods 1-A, 1-B and 1-C, a reasonable indication of the degree of swelling which took place can be obtained by an intercomparison of rod dimensions. However, initial and final thickness measurements taken at the middle of the rod are available for rods 2-A, 2-B and 2-C which had been in the reactor for 320 megawatt hours. These measurements are as follows:

Measurement	Shim-Safety Rod		
	2-A	2-B	2-C
Initial	0.922 in.	0.890 in.	0.913 in.
Final	0.928	0.921	0.925
Change	0.006	0.031	0.012

The inside dimensions of the guide tube of the special fuel elements are presented in the last column of Table I.

TABLE I - SHIM-SAFETY ROD THICKNESS DIMENSIONS

Note: The corresponding internal dimensions of the guide tube inside special fuel element 1-A are given in the last column.

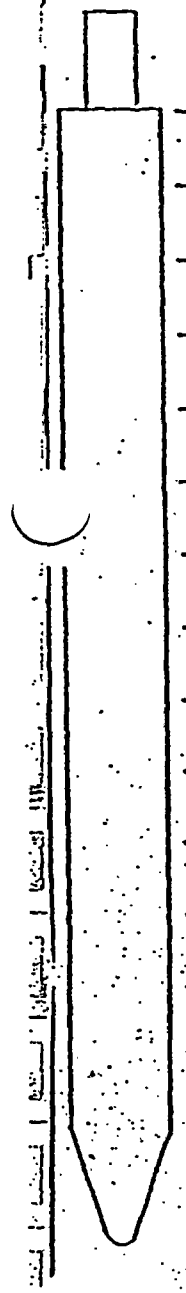

1-A	1-B	1-C	2-A	2-B	2-C	GUIDE TUBE
0.882	0.880	0.865	0.875	0.877	0.875	1.100
0.925	0.920	0.904	0.901	0.883	0.889	1.100
1.078	0.915	0.905	0.910	0.883	0.909	1.100
1.107	0.916	0.905	0.915	0.889	0.914	1.100
1.103	0.912	0.906	0.920	0.892	0.915	1.100
1.097	0.915	0.908	0.922	0.891	0.914	1.100
1.093	0.913	0.909	0.922	0.890	0.913	1.100
1.091	0.913	0.909	0.922	0.890	0.913	1.100
1.087	0.914	0.909	0.922	0.892	0.913	1.105
1.088	0.919	0.909	0.923	0.892	0.914	1.105
1.106	0.920	0.908	0.921	0.892	0.915	1.105
1.090	0.915	0.909	0.922	0.884	0.915	1.105
1.057	0.917	0.909	0.917	0.882	0.910	1.105
1.009	0.886	0.867	0.897	0.872	0.888	1.105
0.875	0.888	0.890	0.886	----	0.870	1.105

TABLE II - SHIM-SAFETY ROD WIDTH DIMENSIONS

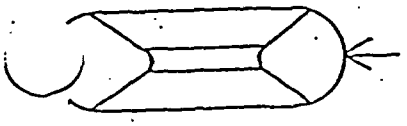

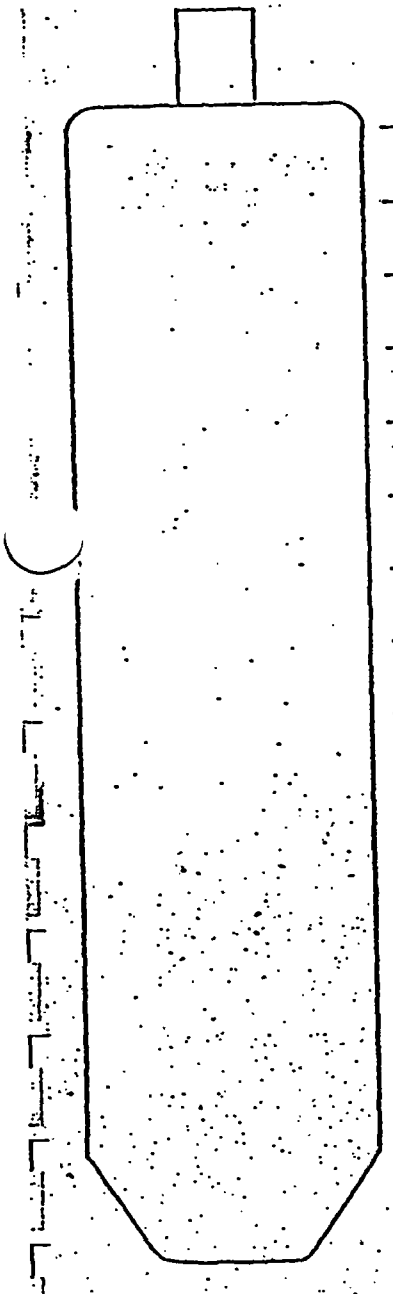

	1-A	1-B	1-C	2-A	2-B	2-C
—	2.242	2.242	2.245	2.251	2.245	2.248
—	2.239	2.249	2.246	2.258	2.245	2.239
—	2.175	2.244	2.249	2.255	2.232	2.227
—	2.187	2.250	2.247	2.255	2.225	2.225
—	2.187	2.247	2.250	2.252	2.225	2.225
—	2.184	2.250	2.250	2.251	2.225	2.225
—	2.187	2.249	2.250	2.250	2.225	2.226
—	2.191	2.248	2.251	2.250	2.225	2.226
—	2.184	2.248	2.253	2.248	2.225	2.226
—	2.183	2.247	2.253	2.251	2.225	2.227
—	2.185	2.247	2.255	2.252	2.225	2.226
—	2.200	2.245	2.255	2.252	2.225	2.226
—	2.227	2.251	2.247	2.255	2.230	2.231
—	2.246	2.250	2.250	2.257	2.245	2.245
—	-----	-----	2.232	2.250	-----	-----

B. Radiographic and Dye Penetrant Studies

Complete radiographs were taken to determine the conditions inside the rods. The most significant finding from these radiographs was the presence of a void above the B_4C powder in the rods. This is shown in Plate II on page 11. Dye penetrant tests indicated pitting on the surface of the rods but no cracks were revealed.

C. Techniques for Collection of Gas and B_4C Powder Samples

The apparatus shown in Sketch II, page 12, was set up to measure any existing pressure and to collect any gas contained in the rod. The apparatus consisted of a self-sealing puncturing device with a pressure-vacuum gauge and an evacuated reservoir for collecting gas samples from the rod. Two rods, 1-A and 1-B, were punctured at the top where the voids were located. After the gas samples were removed, both rods were subjected to internal pressures of 40 psig while immersed in water.

The rods were then opened by cutting out a section on one side of each rod. The section that was removed is shown in Sketch III on page 13. Care was taken to avoid getting aluminum shavings in the B_4C powder. Samples of the powder were removed from different positions along the length of the rod.

D. Analysis of Contents of Shim Rods

Gas Analysis

When pressure measurements were made on the two shim-safety rods, 1-B had a pressure of 20 psig while rod 1-A, the deformed rod, was at atmospheric pressure. The gas samples from 1-A, 1-B and 2-C were analyzed using a mass spectrometer.

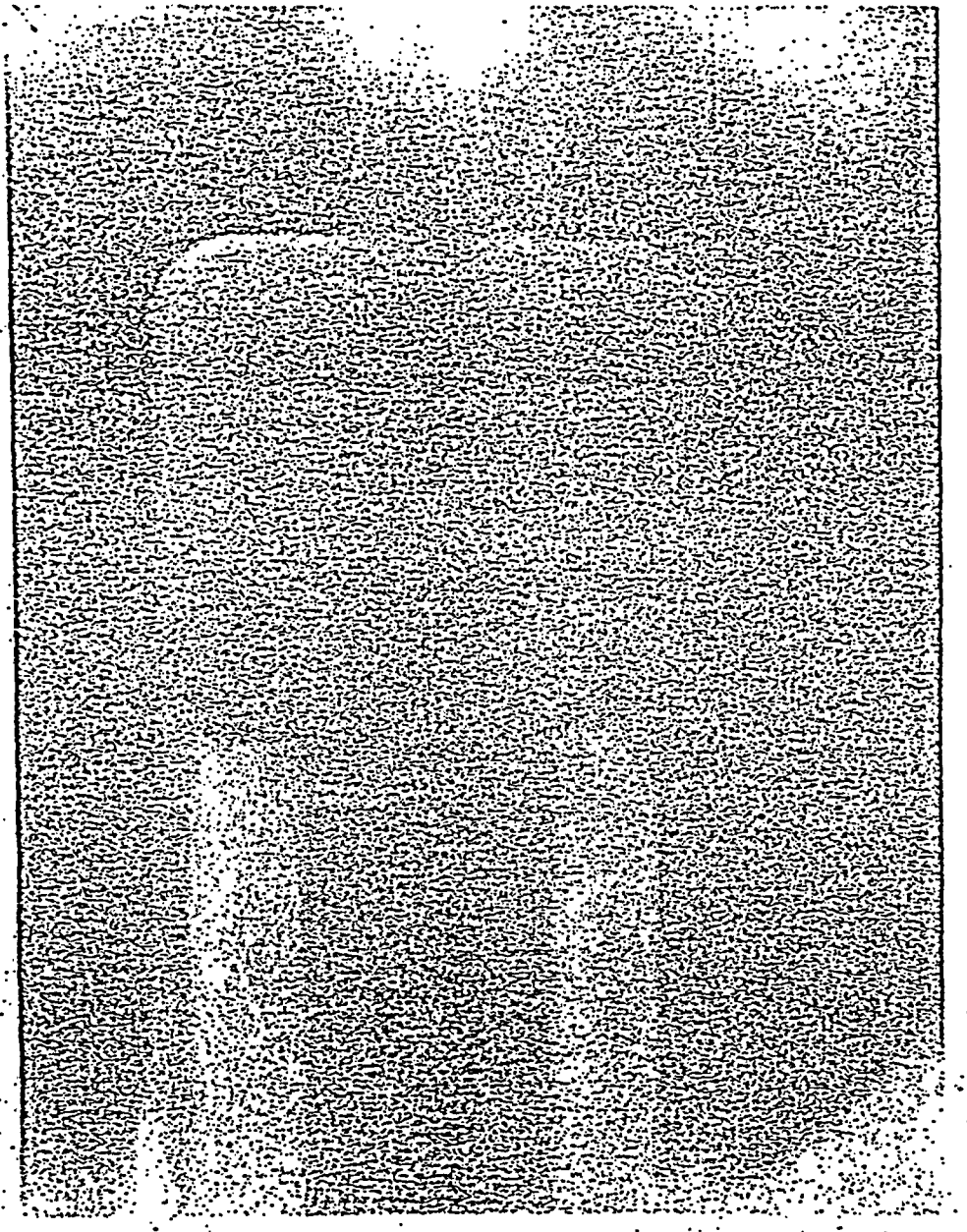

PLATE II - RADIOGRAPH OF THE TOP END OF A SHIM-SAFETY ROD

The light vertical rods are lead filled ballast tubes. The darkest area between the two tubes represents the void above the powder.

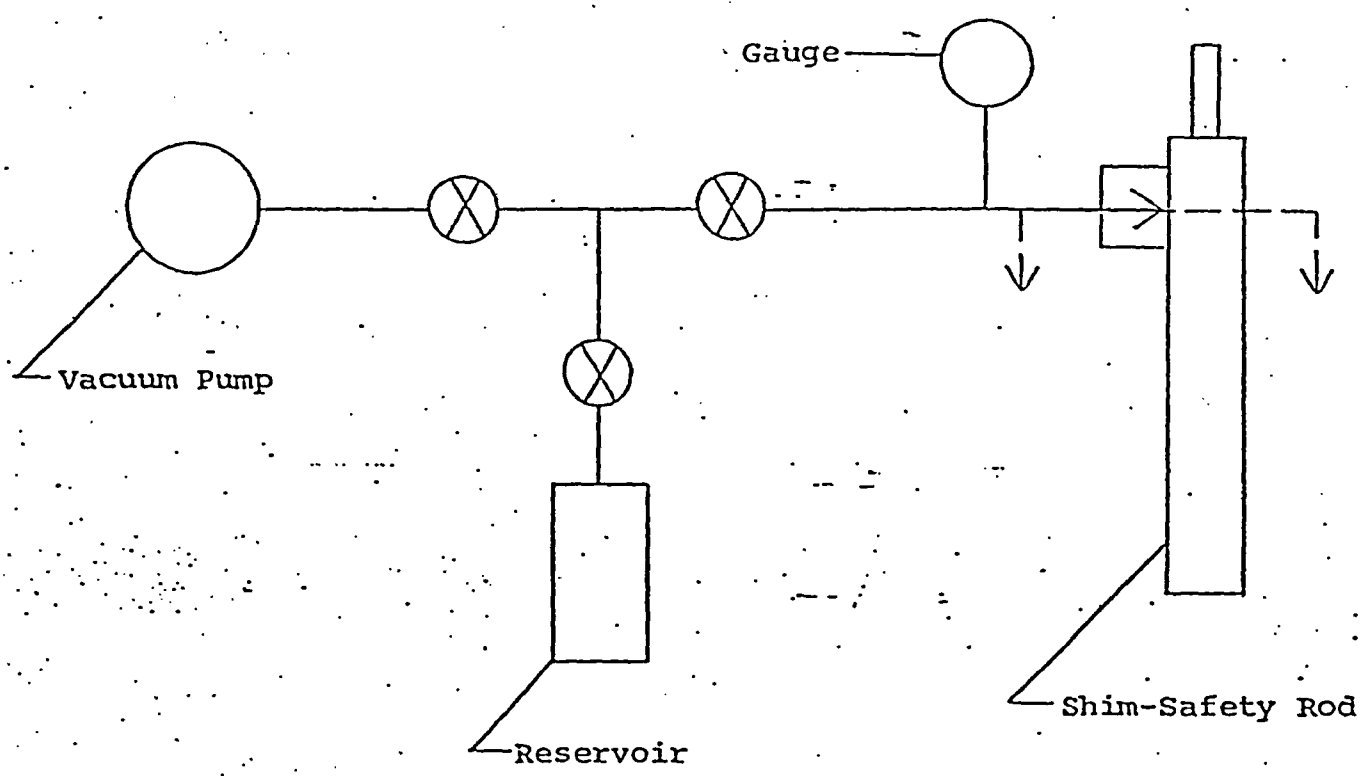

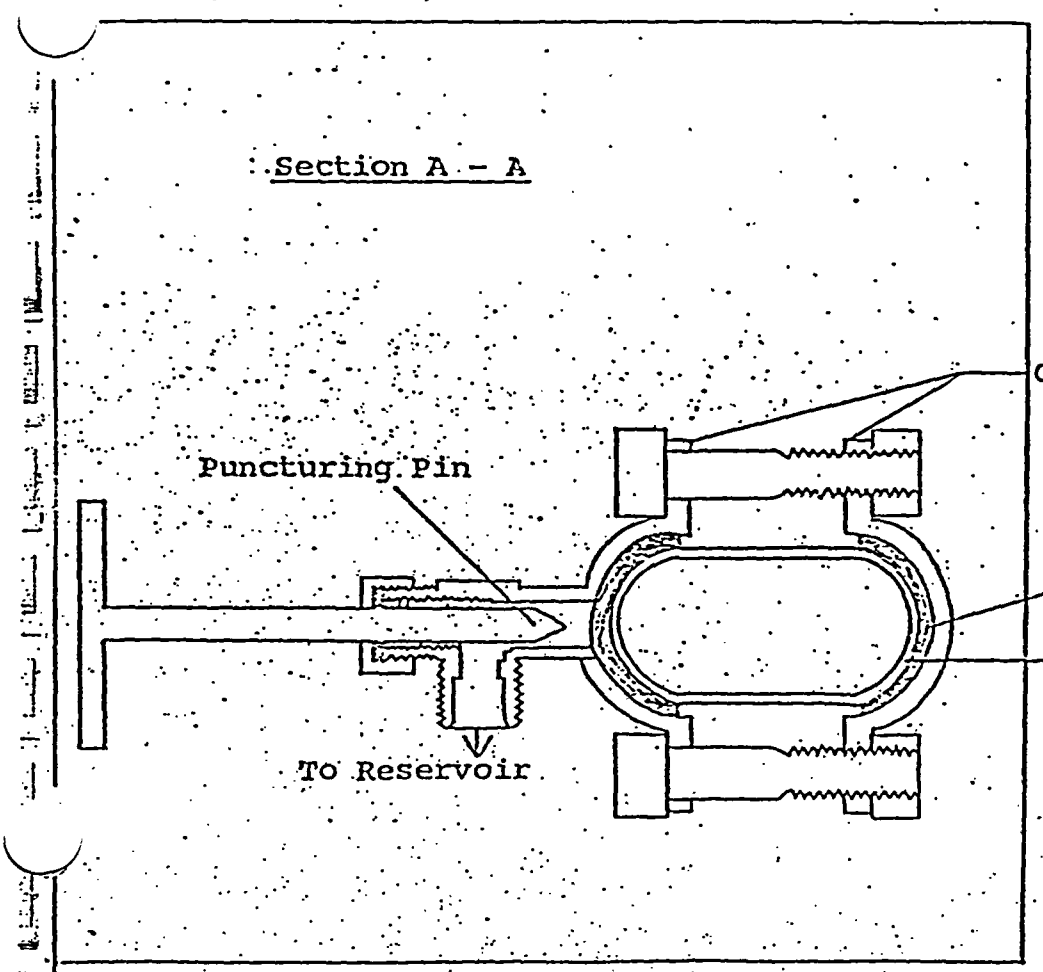

SKETCH II - GAS REMOVAL APPARATUS

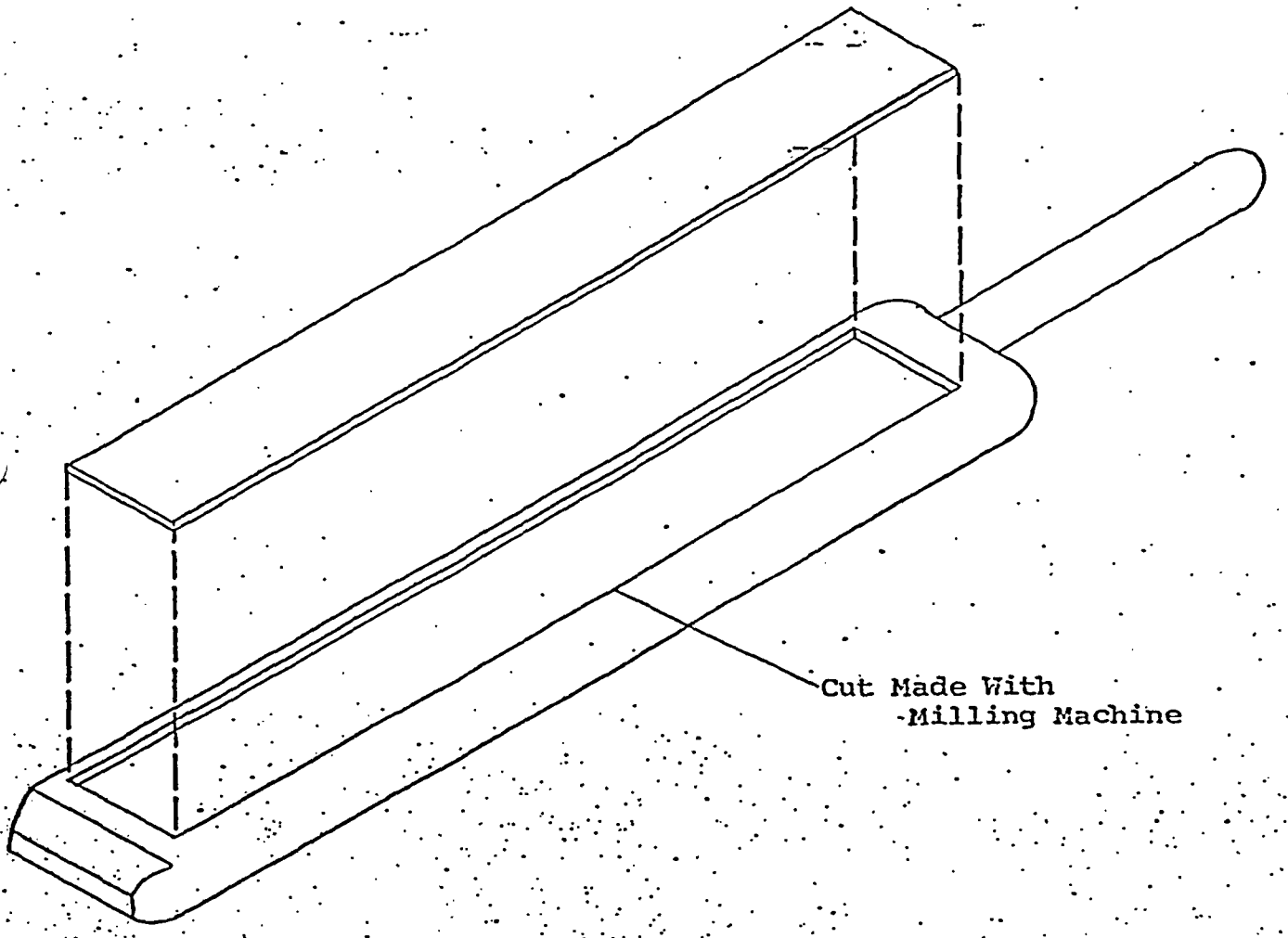

SKETCH III - ROD SECTIONING DIAGRAM

The results are as follows:

Gas Analyses
(in Mole Per Cent)

Rod 1-A Rod which jammed

Rod 1-B "Normal rod"

Rod 2-C Rod which off-gassed

Gas	1-A	1-B	2-C
H_2	36.42	78.6	39.47
O_2	36.00	0.4	14.98
N_2	23.23	15.4	44.54
CO_2	1.70	4.6	0.15
A	0.29	0.35	0.71
He	0.0	0.7	0.0

Note that the hydrogen-oxygen concentrations observed in 1-A and 2-C are in the detonable range.

Analysis of B_4C Powder and Inspection of Rod Interiors

When rod 1-B was opened, the B_4C powder was dry and lightly packed. The interior walls of the rod were not corroded. The powder removed from the lower portion of the rod was radioactive and had a total beta-gamma activity of about 3 mr/hr/gram on contact. A gamma spectral analysis indicated the presence of Mn^{54}, Zn^{65}, and Co^{60}. Analyses of the B_4C by emission spectroscopy showed the most predominant impurities to be Al, Cu, Fe, Zn and Mn. The supplier of the B_4C powder reports 98.79% B, 1.08% C, 0.10% Si, 0.02% Se and 0.02% N.

The B_4C in rod 1-A, the deformed rod, was found to be in a caked rather than a powdered form as in rod 1-B. The hard layer was concentrated between the ballast rods along the lower six inches of the shim rod. This cake had a grayish appearance unlike the characteristically black color of B_4C powder. The powder removed from the lower portion of rod 1-A was found to contain approximately 5 weight per cent water.

Oxidation was prevalent on the interior walls at the lower end of rod 1-A. A crust of Al_2O_3 surrounded the lead filled aluminum ballast rods.

The water found in rod 1-A indicated a leak had occurred. However, the 40 psig pressure test before sectioning failed to show such a leak. Therefore, another attempt was made to locate a leak in rod 1-A with the powder removed and the inner surface cleaned. This was done by replacing and rewelding the removed section and pressurizing to 40 psig. Under these conditions a 30 cc/hr leak was noted at the top of the rod where the endpiece is welded to the extruded tube. The gas leaked from a very small hole which looked much like the pits revealed by the dye penetrant test.

The leakage rate was reduced drastically by evacuating and then re-pressurizing the rod. It appeared that the leak was capable of a valve-like action which was dependent on the internal pressures of the rod.

IV. POSSIBLE EXPLANATION OF DEFORMATION

Consideration has been given to the possible causes of the swelling of rod 1-A. The deformation of rods 2-A, 2-B and 2-C, although not as great as that of 1-A, was also considered.

The hypotheses are:

A. Mechanical stresses resulting from expansion of wet B_4C powder.

B. Internal gas pressure generated by:

1. B^{10} (n, α) Li^7 reactions

2. Chemical reactions between B_4C and H_2O

3. Chemical reactions between Li^7 and H_2O

4. Radiolysis of H_2O

Several experiments and calculations have been made to assist in evaluating these hypotheses.

A. The hypothesis that the deformation of the rod was a result of volumetric changes in wetted B_4C powder appears to be without foundation. Radial measurements of a polyethylene bottle containing wetted B_4C at room temperature showed no dimensional changes during an eight week period of observation.

B-1. It has been demonstrated that a pressure of approximately 110 psig is required to obtain the degree of deformation observed for rod 1-A. Calculations indicate that the generation of this pressure by helium as a result of (n, α) reactions on boron is extremely doubtful. Further, the gas analysis of rods 1-A and 1-B showed a relatively low concentration of helium.

B-2. The hypothesis involving a chemical reaction between B_4C and H_2O has been given little consideration since the reaction rate constant is small even at temperatures of 400°C. (Reference 1)

B-3. Significant pressures from the Li-H_2O reaction are unlikely in view of the low lithium concentrations from the B^{10} (n, α) Li^7 reactions.

B-4. Present data strongly indicates that the necessary pressure to cause the observed rod deformation can be generated inside the rod by the radiolytic decomposition of water into gaseous hydrogen and oxygen. To produce free H_2 and O_2, this reaction requires free radical scavengers which could well be the B_4C powder itself, impurities in the powder, impurities in the water or the component parts of the rod (References 2, 3, 4, 5 and 6). The generation of gases was not the only prerequisite for the rod deformation. In addition, either the hole which allowed water to get into the rod and which allowed gas to escape must have closed off at some time or, the gas generation rate far exceeded the gas leakage rate.

The possibility of having water present at the time the rods were sealed in the fabrication process was considered since a small amount of water is capable of causing rod deformation. This is especially significant since B_4C powder is naturally hygroscopic.

In the case of the deformed rod, the above possibility was discounted in favor of an external leak since the rod was in the reactor for a long period of time before jamming occurred. However, this possibility exists for rods 2-A, 2-B and 2-C. It is therefore imperative that the B_4C powder used in fabricating shim-safety rods be dried and subsequently handled in humidity controlled environments.

In an attempt to demonstrate the feasibility of generating significant quantities of gas in reasonably short periods of time, an experiment was designed which would simulate the conditions that were suspected within the jammed rod. Two

small, aluminum sealed vessels, one containing water and the other water and B_4C powder were installed adjacent to the reactor core in a thermal flux of 5×10^{12} neutrons per square centimeter-second and a gamma field of 5×10^{7} roentgens per hour. Pressures in these chambers were monitored over a period of three days during which time the reactor operated at a power level of one megawatt for 50 hours. The pressure in the chamber containing water and B_4C powder increased linearly with respect to reactor operating time at a rate of 1.2 psig per hour. See Graph I, page 19. This test chamber had a volume of 295 cc and contained 10 grams of water and 25 grams of B_4C powder. The pressure in the chamber containing water only was 1.1 psig after 50 hours of reactor operation as compared to 60 psig in the chamber containing both water and B_4C powder.

Analysis showed that the gas generated in the water-B_4C chamber contained predominantly a hydrogen-oxygen gas mixture in a 2:1 ratio, similar to the finding for rod 2-C.

V. RECOMMENDATIONS

Deformation of shim-safety rods because of internal pressure could lead to the following dangerous conditions:

1. Withdrawal of a special fuel element during start-up. Any subsequent release and drop of this special fuel element could result in a large and rapid increase in the positive reactivity of the reactor.

2. Jamming of the rods during reactor operation. In such an event, it would not be possible to insert the deformed

GRAPH I - TEST CHAMBER PRESSURE VS MEGAWATT HOURS

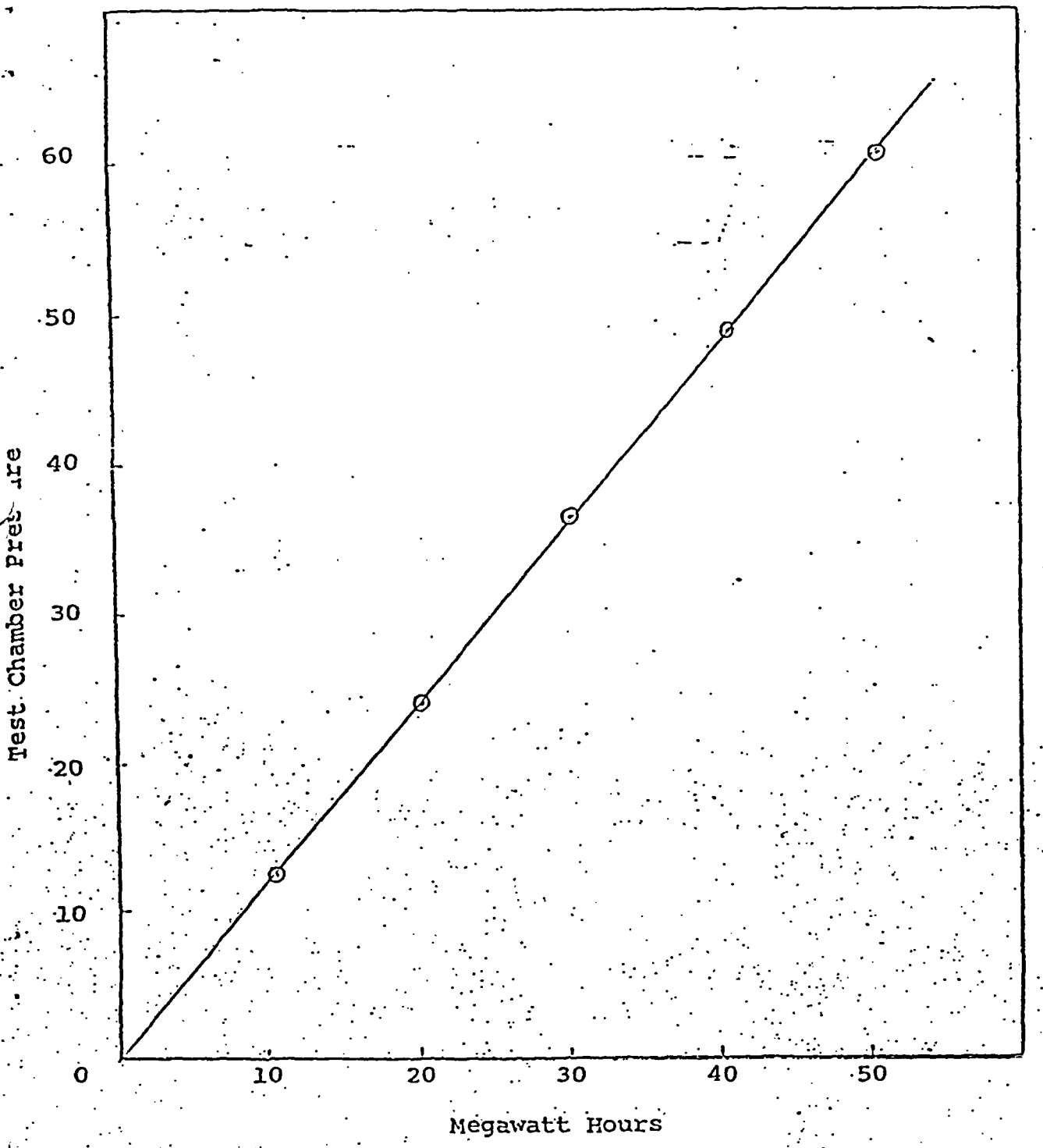

rods into the reactor when unsafe conditions exist or even for routine shut down. This is a particularly serious possibility in reactors which operate at power for long periods of time.

3. Detonation of the hydrogen-oxygen gas mixture contained in the shim-safety rods. This could cause damage to the reactor core in addition to rupturing the rod. Although such a detonation appears to be improbable, it is nevertheless a potential hazard that needs further investigation, especially in strong radiation fields.

Operational Recommendations

In view of the important function of shim-safety rods, a detailed inspection should be made of all rods before installation in a reactor. Records of these inspections, especially weights in water and dimensional measurements, should be maintained for reference purposes. A careful survey of the surface conditions of the rods including all welds is extremely important. Radiographs have proved valuable in determining internal conditions of reactor rods.

In addition to the initial tests, shim-safety rods should undergo periodic inspections. The FNR is presently on a schedule calling for rod inspection every 320 megawatt hours of operation. This inspection requires the rods to be removed from the reactor, the dimensions measured directly and the surface observed for corrosion or any other indication of damage, such as off-gassing.

Close attention should also be given to the potential hazards that exist when water containing free-radical scavengers is present in any sealed experiment or device located in a radiation field.

Recommendations for Design and Fabrication

Consideration should be given to the design of new shim-safety rods which would avoid the possibility of the generation of gases leading to high pressures. Further, consideration should be given to the design of the special fuel elements for these rods which would minimize the possibility of jamming. Any arrangement of element and rod which would make dimensional changes easily and readily detectable would be a decided improvement over our present system.

In the fabrication of shim-safety rods similar to those presently used on the FNR, it is extremely important that all substances capable of producing gases in the presence of radiation be held to a minimum. These substances include volatile degreasing agents, water used for rinsing and any water contained in the B_4C powder.

Proposed Investigations

As a result of this investigation of the shim-safety rod incident, it has become evident that the following subjects should be investigated more thoroughly.

1. The internal pressures necessary for shim-safety rod deformation.
2. Gas and pressure generation in shim-safety rods located in a reactor core as a function of water content in B_4C powder.
3. The effect of alpha particles and lithium recoils from B_4C powder on the radiolytic process.
4. The sources of free-radical scavengers which are required in the radiolytic process.

5. Possible sources of ignition energy for the detonation of hydrogen-oxygen gas mixtures.

Recognizing the importance of the above problems, these investigations will be undertaken at the Phoenix Memorial Laboratory. Financial assistance will be required for a thorough investigation of these problems.

From an operational point of view, the removal of shim-safety rods from their special fuel elements and the reactor for dimensional tests is a time consuming and complicated manipulation. In an attempt to simplify these inspections a study of "in situ" rod inspection techniques will be undertaken. Further, the criteria for the frequency and technique of inspection for shim-safety rods will be re-evaluated in light of the results of the aforementioned experimental investigations.

I. REFERENCES

1. F. F. Mikus, Reactor Technology Quarterly Report No. 6 KAPL-2000-3, 48-49 (1958).

2. J. B. Hoag, Nuclear Reactor Experiments, D. Van Nostrand Co., Inc., Princeton, New Jersey 346-347 (1958).

3. E. J. Hart and P. D. Walsh, Proc. 2nd Intern. Conf. Peaceful Uses of Atomic Energy, Geneva 29, P/763 38-42 (1958).

4. A. O. Allen and H. A. Schwarz, Proc. 2nd Intern. Conf. Peaceful Uses of Atomic Energy, Geneva 29, P/1403 30-37 (1958).

5. E. J. Hart, et al, Proc. 2nd Intern. Conf. Peaceful Uses of Atomic Energy, Geneva 7, P/839 593-598 (1955).

6. C. B. Senvar and E. J. Hart, Proc. 2nd Intern. Conf. Peaceful Uses of Atomic Energy, Geneva 29, P/1128 19-23 (1958).

b+p Brooks & Perkins, Incorporated

Report No. 540

QUANTITATIVE ANALYSIS

OF

BORAL[tm] PANELS

PROGRAM CONDUCTED FOR:

YANKEE ATOMIC ELECTRIC COMPANY
20 Turnpike Road
Westborough, Mass. 01581

PROGRAM CONDUCTED BY:

Brooks & Perkins, Inc.
17515 W. Nine Mile Road
Southfield, Mich. 48075

July 30, 1976

Leslie Mollon

Mr. Leslie Mollon - Director
Nuclear Product Development

TABLE OF CONTENTS

Table of Contents (cont'd)

1. INTRODUCTION

1.1 Purpose. This report provides the results of a quantitative analysis program conducted to determine the amount of boron carbide present in the core (inner layer) of BORAL^{tm} panels. The information obtained for this program was supplemental to the physical characteristics obtained during the routine quality assurance checks which are performed in accordance with Brooks & Perkins, Inc. Specification BPS-9000-01.

1.2 Program. The program envolved the physical measurement of the BORAL^{tm} panels by destructive and non-destructive methods in various locations within each panel. A total of 147 panels were analyzed in five different lots. Four of the lots were randomly selected and the other lot consisted of panels having the lowest content of boron carbide by neutron radiographic examination.

The program included 1,833 thickness measurements taken by metallographic techniques, 66 thickness measurements by ultrasonic techniques and 196 quantitative chemical analyses (See Appendix A thru G

The recorded data was statistically analyzed and for each characteristic in each lot a mean and standard deviation was established. The probability that each characteristic will be above a certain minimum value can now be determined from the statistical data.

1.3 Background. BORAL[tm] is a thermal neutron shielding material that can best be described as a sandwich-type panel. The outer layers or "skins" of the panel are 1100 alloy aluminum. The inner layer or "core" of the panel is a mixture of boron carbide and 1100 alloy aluminum. The interface between a skin and the core is not a clearly discernible surface when viewed with a microscope. The interface is in reality an irregular zone that is approximately five thousands of an inch (.005 in.) in thickness. In this zone there is a linear transition from 100% aluminum and zero % boron carbide in the skin to 65% aluminum and 35% boron carbide particles of various sizes in the core. The appearance of the interface is a series of peaks and valleys. (See Fig. 1

The boron carbide particles is the constituent of the BORAL[tm] panel that absorbs or attenuates the thermal neutrons. The ability of the panel to provide a particular level of neutron attenuation is directly related to the amount of boron carbide contained per unit surface area of the panel.

The BORAL[tm] panel is produced by the rolling of a specially prepared ingot into a sheet (1) that will yield one or more finished panels(1) that are four feet wide and ten feet long. The finished panels are sheared from the oversized sheets by the removal of the scrap material around the

(1) Note term useage, "sheet" - the untrimmed product of rolling, "panel" 48" x 120" product cut from the original rolled product.

10 X 1931B-4

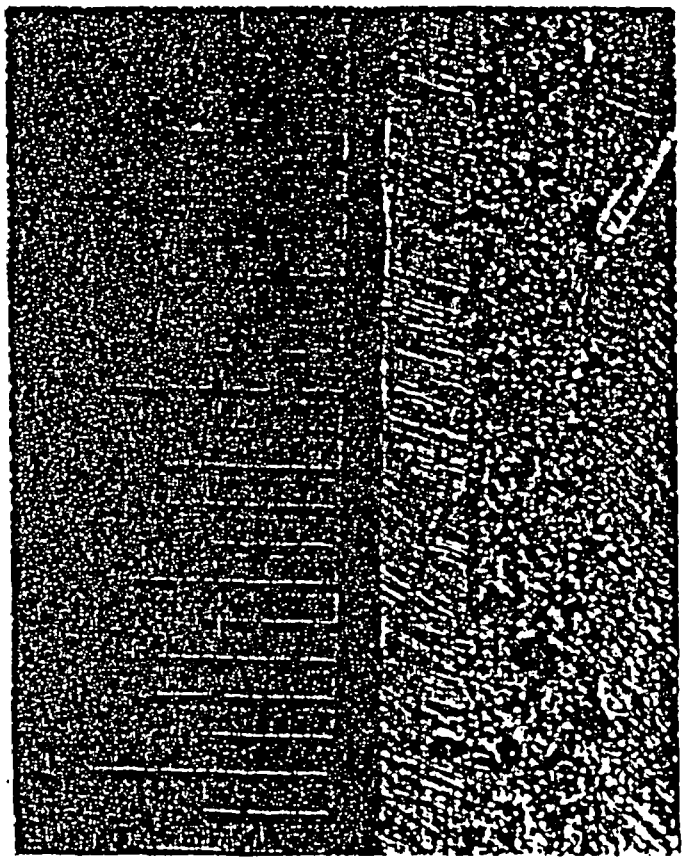

FIGURE 1

MICROSCOPIC VIEW OF THE EDGE OF BORAL™ PANEL NO. 1931-B (10X)

periphery of the oversized sheet. The scrap material contains a core that tapers from zero thickness on the extreme outer edge to a core of full thickness on the edge adjacent to the finished panel. If the shear line is improperly placed on the oversized sheet the finished panels could contain a core thickness along that line that is not of full thickness.

1.4 Methods Used.

1.4.1 Metallographic Technique. The thickness of the core was measured by a 7.5 power optical comparator after the edge of the panel or the retain strip was mechanically and chemically prepared. Approximately one eighth of an inch (.125 in.) was machined away from the edge to remove the material affected by the searing action. The edge was then made smooth by using a sequence of files of decreasing courseness. The edge was then polished with emery paper before chemically etching it to improve the visual contrast and to remove any minute overlapping of the boron carbide by the aluminum from the mechanical removal operations.

The core thickness measurement was established by averaging the one maximum and the one minimum measurement that could be observed within the visual range of the optical comparator.

1.4.2 Ultrasonic Technique. The thickness of the core was measured by a Sonoray Model 303B Ultrasonic Flow and Thickness Tester using a dual element transducer. The tester was calibrated with a standard block before taking any set of thickness measurements. The tester was also frequently checked during the taking of measurements to assure the instrument remained in calibration.

To take a thickness measurement the tester operator would place the dual element transducer on the surface of the BORAL^{tm} panel that had been wetted with a drop of liquid couplant. The operator would adjust the position of the transducer within the spot of couplant until a stable wave pattern was displayed on the scope of the tester. The particular tester used was equipped with a digital readout which eliminated the possibility of human error in reading the grid lines on the scope face of the tester because the displayed number was the actual core thickness at that location.

1.4.3 Quantitative Chemical Analysis. The chemical analysis was performed on samples approximately one inch square which had been removed from a retain strip or the finished BORAL^{tm} panel. The samples were marked with a numbering system which identified the BORAL^{tm} sheet and the location on the sheet from where the sample was taken. The four edges of the samples were filed smooth and straight to prevent erroneous volumetric readings.

The surface area of each sample was determined by dividing the sample's volume by its thickness. The volume was determined by deducting the weight of the sample in water from the weight of the sample in air and correcting the result for the difference of the water temperature from the standard temperature.

The weight of boron carbide in the sample was determined by weighing the dry residue remaining after dissolving the sample in dilute hydrochloric acid and correcting the result for the soluble portion of the boron carbide. It was determined by actual test that 4.12 percent of boron carbide conforming to Type 2 of ASTM C750-73T is soluble in dilute hydrochloric acid (See Appendix

The content of boron carbide per unit area (commonly referred to as the "grams loading") was determined by dividing the total weight of the boron carbide in the sample in grams by the area of the original sample in square centimeters.

The weight factor or percentage of boron carbide present in the core was determined by dividing the total weight of boron carbide by the total weight of the sample less the calculated weight of the aluminum cladding.

The core compaction factor was determined by dividing the total weight of the sample less the calculated weight of aluminum cladding by the theoretical weight of the core based on the weight factor and core thickness.

The core proportionality was determined by dividing the core thickness by the total thickness of the sample.

2. SUMMARY

2.1 Results. The mean core thickness, the weight factor of boron carbide within the panel core and the standard deviation of each are listed in Table I. These results are listed by panel lot number and by the sheet area where the observations were taken. The averages by area and the overall weighted average is also shown in Table I.

2.2 Areas. The location of each observation taken during this program can be determined by the sample serial number and a map of the panels. The observation results were then segregated by area and listed accordingly. The three main sheet areas are: (1) Retain Strip, which is a portion of the scrap that is trimmed from the edge that is immediately adjacent to the end of a finished panel, (2) Outer Edge, which is the area lying in the one inch border strip on the periphery of the finished panel, (3) Central Portion, which is the area lying internal to the one inch border strip (i.e. - the area that is more than one inch in from the finished panel edge).

2.3 Panel Lots. The BORAL^{tm} panels analyzed in this program are listed in Table II by lot number and panel serial number. The lots were established during the progress of the program and can be described as follows:

TECHNICAL ANALYSIS FORM

BY LM DATE	Brooks & Perkins, Incorporated	SHEET OF
CK. DATE	ADVANCED STRUCTURES DIVISION	SUBJECT
REV. DATE		

SUMMARY OF STATISTICAL FACTORS

PANEL LOT NO.	RESULTS BY AREA OF SHEET: STA. FAC.	RETAIN STRIP	OUTER EDGE	CENTRAL PORTION	WEIGHTED AVERAGES
I	$\bar{t}_c$	(26) .0800	(48) .0772	(217) .0894	—
	S.D.	.0059	.0071	.0068	
	W.F.	(38) .3800	(48) .3821	N/A	—
	S.D.	.0173	.0348		
II	$\bar{t}_c$	N/A	(150) .0843	(170) .0924	—
	S.D.		.0056	.0025	
	W.F.	(7) .3902	(2) .3858	(1) .3791	—
	S.D.	.0125	.0216	-0-	
III	$\bar{t}_c$	N/A	(170) .0882	N/A	—
	S.D.		.0031		
	W.F.	N/A	N/A	N/A	—
	S.D.				
IV	$\bar{t}_c$	(167) .0846	N/A	N/A	—
	S.D.	.0045			
	W.F.	(27) .3962	N/A	N/A	—
	S.D.	.0194			
V	$\bar{t}_c$	(1001) .0894	N/A	N/A	—
	S.D.	.0064			
	W.F.	(73) .3878	N/A	N/A	—
	S.D.	.0164			
OVERALL AVERAGES LOTS I, II, III, IV, V	$\bar{t}_c$	(1194) .0847	(318) .0832	(387) .0909	—
	S.D.	.0056	.0053	.0047	
	W.F.	(145) .3886	(50) .3840	(1) .3791	—
	S.D.	.0164	.0282	-0-	
UNBIASED AVERAGES LOTS II, III, IV, V	$\bar{t}_c$	(1168) .0870	(270) .0863	(170) .0924	(1608) .0921 *
	S.D.	.0055	.0044	.0025	.0027
	W.F.	(107) .3914	(2) .3858	(1) .3791	(110) .3911 *
	S.D.	.0161	.0282	-0-	.0162

LEGEND — STA. FAC. = STATISTICAL FACTORS, $\bar{t}_c$ = MEAN CORE THICKNESS (INCHES), S.D. = STANDARD DEVIATION, W.F. = MEAN WEIGHT-FACTOR, (26) = NO. OF OBSERVATIONS, N/A = NOT AVAILABLE.

* BY AREA RATIOS OF .0576 OUTER, .9424 CENTRAL.

* BY NUMBER RATIOS OF .9727 RETAIN, .0182 OUTER, .0091 CENTRAL

Lot I - The thirteen (13) panels which appeared to have the lowest content of boron carbide by inspection of the neutron radiographs previously provided as a routine quality assurance item;

Lot II - The ten (10) panels picked at random to fulfill an incremental shipment release by the customer;

Lot III - The twenty (20) panels picked at random to fulfill a second incremental shipment release by the customer;

Lot IV - The twenty-seven (27) retain strips are from the sheets of previously delivered panels for spent fuel storage racks for Yankee Rowe;

Lot V - The seventy-seven (77) retain strips are from the sheets previously delivered panels for spent fuel racks for Maine Yankee.

2.4 Weighted Average. The "weighted average of the mean core thickness" quoted in Table I, was obtained by multiplying the unbiased average mean core thickness for the outer edge and central portion areas by the percentage factor each area represents of the total finished panel area and then adding the two products. The "weighted average of the mean core

TECHNICAL ANALYSIS FORM

BY LM DATE CK. DATE REV. DATE	Brooks & Perkins, Incorporated ADVANCED STRUCTURES DIVISION	SHEET OF SUBJECT

IDENTIFICATION OF LOTS BY PANEL NO.

LOT NO.	PANEL NUMBER					
I	1000B	1069B	1338B	1372A	1381A	1394A
(13) MIN. B+C	1416A	1426B	1492A	1496B	1533B	1537B
	1568A					
II	1266A	1325A	1325B	1352A	1352B	1402B
(10) RANDOM	1406B	1434A	1462B	1931B		
III	2003A	2004A	2004B	2005A	2005B	2006A
	2006B	2007A	2010A	2013A	2015B	2017B
(20) RANDOM	2019A	2019B	2025B	2028B	2033A	2033B
	2035A	2035B				
IV	1531A	1531B	1535A	1535B	1545B	1552A
	1552B	1555A	1555B	1556A	1556B	1558A
(27) RETAINS (ROWE)	1558B	1565B	1566B	1569A	1569B	1575B
	1581A	1585A	1585B	1589A	1589B	1590A
	1590B	1594A	1594B			
V	1001B	1010A	1012B	1013A	1023A	1025B
	1052A	1055A	1057A	1059B	1064A	1067A
(77) RETAINS (MAINE ETC.)	1072B	1077B	1084B	1086B	1091B	1093B
	1101A	1111A	1112B	1113B	1116A	1118A
	1118B	1124A	1151A	1151B	1152A	1152B
	1155A	1156B	1167A	1182A	1184B	1201A
	1201B	1203A	1203B	1206A	1206B	1207B
	1212A	1222B	1224A	1227A	1228A	1228B
	1233A	1233B	1243A	1243B	1245A	1251B
	1260A	1281A	1302A	1302B	1304A	1307B
	1320A	1323B	1334A	1334B	1335B	1336A
	1336B	1359A	1361B	1364A	1397A	1535B
	1555A	1558A	1590A	1594A	(X)	

thickness" represents the result that will be obtained from a set of observations that are randomly spaced across the entire surface of a panel. The "weighted average of the standard deviation" for the "weighted average of mean core thickness" was also determined by the ratio of areas.

The "weighted average of the mean weight-factor" was determined on the basis of the number of observations in each area because no valid relationship between the value of the weight-factor and the location of the observation was discovered. The number of weight-factor observations taken from the retain strip, outer edge, and central portion areas were 145, 50, and 1 respectively. The number ratios for those areas is therefore .7398, .255, and .0051 respectively. The "weighted average of the mean weight-factor" was determined by multiplying the average weight-factor in each area by the number ratio for that area and then adding the three products. The "weighted average of the mean weight-factor" represents the results that would be obtained from an equal number of observations in each area.

The "weighted average of the standard deviation" for the mean weight-factor was also determined by the ratio of the number of observations. The results from the panels in Lot I were excluded from the averages used to determine all of the weighted averages because the panels

in Lot I do not represent a normal distribution that would be in a randomly selected lot.

2.5 Theory. The statistical factors obtained from the recorded data were determined in the following manners,

2.5.1 Mean. The arithmetic mean for the core thickness and the weight-factor were determined by dividing the summation of those observations separately in each lot by the number of those observations in the lot.

mean core thickness $= \bar{t}_c = \frac{\Sigma t_c}{\text{No. of } t_c \text{ OBSERVATIONS}}$

mean weight-factor $= \overline{W.F.} = \frac{\Sigma W.F.}{\text{No. of W.F. OBSERVATIONS}}$

2.5.2 Standard Deviation. The standard deviation for a set of core thickness observations and weight-factor observations were determined by taking the square root of the average squared residual.

standard deviation (core thickness) $= S.D._{t_c} = \sqrt{\frac{\Sigma t_c^2 - \frac{(\Sigma t_c)^2}{n}}{n-1}}$

Standard deviation (weight-factor) $= S.D._{W.F.} = \sqrt{\frac{\Sigma W.F.^2 - \frac{(\Sigma W.F.)^2}{n}}{n-1}}$

2.5.3 Probability. The probability that a deviation of an individual observation from the mean lies between minus x (S.D.) and infinity is determined from the probability integral.

$$P = \frac{1}{\sqrt{2\pi}} \int_{-x(S.D.)}^{\infty} e^{-\frac{x^2}{2}} dx$$

By consulting a table of probability functions such as is found in "Handbook of Mathematical Tables and Formulas" by Burington, it can be determined that a value of 1.65 times the standard deviation will provide a probability of .9505 for a normal distribution of observations.

3. CONCLUSIONS

The boron carbide content per unit area of the BORAL^{tm} panels is equal to or greater than 0.203 grams per square centimeter with a probability of .9505. This conclusion was arrived at in the following manner:

$$P = \frac{1}{\sqrt{2\pi}} \int_{-1.65\ S.D.}^{\infty} e^{-\frac{x^2}{2}} dx = .9505$$ (SEE PARA. 2.5.2

weighted average of mean core thickness = $\overline{t_c}^w$ = .0921 INCHES

weighted average of standard deviation for t_c = $\overline{S.D.}^w_{t_c}$ = .0027

95% of observation fall between - 1.65 SD and infinity

core thickness at minimum of 95% = $\overline{t_c}^w - 1.65\ \overline{S.D.}^w_{t_c}$

minimum t_c = .0921 - .0044 = .0877 in.

weighted average of mean weight-factor = $\overline{W.F.}^w$ = .3911

weighted average of standard deviation for W.F. = $\overline{S.D.}^w_{W.F.}$ = .0162

95% of observations fall between - 1.65 SD and infinity

weight-factor at minimum of 95% range = $\overline{W.F.}^w - 1.65\ \overline{S.D.}^w_{W.F.}$

minimum W.F. = .3911 - .0267 = .3644

The boron carbide distribution per unit area is directly proportional to the core thickness and the boron carbide content weight factor. The theoretical distribution of boron carbide is 0.1894 grams per square centimeter for a core thickness of 0.085 inches and a weight factor of .3500 (see Appendix L). The actual distribution can be determined from the following relationship:

$$\frac{\text{actual } B_4C \text{ distribution}}{\text{theoretical } B_4C \text{ distribution}} = \frac{t_c \text{ (actual)}}{t_c \text{ (theor.)}} \times \frac{\text{W.F. (actual)}}{\text{W.F. (theor.)}}$$

$$\text{actual } B_4C \text{ distribution} = \frac{.1894}{} \times \frac{.0877}{.0850} \times \frac{.3644}{.3500} = .2035 \text{ gm/square}$$

APPENDIX A

EXPERIMENTAL DATA

PANEL LOT I

PAGES I-1 THRU I-18

SAMPLE No.	1000 BR-1	1000 BR-2	1000 B - EVEN	1000 B-2
t_a (in./cm.)	.185/.4699	.185/.4699	.172/.4369	.173/.439
WT-a (gms.)	6.9252	6.3700	5.3698	6.9181
A-a (sq. cm.)	5.6555	5.2139	4.6343	5.9504
WT-b (gms.)	1.0378	.9463	.5581	.8839
G.L. (gms/sq.cm.)	.184	.181	.120	.149
W.F. —	.3614	.3643	.3630	.3550
t_c (in./cm.)	.081/.2057	.080/.2032	.052/.1321	.065/.16
C.F. / C.P	.9364/.4378	.9303/.4324	.9530/.3024	.9610/.37

SAMPLE No.	1000 B - 000	1000 B-7	1069 BR-1	1069 BR-
t_a (in./cm.)	.178/.4521	.179/.4547	.188/.4775	.188/.477
WT-a (gms.)	6.2887	5.3870	8.1414	7.9152
A-a (sq.cm.)	5.2866	4.5148	6.5893	6.3590
WT-b (gms.)	.9446	.7402	1.3822	1.3654
G.L.	.1787	.1639	.2098	.2147
W.F.	.3474	.3891	.3790	.3771
t_c (in./cm.)	.080/.2032	.067/.1702	.089/.2261	.090/.22
C.F. / C.P	.9591/.4495	.9412/.3743	.9300/.4735	.9462/.4

SAMPLE No.	1338 BR-1	1338 BR-2	1338 B-7	1338 B-
t_s (in./cm.)	.180/.4572	.183/.4648	.175/.4445	.175/.444
WT-s (gm.)	6.7924	6.8312	6.3658	6.4657
A_s (sq. cm.)	5.7478	5.7307	5.4308	5.5524
WT-b (gms.)	1.1416	1.1492	.9319	.8329
G.L.	.1986	.2005	.1716	.1500
W.F.	.3817	.3987	.3603	.3155
t_c (in./cm.)	.084/.2134	.083/.2108	.074/.1880	.075/.19
C.F. / C.P	.9265/.4668	.9078/.4535	.9610/.4229	.9433/.42

SAMPLE No.	1338 B-8	1338 B-10	1372A-4	1372A-6
t_s (in./cm.)	.172/.4369	.170/.4318	.172/.4369	.174/.442
WT_s (gms.)	5.0311	5.0849	6.4842	6.6420
A_s (sq. cm.)	4.4477	4.5862	5.6988	5.8131
WT-b (gms.)	.9006	.8698	1.1717	1.1623
G.L.	.2025	.1897	.2056	.1999
W.F.	.4511	.3829	.3869	.3682
t_c (in./cm.)	.073/.1854	.081/.2057	.084/.2134	.087/.22

SAMPLE No.	1372A-7	1372A-9	1372AR-1	1372AR-
t_a (in./cm.)	.177/.4496	.176/.4470	.182/.4623	.184/.46
WT-a (gms.)	6.9310	6.8497	7.0670	7.1194
A-a (sq. cm.)	5.9144	5.8901	5.7741	5.9125
WT-b (gms.)	1.2253	1.2737	1.0996	1.1318
G.L. (gms/sq.cm.)	.2072	.2162	.1904	.1914
W.F. —	.3663	.4371	.3608	.4101
t_a (in./cm.)	.089/.2261	.079/.2007	.081/.2057	.077/.19
C.F. / C.P.	.9493/.5029	.9407/.4490	.9733/.4449	.9087/.41

SAMPLE No.	1381AR-1	1381AR-2	1381A-4	1381A-2
t_a (in./cm.)	.190/.4826	.190/.4826	.177/.4496	.178/.45
WT-a (gms.)	7.1598	6.2661	7.1400	6.944
A-a (sq.cm.)	5.7663	4.9560	6.1057	5.953
WT-b (gms.)	1.0536	.9205	1.1672	.9975
G.L.	.1827	.1857	.1912	.1676
W.F.	.3623	.3478	.3315	.3842
t_a (in./cm.)	.083/.2108	.084/.2134	.091/.2311	.072/.18
C.F. / C.P.	.9076/.4368	.9483/.4422	.9443/.5140	.9062/.4

SAMPLE No.	1381A-5	1381A-7	1394AR-1	1394AR-
t_s (in./cm.)	.183/.4648	.183/.4648	.185/.4699	.182/.46
WT-s (gms.)	6.2407	5.8232	6.7935	6.929
A_s (sq. cm.)	5.1461	4.8100	5.5205	5.757
WT-b (gms.)	1.0076	.9504	.9135	1.037
G.L.	.1958	.1976	.1655	.1801
W.F.	.4306	.4574	.3719	.404
t_a (in./cm.)	.073/.1854	.070/.1778	.071/.1803	.072/.18
C.F. / C.P.	.9355/.3989	.9287/.3825	.9369/.3837	.9272/.3

SAMPLE No.	1394A-8	1394A-10	1394A-7	1394A-
t_s (in./cm.)	.174/.4420	.171/.4343	.173/.4394	.171/.43
WT_s (gms.)	6.6993	6.4895	6.4685	6.1487
A_s (sq. cm.)	5.7867	5.7199	5.6557	5.369
WT-b (gms.)	1.1563	1.1323	1.9773	.9669
G.L.	.1998	.1980	.1906	.1801
W.F.	.3972	.3849	.3739	.3570
t_a (in./cm.)	.079/.2007	.081/.2057	.081/.2057	.078/.19
C.F. / C.P.	.9521/.4541	.9504/.4721	.9409/.4681	.9456/.4

SAMPLE No.	1416AR-1	1416AR-2	1416A-4	1416A-1
t_a (in./cm.)	.181/.4597	.181/.4597	.174/.4420	.174/.44
WT-a (gms.)	7.0529	6.7357	6.7885	6.5814
A-a (sq. cm.)	5.8066	5.5308	5.8616	5.6606
WT-b (gms.)	1.0290	.9875	.9601	.9211
G.L. (gms/sq.cm.)	.1772	.1785	.1638	.1627
W.F. —	.4064	.3769	.3492	.3488
t_a (in./cm.)	.068/.1727	.073/.1854	.074/.1880	.073/.18
C.F. / C.P.	.9612/.3757	.9704/.4033	.9456/.4253	.9536/.4

SAMPLE No.	1416A-1	1416A-3	1426B-8	1426B-1
t_a (in./cm.)	.178/.4521	.176/.4470	.177/.4496	.176/.447
WT-a (gms.)	6.4845	6.6940	6.4404	6.6156
A-a (sq.cm.)	5.5564	5.7347	5.4540	5.6401
WT-b (gms.)	1.1340	1.1746	1.0796	1.0344
G.L.	.2041	.2048	.1979	.1834
W.F.	.3929	.3791	.3915	.3900
t_a (in./cm.)	.084/.2134	.085/.2159	.079/.2007	.074/.18
C.F. / C.P.	.9257/.4720	.9507/.4830	.9580/.4464	.9512/.4

SAMPLE No.	1426B-3	1426B-5	1426BR-1	1426BR-
t_s (in./cm.)	.177/.4496	.178/.4521	.186/.4724	.186/.47
WT-s (gm.)	6.5744	6.8949	6.5092	6.5127
A_s (sq. cm.)	5.5936	5.8660	5.2164	5.2175
WT-b (gms.)	1.0846	1.2233	.8936	.8664
G.L.	.1939	.2085	.1713	.1661
W.F.	.3724	.3852	.3762	.3588
t_a (in./cm.)	.082/.2083	.086/.2184	.071/.1803	.072/.18
C.F. / C.P.	.9491/.4633	.9421/.4831	.9593/.3817	.9598/.3

SAMPLE No.	1492AR-1	1492AR-2	1492A-2	1492A-1
t_s (in./cm.)	.184/.4674	.186/.4724	.171/.4343	.171/.434
WT_s (gms.)	7.3039	5.8688	6.2767	6.0813
A_s (sq. cm.)	6.0001	4.8289	5.4755	5.4169
WT-b (gms.)	1.1512	.8886	.8614	1.0601
G.L.	.1919	.1840	.1573	.1957
W.F.	.3682	.3742	.2990	.4120
t_a (in./cm.)	.083/.2108	.081/.2057	.081/.2057	.077/.1
C.F. / C.P.	.9384/.4510	.9079/.4354	.9656/.4736	.9251/.4

SAMPLE No.	1492A-1	1492A-7	1496BR-1	1496BR-
t_a (in./cm.)	.173/.4394	.171/.4343	.188/.4775	.188/.477
WT-a (gms.)	6.7973	5.8282	6.3313	7.6183
A-a (sq. cm.)	5.9627	5.1042	5.1066	6.084
WT-b (gms.)	.9391	.8548	1.0426	1.2506
G.L. (gms/sq.cm.)	.1575	.1675	.2042	.2055 .246
W.F. —	.3661	.3755	.4007	.4160 .332
t_c (in./cm.)	.070/.1778	.070/.1778	.082/.2083	.078/.19
C.F. / C.P.	.9184/.4046	.9526/.4094	.9308/.4362	~~1.4149~~ .9502 / .4

SAMPLE No.	1496B-6	1496B-8	1496B-7	1496B-
t_a (in./cm.)	.171/.4343	.171/.4343	.173/.4394	.175/.44
WT-a (gms.)	6.5535	6.3439	6.8716	7.0149
A-a (sq.cm.)	5.7437	5.5447	5.9430	5.9675
WT-b (gms.)	1.1143	1.0409	1.2031	1.1606
G.L.	.1940	.1877	.2024	.1945
W.F.	.3989	.4063	.4334	.4055
t_c (in./cm.)	.076/.1930	.072/.1829	.073/.1854	.074/.18
C.F. / C.P.	.9588/.4444	.9618/.4211	.9613/.4219	.9712/.4

SAMPLE No.	1533BR-1	1533BR-2	1533B-4	1533B-
t_s (in./cm.)	.185/.4699	.184/.4674	.172/.4369	.172/.43
WT-s (gm.)	7.3265	6.7002	6.8814	6.7066
A_s (sq. cm.)	5.9515	5.4448	5.9989	5.8692
WT-b (gms.)	1.1465	1.0568	1.1140	1.1791
G.L.	.1926	.1941	.1857	.2009
W.F.	.3555	.3679	.3826	.4003
t_c (in./cm.)	.085/.2159	.082/.2083	.076/.1930	.079/.20
C.F. / C.P.	.9518/.4595	.9614/.4457	.9557/.4417	.9515/.4

SAMPLE No.	1533B-5	1533B-9	1537BR-1	1537BR-
t_s (in./cm.)	.177/.4496	.174/.4420	.182/.4623	.184/.467
WT_s (gms.)	6.7560	6.9483	7.1220	6.6103
A_s (sq. cm.)	5.6822	5.9340	5.9143	5.4664
WT-b (gms.)	1.1003	.7922	1.1177	.9735
G.L.	.1936	.1335	.1880	.1781
W.F.	.3720	.2853	.3484	.3888
t_c (in./cm.)	.080/.2032	.072/.1829	.086/.2184	.075/.19
C.F. / C.P.	.9726/.4530	.9148/.4134	.9414/.4264	.9141/.4

SAMPLE No.	1537B-5	1537B-7	1537B-8	1537B-10
t_a (in./cm.)	.183/.4648	.178/.4521	.177/.4496	.174/.442
WT-a (gms.)	6.5621	6.4670	5.6993	6.0034
A-a (sq. cm.)	5.3637	5.4723	4.9107	5.2483
WT-b (gms.)	1.1830	1.1530	1.0533	1.1292
G.L. (gms/sq.cm.)	.2206	.2107	.2145	.2152
W.F. —	.3878	.4105	.4127	.4109
t_c (in./cm.)	.088/.2235	.081/.2057	.084/.2134	.084/.213
C.F. / C.P.	.9675/.4809	.9503/.4550	.9278/.4746	.9346/.48

SAMPLE No.	1568AR-1	1568AR-2	1568A-4	1568A-1
t_a (in./cm.)	.180/.4572	.181/.4597	.170/.4318	.170/.43
WT-a (gms.)	6.8920	7.1767	6.7992	6.4068
A-a (sq.cm.)	5.8067	5.9826	5.9639	5.632
WT-b (gms.)	1.1371	1.1779	1.0418	1.0081
G.L.	.1958	.1969	.1747	.1780
W.F.	.3727	.3705	.3874	.3992
t_c (in./cm.)	.084/.2134	.084/.2134	.070/.1778	.070/.17
C.F. / C.P.	.9350/.4668	.9453/.4642	.9642/.4118	.9596/.4

SAMPLE No.	1568A-7	1568A-9		
t_s (in./cm.)	.175/.4445	.173/.4394		
WT-s (gms.)	6.5474	6.5846		
A_s (sq. cm.)	5.5921	5.6802		
WT-b (gms.)	1.1398	1.0550		
G.L.	.2038	.1857		
W.F.	.4057	.3401		
t_c (in./cm.)	.078/.1981	.084/.2134		
C.F. / C.P.	.9654/.4457	.9692/.4857		

SAMPLE No.				
t_s (in./cm.)	26 RETAINS	MEANS	STD.	48 FROM EDGE STR
WT_s (gms.)		(74 OBSERVATIONS)	DEVIATIONS	
A_s (sq. cm.)		↓	↓	
WT-b (gms.)				
G.L.		.1875	.0192	
W.F.		.3803	.0301	
t_c (in./cm.)	MEAN .0800/.0059 SD	.0782/.1986	.0068/.0173	MEAN .0772/.
C.F. / C.P.		.9450/.4390	.0177/.0369	

LEGEND

t_s = thickness of sample (in./cm.)

WT_s = total weight of sample (grams)

A_s = surface area of sample (sq. centimeters)

WT_b = weight of boron carbide (grams)

G.L. = grams loading (distribution of boron carbide per unit area) (gms/sq. cm.)

W.F. = weight factor (content ratio of boron carbide in core by weight)

t_c = thickness of core (in./cm.)

C.F. = compaction factor (ratio of actual density to ideal)

C.P. = core proportion (ratio of core thickness to sample thickness)

Sheet # 10000B Date _____ Customer _____ Inspector _____ Form 502

Dimensional inspection (Indicate acceptance or rejection)

Total thickness: _____
Width: _____
Length: _____
Squareness: _____

Workmanship (Indicate acceptance or rejection) _____

Surface Condition (Indicate acceptance or rejection) _____

Diagram and identify pieces cut, dimensions, location of samples.

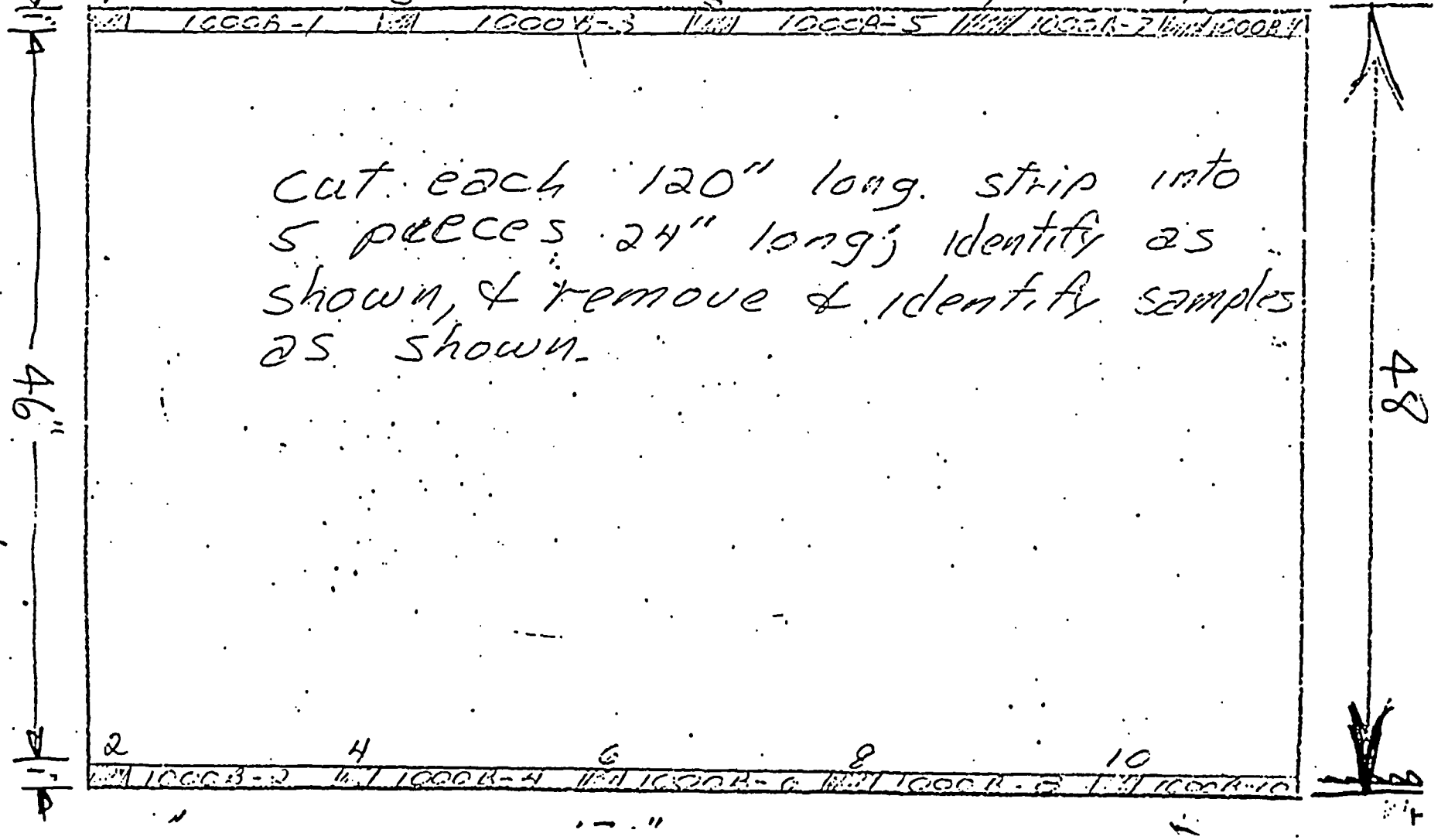

LATERAL PROFILE

1338B-4

	t_p	t_c	C.P.
0	.175	.065	.3714
1	.175	.075	.4286
2	.175	.080	.4571
3	.175	.090	.5143
12	.180	.095	.5278
24	.182	.095	.5220
36	.178	.090	.5056
43	.173	.085	.4913
44	.173	.080	.4624
45	.172	.080	.4651
46	.172	.080	.4651

1492A-4

	t_p	t_c	C.P.
	.175	.080	.4571
	.177	.085	.4802
	.177	.090	.5085
	.177	.090	.5085
	.185	.095	.5135
	.189	.100	.5291
	.185	.095	.5135
	.178	.090	.5056
	.178	.075	.4213
	.176	.075	.4261
	.176	.070	.3977

1537B-4

0	.179	.085	.4749
1	.179	.085	.4749
2	.179	.085	.4749
3	.179	.085	.4749
12	.188	.100	.5319
24	.189	.100	.5291
36	.185	.100	.5405
43	.178	.090	.5056
44	.178	.085	.4775
45	.176	.080	.4545
46	.176	.085	.4830

Sheet # 1537-B Date [illegible] Customer _____ Inspector _____ FORM 502

Dimensional inspection (Indicate acceptance or rejection)

Total thickness: _____
Width: _____
Length: _____
Squareness: _____

Workmanship (Indicate acceptance or rejection) _____

Surface Condition (Indicate acceptance or rejection) _____

Diagram and identify pieces cut, dimensions, location of samples.

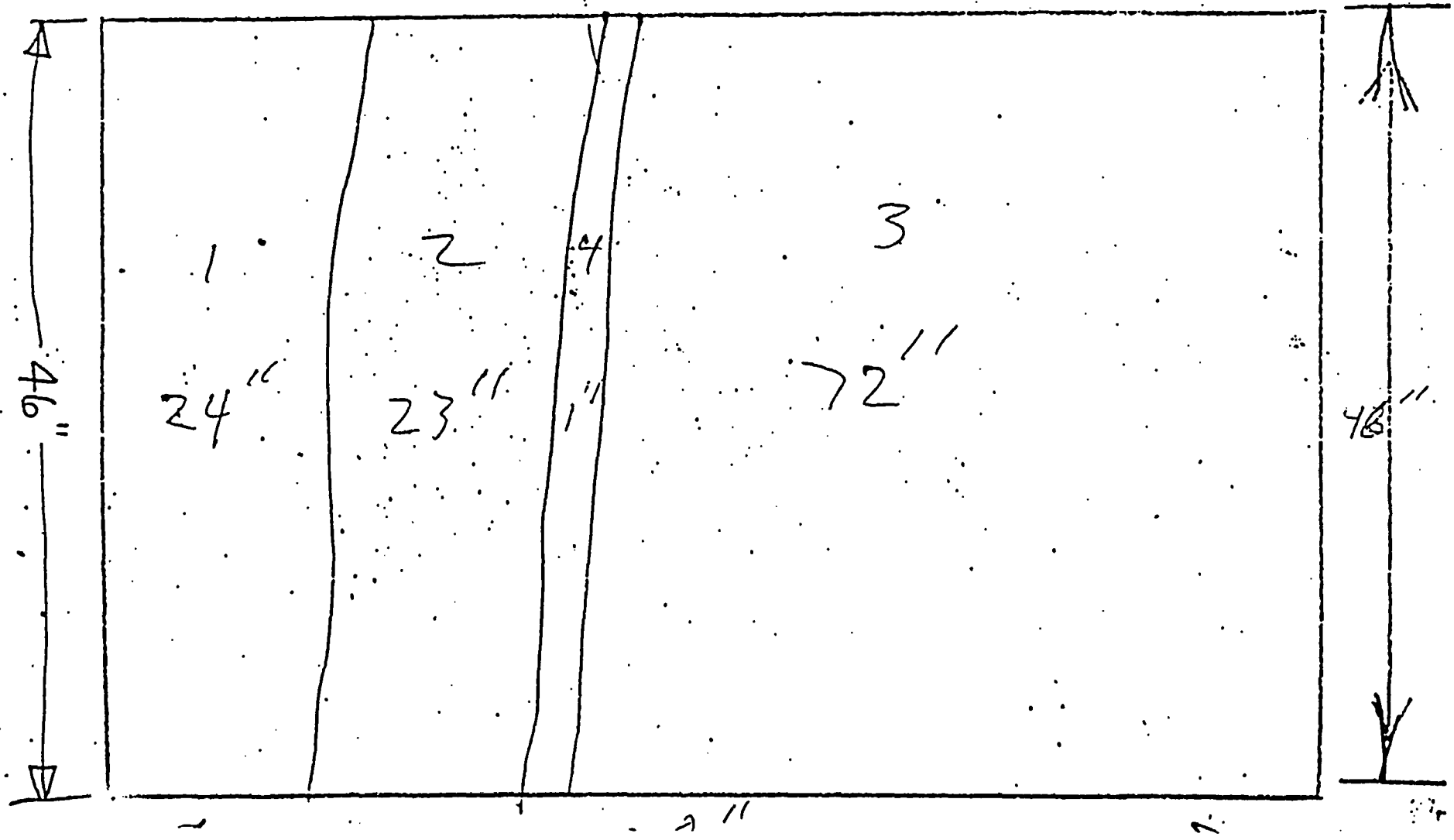

Sheet # 1492-4 Date 5-2-76 Customer _____ Inspector _____ FORM 902

Dimensional inspection (Indicate acceptance or rejection)

Total thickness: _____
Width: _____
Length: _____
Squareness: _____

Workmanship (Indicate acceptance or rejection) _____

Surface Condition (Indicate acceptance or rejection) _____

Diagram and identify pieces cut, dimensions, location of samples.

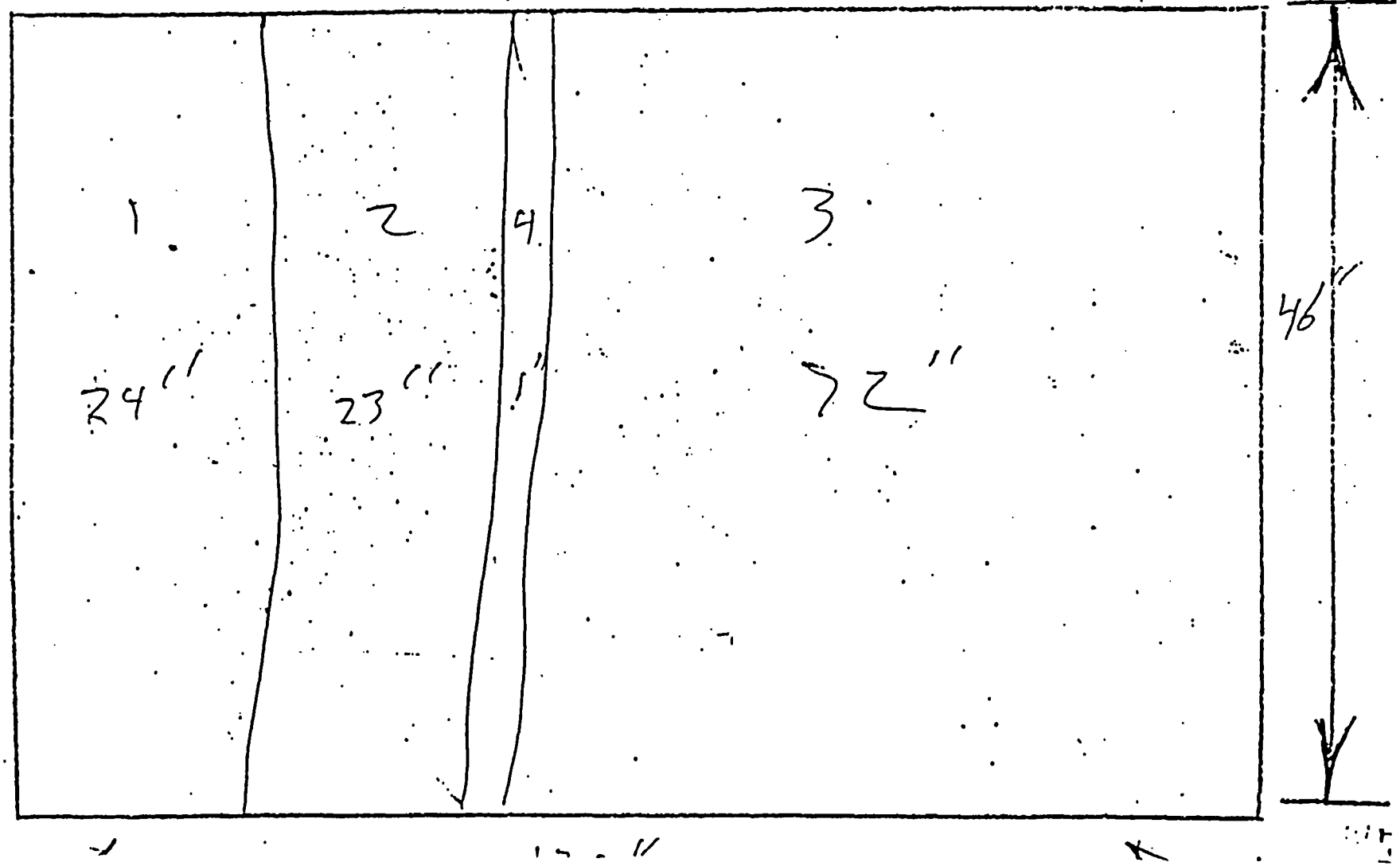

Sheet # 1000-B Date 5-3-76 Customer _____ Inspector J. Richards FORM 502

Dimensional inspection (Indicate acceptance or rejection)

Total thickness: _____
Width: 46
Length: 120
Squareness: _____

Workmanship (Indicate acceptance or rejection) _____

Surface Condition (Indicate acceptance or rejection) _____

Diagram and identify pieces cut, dimensions, location of samples.

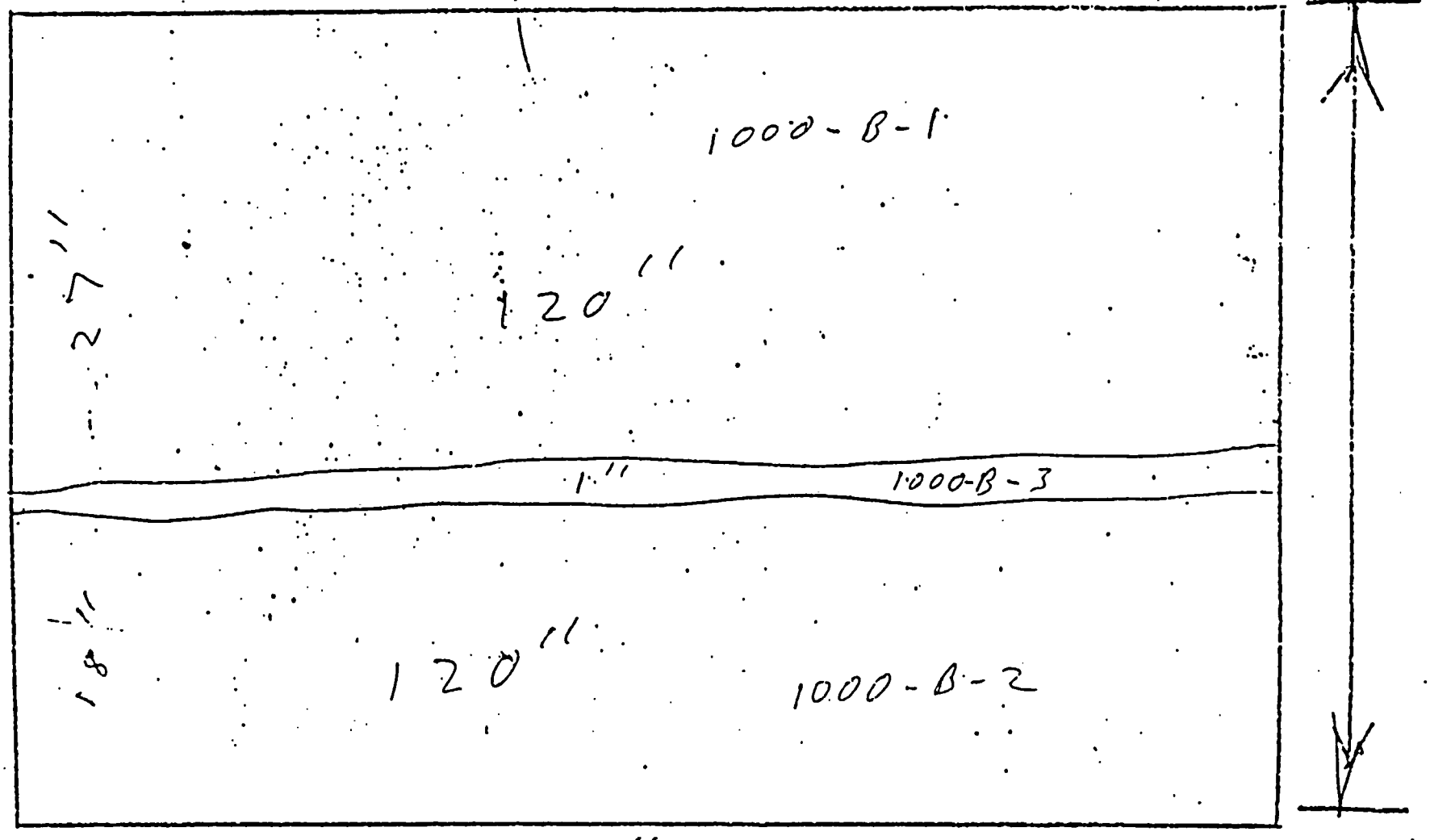

Sheet #1381-A Date [illegible] Customer _____ Inspector _____ FORM 502

Dimensional inspection (Indicate acceptance or rejection)

Total thickness: _____
Width: _____
Length: _____
Squareness: _____

Workmanship (Indicate acceptance or rejection) _____

Surface Condition (Indicate acceptance or rejection) _____

Diagram and identify pieces cut, dimensions, location of samples.

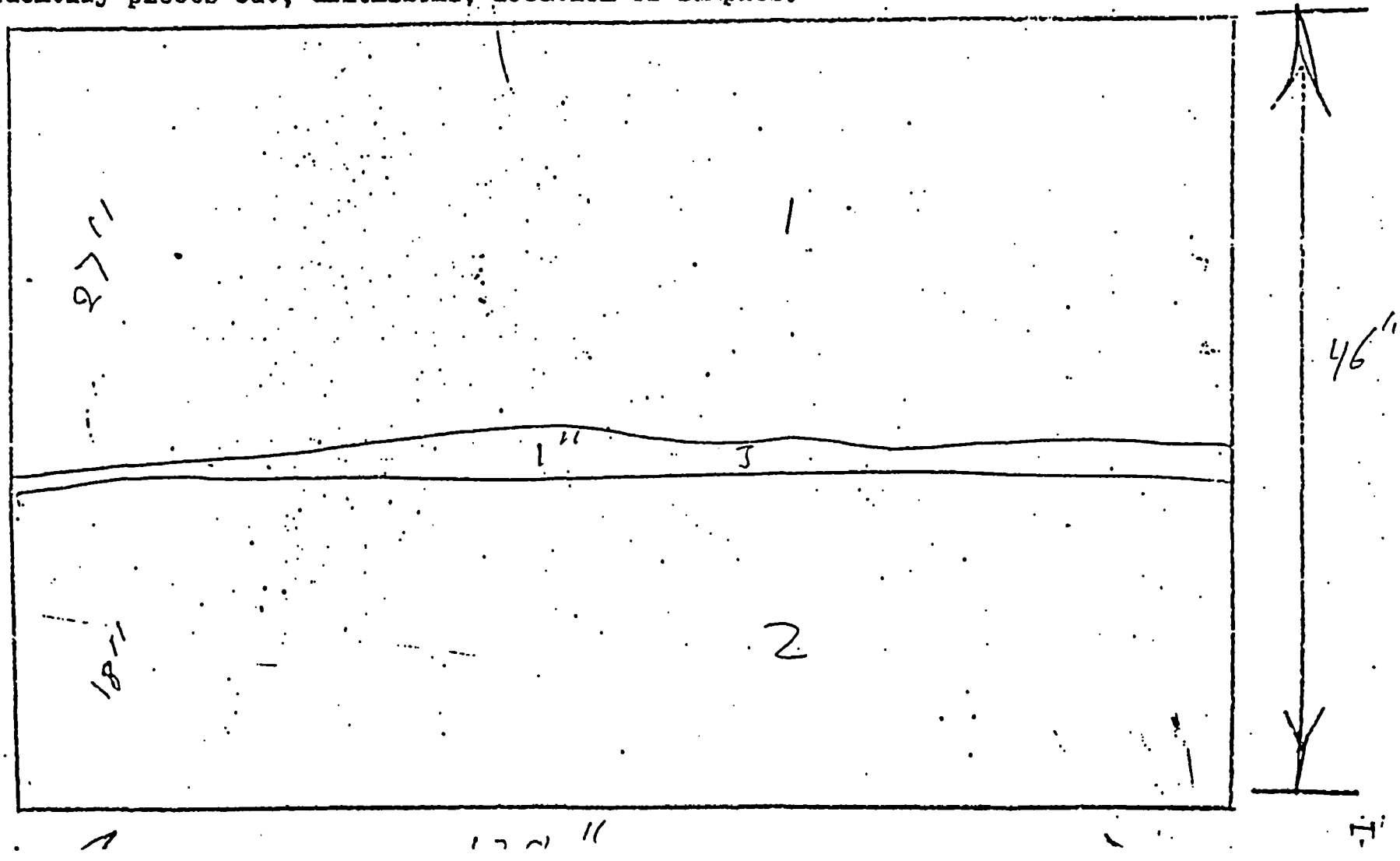

Sheet # 1334-B Date 5-3-24 Customer _____ Inspector _____ Form 50.

Dimensional inspection (Indicate acceptance or rejection)

Total thickness: _____
Width: _____
Length: _____
Squareness: _____

Workmanship (Indicate acceptance or rejection) _____

Surface Condition (Indicate acceptance or rejection) _____

Diagram and identify pieces cut, dimensions, location of samples.

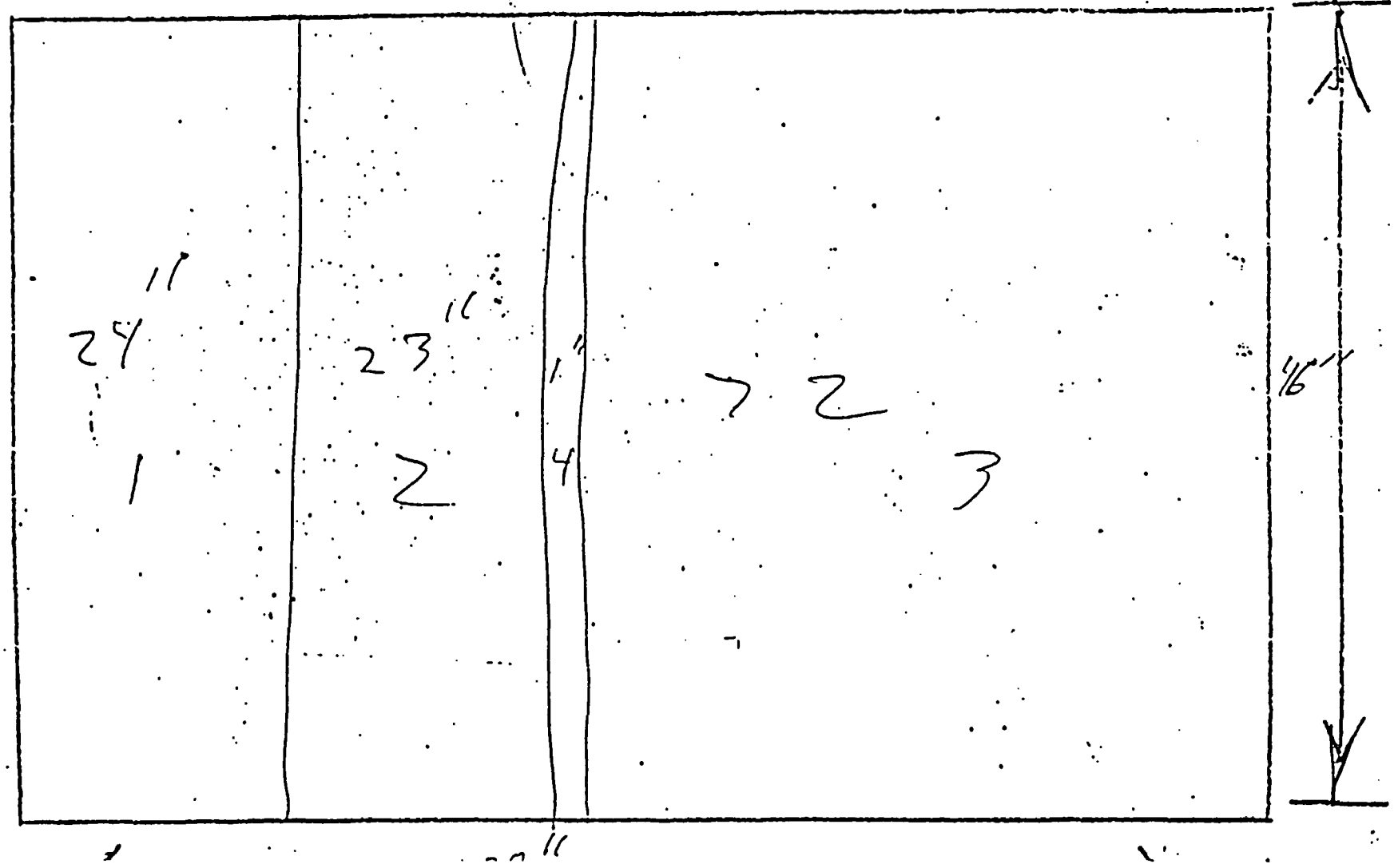

5/4/76
LM

LATERAL PROFILE

LE	1338 B-4		1492 A-4		1537-B-4	
OSITION	THICK	CORE	THICK	CORE	THICK.	CORE
0						
1						
2						
3						
11½						
12						
12½						
23½						
24						
24½						
35½						
36						
36½						
43						
24						
15						
96						
MEAN/STD.DEV.	.0865/.0086		.0891/.0092		.0922/.0066	

LONGITUDINAL PROFILE

	1000 B-3		1381 A-3	
	THK.	CORE	THK.	CORE
1				
12				
24				
36				
48				
60				
72				
84				
96				
108				
19				
	.0923/.0052		.0964/.0023	

eet # 1146B Date 5-6-76 Customer _____ Inspector _____ FORM 9

Dimensional inspection (Indicate acceptance or rejection)

Total thickness: _____
Width: _____
Length: _____
Squareness: _____

Workmanship (Indicate acceptance or rejection) _____

Surface Condition (Indicate acceptance or rejection) _____

agram and identify pieces cut, dimensions, location of samples.

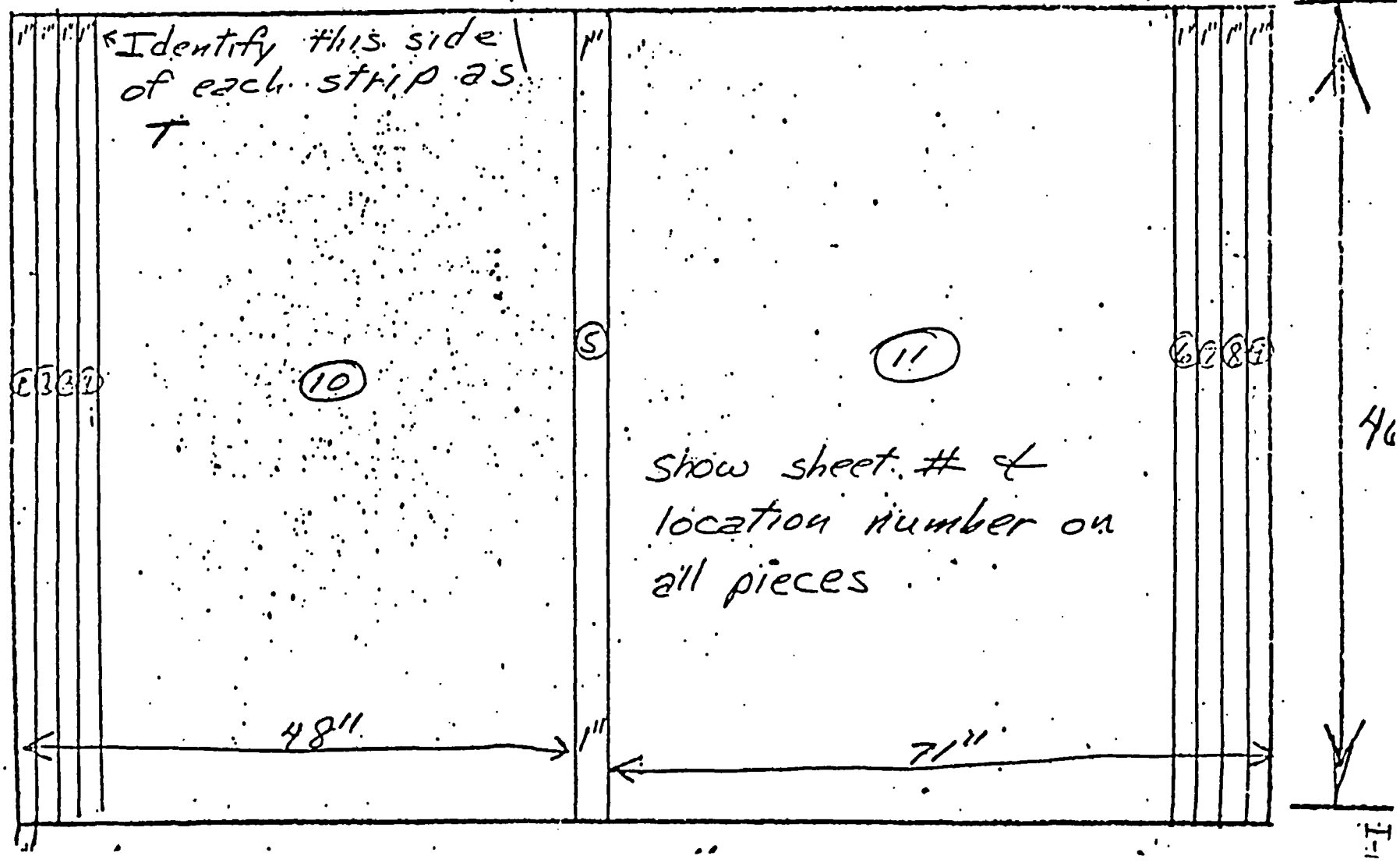

IN"	T	C
0	.174	.080
1	.175	.085
2	.176	.085
3	.177	
4	.178	
5	.179	
6	.180	
7	.181	
8	.181	
9	.182	
10	.183	
11	.183	.090
12	.184	.085
13	.185	.090
14	.185	.090
15	.185	.085
16	.186	.090
17	.186	
18	.187	
19	.187	
20	.188	
21	.187	
22	.187	
23	.188	.090
24	.188	.090
25	.189	.085
26	.187	.085
27	.187	
28	.186	
29	.186	
30	.185	
31	.185	
32	.184	
33	.183	
34	.183	.095
35	.182	.095
36	.181	.085
37	.180	.085
38	.180	
39	.179	
40	.177	
41	.176	
42	.175	.085
43	.174	.085
44	.174	.075
45	.173	.075
MEAN		.0869
STD. DEV		.0056

IN"	T	C
0	.181	.085
1	.151	.085
2	.182	.090
3	.183	.090
4	.184	.095
5	.184	
6	.185	
7	.186	
8	.187	
9	.188	
10	.189	.095
11	.190	.100
12	.190	.095
13	.190	.090
14	.191	
15	.191	
16	.191	
17	.192	
18	.192	
19	.192	
20	.192	
21	.193	
22	.193	.095
23	.193	.100
24	.192	.100
25	.192	
26	.192	
27	.192	
28	.191	
29	.191	
30	.191	
31	.191	
32	.190	
33	.190	
34	.189	.090
35	.189	.095
36	.188	.090
37	.185	.090
38	.185	
39	.184	
40	.183	
41	.181	
42	.180	
43	.180	.085
44	.179	.085
45	.177	.080
46	.177	.075

IN"	T	C
0	.180	.085
1	.181	.085
2	.182	.090
3	.183	.090
4	.184	.085
5	.185	.090
6	.186	
7	.186	
8	.187	
9	.188	
10	.189	.095
11	.190	.090
12	.191	.090
13	.191	.090
14	.192	
15	.192	
16	.192	
17	.192	
18	.194	
19	.193	
20	.194	
21	.194	
22	.194	.095
23	.194	.095
24	.193	.100
25	.193	
26	.193	
27	.193	
28	.192	
29	.192	
30	.192	
31	.192	
32	.191	
33	.191	
34	.190	.095
35	.189	.100
36	.188	.095
37	.187	.090
38	.185	.085
39	.184	
40	.183	
41	.182	
42	.181	
43	.180	.085
44	.178	.085
45	.178	.080
46	.177	.075
		.070
MEAN		.0888
STD. DEV		.0074

IN"	T	C
0	.177	.080
1	.150	.085
2	.151	.090
3	.182	
4	.153	
5	.184	
6	.186	
7	.186	
8	.187	
9	.187	
10	.188	
11	.159	.100
12	.190	.095
13	.190	.090
14	.191	
15	.191	
16	.192	
17	.192	
18	.193	
19	.193	
20	.193	
21	.194	
22	.193	
23	.193	.100
24	.193	.095
25	.192	.100
26	.192	
27	.192	
28	.192	
29	.191	
30	.191	
31	.190	
32	.190	
33	.190	
34	.187	
35	.186	.095
36	.186	.090
37	.185	.100
38	.184	
39	.183	
40	.182	
41	.181	
42	.180	
43	.179	
44	.178	.095
45	.177	.090
46	.177	.055
		.050
		.075
MEAN		.0909
STD. DEV		.0078

IN"	T	C
1	.175	.085
2	.177	.085
3	.178	.085
4	.178	.090
5	.179	.090
6	.180	
7	.180	
8	.181	
9	.182	
10	.183	
11	.184	
12	.184	.085
13	.185	.090
14	.186	.111
15	.186	.095
16	.187	
17	.187	
18	.188	
19	.188	
20	.188	
21	.188	
22	.188	.085
23	.189	.090
24	.189	.111
25	.189	.095
26	.188	
27	.187	
28	.187	
29	.187	
30	.187	
31	.186	
32	.185	
33	.185	
34	.184	
35	.184	.080
36	.183	.090
37	.182	.091
38	.181	.085
39	.181	
40	.180	
41	.179	
42	.178	
43	.177	.085
44	.176	.085
45	.175	.085
46	.174	.085
MEAN		.0887
STD. DEV.		.0048

IN"	T	C
0	.179	
1	.175	.075
2	.176	.080
3	.177	.085
4	.178	.085
5	.179	
6	.180	
7	.181	
8	.181	
9	.182	
10	.183	.085
11	.184	.090
12	.184	.085
13	.185	
14	.186	
15	.186	
16	.187	
17	.187	
18	.187	
19	.188	
20	.188	
21	.188	
22	.188	.095
23	.189	.090
24	.189	.075
25	.189	.095
26	.188	
27	.187	
28	.187	
29	.187	
30	.187	
31	.186	
32	.185	
33	.185	.085
34	.184	.090
35	.184	.085
36	.183	.100
37	.182	.075
38	.181	.100
39	.180	
40	.179	
41	.179	
42	.178	
43	.177	
44	.176	.090
45	.175	.085
46	.174	.075
MEAN		.0843
STD. DEV.		.0081

IN"	T	C
0	.181	
1	.181	.100
2	.182	.095
3	.184	.085
4	.184	.090
5	.185	.095
6	.186	.100
7	.187	.100
8	.188	.100
9	.189	.095
10	.190	.100
11	.190	.095
12	.191	.100
13	.191	.095
14	.191	.095
15	.192	
16	.192	
17	.193	
18	.193	
19	.193	
20	.193	
21	.194	
22	.194	.105
23	.193	.100
24	.193	.100
25	.193	.100
26	.193	
27	.193	
28	.192	
29	.192	
30	.192	
31	.192	
32	.191	
33	.190	
34	.189	.090
35	.188	.085
36	.188	.085
37	.187	
38	.185	
39	.185	
40	.183	
41	.182	
42	.181	
43	.180	.100
44	.179	.095
45	.178	.085
46	.178	.085
		.090
MEAN		.0947
STD. DEV.		.0067

IN"	T	C
0	.173	.095
1	.175	.100
2	.175	.095
3	.175	
4	.177	
5	.178	
6	.179	
7	.180	
8	.181	
9	.182	
10	.183	
11	.184	
12	.184	
13	.184	
14	.185	
15	.185	
16	.185	
17	.186	
18	.186	
19	.186	
20	.186	
21	.187	
22	.187	
23	.187	
24	.187	
25	.187	
26	.187	
27	.186	
28	.186	
29	.186	
30	.185	
31	.185	
32	.184	
33	.184	.085
34	.183	.075
35	.182	.085
36	.182	
37	.181	
38	.180	
39	.179	
40	.178	
41	.177	
42	.176	
43	.175	.085
44	.174	.075
45	.173	.080
46	.173	.075
		.075
MEAN		.0818
STD. DEV.		.0099

IN"	T	C	IN"	T	C	IN"	T	C	IN"	T	C
	.177	.090	0	.170	.080						
	.179	.085	1	.172	.085						
	.179	.095	2	.172	.090						
	.180		3	.174							
	.181		4	.175							
	.182		5	.175							
	.183		6	.176							
	.184		7	.177							
	.184		8	.178							
	.185		9	.180							
	.186		10	.181							
	.187		11	.182	.085						
	.187	.090	12	.182	.090						
	.188	.095	13	.183	.095						
	.188	.100	14	.183							
	.188	.095	15	.184							
	.189		16	.185							
	.190		17	.185							
	.190		18	.185							
	.190		19	.186							
	.190		20	.187							
	.191		21	.187							
	.191		22	.187							
	.191	.085	23	.187	.090						
	.191	.095	24	.187	.095						
	.190	.090	25	.186							
	.190		26	.186							
	.190		27	.186							
	.190		28	.185							
	.189		29	.185							
	.189		30	.184							
	.189		31	.183							
	.188		32	.182							
	.187		33	.181							
	.186		34	.180							
	.186	.085	35	.179							
	.185	.090	36	.178	.085						
	.184	.095	37	.176	.090						
	.183										
	.182										
	.181										
	.180										
	.179										
	.178	.085									
	.177	.090									
	.175	.095									
	.175										
MEAN		.0900			.0891						
STD. DEV.		.0048			.0049						

APPENDIX B

EXPERIMENTAL DATA

PANEL LOT II

PAGES II-1 THRU II-20

THICKNESS MEASUREMENTS FOR BORAL SHEET NO. 1266A

LOCATION	CORE THICKNESS MIN.	MAX.	AVG.	PANEL THICKNESS	
I	.070	.085	.0775	.166	
~~II~~	.080	.085	.0825	.169	
6M	.075	.090	.0825	.171	
III	.075	.085	.080	.173	
1A	.085	.095	.090	.172	
1C	.085	.090	.0875	.175	
1E	.085	.095	.090	.177	
1G	.085	.095	.090	.176	
1J	.075	.090	.0825	.177	
2B	.085	.095	.090	.180	
2D	.085	.095	.090	.182	
2F	.080	.100	.090	.183	
2H	.090	.100	.095	.181	
6L	.090	.100	.095	.187	
7L	.090	.100	.095	.189	
3A	.080	.100	.090	.181	
3C	.085	.095	.090	.183	
3E	.080	.095	.0875	.184	
3G	.090	.100	.095	.184	
3J	.085	.100	.0925	.184	
4B	.085	.095	.090	.179	
4D	.085	.095	.090	.182	
4F	.090	.095	.0925	.182	
4H	.090	.095	.0925	.180	
IV	.065	.075	.070	.170	
5C	.070	.085	.0775	.172	
5E	.080	.090	.085	.174	
V	.080	.100	.090	.174	
5G	.075	.090	.0825	.174	
5J	.075	.090	.0825	.174	
6K	.090	.095	.0925	.176	
VI	.095	.100	.0975	.178	
		MEAN	.0879	.0906	.0850
		STD. DEVIATION	.0061	.0031	.0074
			COMBINED	CENTRAL	PERIPHERY

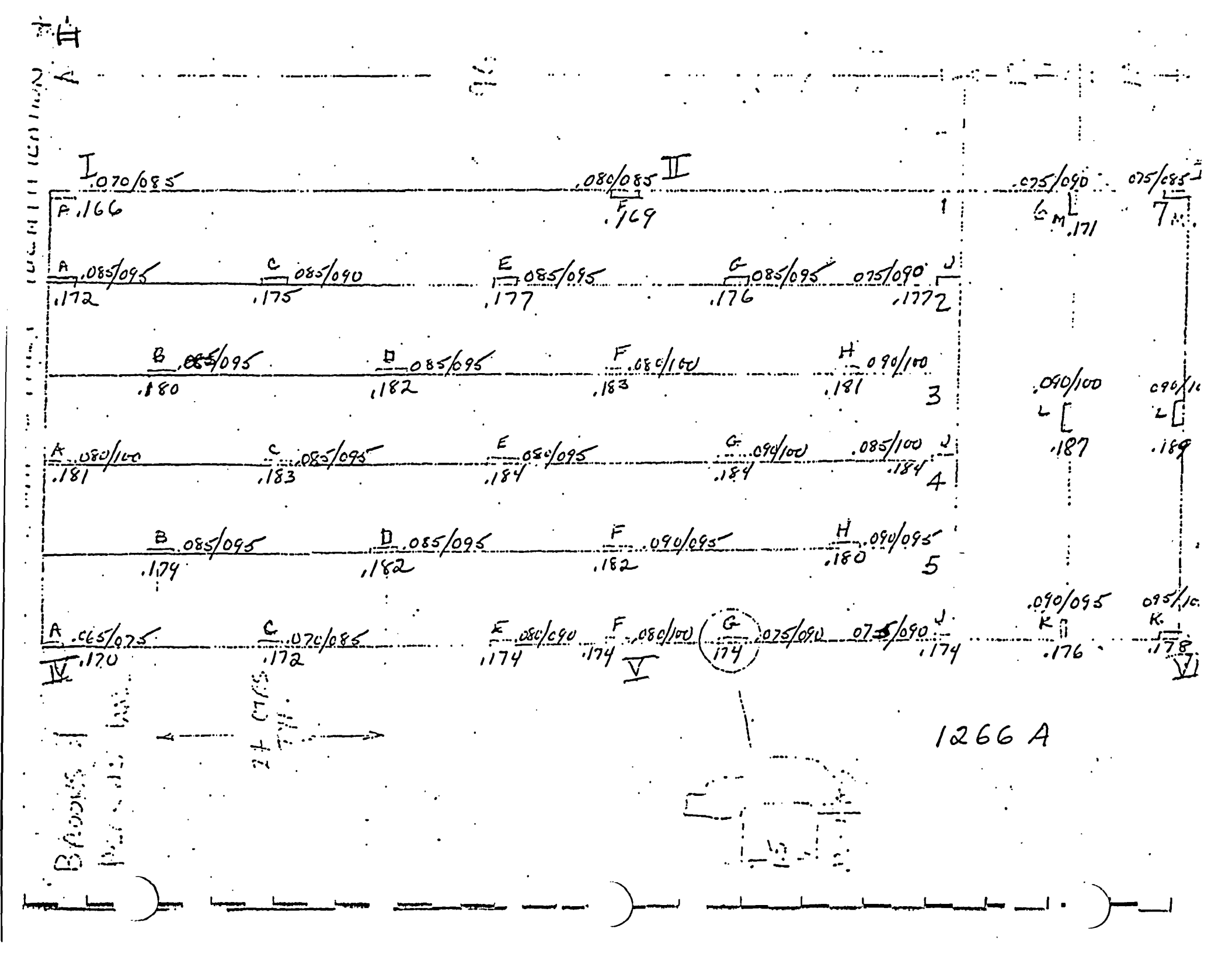
I .070/085
.080/085 II
.075/090
075/085
F .166
F .169
6 M .171
7 M
A .085/095
C .085/090
E .085/095
G .085/095
.075/090 J
.172
.175
.177
.176
.177 2
B .085/095
D .085/095
F .080/100
H .090/100
.180
.182
.183
.181
3
.090/100
.187
.189
A .080/100
C .085/095
E .080/095
G .090/100
.085/100 J
.181
.183
.184
.184
.184 4
B .085/095
D .085/095
F .090/095
H .090/095
.179
.182
.182
.180
5
.090/095
K
.176
095/10
K
.178
A .065/075
C .070/085
E .080/090
F .080/100
G
174
.075/090
.075/090 J
.174
IV .170
.172
.174
.174
V
V
1266 A

THICKNESS MEASUREMENTS FOR BORAL SHEET NO. 1325-A

LOCATION	CORE THICKNESS MIN.	MAX.	AVG.	PANEL THICKNESS	
I	.075	.090	.0825	.169	
~~II~~	.075	.085	.080	.173	
6M	.080	.085	.0825	.174	
III	.075	.085	.080	.175	
1A	.085	.090	.0875	.174	
1C	.085	.100	.0925	.177	
1E	.085	.095	.090	.180	
1G	.090	.095	.0925	.178	
1J	.085	.095	.090	.178	
2B	.085	.095	.090	.180	
2D	.090	.100	.095	.182	
2F	.090	.100	.095	.183	
2H	.090	.100	.095	.180	
6L	.080	.100	.090	.184	
7L	.095	.100	.0975	.186	
3A	.080	.090	.085	.177	
3C	.085	.100	.0925	.180	
3E	.085	.100	.0925	.182	
3G	.085	.100	.0925	.180	
3J	.085	.100	.0925	.180	
4B	.080	.095	.0875	.176	
4D	.085	.100	.0925	.177	
4F	.085	.095	.090	.178	
4H	.085	.100	.0925	.176	
IV	.075	.080	.0775	.166	
5C	.080	.085	.0825	.169	
5E	.080	.085	.0825	.172	
V	.080	.090	.085	.172	
5G	.080	.085	.0825	.170	
5J	.080	.085	.0825	.170	
6K	.075	.090	.0825	.172	
VI	.090	.100	.095	.175	
		MEAN	.0883	.0919	.0843
		STD. DEVIATION	.0054	.0020	.0053
			COMBINED	CENTRAL	PERIPHERY

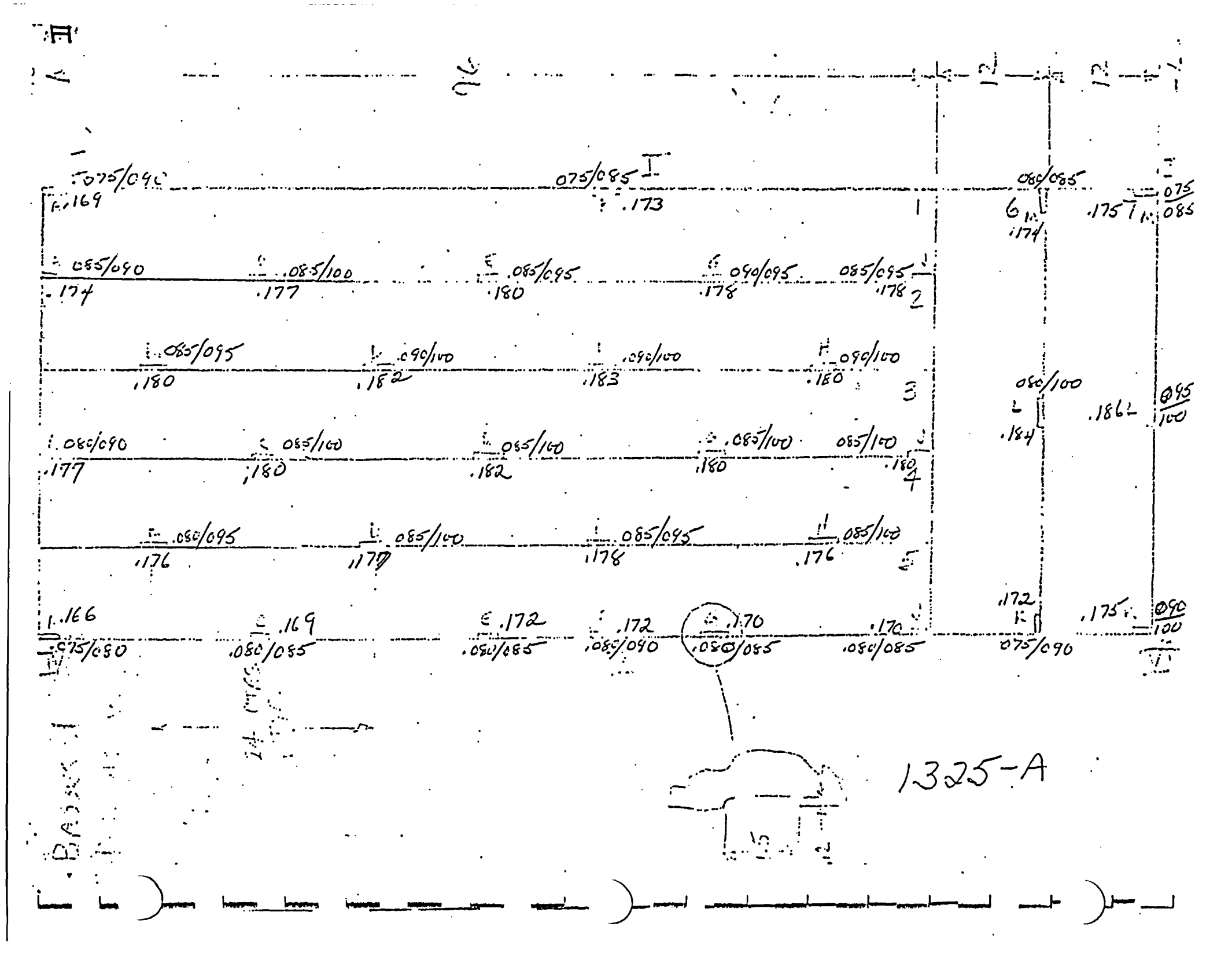
1325-A

THICKNESS MEASUREMENTS FOR BORAL SHEET NO. 1325-B

LOCATION	CORE THICKNESS MIN.	CORE THICKNESS MAX.	CORE THICKNESS AVG.	PANEL THICKNESS	
I	.080	.090	.085	.168	
II	.080	.090	.085	.170	
6M	.085	.095	.090	.172	
III	.090	.095	.0925	.172	
1A	.080	.095	.0875	.174	
1C	.085	.095	.090	.176	
1E	.085	.095	.090	.175	
1G	.090	.095	.0925	.175	
1J	.080	.095	.0875	.177	
2B	.085	.095	.090	.180	
2D	.090	.100	.095	.180	
2F	.085	.095	.090	.180	
2H	.085	.095	.090	.180	
6L	.090	.100	.095	.185	
7L	.085	.095	.090	.185	
3A	.085	.100	.0925	.179	
3C	.090	.100	.095	.180	
3E	.085	.100	.0925	.179	
3G	.090	.100	.095	.180	
3J	.080	.100	.090	.183	
4B	.085	.095	.090	.179	
4D	.090	.100	.095	.178	
4F	.085	.095	.090	.178	
4H	.085	.100	.0925	.178	
IV	.070	.080	.075	.170	
5C	.075	.090	.0825	.171	
5E	.075	.085	.080	.171	
V	.075	.090	.0825	.171	
5G	.080	.090	.085	.171	
5J	.075	.095	.085	.173	
6K	.080	.090	.085	.174	
VI	.080	.090	.085	.174	
		MEAN	.0888	.0917	.0855
		STD. DEVIATION	.0047	.0024	.0046
			CALCULATED	CALCULATED	REQUIRED

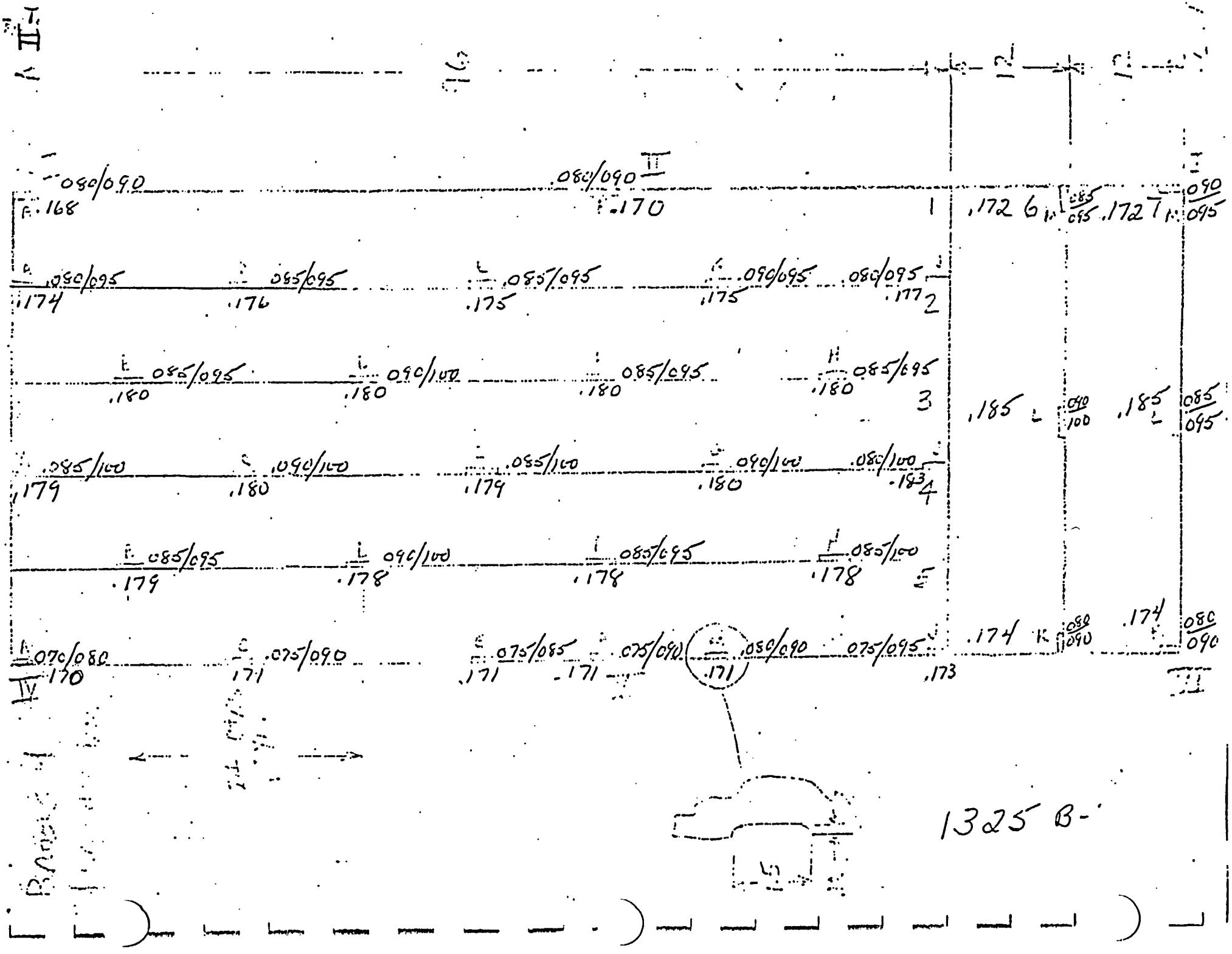
1325 B-

THICKNESS MEASUREMENTS FOR BORAL SHEET NO. 1352-A

LOCATION	CORE THICKNESS MIN.	MAX.	AVG.	PANEL THICKNESS	
I	.075	.085	.080	.163	
~~II~~	.085	.095	.090	.167	
6M	.080	.085	.0825	.166	
III	.085	.090	.0875	.168	
1A	.085	.095	.090	.168	
1C	.085	.090	.0875	.175	
1E	.085	.095	.090	.175	
1G	.080	.095	.0875	.171	
1J	.080	.090	.085	.170	
2B	.085	.100	.0925	.174	
2D	.085	.095	.090	.177	
2F	.085	.095	.090	.178	
2H	.085	.100	.0925	.173	
6L	.090	.100	.095	.178	
7L	.085	.090	.0875	.181	
3A	.075	.095	.085	.173	
3C	.085	.100	.0925	.175	
3E	.085	.095	.090	.180	
3G	.090	.100	.095	.175	
3J	.080	.090	.085	.175	
4B	.085	.095	.090	.170	
4D	.085	.100	.0925	.173	
4F	.080	.090	.085	.174	
4H	.085	.095	.090	.170	
IV	.080	.085	.0825	.164	
5C	.085	.090	.0875	.165	
5E	.085	.095	.090	.169	
V	.080	.090	.085	.167	
5G	.080	.090	.085	.166	
5J	.080	.090	.085	.165	
6K	.080	.085	.0825	.167	
VI	.085	.090	.0875	.169	
		MEAN	.0880	.0900	.0858
		STD. DEVIATION	.0037	.0032	.0031
				CENTRAL	PERIPHERY

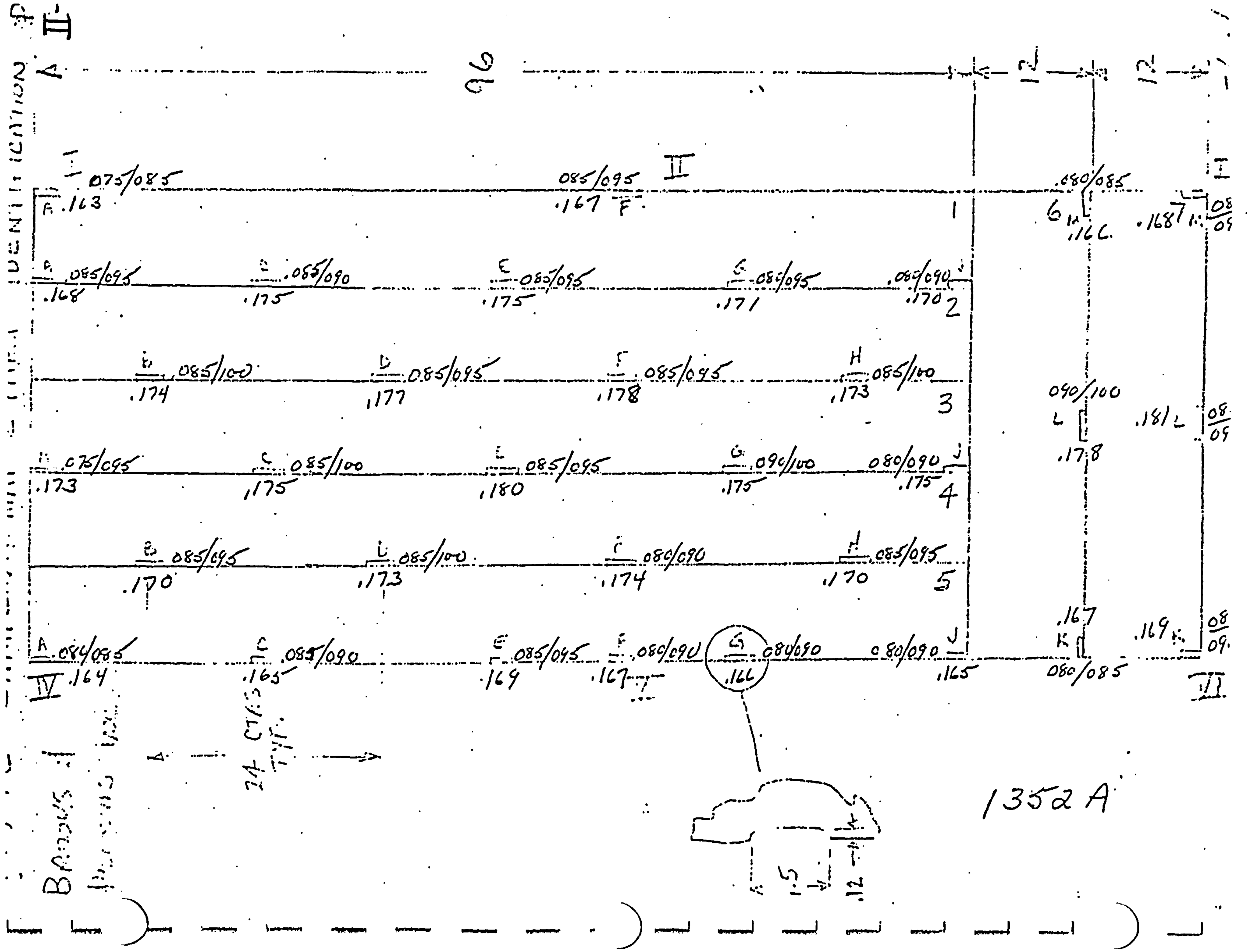
96
12
12
II
I
.075/085
.163
.085/095
.167 F
1
.080/085
6
.166
.168
A .085/095
.168
.085/090
.175
E .085/095
.175
G .085/095
.171
.085/090
.170
2
B .085/100
.174
D .085/095
.177
F .085/095
.178
H .085/100
.173
3
090/100
L
.178
.181 L
.075/095
.173
C .085/100
.175
E .085/095
.180
G .090/100
.175
080/090 J
.175
4
B .085/095
.170
D .085/100
.173
F .080/090
.174
H .085/095
.170
5
.167
K
.169 K
A .080/085
.164
IV
C .085/090
.165
E .085/095
.169
F .080/090
.167
G .080/090
.166
.080/090 J
.165
080/085
II
1352 A
1.5
.12

THICKNESS MEASUREMENTS FOR BORAL SHEET NO. 1352-B

LOCATION	CORE THICKNESS MIN.	CORE THICKNESS MAX.	CORE THICKNESS AVG.	PANEL THICKNESS	
I	.075	.085	.080	.173	
II	.085	.095	.090	.175	
6M	.080	.090	.085	.175	
III	.085	.090	.0875	.176	
1A	.080	.090	.085	.179	
1C	.090	.100	.095	.179	
1E	.085	.100	.0925	.181	
1G	.090	.100	.095	.182	
1J	.090	.100	.095	.183	
2B	.080	.095	.0875	.184	
2D	.085	.095	.090	.183	
2F	.090	.100	.095	.186	
2H	.090	.100	.095	.187	
6L	.085	.095	.090	.187	
7L	.095	.100	.0975	.189	
3A	.075	.085	.080	.183	
3C	.085	.095	.090	.184	
3E	.090	.100	.095	.185	
3G	.090	.100	.095	.188	
3J	.085	.100	.0925	.187	
4B	.080	.090	.085	.180	
4D	.085	.095	.090	.179	
4F	.090	.100	.095	.182	
4H	.090	.100	.095	.183	
IV	.070	.080	.075	.172	
5C	.075	.080	.0775	.172	
5E	.085	.095	.090	.174	
V	.085	.090	.0875	.175	
5G	.085	.095	.090	.176	
5J	.085	.095	.090	.175	
6K	.080	.095	.0875	.175	
VI	.085	.090	.0875	.176	
		MEAN	.0894	.0925	.0860
		STD. DEVIATION	.0055	.0031	.0058
			COMBINED	CENTRAL	PERIPHERY

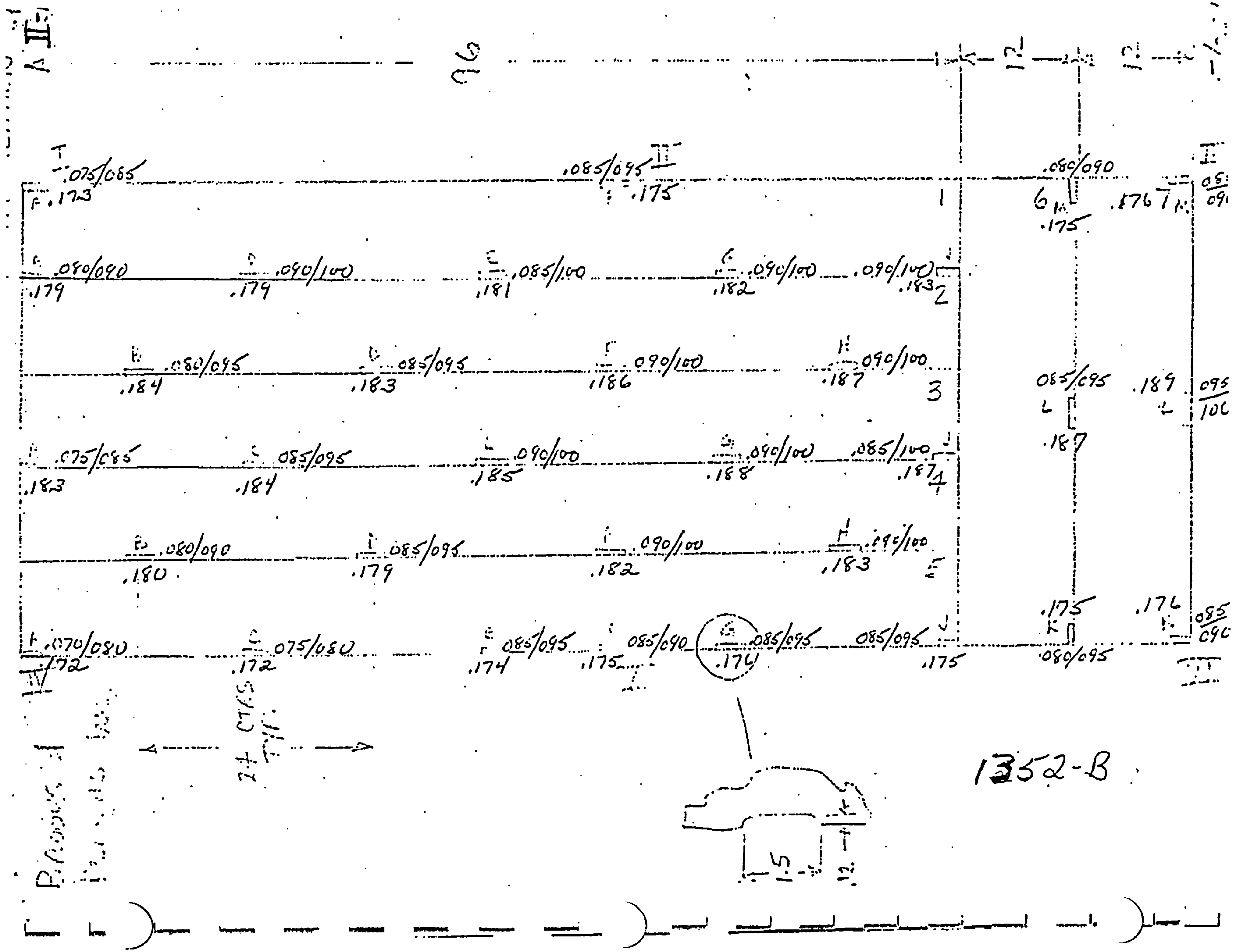

96
12
12
.075/085
.173
.085/095
.175
.080/090
.175
.176
.080/090
.179
.090/100
.179
.085/100
.181
.090/100
.182
.090/100
.183
2
.080/095
.184
.085/095
.183
.090/100
.186
.090/100
.187
3
085/095
.189
095/100
.187
.075/085
.183
.085/095
.184
.090/100
.185
.090/100
.188
.085/100
.187
4
.080/090
.180
.085/095
.179
.090/100
.182
.090/100
.183
.175
.176
085/090
.070/080
.172
.075/080
.172
085/095
.174
.175
085/090
.176
085/095
085/095
.175
.080/095
1352-B

THICKNESS MEASUREMENTS FOR BORAL SHEET NO. 1402-B

LOCATION	CORE THICKNESS MIN.	CORE THICKNESS MAX.	CORE THICKNESS AVG.	PANEL THICKNESS	
I	.065	.080	.0725	.174	
~~II~~	.080	.090	.085	.177	
6M	.080	.090	.085	.176	
III	.090	.100	.095	.180	
1A	.085	.095	.090	.182	
1C	.085	.095	.090	.184	
1E	.090	.100	.095	.185	
1G	.090	.100	.095	.185	
1J	.085	.100	.0925	.185	
2B	.090	.100	.095	.188	
2D	.095	.100	.0975	.188	
2F	.085	.100	.0925	.191	
2H	.085	.100	.0925	.191	
6L	.090	.100	.095	.193	
7L	.090	.100	.095	.194	
3A	.065	.085	.075	.187	
3C	.085	.100	.0925	.188	
3E	.090	.100	.095	.190	
3G	.090	.100	.095	.191	
3J	.090	.100	.095	.191	
4B	.090	.105	.0975	.182	
4D	.090	.100	.095	.182	
4F	.095	.110	.1025	.185	
4H	.090	.100	.095	.185	
IV	.075	.085	.080	.172	
5C	.075	.085	.080	.174	
5E	.075	.085	.080	.175	
V	.075	.085	.080	.176	
5G	.075	.085	.080	.176	
5J	.075	.085	.080	.176	
6K	.070	.090	.080	.179	
VI	.075	.090	.0825	.178	
		MEAN	.0891	.0948	.0826
		STD. DEVIATION	.0077	.0027	.0064
			COMBINED	CENTRAL	PERIPHERY

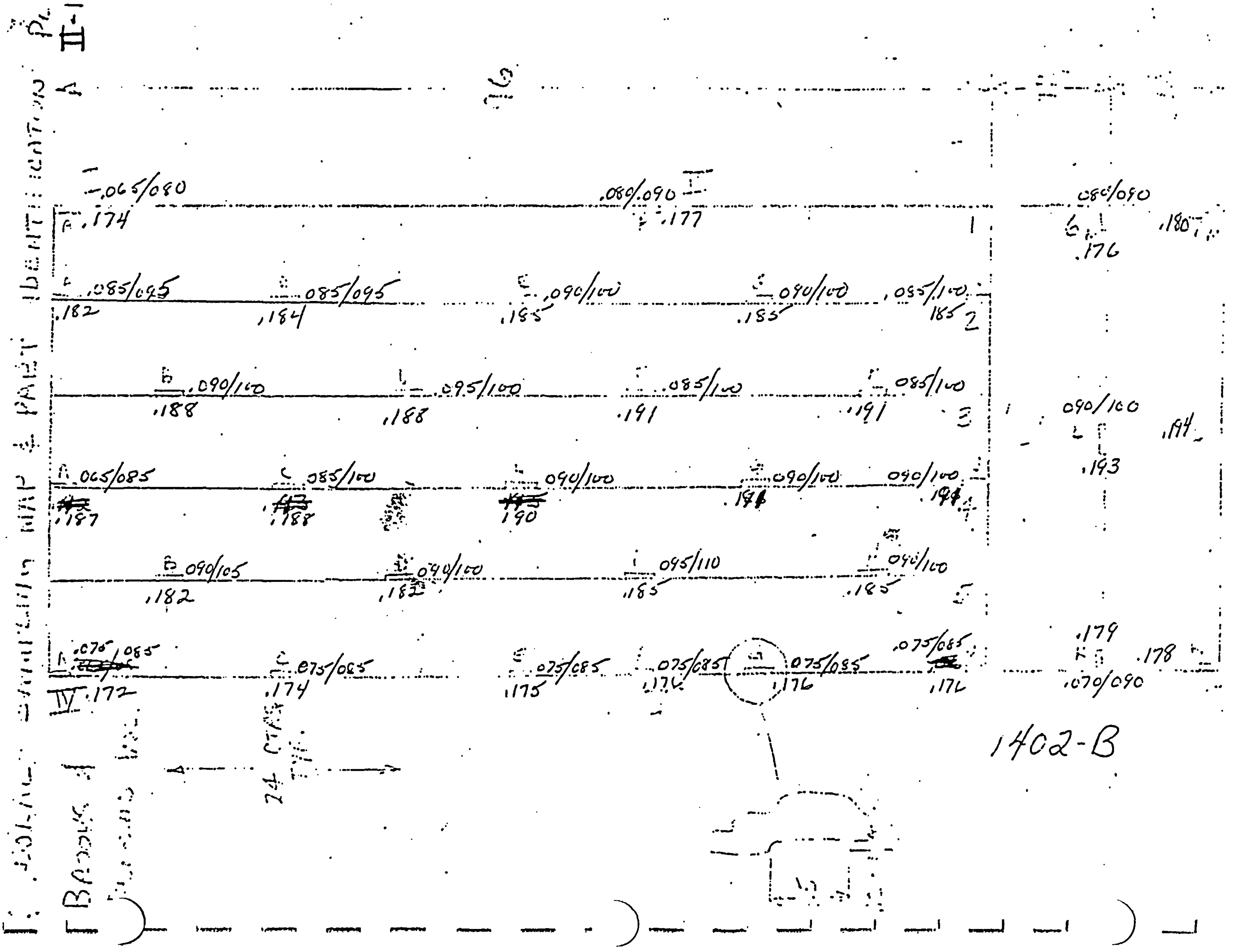

.065/080
.174
.080/.090
.177
.080/090
.176
.180
.085/095
.182
.085/095
.184
.090/100
.185
.090/100
.185
.085/100
185
.090/100
.188
.095/100
.188
.085/100
.191
.085/100
.191
090/100
.194
.193
.065/085
.187
.085/100
.188
090/100
190
090/100
090/100
.182
.090/105
.182
.090/100
.095/110
.185
.090/100
.185
.075/085
.172
.075/085
.174
.075/085
.175
.075/085
.075/085
.176
.075/085
.176
.179
.178
.070/090
1402-B

THICKNESS MEASUREMENTS FOR BORAL SHEET NO. 1406-B

LOCATION	CORE THICKNESS MIN.	CORE THICKNESS MAX.	CORE THICKNESS AVG.	PANEL THICKNESS	
I	.070	.085	.0775	.167	
II	.075	.090	.0825	.170	
6M	.080	.090	.0850	.174	
III	.085	.090	.0875	.171	
1A	.075	.085	.0800	.174	
1C	.090	.100	.095	.175	
1E	.085	.095	.090	.177	
1G	.090	.100	.095	.178	
1J	.090	.095	.0925	.176	
2B	.085	.095	.090	.182	
2D	.090	.100	.095	.182	
2F	.090	.100	.095	.183	
2H	.090	.095	.0925	.183	
6L	.090	.100	.095	.183	
7L	.095	.100	.0975	.187	
3A	.080	.085	.0825	.180	
3C	.085	.095	.080	.181	
3E	.085	.095	.090	.182	
3G	.090	.100	.095	.184	
3J	.085	.100	.0925	.183	
4B	.085	.095	.090	.176	
4D	.085	.100	.0925	.176	
4F	.085	.095	.090	.178	
4H	.085	.095	.090	.177	
IV	.070	.085	.0775	.167	
5C	.075	.085	.080	.168	
5E	.080	.085	.0825	.169	
V	.080	.090	.085	.170	
5G	.075	.090	.0825	.170	
5J	.075	.085	.080	.169	
6K	.080	.090	.085	.169	
VI	.075	.085	.080	.171	
		MEAN	.0879	.0923	.0830
		STD. DEVIATION	.0060	.0022	.0049
			COMBINED	CENTRAL	PERIPHERY

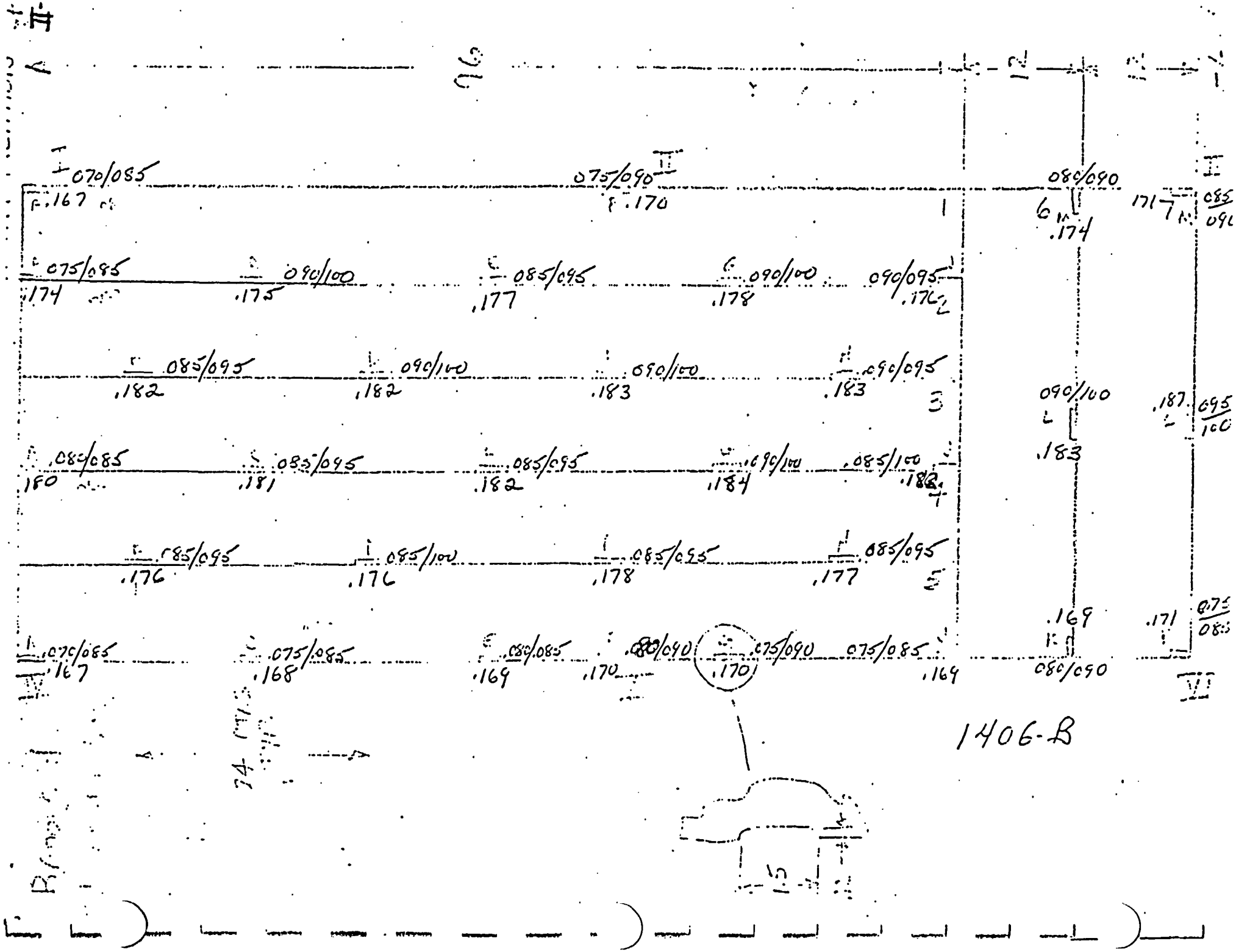
1406-B

THICKNESS MEASUREMENTS FOR BORAL SHEET NO. 1434-A

LOCATION	CORE THICKNESS MIN.	MAX.	AVG.	PANEL THICKNESS	
I	.075	.085	.080	.173	
~~II~~ II	.080	.100	.090	.176	
6M	.075	.095	.085	.173	
III	.075	.085	.080	.174	
1A	.085	.100	.0925	.181	
1C	.090	.100	.095	.179	
1E	.090	.100	.095	.180	
1G	.090	.100	.095	.183	
1J	.085	.100	.0925	.180	
2B	.085	.100	.0925	.184	
2D	.090	.100	.095	.183	
2F	.090	.100	.095	.187	
2H	.090	.100	.095	.185	
6L	.095	.100	.0975	.184	
7L	.090	.100	.095	.185	
3A	.085	.095	.090	.183	
3C	.090	.100	.095	.182	
3E	.085	.100	.0925	.183	
3G	.085	.100	.0925	.185	
3J	.085	.095	.090	.183	
4B	.085	.095	.090	.177	
4D	.090	.100	.095	.176	
4F	.090	.100	.095	.180	
4H	.085	.095	.090	.179	
IV	.075	.085	.080	.169	
5C	.075	.085	.080	.169	
5E	.075	.090	.0825	.170	
V	.080	.090	.085	.171	
5G	.080	.095	.0875	.171	
5J	.080	.095	.0875	.169	
6K	.075	.085	.080	.174	
VI	.080	.090	.085	.170	
		MEAN	.0897	.0937	.0853
		STD. DEVIATION	.0056	.0022	.0050
			COMBINED	~~PERIPHERY~~ CENTRAL	PERIPHERY

96
075/085
080/100
.173
.176
.085/100
.090/100
.181
.179
.180
.183
.180
.085/100
.184
.183
.187
.185
.090/100
085/095
.183
.182
.183
.185
.183
085/095
.177
.176
.180
.179
.085/095
075/085
.169
.169
.170
.171
.171
.080/095
.169
.174
.185
.170
075/085
095/100
14 CTS
1434-A

THICKNESS MEASUREMENTS FOR BORAL SHEET NO. 1462-B

LOCATION	CORE THICKNESS MIN.	CORE THICKNESS MAX.	CORE THICKNESS AVG.	PANEL THICKNESS	
I	.075	.085	.080	.168	
~~II~~	.075	.085	.080	.167	
6M	.075	.085	.080	.165	
III	.060	.080	.070	.165	
1A	.090	.100	.095	.176	
1C	.090	.100	.095	.176	
1E	.085	.090	.0875	.175	
1G	.085	.095	.090	.174	
1J	.085	.100	.0925	.175	
2B	.090	.100	.095	.181	
2D	.090	.100	.095	.182	
2F	.085	.100	.0925	.180	
2H	.080	.100	.090	.180	
6L	.090	.100	.095	.182	
7L	.075	.090	.0825	.180	
3A	.090	.100	.095	.183	
3C	.090	.100	.095	.183	
3E	.085	.100	.0925	.183	
3G	.090	.100	.095	.182	
3J	.085	.100	.0925	.182	
4B	.085	.100	.0925	.180	
4D	.085	.100	.0925	.180	
4F	.090	.100	.095	.179	
4H	.090	.100	.095	.179	
IV	.085	.100	.0925	.171	
5C	.085	.095	.090	.172	
5E	.080	.090	.085	.171	
V	.080	.100	.090	.171	
5G	.085	.095	.090	.171	
5J	.080	.095	.0875	.171	
6K	.080	.095	.0875	.170	
VI	.070	.085	.0775	.170	
		MEAN	.0895	.0930	.0855
		STD. DEVIATION	.0063	.0022	.0070
			COMBINED	CENTRAL	PERIPHERY

Pg. II-1

1462-B

THICKNESS MEASUREMENTS FOR BORAL SHEET NO. 1931-B

LOCATION	CORE THICKNESS MIN.	CORE THICKNESS MAX.	CORE THICKNESS AVG.	PANEL THICKNESS	
I	.075	.085	.080	.180	
II	.070	.080	.075	.175	
6M	.075	.085	.080	.175	.201 GMS/CM²
III	.075	.080	.0775	.174	
1A	.080	.100	.090	.187	
1C	.085	.100	.0925	.188	
1E	.085	.095	.090	.187	
1G	.085	.100	.0925	.184	
1J	.090	.100	.095	.183	
2B	.090	.100	.095	.190	
2D	.090	.100	.095	.187	
2F	.090	.100	.095	.185	
2H	.090	.100	.095	.186	
6L	.090	.100	.095	.186	.230 GMS/CM²
7L	.080	.085	.0825	.185	
3A	.095	.100	.0975	.190	
3C	.090	.100	.095	.187	
3E	.090	.100	.095	.185	
3G	.090	.100	.095	.185	
3J	.090	.100	.095	.185	
4B	.085	.100	.0925	.183	
4D	.085	.100	.0925	.181	
4F	.085	.100	.0925	.180	
4H	.090	.100	.095	.180	
IV	.075	.085	.080	.176	
5C	.070	.085	.0775	.174	
5E	.070	.085	.0775	.173	
V	.070	.075	.0725	.173	
5G	.070	.080	.075	.172	
5J	.070	.085	.0775	.173	
6K	.065	.080	.0725	.172	.177 GMS/CM²
VI	.075	.085	.080	.171	
		MEAN	.0872	.0939	.0796
		STD. DEVIATION	.0085	.0015	.0065
			COMBINED	CENTRAL	PERIPHERY

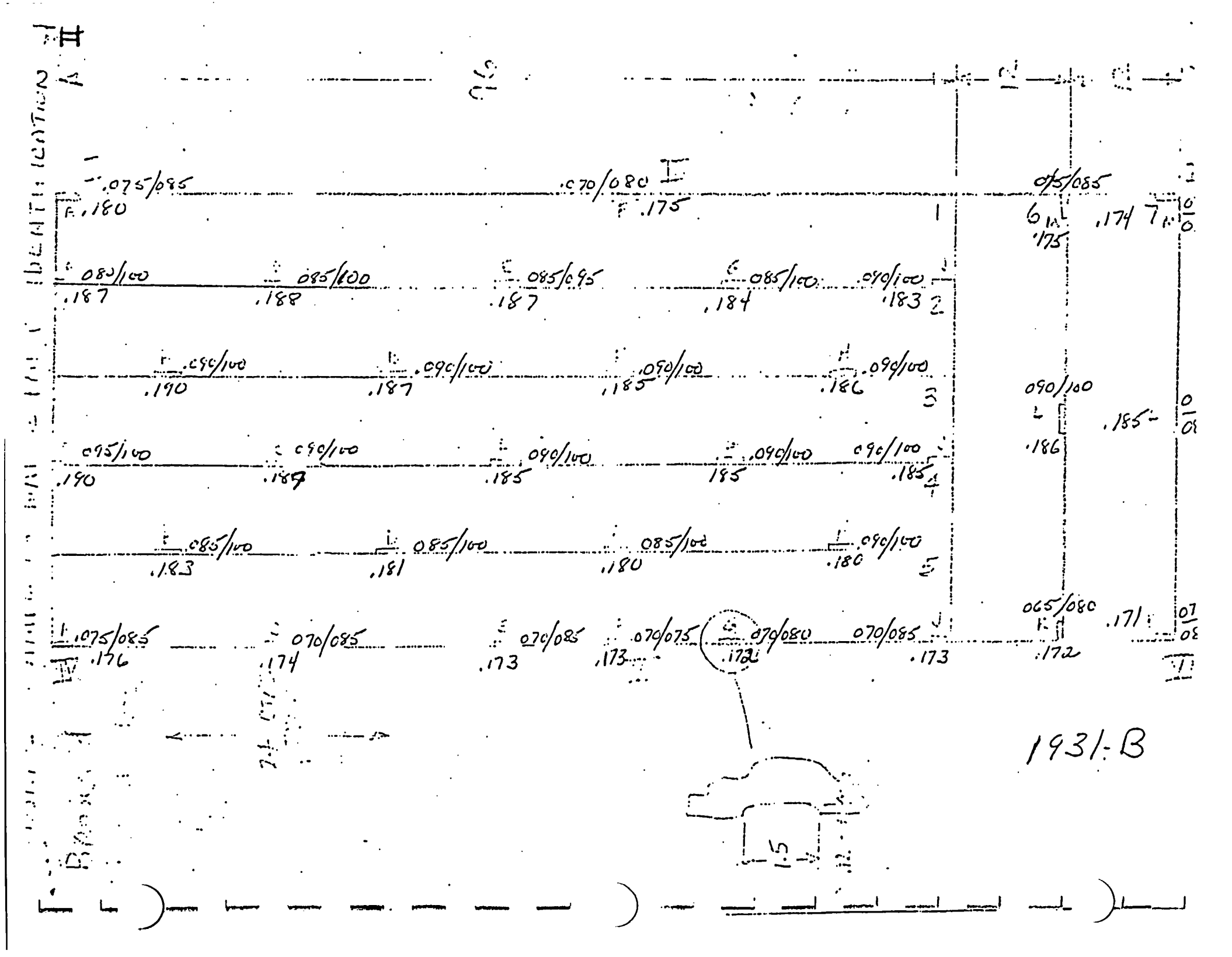
1931-B

APPENDIX C

EXPERIMENTAL DATA

PANEL LOT III

PAGES III-1 THRU III-2

JULY 1, 1976 III
GAGNON
ROSZLER
MOLLON
(PAR)

SET No.		I	II	III	IV	V	VI
2007-A	t_e	.085	.090	.090	.085	.085	.085
	t_s	.168	.169	.172	.165	.168	.170
2019-A	t_e	.085	.085	.085	.090	.085	.085
	t_s	.175	.170	.170	.172	.167	.172
2019-B	t_e	.085	.085	.085	.085	.085	.085
	t_s	.172	.166	.165	.171	.167	.177
2025-B	t_e	.085	.085	.085	.085	.075	.085
	t_s	.176	.168	.168	.166	.168	.174
2005-A	t_e	.085	.085	.085	.085	.090	.085
	t_s	.171	.167	.167	.174	.180	.167
2015-B	t_e	.085	.085	.085	.085	.095	.085
	t_s	.177	.175	.181	.174	.173	.175
2013-A	t_e	.085	.085	.085	.085	.085	.085
	t_s	.172	.171	.173	.168	.170	.171
2035-A	t_e	.085	.085	.085	.085	.090	.085
	t_s	.175	.176	.175	.169	.173	.173
2035-B CAP. OPTIC. PAR U.T.	t_e	.085	.085	.085	.085	.085	.085
	t_s	.174	.173	.176	.169	.170	.171
2003-A	t_e	.095	.085	.090	.095	.095	.095
	t_s	.170	.168	.172	.166	.173	.170
2005-B	t_e	.085	.085	.090	.085	.085	.095
	t_s	.165	.167	.171	.166	.174	.173
2017-B	t_e	.085	.100	.085	.090	.085	
	t_s	.167	.168	.169	.167	.168	.170

SHEET NO.		I	II	III	IV	V	VI
2004-A	t_c	.090	.090	.095	.090	.095	.090
	t_s	.165	.168	.172	.168	.170	.174
2004-B	t_c	.085	.090	.085	.095	.085	.090
	t_s	.168	.170	.170	.168	.170	.172
2010-A	t_c	.090	.095	.095	.095	.095	.095
	t_s	.174	.177	.180	.170	.173	.180
2033-B	t_c	.085	.090	.085	.085	.080	.085
	t_s	.166	.168	.173	.170	.166	.165
2033-A	t_c	.090	.090	.090	.080	.090	.090
	t_s	.167	.170	.174	.170	.168	.166
2006-B	t_c	.095	.095	.090	.095	.090	.095
	t_s	.168	.171	.175	.170	.173	.176
2006-A	t_c	.095	.095	.095	.100	.090	.095
	t_s	.169	.172	.177	.172	.172	.178
2028-B	t_c	.095	.095	.095	.090	.085	.085
	t_s	.168	.168	.171	.168	.169	.172

t_s = total thickness of BORAL sheet - all measurements provided verbally by CAD (taken by micrometer)

t_c = thickness of BORAL core - first nine sheets measurements provided verbally by CAD. (taken by optical comparator - last eleven sheets measured by Krautkramer-Branson USM 2MT Ultrasonic Flaw Detector with Z-103 DUFP transducer (5.0 MHz - 1/4" DIA.)

APPENDIX D

EXPERIMENTAL DATA

PANEL LOT IV

PAGES IV-1 THRU IV-6

T	1552-A	C		1555-A	
	.174		0	.090	
1	.175	.085	1	.190	.100 .100
2	.176	.085 .080	2	.170	
3	.177		3	.190	
4	.178		4	.190	
5	.179		12	.189	
10	.184		13	.190	
11	.185		14	.190	
12	.184		15	.188	.070 .090
13	.185	.085	16	.198	
14	.186	.085	17	.187	
15	.186		18	.187	
	.187		27	.177	
17	.187		28	.177	
26	.189		29	.175	
27	.189		30	.175	
28	.189		31	.173	.080 .080
29	.189	.085			
30	.189	.085			
31	.189				
M		.0843			.0900 M
SD		.0019			.0089 SD

AVERAGE OF 27	
.0846	MEAN
.0045	STD. DE

$\frac{\varepsilon}{2.2946}$

.122

IV.

1558-A

IN"	T	C
0	.171	
1	.171	.060
2	.171	.065
3	.171	
4	.172	
14	.179	
15	.180	
16	.180	
17	.181	.075
18	.181	.075
19	.181	
25	.181	
26	.183	
27	.183	
28	.183	
29	.183	.075
30	.183	.075
31	.183	
	.182 M	.0708
	.181 SD	.0066

1558-B

IN"	T	C
0	.170	
1	.169	.075
2	.170	.075
3	.170	
4	.171	
5	.172	
16	.178	
17	.178	
18	.178	
19	.178	.085
20	.178	.085
21	.179	
22	.178	
27	.179	
28	.179	
29	.179	
30	.179	
31	.179	.055
32	.179	.055
		.0817
		.0052

1589-B

IN"	T	C
0	.172	
1	.172	.080
2	.172	.075
3	.173	
4	.177	
5	.174	
16	.184	
17	.184	
18	.184	.085
19	.184	.085
20	.184	
21	.184	
28	.184	
29	.184	
30	.182	
31	.182	.085
32	.182	.080
33	.184	
		.0817
		.0041

1567B

IN"	T	C
0	.170	
1	.172	
2	.173	
3	.174	.075
4	.174	.080
5	.174	
6	.175	
12	.177	
13	.178	
14		.075
15	.177	.075
16	.179	
17	.178	
28	.179	
29	.178	
30	.178	
31	.177	.080
32	.177	.050
33	.176	
		.0775 M
		.0027 SD

1581-A

T	C
.172	
.173	
.173	.070
.174	.075
.175	
.176	
.177	
.184	
.184	
.184	
.184	
.184	.085
.184	.090
.184	
.185	
.183	
.184	
.184	
.183	.085
.182	.090
M	.0825

1575-B

No.	T	C
0	.176	
1	.172	.085
2	.175	.085
3	.179	
4	.175	
5	.176	
6	.177	
14	.183	
15	.183	
16	.183	
17	.183	.080
18	.183	.070
19	.183	
20	.183	
21	.183	
22	.184	
27	.182	
28	.181	
29	.182	.100
30	.182	.090
31	.182	.085
32	.180	.0
		.0857

1556-B

No.	T	C
0	.173	
1	.173	
2	.179	.085
3	.179	.085
4	.175	
5	.177	
6	.178	
9	.180	
10	.181	
11	.182	
12	.183	.085
13	.189	.090
14	.189	
15	.185	
16	.185	
17	.185	
25	.186	
26	.185	
27	.185	.090
28	.189	.090
29	.184	.090
30	.184	
31	.186	
32	.183	
		.0875

1589-A

No.	T	C
0	.172	
1	.171	
2	.172	.085
3	.173	.085
4		
5	.174	
6	.175	
16	.183	
17	.184	
18	.185	
19	.180	.085
20	.189	.090
21	.184	
22	.189	
23	.184	
28	.184	
29	.183	
30	.183	
31	182	.085
32	.183	.085
33	.183	
		.0858 M

IN	T	C
1	.171	
	.171	
	.172	.085
	.172	.090
	.173	
	.174	
	.175	
	.183	
	.189	
	.189	
18	.189	
	.189	.085
	.184	.085
21	.189	
	.184	
23	.189	
24	.183	
	.183	
30	.182	
31	.182	.085
	.182	.085
33	.182	
M		.0858
SD		.0020

IN	T	C
0	.172	
1	.173	
2	.173	.080
3	.174	.085
9	.175	
5	.177	
6	.177	
11	.182	
12	.183	
13	.183	
19	.183	
15	.155	.085
16	.154	.080
17	.158	
18	.185	
28	.184	
29	.184	
30	.184	
31	.181	.090
32	.181	.085
M		.0842
SD		.0038

IN	T	C
0	.171	
1	.172	.085
2	.172	.095
3	.173	
4	.174	
5	.175	
13	.182	
14	.183	
15	.183	
16	.184	.090
17	.184	.090
18	.185	
19	.185	
20	.184	
21	.185	
26	.184	
27	.184	
28	.184	
29	.183	.100
30	.183	.095
31	.184	
M		.0925
SD		.0052

IN	T	C
0	.170	
1	.171	
2	.171	.055
3	.172	.090
4	.173	
5	.174	
6	.175	
16	.184	
17	.184	
18	.184	
19	.184	.085
20	.185	.090
21	.185	.100
22	.185	
23	.184	
24	.184	
28	.184	
29	.183	
30	.183	.085
31	.183	.085
32	.182	
33	.183	
M		.0886
SD		.0056

IN	1566-B T	C
1	.165	
	.165	.080
	.166	.095
3	.167	
	.167	
	.165	
6	.169	
	.174	
	.175	
14	.175	
	.176	
	.178	.085
17	.177	.090
18	.177	.100
	.177	
	.177	
21	.177	
	.180	
	.178	
	.178	
25	.178	.085
	.177	.090
	.177	
M		.0879
SD		.0064

IN	1569-A T	C
0	.168	.085
1	.169	.085
2	.171	
3	.171	
4	.172	
5	.173	
6	.174	
13	.179	
14	.180	
15	.180	
16	.181	
17	.181	.085
18	.181	.085
M	.182	
20	.182	
21	.183	
22	.183	
26	.183	
27	.183	
28	.183	
29	.183	.085
30	.182	.095
31	.182	
M		.0867
SD		.0041

IN	1531-B T	C
0	.172	
1	.172	.085
2	.173	.085
3	.174	
4	.175	
5	.176	
6	.177	
13	.183	
14	.184	
15	.183	
16	.185	
17	.189	.055
18	.189	.090
19	.189	
20	.189	
21	.189	
25	.189	
26	.189	
27	.183	
28	.183	
29	.183	.055
30	.183	.055
31	.183	
M		.0858
SD		.0020

IN	1530-B T	C
0	.171	
1	.172	.080
2	.172	.085
3	.173	.085
9	.179	
5	.175	
6	.176	
12	.182	
13	.181	
19	.182	
15	.182	
16	.182	.085
17	.183	.090
18	.183	.095
19	.183	
20	.183	
26	.182	
27	.182	
28	.181	
29	.181	
30	.181	.090
31	.181	.090
32	.181	.095
M		.0883
SD		.0050

1552-B		1535-A		1594-B	
.193		0 .168	.065	0 .177	~~.085~~
.183	.080		.080		.085
	.100	1 .168	.075	1 .177	
2 .185		2 .171		2 .177	
.186		3 .171		3 .178	
1 .187		4 .170		4 .179	
1. .193		16 .180		5 .180	
2 .193		17 .180		9 .183	
3 .193	.100	18 .181		10 .183	
4 .194	.100	19 .181	.090	11 .185	
5 .196			.090		.085
16 .196		20 .181		12 .184	.085
7 .195		21 .181		13 .184	
5 .195		22 .181		14 .184	
26 .192		28 .180		15 .184	
27 .192		29 .180		24 .183	
28 .191	.100	30 .180		25 ~~.183~~	
	.100		.080		
29 .192		31 .178	.085	26 .183	
30 .192		32 .178		27 .181	
		33 .178		28 .182	
				29 .181	
				30 .182	
M	.0983		.0807		.0850 M
SD	.0041		.0087		0 S.D.

1635-B T	1635-B C	1531-A T	1531-A C	1555-B T	1555-B C
.173		⊙ .172		0 .171	
.171		1 .172	.085	1 .173	.075
2 .174	.085 .085	2 .175	.085 .085	2 .174	.075
3 .172		3 .174		3 .174	
4 .172		4 .176		4 .174	
5 .173		5 .177		5 .175	
6 .179		6 .178		6 .176	
7 .179		16 .184		15 .185	
8 .181		17 .184		16 .186	
0		18 .184		17 .185	
1		19 .184		19 .186	
11		20 .184	.090	19 .185	
2		21 .185	.085	20 .186	.080 .080
3 .186		22 .185		21 .186	
19 .181		23 .185		22 .187	
.181		28 .184		23 .186	
	.085 .085	29 .183		27 .187	
18 .183		30 .182		28 .186	
9 .183		31 .182	.085 .085	27 .186	
0 .183		32 .182		30 .185	
21		33 .182		31 .185	.085 .085
2				32 .185	
3				33 .183	
24					
5					
6					
27					
28 .183					
9 .184					
0 .182					
31 .182	.085 .085				
2 .182					
3 .182					
M	.0850		.0858		.0800 M
SD	0		.0020		.0045 SD

1594-A		1545-B		1590-A	
T	C	T	C	T	C
0. 173		0 .169		0 .172	
1 .172		1 .170		1 .173	.075 .080
2 .173		2 .170	.055 .060	2 .172	
3 .173	.085 .095	3 .171		3 .173	
4 .173		4 .171		4 .174	
5 .174		5 .173		5 .177	
11 .180		16 .180		14 .182	
12. 181		17 .180		15 .184	
13. .182		18 .181		16 .188	
14 .183	.085 .085	19 .186	.085 .085	17 .187	.080 .085
15 .185		20 .188		18 .191	
16 .189		21 .190		19 .190	
17 .183		22 .197		20 .188	
28 .183		23 .186		21 .184	
29 .182		28 .180		28 .190	
30 .182		29 .180		29 .189	
31 .182		30 .179		30 .189	
32 .183		31 .178	.085 .085	31 .187	.085 .085
		32 .178		32 .182	
		33 .180		33 .182	
M	.0850		.0758		.0817
SD	0		.0143		.0041

APPENDIX E

EXPERIMENTAL DATA

PANEL LOT V

PAGES V-1 THRU V-20

IN"	T	C
0	.168	.075
	.169	.075
	.169	.085
	.170	.095
4	.170	
11	.175	
	.186	.090
14	.176	.090
	.177	.085
24	.179	
	.178	.085
	.179	.095
27	.179	
	MEAN	.0833
	STD DEV	.0086
36	.175	.085
	.174	.090
	174	.085
	.168	
	.161	.075
	.167	.075
47	.166	.065
	.166	

IN"	T	C
0	.178	0
1	.173	.075
2	.173	.075
3	.174	.085
4	.175	
10	.181	
11	.182	.090
12	.182	.090
13	.183	
22	.185	
23	.185	.095
24	.186	.085
25	.185	
		.0862
		.0065
34	.182	.090
35	.182	.085
36	.181	.095
44	.172	
45	.172	.090
46	.171	.095
47	.170	.080

IN"	T	C
17	.173	
2	.175	.095
3	.176	.090
4	.177	.095
5	.177	.085
11	.183	.100
12	.184	.100
13	184	.095
23	.187	.095
24	.185	.105
25	.187	.100
		.0941
		.0096
35	.184	.100
36	.183	.115
37	.182	.095
45	.175	.085
46	.175	.090
47	.174	.090
48	.174	.075

IN"	T	C
0	.170	
1	.170	.085
2	.171	.090
3	.174	.100
12	.180	
13	.180	.090
14	.180	.090
15	.180	.095
24	.181	
25	.182	.100
26	.182	.100
27	.183	
		.0893
		.0102
35	.177	
36	.176	.095
37	.175	.095
38	.175	.090
45	.169	
46	.167	.095
47	167	.080
48	.166	.065
49	166	

1077-B ✓

	T	C
1	.179	.095
	.180	.085
	.181	.095
	.182	
9		
10	.186	
11	.186	.085
12	.187	.085
	.188	.095
14		
	MEAN	.0910
	STD. DEV.	.0087
21		
22	.189	
23	.189	.095
24	.188	.095
	.189	.100
26		
34	.183	
35	.182	.100
36	.181	.100
37	.182	.100
42		
	.171	
	.176	.085
	.175	.075
	.175	.075
45		
47		

X 1001-D ✓

IN"	T	C
1	.174	.085
2	.174	.080
3	.175	.075
4	.175	
5		
11	.177	.085
12	.176	.075
13	.176	.085
14	1	
		.0785
		.0075
22	.174	.085
23	.174	.085
24	.174	.085
25	.172	
34	.166	.075
35	.165	
36	.165	.075
37	164	.065
38	164	.065

X 1084-B ✓

IN"	T	C
1	.164	.080
2	.165	.090
3	.166	.085
4	.167	
5		
11	.175	
12	.175	.095
13	.176	.095
14	.177	
		.0883
		.0113
23	.180	
24	.180	.100
25	.181	.100
26	.181	
34	.181	
35	.178	.095
36	.177	.100
37	.175	
38	174	
44	.167	
45	.166	
46	.165	.075
47	.165	.080
48	.164	.065

1012-D ✓

IN"	T	C
1	.177	.085
2	.178	.090
3	.179	.080
4	.180	
5		
7	.183	.090
8	.184	
9	.185	.085
		.0912
		.0087
18	190	
19	190	.100
20	191	.100
21	191	
30	.189	
31	.189	.105
32	.188	
33	.188	.100
40	.182	.100
41	.182	.080
42	.182	.085
43	.181	.085

ck Core

1086-B ✓

IN"	T	C
	.170	.090
2	.171	.095
	.172	.090
4	.173	~~.095~~
11	.181	.095
	.181	.095
13	.183	.085
MEAN		.0944
S.D.		.0066
	.188	
	.189	.100
24	.188	.100
	.189	.105
35	.190	.105
	.187	.095
37	.187	.100
3	.180	
44	.179	.095
45	.178	.090
	.176	.085

1025-B ✓

IN"	T	C
1	.170	.075
2	.171	.075
3	.172	.075
4	.173	-
10	.178	.085
11	.179	.085
12	.180	~~.095~~
13	.181	
MEAN		.0871
S.D.		.0084
22	.184	
23	.184	.095
24	.185	.095
25	.185	
34	.184	.095
35	.183	.095
36	.183	
37	.184	
38	.182	
39	.181	.095
40	.180	.085
41	.180	.090

1025-H ✓

IN"	T	C
0	.185	.095
1	.185	.100
2	.186	.100
3	.186	.090
4	.187	
11	.190	
12	.191	.100
13	.192	.095
14	.192	
MEAN		.0921
S.D.		.0061
23	.190	
24	.191	.085
25	.190	.100
34	.182	
35	.181	.090
36	.182	.085
37	.181	.055
38	.181	.090
39	.178	.090
40	.178	.085

1010-A ✓

IN"	T	C
0	.165	.060
1	.165	.075
2	.167	.085
	.168	.085
3		
4	.170	
14	.176	
15	.176	.100
16	.176	.085
17	.177	
MEAN		.0868
S.D.		.0119
26	.179	
27	.179	.100
28	.178	.085
29	.178	
36	.176	
37	.176	.100
38	.176	.090
39	.175	.090

1155-FT

IN"	T	C
	.171	085
	.171	085
	.171	095
3	172	095
	173	
12	180	
13	180	.100
14	181	.095
15	181	
M		.0910
SD		.0063
24	184	095
25	184	095
26	184	100
33	183	
34	182	090
35	180	095
43	174	
44	173	085
45	172	085
46	171	085
47	171	080

1162-FT

IN"	T	C
0	.168	075
1	.169	.075
2	.170	.075
3	.171	.075
4	172	
13	.175	.085
14	.179	.085
15	.179	.085
		.0833
		.0056
24	.180	
25	.180	.090
26	.179	090
27		
36	.174	090
37	174	085
38	174	085
45	.167	
46	.167	095
47	.166	085
48	.166	085
49	.166	

1164-N

IN"	T	C
0	.174	~~080~~
1	175	085
2	176	085
3	176	085
4	177	
11	.183	090
12	.184	095
13	.185	095
		.0890
		.0069
23	.189	080
24	.190	095
25	.189	
34	.187	~~095~~
35	.186	095
36	.186	100
43	179	~~085~~
44	178	085
45	176	090
46	.176	085
47	.175	075

1161-FT

IN"	T	C
0	.188	080
1	.178	075
2	.176	080
3	.177	085
4	.177	
11	183	.090
12	184	.100
13	.185	.100
		.0885
		.0084
23	.187	.100
24	.188	.085
25	.187	095
34	183	
35	.182	095
36	.181	095
37	.181	095
44	.174	
45	.173	085
46	.172	085
47	.171	085
48	.170	075

II-
OK
Core

1229-A ✓			1243-A ✓			1281-A ✓			1281-A		
IN	T	C	IN	T	C	IN	T	C	IN	T	C
	179	.095	0	.175	.085	0	.182	.090	0	.182	.095
	.176	.095	1	.175	.085	1	.182	.095	1	.181	.095
	.176	.095	2	.179	.085	2	.181	.085	2	.181	.100
	.176	.090	3	.179	.090	3	.181	.100	3	.181	.105
	.175		4	.173	.	4	.181	.	9	.181	
	.176	.090	11	.172	.	11	.180	.	11	.180	
12	.176	.096	12	.172	.085	12	.179	.090	12	.180	.190
	.176	.090	13	.171	.080	13	.179	.090	13	.179	.100
	.176		19	.171	.	19	.180	.	19	.179	
	.177		22	.172	.	23	.180	.	23	.180	
24	.176	.085	23	.172		29	.180	.090	29	.180	.090
	.175	.090	24	.172	.090	25	.180	.085	25	.180	.085
	.175		25	.172	.085	26	.181	.	26	.180	
			26	.173	.						
31	.175					32	.182	.	32	.182	
	.175	.090	33	.173	.	33	.182	.090	33	.182	.090
33	.175	.085	34	.174	.080	34	.182	.	34	.183	.080
	.175	.085	35	.174	.085	35	.183	.	35	.183	.090
	.175	.085	36	.175	.085	36	.183	.	36	.183	.090
		.0896			.0850			.0906			
		.0038			.0032			.0046			

V-
ck
Core
Thk

1201-0 ✓			1201-17 ✓			1201-11 ✓					
IN	T	C	IN	T	C	IN	T	C	IN	T	C
1	.181	.090	0	.186	.095	0	.179	.090			
	181	.095	1	.186	.100	1	.179	.095			
	181	.085	2	.186	.100	2	.179	.095			
	.181	.090	3	.186	.090	3	.179	.095			
	.181		9	.186		9	.179				
	.180		11	.189		11	.179				
12	.180	.090	12	.189	.085	12	.180	.085			
	.180	.100	13	.189	.100	13	.180	.090			
19	.179		19	.189		19	.180				
						22	.180				
23	.179		23	.183		23	.180				
	.178	.100	29	.182	.085	29	.180	.090			
2	.178	.100	25	.182	.085	25	.180	.085			
26	.178		26	.182		26	.180				
	.179		32	.182		32	.181				
	.180	.100	33	.182		33	.182	.100			
	.180	.100	39	.182	.080	39	.182	.100			
35	.180	.085	35	.182	.085	35	.182	.090			
	.181	.090	36	.183	.085	36	.183				
		.0938			.0900			.0923			
		.0061			.0074			.0052			

V - ok Core 1.

1091-B ✓			1092-B ✓			1093-B ✓ X					
IN"	T	C	IN"	T	C	IN"	T	C	IN"	T	C
	170	.080	1	177	.085	1	.166	.060			
2	169	.090	2	173	.085	2	.168	.075			
3	170	.090	3	172	.090	3	.169	.080			
4	171		4	174		4	.169				
11	.178	.090	11	174		11	.174				
12	.179		12	180	.090	12	.175	.085			
13	182	.090	13	181	.100	13	.176	.085			
		.0871			.0877			.0815			
		.0033			.0075			.0072			
	184		23	184		23	181				
23	184	.090	24	185	.095	24	180	.085			
25	185	.085	25	184	.095	25	181	.085			
	184										
			34	181	.085						
35	.183	.085	35	181	.095	35	179				
	.182	.085	36	180		36	178	.085			
37	.184		37	179		37	.178	.085			
41	.178										
	.176	.090									
	.176	.085									
	.175	.085									
			44	172		45	172				
			45	172	.085	46	.171	.085			
			46	171	.085	47	.170	.083			
			47	170	.075	48	.170	.085			
			48	170	075			.085			

V
ck
Cor

1251-B ✓

IN"	T	C
1	.178	.090
2	.177	.100
3	.179	.100
4	.179	
5	.180	
6	.181	
7		
8		
9	.183	
10	.184	.090
11	.184	.100
12	.184	
13	.185	
14		
15		.0950
16		.0048
17		
18		
19		
20	.189	
21	.187	.090
22	.187	.100
23	.187	
24	.187	
25		
26		
27		
28		
29		
30		
31	.184	
32	.183	.100
33	.182	.090
34	.182	
35	.182	
36		
37		
38		
39		
40		
41	.176	
42	.175	.095
43	.176	.095
44	.171	.090
45	.171	

IN"	T	C
1	.180	.085
2	.178	.100
3	.178	.100
4	.180	.100
5	.180	
6		
7		
8		
9		
10	.186	.100
11	.186	.102
12	.187	
13	.187	
14		
15		.0958
16		.0069
17		
18		
19		
20		
21	.189	
22	.191	.100
23	.190	.100
24	.190	
25	.189	
26		
27		
28		
29		
30		
31		
32		
33	.189	
34	.186	.100
35	.185	.100
36	.184	.100
37	.183	
38		
39		
40		
41		
42		
43	.176	
44	.175	.095
45	.175	.095
46	.173	.085
47	.172	.085

IN"	T	C
1	.169	.085
2	.169	.090
3	.170	.090
4	.171	
5		
6		
7		
8		
9		
10	.178	
11	.178	.090
12	.180	.095
13	.182	.100
14	.181	
15		.0928
16		.0055
17		
18		
19		
20		
21		
22	.186	
23	.187	.100
24	.186	.090
25	.186	.090
26	.187	
27		
28		
29		
30		
31		
32		
33		
34	.186	
35	.185	.095
36	.184	.095
37	.184	.100
38		
39		
40		
41		
42		
43	.177	
44	.176	.100
45	.175	.095
46	.174	.085
47	.174	.085

IN"	T	C
1	.180	.090
2	.180	.085
3	.181	.095
4	.182	
5		
6		
7		
8		
9	187	
10	187	
11	188	.100
12	.189	.100
13	190	
14		
15		.0969
16		.0072
17		
18		
19		
20		
21		
22	.192	.110
23	.191	.105
24	.191	.100
25		
26		
27		
28		
29		
30		
31		
32		
33		
34	.186	
35	.185	.095
36	.185	.100
37	.183	
38		
39		
40		
41		
42		
43	.178	
44	.177	
45	.175	.095
46	.175	.100
47	.176	.095

1124-FF ✓ X			1206-FF ✓			1233-FF ✓			* 1228-FF ✓		
IN"	T	C	IN"	T	C	IN"	T	C	IN"	T	C
	.170	065	0	Ø85	.100	0	.180		0	.182	.095
	.172	075	1	Ø84	095	1	.180	.085	1	.182	.095
	.173	080	2	Ø84	.100	2	180	.090	2	.182	.085
	.174	085	3	Ø84	.095	3	.180	090	3	.182	
4	.174		4	Ø84	-	4	.180		4	.182	
			11	Ø85		11	.180		11	.181	.100
	.182	.090	12	Ø85	.095	12	.180	.085	12	.182	
14	.182	.085	13	Ø84	.095	13	.180	090	13	.181	.095
	182	.095	14	985		14	.181		14	.181	
		.0894			.0946			.0895			.0946
		.0085			.0052			.0052			.0054
1	.184	.100	23	Ø85	.100	23	.182		23	.183	.090
5	183	.085	24	.186	095	24	.182	095	24	.182	.100
6	.183	.090	25	.186	.100	25	.183	.085	25	.182	.085
7	.182		26	.187		26	.182		26	.182	
			29	.186							
36	.179	.090	30	.186	.095	31	.183		31	.182	
37	.178	.090	31	.186	.090	32	.183	.095	32	.183	.100
5	.178	.085	32	.185	085	33	.183	.100	33	.182	.100
39	.176		33	.185	.085	34	.183	085	34	.182	.095
						35	.183	.085	35	.182	095
	.171										
	.170	.085									
0	.170	085									
41	.169	075									
4	.169	075									

1064-A			1013-A			1055-A			1052-A		
IN"	T	C	IN"	T	C	IN"	T	C	IN"	T	C
	.172	.090	1	.181	.080	1	.176		1	.183	.100
	.171	.085	2	.183	.095	2	.177	.085	2	.183	.100
	.173	.080	3	.184	.085	3	.177	.095	3	.185	.100
4	.174		4	.184		4	.178	.045	4	.185	
						5	.178		5		
									10	191	
11	.181	.100	11	.191	.090	12	.184		11	191	.100
	.182	.100	12	.191	.090	13	.184	.100	12	191	.105
	.183	.095	13	.192	.100	14	185	.100			
	.183		14	.193							.0954
		.0923			.0935			.0910			.0090
		.0065			.0080			.0060			
									22	192	
									23	192	.105
	.186	.090	23	.194	.100				24	192	.100
24	.186	.100	24	194	.105	24	.188		25	192	
	.186	.100	25	194	.100	25	.188	.085			
						26	.187	.085			
								.090			
1	.184								34	.188	
35	183	.090	35	.190					35	.187	.095
6	182	.090	36	.187	.100	36	.186	.095	36	.186	.100
7	181	.090	37	.188	.100	37	.183	.095	37	.185	
38	180	085				38	.183	.095			
1	.179	.100									
	.177	.090									
									43	.178	
						45	.178		44	.179	.090
			45	.180		46	176	.090	45	.177	085
			46	.179	085	47	.175	.090	46	176	.085
			47	.178	085		.175	.080	47	176	.075

V

ck
Col

V

1110-M1 ✓

IN"	T	C
	.175	.100
	.175	.095
	.176	.095
	.177	.090
4	.177	
11	.184	.095
1[illegible]	.185	.095
13	.185	.095
		.0947
		.0048
	.190	
23	.189	.095
	.189	.105
25	.189	
	.186	.100
	.186	.095
36	.185	.095
7		
3	.177	
	.177	.090
	.176	.090
	.175	.085
47	.175	

1151-M ✓

IN"	T	C
0	.171	.085
1	.172	.085
2	.172	.085
3	.173	.095
4	.174	--
12	.182	.100
13	.183	.100
14	.183	.095
		.0925
		.0071
23	.188	
24	.188	.100
25	.188	.095
26	.188	
34	.187	
35	.186	.100
36	.186	.100
37	.186	.100
44	.179	.085
45	.178	.085
46	.177	.085
47	.176	.085
48	.175	

1156-B ✓

IN"	T	C
0	.176	.090
1	.176	.085
2	.177	.085
3	.177	.090
4	.178	
11	.183	.095
12	.189	.100
13	.185	.100
		.0910
		.0060
22	.187	
23	.187	.085
24	.187	.100
25	.187	
33	.184	
34	.189	.095
35	.183	.095
36	.182	
43	.176	
44	.175	.085
45	.175	.085
46	.174	.085
47	.174	.090

1151-D ✓

IN"	T	C
0	.176	.075
1	.177	.075
2	.177	.085
3	.178	.085
4	.181	
11	.187	.085
12	.187	.095
13	.189	.095
		.0924
		.0092
23	.194	.100
24	.195	.100
25	.195	.105
35	.194	.100
36	.193	.100
37	.193	.100
44	.186	
45	.186	100
46	.184	.090
47	.183	.085
48	.182	.085

1101-A

	T	C
	.168	.075
	.169	.085
2	.169	.085
	.170	.085
4	.171	
10	.176	.090
	.177	.090
12	.177	.100
13	.178	
		.0894
		.0075
22	.181	.100
23	.181	.100
24	.182	090
25	.182	
34	.180	.100
35	.180	.090
36	.178	095
44	.172	
45	171	.085
45	170	.085
46	170	.085
		.080

1152-A

IN"	T	C
0	174	
1	174	.085
2	175	085
3	177	085
4	178	085
5	179	
11	184	
12	184	.100
13	185	.105
14	185	
		.0886
		.0072
23	186	
24	186	095
25	186	095
26	185	
35	180	
36	179	085
37	179	085
44	171	
45	171	085
46	170	095
47	169	080

1152-B

IN"	T	C
0	.168	.085
1	.168	.090
2	.170	.085
3	.171	085
4	.172	
11	178	
12	178	.100
13	.179	085
14	.179	
		.0863
		.0079
23	.180	.100
24	.179	.090
25	.180	085
26	.179	
34	.174	
35	.174	085
36	.172	090
37	.172	085
44	.165	
45	.166	.085
46	.163	085
47	.161	080

1184-B

IN"	T	C
0	.178	
1	.179	.085
2	180	.090
3	.181	095
4	.182	105
12	.190	
13	.190	.100
14	.191	.095
15	.191	
		.0932
		.0071
24	.193	.100
25	.193	.100
26	.193	.100
36	.189	085
37	.189	.100
38	.187	095
44	.181	090
45	.180	090
46	.180	090
47	175	085

1233-B ✓

	T	C
1	.178	.090
2	.178	.095
3	.178	.095
4	.178	.100
5	.178	
6		
7		
8		
9		
10	.178	
11	.178	.090
12	.179	.095
13	.179	
14		
15		
16		
17	.180	
18	.180	.095
19	.180	.100
20	.180	
21		
22		
23		
24		
25		
26		
27		
28		
29		
30		
31	.181	
32	.181	.090
33	.182	.090
34	.182	.085
35	.182	.090
	.0929	
	.0045	

1207-B ✓

IN"	T	C
0	.182	.085
1	.182	.085
2	.182	.085
3	.182	.085
4	.183	
5		
6		
7		
8		
9		
10		
11	.183	
12	.183	.090
13	.183	.095
14	.183	
15		
16		
17		
18		
19		
20		
21		
22		
23	.185	
24	.185	.100
25	.185	.100
26	.185	
27		
28		
29		
30	.185	
31	.187	.090
32	.186	.090
33	.186	.100
34	.186	.100
	.0921	
	.0066	

1228-B ✓

IN"	T	C
0	.180	.090
1	.180	.090
2	.180	.090
3	.180	.085
4	180	
5		
6		
7		
8		
9		
10		
11	.179	
12	.179	.095
13	.179	.090
14	.179	
15		
16		
17		
18		
19		
20		
21		
22		
23	.178	
24	.178	.095
25	.178	.095
26		
27		
28		
29		
30	.179	
31	.178	.085
32	.178	.090
33	.178	.095
34	.178	.090
	.0908	
	.0036	

1555-A ✓

IN"	T	C
0	—	.085
1	—	.085
2	—	.090
3		
4		
5		
6		
7		
8		
9		
10		
11		
12		
13		
14		
15		
16	.100	.100
16	.100	.100
17	—	.100
18		
19		
20		
21		
22		
23		
24		
25		
26		
27		
28		
29	—	.100
30	—	.100
	.0950	
	.0071	

IN	T	C
0	.181	.085
1	.181	.085
2	.181	.085
3	.181	.090
4	.181	
10	.182	
11	.181	.090
12	.181	.095
13	.181	
14	.182	
23	.181	.095
24	.181	.095
25	.181	
26	.181	
30	.181	
31	.181	.085
32	.181	.090
33	.181	.085
34	.181	.090
		.0892
		.0042

IN	T	C
0	.183	.090
1	.183	.090
2	.183	.090
3	.183	.095
4	.3	-
10	.184	
11	.184	.100
12	.184	.090
13	.184	.100
14	.184	
22	.183	
23	.183	
24	.182	.095
25	.183	.095
26	.182	
30	.181	
31	.180	.100
32	.180	.100
33	.180	.095
34	.180	.096
		.0950
		.0041

IN	T	C
0	.186	.100
1	.185	.096
2	.185	.100
3	.185	.096
4	.185	
11	.185	
12	.186	.095
13	.184	.095
14	.183	
23	.183	
24	.189	.095
26	.183	.095
26	.183	
30	.184	
31	.189	.095
32	.189	.095
33	.183	.090
34	.184	.100
		.0958
		.0029

IN	T	C
0	.192	
1	.192	.090
2	.192	.100
3	.192	.100
4	.192	
11	.192	
12	.192	.100
13	.192	.095
14	.192	
23	.194	
24	.195	.085
25	.196	.100
26	.196	
31	.195	
32	.195	.095
33	.195	.095
34	.195	.100
		.0970
		.0035

1227-1A

	T	C
	.176	.085
	.177	.090
	.178	.090
	.177	.090
4	.177	
11	.178	
12	.178	.090
13	.178	.095
19	.178	
23	.178	
24	.179	.085
25	.178	.090
26	.178	
32	.180	
33	.180	.096
35	.180	.085
36	.180	.085
		.0891
		.0038

1222-B

IN	T	C
0	.184	.090
1	.184	.090
2	.183	.090
3	.183	.085
9	.183	
11	.182	
12	.182	.100
13	.182	.095
19	.182	
23	.184	
29	.184	.090
25	.184	.090
26	.184	
32	.186	
33	.187	.090
39	.187	.095
35	.187	.090
		.0914
		.0039

1260-A

IN	T	C
0	.175	.090
1	.175	.085
2	.179	.090
3	.179	.095
9	.179	
11	.175	
12	.175	.100
13	.175	.100
19	.175	
23	.177	
29	.177	.095
25	.177	.095
26	.177	
33	.177	
39	.177	.090 ~~.080~~
35	.177	.085
36	.176	.085
		.0918
		.0056

1295-A

IN	T	C
0	.180	.095
1	.180	.090
2	.180	.090
3	.180	.085
4	.180	
11	.181	
12	.181	.100
13	.180	.100
19	.180	
15	.180	
23	.180	
24	.180	.090
25	.180	.090
26	.180	
31	.180	
32	.180	
33	.180	.096
39	.180	.095
35	.179	.095
~~36~~	~~.179~~	
		.0932
		.0046

V-1

1339-B			1339-A			1336-A			?			
IN	T	C	IN	T	C	IN	T	C	IN	T	C	ck Core Thk.
	.169	.085	0	.173	.085	0	.169	.075	0	.173	.070	
	.170	.085	1	.170	.085	1	.169	.075	1	.173	.075	
	.170	.090	2	.170	.090	2	.170	.075	2	.173	.085	
	.171	.085	3	.171	.090	3	.171	.085	3	.173	.085	
	.172		4	.172		4	.172		4	.179		
	.176	.090	11	.177		7	.179		11	.176		
	.177	.090	12	.178	.090	8	.175	.090	12	.179	.095	
	.179	.085	13	.178	.090	9	.176	.090	13	.179	.095	
	.178		14	.179		10	.177		14	.180		
	.181		23	.182		19	.182		23	.182		
	.181	.090	24	.183	.090	20	.182	.085	24	.182	.095	
	.181	.090	25	.182	.095	21	.182	.090	25	.181	.095	
	.181		26	.183		22	.184		26	.181		
	.180		28	.182		29	.183	.085	29	.181		
	.180	.090	29	.182	.090	30	.183	.085	30	.180	.095	
	.180	.090	30	.182	.090	31	.183	.090	31	.180	.090	
	.180	.085	31	.182	.095	32	.183		32	.180	.095	
	.180	.085	32	.182	.090	33	.183					
	.179		33	.182								
		.0877			.0900			.0841			.0886	
		.0026			.0030			.0063			.0090	

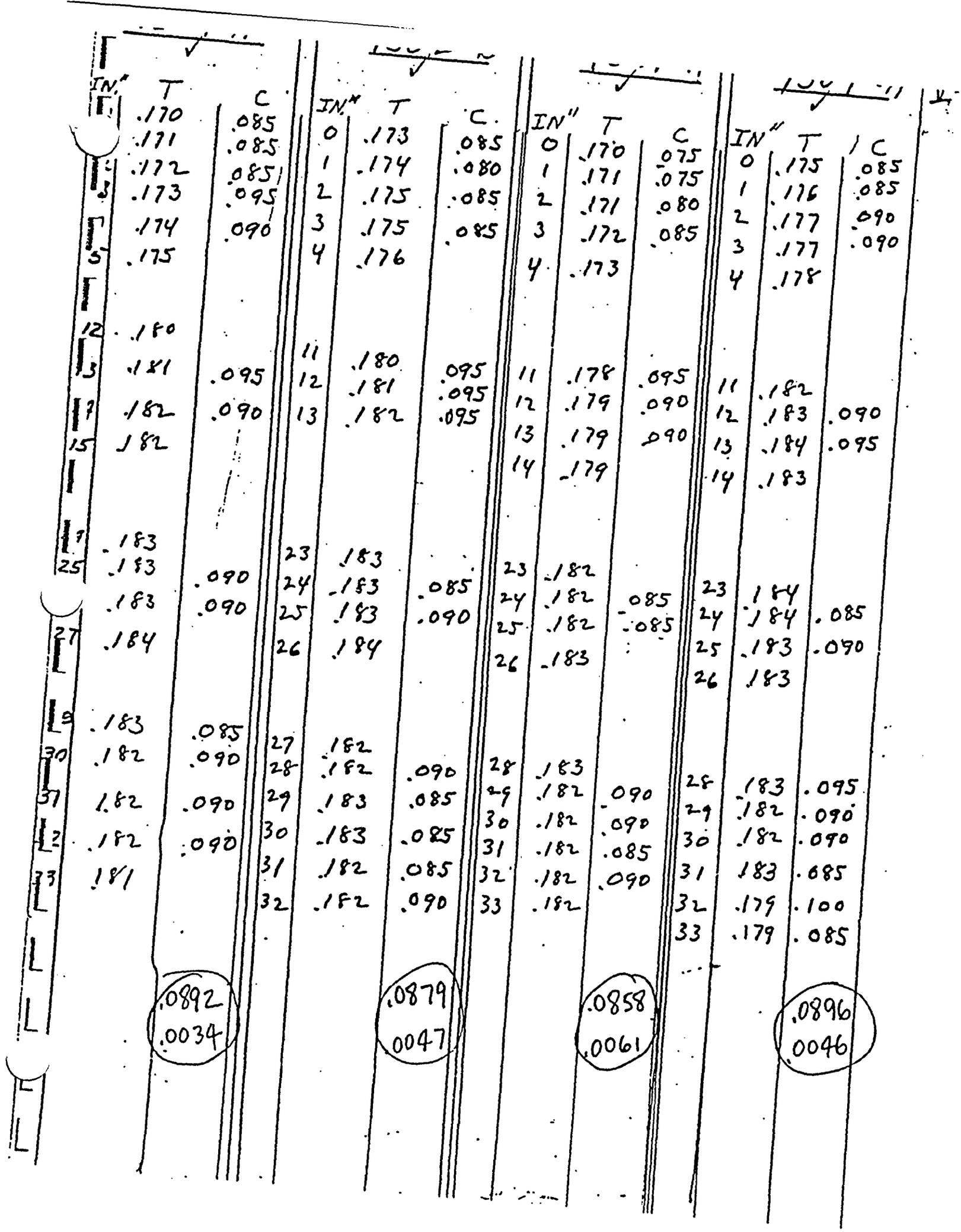

IN"	T	C
	.170	.085
	.171	.085
	.172	.085
3	.173	.095
	.174	.090
5	.175	
12	.180	
13	.181	.095
7	.182	.090
15	182	
7	.183	
25	.183	.090
	.183	.090
27	.184	
9	.183	.085
30	.182	.090
31	182	.090
2	.182	.090
33	181	
	.0892	
	.0034	

IN"	T	C
0	.173	.085
1	.174	.080
2	.175	.085
3	.175	.085
4	.176	
11	.180	
12	.181	.095
13	.182	.095
23	.183	
24	.183	.085
25	.183	.090
26	.184	
27	.182	
28	.182	.090
29	.183	.085
30	.183	.085
31	.182	.085
32	.182	.090
	.0879	
	0047	

IN"	T	C
0	.170	.075
1	.171	.075
2	.171	.080
3	.172	.085
4	.173	
11	.178	.095
12	.179	.090
13	.179	.090
14	.179	
23	.182	
24	.182	.085
25	.182	.085
26	.183	
28	.183	
29	.182	.090
30	.182	.090
31	.182	.085
32	.182	.090
33	.182	
	.0858	
	.0061	

IN"	T	C
0	.175	.085
1	.176	.085
2	.177	.090
3	.177	.090
4	.178	
11	.182	
12	.183	.090
13	.184	.095
14	.183	
23	.184	
24	.184	.085
25	.183	.090
26	.183	
28	.183	.095
29	.182	.090
30	.182	.090
31	.183	.085
32	.179	.100
33	.179	.085
	.0896	
	.0046	

1397-A

IN"	T	C
	169	.085
	170	.080
	171	.085
	171	.085
4	.172	
	173	
12	.180	
13	.181	.085
14	.181	.090
15	.182	
24	.182	
25	.184	.090
26	.183	.090
27	.183	
30	.182	.090
31	.182	.090
32	.181	.085
33	.180	
		.0868
		.0034

1336-B

IN"	T	C
0	.179	.085
1	.180	.085
2	.180	.080
3	.180	.090
4	.181	
5		
11	.183	
12	.182	.090
13	.182	.085
14	.182	
23	.180	
24	.179	.085
25	.178	.085
26		
29	.175	
30	.174	.080
31	.173	.085
32	.173	.075
		.0841
		.0044

1323-D

IN"	T	C
0	.174	.080
1	.175	.090
2	.177	.090
3	.178	.090
4	.178	
11	.184	
12	.185	.095
13	.186	.095
23	.190	
24	.190	.095
25	.190	.095
26	.191	
27	.190	
28	.190	.095
29	.191	.095
30	.191	.095
		.0923
		.0047

1307-D

IN"	T	C
0	174	.055
1	.175	.065
2	.176	.075
3	.177	.075
4	.178	
6	.180	
7	.181	.085
8	.182	.095
9	.182	
18	.188	
19	.188	.095
20	.188	.095
21	.188	
29	.190	
30	.190	.085
31	.189	.085
32	.189	.085
		.0819
		.0129

Co
Thi
Gr
V

V

1361-B			1335-B			1320-A			1392-A		
IN"	T	C	IN"	T	C	IN"	T	C	IN"	T	C
	.181	.090	0	.172	.080	0	.180	.090	0	.171	.080
	.181	.085	1	.173	.080	1	.180	.085	1	.172	.085
2	.181	.085	2	.174	.085	2	.181	.085	2	.172	.085
	.181	.090	3	.175	.090	3	.182	.095	3	.172	.090
4	.181	.090	4	.175		4	.183		4	.173	
	.181	.085									
6	.181										
			6	.177							
			7	.178	.090						
			8	.178	.090	11	.189		11	.179	
	.179		9	.179		12	.189	.095	12	.179	.095
10	.179	.090				13	.190	.095	13	.180	.095
	.178	.085				14	.190		14	.180	
18	.178										
			18	.185							
			19	.186	.090	23	.193		23	.183	
			20	.186	.085	24	.193	.100	24	.183	.095
26	.173		21	.186		25	.193	.100	25	.183	.095
27	.173	.085				26	.193		26	.183	
28	.172	.085				27	.193				
29	.172	.080				28	.192	.100			
			28	.187		29	.192	.100	29	.183	.090
			29	.187		30	.192	.105	30	.183	.090
			30	.187	.075				31	.182	.090
			31	.186	.075				32	.182	
			32	.187	.085				33	.182	
		.0864			.0841			.0955			.0900
		.0032			.0058			.0065			.0050

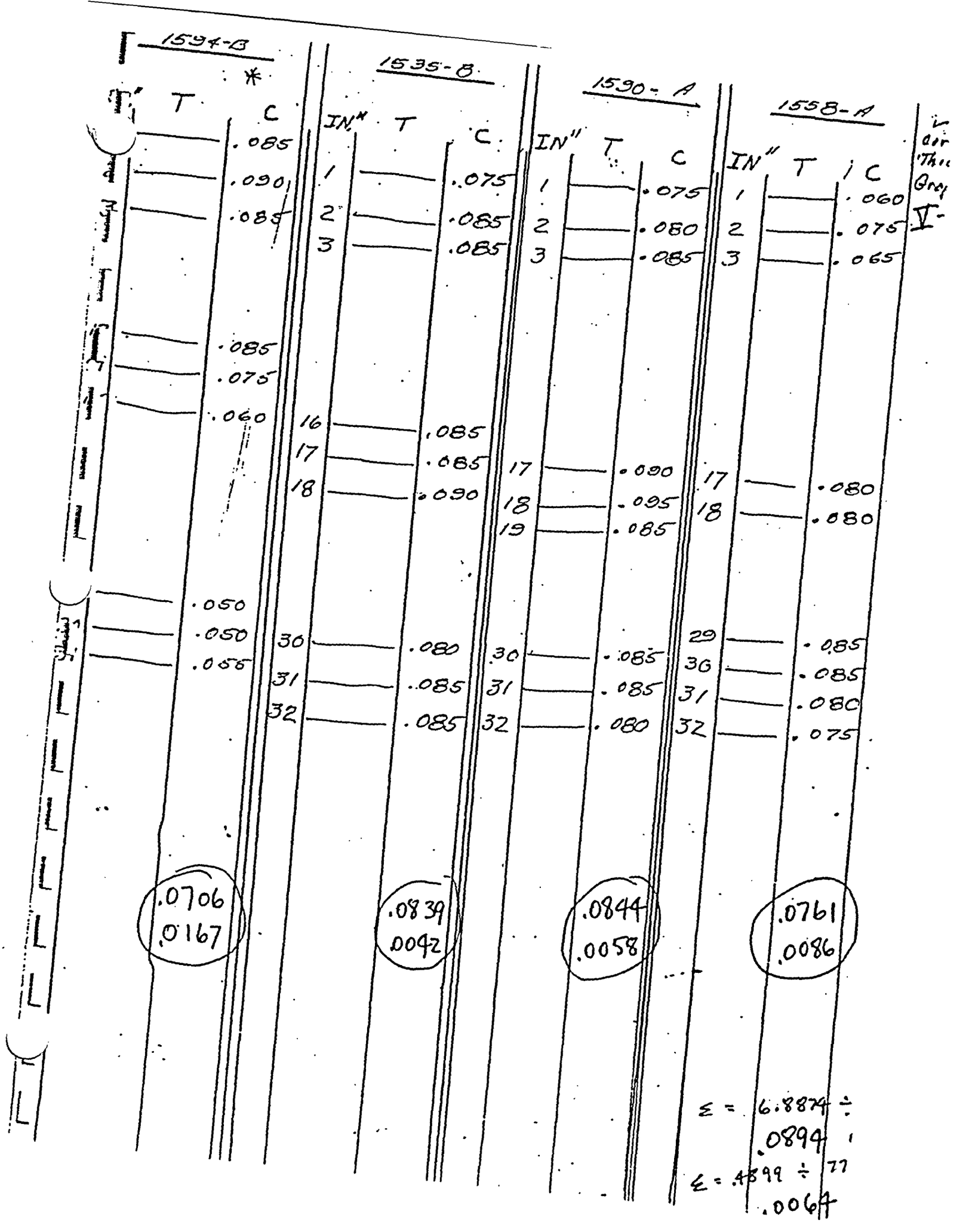
1594-B
T
C
.085
.090
.085
.085
.075
.060
.050
.050
.056
.0706
.0167
1535-B
IN"
T
C
1
.075
2
.085
3
.085
16
.085
17
.085
18
.090
30
.080
31
.085
32
.085
.0839
.0042
1590-A
IN"
T
C
1
.075
2
.080
3
.085
17
.090
18
.095
19
.085
30
.085
31
.085
32
.080
.0844
.0058
1558-A
IN"
T
C
1
.060
2
.075
3
.065
17
.080
18
.080
29
.085
30
.085
31
.080
32
.075
.0761
.0086
ε = 6.8874 ÷ .0894
ε = .4899 ÷ 77
.0064

APPENDIX F

EXPERIMENTAL DATA

SOLUBILITY TESTS OF BORON CARBIDE IN DILUTE HYDROCHLORIC ACID

PAGE VI-1

BY_____ DATE_____
CK._____ DATE_____
REV._____ DATE_____

b+p Brooks & Perkins, Incorporated
ADVANCED STRUCTURES DIVISION

SHEET_____ OF_____
SUBJECT_____

SOLUBILITY OF B_4C IN DILUTE HCL

TEST METHOD - PARA. 4.3 OF BPS-9000-01
BORON CARBIDE - TYPE 2 OF ASTM C750-73T
WEIGHT IN GRAMS

ITEM	TEST NUMBER			AVERAGE OF THREE TESTS
	1	2	3	
WEIGHT OF WET SAMPLE	2.0683	2.0402	2.4373	
WEIGHT OF DRY SAMP & CRUC.	29.3333	29.4627	29.7916	
WEIGHT OF CRUCIBLE	27.2885	27.4476	27.3832	
WEIGHT OF DRY SAMPLE	2.0448	2.0151	2.4084	2.1561
% LOSS OF MOISTURE	1.1362	1.2303	1.1857	
WEIGHT DRY RESIDUE & CRUC.	19.8131	19.6797	24.5031	
WEIGHT OF CRUCIBLE	17.8547	17.7504	22.1893	
WEIGHT OF DRY RESIDUE	1.9584	1.9293	2.3138	2.0672
WEIGHT LOSS OF B_4C	.0864	.0858	.0946	.0889
% LOSS OF B_4C	4.2254	4.2579	3.9279	4.12

APPENDIX G

EXPERIMENTAL DATA

CORE TAPER IN SCRAP AREA OF PANEL

PAGES VII-1 THRU VII-3

TECHNICAL ANALYSIS FORM

BY_____ DATE_____
CK._____ DATE_____
REV._____ DATE_____

b+p Brooks & Perkins, Incorporated
ADVANCED STRUCTURES DIVISION

SHEET_____ OF_____
SUBJECT_____

CORE TAPER IN SCRAP AREA OF PANEL

SCRAP SAMPLE TAPERING ZONE	CORE THICKNESS AT TRANSITION POINT	TAPER LENGTH FROM ZERO CORE TO TRANSITION PT.	CORE TAPER (INCHES PER INCH)
#1 LEFT	.080	2.71	.0295
#2 LEFT	.070	2.01	.0348
#3 LEFT	.075	1.90	.0395
#1 RIGHT	.075	4.11	.0182
#2 RIGHT	.075	3.00	.0250
#3 RIGHT	.085	3.30	.0258
	AVERAGE CORE TAPER		.0288

CHKD. BY.....DATE.....

JOB NO.....

#1 LEFT

#1 RIGHT

#2 LEFT

#2 RIGHT

#3 LEFT

#3 RIGHT

APPENDIX H

SUPPLEMENTAL DATA

TOTAL BORON CONTENT

IN

BORON CARBIDE

PAGE VIII-1

BORON CARBIDE

LOT OR ORDER NO.		AMOUNT (LBS)	% TOTAL BORON (1)
01-123-312	7/73	2250	71.84
01-336-005	1/75 ITEM 1	5000	74.63
585-35-3	2/75	5000	73.64
585-35-7	4/75	7000	74.13
585-35-9	5/75	7000	73.26
585-34-11	6/75	3500	74.02
585-35-10	6/75	3500	74.81
585-36-1	8/75	7000	75.37
585-36-2	9/75	7000	73.82
585-36-4	10/75	7000	73.28
585-36-6	11/75	7000	71.30
585-36-11	1/76	7000	73.73
585-36-12	1/76	7000	74.25
585-37-1	2/76	7000	73.94
		82,250 LBS	73.72 MEAN
			1.08 STD. DEV.
(1) PER VENDOR CERTIFICATIONS			75.37 HIGH

APPENDIX J

SUPPLEMENTAL DATA

BORON CARBIDE DISTRIBUTION

VERSUS

CORE THICKNESS & B_4C CONTENT RATIO

PAGE IX-1

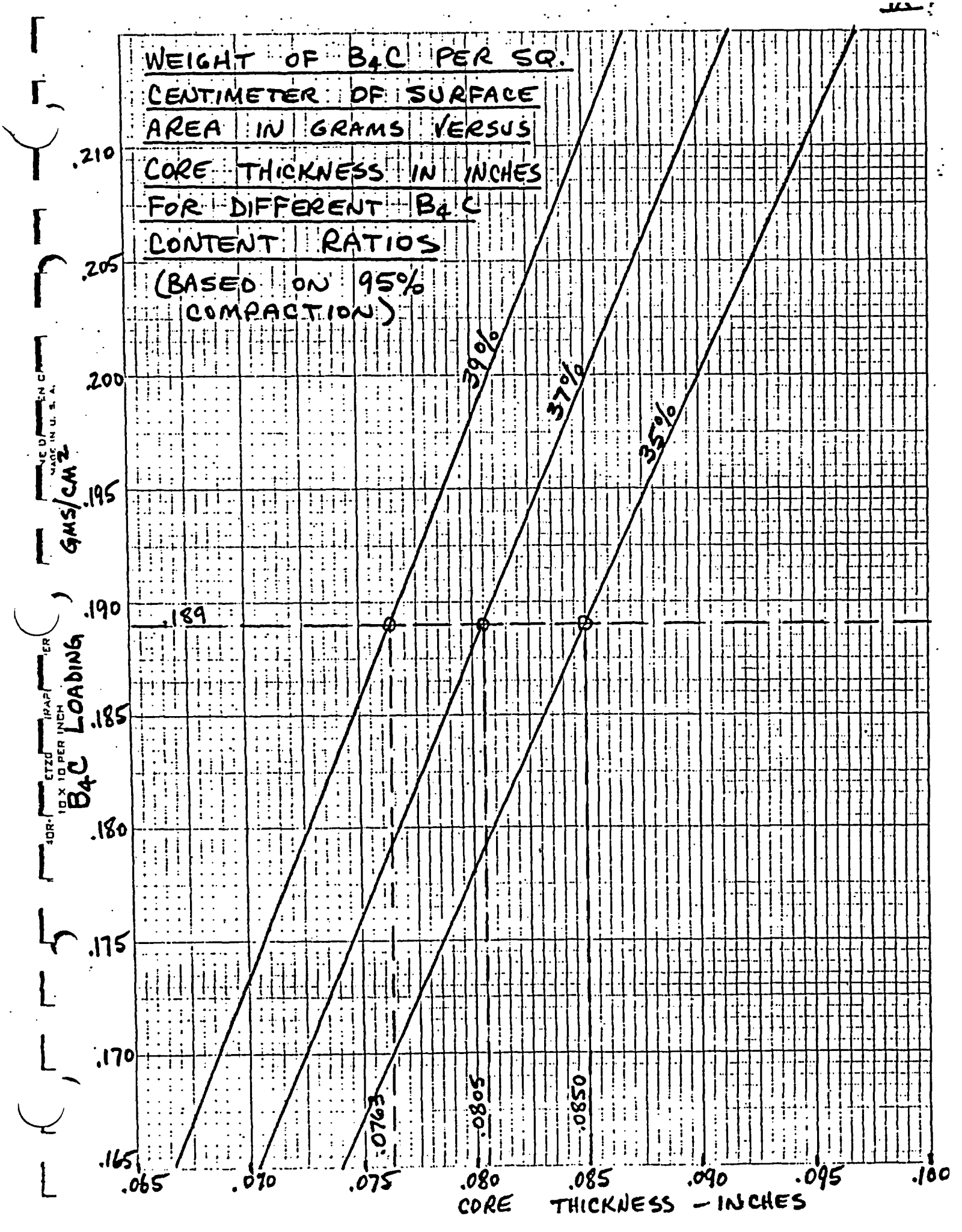
WEIGHT OF B_4C PER SQ. CENTIMETER OF SURFACE AREA IN GRAMS VERSUS CORE THICKNESS IN INCHES FOR DIFFERENT B_4C CONTENT RATIOS (BASED ON 95% COMPACTION)
39%
37%
35%
.189
.0765
.0805
.0850
.210
.205
.200
.195
.190
.185
.180
.175
.170
.165
.065
.070
.075
.080
.085
.090
.095
.100
GMS/CM²
B4C Loading
CORE THICKNESS – INCHES

APPENDIX K

SUPPLEMENTAL DATA

ITEM SPECIFICATION FOR BORAL™

BPS-9000-01

PAGES 1 THRU 7

B+P Brooks & Perkins, Incorporated

BROOKS & PERKINS, INCORPORATED
Specification Number
BPS-9000-01
Date of original issue: March 19, 1975
Date of revision: May 18, 1977
Date of revision: July 18, 1980
Jan. 6, 1981

Item Specification for BORAL^{tm}
A Neutron Shielding Material

1.0 GENERAL

1.1 Description: BORAL^{tm} is a sandwich material having exterior faces of an aluminum alloy and a core composed of aluminum and boron carbide. This sandwich material has a unique ability to absorb thermal neutrons without producing hard gamma radiation.

1.2 Scope: This specification establishes the standard for the manufacture, quality assurance, certification documentation, marking, packaging and preparation for shipment for BORAL^{tm} sheet and plate material. This specification shall form a part of all purchase orders, agreements and contracts for BORAL^{tm} and shall take precedence over any and all conflicting requirements unless specifically and mutually agreed upon to the contrary in writing by Brooks & Perkins, Inc. and the customer.

1.3 Classification: The BORAL^{tm} sandwich material will be manufactured with a boron carbide content that will provide the minimum weight of total boron per unit area as specified in Paragraph 3.4.

2.0 APPLICABLE DOCUMENTS: The following specifications and standards of the issue in effect on the date of the purchase agreement shall form a part of this specification.

2.1 Specifications:

ASTM B209

B&P Nuclear Quality Assurance Program Manual, Sections BP-1000 QA through BP-18000 QA

QA Approval	Engr. Approval	Supercedes Issue	Document No.
W. Jurgens	L. Moller	May 18, 1977	BPS-9000-01

M-100

3.0 REQUIREMENTS: The finished product BORAL^{tm} and the components from which it is produced will conform to the following requirements.

3.1 Cladding: The exterior faces or cladding of the sandwich panel will be the 1100 series aluminum in accordance with ASTM B209.

3.2 Boron Carbide Powder: The boron carbide powder contained in the core of the sandwich material will contain a minimum total boron content of 70.0% minimum by weight. Boric oxide will not exceed 3.0% maximum and iron will not exceed 2.0% maximum. The B^{10} isotopic content of the boron shall be that which is found in nature.

3.3 Boron Carbide Content (in-process): The core ingredients will be prepared such that any random sample taken from an in-process batch will contain by chemical analysis the minimum weight percentage of boron carbide required to meet Paragraphs 1.3 and 3.4.

3.4 Total Boron Content (sandwich): The minimum weight of total boron per unit area of sandwich material for the overall thickness will be as follows:

Sandwich Material Overall Thickness		Minimum Weight of Total Boron/Unit Area	
in.	(cm.)	oz./sq.in.	(gm/sq.cm.)
.177	(.450)	.029	(.126)
.265	(.673)	.059	(.251)

3.5 Tolerances: The dimensions of the Boral^{tm} sandwich material will be as specified within the following tolerances:

Dimension	Tolerance (plus or minus)	
(1) thickness, .177 in (.450 cm)	0.012 inch	(.0305 cm)
(1) thickness, .265 in (.673 cm)	0.015 inch	(.0381 cm)
width	3/16 inch	(.4763 cm)
length	5/32 inch	(.3969 cm)
(2) squareness	5/16 inch	(.7938 cm)
(3) flatness	1/2 inch	(1.27 cm)

QA Approval	Engrg Approval	Supercedes Issue	Document No.
W.R. Jacoyan	L. Mollon	May 18, 1977	BPS-9000-01

(1) total thickness of sandwich including core and two faces.
(2) maximum difference between diagonals of panel.
(3) rise from flat surface within 36 inches from where hand pressure (not exceeding 25 lbs.) is applied.

3.6 Workmanship: The workmanship provided during the manufacture of the BORAL^{tm} sandwich material in accordance with this specification will be of a high level to insure the requirements established herein have been met.

3.6.1 Surface Condition: The surface condition of the BORAL^{tm} sandwich material will conform to the requirements of the Aluminum Association for mill products in the "as-rolled" condition.

3.7 Marking: The BORAL^{tm} sandwich material will be spot marked for identification purposes with the following information on both the product and on the shipping container. The size of marking characters will be commensurate with the size of the product provided.

3.7.1 Trademark and Identification: The trademark and manufacturer's identification will be shown on a decal attached to the shipping container.

3.7.2 Serial Number: The serialized batch number will be permanently marked on each sheet or plate.

3.8 Packaging: The BORAL^{tm} sandwich material will be packaged in accordance with the following:

3.8.1 Lay two (2) thicknesses of polyethylene sheet into box, allowing to drop over sides and ends. Box is a general usage box to be used for BORAL^{tm} that will fit within its envelope. Number of pieces that can be shipped in this box will vary with BORAL^{tm} thickness, width, length and flatness.

3.8.2 Line bottom and sides of box with corrugated fiberboard sheets.

QA Approval	Engr. Approval	Supercedes Issue	Document No.
W.R. Jueyon	L. Mollon	May 18, 1977	BPS-9000-01

3.8.3 Load BORAL^{tm} into box stacking tight to one side and end of box. Boral shall be separated from each other by corrugated fiberboard sheet.

3.8.4 Block and brace BORAL^{tm} with suitable lumber to prevent any shifting within box.

3.8.5 Lay corrugated fiberboard sheet over BORAL^{tm} stack. Fold polyethylene sheet over top of BORAL^{tm} and tape in place.

3.8.6 Secure box top with lag screws and metal band box four (4) places around girth of box and two (2) places around length of box.

3.9 Preparation for Shipment: The exterior of the shipping container will be suitably marked with the following information:

Customer:

Shipping Destination:
Name and Address of Shipper:

4.0 QUALITY ASSURANCE PROVISIONS: Unless otherwise specified in the purchase agreement, Brooks & Perkins, Inc. will perform the following examinations to assure and certify the BORAL^{tm} furnished to the customer complies with the requirements specified herein in regards to materials, workmanship, boron content, marking, packaging and preparation for shipment.

4.1 Cladding: Each lot of raw material will be inspected for certification of compliance from the supplier and any additional tests required to assure the material conforms to the requirements of 3.1.

4.2 Boron Carbide: Each lot of raw material will be inspected for certification of compliance from the supplier and any additional tests required to assure the material conforms to the requirements of 3.2. A sample from each lot of raw material will be subjected to the quantitive analysis described in Paragraph 4.3.1 through 4.3.6 to determine the percentage of raw material remaining after analysis.

QA Approval	Engrg Approval	Supercedes Issue	Document No.
		May 18, 1977	BPS-9000-01

4.3 Boron Carbide Content (in-process): Each batch of blended core ingredients will have a minimum of one (1) sample retained for quantitive analysis to assure the material conforms to the requirements of Paragraph 3.3. Each sample will be identified with the serialized batch number. The percentage content of boron carbide in the sample will be determined as follows:

4.3.1 Heat sample in oven at 600°F (316°C) for 30 minutes and cool in a dessicator.

4.3.2 Record net weight of dry samples (gms).

4.3.3 Place the sample in hot dilute hydrochloric acid until the chemical action (bubbling) stops.

4.3.4 Filter the residue out of the solution.

4.3.5 Heat the residue in oven at 600°F (316°C) for one hour and cool in a dessicator.

4.3.6 Record the net weight of the dry residue (gms).

4.3.7 Divide the dry residue weight by the percentage of raw material remaining after analysis determined in Paragraph 4.2 for the particular lot of material.

4.3.8 Compute the percentage content in the sample dry weight (Paragraph 4.3.2) of the residue dry weight divided by the percentage of raw material remaining after analysis (Paragraph 4.3.7).

4.3.9 Compute the percentage content by weight of the total boron by multiplying the percentage determined in Paragraph 4.3.8 by the total boron percentage content stated on raw material certification.

4.4 <u>Boron Carbide Content (sandwich):</u> Each finished sheet or plate of BORAL^tm sandwich material will have a minimum of one (1) sample retained from the trim material cut from the short edges for quantative analysis to assure the material conforms to the requirements of Paragraph 3.4. The remaining portion of the sample will be retained by Brooks & Perkins Inc. for a period of one year and then will be disposed of unless instructed otherwise. Each sample will be identified with the serialized batch number. The percentage content of boron carbide and total boron in the samples will be determined as follows:

4.4.1 Record the overall thickness (cms) of the sample, including the cladding and core thickness.

4.4.2 Heat sample in oven at 600°F (316°C) for one hour and cool in dessicator.

4.4.3 Record the net dry weight (gms) of the sample in air and also in distilled water, and determine the difference between the two, which is the volume in cubic centimeters.

4.4.4 Compute the density of the sample by dividing the net dry weight in air by the volume of the sample determined in Paragraph 4.4.3 (gms/cc).

4.4.5 Place the sample in hot dilute hydrochloric acid until the chemical action (bubbling) stops.

4.4.6 Filter the residue out of the solution.

4.4.7 Wash the residue at least three times in hot dilute hydrochloric acid, followed each time by a rinse in distilled water.

4.4.8 Filter the residue through a Gooch crucible.

4.4.9 Heat the residue in oven at 600°F (316°C) for one hour and cool in a dessicator.

4.4.10 Record the net weight of dry residue (gms).

4.4.11 Divide the dry residue weight by the percentage of raw material remaining after analysis determined in Paragraph 4.2 for the particular lot of material.

4.4.12 Compute the boron carbide weight per unit area (gms/sq. cm.) by multiplying the corrected residue weight from Paragraph 4.4.11 by the sample thickness from Paragraph 4.4.1 and dividing by the volume from Paragraph 4.4.3.

4.4.13 Compute the total boron per unit area (gms/sq.cm.) by multiplying the boron carbide weight per unit area from Paragraph 4.4.12 by the total boron percentage content stated on raw material certification.

QA Approval	Engr. Approval	Supercedes Issue	Document No.
W. Jurgens	L. Moller	May 18, 1977	BPS-9000-01

4.5 Visual Examination: Each finished sheet or plate of BORAL[tm] sandwich material will be visually examined to assure the material conforms to the requirements of Paragraphs 3.5, 3.6, 3.7, 3.8 and 3.9.

4.6 X-Ray Radiographic Examination: When specifically required by the purchase order, the following additional testing will be performed. X-Ray radiographs will be taken in accordance with MIL-STD-00453 or the ASME Boiler and Pressure Vessel Code, Section 5, Subsection A, Article 2. The quantity and location of radiographs to be taken will be in accordance with the purchase order requirements. The radiograph film will be examined visually to determine the presence of any of the following defects which are unacceptable.

(a) Cracks or fractures in the aluminum cladding.
(b) Internal inclusions, discontinuities or voids in the core.
(c) Inclusions in the cladding that cannot be removed without destroying the integrity of the cladding.

4.7 Neutron Radiographic Examination: When specifically required by the purchase order, the following additional testing will be performed. Required additional samples will be retained from the trim material obtained in Paragraph 4.4 for neutron radiograph examination to assure the uniform dispersion of the boron. Each sample will be identified with the serialized batch number. The neutron radiograph will be taken in accordance with BP-9004QAP. The radiograph film will be examined visually or with a MacBeth Densitometer or equivalent for areas not having comparable density to the standard for the boron content requirement of Paragraph 1.3.

5.0 CERTIFICATION DOCUMENTATION: Documentation will be issued to the purchaser to certify that the material supplied hereunder has been inspected and tested and has been found to meet the requirements specified herein, including any additional testing that has been mutually agreed upon and so stated in the purchase order.

QA Approval	Engr. Approval	Supercedes Issue	Document No.
W.R. Lueyene	L. Mellon	May 18, 1977	BPS-9000-01

APPENDIX L

SUPPLEMENTAL DATA

BORAL™ THEORETICAL PHYSICAL CHARACTERISTICS

PAGES X-1 & X-2

TECHNICAL ANALYSIS FORM

BY LM DATE CK. DATE REV. DATE	Brooks & Perkins, Incorporated ADVANCED STRUCTURES DIVISION	SHEET OF SUBJECT

BORAL THEORETICAL WEIGHT FACTORS

DENSITIES

ALUM. (1100) = .098 LBS/IN^3 = 2.713 GM/CC
BORON CARBIDE (B_4C) = 2.510 GM/CC

BORAL CORE		35%	50%
ALUM.	6.5 gm	2.3959 cc	1.8430
B_4C	3.5 gm	1.3944 cc	1.9920
	10.0 gm	3.7903 cc	3.8350 cc

$\frac{10 \text{ gm}}{3.7903 \text{ cc}} = 2.6383 \text{ gm/cc}$ 2.6076 gm/cc

PANEL THICKNESSES CM. (INCHES)

.178	MIN.	NOM.	MAX.
CLAD	.1016 (.0400)	.1090 (.0429)	.1163 (.0458)
CORE	.2159 (.0850)	.2316 (.0912)	.2474 (.0974)
CLAD	.1016 (.0400)	.1090 (.0429)	.1163 (.0458)
TOTAL	.4191 (.1650)	.4496 (.1770)	.4800 (.1890)

.265	MIN.	NOM.	MAX.
CLAD	.1016 (.0400)	.1077 (.0424)	.1138 (.0448)
CORE	.4318 (.1700)	.4577 (.1802)	.4836 (.1904)
CLAD	.1016 (.0400)	.1077 (.0424)	.1138 (.0448)
TOTAL	.6350 (.2500)	.6731 (.2650)	.7112 (.2800)

BY LM DATE	Brooks & Perkins, Incorporated	SHEET OF
CK. DATE	ADVANCED STRUCTURES DIVISION	SUBJECT
REV. DATE		

BORAL CORE - MINIMUM CONTENTS (THEOR.)

CORE THICKNESS INCHES/CM.	% OF THEOR. DENSITY	% OF B_4C IN CORE ①	DISTRIBUTION OF B_4C GMS/SQ.CM.	DISTRIBUTION OF TOTAL BORON ② GMS/SQ.CM.	DISTRIBUTION OF B^{10} ISOTOPES ③ GMS/SQ.CM.
.085/.2159	100 (IDEAL)	35	.1994	.1396	.0251
.085/.2159	95 (MEAN)	35	.1894	.1326	.0239
.085/.2159	90 (MIN.)	35	.1795	.1256	.0226
.170/.4318	100 (IDEAL)	35	.3987	.2791	.0503
.170/.4318	95 (MEAN)	35	.3788	.2651	.0477
.170/.4318	90 (MIN.)	35	.3588	.2512	.0452

① B_4C PER ASTM C750-73T - TYPE 2

② 70.0 % MINIMUM - BY WEIGHT

③ 19.75 ± 0.30 ATOM % = 18.29 ± .28 % BY WEIGHT

ACR
DGW
RCK
FILE —

THE UNIVERSITY OF MICHIGAN
PHOENIX MEMORIAL LABORATORY
FORD NUCLEAR REACTOR
ANN ARBOR, MICHIGAN 48105

December 2, 1976

Mr. Les Mollon
Brooks and Perkins, Inc.
P. O. Box 2067
Livonia, Michigan 48151

Dear Les:

Enclosed are data and rough graphs per our telephone conversation. The three data sheets are for the 115 crystal plane which affords the least higher order neutron interference.

Figure 1 shows the transmission versus B4C mesh size. Each plot is for a different energy. As you can see transmission drops drastically down to 50-60 mesh, but not so much from that point on. We could use several in between size samples to verify this figure.

Figure 2 provides experimental transmission versus energy. Figure 3 shows the experimental transmission constant versus energy.

Figures 4, 5, and 6 show the individual experimental plots from Figure 3 with the theoretical plot imposed for comparison.

Very truly yours,

Reed R. Burn/D.Z.

Reed R. Burn
Reactor Manager
Ford Nuclear Reactor

RRB:dmz

cc: J. Lee
Enclosures

DATE: 11-24-76

SPECTROMETER DATA SHEET

TITLE: BROOKS AND PERKINS BORAL SAMPLES

E, Neutron Energy, eV	Sample Identification	Counting Time, Seconds	I_0, Beam Intensity, Counts	B_0, Beam Background, Counts	I, Transmitted Intensity, Counts	B, Transmitted Background, Counts	T, Transmission, $I-B/I_0-B_0$	t, Thickness, Inches	C, Transmission Constant $(\sqrt{E}/t)\ln(1/T)$
115	Crystal	P-Lane							
0.100	25/30-1	100	29878	161	3484	359	.1062	.087	8.15
0.125	25/30-1	100	30149	612	3733	459	.1108	.087	8.94
0.150	25/30-1	100	44502	730	6254	541	.1305	.087	9.06
0.175	25/30-1	100	40833	748	5889	553	.1331	.087	9.70
0.200	25/30-1	100	30715	809	5521	680	.1619	.087	9.36
0.250	25/30-1	100	33538	1346	6677	934	.1784	.087	9.91
0.300	25/30-1	100	23130	1632	5002	1168	.1783	.087	10.85

Comments:

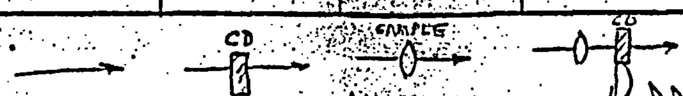

Attest:

Signature

DATE: 11-24-76

SPECTROMETER DATA SHEET

TITLE: BROOKS AND PERKINS BOREAL SAMPLES

E, Neutron Energy, eV	Sample Identification	Counting Time, Seconds	I_0, Beam Intensity, Counts	B_0, Beam Background, Counts	I, Transmitted Intensity, Counts	B, Transmitted Background, Counts	T, Transmission, $I-B/I_0-B_0$	t, Thickness, Inches	C, Transmission Constant $(\sqrt{E}/t)\ln(1/T)$
115	Crystal	A. Lane							
0.100	50/60-1	100	29878	461	1804	373	.0487	.087	10.99
0.125	50/60-1	100	30149	612	1953	423	.0518	.087	12.03
0.150	50/60-1	100	44502	730	3441	516	.0684	.087	11.94
0.175	50/60-1	100	40833	748	3350	524	.0705	.087	12.75
0.200	50/60-1	100	30715	809	3433	631	.0937	.087	12.17
0.250	50/60-1	100	33538	1346	4327	840	.1083	.087	12.77
0.300	50/60-1	100	23103	1632	3773	1047	.1268	.087	13.00

Comments:

Attest: Lloyd R. Perkins
Signature

DATE: 11-24-74

SPECTROMETER DATA SHEET

TITLE: BROOKS AND PERKINS BARAL SAMPLES

E, Neutron Energy, eV	Sample Identification	Counting Time, Seconds	I_0, Beam Intensity, Counts	B_0, Beam Background, Counts	I, Transmitted Intensity, Counts	B, Transmitted Background, Counts	T, Transmission, $I-B/I_0-B_0$	t, Thickness, Inches	C, Transmission Constant $(\sqrt{E}/t)\ln(1/T)$
115	Crystal	plane							
0.100	170-1	100	29878	461	1467	368	.0374	.087	11.95
0.125	170-1	100	30149	612	1713	458	.0425	.087	12.84
0.150	170-1	100	44562	730	2978	548	.0555	.087	12.87
0.175	170-1	100	40833	748	3017	547	.0616	.087	13.40
0.200	170-1	100	30715	809	3016	632	.0797	.087	13.00
0.250	170-1	100	33538	1346	4067	887	.0988	.087	13.30
0.300	170-1	100	23130	1632	3672	1049	.1220	.087	13.24

Comments:

Attest: Reed R Barr
Signature

FIGURE 1

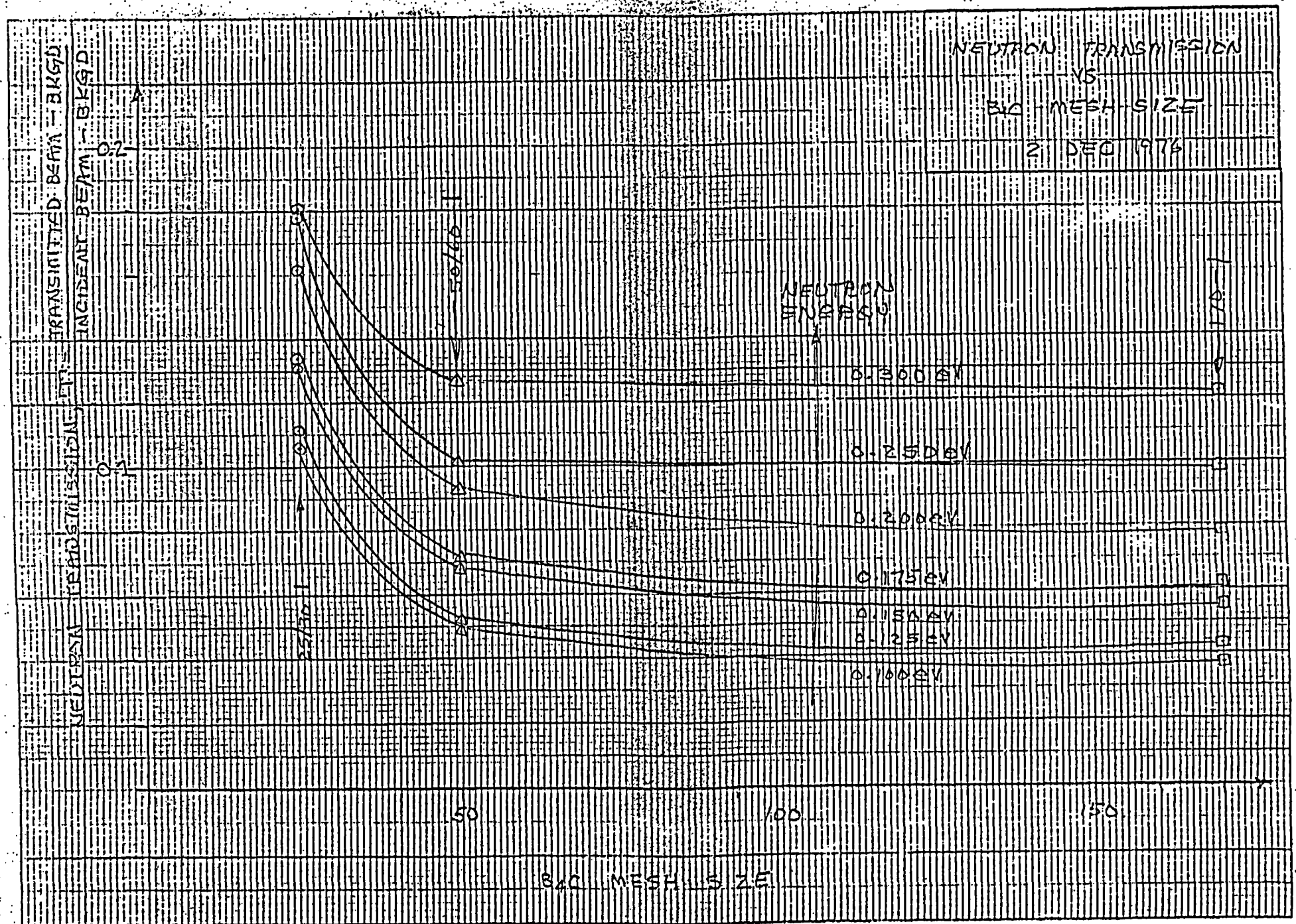

FIGURE 2

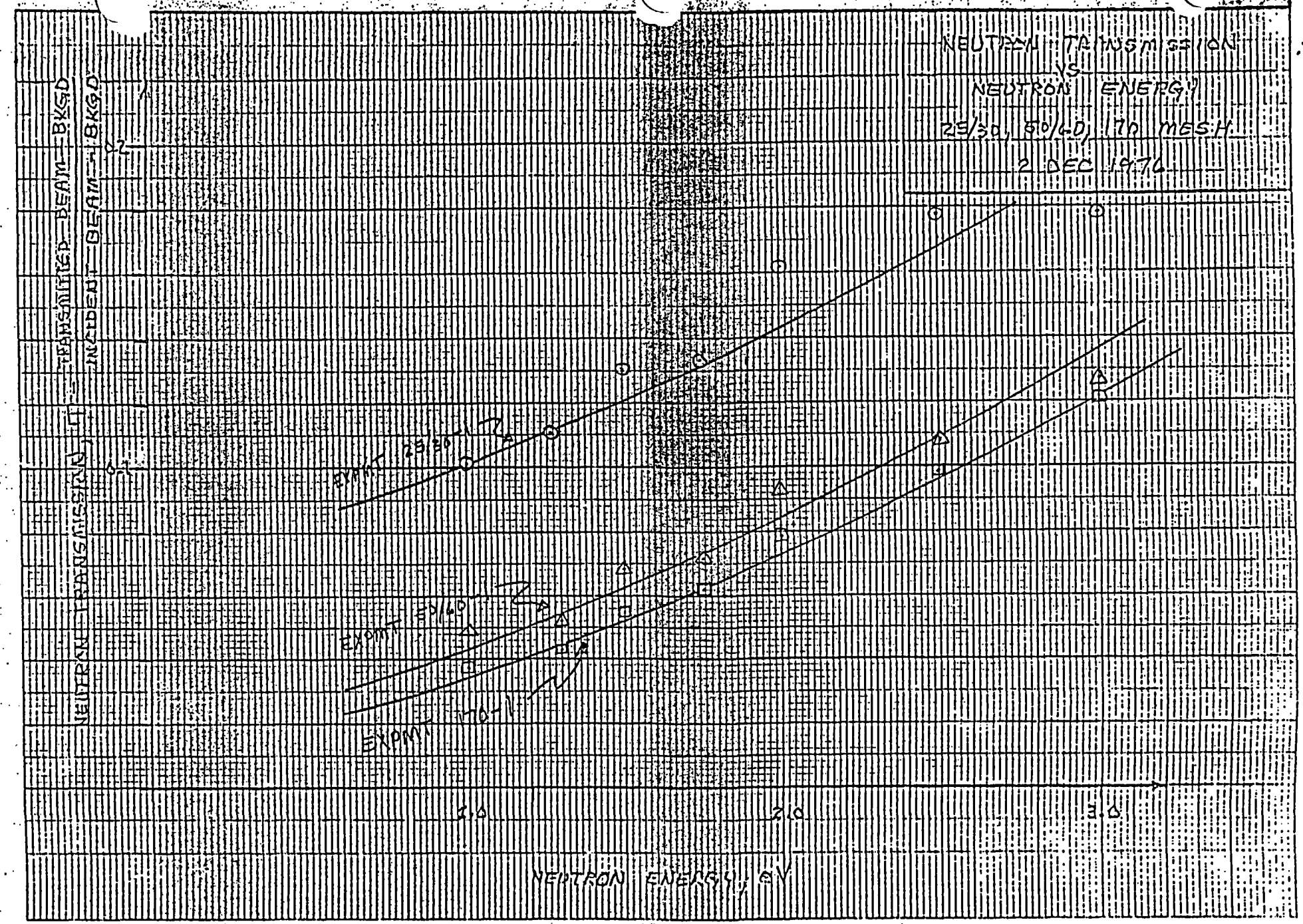
NEUTRON TRANSMISSION
VS
NEUTRON ENERGY
25/30, 50/40, 12in MES.H.
2 DEC 1974
TRANSMITTED BEAM - BKGD
INCIDENT BEAM - BKGD
EXPT 25/30
EXPT 50/40
EXPT 12-0
1.0
2.0
3.0
NEUTRON ENERGY, eV

46 1320

FIGURE 3

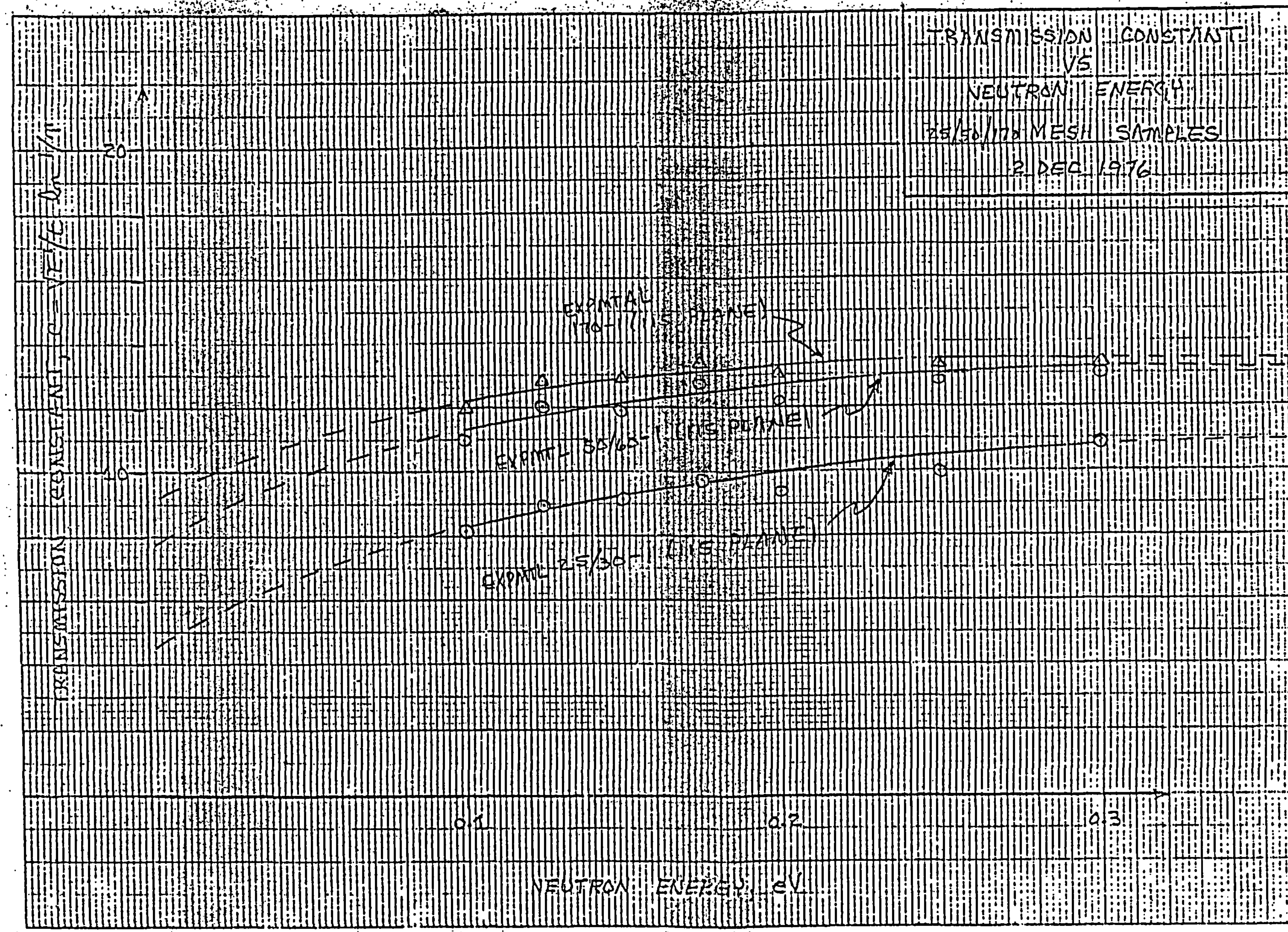

KEUFFEL & ESSER CO. MADE IN U.S.A.

FIGURE 4

TRANSMISSION CONSTANT
VS
NEUTRON ENERGY
25/30 MESH SAMPLES
2 DEC 1976

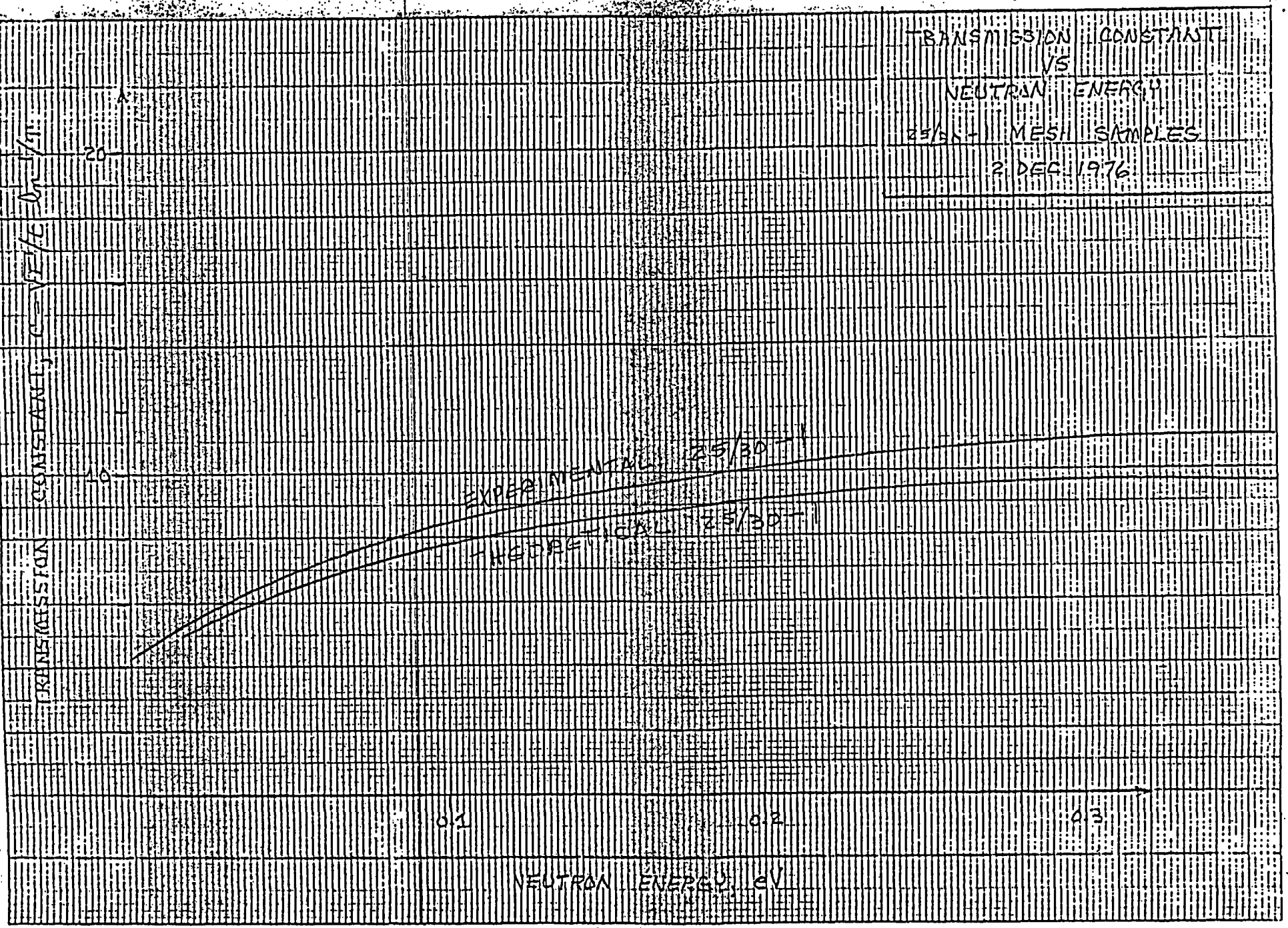

FIGURE 5

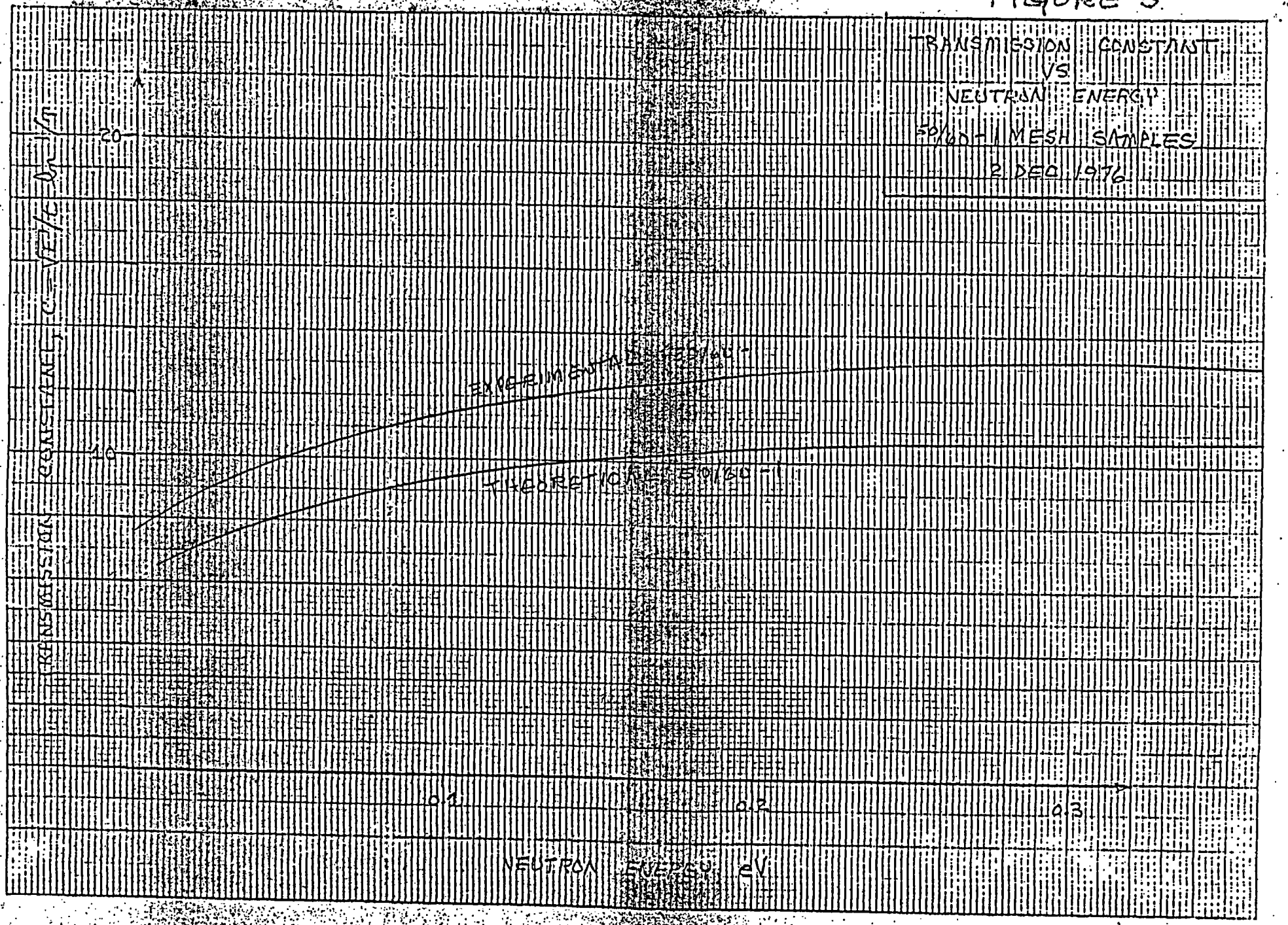

FIGURE 6

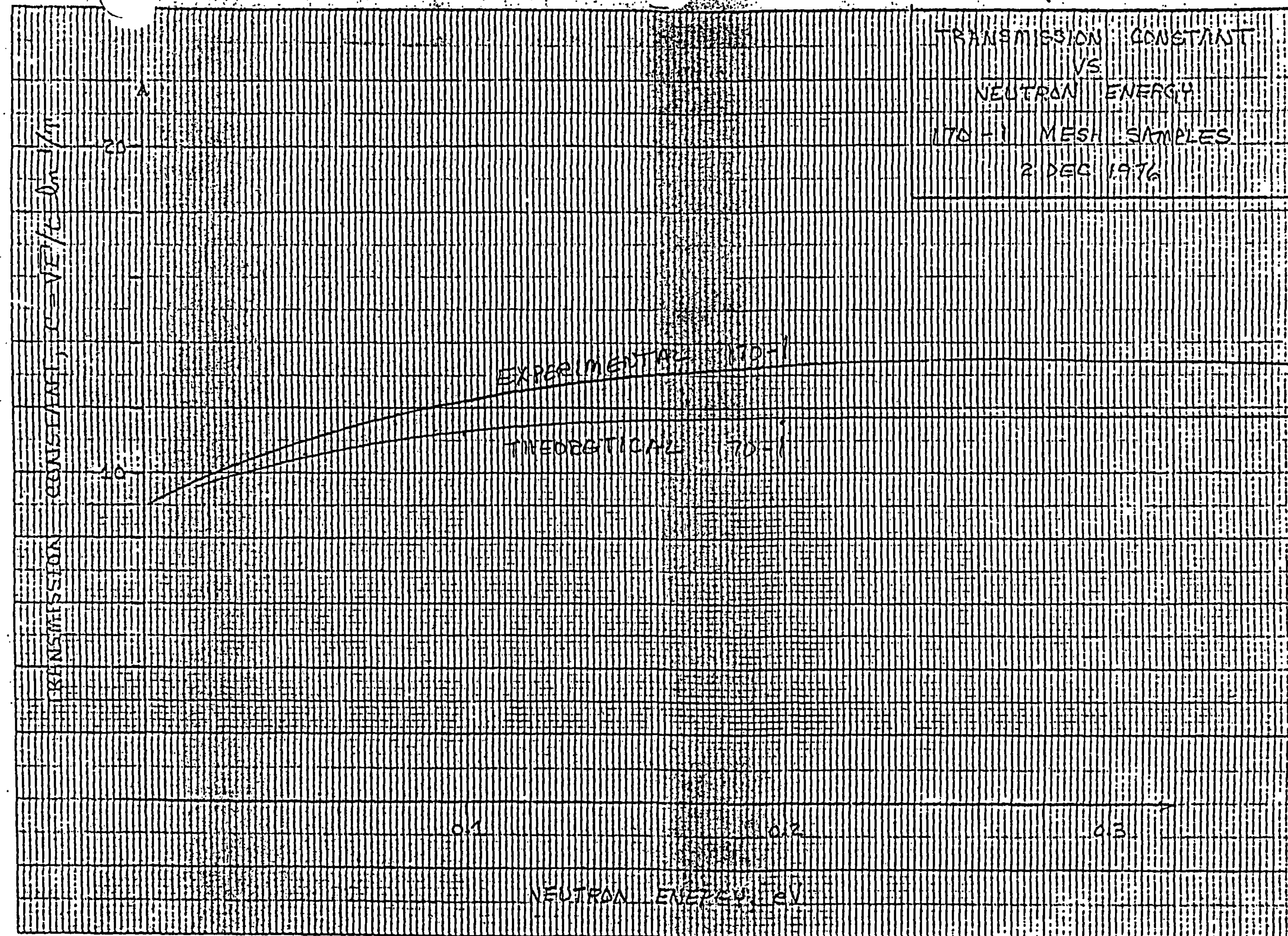
TRANSMISSION CONSTANT
VS
NEUTRON ENERGY
170-11 MESH SAMPLES
2 DEC 1976
EXPERIMENTAL 170-1
THEORETICAL 170-1
20
10
0.1
0.2
0.3
NEUTRON ENERGY, eV

MICHIGAN MEMORIAL PHOENIX PROJECT
THE UNIVERSITY OF MICHIGAN

NEUTRON TRANSMISSION THROUGH BORAL SHIELDING MATERIAL

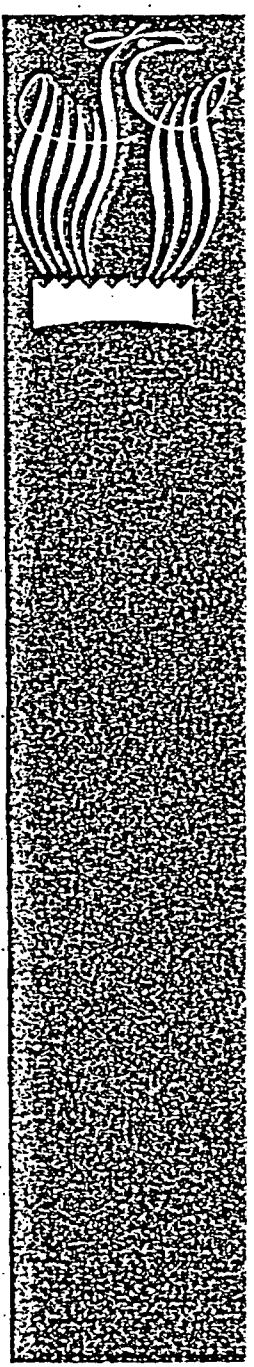

January, 1978

Prepared For

Brooks and Perkins, Incorporated
12633 Inkster Road
Livonia, Michigan 48150

ANN ARBOR MICHIGAN

This report provides neutron transmission information for Brooks and Perkins BORAL shielding material.

Combinations of boron-10 loading (gm/cm^2) and core thickness (in) for nine BORAL case evaluations are listed in TABLE 1. Boron-10 loading ranges from 0.01 gm/cm^2 to 0.03 gm/cm^2. Core thickness varies linearly with boron-10 loading. The BORAL core is a compaction of aluminum and boron carbide (B_4C). Boron carbide core volume fraction is the volume fraction of the core compaction that is boron carbide. Because of the linear relationship between boron-10 loading and core thickness, volume fraction is essentially constant.

Boron carbide particle sizes are expressed in terms of Tyler screen mesh numbers. Screen mesh openings correspond to particle diameters under the assumption that the particles are spherical. The mesh number range for boron carbide in the BORAL core is 60-200. TABLE 2 shows the actual sizes and percentage distributions of core particles.

BORAL neutron transmission versus neutron energy is presented in TABLE 3 for the various boron-10 loading-core thickness cases listed in TABLE 1. Transmission values are based upon a collimated beam theory developed at the University of Michigan which has been verified by transmission measurement experiments.[1]

FIGURE 1 is a linear plot of neutron transmission versus neutron energy over the energy range 0 - 0.55 eV. FIGURE 2 is a similar logarithmic plot over the narrower energy range 0 - 0.1 eV.

Integrated transmission shown on FIGURE 1 represents the integral of (Source Flux (E) X Neutron Transmission (E)) divided by the integral of (Source Flux (E)) over the energy range 0 - 0.55 eV. Source flux is assumed to be the Maxwell-Boltzmann flux distribution.

---

[1] J. W. Bryson, J. C. Lee, and R. R. Burn, "Neutron Transmission Through BORAL Shielding Material: Theoretical Model and Experimental Comparison", Department of Nuclear Engineering, Michigan Memorial-Phoenix Project, The University of Michigan, November, 1977.

TABLE 1

BORAL PARAMETRIC COMBINATIONS FOR CASE EVALUATIONS

Case	Boron-10 Loading (gm/cm^2)	Core Thickness (in)	Boron Carbide Particle Size (Mesh Number)	Boron Carbide Core Volume Fraction
1	.0100	.0274	60 - 200	.4468
2	.0125	.0336	60 - 200	.4557
3	.0150	.0402	60 - 200	.4569
4	.0175	.0463	60 - 200	.4628
5	.0200	.0533	60 - 200	.4594
6	.0225	.0598	60 - 200	.4607
7	.0250	.0662	60 - 200	.4625
8	.0275	.0728	60 - 200	.4625
9	.0300	.0796	60 - 200	.4614

TABLE 2

60 - 200 BORON CARBIDE PARTICLE SIZE DISTRIBUTION FOR CASE EVALUATIONS

Particle Size (Mesh Number)	Mesh Opening Particle Diameter (in)	Particle Radius (cm)	Particle Percentage (%)
70	.0077	.0098	11.5
90	.0063	.0080	39.7
130	.0046	.0058	38.6
170	.0035	.0044	8.6
200	.0029	.0037	1.6
Average		.0070	100.0

TABLE 3

BORAL NEUTRON TRANSMISSION VERSUS NEUTRON ENERGY (eV)

For Parametric Combinations of
Boron-10 Loading (B, gm/cm^2) and Core Thickness (T, in)

Neutron Energy	1. B .0100 T .0274	2. B .0125 T .0336	3. B .0150 T .0402	4. B .0175 T .0463	5. B .0200 T .0533	6. B .0225 T .0598	7. B .0250 T .0662	8. B .0275 T .0728	9. B .0300 T .0796
0.01	.0530	.0249	.0119	.0056	.0027	.0013	.0006	.0003	.0001
0.02	.1077	.0610	.0348	.0197	.0113	.0064	.0037	.0021	.0012
0.03	.1533	.0952	.0594	.0368	.0231	.0144	.0090	.0056	.0035
0.04	.1915	.1260	.0831	.0546	.0362	.0239	.0157	.0104	.0069
0.05	.2240	.1534	.1054	.0721	.0496	.0341	.0234	.0161	.0110
0.06	.2522	.1780	.1260	.0889	.0630	.0446	.0315	.0223	.0158
0.07	.2770	.2002	.1451	.1048	.0761	.0551	.0399	.0289	.0210
0.08	.2990	.2204	.1628	.1200	.0888	.0655	.0484	.0357	.0264
0.09	.3188	.2389	.1793	.1343	.1010	.0757	.0568	.0427	.0320
0.10	.3367	.2558	.1947	.1479	.1127	.0857	.0652	.0496	.0378
0.15	.4065	.3241	.2586	.2061	.1646	.1313	.1048	.0836	.0668
0.20	.4560	.3743	.3074	.2522	.2073	.1703	.1398	.1149	.0944
0.25	.4937	.4134	.3464	.2900	.2432	.2037	.1707	.1430	.1199
0.30	.5238	.4452	.3786	.3218	.2738	.2328	.1980	.1684	.1432
0.35	.5486	.4718	.4059	.3491	.3004	.2584	.2224	.1913	.1646
0.40	.5696	.4945	.4295	.3728	.3239	.2813	.2443	.2122	.1843
0.45	.5876	.5142	.4501	.3938	.3448	.3018	.2642	.2313	.2025
0.50	.6034	.5316	.4684	.4126	.3637	.3204	.2823	.2488	.2193
0.55	.6174	.5470	.4848	.4295	.3807	.3374	.2990	.2650	.2349
Integrated Transmission	.1810	.1240	.0863	.0606	.0431	.0307	.0222	.0161	.0018

FIGURE 1 BORAL NEUTRON TRANSMISSION VERSUS NEUTRON ENERGY

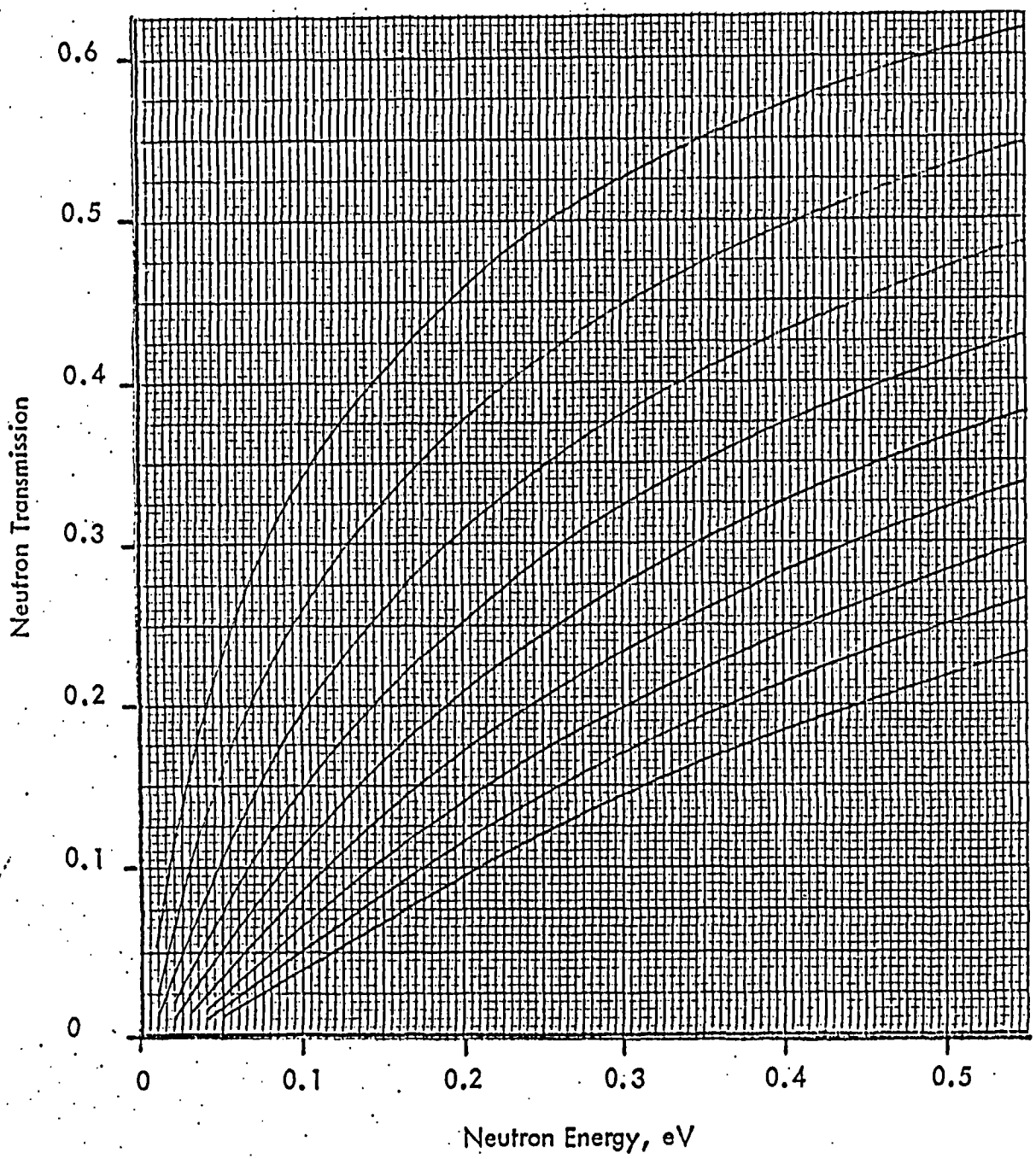

Boron-10 Loading	Integrated Transmission
0.0100 gm/cm^2	0.1810
0.0125	0.1240
0.0150	0.0863
0.0175	0.0606
0.0200	0.0431
0.0225	0.0307
0.0250	0.0222
0.0275	0.0161
0.0300	0.0118

FIGURE 2

BORAL NEUTRON TRANSMISSION VERSUS NEUTRON ENERGY

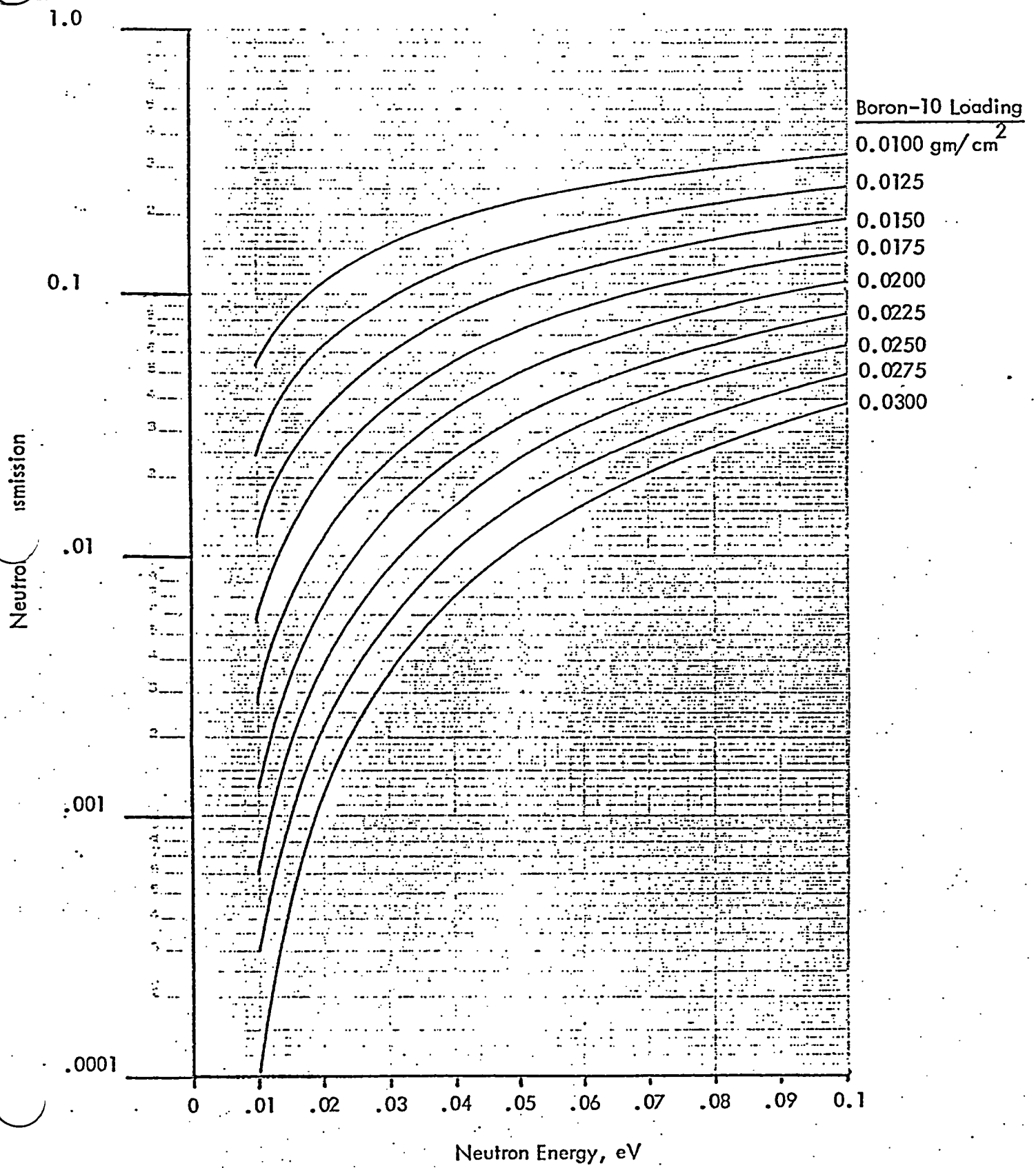

TOPICAL REPORT
REFERENCE DOCUMENTS
BOOK 2 of 2

Credit for 90% of the ^{10}B in BORAL

Submitted by:
AAR Manufacturing
12633 Inkster Road
Livonia, Michigan 48150
Tel: 734-522-2000
Fax: 734-522-2240

AAR Report 1829, Revision 0

October 27, 2004

MICHIGAN MEMORIAL PHOENIX PROJECT

THE UNIVERSITY OF MICHIGAN

NEUTRON TRANSMISSION THROUGH BORAL SHIELDING MATERIAL

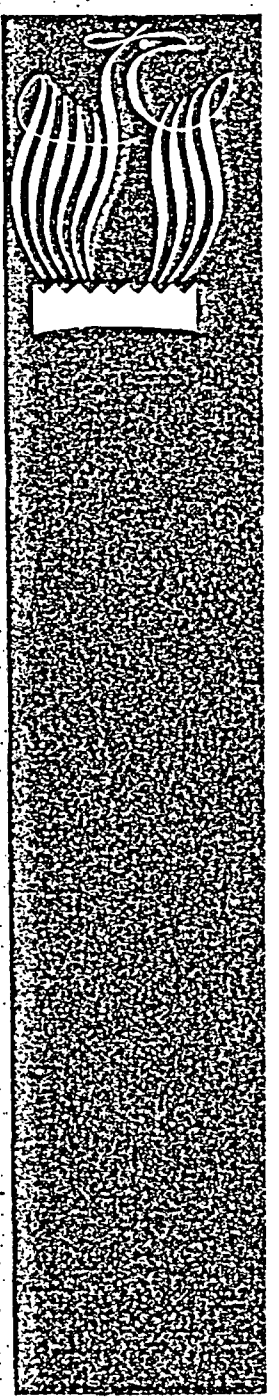

January, 1978

Prepared For

Brooks and Perkins, Incorporated
12633 Inkster Road
Livonia, Michigan 48150

ANN ARBOR MICHIGAN

This report provides neutron transmission information for Brooks and Perkins BORAL shielding material.

Combinations of boron-10 loading (gm/cm^2) and core thickness (in) for nine BORAL case evaluations are listed in TABLE 1. Boron-10 loading ranges from 0.01 gm/cm^2 to 0.03 gm/cm^2. Core thickness varies linearly with boron-10 loading. The BORAL core is a compaction of aluminum and boron carbide (B_4C). Boron carbide core volume fraction is the volume fraction of the core compaction that is boron carbide. Because of the linear relationship between boron-10 loading and core thickness, volume fraction is essentially constant.

Boron carbide particle sizes are expressed in terms of Tyler screen mesh numbers. Screen mesh openings correspond to particle diameters under the assumption that the particles are spherical. The mesh number range for boron carbide in the BORAL core is 60-200. TABLE 2 shows the actual sizes and percentage distributions of core particles.

BORAL neutron transmission versus neutron energy is presented in TABLE 3 for the various boron-10 loading-core thickness cases listed in TABLE 1. Transmission values are based upon a collimated beam theory developed at the University of Michigan which has been verified by transmission measurement experiments.[1]

FIGURE 1 is a linear plot of neutron transmission versus neutron energy over the energy range 0 - 0.55 eV. FIGURE 2 is a similar logarithmic plot over the narrower energy range 0 - 0.1 eV.

Integrated transmission shown on FIGURE 1 represents the integral of (Source Flux (E) X Neutron Transmission (E)) divided by the integral of (Source Flux (E)) over the energy range 0 - 0.55 eV. Source flux is assumed to be the Maxwell-Boltzmann flux distribution.

---

[1] J. W. Bryson, J. C. Lee, and R. R. Burn, "Neutron Transmission Through BORAL Shielding Material: Theoretical Model and Experimental Comparison", Department of Nuclear Engineering, Michigan Memorial-Phoenix Project, The University of Michigan, November, 1977.

TABLE 1

BORAL PARAMETRIC COMBINATIONS FOR CASE EVALUATIONS

Case	Boron-10 Loading (gm/cm^2)	Core Thickness (in)	Boron Carbide Particle Size (Mesh Number)	Boron Carbide Core Volume Fraction
1	.0100	.0274	60 - 200	.4468
2	.0125	.0336	60 - 200	.4557
3	.0150	.0402	60 - 200	.4569
4	.0175	.0463	60 - 200	.4628
5	.0200	.0533	60 - 200	.4594
6	.0225	.0598	60 - 200	.4607
7	.0250	.0662	60 - 200	.4625
8	.0275	.0728	60 - 200	.4625
9	.0300	.0796	60 - 200	.4614

TABLE 2

60 - 200 BORON CARBIDE PARTICLE SIZE DISTRIBUTION FOR CASE EVALUATIONS

Particle Size (Mesh Number)	Mesh Opening Particle Diameter (in)	Particle Radius (cm)	Particle Percentage (%)
70	.0077	.0098	11.5
90	.0063	.0080	39.7
130	.0046	.0058	38.6
170	.0035	.0044	8.6
200	.0029	.0037	1.6
Average		.0070	100.0

TABLE 3

BORAL NEUTRON TRANSMISSION VERSUS NEUTRON ENERGY (eV)

For Parametric Combinations of
Boron-10 Loading (B, gm/cm^2) and Core Thickness (T, in)

Neutron Energy	1. B .0100 T .0274	2. B .0125 T .0336	3. B .0150 T .0402	4. B .0175 T .0463	5. B .0200 T .0533	6. B .0225 T .0598	7. B .0250 T .0662	8. B .0275 T .0728	9. B .0300 T .0796
0.01	.0530	.0249	.0119	.0056	.0027	.0013	.0006	.0003	.0001
0.02	.1077	.0610	.0348	.0197	.0113	.0064	.0037	.0021	.0012
0.03	.1533	.0952	.0594	.0368	.0231	.0144	.0090	.0056	.0035
0.04	.1915	.1260	.0831	.0546	.0362	.0239	.0157	.0104	.0069
0.05	.2240	.1534	.1054	.0721	.0496	.0341	.0234	.0161	.0110
0.06	.2522	.1780	.1260	.0889	.0630	.0446	.0315	.0223	.0158
0.07	.2770	.2002	.1451	.1048	.0761	.0551	.0399	.0289	.0210
0.08	.2990	.2204	.1628	.1200	.0888	.0655	.0484	.0357	.0264
0.09	.3188	.2389	.1793	.1343	.1010	.0757	.0568	.0427	.0320
0.10	.3367	.2558	.1947	.1479	.1127	.0857	.0652	.0496	.0378
0.15	.4065	.3241	.2586	.2061	.1646	.1313	.1048	.0836	.0668
0.20	.4560	.3743	.3074	.2522	.2073	.1703	.1398	.1149	.0944
0.25	.4937	.4134	.3464	.2900	.2432	.2037	.1707	.1430	.1199
0.30	.5238	.4452	.3786	.3218	.2738	.2328	.1980	.1684	.1432
0.35	.5486	.4718	.4059	.3491	.3004	.2584	.2224	.1913	.1646
0.40	.5696	.4945	.4295	.3728	.3239	.2813	.2443	.2122	.1843
0.45	.5876	.5142	.4501	.3938	.3448	.3018	.2642	.2313	.2025
0.50	.6034	.5316	.4684	.4126	.3637	.3204	.2823	.2488	.2193
0.55	.6174	.5470	.4848	.4295	.3807	.3374	.2990	.2650	.2349
Integrated Transmission	.1810	.1240	.0863	.0606	.0431	.0307	.0222	.0161	.0018

FIGURE 1 BORAL NEUTRON TRANSMISSION VERSUS NEUTRON ENERGY

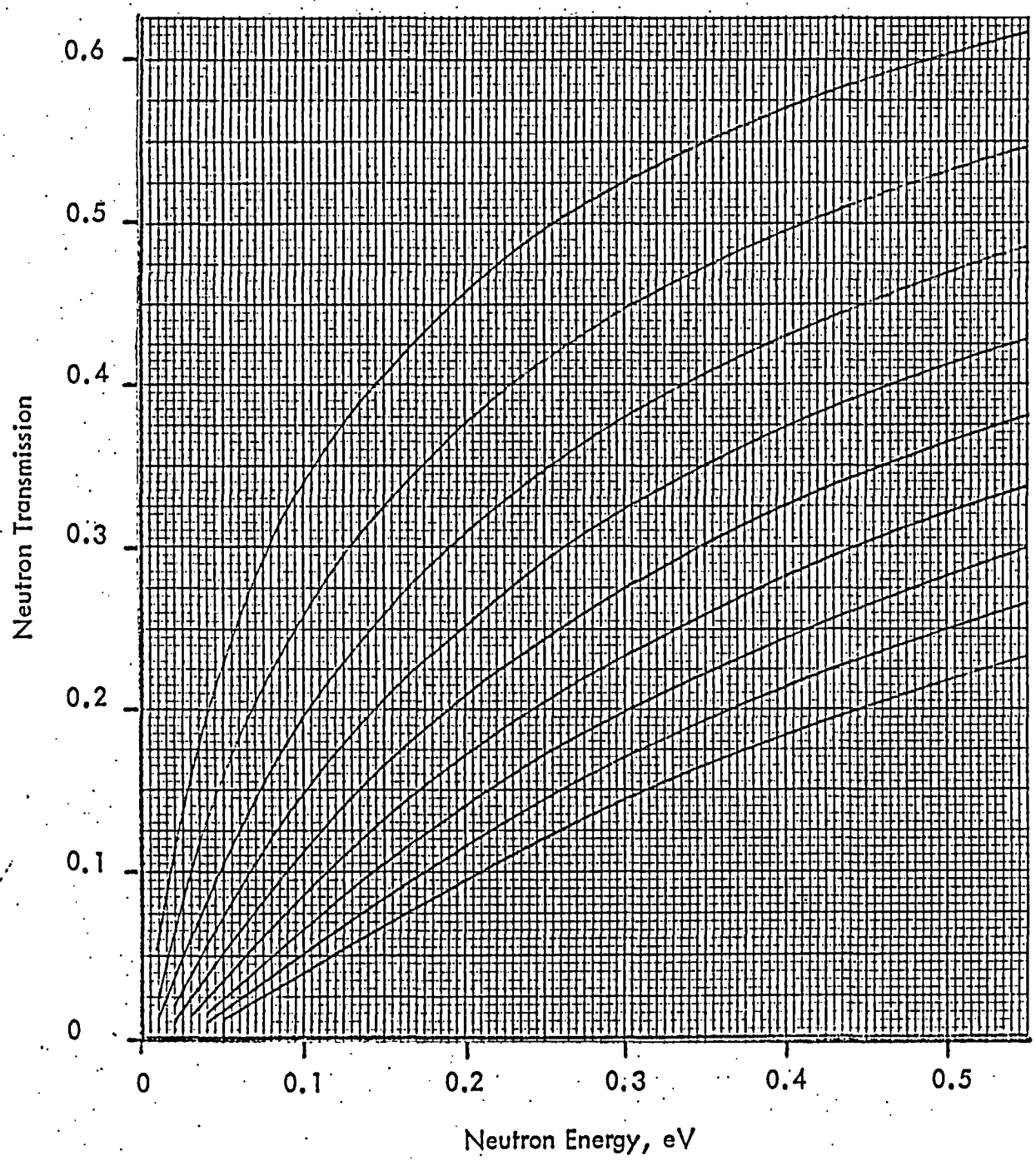

Boron-10 Loading	Integrated Transmission
0.0100 gm/cm^2	0.1810
0.0125	0.1240
0.0150	0.0863
0.0175	0.0606
0.0200	0.0431
0.0225	0.0307
0.0250	0.0222
0.0275	0.0161
0.0300	0.0118

FIGURE 2

BORAL NEUTRON TRANSMISSION VERSUS NEUTRON ENERGY

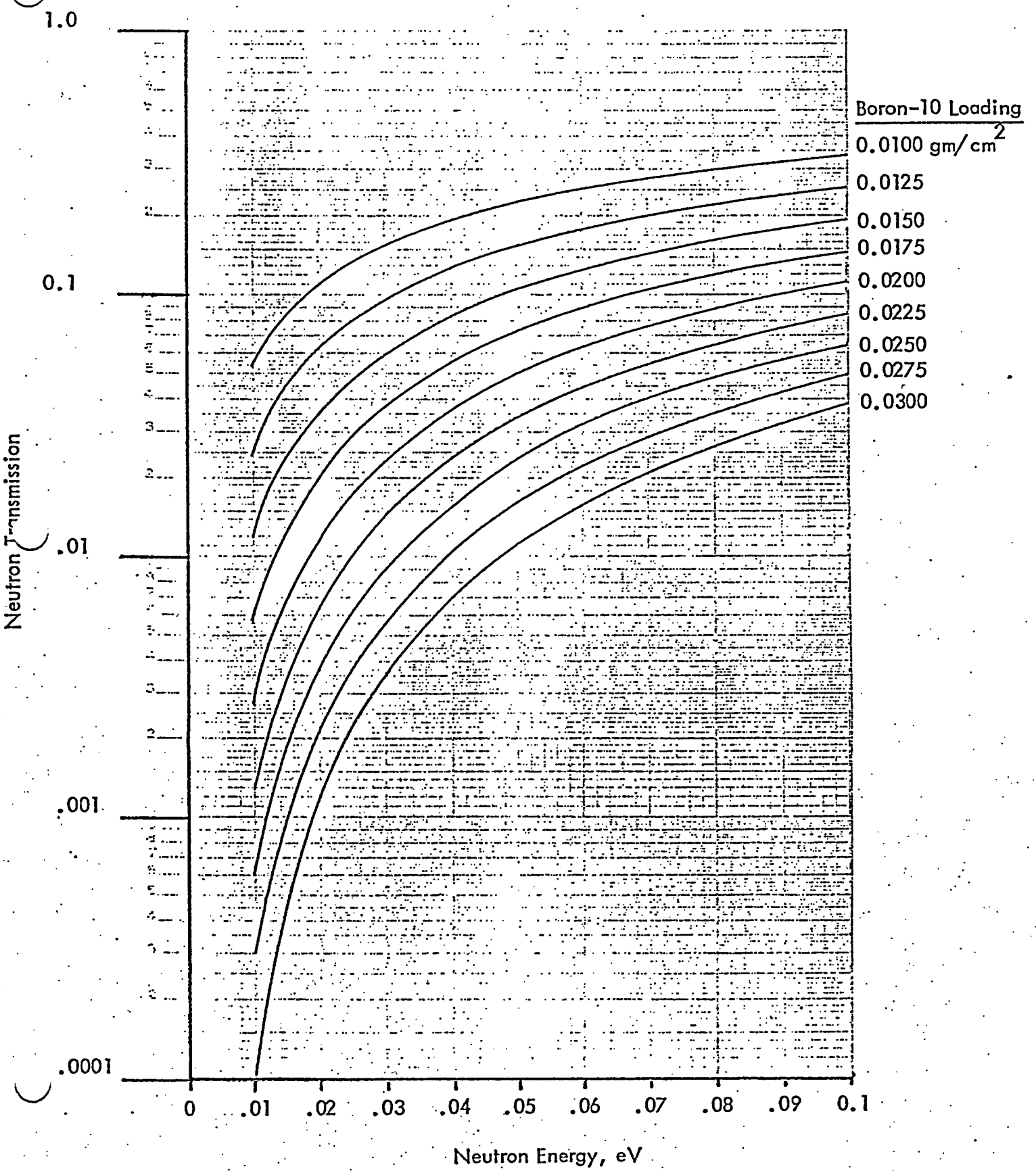

BROOKS & PERKINS
ADVANCED STRUCTURES
An AAR Company

AAR BROOKS & PERKINS CORP.
12633 Inkster Road
Livonia, Michigan 48150

Report 624

Boral
Neutron Absorbing/Shielding Material

Product Performance Report

Prepared By:

L. Mollon
Nuclear Programs Manager
July 20, 1982

BROOKS & PERKINS
ADVANCED STRUCTURES
An AAR Company

TABLE OF CONTENTS

BROOKS & PERKINS
ADVANCED STRUCTURES
An AAR Company

BORAL
NEUTRON ABSORBING/SHIELDING MATERIAL

Product Performance Report

GENERAL

Boral is a thermal neutron poison material composed of boron carbide and the 1100 alloy aluminum. Boron carbide is a compound having a high boron content in a physically stable and chemically inert form. The 1100 alloy aluminum is a light-weight metal with high tensile strength which is protected from corrosion by a highly resistant oxide film. The two materials, boron carbide and aluminum, are chemically compatible and ideally suited together for long-term use in the radiation environment of a nuclear reactor or in spent fuel containment.

Boral is an ideal neutron absorbing/shielding material because of the following reasons:

1. The content and placement of boron carbide provides a very high removal cross section for thermal neutrons.
2. Boron carbide, in the form of fine particles, is homogenously dispersed throughout the central layer of the Boral panels.
3. The boron carbide and aluminum materials in Boral are totally unaffected by long-term exposure to gamma radiation.
4. The neutron absorbing central layer of Boral is protected by permanently attached surfaces of aluminum.

5. Boral is stable, strong, durable, and corrosion resistant.

Boral is manufactured under the control and surveillance of a computer-aided Quality Assurance/Quality Control Program that conforms to the requirements of 10CFR50 Appendix B entitled, "Quality Assurance Criteria for Nuclear Power Plants". For further discussion on Quality Control see Brooks & Perkins Bulletin No. 102.

Boral has been licensed by the USNRC for use in BWR and PWR spent fuel storage racks, shipping and storage containers and for many other shielding uses including control blades. For specific applications see later in this report.

Boral panels can be used in the flat panel form or fabricated into a variety of geometrical shapes by standard metal working methods and techniques. The shielding capability of Boral is assured by wet chemical analysis or neutron attenuation testing and is specified as a minimum of grams of B^{10} per square centimeter of surface area. Boral can be provided at any B^{10} loading up to 0.06 gm/sq cm as required.

BORAL MATERIAL CHARACTERISTICS

Aluminum. Aluminum is a silvery-white, ductile metallic element that is the most abundant in the earth's crust. The 1100 alloy aluminum is used extensively in cooking utensils, heat exchangers, pressure and storage tanks, chemical equipment, reflectors and sheet metal work.

It has high resistance to corrosion in rural, industrial and marine atmospheres. Aluminum has atomic number of 13, atomic weight of 26.98, specific gravity of 2.69 and valence of 3. The physical and mechanical properties of the 1100 alloy aluminum are listed in Table 1.

Table 1 - 1100 Alloy Aluminum

Density	0.098	lb/cu.in.
	2.713	gm/cc
Melting Range	1190-1215	deg.F
	643-657	deg.C
Thermal Conductivity (77 deg.F)	128	BTU/hr/sq ft/deg.F/ft
	0.53	cal/sec/sq cm/deg.C/cm
Coef. of Thermal Expansion (68-212 deg.F)	13.1×10^{-6}	/deg.F
	23.6×10^{-6}	/deg.C
Specific Heat (212 deg.F)	0.22	BTU/lb/deg.F
	0.23	cal/gm/deg.C
Modulus of Elasticity	10×10^{6}	psi
Tensile Strength (75 deg.F)	13,000	psi annealed
	18,000	psi as rolled
Yield Strength (75 deg.F)	5,000	psi annealed
	17,000	psi as rolled
Elongation (75 deg.F)	35-45%	annealed
	9-20%	as rolled
Hardness (Brinell)	23	annealed
	32	as rolled
Annealing Temperature	650	deg.F
	343	deg.C

BROOKS & PERKINS
ADVANCED STRUCTURES
An AAR Company

Chemical Composition - Aluminum (1100 Alloy)

99.00% min. - Aluminum

1.00% max. - Silicon and Iron

.05-.20% max. - Copper

.05% max. - Manganese

.10% max. - Zinc

.15% max. - others each

The excellent corrosion resistance of the 1100 alloy aluminum is provided by the protective oxide film that develops on its surface from exposure to the atmosphere or water. This film prevents the loss of metal from general corrosion or pitting corrosion and the film remains stable between a pH range of 4.5 to 8.5. More detailed corrosion data is provided later in this report and in Brooks & Perkins Bulletin No. 101.

Boron Carbide. The boron carbide contained in Boral is a fine granulated powder that conforms to ASTM C-750-80 nuclear grade Type III. The particles range in size between 60 and 200 mesh and the material conforms to the chemical composition listed in Table 2.

Table 2 - Boron Carbide Chemical Composition, Weight %

Total boron	70.0 min.
B^{10} isotopic content in natural boron	18.0 min.
Boric oxide	3.0 max.
Iron	2.0 max.
Total boron plus total carbon	94.0 min.

The general physical properties of the boron carbide powder are listed in Table 3.

Table 3 - Boron Carbide Physical Properties

Chemical formula	B_4C
Boron content (weight)	78.28%
Carbon content (weight)	21.72%
Crystal structure	rombohedral
Density	2.51 gm/cc-0.0907 lb/cu. in.
Melting point	2450°C-4442°F
Boiling point	3500°C-6332°F
Microscopic capture cross section	600 barn

Materials Compatibility. The materials contained in Boral are compatible with all parts of a spent fuel storage system in either a boiling-water (BWR) or pressurized-water reactor including the fuel assemblies, the cooling system, the cleanup system, the pool liner and the structures of the storage racks. This compatibility is evidenced by more than seventeen years of continuour service in both types of pool water (1) (3). None of the following materials are contained in Boral nor do they come in contact with Boral during its manufacture and therefore Boral can not cause these materials to come in contact with the fuel assemblies:

a. Any material that contains halogens in amounts exceeding 50 ppm, including chlorinated cleaning compounds.
b. Lead
c. Mercury
d. Sulfur
e. Phosphorus
f. Zinc
g. Copper and Copper alloys
h. Cadmium
i. Tin
j. Antimony
k. Bismuth
l. Mischmetal
m. Carbon steel, e.g., wire brushes
n. Magnesium oxide, e.g., insulation
o. Neoprene or other similar gasket materials made of halogen-containing elastomers.
p. Viton
q. Saran
r. Silastic Ls-53
s. Rubber-bonded asbestos
t. TFE (Teflon) containing more than 0.075% total chlorine (glass-filled) and TFE films containing more than 0.05% total chlorine.

u. Nylon containing more than 0.07% total chlorine.
v. Polyethylene film (colored) with pigments over 50 ppm fluorine, measurable amounts of mercury or halogens, or more than 0.05% lead.
w. Grinding wheels that have been used on other than stainless steel or Inconel material.
x. Water containing more than 25 ppm halogens during any cleaning operation.
y. Any material that forms alloys or deposits on the fuel assembly.

BORAL PHYSICAL CHARACTERISTICS

Boral is a clad composite of aluminum and boron carbide. The Boral panel consists of three distinct layers. The outer protective layers are solid 1100 alloy aluminum. The central layer contains a uniform aggregate of fine boron carbide particles tightly held within an aluminum alloy matrix. The boron carbide particle in the central layer averages 85 micons in diameter. The average spacial separation is 1.25 to 1.50 particle diameters. The overall thickness of the three layers will vary depending on the B^{10} content in accordance with Figure 1.

The physical characteriestics of a Boral panel will vary of course, according to clad thickness, overall thickness and B^{10} content. A typical Boral panel for spent fuel storage can be described as having 0.020 grams of B^{10} per sq. cm with an overall thickness of .075 $\pm$ .004 inches including a nominal clad of .0095 inches on each side. The physical characteristics for that typical panel is as shown in Table 4.

BROOKS & PERKINS
ADVANCED STRUCTURES
An AAR Company

Figure 1

Boral Thickness Versus B10 Content

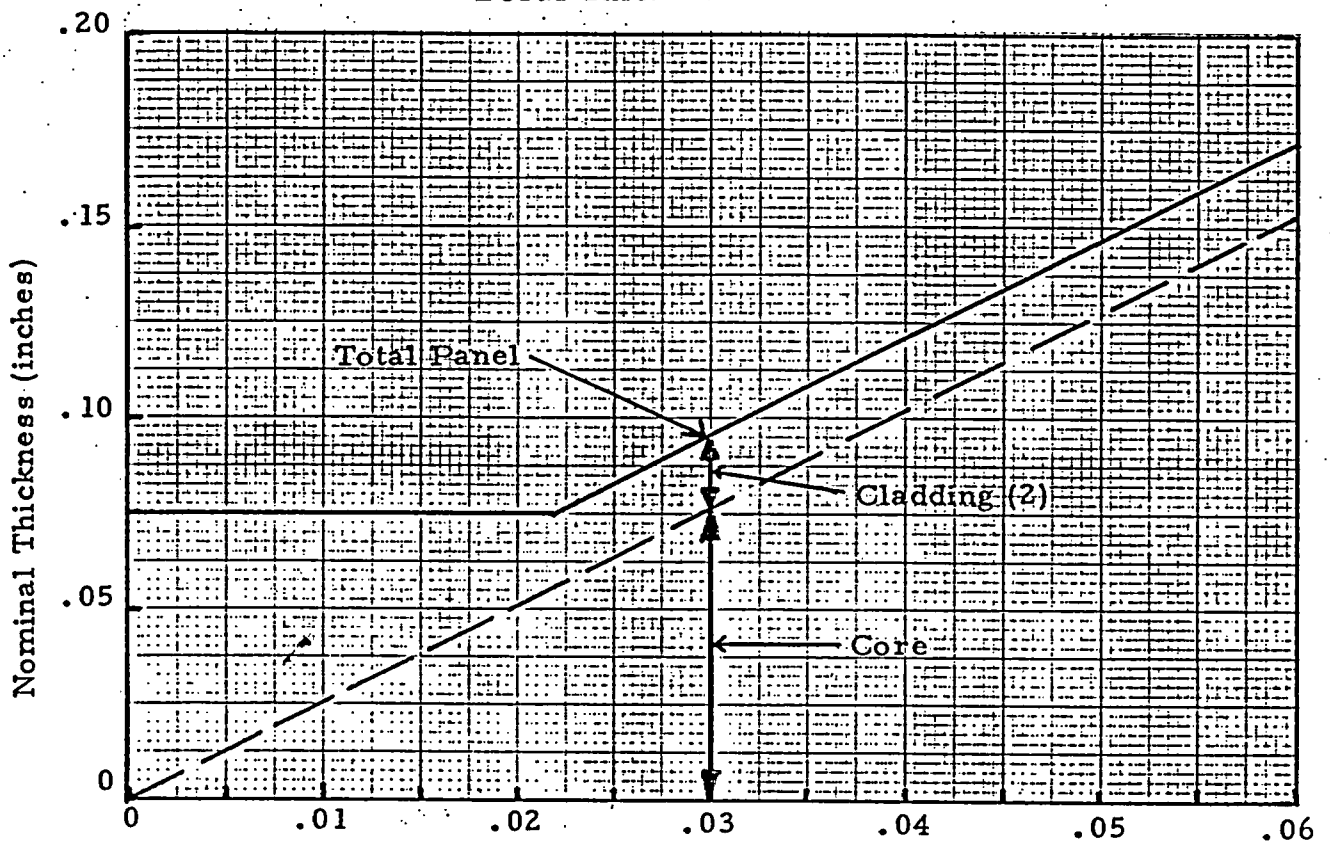

B10 Content	Equiv. Boron	Total Thickness Including Cladding			
		Inches	± Tol.	mm	± Tol.
.005	.028	.075	.004	1.91	.10
.010	.056	.075	.004	1.91	.10
.015	.083	.075	.004	1.91	.10
.020	.111	.075	.004	1.91	.10
.025	.139	.083	.004	2.11	.10
.030	.167	.096	.005	2.41	.13
.035	.194	.108	.006	2.74	.15
.040	.222	.121	.006	3.07	.15
.045	.250	.133	.006	3.38	.15
.050	.278	.146	.007	3.71	.18
.055	.306	.158	.007	4.01	.18
.060	.333	.172	.009	4.37	.23

This tabulation is for Boral with thin cladding for use in high density spent fuel racks. Boral with thicker cladding is also available for other applications.

Table 4 - Boral Panel

B^{10} content	0.020 gm/sq cm
Boron content	.111 gm/sq cm
Thickness-overall	.075 $\pm$ .004 inches .190 $\pm$ .010 cm
Thickness-clad (nominal)	.0095 inches .024 cm
Neutron attenuation (at 0.06 eV)	.935
Total weight	.42 gm/sq cm .86 lb/sq ft.

Dispersion Uniformity. The aluminum and boron carbide ingredients in the central core of the Boral panel are combined in powder form. The methods used to weigh and blend the powders as well as the design and construction of the ingots necessary to produce acceptable Boral panels are patented and proprietary processes of Brooks & Perkins. The manufacturing methods used include a sintering process and hot rolling. The final outcome of the entire manufacturing cycle is Boral panels having boron carbide uniformly dispersed throughout the central core. The amount of boron carbide per unit area is directly related to the panel thickness. The minimum B^{10} content per unit area and the uniformity of dispersion within a panel is verified by wet chemical analysis or neutron attenuation testing. For details of the verification methods see Brooks & Perkins Quality Assurance Procedures BP-11002-QAP and BP-11004-QAP.

The acceptance standards in these procedures are controlled by statistical data to assure the minimum requirements are achieved with 95/95 confidence level. The maximum variation in the manufacturing processes (statistical tolerance interval) over a significantly large sample size has been determined and is utilized in the establishment of acceptance criteria.

CORROSION RESISTANCE

The useful service life of Boral will exceed 40 years when in contact with the storage pool water of either a boiling-water or pressurized-water reactor. This fact is evident through laboratory testing and is further supported by the longest continuous, in-pool, service by Boral over any other thermal neutron shielding material. This excellent corrosion resistance is provided by the protective nature of the aluminum cladding that is an integral facing on the Boral panels. The corrosion of aluminum is negligible in fuel storage pools of either type reactor when the water quality and temperatures are maintained within the normal operating limits as listed in Table 5. The boron content in the Boral will not be reduced below the specified limit during the forty or more years of exposure under those operating conditions.

In order to understand the total corrosion resistance of aluminum within the normal operating conditions of the storage pools a discussion of that resistance must consider all forms of corrosion. A detailed discussion follows for general, galvanic, pitting, crevice, intergranular, and stress forms of corrosion.

Table 5 - Chemistry of Pool Waters

Reactor type	PWR	BWR
Cooling medium	* D-M water	D-M water
Boron content, ppm	0 to 2000	0
pH range	4.5 to 6.0	6.0 to 7.5
Temp range, °F °C	80 to 140 26 to 60	80 to 125 26 to 52
Conductivity @ 25°C micro mho/cm	1 to 30	1
Chloride ions, ppm, max.	0.15	0.20
Fluoride ions, ppm, max.	0.10	----
Total solids, ppm, max.	1.00	0.50
Heavy metals, ppm, max.	----	0.10
Halogens, ppm, max.	0.15	----

* demineralized water

General Corrosion. General corrosion is a uniform attack of the metal over the entire surfaces exposed to the corrosive media. General corrosion is measured by weight loss or decrease in thickness and is generally expressed in mils per year (mpy). The severity of general corrosion of aluminum depends upon the chemical nature and temperature of the electrolyte and can range from superficial etching and staining to dissolution of the metal.

Figure 2 shows a potential - pH diagram for aluminum in high purity water at 25°C (77°F). The potential for aluminum coupled with stainless steel and the limits of pH for BWR and PWR pools are shown on the diagram to be well within the passivation domain. The passivated surface of aluminum (hydrated oxide of aluminum) affords protection against corrosion in the domain shown because the coating is insoluble, non-porous and adherent to the surface of the aluminum. The protective surface formed on the aluminum (gibbsite and bayerite) is known to be stable up to 135°C (275°F) [5] and in a pH range of 4.5 to 8.5 [6].

Figure 3 is also a potential-pH diagrams for the aluminum-water system but at 60°C (140°F) which also shows the potential for the aluminum/stainless steel couple and the BWR and PWR limits for pH at this upper limit of temperature.

The ability of aluminum to resist corrosion from the boron ions is evident from the wide useage of aluminum in the handling of borax and in the manufacture of boric acid. (7) Aluminum racks with Boral plates in contact with the 800 ppm max. boron water showed only small amount of pitting but maintained good structural integrity after seventeen years in the pool [1].

BROOKS & PERKINS
ADVANCED STRUCTURES
An AAR Company

Figure 2

Potential Versus pH Diagram

For Aluminum-Water System
At 25°C (77°F) (10)

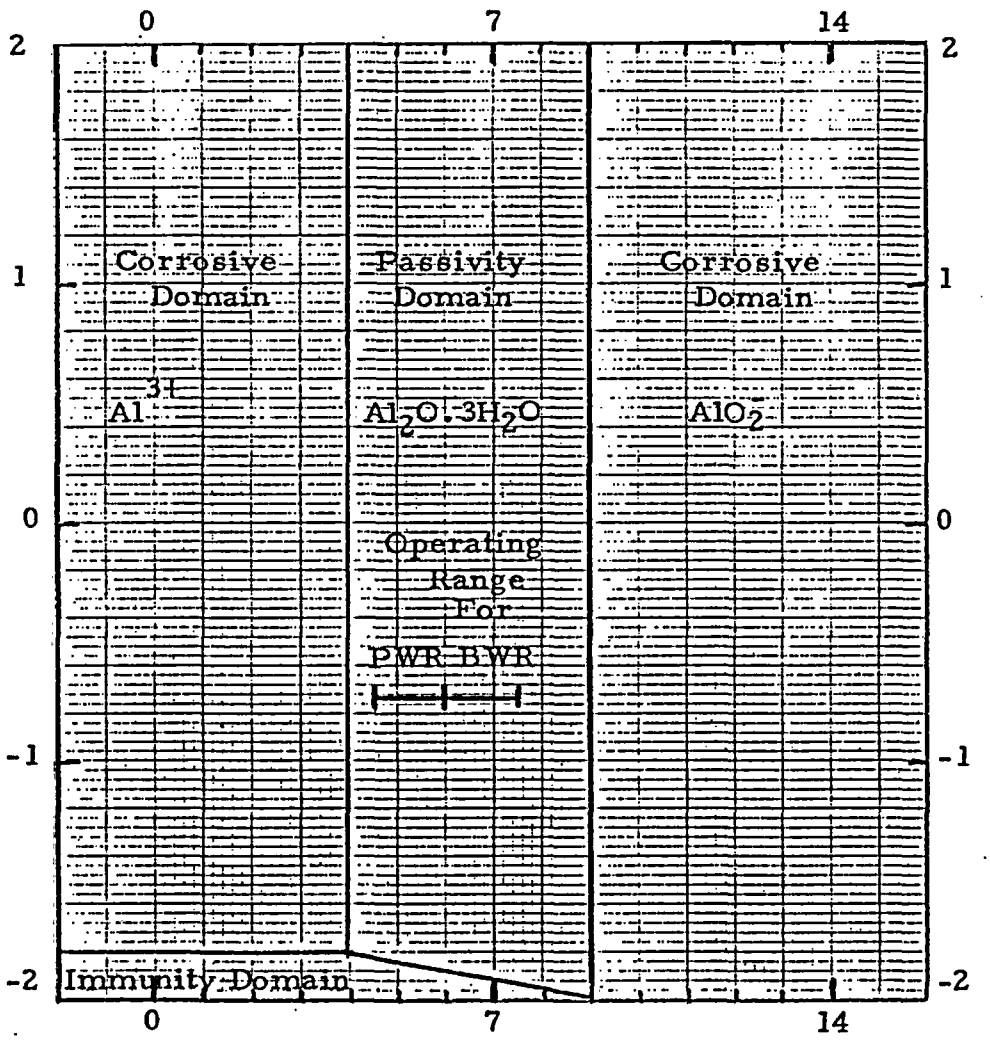

BROOKS & PERKINS
ADVANCED STRUCTURES
An AAR Company

Figure 3

Potential Versus pH Diagram

For Aluminum-Water System

At 60°C (140°F) (5)

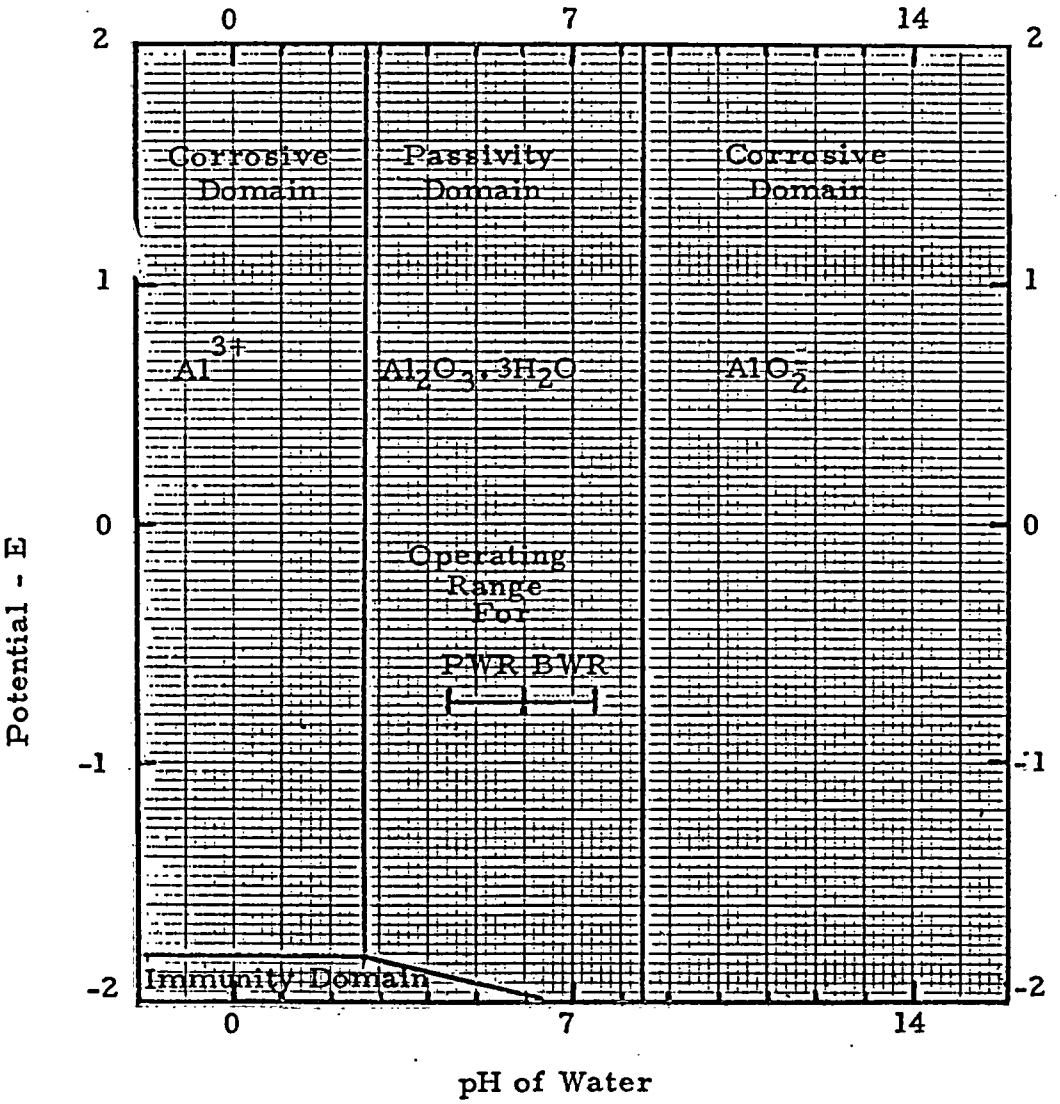

Galvanic Corrosion. Galvanic corrosion is associated with the current of a galvanic cell consisting of two dissimilar conductors in an electrolyte. The two dissimilar conductors of most interest in this discussion are aluminum and stainless steel while in an electrolyte similiar to the pool water from either a BWR or PWR. There is less galvanic current flow between the aluminum-stainless steel couple than the potential difference would indicate because of the greater than normal resistance at the metal-liquid interface on stainless steel which is known as polarization. (6) It is because of this polarization characteristic that stainless steel is compatible with aluminum in all but severe marine, or high chloride, environmental conditions. Test data for aluminum coupled with 304 stainless steel in 5.0 pH water at 100°C (212°F) with flow rates ranging from 0.5 fpm to 81 fps show weight losses of 0.1 to 0.2 mpy and randomly spread pits that were not of major consequence. (8) This performance indicates a projected service life much greater than forty years.

Pitting Corrosion. Pitting corrosion is the forming of small sharp cavities in a metal surface. The first step in the development of corrosion pits is a local destruction of the protective oxide film. Pitting will not occur on commercially pure aluminum when the water is kept sufficiently pure, even when the aluminum is in electrical contact with stainless steel. (9)

Pitting of aluminum has been observed when in contact with stainless steel where the electrolyte can stagnate and the conductivity of the electroylyte increases.

This pitting has not been significant in spent fuel environments and it is not likely that pitting of the aluminum would have any influence on the neutron shielding performance of the Boral. (4)

Crevice Corrosion. Crevice corrosion is the corrosion of a metal that is caused by the concentration of dissolved salts, metal ions, oxygen or other gases in crevices or pockets remote from the principal fluid stream, with a resultant build up of differential galvanic cells that ultimately cause pitting. Testing has confirmed that after 2000 hours, under a controlled environment, the Boral and 304 stainless steel combination exhibited little or no corrosion of the aluminum cladding of the Boral. In a separate 2000 hour test at 90° to 180°C the maximum pit depth of corrosion of the Boral surface was reported at less than five mils giving a projected life much greater than forty years. (8)

Intergranular Corrosion. Intergranular corrosion is corrosion occurring preferentially at grain boundaries or closely adjacent regions without appreciable attack of the grains or crystals of the metal themselves. Intergranular corrosion does not occur with the commercially pure aluminum (alloy 1100) and other common work hardening alloys.

Stress Corrosion. Stress corrosion cracking is failure of the metal by cracking under the combined action of corrosion and high stresses approaching the yield stress of the metal. The 1100 alloy used in Boral is not susceptable to stress corrosion and Boral is seldom if ever subjected to high stresses when used as a neutron shield in a spent fuel rack.

$$Al^{+++} + H_2O \longrightarrow Al(oH)^{++} + H^+$$

$$2\,Al + 6\,H_2O \longrightarrow Al_2O_3 \cdot 3H_2O + 6H^+ + 6 \text{ electrons}$$

$$2\,H^+ + 2 \text{ electrons} \longrightarrow H_2\uparrow \qquad (5)$$

The water-aluminum reactions are self-limiting because the surface of the aluminum becomes passive by the formation of a protective and impervious coating making further reaction impossible until that coating is removed by mechanical or chemical means.

The volumes and types of gases collected from the Boral in demineralized and borated water strongly indicate the gases resulted from one or both of the two described mechanisms and did not result from cross linking or oxidative scission of any of the Boral materials.

In summary Boral does not out-gas or change physically or chemically as a result of exposure to gamma radiation. Water in contact with aluminum will release hydrogen chemically until the aluminum surface is passivated and water will disassociate through hydrolysis from gamma radiation. It is therefore necessary to provide a means for venting the hydrogen and oxygen gases if water is allowed to come in contact with Boral in spent fuel storage applications.

NEUTRON SHIELDING PERFORMANCE

The thermal neutron shielding performance of Boral is obtained from the B^{10} isotopes contained within the boron carbide particles in its core. This performance is directly related to the amount of boron carbide provided and the spacial relationship between the particles of boron carbide. Figure 4 shows the actual performance of Boral as compared to an ideal (unobtainable) layer of B^{10} isotopes. The shielding performance is measured as a neutron attenuation factor and is plotted against the surface density of B^{10} isotopes in grams per square centimeter. For further discussion on the shielding properties of Boral see Brooks & Perkins Bulletin No. 100. The neutron shielding performance of Boral was unaffected after exposure to 1.03×10^{11} rads gamma and 5.3×10^{19} thermal neutrons per sq cm.

Boron and Halogen Leachability. The boron leachability and the halogen leachability was evaluated for Boral during irradiation testing conducted at the University of Michigan. The test solutions were analized for boron and halogen contents before and after radiation exposure when sufficient solution was remaining after the test. The volume of solution was reduced to zero in some cases by the radiation. The analysis of the test solutions showed no increase in boron or halogen that cannot be accounted for by the decrease in test solution volume or pickup of the soluble boron on the external edges of the Boral. The boron carbide is allowed to contain, by the ASTM Specification C750-80, up to a maximum of three percent (3.0%) soluble boron in the form of boric oxide (B_2O_3).

Figure 4

Neutron Attenuation Versus B^{10} Content

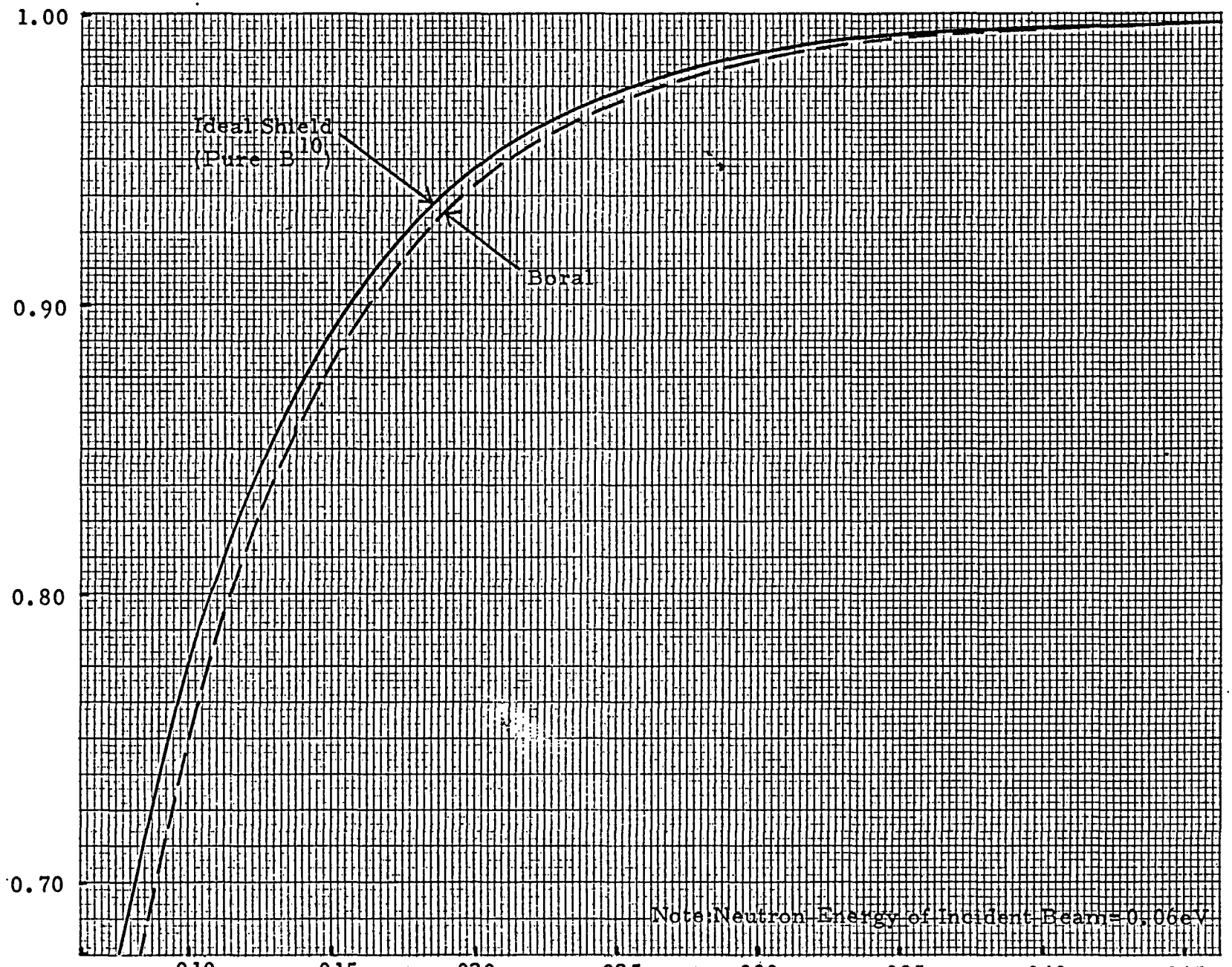

BROOKS & PERKINS
ADVANCED STRUCTURES
An AAR Company

Report 624

The amount of boron carbide that can come in contact with water is limited to that which is confined to the outer edges of the Boral panel. This wettable amount of boron carbide is of course influenced by the geometrical size and shape of the panel but is less than one percent (1.0%) of the total boron carbide contained therein. In any regard, the total boron content of the panel will remain above the specified minimum content in the event the total soluble boron content were somehow lost through dissolution.

Residual Activity. The residual radioactivity of the Boral was measured following the irradiation testing conducted at the University of Michigan. The activation was limited to trace amounts of impurities contained in the boron carbide and aluminum materials from which Boral is produced. The specific results are available upon request.

BROOKS & PERKINS
ADVANCED STRUCTURES
An AAR Company

Installations Using Boral

I. Spent Fuel Storage Racks

A. Pressurized Water Reactors

	Reactor	Utility	Water Contact	Service Date
1.	Yankee Rowe	Yankee Atomic Electric Co.	Yes	1964
2.	Maine Yankee	Maine Yankee Atomic Power Co.	No	1977
3.	Cook 1&2	Indiana & Michigan Electric Co.	No	1979
4.	Sequoyah 1&2	Tenn Valley Authority	No	1979
5.	Zion 1&2	Commonwealth Edison Co.	Yes	1980
6.	Salem 1&2	Public Service Electric & Gas Co.	No	1980
7.	Bellefonte 1&2	Tenn Valley Authority	No	1981
8.	Yellowcreek 1&2	Tenn Valley Authority	No	Indef.

B. Boiling Water Reactors

	Reactor	Utility	Water Contact	Service Date
1.	LaCrosse	Dairyland Power Coop.	Yes	1976
2.	Pilgrim 1	Boston Edison Co.	No	1978
3.	Monticello	Northern States Power Co.	Yes	1978
4.	Vermont Yankee	Vermont Yankee Nuclear Power	No	1978
5.	Peach Bottom 2&3	Philadelphia Electric Co.	No	1978
6.	Fitzpatrick	Power Authority of State NY	No	1978
7.	Cooper	Nebraska Public Power District	Yes	1979
8.	Duane Arnold 1	Iowa Electric Light & Power Co.	No	1979
9.	Susquehanna 1&2	Pennsylvania Power & Light Co.	No	1979
10.	Perry 1&2	Cleveland Electric Illuminating Co.	No	1979
11.	Limerick	Philadelphia Electric Co.	No	1980
12.	Browns Ferry 1,2, &3	Tenn Valley Authority	Yes	1980
13.	Dresden 1,2, &3	Commonwealth Edison Co.	Yes	1981
14.	Hatch 1&2	Georgia Power Co.	Yes	1981
15.	Brunswick 1&2	Carolina Power & Light Co.	Yes	1981
16.	Clinton	Illinois Power Co.	Yes	1981
17.	Hartsville 1&2	Tenn Valley Authority	Yes	Indef.
18.	Phipps Bend 1&2	Tenn Valley Authority	Yes	Indef.

BROOKS & PERKINS
ADVANCED STRUCTURES
An AAR Company

References

1. Yankee Rowe, Rowe, Mass., Boral Spent Fuel Storage Rack in 800 ppm boron max. water, installed Aug. 1964, removed in 1981, small amount of pitting, good structural integrity (2).

2. F.M. Kustas, S.O. Bates, B.E. Opitz, A.B. Johnson Jr., J.M. Perez Jr., R.K. Farnsworth, "Investigation of the Condition of Spent Fuel Pool Components", Battelle-Pacific Northwest Laboratory, PNL-3513/UC-85 Sept. 1981 pg. 5.

3. Brookhaven Medical Research Reactor, Boral in fuel storage area since Jan. 1959, in demineralized water, no loss of boron carbide after more than 19 years (4).

4. C. Czajkowski, J.R. Weeks, and S.R. Protter, "Corrosion of Structural and Poison Material in Spent Fuel Storage Pools", Paper No. 163 presented at Corrosion 81, Apr. 1981, Toronto, Canada.

5. D.D. Mac Donald and P. Butler, "The Thermo-dynamics of the Aluminum -Water System at Elevated Temperatures" Corrosion Science 1973 Vol. 13 pgs. 264, 265 & 266.

6. K.R. Van Horn, "Aluminum", American Society for Metals, 1967 Vol. 1 pgs. 211, 220 & 221.

7. T. Lyman, "Metals Handbook" 8th Edition, 1961 Vol. 1 pg. 930.

8. J. L. English and J. C. Griess, "Dynamic Corrosion Studies for High Flux Isotope Reactor" ORNL-TM-1030 Sept. 1966 pgs. 1, 2, 3, 4, 23, 26, 27 & 31.

9. K. Videm, "Pitting Corrosion of Aluminum in Contact with Stainless Steel" Institute for Atomenergi, Kjeller Research Establishment, Lillestrom, Norway.

10. E. Deltombe, C. Vanleugenhaghe and M. Pourbaix, "Aluminum", pg. 172

BROOKS & PERKINS
ADVANCED STRUCTURES
An AAR Company

Effect of Gamma Radiation on the Neutron Attenuation Properties of Boral™

Report #637

BROOKS & PERKINS
ADVANCED STRUCTURES
An AAR Company

Effect of Gamma Radiation on the Neutron Attenuation Properties of Boral™

Report #637

Prepared by:

Thomas B. Brown
AAR Brooks & Perkins
Advanced Structures Div.
Livonia, MI

February, 1985

Submitted to:

GCA/PAR Systems
St. Paul, MN

Bechtel Power Corp.
San Francisco, CA

BROOKS & PERKINS
ADVANCED STRUCTURES
An AAR Company

Contents

Tables

Sketches

Photograph

BROOKS & PERKINS
ADVANCED STRUCTURES
An AAR Company

Abstract:

The results of neutron attenuation measurements of irradiated Boral[tm] specimens are presented. Irradiation and neutron attenuation measurements were performed by the Phoenix Memorial Laboratory of the University of Michigan. No significant change in the neutron attenuation properties of Boral[tm] was detected up to radiation exposure levels to 7 x 10" rads. Test background and methodology are discussed.

BROOKS & PERKINS
ADVANCED STRUCTURES
An AAR Company

INTRODUCTION:

Boral[tm] is the trade mark of a neutron absorbing material manufactured by AAR Brooks & Perkins, Inc. (B&P)and is used around the world in a wide variety of shielding and criticality control applications. Boral[tm] is a composite material consisting of an aluminum and boron carbide core clad with pure aluminum face sheets. Boral[tm] properties are fully described in B&P's Product Performance Report 624.(1)

The application being studied in this report is the use of Boral[tm] as the neutron absorber in high density storage racks for spent nuclear fuel. These racks are submerged in the fuel pool at a nuclear reactor site and hold spent fuel discharged from the reactor during refueling. This spent fuel will be stored in the fuel racks for as long as 40 years.

The function of Boral[tm] in this application is criticality control to insure the closely spaced fuel assemblies cannot reach a critical condition even during accident situations (e.g. fuel assembly drops, earthquakes, improper fuel positioning etc.). Since this is a safety related function the U.S. NRC is particularly interested in the effectiveness of the poison both when installed, and over the rack service life.

Applicants for fuel storage licenses must furnish a considerable amount of data on the neutron absorbing poison they intend to use in the fuel racks. In addition to documenting the initial effectiveness of the poison the NRC requires that "methods for verification of long-term material stability and mechanical integrity of special poison materials utilized for neutron absorption should include actual tests".(2)

Boral,[tm] or any neutron poison used in spent fuel racks is exposed to an extremely harsh environment. The Boral[tm] is subjected to high gamma radiation fields, high temperature of discharged fuel assemblies and pool water chemistry. The impact of these factors acting over long periods must be assessed in order to judge the capability of the poison to perform its function and live in this environment.

PURPOSE OF REPORT:

This paper will report some results from a test-in-progress on Boral[tm]. This is an accelerated type test intended to subject the Boral[tm] to a total integrated life dose of 1×10^{12} rads gamma radiation. The testing is being done in the Ford Nuclear Reactor at the University of Michigan in Ann Arbor. The test conditions also subject the Boral[tm] specimens to pool water chemistry and temperature thereby simulating the fuel pool environment.

These test results are offered as documentation that Boral[tm] can withstand total integrated gamma doses of 7 x 10" rads with no change in the neutron attenuation properties nor loss of physical integrity or durability.

Boral[tm] has been selected as the neutron absorber to be used in the high density spent fuel storage racks for Hope Creek 1 belonging to Public Service Electric & Gas Co. (NJ). Bechtel Power Corp. is the architect-engineer and has developed the fuel rack specifications and defined the operating environment. The specified environment was dimineralized water at 135° F maximum with a radiation dose of 5.12 x 10" rads gamma integrated over 40 years. (3)

The actual integrated lifetime radiation dose to which the fuel racks will be subjected is unknown. However, a "worst case" scenario can be established if it is assumed that freshly discharged fuel is always loaded into the same storage cells at each refueling outage over the life of the plant. Qualification of the rack materials, including Boral[tm], to this "worst case" radiation level will allow for maximum flexibility in fuel handling.

This "worst case" level of radiation exposure would be approached if the freshly discharged fuel were always placed in the same area of the storage racks-such as the full core discharge area. After the outage, when time is less critical and man power more available, the fuel can be transferred to another rack section for long term storage. This is, in fact, the way that many utilities handle their discharged fuel.

The cells would experience lower radiation doses if discharged fuel were placed in the long term storage position directly upon discharge. This system reduces fuel management flexibility somewhat and requires the plant operator to institute a system for managing the radiation exposure of the rack.

BACKGROUND:

The University of Michigan Phoenix Memorial Laboratory initiated a study of the radiation aging of various commercial poison materials in 1978.(4) One of the objectives of this study was to subject several commercial poisons to radiation in U of M's Ford Reactor to investigate the phenomenon of radiation induced out-gassing. The gases evolved would be measured for amount and analyzed for composition.

The reason for this study is that there had been several occurances of individual storage cells in fuel storage racks swelling due to gas build-up in the cavity holding the poison. As this had happened at several reactor sites with different poisons the U.S. NRC was concerned that all poisons may suffer from a generic defect.(5)

In addition to measuring and analyzing the evolved gas, the U of M study measured the pre-and post-irradiation mechanical properties of the poisons tested. The suspicion existed that radiation induced out-gassing was a symptom of radiation damage occuring in the poison matrix material. This data would be taken to determine the extent of any damage and to assess the ability of irradiated poisons to withstand the NRC postulated accidents.

Interim test results describing the quantity and constituents of the evolved gasses were published in 1979.(6) This reports that of the poisons tested only Boral^{tm} produced no off-gases due to irradiation. This data was taken at a total gamma dose of 1×10^{10} rads. The report further states that testing would continue to reach a total integrated dose of 1×10^{12} rads. The tests have currently reached a level in excess of 7×10^{11} rads which is believed to be greater than a "worst case" scenario for the Hope Creek fuel racks.

METHODOLOGY:

The Ford Nuclear Reactor is a 2 megawatt Babcock & Wilcox pool type reactor used for educational and research purposes.(7) This reactor was used for accelerated irradiation tests on various commercial poisons including Boral as described in references (4) and (6). A follow-on irradiation test was performed to extend the data to higher radiation levels than achieved in earlier tests. The purpose of the test is "to determine physical properties and changes to physical properties of shielding materials as a result of irradiation under conditions similar to those encountered in PWR and BWR spent fuel storage pools."(8)

Thirteen groups of samples, with three specimens per group, were irradiated to various radiation levels as shown in Table 1. The following tests and measurements were taken prior to irradiation and it was planned to make similar measurements following irradiation.

weight
specific gravity
hardness
mechanical strength
neutron attenuation

The neutron attenuation and physical/mechanical properties were measured before irradiation. The post irradiation neutron attenuation measurements were made and are presented in the results section. The researcher elected not to perform post-irradiation mechanical tests on the Boral specimens because of concern over possible mechanical test lab contamination and the inability to acquire comparable data.(9)

The samples to be irradiated were loaded in sample holders as shown in the attached sketch and placed in reactor test locations where they would be subjected to approximately 7×10^7 rad/hour.

Table 1 gives the sample identification and test conditions.(10)

BROOKS & PERKINS
ADVANCED STRUCTURES
An AAR Company

TABLE 1
NEUTRON SHIELDING MATERIAL TEST SAMPLE SERIES

Sample Set Identification	Gamma Dose (rad)	Neutron Dose		Estimated Irradiation Time (hr)
		Thermal (n/cm2)	Fast 1 MeV (n/cm2)	
Pre Irradiation	0	0	0	0
Control	286	0	0	14,290
S1E9	1.0×10^{9}	5.66×10^{17}	5.66×10^{15}	15
S5E9	5.0×10^{9}	2.83×10^{18}	2.83×10^{16}	75
S1E10	1.0×10^{10}	5.66×10^{18}	5.66×10^{16}	143
S5E10	5.0×10^{10}	2.83×10^{19}	2.83×10^{17}	715
S1E11	1.0×10^{11}	5.66×10^{19}	5.66×10^{17}	1,429
S2E11	2.0×10^{11}	1.13×10^{20}	1.13×10^{18}	2,858
S3E11	3.0×10^{11}	1.70×10^{20}	1.70×10^{18}	4,287
S4E11	4.0×10^{11}	2.26×10^{20}	2.26×10^{18}	5,716
S5E11	5.0×10^{11}	2.83×10^{20}	2.83×10^{18}	7,145
S6E11	6.0×10^{11}	3.40×10^{20}	3.40×10^{18}	8,574
S7E11	7.0×10^{11}	3.96×10^{20}	3.96×10^{18}	10,003
S8E11	8.0×10^{11}	4.53×10^{20}	4.53×10^{18}	11,432
S9E11	9.0×10^{11}	5.09×10^{20}	5.09×10^{18}	12,861
S1E12	1.0×10^{12}	5.66×10^{20}	5.66×10^{18}	14,290

Sample Environment: Demineralized Water
Estimated Gamma Dose Rate: 7.0×10^{7} rad/hr.
Estimated Neutron Dose Rate:
Thermal 1.1×10^{13} n/cm^2/sec
Fast 1MeV 1.1×10^{11}n/cm^2/sec
Number of Samples In Set: 3

BROOKS & PERKINS
ADVANCED STRUCTURES
An AAR Company

RESULTS:

Neutron transmission measurements were taken using a standard procedure developed by Phoenix Lab personnel.[11] The results are tabulated in Table 2.

TABLE 2[12]

Neutron Attenuation Properties of Boral^{tm} Specimens *

neutron energy = 0.06 eV

Sample Set Identification	Gamma Dose (rads)	Pre-irradiation attenuation	Post-irradiation attenuation
S1E11			
sample 1	9.72×10^{10}	.990	.991
sample 2	9.72×10^{10}	.991	.992
sample 3	9.72×10^{10}	.990	.992
S2E11			
sample 1	2.04×10^{11}	.991	.993
sample 2	2.04×10^{11}	.992	.993
sample 3	2.04×10^{11}	.993	.993
S3E11			
sample 1	3.00×10^{11}	.992	.994
sample 2	3.00×10^{11}	.992	.994
sample 3	3.00×10^{11}	.992	.993
S4E11			
sample 1	4.00×10^{11}	.991	.992
sample 2	4.00×10^{11}	.990	.991
sample 3	4.00×10^{11}	.992	.994
S5E11			
sample 1	5.02×10^{11}	.992	.989
sample 2	5.02×10^{11}	.992	.990
sample 3	5.02×10^{11}	.992	.992
S6E11			
sample 1	6.05×10^{11}	.991	.993
sample 2	6.05×10^{11}	.990	.993
sample 3	6.05×10^{11}	.992	.992
S7E11			
sample 1	6.99×10^{11}	.992	.993
sample 2	6.99×10^{11}	.991	.992
sample 3	6.99×10^{11}	.992	.993

*attenuation = 1-transmission = $1 - \frac{\text{transmitted neutron beam}}{\text{incident neutron beam}}$

Visual examination of the specimens revealed no observable degradation of the Boral[tm] specimens irradiated. There was no apparent shrinkage, material loss, cracking, breaking or other deformation.

The specimens did exhibit the characteristic darkening or tarnishing due to water contact with the aluminum cladding as a passivating film forms.(13) This darkening is illustrated in the attached photograph of test specimens. The amount of discoloration appears to stabilize sometime after 30 days of water contact time.

A few specimens developed small blisters on the cladding. A sketch is attached showing typical blisters. This phenomenon occured only on the outside surface of the outermost specimens loaded in the specimen holder. Neither the inside surface nor any of the other specimens in the specimen holder developed blisters.(14) The researcher hypothesized that this could be a neutron flux induced phenomenon where the outside specimen absorbed most of the neutron flux shielding the inside specimens. The hypothesized mechanism is neutron capture by the B^{10} molecules form lithium and helium which is trapped under the aluminum cladding. Neutron heating may have loosened the bond between cladding and core allowing local blistering of the cladding.

The specimens had good physical integrity and could be struck together sharply with no damage to the Boral[tm].

CONCLUSIONS:

Neutron attenuation measurements of irradiated Boral[tm] specimens showed no degradation in shielding properties up to radiation levels of 7×10^{11} rads. This exceeds the maximum 40 year life gamma dose expected for Hope Creek spent fuel racks. Therefore gamma radiation does not appear to be a creditable threat to a Boral[tm] service life of 40 years.

Visual examination and rough handling showed no degradation or loss of physical integrity. Although a superficial surface tarnish formed on the specimens, the subjective appraisal is the properties of the irradiated Boral[tm] are essentially unchanged by gamma radiation exposure. The specimens are available for further testing, including mechanical tests, should the NRC wish to fund this work.

The test results do not provide any data or reveal any trends which would allow an end-of-qualified life prediction. The combination of radiation, pool water temperature and water chemistry do not appear to degrade Boral.[tm]

NEUTRON POISON SPECIMEN HOLDER

Hollow square aluminum extrusion
with bottom closed

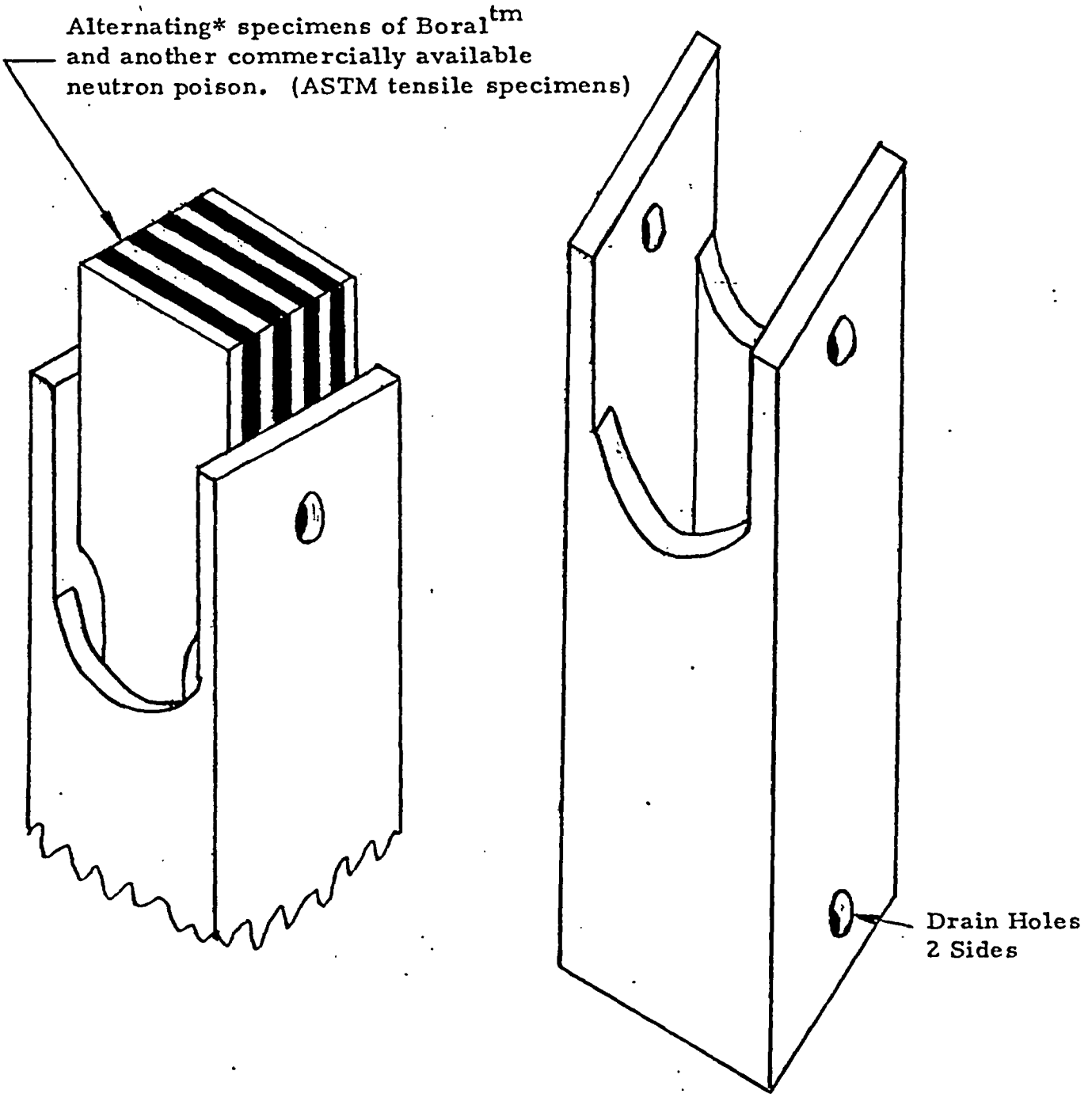

SPECIMENS IN HOLDER

EMPTY HOLDER

*Boral™ always used for first and last specimens to support adjacent flexible poison specimens

Post-Irradiation
Boral Specimen
Full Scale

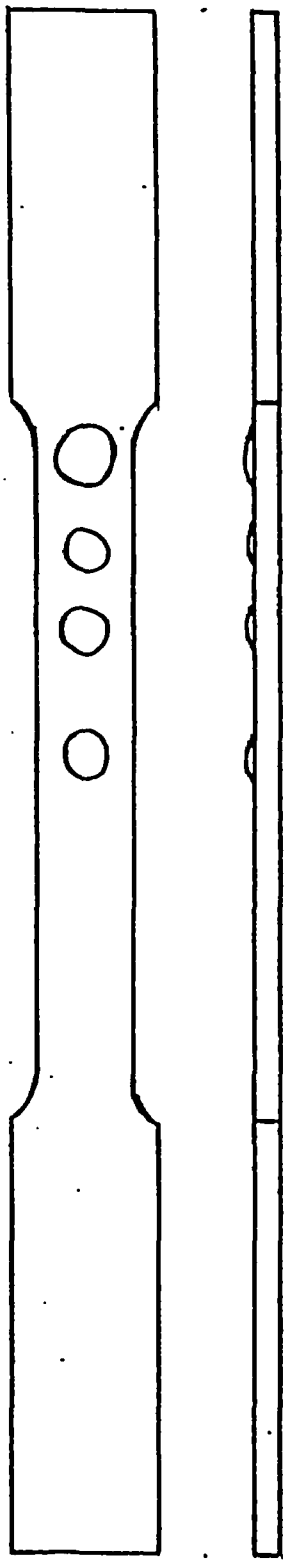

Typical
Blister
Pattern
on outside
surface

Arrangement of Poison
Specimens during Irradiation
(White Specimens-Boral)

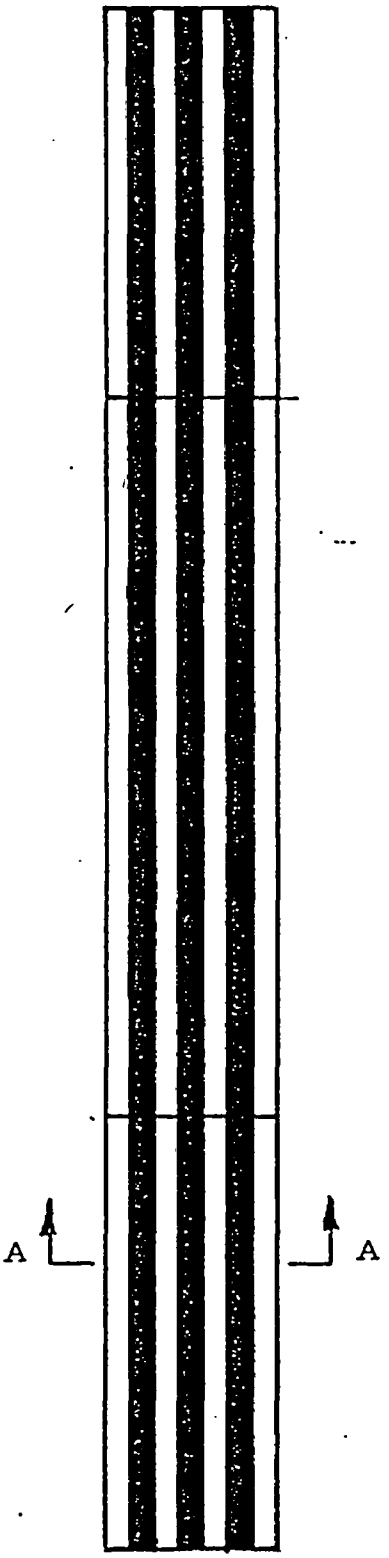

Pre-Irradiation

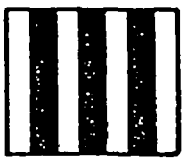

Sec A-A

Post-Irradiation

Sec. A-A

Blister Pattern On Outermost Surface Of
Boral Specimens

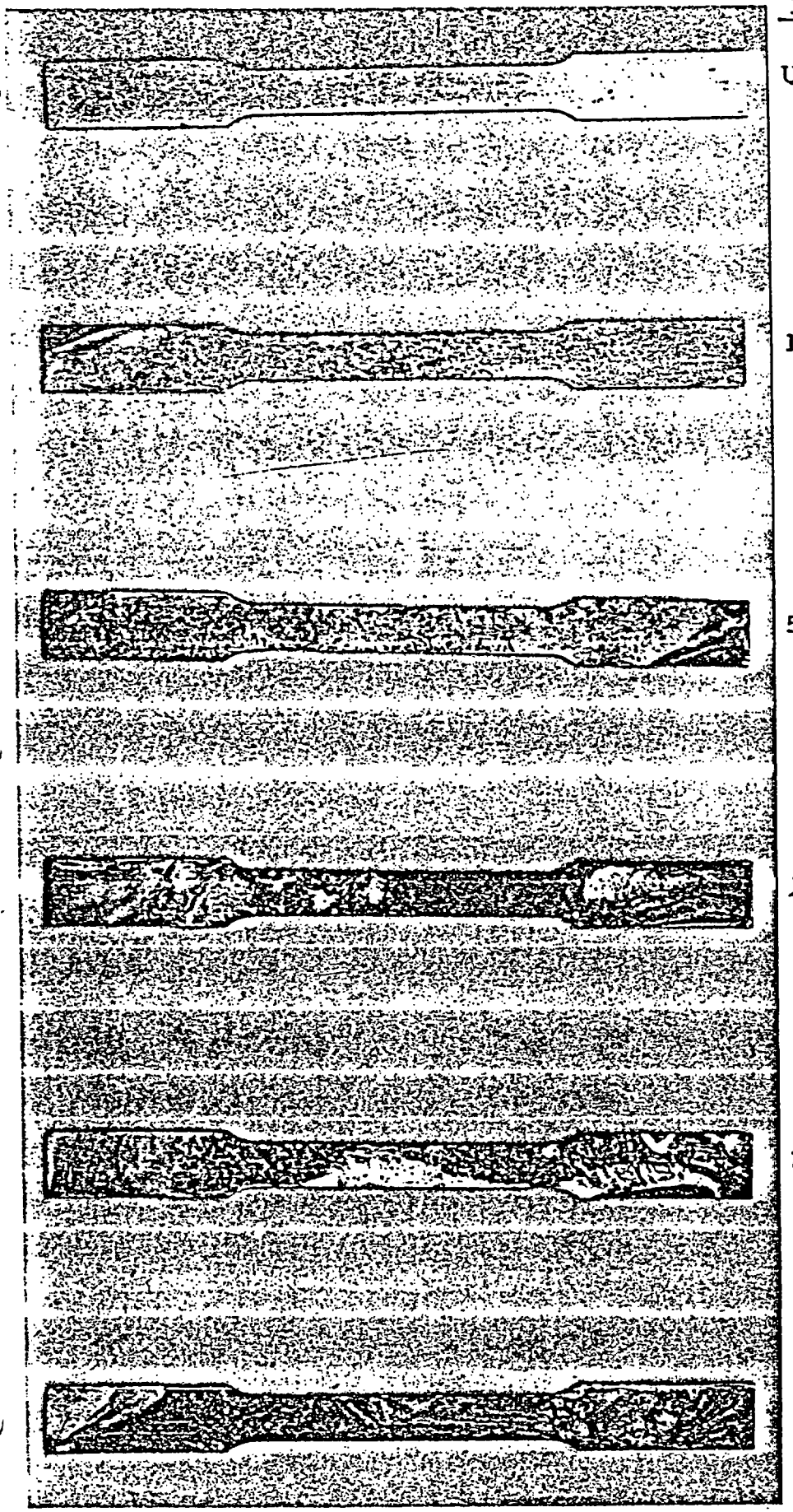

Irradiation Level	Water Contact Time
Un-irradiated	None
1×10^{10} rads	6 Days
5×10^{10} rads	30 Days
1×10^{11} rads	60 Days
2×10^{11} rads	120 Days
3×10^{11} rads	180 Days

IRRADIATED BORAL SPECIMENS

REFERENCES

(1) AAR Brooks & Perkins, Boral, The Neutron Absorber Product Performance Report #624 Livonia MI.

(2) U.S. Nuclear Regulatory Commission, Office of Technology Position for Review and Acceptance of Spent Fuel Storage and Handling Applications Washington DC Apr. 4, 1978.

(3) Bechtel Power Corp., Design Specification for High Density Spent Fuel Storage Racks 10855-M-178(Q) Rev 1 San Francisco CA.

(4) Brand Industrial Services, Inc., Report 748-10-1 Irradiation Study of Boraflex Neutron Shielding Materials July 25, 1979 Rev. Aug. 12, 1981 Park Ridge, IL.

(5) U.S. Nuclear Regulatory Commission, Generic Issue-Spent Fuel Storage Rack Swelling Due to Gas Generation Washington DC Jan 15, 1978.

(6) R. R. Burn & G. Blessing Radiation Effects on Nuetron Shielding Materials Transactions of the American Nuclear Society TANSAO32 (Suppl. 1) 1-67 Aug. 1979.

(7) University of Michigan, Phoenix Memorial Laboratory, Radiation, Analytical, Test and Training Services Ann Arbor MI July 1980.

(8) University of Michigan, Phoenix Memorial Laboratory, Procedure for Test Program-Irradiation Studies of Neutron Shielding Materials Ann Arbor MI Nov. 1980.

(9) T. B. Brown personal conversation with R.R. Burn Ford Nuclear Reactor Manager.

(10) U of M, Procedure for Test Program-Irradiation Studies of Neutron Shielding Materials Table 1.

(11) University of Michigan, Phoenix Memorial Laboratory, Neutron Transmission Measurement Procedure Ann Arbor Jan 1978.

(12) R. R. Burn, Transmittal of neutron attenuation measurements of irradiated Boral^{tm} specimens Nov. 21, 1983.

(13) AAR Brooks & Perkins, Boral, The Neutron Absorber page 5.

(14) T. B. Brown-personal examination of Boral^{tm} specimens at Phoenix Memorial Laboratory.

b+p Brooks & Perkins, Incorporated

Report No. 551

Prepared by:

Brooks & Perkins, Inc.
12633 Inkster Road
Livonia, MI 48150

February, 1977

Corrosion Resistance of BORAL™ to One Year of Exposure to BWR Storage Pool Water

b+p Brooks & Perkins, Incorporated

CORROSION RESISTANCE OF BORAL™ TO ONE YEAR OF EXPOSURE TO BWR STORAGE POOL WATER

PURPOSE: The purpose of this test was to determine the physical changes to unprotected samples of BORAL after one year of exposure to an aqueous solution representing a BWR storage pool water.

METHOD: Three bare and unclad samples of BORAL were placed in a covered beaker containing demineralized water. The samples were the standard 35% B_4C type BORAL panels that measured .177 x 2 x 2 inches. The samples and the solution were periodically examined and the progression of the changes were recorded. The samples were carefully left undisturbed during the test period without any change or alteration being made to the water solution.

TEST DATA:

Sample	Size (cm)	Surface Area Two Sides (cm^2)	Initial Weight (gms)	Final Weight (gms)	Total Weight Loss (gms)	Unit Wt. Loss Per Year ($mgms/cm^2/yr$)	Penetration Per Year (mils/yr)
A	.45x4.92x4.92	48.4	29.8564	29.7612	.0952	1.97	.29
B	.45x5.08x5.08	51.6	31.2759	31.2042	.0717	1.39	.20
C	.45x5.08x5.24	53.2	32.3222	32.1962	.1261	2.37	.34
					Average	1.91	.276

RESULTS: The pH of the solution increased in number from the original 5.6 to 7.7 in the first two and one-half months and remained at that approximate level for the remainder of the year.

The BORAL samples experienced weight losses through general corrosion with no evidence of pitting, galvanic or intergranular types of corrosion. The average rate of weight loss after one year of exposure was 1.91 milligrams per square centimeter per year or .28 mils per year.

CONCLUSION: The period of time necessary for the total loss of the outer cladding of the BORAL by general corrosion at the corrosion rate after one year would be a minimum of 144 years.

TECHNICAL ANALYSIS FORM

BY_____ DATE_____ CK._____ DATE_____ REV._____ DATE_____	b+p Brooks & Perkins, Incorporated ADVANCED STRUCTURES DIVISION	SHEET_____ OF_____ SUBJECT_____

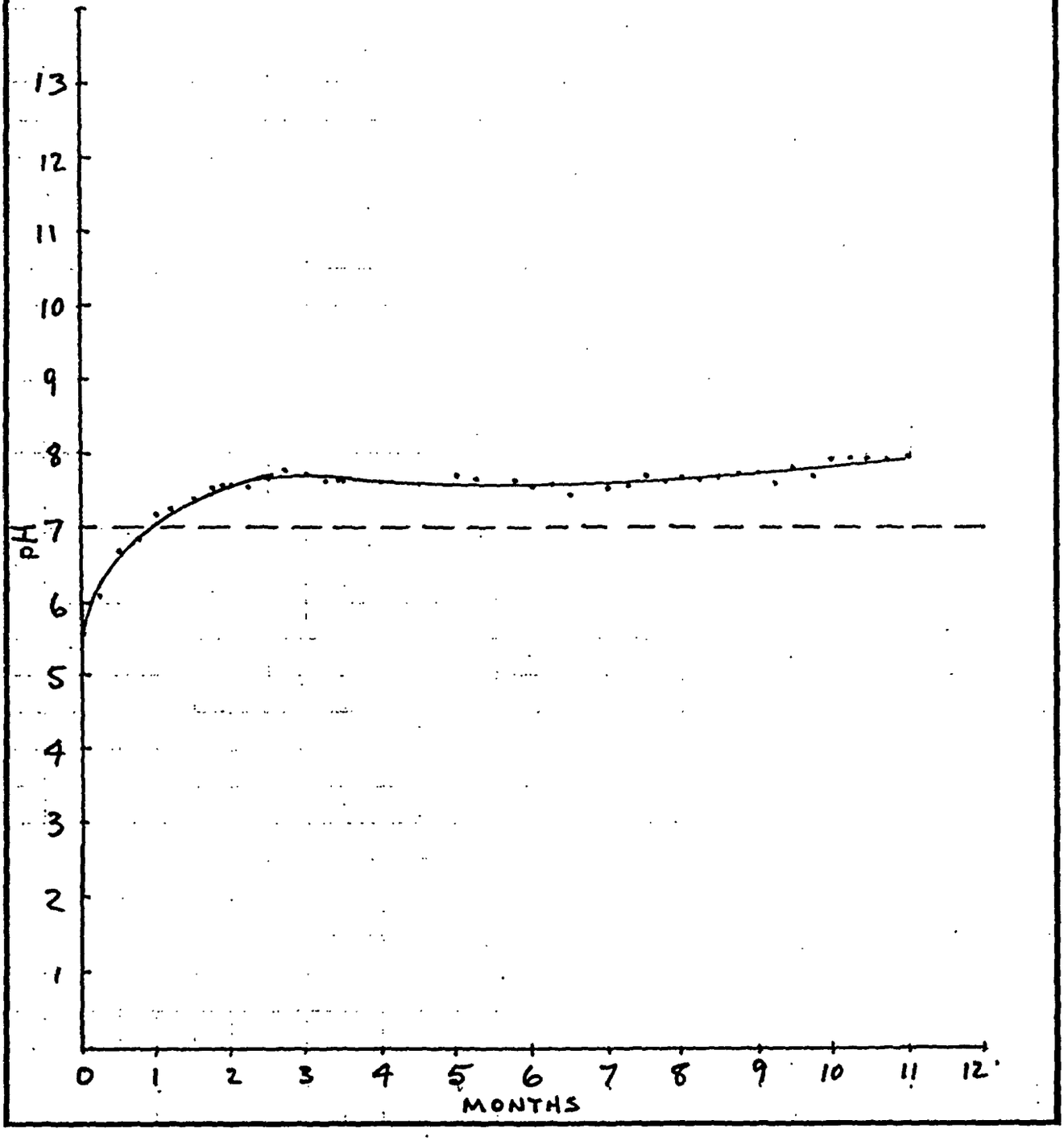

Ucral 2X2"
(A) FILED ALL EDGES. (B) AS SHEARED. } BAKE LAB OVEN (1) 600°F/1HR. WEIGH. (2) SOAK IN DE-MINERALIZED WATER 168 HRS. (3) REWEIGH

(DE-MIN WATER 5.66 pH.)

Date		WT AFTER 168 HR WATER SOAK	WT AFTER 600°F/1HR	pH	CHANGE IN WT	
3-23-76 H_2O 5.66 pH	(A)	—	29.8562	5.66 pH.		
	(B)	—	31.2759			
3-31-76	(A)	30.0933		6.09 pH.	+ [illegible]	SLIGHT CORROSION
	(B)	31.4948			+ [illegible]	
	(C)		32.3222			
4-7-76	(A)	30.1121		6.68 pH	+ [illegible]	EDGE CORROSION
	(B)	31.5248			+ [illegible]	
4-11-76	(A)	30.1045		6.88 pH	[illegible]	EDGE CORROSION
	(B)	31.4891			[illegible]	
4-21-76	(A)	30.1119		7.21 pH / 72°F	[illegible]	EDGE CORROSION
	(B)	31.5337			[illegible]	
4-28-76	(A)	30.1139		7.31 pH / 68°F		EDGE CORROSION
	(B)	31.5414				
	(C)	32.6033				
5-5-76	(A)	30.1129		7.13 pH / 72°F		EDGE CORROSION
	(B)	31.5334				
5-12-76	A	30.1117		7.62 pH / 69°F		EDGE CORROSION
	B	31.5397				
5-19-76	A	30.1067		7.68 pH / 74°F		EDGE CORROSION
	B	31.5291				
5-26-76	A	30.1073		7.62 / 73°F		EDGE CORR.
	B	31.5358				
	C	32.5967				
6-2-76	A	30.1061		7.59 / 72°F		EDGE CORROSION
	B	31.5453				

		WT	pH & Temp.
6-9-76	A	30.0994	7.72pH/76°F
	B	31.5335	
6-23-76	A	20.1036	7.87/71°F
	B	31.5490	
	C	32.6215	
6-30-76	A	30,1015	7.74pH/70°F
	B	31.5491	
7-7-76	A	30,0951	7.61pH/72°F
	B	31,5377	
7-14-76	A	30,0878	7.67pH/74°F
	B	31,5387	
7-21-76	A	30.0892	7.68pH/78°F
	B	31.5359	
	C	32,6009	
VACATION			
8-11-76	A	30,0733	7.62pH/72°F
	B	31.5265	
	C	32.5704	
7-25-76	A	30,0665	7,78pH/74°F
	B	31.5263	
7-1-76	A	30,0706	7.72pH/72°F
	B	31.5301	
9-14-76	A	30.0623	7.72pH/73°F
	B	31.5252	
	C	32.6017	
9-25-76	A	30.0411	7.55pH/72°F
	B	31.4767	

TO PAGE 146

DATE		WEIGHT	pH & TEMP
10-7-76	A	30.0414	7.62/75°F
	B	31.5236	
10-13-76	A	30.0433	7.48/76°F
	B	31.4892	
	C	32.5401	
10-22-76	A	30.0485	7.51/73°F
	B	31.5061	
10-27-76	A	30.0507	7.58pH/74°F
	B	31.5124	
11-3-76	A	30.0278	7.71pH/71°F
	B	31.4965	
11-10-76	A	30.0404	7.61/74°F
	B	31.4875	
	C	32.5167	
11-17-76	A	30.0242	7.65pH/74°F
	B	31.4858	
11-24-76	A	30.0450	7.68pH/73°F
	B	31.4996	
12-1-76	A	30.0443	7.68/74°F
	B	31.4972	
12-8-76	A	30.0345	7.68pH/75°F
	B	31.4811	
	C	32.5265	
12-15-76	A	30.0374	7.73pH/72°F
	B	31.5019	

	DATE		WEIGHT	pH & TEMP
	12-21-76	A	30.0162	7.81pH/
		B	31.4762	
	12-29-76	A	30.0268	7.72pH/ 7
		B	31.4934	
	1-5-77	A	30.0245	7.59pH/7
		B	31.4594	
		C	32.5026	
	1-12-77	A	30.0377	7.19/68
		B	31.4954	
	1-19-77	A	30.0323	7.68/73
		B	31.4792	
	1-26-77	A	30.0093	7.11/70 (A)
		B	31.4552	
	2-2-77 IN AIR 1HR BEFORE WEIGHING TEST.	A	29.9882	7.93/
		B	31.4283	
		C	32.4667	
	2-10-77	A	30.0144	7.90/7
		B	31.4905	
	2-16-77	A	30.0001	7.45pH/7
		B	31.4584	
	2-23-77	A	30.0009	7.98pH/
		B	31.4707	
		C	32.5186	
DRY IN OVEN 24HRS/66°C	2-24-77	A	29.8057	-.0560
		B	31.2735	-.0024
		C	32.2764	-.0458

DATE		WEIGHT	PH & TEMP
10-7-76	A	30.0474	7.62 / 75°F
	B	31.5236	
10-13-76	A	30.0433	7.48 / 76°F
	B	31.4892	
	C	32.5401	
10-22-76	A	30.0485	7.51 / 73°F
	B	31.5061	
10-27-76	A	30.0507	7.58 PH / 74°F
	B	31.5124	
11-3-76	A	30.0278	7.71 PH / 71°F
	B	31.4965	
11-10-76	A	30.0404	7.61 / 74°F
	B	31.4875	
	C	32.5167	
11-17-76	A	30.0242	7.65 PH / 74°F
	B	31.4858	
11-24-76	A	30.0450	7.68 PH / 73°F
	B	31.4996	
12-1-76	A	30.0443	7.68 PH / 74°F
	B	31.4972	
12-8-76	A	30.0345	7.68 PH / 75°F
	B	31.4811	
	C	32.5265	
12-15-76	A	30.0377	7.73 PH / 72°F
	B	31.5019	

DRY IN OVEN 24 HRS / 66°C

DATE		WEIGHT	PH & TEMP
12-21-76	A	30.0162	7.81 PH /
	B	31.4762	
12-29-76	A	30.0268	7.72 PH / 72
	B	21.4934	
1-5-77	A	30.0245	
	B	31.4594	7.59 PH /
	C	22.5026	
1-12-77	A	30.0377	7.79 / 68°
	B	31.4954	
1-19-77	A	30.0323	7.68 / 73
	B	31.4792	
1-26-77	A	20.0093	7.91 / 70° (A)
	B	31.4552	
2-2-77	A	29.9882	
	B	31.4283	7.93 /
	C	32.4667	
WAIR 1HR BEFORE ENDING TEST			
2-10-77	A	30.0144	7.90 / 72
	B	31.4905	
2-16-77	A	30.0001	7.45 PH / 7
	B	31.4584	
2-23-77	A	30.0009	7.98 PH /
	B	31.4707	
	C	32.5186	
2-24-77	A	29.8057	-.0500
	B	31.2735	-.0024
	C	32.2764	-.0458

DATE					DATE	
2-27-77	A	29,7612	-.0952	.3181 %		
300°F	B	31.2042	-.0717	.2212 %		
1 HR	C	32.1962	-.1260	.3772 %		

(WAS CLEANED AFTER PICTURES)

0.167 %
0.0077%
0.142%

Report 554

Prepared by:

Leslie Mollon
Director - Nuclear Product
Development
Brooks & Perkins, Inc.
12633 Inkster Road
Livonia, MI 48150

June 1, 1977

Brooks & Perkins, Inc. Spent Fuel Storage Module Corrosion Report

ABSTRACT

Brooks & Perkins, Inc. Spent Fuel Storage
Module Corrosion Report No. 554

A determination is made from published data of the expected life of a storage module following a rupture in the water barrier covering. The environmental conditions external and internal to the module are defined. The various types of corrosion which can occur are also defined and their experimentally determined corrosion rates are listed. Results show an expected life to be at least greater than fifty three (53) years and probably greater than sixty (60) years following the occurrence of the rupture to the water barrier covering.

BROOKS & PERKINS, INC. SPENT FUEL STORAGE MODULE CORROSION REPORT

PURPOSE: The purpose of this report is to determine from published data the extent of any deterioration that is likely to occur over a forty year period to the shielding capability of a Brooks & Perkins, Inc. spent fuel storage module following a water leak in the stainless steel covering.

BACKGROUND: The spent fuel storage module (SFSM) is a slender square-shaped tube with open ends that is used for the storing and the shielding of one spent fuel assembly in a light water nuclear reactor storage pool. The tube is constructed with the inside and outside coverings being made of type 304 stainless steel. These two stainless steel surfaces are welded together at the top and bottom of the tube over an inner layer of a thermal neutron shielding material called BORAL^{tm}.

A group of SFSM's are assembled into a tightly packed array called a high-density storage rack. A network of horizontal and diagonal members separate the modules within the rack and provide the necessary lateral support. The racks stand in a vertical position on the bottom of a forty foot deep storage pool.

The water in the storage pools is constantly circulated through a series of filters which causes a constant water flow within the pool. The water is monitored and controlled for pH and temperature within specific limits depending on the type of nuclear reactor.

The quality of the water in the storage pool of the two types of reactors is controlled within the following ranges:

Pressurized Water Reactor (PWR)

water type	demineralized
water temperature	70° to 150°F (21° to 66° C)
pH at 77°F (25°C)	4.0 to 8.0*
boron, ppm	1800 to 2200
chloride ion, ppm, max.	0.1

* (4.5 to 10.6 at Combustion Engineering Reactors)

fluoride ion, ppm, max.	0.1
total suspended solids, ppm, max.	1.0
solids filtration, microns, max.	25

Boiling Water Reactor (BWR)

water type	demineralized
water temperature	70° to 150°F (21° to 66°C)
pH at 77°F (25°C)	5.8 to 7.5
chloride ion, ppm, max.	0.5
total heavy element, ppm, max.	0.1
total suspended solids, ppm, max.	1.0
solids filtration, microns, max.	25

The thermal neutron absorbing material BORAL^{tm} is a sandwich type panel that has outer surfaces of type 1100 aluminum and a core of boron carbide uniformly dispersed in a matrix of type 1100 aluminum.

DISCUSSION: The shielding capability of a BORAL panel is due to its ability to capture thermal neutrons. The capture of thermal neutrons is accomplished by the B^{10} (boron-ten) isotopes that are contained within the boron carbide particles. These boron carbide particles are chemically inert (unreactive), heat resistant, highly crystalline and nearly equivalent to diamond in hardness.

In order for corrosion to cause a reduction in the shielding capability of a BORAL panel, the boron carbide particles have to be physically displaced from the panel. A displacement of the boron carbide particles to occur would require the following sequence of events.

(1) the complete removal of the outer protective aluminum surfaces on the BORAL panel.

(2) the complete removal of the aluminum matrix surrounding each boron carbide particle.

(3) the physical displacement of the boron carbide particles.

It is interesting to note that BORAL has been used in fuel storage pools [1] [2] since 1964 and samples have been subjected to many corrosion studies [3] [4] for long periods of time. In none of these exposures has it been reported that any boron carbide particles were displaced.

The progression of corrosion to the outer surface is directly dependent upon the area in contact with the water. The outer surface will reduce in thickness at the same rate in mils per year as the edge will be attacked if the entire panel is in contact with the water. If only the edges of the BORAL are exposed to the water, the corrosion rate would be the same but a much longer period of time would be required for the total failure of the panel to occur.

In order to effectively extrapolate from previous test results, it is often necessary to make reasonable interpolations or projections from the published data because of differences between test and actual conditions. It must also be kept in mind that most, if not all, tests are conducted with constant or precisely controlled conditions throughout the test period which would not be the case in an actual leak.

Alwitt et al [5] states, "Aluminum reacts readily with water to form a hydrous oxide film. Depending upon the conditions of film formation, the film is more or less protective against subsequent corrosion. Growth occurs in two states: a pseudoboehmite film is produced initially and then is covered with a layer of bayerite crystals. By analogy with the aging mechanism in a colloidal suspension, it is thought that the pseudoboehmite dissolves and re-precipitates as bayerite crystals. The growth of bayerite is inhibited at higher temperatures (80°-100°C), presumably because the pseudoboehmite is better crystalized and dissolves more slowly."

"The growth kinetics and properties of the pseudoboehmite film produced at 100°C have been studied extensively. Less is known about the layers produced at low temperatures, but Hart has reported the weight gain and electron diffraction analyses for aluminum samples immersed in water at temperatures between 20° and 80°C."

There are at least four significant changes that will occur immediately to the water that enters into the internal voids in the storage module. Those changes are as follows:

1. Flow Rate. The pool water surrounding the storage module is constantly flowing and therefore its chemistry, purity and temperature can be controlled within precise limits. The water entering through a hole into the internal voids of the storage module will cease flowing and will become stagnant once the voids are filled. The internal water will change from the external water and will be the corrodent media to consider for the long term affects of corrosion. As pointed out by Godard, [6] "Movement of the corrosive liquid usually accelerates the rate of corrosion."

2. Shift in pH. The internal water will react with the aluminum upon contact and cause the pH to change. The pH will increase or decrease towards a steady pH near neutral depending on whether the initial condition is acidic or alkaline. This change in pH is reported by the following:

   A. Sedriks et al [7] "The change of pH with time for initially acidic solutions (i.e., pH <2) in the presence of dissolving aluminum is shown in Figures 1 and 2. (The curves shown could be reproduced within ± 0.05 of a pH unit.) In general, the change can be characterized by (1) an initial increase in pH, and (2) the subsequent attainment of a steady pH value."

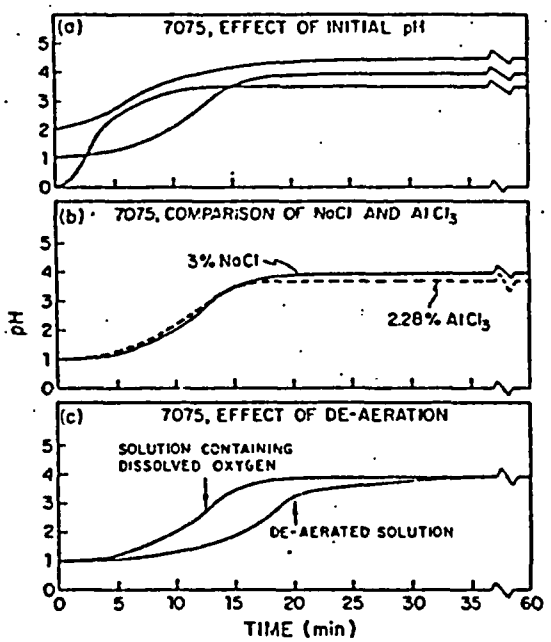

FIGURE 1 — The change of pH with time as a function of (a) initial pH of solution, (b) presence of aluminum ions, and (c) effect of oxygen.

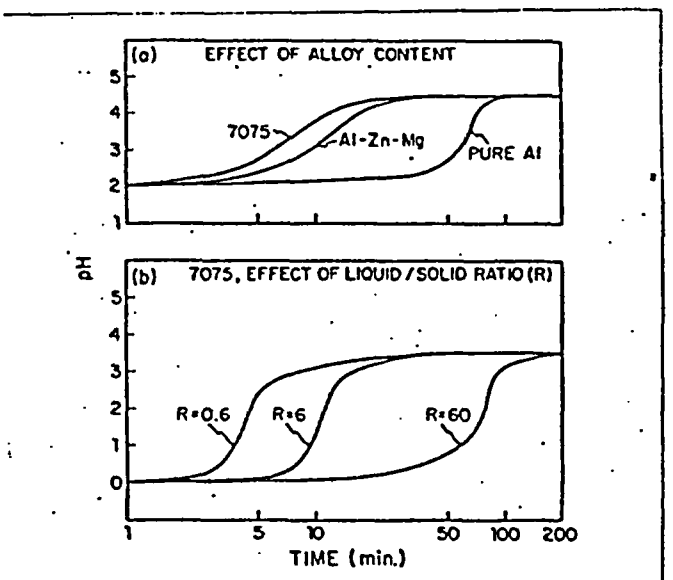

FIGURE 2 — The change of pH with time as a function of (a) alloy content, and (b) liquid/solid ratio.

"The steady pH value is related to the concentration of aluminum ions in solution....and is associated with the onset of precipitation of aluminum hydroxide, AL $(OH)_3$."

B. "Peterson et al [8] report that in sea water (pH 8.2) the corrodent in crevices in Type 304 stainless steel was less than 2(pH). The pH at the growing front of exfoliation crevices in aluminum alloys does not appear to have been reported, but it is postulated to be acid, having a pH of possibly as low as 3.2 based upon measurements of pH at the tips of stress corrosion cracks in aluminum alloys."

C. B. F. Brown. [9] "The acidity is caused by hydrolysis of one or more components of the metal or alloy, and the acidity persists because of the restricted interchange between the corrosion cell and the bulk environment."

D. Peterson et al [10] "Figures 3 and 4 show that regardless of the initial potential and pH, the crevices on stainless steel polarized the pH shifted in the alkaline direction to the domain where water is unstable and hydrogen discharge would be expected. One would therefore expect that cathodic protection has been achieved, since the potential of the surface has been shifted into a region where stainless steel is known to be cathodically protected. In addition, the pH has shifted to a value which indicates that the solution within the crevice is benign to stainless steel."

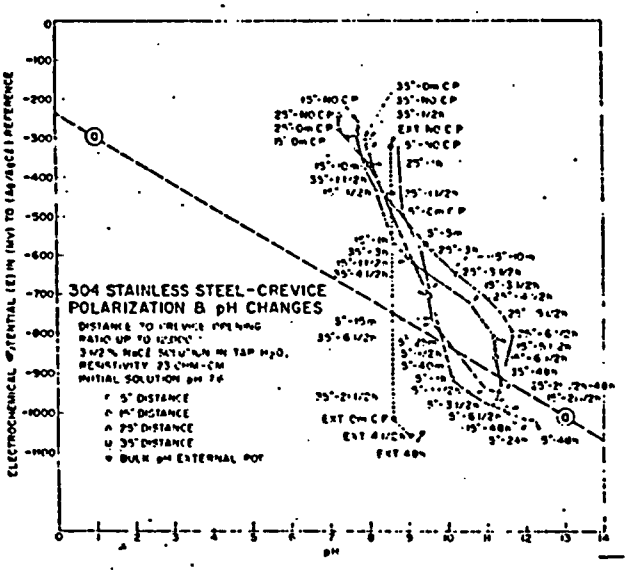

FIGURE 3 – Type 304 stainless steel, crevice polarization and pH data at various distances from the crevice opening and at various times. Shown on a partial Pourbaix diagram. The 0.6 M NaCl solution had an initial pH of 7.6

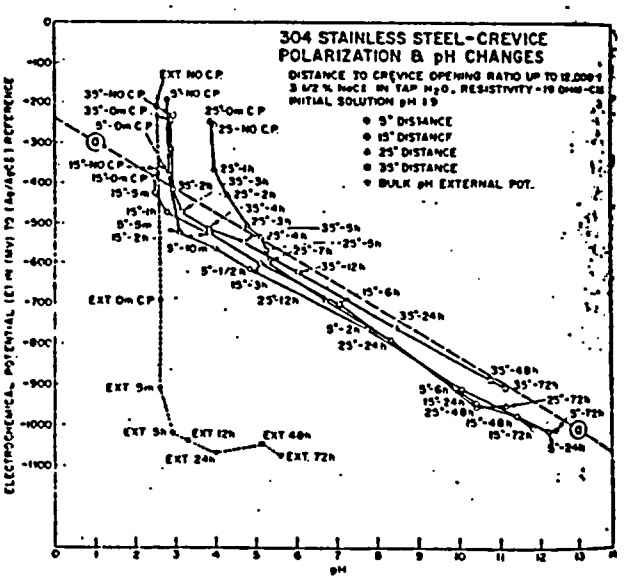

FIGURE 4 – Type 304 stainless steel, crevice polarization and pH data at various distances from the crevice opening and at various times. Shown on a partial Pourbaix diagram. The 0.6 M NaCl solution had an initial pH of 1.9.

E. B&P Report No. 553 11

Samples of the SFSM were placed in water baths having a pH of 4.5 and 10.5. Within a few hours the pH of the water that entered the SFSM had changed and was steady at 7.1 and 7.7 respectively.

3. Oxygen Content. The content of dissolved oxygen in the internal water will be depleted by the oxidation of the metal surfaces. The decelerating effect on the reactivity of the solution by this de-aeration can be seen in Figure 1(c) [1]. The de-aerated solution required 38% more time to change pH from 1.0 to 3.0 and 80% more time to change from 1.0 to 4.0 than the solution containing dissolved oxygen. This delay in reaction time is also caused by the development of a protective oxide film on the surface of the aluminum which tends to arrest further corrosion action.

4. Ion Concentration. The volume of the internal water will be small compared to the surface area of the metal faces and will therefore become saturated with ions very quickly. The further ionization of the aluminum surfaces can proceed only to the extent that aluminum ions precipitate out of solution in the form of an insoluble compound. A study of a potential-pH diagram (Pourbaix) for the aluminum-water system (see Figures 5 and 6 of MacDonald [12] et al) discloses the following reaction will occur within a pH range of 3 to 8.5 and a temperature range of 77° to 140°F.

$$2\,Al + 6\,H_2O \rightarrow Al_2O_3 3H_2O \downarrow + 6H^+ + 6 \text{ electrons}$$

A dissolved aluminum atom will react directly with water to form the precipitate gibbsite and bayerite ($Al_2O_3\ 3H_2O$).

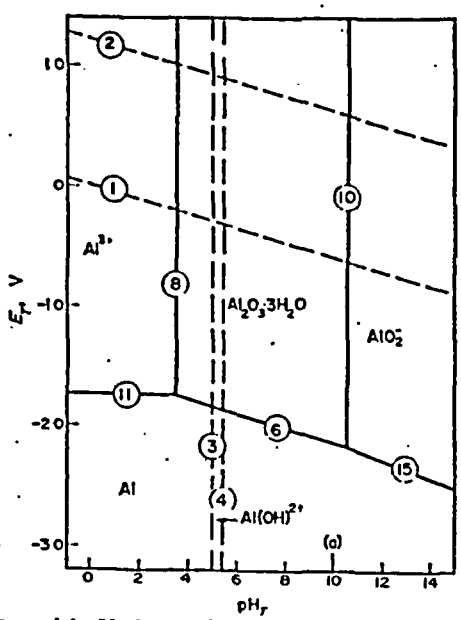

FIG. 5 Potential-pH diagram for the aluminium-water system at 25°C. (a) refers to the pH_r of a 10^{-4}m OH^- solution.

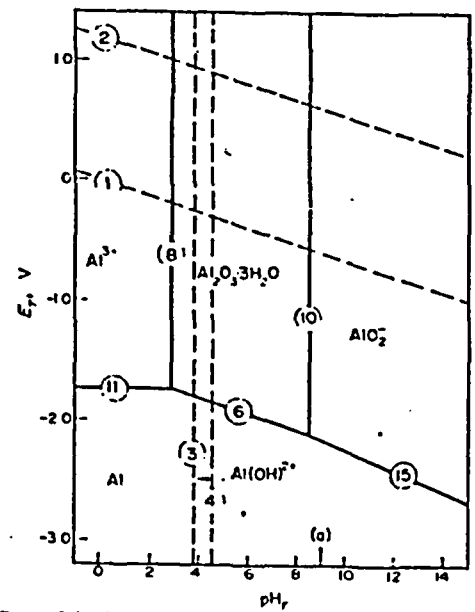

FIG. 6 Potential-pH diagram for the aluminium-water system at 60°C. (a) refers to the pH_r of a 10^{-4}m OH solution.

The precipitate is a hydrated oxide of aluminum which is stable up to 135°C (275°F). The entrapped water will become saturated by the forming of the gibbsite and bayerite, and therefore would be a self-limiting influence to the corrosion.

CORROSION DATA

BORAL

1. One year test results [3]

water type	BWR
pH	5.6 to 7.7
temp.	68° to 78°F (20° to 26° C)
corrosion rate, mpy	0.28
expected life (at 15 mils thickness)*	> 53 years

*10 Mils of Clad Plus 5 Mils of Matrix Holding Boundary Layers of B_4C.

2. 2000 hour test results [4]

water type	BWR
pH	7.0
temp.	190°F (88°C)
corrosion rate, mpy	1.2 to 2.1
estimated corrosion rate @ 70° to 150°F., mpy	.18 to .32
expected life (at 15 mils thickness)*	>45 years

3. Twelve years of service [1]

water type	PWR
boron	nil
pH	4.0 to 8.0 (est.)
temp.	70° to 150°F (21° to 66°C) (est.)
corrosion rate, mpy	nil
expected life (at 15 mils thickness)*	> 60 years

STAINLESS STEEL - type 304

1. General Corrosion [13]

water type	BWR or PWR
pH	7.0 to 11
temp.	572°F (300°C)
oxygen, ppm	< .01 to 2
chlorides, ppm	< .1
corrosion rate, mpy	< 2
estimated corrosion rate @ 150°F, mpy	<.6
expected life (at 60 mils thickness)	> 60 years

* 10 mils of Clad plus 5 mils of Matrix Holding Boundary Layers of B_4C.

2. General Corrosion after 3000 hours [14]

water type	high purity, demineralized
hydrazine, ppm	.01 to .07
oxygen, ppm	< .005
chlorine, ppm	< .05
pH	6.95 to 9.58
flow rate, gal/hr.	3.5
temp.	320°F (160°C)
corrosion rate, mpy	.01
expected life (at 60 mils thickness)	> 60 years

3. Stress-Corrosion-Cracking after 3000 hours [14]

water quality same as 2 above	
stress % of .2% yield	120
results	"Metallographic examination of selected samples also failed to reveal any cracking."
expected life (at 60 mils thickness)	> 60 years

ALUMINUM - type 1100F

1. General Corrosion after 14,200 hours [15]

water type	high purity, demineralized
oxygen, ppm	4 to 5
pH	5.0 to 6.0
flow rate, fps	7.6
temp.	194° to 356°F (90° to 180°C)
corrosion rate, mpy	0.16
expected life (at 15 mils thickness)	> 60 years

STAINLESS STEEL (type 304) coupled with ALUMINUM (type 1100F)

1. Crevice and Galvanic Corrosion [15]

water type	high purity, demineralized		
oxygen, ppm	4 to 5		
pH	5.0 to 6.0		
flow rate, fpm	0.5		
temp.	194° to 356°F (90° to 180°C)		
time, hrs.	1100	1775	2000
Al max. pit depth, mils	2	< 3	< 5
Al corrosion rate, mpy	0.1	0.1	0.1
S.S. Corrosion rate, mpy	0	0	0
expected life (at 15 mils thickness of Al)	> 60 yrs	> 60 yrs	> 60 yrs

CONCLUSION: A thorough review of the published test data indicates the materials used in the Brooks and Perkins Inc. spent fuel storage module (namely 304 Stainless Steel and 1100F Aluminum) provide adequate corrosion resistance to achieve a life expectancy of forty years without a reduction of neutron absorbing capability when used in a BWR or PWR storage pool with a rupture in the stainless steel covering.

REFERENCES:

[1] Yankee-Rowe, Fuel Storage Rack, Part No. YM-H-1-2, Aug, 1964

[2] Dairyland Power Cooperative, LaCrosse Plant, BWR, Mar,1975

[3] B&P Report No. 551, Corrosion Resistance of Boral to 1 Yr. Exposure to BWR Pool, Feb, 77

[4] L. Marti-Balaguer and W. R. Smalley, "Evaluation of Control Rod Materials; CVTR Project", CVNA-86. Carolinas-Virginia Nuclear Power Associates, Inc. (1960)

[5] R. S. Alwitt & L. C. Archibald, Some Observations on the Hydrous Oxide Film on Aluminum Immersed in Warm Water, Corrosion Science, Vol. 13, pg. 687

[6] H. P. Godard, The Corrosion Behavior of Aluminum, NACE-Corrosion, Vol. 11, Dec. 1955, pg. 55

[7] A. J. Sedriks, J. A. S. Green and D. L. Novak. On the Chemistry of the Solution at Tips of Stress Corrosion Cracks in Al Alloys. NACE-Corrosion, Vol. 27, No. 5, May 71, pg. 199

[8] M. H. Peterson, T. J. Lennox, Jr., and R. E. Groover, A Study of Crevice Corrosion in Type 304 Stainless Steel, Proceedings of 25th NACE Conference, 314-317, National Association of Corrosion Engineers, Houston (1970). Quotation from [9].

[9] B. F. Brown. Concept of the Occluded Corrosion Cell. NACE-Corrosion, Vol. 26, No. 8, Aug. 70, pg. 249

[10] M. H. Peterson and T. J. Lennox, Jr. A Study of Cathodic Polarization and pH Changes in Metal Crevices NACE-Corrosion, Vol. 29, No. 10, Oct. 73 Pg 409

[11] B&P Report No. 553, pH Shift of Water Inside Spent Fuel Storage Module, Feb., 77.

[12] D. D. MacDonald and P. Butler, The Thermodynamics of the Aluminum-Water System at Elevated Temperatures. Corrosion Science 1973, Vol. 13, pg. 265

[13] National Assoc. of Corrosion Engineers, Corrosion Data Survey, 1974, pp. 34 & 252

[14] A. P. Larrick, Corrosion Studies in Simulated N-Reactor Secondary System Water Encironment. Atomic Energy Commission Research and Development, Report HW-76358, Hanford Atomic Products Operation, May 1963, pg. 7, 10 & 22.

[15] J. L. English and J. C. Griess, Dynamic Corrosion for the High - Flux Isotope Reactor, ORNL - TM - 1030, September, 1966, pg. 1, 2, 3, 4, 23, 26, 27, 31

Brooks & Perkins, Incorporated

Report No. 561

Testing conducted in
accordance with BPS-384
by:

Brooks & Perkins, Inc.
Advanced Structures Division
12633 Inkster Road
Livonia, Michigan 48150

STORAGE MODULE

CORROSION TESTING

Final Report

Abstract

1. The corrosion testing of the storage module has been completed in accordance with test procedure BPS-384.

2. All test samples were exposed approximately 90 days.

3. The final weights of the test samples are reported with the corrosion products removed with the exception of the Cadmium samples.

I. Purpose

The purpose of this program is to substaniate by laboratory tests the ability of the Brooks & Perkins storage module to satisfactorily resist the envoronment of a BWR and PWR fuel storage pool. The test conditions represent a postulated leak in the stainless steel covering and the most adverse environmental conditions likely to occur during normal operation of the storage pool.

II. Factual Data

A. Test Samples

The test samples were fabricated in accordance with paragraph 5.1 of BPS-384 and placed in the specified test environmental as available.

B. Testing

The test samples and solutions were under daily visual surveillance. The test solutions were monitored and either replaced on adjusted as required to maintain the proper pH. The frequency of this monitoning depended on the solution - sample combination and varied from 3 to 7 days.

C. Changes in Procedures

1. After the completion of the exposure period, all samples were cleaned by scrubbing with a soft bristle brush using a mild detergent and 600 grit silicon carbide polishing compound.

2. In addition to the above cleaning method, all Aluminum and BORAL^{tm} samples were immersed for 15 minutes in a 25% Nitric Acid solution at room temperature in order to remove corrosion by-products.

3. In order to completely dry the BORAL^{tm} samples in a reasonable time it was necessary to raise the final drying temperature to 600°F for a minimum of 3 hours. To minimize scattering of results all samples received this final drying treatment.

III. Conclusions

The results of the test program confirmed the anticipated reactions of the materials to the pH of the test solutions. Namely, no reaction with Stainless Steel, Aluminum and BORAL^{tm} showing the greatest reaction with the highest pH, and Cadmium being dissolved at the lowest pH. Detailed observation listed below.

A. 304 Stainless Steel.

No appreciable change in all solutions and combination of materials. All samples exhibited a gain in weight and varied from a MDD (Milligrams per sq. decimeter per day) of a + 0.37 in a 4.5 pH solution to a low of + .002 in a 7.0 pH solution. Visual change of the Stainless Steel was minor and varied from light golden color in sample #1, pH 4.5 to a frosted appearance in sample #10, pH 7.0 A light dense coating formed on the side of sample #6 that was in contact with the BORAL^{tm} and gained 0.144 MDD. In all samples the MPY(Milsper year) was considered too low to be meaningful.

B. BORAL^{tm}

The greatest unit change (Table I) occured in a single sample (#34) of BORAL^{tm} at temperature of 150°F and a pH of 10.5, PWR water. The addition of stainless steel, sample #5, in the same solution resulted in a marked decrease in unit change.(Table I). With the inclusion of a sacrificial material, 7072-0 Aluminum Alloy, to the stainless steel and BORAL^{tm} (sample #6) the corrosion rate was further lowered, Table I.

Table I

Sample	pH	Temperature	MPY	MDD	Combination
34	10.5	150°F	-3.29	-6.67	BORAL^{tm}
5	10.5	150°F	-1.988	-4.03	SS-BORAL-SS
6	10.5	150°F	-.815	-1.65	AL-BORAL-SS

The combination of stainless steel and BORAL^{tm} exhibited a decrease in unit change with an increase of temperature in all solutions. The higher temperatures probably aided in the formation of a more corrosion resistant film on the surfaces of the BORAL^{tm}. Though the anodized BORAL^{tm}, sample #13, with stainless steel resulted in unit loss, -.767 MPY and -1.555 MDD, there was no visual change in the anodized film on the surface of the BORAL^{tm}, indicating the losses occured in the sheared edges of the samples. Prior to the exposure test, the core section of the sheared edges did not exhibit the formation of the anodized film.

The same combination of materials listed in Table I exhibited the same pattern of unit change when exposed in a 4.5 pH solution. The results are given in Table II.

Table II

Sample	pH	Temperature	MPY	MDD	Combination
33	4.5	150°F	-.8634	-1.75	BORAL^{tm}
2	4.5	150°F	-.6066	-1.23	SS-BORAL-SS
3	4.5	150°F	-.4114	-.835	AL-BORAL-SS

C. Aluminum-BORAL^{tm}

This combination of material exhibited minor unit changes in solutions of 5.3 and 7.5 pH at a temperature of 150°F. The BORAL^{tm} showed a weight loss with 6061-0 aluminum alloy and a slight gain with alloys 5083 and 6061-4, Table III. Major changes were inhibited by the development of a passivating coating on the surface of the samples.

Table III

Sample	pH	Temperature	MPY	MDD	Combination
15	5.3	150°F	-.1944	-.394	6061-0, Boral, 6061-
17	5.3	150°F	+.1727	+.35	5083, Boral, 5083
19	5.3	150°F	+.1359	+.275	6061-T4, Boral, 6061-T4
16	7.5	150°F	-.3354	-.68	6061-0, Boral, 6061
18	7.5	150°F	+.117	+.237	5083, Boral, 5083

D. Cadmium

Severe attack occured at a pH of 4.5. In combination with stainless steel, sample #21, the cadmium had a MPY of -4.25 indicating being completely dissolved in 6 years. In all solutions and temperatures heavy corrosion products developed which were not removable by the standard cleaning method. After recording the results, chemical cleaning was attempted but abandoned because any chemical that removed the corrosion also attached the parent material.

IV. Visual

A. Blisters

Blisters in the BORAL^{tm} were a result of heating the wet samples to 500°F without prior heating at lower temperatures. The rapid heating resulted in a internal pressure differential causing the cladding to part from the core section. A preliminary heat-treatment at 300°F maximumum for 3 to 6 hours eliminates this problem.

B. Color

Stainless steels varied from no change to a light straw color. Corrosion of the cadmium developed in various colors ranging from red to yellow brown.

C. Etched

Surfaces lightly etched delineating grain boundaries with no measurable dimension loss. Welds are outlined and darkened.

D. Pitting

Except as noted, pitting was minor and unmearsurable. Where pitting penetrated the cladding the average depth was .010 inches.

E. Coated Surface

A light uniform on the surfaces of the samples which inhibited major unit changes.

Final Result 90 day Exposure

Sample Solut.	Material	Ph Range	Days	% Wt Change	MPY	MDD	Visual
	304 ss	4.5-5.38	89.79	+ .009		+0.37	Slight discoloration
#1 #1-75°F	Boral			- .558	-.6969	-1.41	Blister, light attack sheared edges
	304 ss			+ .002		+.009	Slight discoloration
	304 ss	4.5-6.0	89.79	+ .0032		+.013	Slight discoloration
#2 #1-150°F	Boral			- .477	-.6066	-1.23	16 pits. .001 max depth
	304 ss			+ .0073		+.031	Slight discoloration
	AL 7072-0	4.5-6.0	90.74	- .183	-.135	-.265	Light etch; 4 corners thickness tapered
#3 #1-150°F	Boral			- .329	-.4114	-.835	5 pits max .003 depth x .030 dia.
	304 ss			+ .0016		+.006	No change
	304 ss	10.05-10.78	94.88	+ .0016		+.006	No change
#4 #2-75°F	Boral			-1.816	-2.187	-4.43	Small pits .001 etched
	304 ss			+ .0016		+.006	No change
	304 ss			+ .074		+.288	No change
#5 #2-150°F	Boral	10.08-10.92	94.63	-1.653	-1.9879	-4.03	Numerous pits pentrating cladding
	304 ss			+ .073		+.288	No change

Final Results 90 day Exposure

Sample	Material	Ph Range	Days	% Wt Change	MPY	MDD	Visual
Solut. #6 #2-150°F	AL 7072-0	10.05-10.88	92.75	- .457	-.340	-.669	Light etch, no pitting
	Boral			- .653	-.8149	-1.654	Numerous pits .001 on surface facing Al.
	304 ss			+ .036		+ .144	Coating on surface touching boral.
#7 #3-75°F	304 ss	4.98-7.9	93.58	+ .021		+ .081	Frosted
	Boral			- .851	-1.0306	- 2.09	No pitting, light attack sheared edges
	304 ss			+ .036		+ .139	Frosted
#8 #3-150°F	304 ss	5.3-8.91	93.58	+ .009		+ .035	Frosted
	Boral			- .223	-.2736	-.555	Pits. .007" deep x .050" wide
	304 ss			+ .005		+ .018	Discolored
#9 #3-150°F	AL 7072-0	5.3-8.8	89.79	- .350	-.2675	-.526	Etched
	Boral			- .503	-.6517	-1.322	Etched, pitted .0095" x .055"
	304 ss			- .011		- .043	Slight color
#10 #4-75°F	304 ss	7.0-8.8	94.5	+ .021		+ .08	Frosted
	Boral			- .446	-.5314	-1.08	Very light pitting
	304 ss			+ .026		+ .098	Frosted

Final Results 90 day Exposure

Sample	Material	Ph Range	Days	% Wt Change	MPY	MDD	Visual
Solut. #11 #4-150°F	304 ss	7.0-8.4	94.5	+ .001		+ .004	Clean
	Boral			- .346	-.4215	- .855	Very slight pitting
	304 ss			+ .001		+ .002	Clean
#12 #4-150°F	AL 7072-0	7.0-8.45	94.83	- .304	-.219	-.431	Etched
	Boral			- .486	-.5909	- 1.199	Etched, pitted .008" x .025" surface facing S.S.
	304 ss			- .006		-.025	Clean
#13 #2-150°F	304 ss	10.03-10.79	90.08	+ .001		+ .002	Clean
	ANOD Boral			- .614	-.7673	-1.555	No change anodized surface
	304 ss			- .014		-.239	Clean
#14 #4-150°F	304 ss	7.0-8.15	90	- .013		- .054	Clean
	ANOD Boral			+ .35	-.4221	-.856	No change anodized surface
	304 ss			- .013		-.052	Clean
#15 #3-150°F	AL 6061-0	5.3-7.98	91.13	+ .311	+.2298	+ .449	Light etch, coated surface
	Boral			- .156	-.1944	-.394	Light etch, no pitting
	AL 6061-0			+ .334	+.2522	+.493	Light etch, coated surface

Final Results 90 Day Exposure

Sample Solut.	Material	Ph Range	Days	% Wt Change	MPY	MDD	Visual
#36 #4-150°F	Boral	7.0-8.58	92.42	- .462	-.5851	-1.187	Etched, few small pits
#37 #1-150°F	Cadmium	4.5-7.12	93.79	- 12.07	- 5.4987	-33.861	Heavy etched surfaces
#38 #2-150°F	Cadmium	9.92-10.98	94.875	+ .305	+ .1333	+ .821	Corrosion products on surface
#39 #3-150°F	Cadmium	5.3-9.68	92.875	+ .256	+ .1155	+.711	Heavy corrosion products on surface
#40 #4-150°F	Cadmium	7.0-9.2	92.92	+ .321	+ .148	+.911	Heavy corrosion products on surface

Final Results 90 day Exposure

Sample	Material	Ph Range	Days	% Wt Change	MPY	MDD	Visual
Solut. #16 #4-150°F	AL 6061-0	7.0-7.92	90	+ .35	+ .2682	+ .524	Etched, coated surface
	Boral			- .262	- .3354	- .68	Etched, no pitting
	AL 6061-0			+ .27	+ .2119	+ .414	Etched, coated surface
#17 #3-150°F	AL 5083	5.3-7.5	90	+ .064	+ .2578	+ .477	Etched, coated surface
	Boral			+ .137	+ .1727	+ .35	No pitting, light etch
	AL 5083			+ .091	+ .3909	+ .724	Etched, coated surface
#18 #4-150°F	AL 5083	7.0-7.81	90	+ .171	+ .692	+1.28	Etched, coated surface
	Boral			+ .093	+ .117	+ .237	No pitting, etched, coated surface
	AL 5083			+ .104	+ .4415	+ .817	Etched, coated surface
#19 #3-150°F	AL 6061 T4	5.3-7.75	90	+ .328	+ .2501	+ .481	Etched, coated surface
	Boral			+ .109	+ .1359	+ .275	No pits, etched coated surface edges chewed
	6061 T4			+ .344	+ .2728	+ .525	Etched coated surface
#20 #1-75°F	304 ss	4.5-7.1	90	- .0016		- .006	Discolored on surface facing cadmium
	Cadmium			-11.626	- 5.6195	-34.638	Chewed, outer edges dissolve
	304 ss			- .0032		- .013	Discolored on surface facing cadmium

Final Results - 90 day Exposure

ample	Material	Ph Range	Days	% Wt Change	MPY	MDD	Visual
olut.							
	304 ss	4.5-6.9	90	+ .0027		+ .011	Discoloration surface facing cadmium
#21 .-150°F							
	Cadmium			- 8.863	- 4.2533	-26.216	Pitted, outer edges dissolved
	304 ss			- .001		- .002	Discoloration surface facing cadmiu
	304 ss	10.0-11.09	90	+ .0101		+ .039	Discolored
#22 :-150°F	Cadmium			- .592	-..2679	-1.651	Etched
	304 ss			+ .017		+ .065	Discolored
	304 ss	5.3-8.9	92.17	- .0047		- .019	Stained
#23 #3-150°F	Cad.			- .776	- .3464	- 2.135	Pitted; heavy build-up corrosio products.
	304 ss			- .006		- .025	Stained
	304 ss	7.0-9.95	92.17	+ .0175		+ .069	Stained
#24 #4-150°F	Cad.			- .694	- .3217	-1.983	Pitted, heavy corrosion products
	304 ss			+ .00		+ .006	Stained
	AL 6061-0	5.3-7.3	91	- .562	- .4244	-8,29	Etched, small pits, stained side facing Cad.
#25 #3-75°F	Cad.			- .594	- .2748	-1.694	Stained, heavy corrosion products
	AL 6061-0			- .541	- .3914	-7.65	Etched, stained side facing Cad.

Final Resu 90 day Exposure

Sample	Material	Ph Range	Days	% Wt Change	MPY	MDD	Visual
#26 #3-150°F	AL 6061-0	5.3-8.22	91.25	- .202	- .1524	- .298	Etched, small pits, stained side facing Cad.
	Cadmium			- .579	- .2715	-1.673	Heavy corrosion products on surface
	AL 6061-0			- .252	- .192	- .375	Etched, small pits, stained side facing Cad.
#27 #4-150°F	AL 6061-0	7.0-8.6	90	+ .293	+ .2241	+ .438	Etched, coated surface
	Cadmium			- .204	- .0944	- .582	Heavy corrosion products on surface
	AL 6061-0			+ .206	+ .1583	+ .309	Etched, coated surface
#28 #3-75°F	AL 5083	5.3-8.35	90	- .142	- .5729	-1.06	Etched, numerous small pits
	Cadmium			- .261	- .124	- .764	Heavy corrosion products on surface
	AL 5083			- .162	- .6699	-1.24	Etched, numerous small pits
#29 #3-150°F	AL 5083	5.3-8.0	90	+ .078	+ .3138	+ .581	Etched, coated surface
	Cadmium			- .668	- .3153	-1.943	Heavy corrosion products on surface
	AL 5083			+ .073	+ .3087	+ .571	Etched, coated surface
#30 #4-150°F	AL 5083	7.0-8.58	90	+ .074	+ .2997	+ .555	Etched, coated surface
	Cadmium			- .541	- .2564	-1.58	Heavy corrosion products on surface
	AL 5083			+ .064	+ .2686	+ .497	Etched, coated surface

Final Results 90 day Exposure

Sample	Material	Ph Range	Days	% Wt Change	MPY	MDD	Visual
Solut.							
	AL 6061-T4	5.3-8.1	90	+ .304	+ .2282	+.446	Etched, coated surface
#31 #3-150°F	Cadmium			- .816	- .3857	-2.389	Heavy corrosion products on surface
	AL 6061-T4			+ .271	+ .2065	+.403	Etched, coated surface
#32 #3-150°F	AL 5083	5.3-8.42	90	+ .071	+ .2873	+.532	Etched coated surface
#33 #1-150°F	Boral	4.5-7.6	93.42	- .715	- .8634	-1.75	Etched, no pitting blister
#34 #2-150°F	Boral	9.97-10.9	92.71	- 2.6102	- 3.29	-6.67	Etched, 2 small blisters, stained pitted .0065 "x 150"
#35 #3-150°F	Boral	5.3-7.91	91.5	- .595	- .7649	-1.552	Etched, no pits, blister

b+p Brooks & Perkins, Incorporated

Report No. 578

Prepared by:

Brooks & Perkins, Inc.
12633 Inkster Road
Livonia, Michigan 48150

Date: July 7, 1978

THE SUITABILITY OF BROOKS & PERKINS SPENT FUEL STORAGE MODULE FOR USE IN PWR STORAGE POOL

ABSTRACT

A. A program of testing and research has been conducted concerning the suitability of the Brooks & Perkins spent fuel storage module (SFSM) for use in a pressurized water reactor storage pool.

B. The following is an outline of the investigation:

1. Corrosion Resistance Testing and Research
   - 1.1 SFSM Without A Leak In The Stainless Steel Covering
   - 1.2 SFSM With A Leak In The Stainless Steel Covering
2. Irradiation Testing and Research
   - 2.1 Gas Generation Test of BORON CARBIDE/ ALUMINUM Matrix Blend
   - 2.2 Irradiation of SFSM With And Without A Leak In The Stainless Steel Covering
   - 2.3 Helium Generation

C. The research and testing that have been conducted indicate that the Brooks & Perkins SFSM is suitable for use in a PWR spent fuel storage pool.

THE SUITABILITY OF BROOKS & PERKINS SPENT FUEL STORAGE MODULE FOR USE IN PWR STORAGE POOL

PURPOSE

The purpose of this report is to exhibit test results and literature research that illustrates the suitability of the Brooks & Perkins Spent Fuel Storage Module (SFSM) for use in a pressurized water reactor (PWR) storage pool.

BACKGROUND

Spent Fuel Storage Module: The SFSM is a slender square-shaped tube with open ends that is used for the storing and the shielding of one spent fuel assembly in a light water nuclear reactor storage pool. The tube is constructed with the inside and outside coverings being made of type-304 stainless steel. These two stainless steel surfaces are welded together at the top and bottom of the tube over an inner layer of a thermal neutron shielding material called BORAL tm. Boral is a sandwhich type panel that has outer surfaces of type 1100 aluminum and a core of boron carbide uniformly dispersed in a matrix of type 1100 aluminum.

A group of SFSM's are assembled into a tightly packed array called a high-density storage rack. A network of horizontal and diagonal members separate the modules within the rack and provide the necessary lateral support. The racks stand in a vertical position on the bottom of a 40-foot deep storage pool.

The water in the storage pools is constantly circulated through a series of filters which causes a constant water flow within the pool. The water is monitored and controlled for pH and temperature within specific limits depending on the type of nuclear reactor.

Environment of SFSM: In a PWR, the high density storage rack is exposed to the following conditions.

Radiation Exposure	10^{11} rads gamma total. 10^{4} neutrons/cm^2/ sec average flux.
Water Type	demineralized.
Water Temperature	70 °to 150 °F (21 °to 66 °C).
pH at 77°F (25 °C)	4.0 to 8.0*
boron, ppm	1800 to 2200

* (4.5 to 10.6 at Combustion Engineering Reactors)

chloride ion, ppm, max.	0.1
fluoride ion, ppm, max.	0.1
total suspended solids, ppm, max.	1.0
solids filtration, microns, max.	25

The storage racks are expected to withstand these conditions over a 40-year period.

Shielding Capability of Boral: The shielding capability of a Boral panel is due to its ability to capture thermal neutrons. The capture of thermal neutrons is accomplished by the B^{10} (boron-ten) isotope that is contained within the boron carbide particles. These boron carbide particles are chemically inert (unreactive), heat-resistant, highly crystalline and nearly equivalent to diamond in hardness.

In order for corrosion to cause a reduction in the shielding capability of a Boral panel, the boron carbide particles have to be physically displaced from the panel. A displacement of the boron carbide particles to occur would require the following sequence of events:

(1) The complete removal of the outer protective aluminum surfaces on the Boral panel.

(2) The complete removal of the aluminum matrix surrounding each boron carbide particle.

(3) The physical displacement of the boron carbide particles.

TESTING AND RESEARCH

Testing and research were conducted to substantiate the ability of the Brooks & Perkins SFSM to satisfactorily resist corrosion and reaction to irradiation in the environment of a pressurized water reactor spent fuel storage pool.

1. Corrosion Resistance Testing and Research

1.1 SFSM Without A Leak in The Stainless Steel Covering

The corrosion resistance of the stainless steel covering of the SFSM

has been investigated through research of published data. The following information indicates that the stainless steel covering of the Brooks & Perkins SFSM provides adequate corrosion resistance for the storage module to achieve a life expectancy of 40 years when used in a PWR storage pool.

CORROSION DATA - Stainless Steel - Type 304:

A. General Corrosion[1]

Water Type	PWR
pH	7.0 TO 11
Temperature	572° F (300° C)
Oxygen, ppm	< .01 to 2
Chlorides, ppm	< .1
Corrosion Rate, mpy	< 2
Estimated Corrosion Rate @ 150 °F, mpy	< .6
Expected Life (at 36 mils thickness)	> 60 years

B. General Corrosion After 3000 Hours[2]

Water Type	high purity, demineralized
Hydrazine, ppm	.01 to .07
Oxygen, ppm	< .005
Chlorine, ppm	< .05

[1] National Assoc. of Corrosion Engineers, Corrosion Data Survey, 1974, ppl 34 and 252.

[2] A.P. Larrick, Corrosion Studies in Simulated N-Reactor Secondary System Water Environment. Atomic Energy Commission Research and Development, Report HW-76358, Hanford Atomic Products Operation, May 1963, pp. 7, 10 and 22.

boron	nil
pH	4.0 to 8.0 (est.)
temp.	70 °to 150 °F (21 °to 66 °C) (est.)
corrosion rate, mpy	nil
expected life (at 15 mils thickness)*	> 60 years

ALUMINUM - type 1100F

General Corrosion after 14,200 hours [4]

water type	high purity, demineralized
oxygen, ppm	4 to 5
pH	5.0 to 6.0
flow rate, fps	7.6
temp.	194 °to 356 °F (90 °to 180 °C)
corrosion rate, mpy	0.16
expected life (at 15 mils thickness)	> 60 years

STAINLESS STEEL (type 304) coupled with ALUMINUM (type 1100F)

Crevice and Galvanic Corrosion [4]

water type	high purity, demineralized
oxygen, ppm	4 to 5

* 10 mils of Clad plus 5 mils of Matrix Holding Boundary Layers of B_4C.

4 J. L. English and J. C. Griess, Dynamic Corrosion for the High - Flux Isotope Reactor, ORNL -TM - 1030, September, 1966, pg. 1, 2, 3, 4, 23, 26, 27, 31.

pH	5.0 to 6.0		
flow rate, fpm	0.5		
temp.	194°to 365°F (90°to 180°C)		
time, hours	1100	1775	2000
Al. max. pit depth, mils	2	<3	<5
Al. corrosion rate, mpy	0.1	0.1	0.1
S.S. Corrosion rate, mpy	0	0	0
expected life (at 15 mils thickness of Al.)	>60 yrs	>60 yrs	>60 yrs

1.2.2 Corrosion Resistance Tests

1.2.2.1 SFSM Materials Test

PURPOSE: A test was conducted to show and describe the extent of corrosion occuring after one year of exposure to PWR storage pool water inside a stainless steel enclosure containing a sample of BORAL.

METHOD: A sample of BORAL™ having bare edges was sealed inside a stainless steel enclosure (see Figure 1). Twenty milliliters (20 ml) of a boron solution (2000 ppm B, pH of 5) was added through a threaded nipple to the void between the BORAL sample and the stainless enclosure. The BORAL was the standard 35% B_4C type and measured .177 x 9 x 9 inches. The stainless steel enclosure was Type 304 and was .018 inches thick. The sample with the boron solution inside was supended in the pool of the Ford Reactor at the University of Michigan for a period of one year. The sample had been irradiated during a prior test with neutron and gamma fluxes. Following the one year of storage in the pool, the sample still retained levels of radioactivity which somewhat restricted the analysis of the sample components, particularly the stainless steel. The sample was suspended in the pool by one corner and the boron solution filled about one-quarter of the inner void volume.

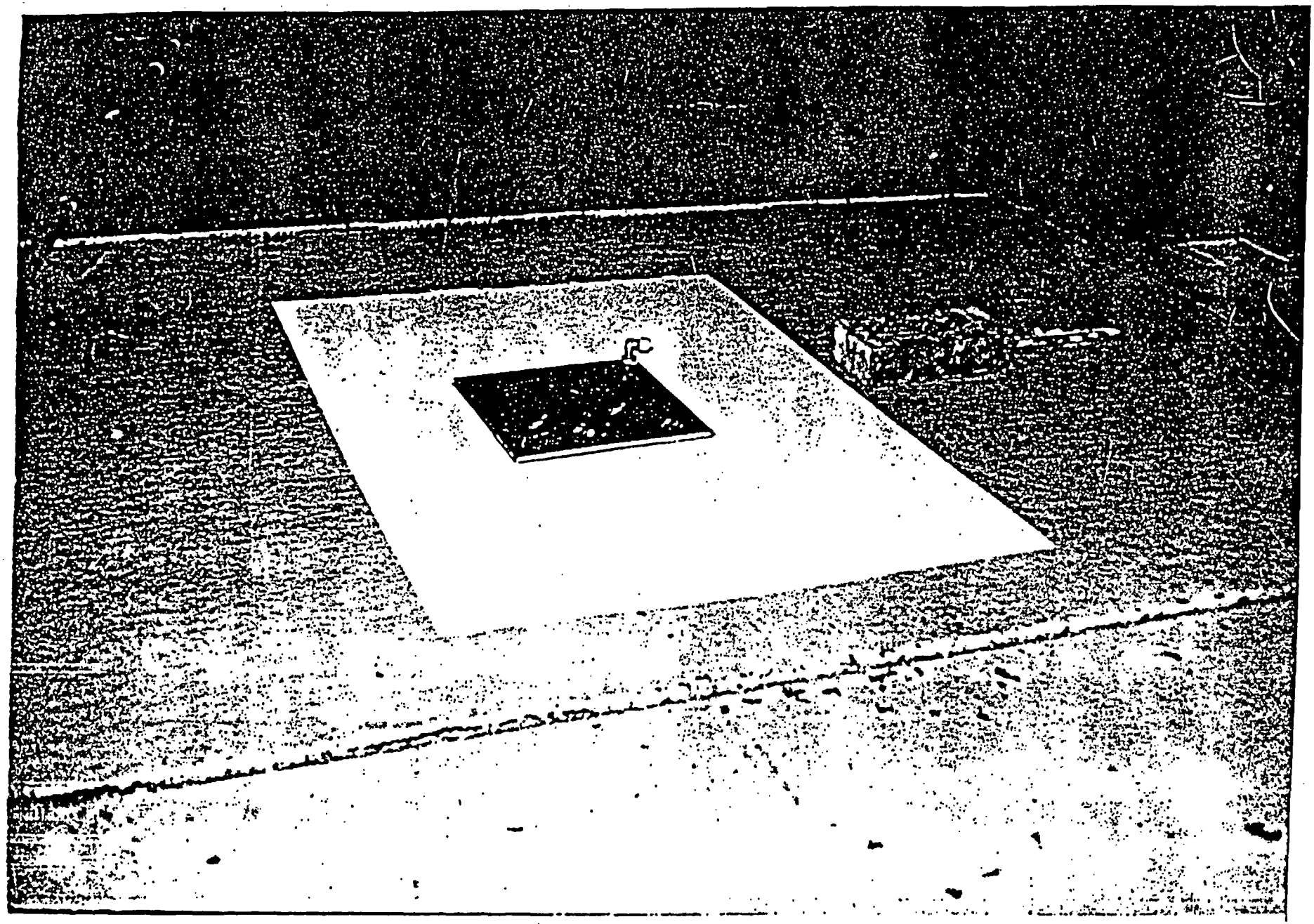

BORAL Enclosed in 304 Stainless Steal Showing
Nipple Through Which Water Was Inserted
FIGURE 1

DATA:

BORAL: 35% B_4C, .177 x9 x9 inches.

Enclosure: Type 304 stainless steel, .018" thick.

Solution: 20 ml of 2000 ppm boron, pH of 5
1.23 gm of H_3BO_3 per 100 ml distilled water

Storage Pool Temperature: approx. 100° F.

Storage Period: January 1976 to February 1977.

RESULTS: On February 8, 1978, the stainless enclosure was removed from the BORAL™ plate. The BORAL™ plate was lightly rust colored in the areas that had been covered with boric acid solution. No pitting, corrosion damage, or other physical damage was observed.

CONCLUSION OF MATERIALS TEST: The total lack of corrosion damage, except for the surface discoloration, indicates the probable useful life of BORAL™ when in contact with the PWR pool and stainless steel to be several times greater than the test period of one year. It is therefore assumed that this design will provide a useful life greater than forty years when used in a pressurized water reactor (PWR) storage pool even in the event a leak should occur in the stainless enclosure.

1.2.2.2 SFSM Test

A test of the ability of the Brooks & Perkins SFSM to withstand the environment of a PWR storage pool has been conducted. The test conditions represented a postulated leak in the stainless steel covering and the most adverse environmental conditions likely to occur during normal operation of the storage pool.

Twelve (12) test samples were fabricated in accordance with Figure 2. The four Boral panels in each sample were weighed prior to assembly. The ends were sealed by welding and two (2) 0.062 dia. holes were drilled through the outer skin at the weld point.

Two water baths were prepared as shown in Figure 2, one with a pH of 4.0 and the second with a second with a pH of 10.5. The test solutions were monitored and adjusted every seven days to maintain the proper pH value. Temperature of each bath was 100° F. The samples were then removed from the baths in the order shown in Table 1 so as to not lose any entrapped water within the tubes.

TABLE 1

	Bath 1	Bath 2	Total Test Days
Sample No.	1	7	7
	2	8	30
	3	9	60
	4	10	90
	5	11	180
	6	12	365

The water entrapped within the walls of the samples was drained into a beaker and the p H value record. The samples were cut open at the corner, in order to not damage the center Boral panels. However, damage did occur to Samples 1, 2, 3, 5, and 6, as noted in Appendix A.

The samples were then washed with a soft brush in a mild abrasive and detergent solution, followed by a rinse of clean water and alcohol. Finally, the panels were dried in a 250 °F oven for three hours, followed by a cycle at 600 °F for three hours.
The following measurements were then made:

1. Weight of each Boral panel were recorded and the corrosion weight change in milligrams per square centimeter per year was calculated.

2. If pitting was present, the depth of the four major pits are to be recorded and the average pit penetration in mils of an inch per year determined.

DISCUSSION: The samples taken from the first bath had an average pH value of 5.67 and the entrapped water taken from the tubes averaged 6.33. Sample No. 5 did not have enough liquid to measure. All samples experienced a weight gain which varied from a MCY (milligrams per square centimeter per year) of +0.238 to +10.285. Sample No. 2 had a blue coating which was attributed to some copper wire or particles that came in contact with the bath.

The second bath had an average pH value of 10.22 during the period. The entrapped water in samples No. 7 through No. 12 which which were in this solution, had an average pH reading of 10.90. Table 2 shows a MCY range of +1.302 to + 74.39 for Samples No. 12 and No. 7.

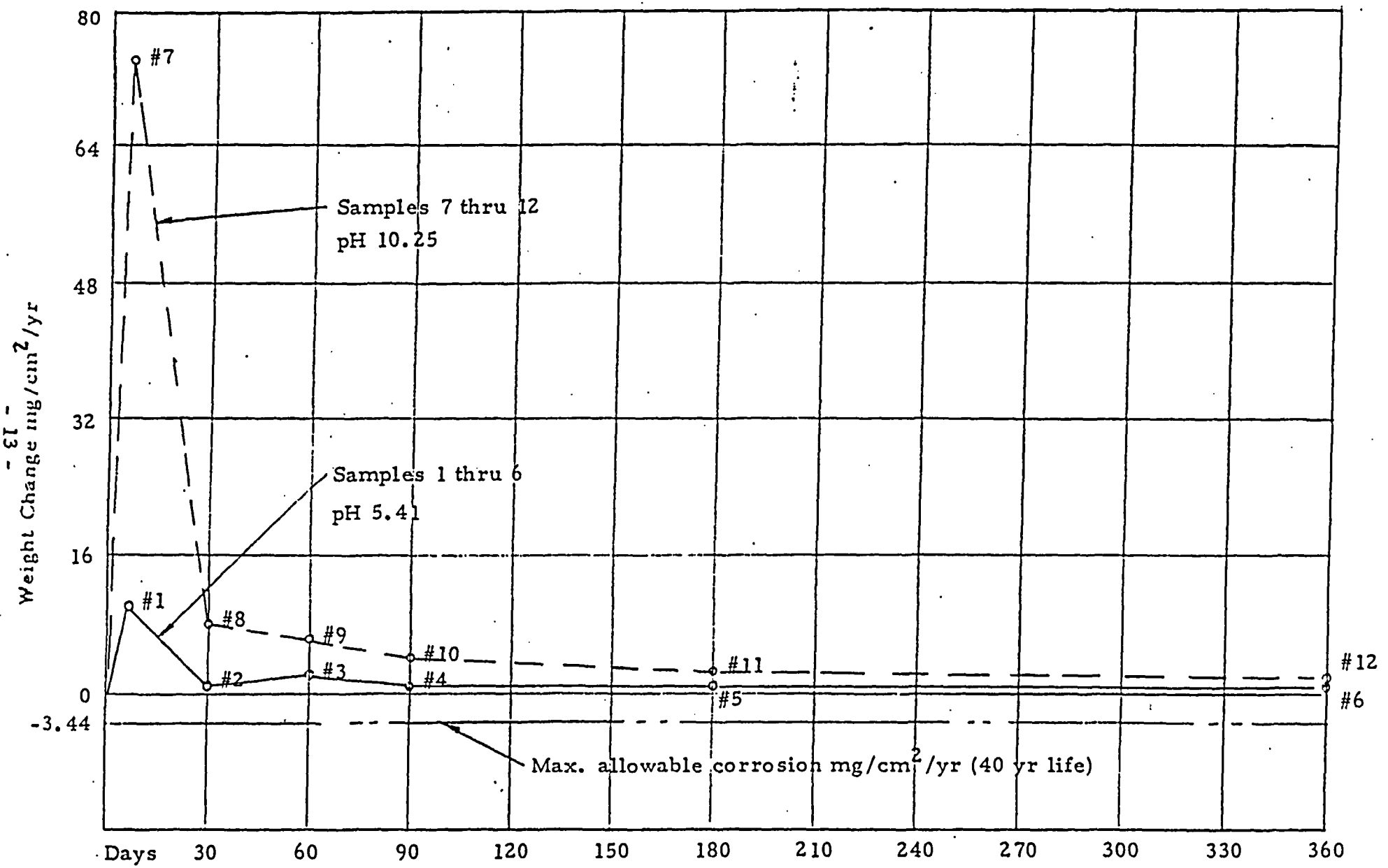

Figure 3- Corrosive Rate
Samples 1 - 6 and 7 - 12, 7 to 360 Days

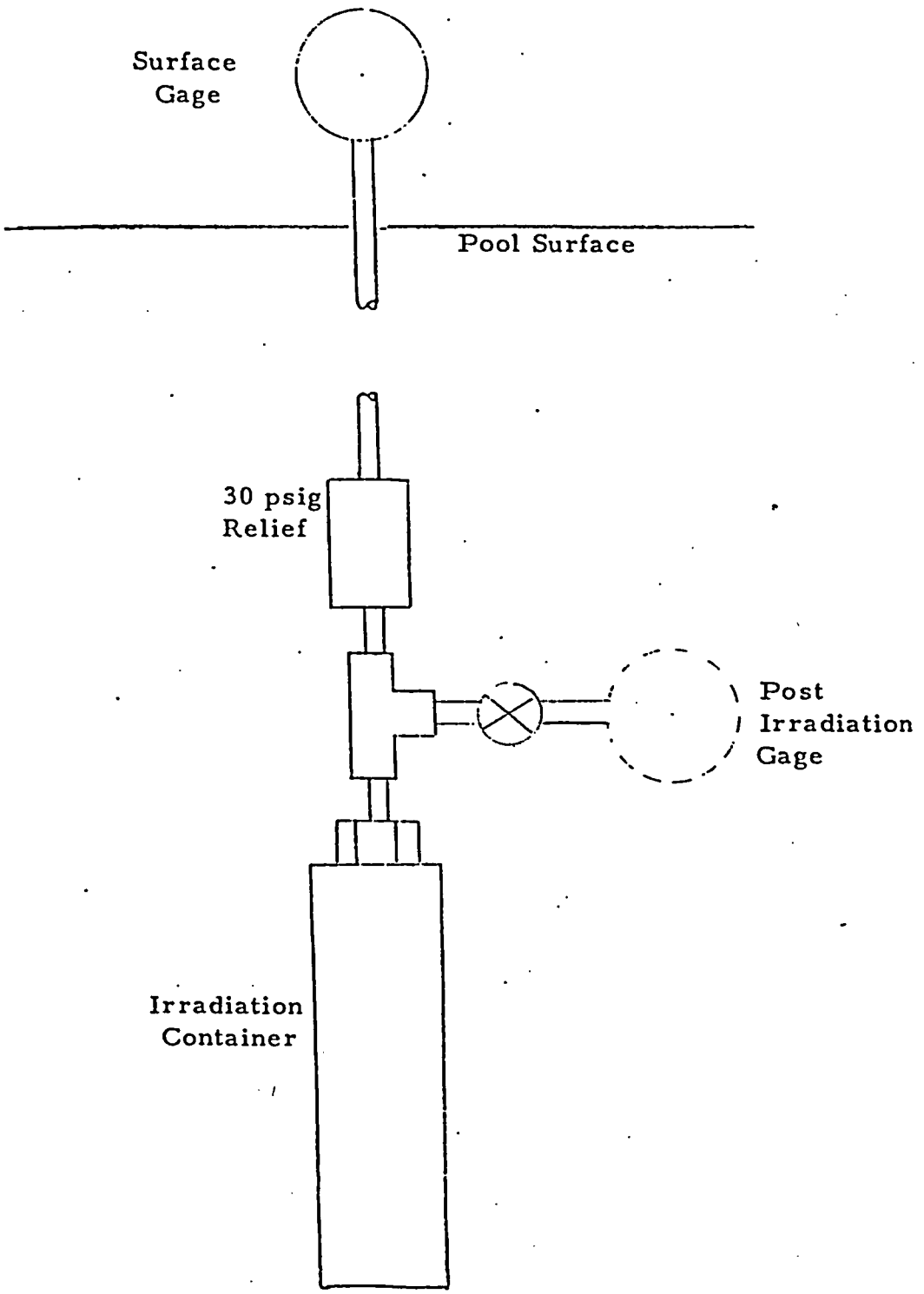

MATRIX MATERIAL IRRADIATION CONTAINER

Figure 4

attached to a threaded fitting at the top of the cylinder to enable: 1) Attachment of a pressure relief valve set at 30 psig and 2) Attachment of a valved gage tapoff for pressure measurement. The total volume of tubing and connectors was approximately 0.8cc. The in line relief valve relieved to a long aluminum tube that extended from the irradiation position to the pool surface. A gage was attached to the tube above the pool surface.

If gas pressure built up during irradiation above the point of lifting the relief valve, the pressure would have been detected on the surface gage. Following irradiation, a gage was attached to the container to measure pressure built up by gas evolution during irradiation.

The samples were exposed to radiation over 5 minute and 75 hour periods. The radiation exposure of these tests is listed in Table 3.

TABLE 3

40 YEAR AND TEST CUMULATIVE

RADIATION EXPOSURE

Radiation Type	40 Year Exposure	5 Min. Test Exposure	75 Hr. Test Exposure
Neutron (n/cm^2)			
Thermal (< 1 Mev)	4.29×10^{13}	4.50×10^{13}	4.05×10^{16}
Epithermal	-	1.38×10^{11}	1.24×10^{14}
Fast (1 Mev)	-	6.00×10^{12}	5.40×10^{15}
Gamma (rad)	8.00×10^{12}	1.67×10^{6}	1.50×10^{9}

RESULTS: Test resulted in no gas evolution detected during or following the 5 minute and 75 hour irradiation.

2.2 Irradiation of SFSM With and Without Leak in Stainless Steel Covering

A test was conducted to observe the reaction of BORAL plates encased in stainless steel jackets under gamma and neutron flux irradiations.

METHOD: Each BORAL sample was a 9 inch x 9 plate of 0.26 inch thickness. Each plate was encased in a thin, watertight jacket of stainless steel welded around the edges. A threaded connection was welded in the upper right corner of the face on one side of the stainless steel jacket. Irradiations were conducted in the Ford Nuclear reactor pool at depths of 12 and 20 feet. An aluminum tube was run from the connection to the surface of the reactor pool for pressure measurements and gas collection.

Prior to testing, each sample plate was baked at 200 °C for seven hours ina vacuum oven to remove moisture.

Each sample was tested to 10 P SIG internal pressure. Experimental pressures were limited to 5 P SIG as a reactor safety precaution.

Experimental measurements were made of pressure within each sample. Gas evolved during the tests was collect and analyzed. It was decided that temperature would not be measured. Each sample was observed after irradiation for damage due to pressure, temperature, or other effects.

Each sample was pressurized momentarily to 10 P SIG as it was inserted into the reactor pool to verify watertightness. Once each sample was placed in its experimental position, a 30 inch Hg vacuum was drawn to evacuate as much air as possible. The starting pressure for each test was the 30 inch Hg vacuum.

EXPERIMENTAL CONDITIONS: The experimental sequence consisted of twelve steps derived from a combination of four different sample plates being subjected to three different irradiation conditions.

Sample 1 was a sealed, dry sample vented only through the gas collection line to the surface of the reactor pool. Sample 2 was identical to Sample 1 except that 25 ml of distilled water was injected within the stainless steel jacket. Sample 3 and Sample 4 were identical to Sample 1 except that 70 ml and 20 ml, respectively, of 2000 PPM boron solution were injected within the stainless steel jacket. The 2000 PPM boron solution was obtained by dissolving 1.23 grams of boric acid, H_3BO_3, in 100 ml of distilled water.

Initially, in Condition 1, each sample was irradiated adjacent to spent reactor fuel in a gamma flux of 2×10^5 rad/hr. In Condition 2 each sample was placed in a holder adjacent to the reactor operating at a power level of 2 MW. The Condition 2 gamma flux was 4×10^7 rad/hr and thermal neutron flux was approximately 1×10^{12} N/cm^2/sec, or 1×10^7 rad/hr. Finally, in Condition 3, each sample was left adjacent to the reactor core immediately after shutdown. Neutron flux was quite low, approximately five orders of magnitude below operating levels, while gamma flux was measured as 1.2×10^6 rad/hr.

RESULTS: Table 4 summarizes the observed effects of irradiation conditions on the BORAL samples. The total hours of irradiation per sample are noted in the array.

No pressure increase or gas evolution was observed under any condition for Sample 1, the dry sample, or Sample 2, the sample containing 25 ml of distilled water.

Sample 3 and Sample 4, the samples containing boron solutions, both generated gas when subjected to Condition 2, reactor at power and an irradiation flux of gamma rays and neutrons. Figure 5 is a plot of sample pressure increase as a function of time and dose. Gas was drawn from each sample and analyzed with a gas chromatograph. The results were:

Sample Gas Constituents (%)

Sample	Hydrogen	Oxygen	Nitrogen
3	6.5	20.4	73.1
4	41.1	21.6	37.3
4	41.0	21.8	37.2

The hydrogen percentage of Sample 3 was lower than might be expected, an approximate 2:1 hydrogen - oxygen ratio, because Sample 3 was not purged extensively prior to sampling. The chromatograph analysis results are included in Appendix B.

When Sample 3 and Sample 4 were subjected to gamma flux alone, gas was not evolved and no pressure increase was detected with irradiation time.

CONCLUSION: Under irradiation fluxes and water conditions expected in a power reactor spent fuel pool, the BORAL samples tested exhibited no detectable gas evolution, pressure build-up, or damage due to temperature or other effects.

2.3 Helium Generation.

The well known reaction

$$ {}_0N^1 + {}_5B^{10} \longrightarrow {}_3Li^7 + {}_2He^4 $$

	SAMPLE 1 9" x 9" BORAL Plate Stainless Steel Jacket Dry	SAMPLE 2 9" x 9" BORAL Plate Stainless Steel Jacket 25 ml Distilled Water	SAMPLE 3 9" x 9" BORAL Plate Stainless Steel Jacket 70 ml - 2000 PPM Boron	SAMPLE 4 9" x 9" BORAL Plate Stainless Steel Jacket 20 ml - 2000 PPM Boron
CONDITION 1 Spent Fuel γ - 2×10^5 Rad/hr N - Negligible	42 Hours No Detectable Effect	25 Hours No Detectable Effect	19 Hours No Detectable Effect	4 Hours No Detectable Effect
CONDITION 2 Reactor at 2 MW γ - 4×10^7 Rad/hr N - 1×10^7 Rad/hr	24 Hours No Detectable Effect	6 Hours No Detectable Effect	48 Hours Linear pressure increase with irradiation time. Gas Analysis: 6.5% Hydrogen 20.4% Oxygen	152 Hours Linear pressure increase with irradiation time. Gas Analysis: 41.1% Hydrogen 21.6% Oxygen
CONDITION 3 Reactor Shutdown γ - 1.2×10^6 Rad/hr N - Negligible	4 Hours No Detectable Effect	4 Hours No Detectable Effect	12 Hours No Detectable Effect	96 Hours No Detectable Effect

Table 4

Observed Effects of Irradiation Conditions on BORAL Samples

Figure 5

Sample Pressure Profile

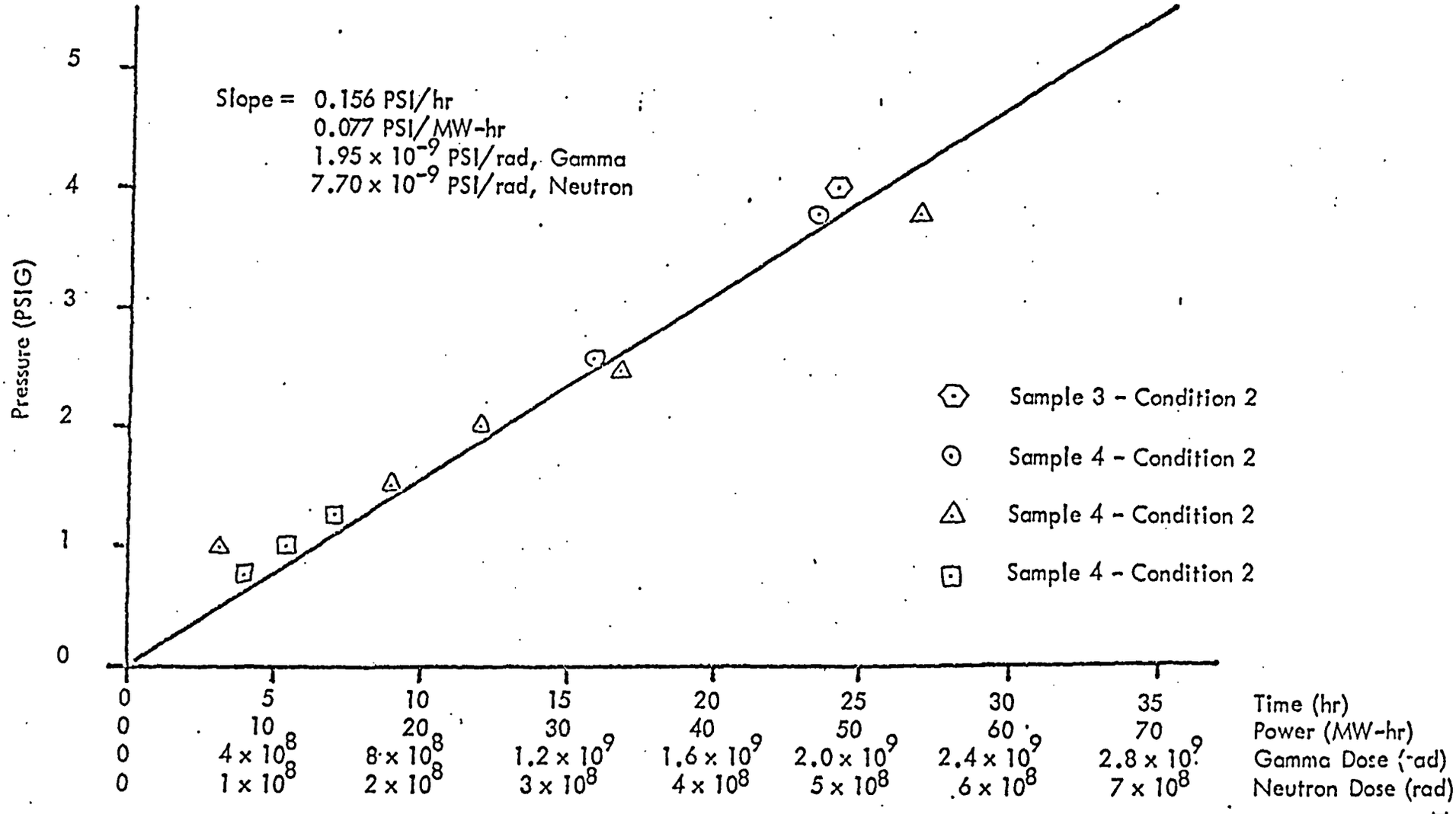

has been cause for concern over the possibility of Helium gas generation and consequential pressure build-up in a storage tube during irradiation. Testing has shown no detectible generation of Helium during irradiation. This concern may be further satisfied by considering that all neutrons which strike the BORAL are thermal neutrons and are absorbed by boron - 10.

Then consider the following calculations:

$\phi = 10^4$ n/cm^2/sec Average Flux

BORAL Area/tube = 3.4×10^4 cm^2

Void between BORAL and tube = 130cc

Void in BORAL core/tube = 300cc

Seconds in 40 years = 1.26×10^9

$\phi = 10^4 \times 1.26 \times 10^9 = 1.26 \times 10^{13}$ molecules/cm^2 over 40 years

$1.26 \times 10^{13} \div 6.023 \times 10^{23} = 2.1 \times 10^{-11}$ moles/cm^2 of He over 40 years

$2.1 \times 10^{-11} \times 3.4 \times 10^4 = 7 \times 10^{-7}$ moles/tube of He over 40 years

$7 \times 10^{-7} \times 22.4 \times 10^3 = 1.6 \times 10^{-2}$ cc/tube @ STP of He in 40 years

Pressure @ 150 F = 1 atm $\times 1.6 \times 10^{-2} \times [(273 + 66) \div (273 \times 430)]$
$= 4.6 \times 10^{-5}$ atm

The pressure rise for the 40 year period of 4.6×10^{-5} atmosphere or .0007 pounds per square inch is insignificant when considering the internal gauge pressure to cause a buckling of the tube walls is in excess of 5 pounds per square inch and that the pool water exerts an external pressure of 17 psi under 40 feet of water.

APPENDIX A

SFSM TEST, FINAL RESULTS

Sample No.	Days	pH Bath	pH Sample	Area (inches)	Area (cm)	Exposed Area (cm)	Mg. Wt. Change	mg/cm^2/yr
1-1	7	6.85	6.40	25.32	156.903	313.806	+ 60.3	+10.020
1-2	7	6.85	6.40	25.32	156.903	313.806	N/A	N/A
1-3	7	6.85	6.40	25.32	156.903	313.806	+ 67.4	+11.199
1-4	7	6.85	6.40	25.32	156.903	313.806	+ 58.0	+ 9.637
Avg.								+10.285
2-1	31	6.6	6.0	24.40	157.42	314.84	+ 20.8	+ 0.778
2-2	31	6.6	6.0	24.54	158.32	316.64	N/A	N/A
2-3	31	6.6	6.0	24.71	159.42	318.84	+ 23.4	+ 0.864
2-4	31	6.6	6.0	24.50	158.06	316.12	+ 13.5	+ 0.503
Avg.								+ 0.715
3-1	60	4.6	6.4	25.11	162.00	324.00	+206.2	+ 3.872
3-2	60	4.6	6.4	24.73	159.55	319.10	N/A	N/A
3-3	60	4.6	6.4	24.40	157.42	314.84	N/A	N/A
3-4	60	4.6	6.4	24.40	157.42	314.84	+ 18.3	+ 0.354
Avg.								+ 2.113
4-1	90	5.41	6.5	24.38	157.295	314.590	+153.9	+ 1.984
4-2	90	5.41	6.5	24.38	157.295	314.590	+138.6	+ 1.787
4-3	90	5.41	6.5	24.40	157.428	314.856	+ 23.4	+ 0.301
4-4	90	5.41	6.5	24.34	157.032	314.064	+ 53.6	+ 0.692
Avg.								+ 1.191
5-1	180	4.9	*	24.19	156.06	312.12	N/A	N/A
5-2	180	4.9	*	24.22	156.28	312.56	+154.5	+ 1.002
5-3	180	4.9	*	24.10	155.48	310.96	+135.4	+ 0.883
5-4	180	4.9	*	24.25	156.45	312.90	+ 76.4	+ 0.495
Avg.								+ 0.793
6-1	360	4.1	*	24.20	156.129	312.258	N/A	N/A
6-2	360	4.1	*	24.30	156.774	313.548	+ 22.8	+ 0.074
6-3	360	4.1	*	24.34	157.032	314.064	+ 55.5	+ 0.175
6-4	360	4.1	*	24.34	157.032	314.064	+147.9	+ 0.466
Avg.								+ 0.238
Avg.		5.41	6.33					

*. No measurable amount; "N/A"= Not Applicable because sample damaged during removal from stainless steel shrouds.

FINAL RESULTS - BATH NO. 1

Sample No.	Days	pH Bath	pH Sample	Area (inches)	Area (cm)	Exposed Area (cm)	Mg. Wt. Change	mg/cm^2/yr
7-1	7	10.97	12.0	24.32	156.903	313.806	+484.7	+80.539
7-2	7	10.97	12.0	24.36	157.161	314.322	+452.9	+75.132
7-3	7	10.97	12.0	24.40	157.419	314.838	+459.3	+76.068
7-4	7	10.97	12.0	24.34	157.025	314.05	+392.6	+65.848
Avg.								+74.397
8-1	31	9.3	*	25.93	167.295	334.590	+315.1	+11.088
8-2	31	9.3	*	25.95	167.439	334.878	+241.3	+ 8.484
8-3	31	9.3	*	25.89	167.022	334.044	+195.4	+ 6.887
8-4	31	9.3	*	25.91	167.165	334.330	+154.2	+ 5.431
Avg.								+ 7.973
9-1	60	10.38	*	24.17	155.94	311.88	+344.5	+ 6.719
9-2	60	10.38	*	24.14	155.74	311.48	+345.3	+ 6.744
9-3	60	10.38	*	24.36	157.16	314.32	+375.1	+ 7.260
9-4	60	10.38	*	24.71	159.42	318.84	+354.8	+ 6.769
Avg.								+ 6.873
10-1	90	10.25	10.5	24.50	158.071	316.143	+194.6	+ 2.496
10-2	90	10.25	10.5	24.06	155.225	310.450	+524.0	+ 6.845
10-3	90	10.25	10.5	24.40	157.419	314.838	+352.3	+ 4.545
10-4	90	10.25	10.5	24.44	157.677	315.354	+218.0	+ 2.804
Avg.								+ 4.173
11-1	180	10.2	10.2	24.42	157.549	315.098	+395.4	+ 2.545
11-2	180	10.2	10.2	24.46	157.807	315.614	+388.2	+2.494
11-3	180	10.2	10.2	24.339	157.026	314.052	+428.8	+ 2.769
11-4	180	10.2	10.2	24.269	156.575	313.150	+459.8	+ 2.927
Avg.								+ 2.696
12-1	360	10.4	*	23.99	154.774	309.548	+362.1	+ 1.157
12-2	360	10.4	*	24.06	155.225	310.450	+359.6	+ 1.146
12-3	360	10.4	*	24.40	157.419	314.838	+511.7	+ 1.608
12-4	360	10.4	*	24.36	157.161	314.322	+411.5	+ 1.295
Avg.								+ 1.302
Avg.		10.25	10.9					

* No measurable amount

FINAL RESULTS - BATH NO. 2

APPENDIX B

CHROMATOGRAPH ANALYSIS OF

GAS EVOLVED BY IRRADIATION OF SFSM

G.C.# 13 V.S.# 16

TABLE II

ANALYSIS SHEET
Van Slyke Apparatus

Rad No. _____

Run No. 1 Vessel No. 2

Original Sample SAMPLE 5 - BORAL PLATE IN STAINLESS JACKET

Sample, as measured _____

Radiation Source/Location CUP 2 - REACTOR Date 1-29-76

Dose Rate γ - 4×10^7 ON' - 1×10^7 rads/hr

Irradiation Time _____ Total Dose _____ rads

Flow Rate 300 cc/MIN Col.#1 10 cc/20.0 sec Col.#2 10 cc/20.0 sec

Baragraph 29.95 Humid. 25 % Temp. 73°F

V.S. Temp. 22.4 Vol. 0.823 cc

1ST SAMPLE, AFTER 1 PURGE

	P_i	P_o
	522.1 mm	138.4 mm
	522.4 mm	138.6 mm
	522.0 mm	138.5 mm
3	1566.5	
		3)
P_i ave	522.17 mm	P_o ave 138.5 mm
P_o ave	138.5 mm	
P_T	353.67 mm	

TF2 Closed 2:30 time

Loop Loaded _____ time

Run Start 2131 time

Total Time 1 MIN

Integrator Data

1 FILE 3
1296 ID

40	20	10	PW
30	30	30	SS
3	3	3	FR
5	5	5	BL
400	200	1	TI
		2	T4
		70	T5
		100	MA
		50	PL
		50000	ML
			SP

830 SEC RUN

Sensitivity Factors Used — Summary Sheet — Date CALC. PRESS

1	H_2	1.400×10^{-4}	H_2/1-6	5-2-75	146.20 mm = 41.1%
2	O_2	1.408×10^{-3}	O_2/1-2	9-8-75	76.77 = 21.6%
3	N_2	1.704×10^{-3}	N_2/1-2	9-10-75	132.59 = 37.3%
4	WITHIN 7.3% OF MEASURED = 355.56 mm				100.0%
5					
6					
7					

TIME		AREA
127	H_2	1044272
250	O_2	54527
587	N_2	77813
		1176612

TIME	CONC
127	88.752
250	4.634
587	6.613
	99.999

COMMENTS:

attest: Reed R Burn

2/12/76

G.C.# 1 & V.S.# 1

TABLE I

ANALYSIS SHEET
Van Slyke Apparatus

Rad No. _____

Run No. 1 Vessel No. NO I.D.

Original Sample SAMPLE 2 - BORAL PLATE IN STAINLESS JACKET

Sample, as measured _____

Radiation Source/Location CUP 2 - REACTOR Date 1-19-76

Dose Rate γ - 4×10^7 $\alpha N'$ - 1×10^7 rads/hr

Irradiation Time _____ Total Dose _____ rads

Flow Rate 30.3 cc/MIN. Col.#1 10 cc/19.8 sec Col.#2 10 cc/20.0 sec

Baragraph 30.15 Humid. 21 % Temp. 74°F

V.S. Temp. 22.3°C Vol. 0.823 cc

	P_i	P_o
	474.0 mm	138.6 mm
	473.0 mm	138.8 mm
	472.7 mm	138.7 mm
	3) 1419.7	3) —
P_i ave	473.23 mm	P_o ave 138.7 mm
P_o ave	138.7 mm	
P_T	334.53 mm	

TF2 Closed 2:32 time

Loop Loaded _____ time

Run Start 2:33 time

Total Time 1 MIN.

Integrator Data

\# 1 FILE 3
1196 ID

40	20	10 PW
30	30	30 SS
3	3	3 FP
5	5	5 BL
400	200	1 T1
		2 T4
		70 T5
		100 HA
		50 PL
		50000 HL
		SP

900 SEC RUN

	Sensitivity Factors Used		Summary Sheet	Date
1	H_2	1.40×10^{-4}	H_2 1-6	5-2-75
2	O_2	1.408×10^{-3}	O_2 1-2	9-8-75
3	N_2	1.704×10^{-3}	N_2 1-2	9-10-75
4				
5				
6				
7				

CALC. PRESS.

21.14 = 6.5%

66.14 = 20.4%

237.37 = 73.1%

324.65 mm

WITHIN 3% OF MEASURED

TIME		AREA	
124	N_2	151011	
249	O_2	46972	3
415	NOISE	370	2
587	N_2	139299	3
		337652	

TIME	CONC	
124	44.734	
249	13.911	3
415	.110	2
587	41.255	3
	100.000	

COMMENTS:

Attest: Rad R Burn
2/12/76

G.C.# 1B V.S.# 1B

TABLE III

ANALYSIS SHEET
Van Slyke Apparatus

Rad No. ______

Run No. 2 Vessel No. 2

Original Sample SAMPLE 3-BARAL PLATE IN STAINLESS JACKET

Sample, as measured ______

Radiation Source/Location CUP 2 - REACTOR Date 1-27-76

Dose Rate γ - 4X10^7 n' - 1X10^7 rads/hr

Irradiation Time ______ Total Dose ______ rads

Flow Rate 30.0 cc/MIN Col.#1 ____ cc/ ____ sec Col.#2 ____ cc/ ____ sec

Baragraph ______ Humid. ______ % Temp. ______

V.S. Temp. 22.7°C Vol. 0.823 cc

P_i	357.1 mm	P_o	138.1 mm
	356.6 mm		138.1 mm
	356.6 mm		138.3 mm
3)	1070.3	3)	414.5
P_i ave	356.77 mm	P_o ave	138.17 mm
P_o ave	138.17 mm		
P_T	218.6 mm		

TF2 Closed 3:00 PM time

Loop Loaded ______ time

Run Start 3:01 time

Total Time 1 MIN.

Integrator Data

\# 2 FILE 3
1296 ID

40	20	10	PW
30	30	30	SS
3	3	3	FP
5	5	5	BL
400	200	1	T1
		2	T4
		70	T5
		100	MA
		50	PL
		50000	HL
			SP

840 SEC RUN

TIME		AREA
126	H_2	596793
251	O_2	31622
587	N_2	44487
		672902

TIME	CONC
~~126~~	~~88.669~~
~~251~~	~~4.699~~
~~587~~	~~6.611~~
	~~99.999~~

	Sensitivity Factors Used		Summary Sheet	Date	CALC. PRESS	
1	H_2	1.520×10^{-4}	H_2/1-6	5-2-75	83.55mm	= 41.0%
2	O_2	1.408×10^{-3}	O_2/1-2	9-8-75	44.52	= 21.8
3	N_2	1.704×10^{-3}	N_2/1-2	9-10-75	75.81	= 37.2
4			WITHIN 6.7% OF MEAS. PRESS.		203.88	100.0%
5						
6						
7						

COMMENTS:

Attest: Reed R Burn
2/12/76

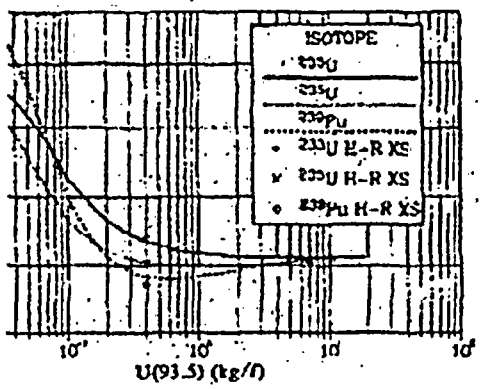

isotope worth of H_2O: reflected optimal cylin- fuel body.

he code provides this ratio as a function of the he absorbing material along a selected trace ore.
udy, a trace along the central axis of an optimal ider was used. For the comparison of the isotope alue at the center of the system was chosen to effects of the boundaries. The results of the cal- shown in Table I and plotted in Fig. 1. The val- shown correspond to the peak values at the : cylinders.
rvative for fuel storage purposes to use storage n optimum moderation and the following equiv- la:

$$\text{alent g } ^{233}U = 1.0(\text{g } ^{235}U) + 1.4(\text{g } ^{233}U) + 1.7(\text{g } ^{239}Pu) .$$

ased on optimum moderation and the above for- conservative for all moderation ratios due to the e in the critical mass for all isotopes as the mod- moves away from optimum. If it were desirable t for the nonoptimum moderation in an actual , for increasing the storage limits, the effects of tion processing on the results would have to be r LWBR fuel, the ^{233}U equivalent of the bred stimated by multiplying the initial thorium load- ctor of 0.07 (based on the LWBR operating

its show that criticality limits based on optimum nd the ratios of the minimum critical masses will ve. A comparison of the results of this study and the minimum critical masses for systems of the s from several references is shown in Table II.

TABLE II

Relative Minimum Mass

RH-600 Minimum Critical[a]		TID-7016 Limit Mass[b]		TID-7028 Minimum Critical		This Study
g	Ratio	kg	Ratio	kg	Ratio	
20	1.0	0.70	1.0	0.81	1.0	1.0
70	1.54	0.52	1.32	0.59	1.37	1.3
31	1.44	0.45	1.56	0.51	1.59	1.7

critical mass.
m slurry single parameter mass limit.

Due to the uncertainties in cross-section sets used in this study, it would not be prudent to plot a set of safe curves for all moderator fuel ratios. Work is currently under way to develop such data using the SCALE physics data processors and ENDF/B-IV cross sections. However, the lack of experimental critical benchmarks for mixed isotopes in this range of moderator fuel ratios would still leave large uncertainties in the results.

1. E. D. CLAYTON, "Anomalies of Nuclear Criticality," PNL-SA-4868, Rev. 5, p. 27, Pacific Northwest Lab. (June 1979).
2. W. W. LITTLE, Jr., R. W. HARDIE, "2DB User's Manual," Rev. 1, BNWL-831, Battelle-Pacific Northwest Lab. (Aug. 1969).
3. R. W. HARDIE, W. W. LITTLE, Jr., "PERT-V—A Two Dimensional Perturbation Code for Fast Reactor Analysis," BNWL-1162, Battelle-Pacific Northwest Lab. (Sep. 1969).
4. C. R. RICHEY, "EGGNIT: A Multigroup Cross Section Code," BNWL-1203, Battelle Pacific Northwest Lab. (Nov. 1969).
5. M. A. LEWALLEN, T. J. TRAPP, "EGGNIT-II: A Multipurpose Criticality Safety Cross Section Code," draft, Battelle Pacific Northwest Lab. (Feb. 1977).
6. L. M. PETRIE, N. F. CROSS, "KENO-IV—An Improved Monte Carlo Criticality Program," ORNL-4938, Oak Ridge National Lab. (Nov. 1975).
7. G. I. BELL et al., "Los Alamos Group-Averaged Cross Sections," LAMS-2941, Los Alamos National Lab.
8. H. F. RAAB, Bettis Atomic Power Lab., Private Communication (1966).

2. Criticality Effect of Neutron Channeling Between Boron Carbide Granules in Boral for a Spent-Fuel Shipping Cask, *Alan H. Wells, Donna R. Marnon (Nuclear Assurance Corp), Ratib A. Karam (Georgia Tech)*

Commercial fixed-neutron poison materials typically consist of a mixture of a neutron absorber such as boron in an aluminum or steel matrix. The neutron absorber is not evenly distributed (homogenized) within the matrix if the boron is in the form of boron carbide particles as is the case for Boral, which can allow neutrons to pass through the Boral between the boron carbide granules without being attenuated. This intergranular channeling effect increases the transmission of neutrons through a Boral sheet and reduces the effectiveness for criticality control or neutron shielding.

A spent-fuel shipping cask fuel basket recently licensed and built by Nuclear Assurance Corporation was tested at the Georgia Institute of Technology reactor facility using a monoenergetic 0.037-eV neutron beam and a moderated ^{252}Cf source. The purpose of these tests was to demonstrate that the fuel baskets were properly manufactured with the specified 0.040 g/cm^2 ^{10}B areal density Boral sheets prior to use for shipment of Fermi-1 and EBR-II spent fuel. Calculations were later performed using the XSDRNPM computer code[1] to evaluate the effect of boron granules on the neutron transmission. The measurements and calculations showed that intergranular channeling effect is a significant phenomenum for Boral of the thicknesses typically used in spent-fuel casks, as shown in Table I. These results agree well with a previous investigation[2] and show that the granulated boron carbide

TABLE I

Experimental and Calculated Transmission Coefficients for Boral

Areal Density (g/cm² ¹⁰B)	W.R.Burrus		Wells, Marnon, Koran	
	Exp.	Calc.	Exp.	Calc.
0.030	7.0×10^{-3}	2.0×10^{-3}	---	---
0.040	---	---	4.8×10^{-6}	9.1×10^{-5}
0.060	5.6×10^{-4}	4.5×10^{-5}	---	---

Note: The experimental measurement for 0.040 g/cm² ¹⁰B includes the effect of the stainless steel of the shipping cask basket.

areal density of 0.040 g/cm² ¹⁰B is equivalent to a homogeneous areal density of 0.033 g/cm² ¹⁰B. The cask licensing calculations[3] indicated that a 25% decrease in boron content, from 0.040 g/cm² ¹⁰B to 0.030, would result in a $\Delta k/k$ of 1.7%. Thus the decrease in Boral effectiveness caused by intergranular channeling for this spent-fuel cask basket would result in an increase in k_{eff} of ~1½%.

In conclusion, the channeling of neutrons between neutron absorber particles in fixed neutron poison materials can reduce the criticality control effectiveness of the material. This effect must be included in shipping cask licensing calculations and typically could result in a change in k_{eff} of 1 or 2%. The intergranular channeling effect is caused by a particulate form of the neutron absorber and would be less significant for poison materials consisting of alloys of steel or aluminum with a boron or gadolinium neutron absorber. Such alloys could be used in future cask designs because of their contribution to the structural strength of a fuel basket and their relative insensitivity to intergranular channeling effects.

1. SCALE-2, "XSDRNPM-S, A One Dimensional Discrete Ordinates Program for Transport Analysis," CCL-430, Reactor Shielding Information Center, Oak Ridge National Lab.
2. W. R. BURRUS, "How Channeling Between Chunks Raises Neutron Transmission Through Boral," *Nucleonics*, 16, *1*, 91 (Jan. 1958).
3. "Safety Analysis Report for the NLI-1/2 Spent Fuel Shipping Cask," Rev. 17, Certificate of Compliance No. 9010 (Aug. 1986).

3. A Shielded Annular Tank for the Storage of Plutonium Solutions, *Jerry N. McKamy (Rockwell Int)*

Rockwell International's Rocky Flats plant has been involved in the investigation of cost-effective, reliable, and safe methods for the storage of high-concentration plutonium nitrate solutions during the past several years. The latest concept is the shielded annular tank (SAT). This tank design offers the advantages of high volume, relatively high floor space utilization, reduced neutron doses to operators, low maintenance costs, and easy shielding verification in a proven technology design. This paper reports results of an initial calculational study to investigate design parameters for a fissile solution storage tank based on the SAT concept. The KENO-IV code with the 16-group Hansen-Roach cross-section set was used for all the calculations.

The SAT incorporates some of the better attributes both Raschig Ring filled tanks and ordinary unshielded an lar tanks. With a floor space utilization factor of 32 ℓ/ the SAT cannot duplicate the floor space utilization c Raschig Ring filled tank but does provide a factor o improvement over that of a standard annular tank. The tron shield is not in contact with the fissile solution, wl makes inspection of the shield relatively straightforw Because the SAT is essentially isolated, spacing restricti imposed from a nuclear criticality safety standpoint are r imized. The SAT is relatively insensitive to changes in solu concentration, as are Raschig Ring filled tanks. The shiel virtually indestructible, so concerns about a sudden los absorber are mitigated. Finally, an added bonus of the S design is that it should reduce neutron radiation doses to o ators by a factor of 5.

The SAT model used in this KENO-IV calculational st is basically an annular tank with a 7.62-cm solution ann surrounded symmetrically on the inner and outer surfaces a close-fitting neutronically isolating jacket. The isolator sists of a sandwich of 0.318 cm of borated rubber, 6.35 cr polyethylene, and another 0.318 cm of borated rubber. borated rubber is a product made by Bisco called Rad-S Rad-Stop has a boron density of 0.6 g/cm³. This jacket sign has the advantage of minimizing the thicknesses of t the absorbing and moderating materials. Figure 1 shows effect of using different moderator materials. The model t has a 740-ℓ solution capacity with a 152-cm o.d. and a he of 214 cm. The nominal solution concentration of interc 150 g Pu/ℓ plutonium nitrate.

The advance in technology is due primarily to the de of the neutron absorber itself. The idea of isolating fissile s tion systems is certainly not new. This sandwich design ac a "high-pass" thermal conversion filter for neutrons. The pose is to neutronically isolate the system, while at the s time minimizing neutron return to the tank by the shield it Conventional shielding materials, such as borated polye ene, return a significant thermal neutron flux to the fi material as well as requiring an overall increase in abso thickness. The isolator used in the SAT allows the relat energetic neutron flux to exit the tank and pass through Rad-Stop without encountering a significant hydrogen cor tration. Once in the moderator, the neutrons begin to ther ize and the thermal neutrons backscattering into the tank preferentially absorbed by the boron in the Rad-Stop. neutrons that proceed outward through the moderator subsequently captured by both the hydrogen in the plastic the outer boron layer. This results in a SAT that does interact significantly with other fissile material. All th

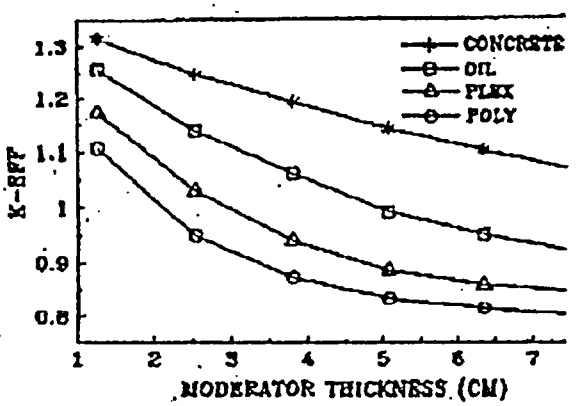

Fig. 1. Representative plot of k_{eff} as a function of mode thickness.

Please Note

Complete text contained on CD enclosed in Book 1

NUREG/CR-6407
INEL-95/0551

Classification of Transportation Packaging and Dry Spent Fuel Storage System Components According to Importance to Safety

Manuscript Completed: January 1996
Date Published: February 1996

Prepared by
J. W. McConnell, Jr., A. L. Ayers, Jr., M. J. Tyacke

Idaho National Engineering Laboratory
Managed by the U.S. Department of Energy

Lockheed Martin Idaho Technologies
Idaho Falls, ID 83415

S. C. O'Connor, NRC Technical Monitor

Prepared for
Division of Industrial and Medical Nuclear Safety
Office of Nuclear Material Safety and Safeguards
U.S. Nuclear Regulatory Commission
Washington, DC 20555-0001
NRC Job Code J5052

The Surface Treatment and Finishing of Aluminum and Its Alloys, Edition

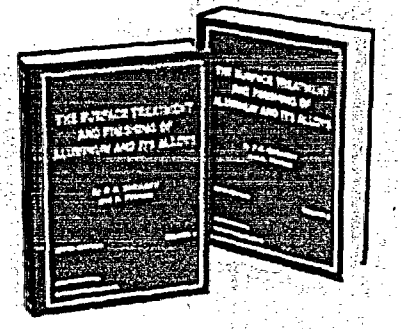

Non-Member Price: $425.0
Member Price: $375.0
Save: **$50.0**

Get EXTRA BENEFITS with a ASM Membership
Learn More

Add to Cart

Publisher: Co-published by Finishing Publications Ltd and ASM International

Stock Status: In Stock

Product Code: 06945G

Author: P.G. Sheasby and R. Pinner

ISBN/ISSN: 0-904477 5, 0-904 22-3, 0-904477-2

Format: Book & CD ROM

Product Description

Contents:
Volume 1: Introduction • Mechanical Surface Treatments And Finishes • Electrolytic and Chemical Polishing • Chemical Cleaning And Etching • Chemical Conversion Coatings and Pretreatment Films • The Fundamentals Of Anodizing • Decorative and Protective Anodizing

Volume 2: Anodizing In Architecture • Hard Anodizing • Colouring Anodic Coatings With Dyes And Pigments • Sealing Anodic Oxide Coatings • Prop And Tests Of Anodic Oxide Coatings • Plating On Aluminum • Organic Fin Vitreous Enameling • Effluent From Aluminum Finishing Operations Appendix A: Composition And Properties Of Major European And U.S. Alu Alloys Appendix B: Finishing Specifications Subject Index

Published: 2001
Pages: 1387

Format: 2 Volume Set and CD ROM

VOL. 1 0-904477-21-5; VOL. 2 0-904477-22-3; CD ROM 0-904477-23-1

Related Product(s)

ASM Handbook Volume 05: Surface Engineering
ASM Specialty Handbook: Aluminum and Aluminum Alloys
Coatings and Coating Processes for Metals
Anodizing and Coloring of Aluminum Alloys (Book and CD ROM)

Add to Cart

Customers who bought this product also bought

Membership/Subscription Renewal
Anodizing and Coloring of Aluminum Alloys (Book and CD ROM)
ASM Handbook Volume 13A: Corrosion: Fundamentals, Testing, and Pr

Oxidation of Al Powder: Report for AAR Cargo

Objectives

The report presents results from an investigation into the oxidation behaviour of pure Al powder in the range 500-550°C. The effect of heating temperature and time are discussed, as is the oxidation mechanism.

Experimental Methods

Powder Heat Treatment

Heat treatment of Al powders was performed at different temperatures, for various times, in order to vary the degree of oxidation. 150 g of powders were spread on a rectangular stainless steel tray to form a thin layer <5 mm, to ensure that air would uniformly penetrate the powder bed. The powders were oxidised in a pre-heated fan oven, in ambient air, at temperatures of 500°C and 550°C for 60, 120, 180, 240, 300, 360, 420, 480, 600 and 1200 min. After oxidation, the powders were removed and allowed to cool in air.

Oxygen and Surface Area Analysis

Oxygen and surface area analysis were performed by London & Scandinavian Metallurgical Co Limited. Oxygen analysis was carried out using a LECO TC-436AR instrument. The equipment measures oxygen content (in wt.%), to 3 decimal places, as CO_2, using an infrared detector cell. BET surface analysis of powders heat-treated at 500°C and 550°C for 60, 300, 600 and 1200 min, was performed using a Beckman Coulter SA 3100 instrument.

Characterisation

A study of the powder morphology was performed using a Philips XL30 FEG scanning electron microscopy (SEM). To prepare samples for SEM, powders were spread onto an adhesive tab mounted on a sample holder, followed by gold coating to ensure maximum conductivity. SEM was operated using a voltage of 20 kV in secondary electron mode with a spot size of 4 μm and working distance of 20 mm.

Thermogravimetric Analysis (TGA)

To study the oxidation kinetics of Al powder, thermogravimetric analysis was performed using a TA Q600 Series Thermal Analyser. Heating of as-received powders was carried out under compressed air, supplied from gas cylinders, with a flow rate of 100 ml/min at isothermal heating temperatures of 475, 500, 525 and 550°C for 1200 min. Heating up to the target temperature was conducted under nitrogen. In all cases, approximately 20 mg of powder was placed in an alumina crucible and normalisation of results for equal mass was conducted.

X-ray Diffraction (XRD)

X-ray diffraction (XRD) using a Siemens D500 Diffractometer with CuKα (λ = 1.5406) radiation was used to identify the phases present in powders. To prepare samples for XRD, powders were sprinkled onto an adhesive tab mounted on a sample holder. The diffractometer was operated at 40 kV and 20 mA with diffraction angles (2θ) ranging from 20° to 90°. A 0.01° s^{-1} step size and a 4 s dwell per step were employed. Phases present in the spectra were identified with the aid of JCPDS diffraction files.

Results and Discussion

Fig. 1 presents the variation in oxygen content for Al powder after heat treatment at 500 and 550°C for different holding times. Although there is a large scatter in the data, the general trend is that heat treatment at both 500 and 550°C results in an increase in oxygen content with heating time. The scatter, however, makes differentiation between the behaviour at 500 and 550°C difficult. Although oxidation at 550°C appears to be more rapid in the first 60 min, similar weight gains are observed for holding times longer than 600 min. This trend is also reflected in the weight gains measured after heat treatment, the results of which are shown in table 1.

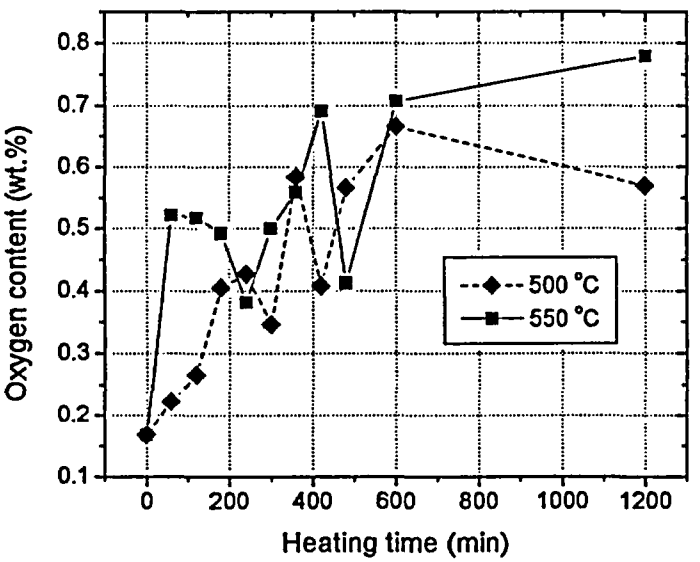

Fig. 1 Oxygen contents for Al powders heat-treated at 500 and 550°C

The large scatter in the experimental data, for both mass gain and oxygen content, is likely to be due to the changing environmental conditions in the heat treatment furnace. Due to the reasonably large powder batch sizes, the oxidation trials were conducted individually over a period of several weeks. This is likely to have lead to

variations in moisture content in the air being experienced throughout the heat treatment trials. Moisture content has been observed, by Wefers, to have a significant influence on the degree of oxidation experienced, with up to a 20% increase in oxidation in moisture-saturated air.

Heating time (min)	Weight gain (g)	
	500°C	550°C
60	0.08	0.77
300	0.47	0.93
600	0.80	0.98
1200	0.87	1.00

Table 1 Weight gains for powders heat-treated at 500 and 550°C

Table 2 shows the surface areas for as-received and heat-treated Al powders as measured by BET. Little or no increase in the surface area of heat-treated powders was observed compared with that of as-received powder. The highest surface area, of 0.15 m^2/g was measured for powders heat-treated at 500°C for 10 h and 550°C for 20 h, in keeping with the oxygen data. Wefers measured, on average, a 50nm increase in thickness of the oxide layer after prolonged heat treatment. This is less than a 0.2% increase in radius for 50-100 micron diameter powders and less than a 0.4% increase in surface area (in this case an increase of 0.00056 m^2/g). The measurements indicate that the variation in powder surface area is most likely due to experimental scatter, as real increases are expected to be below the resolution of the instrument.

Powder	Surface area (m^2/g)			
	60 min	300 min	600 min	1200 min
500°C	0.14	0.13	0.15	0.14
550°C	0.14	0.14	0.13	0.15
As-received	0.13			

Table 2 Surface area for as-received and heat-treated powders

Fig. 2 shows the morphologies of as-received and heat-treated powders. No significant difference in shape and surface roughness is observed between two powders, with no obvious signs of either nodular or thick continuous oxide film development even after prolonged heat treatment. The resolution of the instrument is roughly 50nm thus making it difficult to see all but the thickest of oxide layers.

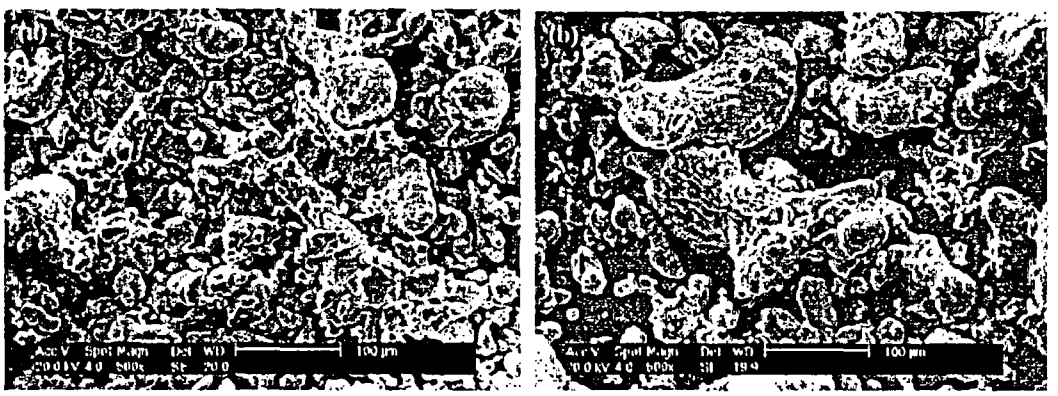

Fig. 2 Morphologies of (a) as-received and (b) powder heat-treated at 550°C for 1200 min

Fig. 3 shows TGA traces for as-received Al powders during isothermal heat treatment between 475 and 550°C for 1200 min. It is clear that in all cases the weight of the powders increases as the heat treatment time increases and that oxidation is more extensive as the heat treatment temperature increases. Different forms of the weight gain - time curves can, however, be appreciated.

At 475 and 500°C, 3 distinct regions are observed. At short times a parabolic dependence is evident which, after mass gains of roughly 0.1% becomes linear. Above weight gains of roughly 0.4-0.5%, this linear dependence becomes parabolic

once more. For oxidation at 525 and 550°C, the first parabolic stage is not clearly observed but the second transition from linear to parabolic is once more observed for weight gains in the region 0.4-0.5%.

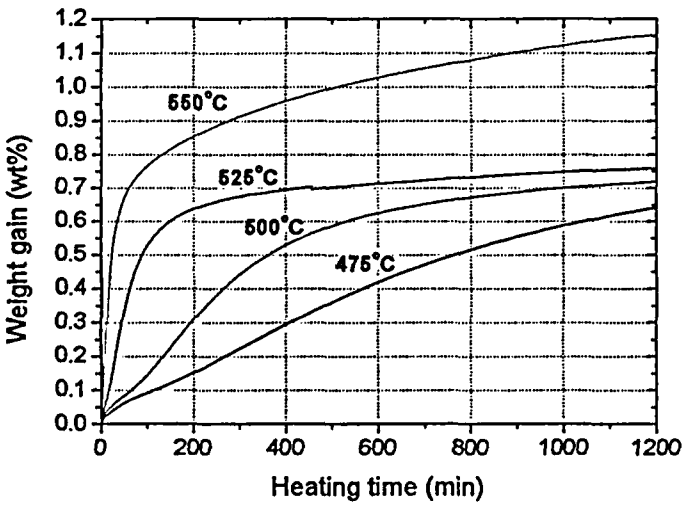

Fig. 3 TGA traces for as-received Al powders isothermally heated at 475, 500, 525 and 550°C for 1200 min

These profiles agree well with those presented by Wefers and indicate that the oxidation mechanism follows that which he proposed namely: at short holding times an amorphous oxide layer is developed and its growth requires diffusion of oxygen through this film, following a parabolic dependence. With longer holds, crystallisation of γ-Al_2O_3 occurs in the film and this cracks the protective layer, allowing oxygen to reach the underlying metal more easily. Oxidation by this mechanism is more rapid and follows a linear dependence. At longer holds still, lateral growth of the γ-Al_2O_3 occurs, blocking the cracks, eventually forming a continuous protective layer. Growth again requires diffusion of oxygen through this film, slowing down the rate of oxidation and once more following a parabolic

dependence. It should be noted that for higher temperature heat treatments the formation of γ-Al_2O_3 occurs very rapidly (within the first 5 min) thus yielding an apparent linear oxidation rate at the outset.

Fig. 4 presents an XRD pattern for powder heat-treated at 550°C for 1200 min compared with as-received powder. Although it appears that heat treatment of Al powder results in little change in the XRD pattern, the presence of a small peak corresponding to γ-Al_2O_3 can just be observed. No such peak could be observed for holds at shorter times or after 1200 min at 500°C. The level of oxide is clearly present at levels close to the resolution level of the instrument, of the order of 1-2wt%.

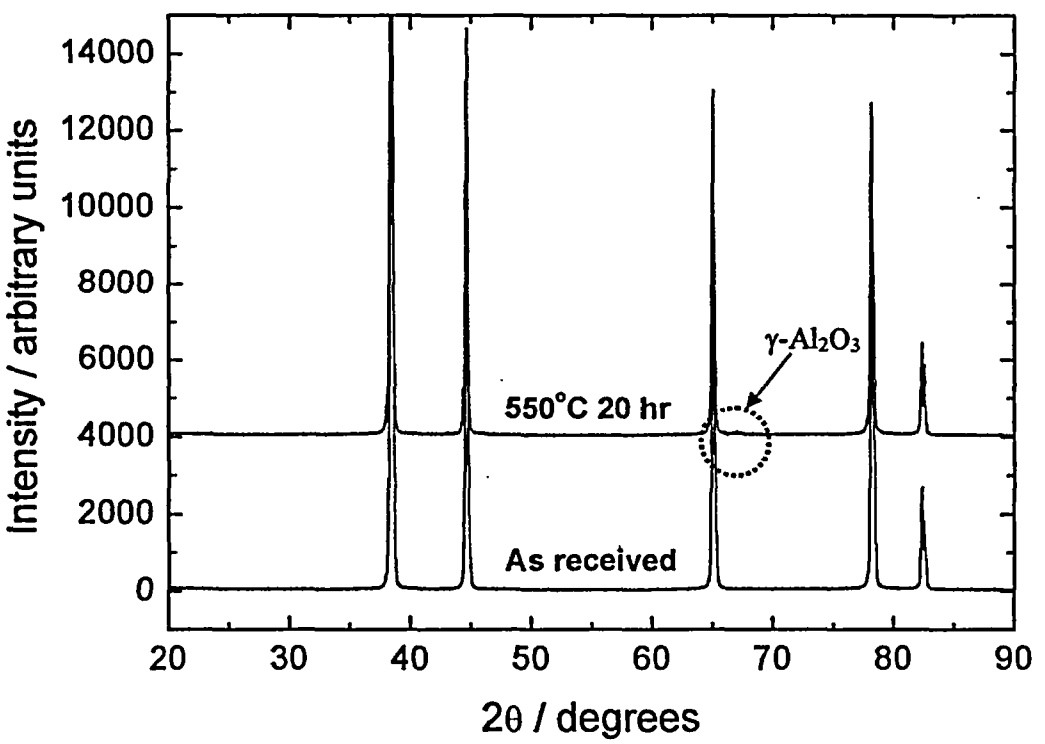

Fig. 4 XRD patterns for as-received Al powder and powder heat-treated at 550°C for 1200 min

XRD clearly shows that γ-Al_2O_3 forms during the oxidation process. TGA plots indicate that for 600 min holds, γ-Al_2O_3 should be present (as oxidation becomes parabolic once more). The low oxide to metal ratio, however, means that it is difficult to confirm or dispute the oxidation mechanism. It is not clear whether either crystallisation has not taken place at this stage or that simply the quantity of oxide present is below the resolution level of the instrument.

A note of caution

Whilst the evidence presented in Fig 3. is convincing, there was initially a great deal of confusion over the results obtained. Figs. 5 presents TGA traces at 500°C and 550°C using compressed air supplied from different gas bottles (A, B and C). Whilst it should be noted that the effect on the form of the plots, and hence the sequence of oxidation steps is unchanged, the effect on the magnitude of the weight gains is dramatic, particularly at 550°C. It was found that the moisture content in the gas bottles is variable and that this had led to the different oxidation behaviour. These measurements indicate that great caution must be taken to compare like-with-like conditions during oxidative studies.

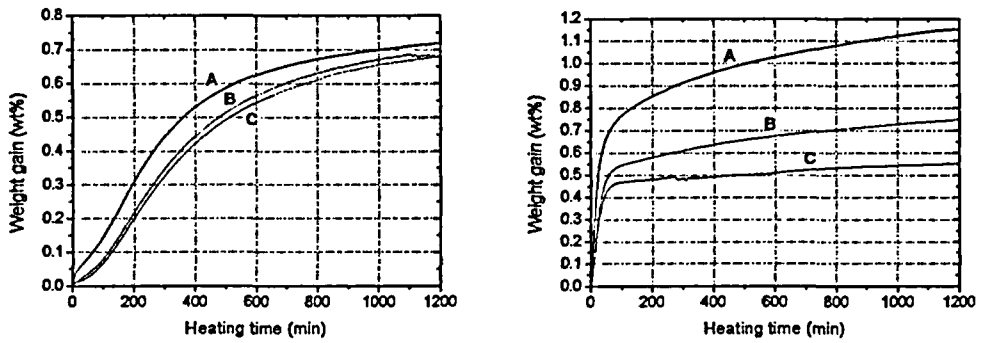

Fig. 5 TGA traces for powders isothermally heated at 500°C (left) and 550°C (right) for 1200 min, using different air cylinders

Summary

The low quantity of oxide generated during oxidation of Al powder makes measurement of oxide film thickness and structure very difficult by SEM, XRD and BET methods. Weight gain measurements enable the progression of oxidation to be studied more accurately, but care must be taken to eliminate variations in moisture content in the air (ambient or bottled) from test to test. Failure to do so can result in a large scatter in results and confusion over the relative magnitudes of oxidation at different temperatures. A reduction in scatter could be best achieved by using air first passed through a drying system.

TGA experiments enable the most precise measurement of the oxidation process and can help elucidate the oxidation mechanisms. The rate and magnitude of oxidation was found to increase with holding temperature. The oxidation behaviour of Al was found to follow three distinct stages; firstly a parabolic dependence of oxidation upon time was observed, followed by a transition to a fast linear rate and finally, after longer holding times, a slow parabolic rate was again established. The results closely follow the behaviour found by Wefers and the mechanism of oxidation proposed by him is thought to be valid for pure Al. The transition to a fast linear oxidation rate is thought to be due to cracking of the initially amorphous oxide coating as a result of crystallisation of γ-Al_2O_3. Passage of oxygen along these cracks accelerates the rate of oxidation compared to slow diffusion through the continuous amorphous layer.

Reference

Wefers, K, Properties and characterisation of surface oxides on aluminium alloys, Aluminium, 57, 11, 1981, 722-726.

Report No. : NET 230-01

Review and Evaluation of B_{10} Areal Density Measurements of BORAL Coupons

February 2004

Prepared
for
AAR Cargo Systems, Inc.
under
Purchase Order No.: 219535

Prepared
by
Northeast Technology Corp.
108 North Front Street
UPO Box 4178
Kingston, NY 12402

Rev.	Date	Prepared by:	Reviewed by:	Approved (QA):
-0-	3/25/04			

Table of Contents

Review and Evaluation of ^{10}B Areal Density Measurements of BORAL Coupons

1.0 Introduction

BORAL is the trade name for a neutron absorber manufactured by AAR Corporation of Livonia, Michigan. BORAL is a laminated panel with solid aluminum cladding and a core of blended boron carbide (B_4C) and aluminum powders, compressed by hot rolling. Boral is manufactured according to established processes and procedures.

The purpose of this test program is to provide applicants for dry fuel storage systems supporting data to request NRC approval for credit for 90% of the ^{10}B contained in BORAL used in the system. NRC Standard Review Plans limit the credit for ^{10}B contained in fixed neutron absorbers for dry fuel storage systems to 75%, unless comprehensive tests are performed to verify that the fabrication process for the neutron absorber assures the presence and uniformity of the neutron poison (^{10}B) in the absorber material.

A method has been proposed (Reference 1) for the computation of percent credit for boron-based neutron absorbers. This method specifies that "material for which data is presented to show the measured attenuation for thermal neutrons to be at or above the acceptance attenuation (A_a), is given the full credit of 90 percent." This test program was developed to meet the test requirement for 90% credit. The neutron attenuation tests, combined with the established BORAL manufacturing procedures, provide verification of the presence and uniformity of the ^{10}B in BORAL panels.

The coupons tested used in this program were provided by AAR. AAR selected the coupons from a commercial production run of 3236 BORAL panels. Production required 114 powder batches; each powder batch yields 30 panels. One panel was randomly selected from each group of 30 panels made from each unique powder batch. Two coupons were cut from random locations from each of the 114 BORAL panels selected for the test, for a total of 228 BORAL test coupons.

The coupons were rectangular and approximately 5.5 inches wide by 11.0 inches long. The minimum certified areal density for these coupons is 0.020 gms B-10/cm^2. The areal densities were measured at 4 locations on each coupon providing a total of 912 measurements. The measurements were made via neutron attenuation testing using known calibration standards to determine the areal densities.

This report documents a statistical analysis of the 912 areal density measurements which demonstrates compliance with requirements for 90% boron credit in dry storage casks. The analysis described subsequently serves to demonstrate that this criteria is satisfied for the 912 areal density measurements on BORAL coupons.

2.0 Methodology

The proposed method specifies that it "is to be used to compute the level of credit to be allowed for 1/v neutron absorber materials, such as boron or lithium. The computation of the allowed level of credit uses the results of neutron attenuation measurements performed on samples of the absorber material placed in a beam of thermal neutrons."

The standard specifies the following variables among its definitions:

A = neutron attenuation, a measured value taken on a given absorber material in a beam of thermal neutrons with fixed energy spectrum. A is assumed to be normally distributed with mean μ and standard deviation σ.

A_a = acceptance value of neutron attenuation, based on a qualified homogeneous absorber standard such as ZrB_2, evaluated at 111% (i.e.1/0.90) of the poison density assumed in the criticality computational model.

A_{tl} = attenuation tolerance limit, a statistic of the data

n = number of coupon measures of attenuation A

P = probability

μ = true mean of A

$\bar{x}$ = estimate of μ

σ = true standard deviation of A

S = estimate of σ

C_p = exact number of standard deviations required at probability P

K_p = tolerance coefficient that is substituted for C_p when μ and σ are estimated by $\bar{x}$ and S, respectively

γ = confidence level

The method specifies that, "data taken under the above rules are used to bound the probability P that the value of neutron attenuation A at an arbitrary location on the material is greater than the acceptance attenuation A_a. This is done by computing an attenuation tolerance limit, A_{tl}, such that, with 95 percent confidence, the probability is less than 0.001 that $A < A_{tl}$."

In the current analysis, the areal density has been computed instead of the neutron attenuation. The areal density is directly proportional to the neutron attenuation. The analysis described subsequently demonstrates that with 95 percent confidence the probability is less than 0.001 that the measured areal density will be less than 111% of the minimum certified areal density.

Implicit in the proposed method is the assumption that the data is normally distributed. To satisfy that this requirement has been met, two tests for normality, Kolmogorov-Smirnov and Anderson-Darling, have been applied to the test data. In addition, the cumulative probability versus areal density has been examined as a further test of normality.

3.0 Test Data

3.1 Test Method

Tests have been performed by NETCO in the Beam Hole Laboratory of the Breazeale Reactor Facility at Penn State University. In these tests a collimated thermal beam of neutrons from the reactor is passed through the Boral coupons placed perpendicular to the incident beam. The intensity of the incident and attenuated beams are measured with BF_3 detectors. These attenuation values were then converted to areal density measurements using a curve fit based on attenuation measurements on coupons of known areal density.

Four locations on each coupon were tested in this manner and the resulting data has been compiled into a single data file that was utilized for this analysis.

3.2 Raw Data

The coupon test results are contained in Appendix A. A subset of the data containing only the areal density measurements is constructed for use in the subsequent statistical analyses. The data is structured in four columns with each column representing a different measurement location on each coupon. All of the data points are plotted here to illustrate the distribution of measured areal density values.

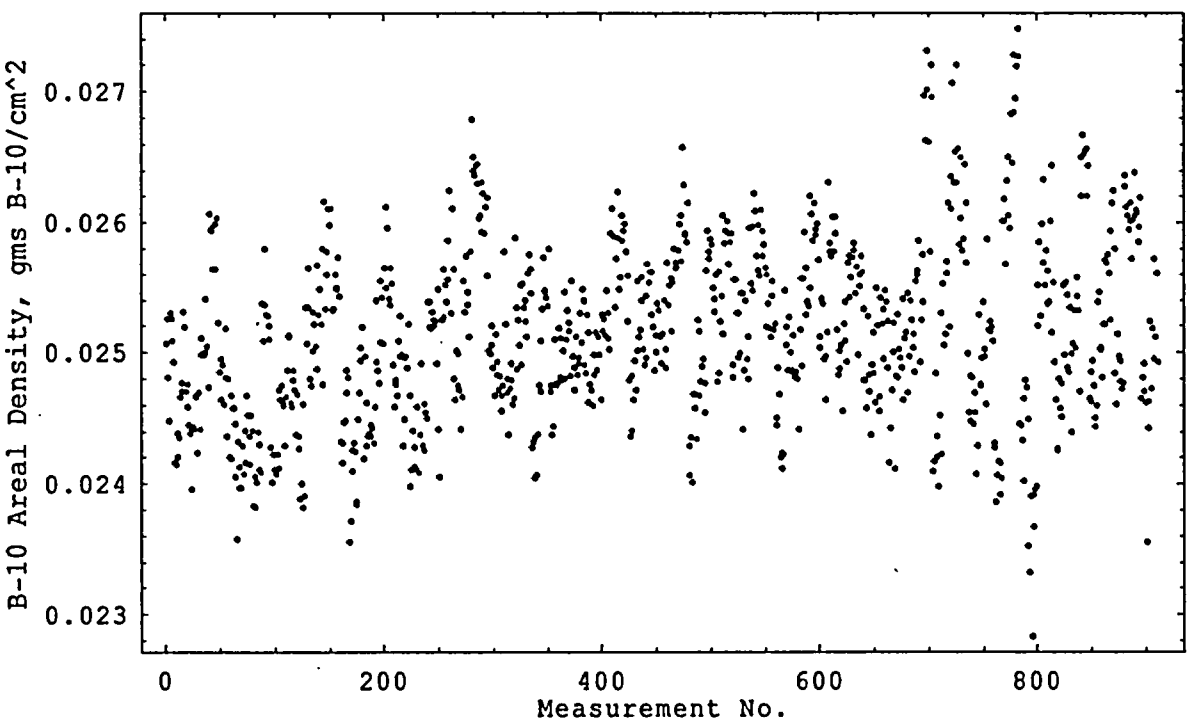

Figure 3-1: Measured Areal Density versus Measurement Number

3.3 One-Sided Tolerance Factor Calculation

The proposed method specifies that a one-sided tolerance factor be calculated to determine, with 95% confidence, the value above which 99.9% of the areal density measurements lie. The tolerance factor itself varies with the degree of confidence, fraction of data in question, and number of samples being tested. Factors have been calculated in tables for several different parameters, however, none of the available tables contain the parameters specified for this test. As such, an approximate formula for the tolerance factor is utilized to provide the necessary value given the parameters of this analysis.

The approximate calculation of a one-sided tolerance factor κ, comes from the following formulas (Reference 2):

$$K = \frac{Z_{1-P} + \sqrt{Z_{1-P}^2 - ab}}{a}$$ **Equation 1**

$$a = 1 - \frac{Z_{1-P}^2}{2(N-1)}; b = Z_{1-P}^2 - \frac{Z_{1-\gamma}^2}{N}$$ **Equation 2**

where:

Z_{1-P} = Standard Normal Score at 1 - P level of significance

N = Number of Samples (912)

These equations are an approximation, however and deviate conservatively from the tabular values in Reference 2 for smaller samples sizes. The difference between the two methods quickly approaches zero after as few as 40 samples. Given that we are working with a sample size of 912, the approximation formula will produce an adequately precise value.

The one-Sided Tolerance factor for P=0.999, α=0.05 & n=912 is calculated to be 3.22572

4.0 Analysis of Areal Density Measurements

4.1 Distributed Properties of the Areal Density Measurements

In order to apply the one sided tolerance factors described in Section 4.1, it must be demonstrated that the areal density data are normally distributed. Figure 4-1 shows the areal density measurements distribution. Table 4-1 contains a summary of the properties of the distributed data. The tests show what appears to be a normally distributed data set with a mean coupon areal density of 0.025 gms B-10/cm^2. There is a slight skewing of the data towards higher areal density values and the kurtosis shows that there is more concentration of data near the mean than in a completely normal distribution. However, these values represent a small deviation from a normal distribution and are conservative with respect to a minimum areal density evaluation.

Figure 4-1: Areal Density Measurements: Distributed Data

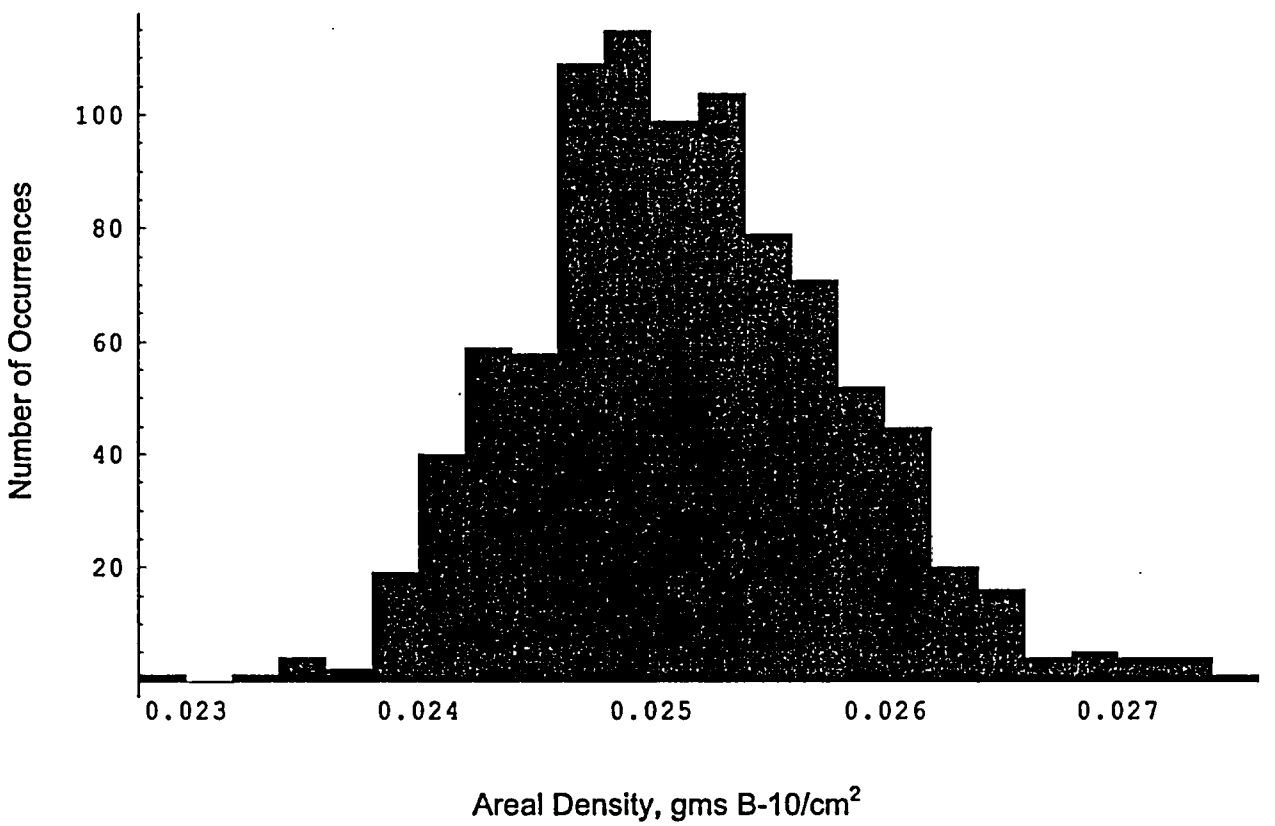

Table 4-1

Properties of the Distributed Data

Location Statistics		Dispersion Statistics		Shape Statistics	
Mean	0.0251432	Variance	4.587×10^{-7}	Skewness	0.309405
Harmonic Mean	0.0251251	Standard Deviation	0.000677	Quartile Skewness	0.056328
Median	0.0251133	Mean Deviation	0.0005399	Kurtosis Excess	0.177064
		Median Deviation	0.000447		

4.2 Test for Normality

The first step in testing for normality is to construct a cumulative probability plot from the data set. This is accomplished by arranging the data set in order of ascending areal density and computing the cumulative frequency for each data point as:

$$\frac{(j-0.05)}{10} \qquad \textbf{Equation 3}$$

For j = 1...912

Figure 4-2 is plot of the cumulative probability versus areal density. It is noted that the data appears to be clustered toward the center of the distribution. This is expected based on the Kurtosis excess shown in Table 4-1. It is also noted that with the exception of a few data points at the upper and lower tails of the distribution, the cumulative probability is well approximated by a straight line. This confirms that a normal distribution is an appropriate model.

The Anderson-Darling and Kolmogorov/Smirnoff test statistics are calculated subsequently as further tests of normality.

Figure 4-2: Cumulative Probability versus Areal Density

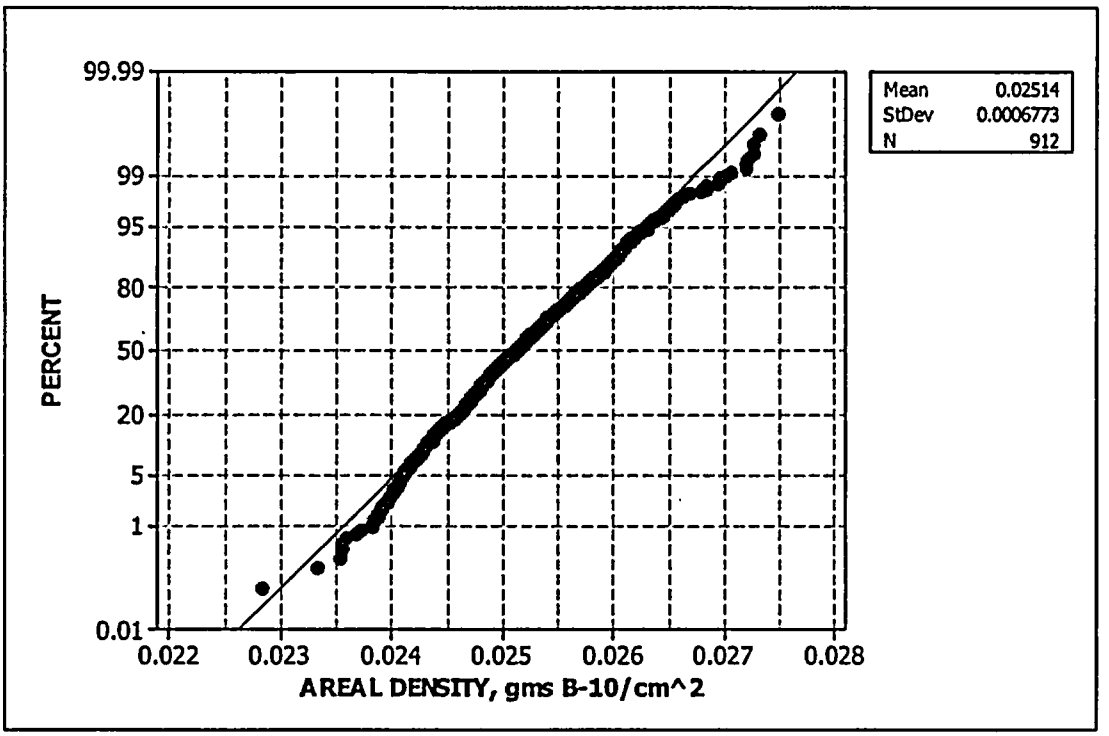

4.2.1 Kolmogorov-Smirnov Test for Normality

In applying the Kolmogorov/Smirnoff test for normality, a test statistic D is calculated for the data distribution. D is the difference between the ordered areal density values and their predicted cumulative probability under the assumption of a normal distribution. The calculated value for the BORAL areal density data is 0.0329.

Under the Kolmogorov/Smirnoff test, D must be less than a certain critical value. The large sample critical value at a 95% confidence is 0.24. Accordingly, we cannot reject the hypothesis that the density are normal distributed.

4.2.2 Anderson-Darling Test for Normality

The Anderson-Darling test is based on the test statistic, A^2, which examines the differences between the tails of the normal distribution and the tails of the test data. The null hypothesis (that the data is normally distributed) is rejected for measures of the test statistic that exceeds a certain critical value.

The test statistic can be calculated numerically from:

$$A^2 = -\left[\sum_{i=1}^{n}(2i-1)(\ln(u_i)+\ln(1-u_{n+1-i}))\right]/n - n \qquad \textbf{Equation 4}$$

where u_i is the value of the theoretical cumulative distribution at the i^{th} largest observation. The test statistic calculated for the Boral areal density values is 1.3018.

The large sample critical value for the Anderson-Darling test is 2.492 at 95% confidence and 3.857 at 99% confidence. Thus we cannot reject the null hypothesis that the data are normally distributed. It is noted that there is some significant deviation in the tails of the data, a situation to which the Anderson-Darling test is very sensitive. This is reflected in the relatively high test statistic value (1.3018) for the test data.

4.3 One-Sided Tolerance Limit and Assessment of 90% Boron Credit

The following equation provides the one sided tolerance limit to the observed coupon areal density:

$$A_{tl} = \bar{x} - K_{912}S \qquad \textbf{Equation 5}$$

where the variable definitions are identical to those outlined previously. Given that the data passes the test for normality, the calculation for the above one-sided tolerance limit is applicable.

Thus the lower tolerance areal density limit is 0.0229 gms B-10/cm^2. The minimum certified areal density is 0.020 gms B-10/cm^2 for the Boral samples tested. The areal density at 111% of the minimum certified value of 0.020 is 0.0222 gms B-10/cm^2. Thus 0.0229 gms B-10/cm^2 > 0.0222 gms B-10/cm^2 and $A_{tl} \geq A_a$ and 90% boron credit is demonstrated.

5.0 Summary and Conclusions

Areal density measurement obtained via neutron attenuation testing at 4 locations each on 228 Boral coupons have been evaluated. The data have been demonstrated to be normally distributed. Accordingly, a one sided tolerance factor for normally distributed data can be applied. This has been computed following the method of Natrella and is 3.226 at 99.9% probability and 95% confidence level.

The proposed method of Reference 1 has been applied to the data set. The minimum certified areal density for this Boral is 0.020 gms B-10/cm^2. The mean of the measured data is 0.02514 gms B-10/cm^2. At a 99.9% probability and a 95% confidence level the one sided lower tolerance limit is 0.0229 gms B-10/cm^2 which exceeds 111% of the minimum certified areal density. Accordingly 90% credit for boron-10 is demonstrated.

6.0 References

1) Standard Guide for Thermal Neutron Absorber (Poisons) for Criticality Control in Dry Cask Storage Systems (DCSS) or Transportation Packages Containing Fissile Materials, Proposed by ASTM Subcommittee c26.03, 5/8/2003.

2) Natrella, M.G., Experimental Statistics, National Bureau of Standards Handbook 91, 8/1/63.

Appendix A

BORAL Coupon B-10 Areal Density Test Data

(For each coupon B-10 areal density $\left(\frac{gm}{cm^2}\right)$ is provided for locations A, B, C and D)

Appendix A

Test Data

Coupon ID	A	B	C	D
WN310009-1-1	0.025062784	0.024806101	0.025250876	0.024480108
WN310009-1-2	0.025295658	0.025086125	0.025252807	0.024921785
WN310010-1-1	0.024152418	0.024151064	0.024378336	0.024202582
WN310010-1-2	0.024352811	0.024659791	0.024761737	0.024701446
WN310025-1-1	0.025310048	0.02518946	0.024700361	0.024747781
WN310025-1-2	0.024580798	0.024444167	0.024380079	0.02440745
WN310039-1-1	0.023953087	0.024438754	0.024408661	0.02465363
WN310039-1-2	0.024672659	0.024228369	0.024687562	0.024413707
WN310048-1-1	0.025107024	0.024973144	0.0249895	0.02497466
WN310048-1-2	0.025397755	0.025000009	0.025044618	0.024732663
WN310057-3-1	0.026060044	0.025943994	0.02593695	0.025635984
WN310057-3-2	0.02597623	0.025634738	0.025991252	0.026032276
WN310061-1-1	0.025224999	0.024849114	0.024948213	0.024638632
WN310061-1-2	0.024898957	0.024600053	0.025178941	0.02480407
WN310075-3-1	0.024364684	0.024797911	0.024201101	0.024193524
WN310075-3-2	0.024664107	0.024569897	0.024569525	0.024457774
WN310089-2-1	0.024046765	0.023573319	0.024314851	0.023963183
WN310089-2-2	0.02412745	0.02396863	0.024289791	0.024072452
WN310092-1-1	0.024400776	0.024162693	0.02467133	0.024521085
WN310092-1-2	0.02436154	0.024143137	0.024520822	0.024401198
WN310104-1-1	0.023831937	0.024049098	0.023821381	0.02400616
WN310104-1-2	0.024390186	0.024299037	0.024099889	0.024080493
WN310110-1-1	0.025373166	0.025079003	0.025794203	0.025359912
WN310110-1-2	0.025280417	0.025269293	0.025199859	0.025094384
WN310121-1-1	0.024272875	0.024006694	0.024225933	0.024220253
WN310121-1-2	0.024102052	0.024075745	0.02421622	0.024114638
WN310139-2-1	0.024712177	0.024640813	0.024742599	0.024591163
WN310139-2-2	0.02461095	0.024280069	0.024661688	0.024862879
WN310146-2-1	0.025119246	0.025126485	0.024612966	0.024587419
WN310146-2-2	0.02486097	0.024785377	0.02470586	0.024366957
WN310159-1-1	0.024683577	0.024266206	0.024359331	0.023880987
WN310159-1-2	0.023998171	0.023817214	0.024607315	0.023905208

WN310160-3-1	0.025342119	0.025062351	0.025643139	0.025336303
WN310160-3-2	0.024797053	0.02473757	0.025010589	0.025302956
WN310178-3-1	0.025207332	0.025038543	0.025669036	0.024866697
WN310178-3-2	0.025284033	0.025471761	0.025206727	0.024754864
WN310189-3-1	0.025791584	0.02616027	0.025330142	0.025774087
WN310189-3-2	0.025591125	0.026108237	0.025977552	0.026101363
WN310191-1-1	0.025329923	0.025311747	0.025331261	0.025591665
WN310191-1-2	0.025491384	0.025480582	0.02572866	0.025418951
WN310203-3-1	0.024319779	0.024152398	0.024305606	0.024461341
WN310203-3-2	0.024471521	0.024689251	0.024861995	0.024804559
WN310219-3-1	0.023548182	0.023711944	0.024098474	0.024253562
WN310219-3-2	0.024307312	0.024244783	0.02386301	0.023837085
WN310229-3-1	0.024489568	0.024689865	0.025025203	0.024938471
WN310229-3-2	0.025186076	0.024188899	0.024962587	0.024289017
WN310231-3-1	0.024612605	0.024355676	0.024385391	0.024363196
WN310231-3-2	0.024447336	0.024428654	0.02430794	0.0245779
WN310248-2-1	0.025387475	0.024924922	0.024860293	0.024765164
WN310248-2-2	0.025536062	0.025070611	0.025410071	0.025061323
WN310253-3-1	0.025646942	0.025484394	0.026117152	0.025959746
WN310253-3-2	0.025397081	0.025362524	0.025650442	0.025515734
WN310269-1-1	0.024897995	0.024583602	0.02478124	0.024753167
WN310269-1-2	0.024664961	0.025079898	0.025277477	0.024967961
WN310270-2-1	0.024975498	0.024282817	0.024952272	0.024487692
WN310270-2-2	0.024964347	0.024884132	0.025208686	0.024663578
WN310284-3-1	0.023974464	0.024105729	0.024405032	0.024127656
WN310284-3-2	0.024273225	0.024117766	0.024584294	0.02408033
WN310295-3-1	0.024372285	0.02436898	0.024914282	0.024282916
WN310295-3-2	0.024605536	0.024256535	0.024545289	0.024495201
WN310309-3-1	0.025377409	0.025378078	0.025188766	0.025179848
WN310309-3-2	0.025307682	0.025199705	0.02524281	0.025231378
WN310312-3-1	0.024912399	0.024416244	0.025476981	0.024053059
WN310312-3-2	0.025239974	0.025239084	0.025265478	0.025639317
WN310327-1-1	0.025504648	0.025385105	0.025855037	0.02555185
WN310327-1-2	0.026239722	0.025292016	0.026102825	0.025639398
WN310331-1-1	0.024798475	0.024638805	0.025009472	0.024991368
WN310331-1-2	0.024741325	0.02471565	0.024410207	0.024655964
WN310343-1-1	0.025540763	0.025536554	0.025310426	0.025738992

WN310343-1-2	0.025364315	0.025453822	0.025116241	0.025771357
WN310359-2-1	0.026783062	0.026392283	0.026498241	0.026358498
WN310359-2-2	0.026428689	0.026293496	0.026444899	0.026025109
WN310367-2-1	0.026053634	0.026302659	0.025920976	0.0262237
WN310367-2-2	0.025909552	0.02610902	0.025577502	0.02618893
WN310371-1-1	0.025011299	0.024982683	0.02520151	0.025050198
WN310371-1-2	0.024884052	0.024664818	0.025132229	0.024827907
WN310388-3-1	0.024923048	0.024715196	0.024817084	0.024668895
WN310388-3-2	0.024546168	0.024745426	0.025770323	0.025209445
WN310390-3-1	0.02479099	0.02469223	0.024367891	0.024716781
WN310390-3-2	0.024784283	0.024908228	0.024600173	0.024642192
WN310401-2-1	0.025878628	0.025339147	0.024874567	0.025243269
WN310401-2-2	0.025052215	0.02550945	0.024901818	0.025521616
WN310418-3-1	0.025339326	0.025232267	0.025390233	0.025117152
WN310418-3-2	0.02560807	0.025748131	0.025442231	0.025637384
WN310428-3-1	0.024271066	0.024319813	0.02435357	0.024035317
WN310428-3-2	0.024063883	0.024367709	0.024739131	0.024698693
WN310433-3-1	0.025082176	0.025327353	0.025729351	0.025461976
WN310433-3-2	0.025456227	0.025409627	0.025349646	0.025793764
WN310443-1-1	0.024743934	0.024702981	0.024372821	0.024436573
WN310443-1-2	0.024754107	0.025098629	0.02473717	0.024766014
WN310452-3-1	0.02518011	0.024802825	0.025108593	0.024785904
WN310452-3-2	0.025004612	0.024793911	0.025460044	0.025097562
WN310464-3-1	0.025312942	0.025217135	0.02516141	0.024815393
WN310464-3-2	0.025541755	0.024962146	0.024711228	0.02487988
WN310471-1-1	0.025109669	0.02482858	0.02495189	0.024909421
WN310471-1-2	0.025300498	0.025069008	0.025478954	0.025385999
WN310486-3-1	0.024901833	0.024838183	0.025281738	0.024611482
WN310486-3-2	0.025148373	0.024755141	0.024710614	0.024588301
WN310493-3-1	0.024829724	0.024976731	0.025151142	0.024861691
WN310493-3-2	0.024975819	0.025118687	0.024972047	0.02463536
WN310501-1-1	0.025157272	0.025279835	0.025253202	0.025126509
WN310501-1-2	0.025462926	0.025298829	0.025104468	0.025019828
WN310510-2-1	0.025908263	0.026099029	0.026107352	0.025887887
WN310510-2-2	0.025336303	0.02572533	0.026233009	0.025884894
WN310527-1-1	0.025481268	0.025568707	0.026055574	0.025854099
WN310527-1-2	0.025931636	0.025983497	0.025776582	0.025578602

WN310532-2-1	0.025230941	0.02478146	0.02436056	0.024817718
WN310532-2-2	0.024401762	0.024631024	0.024934355	0.024711376
WN310545-2-1	0.0255409	0.025012667	0.025112927	0.025171974
WN310545-2-2	0.025388614	0.025577035	0.025018442	0.024898188
WN310550-2-1	0.02542234	0.024949884	0.025673425	0.025528334
WN310550-2-2	0.025609758	0.02561872	0.02528044	0.025184991
WN310564-1-1	0.024860678	0.025124858	0.0249959	0.025364587
WN310564-1-2	0.025321788	0.025116591	0.025140268	0.024912686
WN310570-3-1	0.025132215	0.025390106	0.024876752	0.02502303
WN310570-3-2	0.025690245	0.025363542	0.025505345	0.02515642
WN310588-2-1	0.025560333	0.025525504	0.025797359	0.025692725
WN310588-2-2	0.025650119	0.025653986	0.025779399	0.025985878
WN310597-2-1	0.026055311	0.025695887	0.026571999	0.026289661
WN310597-2-2	0.025902261	0.025907078	0.025846972	0.026147002
WN310606-2-1	0.024062615	0.024282215	0.024343733	0.024010414
WN310606-2-2	0.024683882	0.024569179	0.024676478	0.024333554
WN310614-1-1	0.025242764	0.025152711	0.024665262	0.024779327
WN310614-1-2	0.024891686	0.024948751	0.024760994	0.024545099
WN310622-1-1	0.02562412	0.025937174	0.025725776	0.025771429
WN310622-1-2	0.025867963	0.025825565	0.025490722	0.025401633
WN310636-2-1	0.025303872	0.025593779	0.024771754	0.024836724
WN310636-2-2	0.025618324	0.025231276	0.025427714	0.02514052
WN310641-1-1	0.026045256	0.025834679	0.025928522	0.026006486
WN310641-1-2	0.02591236	0.025681345	0.025849059	0.025909118
WN310659-3-1	0.024810211	0.024904006	0.025549148	0.025552879
WN310659-3-2	0.025290864	0.024956939	0.025295604	0.024990644
WN310661-3-1	0.02544206	0.024415477	0.025443774	0.024864616
WN310661-3-2	0.025389151	0.024943107	0.025113668	0.024795219
WN310673-1-1	0.02595298	0.025514257	0.025964729	0.025461431
WN310673-1-2	0.026222721	0.026083706	0.025741865	0.025626861
WN310681-3-1	0.025977647	0.025577403	0.026092906	0.025741408
WN310681-3-2	0.025933166	0.02582296	0.025644319	0.025185094
WN310693-3-1	0.025591089	0.02537274	0.025175017	0.02511485
WN310693-3-2	0.02542702	0.025543833	0.025167034	0.025210573
WN310701-1-1	0.024501274	0.024448863	0.024885668	0.02468246
WN310701-1-2	0.024198248	0.024231005	0.024119184	0.024216958
WN310710-1-1	0.025467378	0.025051779	0.025193495	0.024864528

WN310710-1-2	0.025260051	0.024998043	0.024850422	0.024861822
WN310728-3-1	0.025127696	0.024810021	0.024846345	0.024802291
WN310728-3-2	0.024799985	0.024407892	0.025170221	0.02489289
WN310733-3-1	0.025559264	0.025559608	0.025921588	0.025649635
WN310733-3-2	0.025288257	0.025378526	0.025346304	0.025489753
WN310745-1-1	0.026202934	0.026056797	0.02586212	0.026145506
WN310745-1-2	0.025902687	0.025943795	0.025983518	0.025710089
WN310759-1-1	0.025112095	0.025030996	0.025404133	0.025366216
WN310759-1-2	0.0249411	0.024964823	0.024631391	0.025148673
WN310763-1-1	0.026301315	0.025773783	0.025842904	0.025742988
WN310763-1-2	0.026041929	0.025777342	0.026038304	0.025915963
WN310776-1-1	0.025165627	0.024825168	0.02500519	0.024872873
WN310776-1-2	0.025053279	0.024550734	0.025212468	0.025086737
WN310786-3-1	0.025378184	0.024921798	0.025683668	0.025412133
WN310786-3-2	0.025737209	0.025573234	0.025733904	0.025787788
WN310791-3-1	0.02584014	0.025442477	0.025660619	0.024975916
WN310791-3-2	0.025592207	0.025497983	0.025744519	0.025609594
WN310807-3-1	0.025322167	0.024785026	0.024785919	0.024568568
WN310807-3-2	0.025278884	0.024695299	0.024828751	0.024367554
WN310813-3-1	0.02490395	0.024836401	0.02514519	0.024618467
WN310813-3-2	0.025491691	0.025197242	0.024552158	0.024657685
WN310825-2-1	0.02541107	0.025205095	0.025328842	0.0249446
WN310825-2-2	0.025466841	0.025385065	0.025232287	0.024883781
WN310836-3-1	0.024162393	0.02442615	0.024711995	0.024999296
WN310836-3-2	0.025221841	0.024116583	0.024815298	0.024801459
WN310846-3-1	0.025279596	0.025021011	0.024959364	0.024881907
WN310846-3-2	0.025405526	0.024636274	0.025104153	0.025145653
WN310851-1-1	0.025443351	0.024686542	0.024967928	0.02539637
WN310851-1-2	0.025241852	0.025135294	0.025028236	0.024853993
WN310866-3-1	0.025539447	0.025625909	0.025589767	0.025862206
WN310866-3-2	0.02492544	0.025240426	0.025382668	0.025750327
WN310871-3-1	0.026961002	0.026626005	0.027308424	0.027002474
WN310871-3-2	0.026609806	0.02577504	0.026958406	0.02720173
WN310885-3-1	0.024095254	0.024168342	0.024839255	0.024363037
WN310885-3-2	0.02420533	0.023981384	0.024518909	0.024221127
WN310897-3-1	0.025290828	0.02552143	0.025045637	0.025141162
WN310897-3-2	0.025697439	0.025605473	0.026143261	0.025188571

WN310907-3-1	0.026344906	0.026100927	0.027060588	0.026301247
WN310907-3-2	0.02653737	0.026309943	0.027197811	0.026561292
WN310912-3-1	0.025829769	0.026024011	0.026502411	0.025788299
WN310912-3-2	0.025870462	0.026447015	0.026145357	0.025692452
WN310928-3-1	0.024981785	0.024540925	0.02481346	0.024472949
WN310928-3-2	0.024807789	0.02445237	0.024691669	0.024543779
WN310931-3-1	0.024069098	0.024284694	0.025289389	0.024737283
WN310931-3-2	0.024748683	0.024955737	0.025378319	0.024968369
WN310946-3-1	0.025020172	0.024603974	0.025869272	0.025167781
WN310946-3-2	0.025156528	0.025233171	0.025188455	0.025083087
WN310952-1-1	0.024304976	0.024271267	0.023861064	0.024061947
WN310952-1-2	0.02417239	0.023912524	0.024154305	0.024041451
WN310966-3-1	0.026009042	0.026009858	0.026173751	0.025679621
WN310966-3-2	0.026311714	0.026050909	0.026495584	0.025950786
WN310971-2-1	0.026828762	0.026454073	0.0272698	0.026834928
WN310971-2-2	0.026942264	0.027188124	0.027260417	0.027476265
WN310986-2-1	0.02446054	0.024442969	0.02432269	0.024020344
WN310986-2-2	0.024649469	0.024779945	0.024734018	0.024488035
WN310997-3-1	0.023521666	0.023314106	0.023897216	0.022831721
WN310997-3-2	0.023666809	0.023909867	0.023957032	0.023974017
WN311002-3-1	0.025506813	0.025195715	0.025845998	0.025278931
WN311002-3-2	0.025990362	0.025691342	0.026321948	0.025512048
WN311016-3-1	0.025784427	0.025366324	0.025628456	0.02538139
WN311016-3-2	0.026009691	0.025147917	0.026432893	0.02552978
WN311027-1-1	0.024918312	0.024638023	0.024260028	0.024254805
WN311027-1-2	0.024792061	0.024573407	0.02476535	0.02450682
WN311034-2-1	0.02550881	0.024981448	0.025525401	0.024877124
WN311034-2-2	0.025429175	0.024848053	0.025333782	0.024388988
WN311047-1-1	0.02498632	0.025059344	0.025316043	0.025031688
WN311047-1-2	0.025573643	0.025424281	0.025317077	0.024701745
WN311053-1-1	0.026495456	0.026194857	0.026672636	0.026519733
WN311053-1-2	0.026551271	0.026199289	0.026565494	0.026434853
WN311065-1-1	0.024642446	0.024621218	0.024849719	0.024933374
WN311065-1-2	0.024746579	0.024435316	0.024497935	0.024591602
WN311077-2-1	0.025384107	0.025458075	0.025031535	0.025015043
WN311077-2-2	0.024801187	0.02520689	0.025708875	0.025212974
WN311081-1-1	0.025690483	0.025756339	0.025601634	0.025241545

WN311081-1-2	0.025938463	0.026148243	0.026236717	0.025799113
WN311099-2-1	0.024842107	0.024606005	0.025133383	0.024965113
WN311099-2-2	0.02477038	0.024938619	0.024725744	0.024760487
WN311109-2-1	0.026271628	0.026359608	0.026117825	0.026050723
WN311109-2-2	0.025940697	0.026141315	0.02600297	0.025718767
WN311111-2-1	0.026021941	0.02605259	0.026378062	0.026090108
WN311111-2-2	0.026068011	0.025967582	0.025846989	0.026184472
WN311120-1-1	0.024642737	0.024805468	0.024916453	0.024702933
WN311120-1-2	0.024617647	0.023551083	0.024418997	0.024628727
WN311139-3-1	0.025230235	0.024722828	0.025182761	0.024944969
WN311139-3-2	0.02571714	0.025109932	0.025598794	0.02492805

Please Note

Complete text contained on CD enclosed in Book 1

Spent Fuel Project Office
Interim Staff Guidance - 15
MATERIALS EVALUATION

Issue

Due, in part, to a number of material-related issues identified during dry cask storage system (DCSS) and transportation package application reviews and field implementation, the staff has recognized the need for specific guidance for the review of materials selected by the applicant for its DCSS or transportation package.

Regulatory Basis

See the Attachment, Section III, "Regulatory Requirements."

Applicability

This guidance applies to DCSS and radioactive material transportation package reviews conducted in accordance with NUREGs 1536, "Standard Review Plan for Dry Cask Storage Systems" (January 1997), 1567, "Standard Review Plan for Spent Fuel Dry Storage Facilities" (March 2000), 1609, "Standard Review Plan for Transportation Packages for Radioactive Material" (Draft, November 1997), and 1617, "Standard Review Plan for Transportation Packages for Spent Nuclear Fuel" (March 2000).

Discussion

There is no existing materials evaluation chapter in either NUREG-1536 or NUREG-1567 for the review of DCSS. Therefore, the staff has developed a materials evaluation chapter to address this need. Parts of this chapter also apply to NUREG-1609 and NUREG-1617. The materials evaluation chapter provides guidance to the staff in the Spent Fuel Project Office (SFPO) for performing materials reviews of DCSSs and transportation packages. The materials evaluation chapter will ensure quality and uniformity in reviews performed by new or current staff members in SFPO.

With respect to NUREGs-1536,-1567, and -1617, ISG-15 will supercede the following ISGs in their entirety:

ISG-4, R1 - Cask Closure Weld Inspections
ISG-11, R0 - Storage of Spent Fuel Having Burnups in Excess of 45,000 MWd/MTU
ISG-11, R1 - Transportation and Storage of Spent Fuel Having Burnups in Excess of 45 GWd/MTU

Recommendation

NUREG-1536 should be revised as follows:

Replace the current contents of Chapter 8, "Operating Procedures," with the attachment to this ISG in its entirety. This ISG then becomes a new Chapter 8. "Operating Procedures" becomes Chapter 9, and the following chapters will be renumbered sequentially. Revise the Table of Contents and Chapter references throughout the NUREG to reflect the new chapter numbers. Add reference to Chapter 8, as appropriate, to other chapters, and delete redundant material.

Revise Appendix C, "Glossary," to include the following terms:

Commercial Spent Fuel Management program (CSFM)
Heat Affected Zone (HAZ)
Megawatt days per Metric Ton Uranium (MWd/MTU)
Nondestructive Examination (NDE)
Post-Weld Heat Treatment (PWHT)

NUREG-1567 should be revised as follows:

Replace the current contents of Chapter 10, "Conduct of Operations Evaluation," with the attachment to this ISG in its entirety. This ISG then becomes the new Chapter 10. "Conduct of Operations Evaluation" becomes Chapter 11, and the following chapters will be renumbered sequentially. Revise the Table of Contents and Chapter references throughout the NUREG to reflect the new chapter numbers. Add reference to Chapter 10, as appropriate, to other chapters, and delete redundant material.

Revise the "Acronyms and Abbreviations" section to include the following terms:

Commercial Spent Fuel Management Program (CSFM)
Heat Affected Zone (HAZ)
Megawatt Days per Metric Ton of Uranium (MWd/MTU)
Post-Weld Heat Treatment (PWHT)

NUREG-1609 should be revised as follows:

Revise the listed NUREG-1609 section to incorporate the applicable material from this ISG:

NUREG section 2.5.2.1	ISG sections X.5.1 and X.5.2.4
NUREG section 2.5.2.2	ISG section X.5.3.1
NUREG section 4.5.1.1	ISG section X.5.2.9
NUREG section 5.5.1.1	ISG section X.5.2.6
NUREG section 6.5.3.2	ISG section X.5.2.7

Revise the "Acronyms and Abbreviations" section to include the following terms:

American Concrete Institute (ACI)
Safety Analysis Report (SAR)

NUREG-1617 should be revised as follows:

Revise the listed NUREG-1617 section to incorporate the applicable material from this ISG:

NUREG section 1.3.3	ISG section X.5.1.1
NUREG section 1.5.2.6	ISG section X.5.2.3
NUREG section 1.5.3.1	ISG section X.5.1
NUREG section 2.3.2	ISG section X.5.2.2
NUREG section 2.4.2	ISG section X.5.2.2
NUREG section 2.5.2.1	ISG sections X.5.2.2 and X.5.2.4
NUREG section 2.5.2.2	ISG section X.5.3.1
NUREG section 2.5.2.3	ISG section X.5.2.9
NUREG section 3.5.2.1	ISG section X.5.2.2
NUREG section 3.5.2.3	ISG section X.5.4
NUREG section 4.5.1.1	ISG sections X.5.2.9 and X.5.3.1
NUREG section 5.5.3.2	ISG section X.5.2.6
NUREG section 6.5.3.2	ISG section X.5.2.7

Revise the "Acronyms and Abbreviations" section to include the following terms:

American Concrete Institute (ACI)
American Welding Society (AWS)
Commercial Spent Fuel Management program (CSFM)
Dry Cask Storage System (DCSS)
Heat Affected Zone (HAZ)
Independent Spent Fuel Storage Installation (ISFSI)
Magnetic Particle examination (MT)
MegaWatt days per Metric Ton Uranium (MWd/MtU)
Nondestructive Examination (NDE)
Dye Penetrant examination (PT)
Post Weld Heat Treatment (PWHT)
Ultrasonic examination (UT)

Approved _____ */RA/* _____ 01/10/2001

E. William Brach **Date**

Attachment: "Materials Evaluation"

X MATERIALS EVALUATION

X.I Review Objective

In this portion of the dry cask storage system (DCSS) review, the NRC staff evaluates the DCSS to ensure adequate material performance of components important to safety of an independent spent fuel storage installation (ISFSI) or monitored retrievable storage facility (MRS) under normal, off-normal and accident conditions. To ensure an adequate margin of safety in the design basis of the ISFSI or MRS, the reviewer should obtain reasonable assurance that:

- The physical, chemical, and mechanical properties of components important to safety meet their service requirements.
- Materials for components important to safety have sufficient requirements to control the quality of the raw material, handling, and fabrication and test activities.
- Materials for components important to safety are selected to accommodate the effects of, and to be compatible with, the ISFSI or MRS site characteristics and environmental conditions associated with normal, off-normal and accident conditions.
- The spent fuel cladding is protected from gross rupture and from conditions that could lead to fuel redistribution.
- DCSS must be designed to allow ready retrieval of spent fuel.

X.2 Areas of Review

The principal purpose of the materials review is to obtain reasonable assurance that materials selected for each component are adequate for performance of the safety function(s) required of that component. As defined in Section 5 of this Chapter, the materials evaluation encompasses the following areas of review:

X.2.1 General

a. cask design/materials, fuel specifications, and environmental conditions
b. engineering drawings

X.2.2 Materials Selection

a. applicable codes and standards
b. material properties
c. weld design and specification
d. bolt applications
e. coatings
f. gamma and neutron shielding materials
g. neutron absorbing/poison materials for criticality control

h. concrete and reinforcing steel
i. seals

X.2.3 Chemical and Galvanic Reactions

a. loss of corrosion resistance
b. flammable gas generation

X.2.4 Cladding Integrity

a. temperature limits
b. high burnup fuel
c. cask reflooding

X.3 Regulatory Requirements

X.3.1 General

a. Structures, systems and components (SSCs) important to safety must be described in sufficient detail to enable reviewers to evaluate their effectiveness. [10 CFR 72.24(c)(3)]

b. In the design, consideration should be given to compatibility of the cask with wet or dry spent fuel loading and unloading facilities and with the requirements for removal from the reactor site. [10 CFR 72.236(m)]

X.3.2 Materials Selection

a. The SSCs important to safety must be designed, fabricated, erected, and tested to quality standards commensurate with the importance to safety of the function to be performed. [10 CFR 72.122(a)]

b. The materials used for shielding and criticality functions shall be adequate for performance of intended functions. [10 CFR 72.104(a), 106(b), 124, 128(a)(2)]

c. The materials of construction shall have adequate properties for anticipated service and environmental conditions, and quality standards shall be used to verify that the design bases for the SSCs are satisfied. [10 CFR 72.122(a), (b) and (c)]

d. Sufficient information shall be included for materials of construction to satisfy the design bases with an adequate margin for safety. [10 CFR 72.24(c)(3)]

e. The DCSS must be designed to store spent fuel safely for a minimum of 20 years and permit maintenance as required. [10 CFR 72.236(g)]

f. Non-combustible and heat resistant materials must be used wherever practical throughout the ISFSI or MRS so that the materials can perform their safety functions under credible fire and explosion exposure conditions. [10 CFR 72.122(c)]

g. The DCSS must reasonably maintain confinement of radioactive material under normal, off-normal, and credible accident conditions. [10 CFR 72.236(l)]

X.3.3 Chemical and Galvanic Reactions

The cask, and cask components, must be compatible with wet or dry spent fuel loading and unloading facilities. [10 CFR 72.236(h)]

X.3.4 Cladding Integrity

a. The spent fuel cladding must be protected from degradation which could lead to gross rupture and pose operational safety problems with respect to spent fuel retrievability. [10 CFR 72.122(h)(1)]

b. In the design of the DCSS, consideration should be given to removal of the spent fuel from a reactor site, transportation and ultimate disposition by the Department of Energy. [10 CFR 72.236(m)]

X.4 Acceptance Criteria

X.4.1 General

For this section, items that follow the acceptance criteria in square brackets ([ ]) refer to lettered paragraphs in Section X.3 of this Chapter.

The safety analysis report (SAR) should describe all materials used for DCSS components important to safety, and the reviewer should consider the suitability of those materials for their intended functions in sufficient detail to evaluate their effectiveness in relation to all safety functions. [1a, 2a]

The DCSS should employ materials that are compatible with wet and dry spent fuel loading and unloading operations and facilities. These materials should not degrade to the extent that a safety concern is created. [1b, 2c]

X.4.2 Materials Selection

The materials properties of a DCSS component should meet its service requirements in the proposed cask system for the duration of the license period. [2a, 2b, 2e]

The materials that comprise the DCSS should sufficiently maintain their physical and mechanical properties during all conditions of operations. The spent fuel should be readily retrievable without posing operational safety problems. [2a, 2b, 2c]

Over the range of temperatures expected prior to and during the storage period, any ductile-to-brittle transition of the DCSS materials, used for structural and nonstructural components, should be evaluated for its effects on safety. [2a, 2e, 2f, 2g]

DCSS gamma shielding materials (e.g., lead) should not experience slumping or loss of shielding effectiveness to an extent that compromises safety. The shield should perform its intended function throughout the licensed service period. [2b, 2e, 2f, 2g]

DCSS materials used for neutron absorption should be designed to perform their safety function. [2b, 2c]

DCSS protective coatings should remain intact and adherent during all loading and unloading operations within wet or dry spent fuel facilities, and during long-term storage. [1b, 2c, 2g, 3]

X.4.3 Chemical and Galvanic Reactions

The DCSS should prevent the spread of radioactive material and maintain safety control functions using, as appropriate, noncombustible and heat resistant materials. [2f, 3]

A review of the DCSS, its components, and operating environments (wet or dry) should confirm that no operation (e.g., short-term loading/unloading or long-term storage) will produce adverse chemical and/or galvanic reactions which could impact the safe use of the storage cask. [1b, 2c, 3]

Components of the DCSS should not react with one another, or with the cover gas or spent fuel, in a manner that may adversely affect safety. Additionally, corrosion of components inside the containment vessel should be effectively prevented. [1b, 3]

The operating procedures should ensure that no ignition of hydrogen gas should occur during cask loading or unloading. [3]

Potential problems from uniform corrosion, pitting, stress corrosion cracking, or other types of corrosion, should be evaluated for the environmental conditions and dynamic loading effects that are specific to the component. [1b, 2c]

X.4.4 Cladding Integrity

The integrity of the cladding should be protected by ensuring that non-combustible and heat-resistant materials are used wherever practical throughout the ISFSI. [2f, 4a]

The cladding temperature should be maintained below maximum allowable limits, and an inert environment should be maintained inside the cask cavity to maintain reasonable assurance that the spent fuel cladding will be protected against degradation that may lead to gross rupture, loss of retrievability, or severe degradation. DCSS distortions from debris, corrosion, or spalled coatings, should not impair removal of the spent fuel from the cask. [4a, 4b]

For Zircaloy-clad fuel, the temperature should be maintained below 570° C (1058° F) for short-term accident conditions, short-term off-normal conditions, and fuel transfer operations, as described in PNL-4835[1]. [4a]

Cladding should not rupture during re-flood operations. [2g, 4a]

Any degradation of DCSS coating material, including vapors or particulate that originate from a deteriorating coating, should not affect the safety functions of the cladding or the cask components. [1b, 2a, 2c, 2d, 2e, 2f 2g, 4a]

DCSS materials should be durable and compatible to demonstrate that the spent fuel is retrievable and the geometry of the spent fuel is maintained in a sub-critical configuration under all credible operating and accident conditions. [1b, 2g, 3, 4b]

X.5 Review Procedures and Guidance

Since the materials review is interdisciplinary, the materials reviewer should coordinate with other reviewers (e.g., structural, thermal, shielding, criticality), as necessary, for identification of materials related issues in other SAR chapters.

X.5.1 General

X.5.1.1 Cask Design/Materials, Fuel Specifications, and Environmental Conditions

The materials reviewer should consider the cask design and materials specifications, fuel specifications, environmental conditions (e.g., time, temperature, radiation, liquid and vapor exposures), and operating conditions of the DCSS, including conditions during loading/unloading, storage, and transfer operations. The reviewer should verify that material properties of the major nonstructural components (e.g., neutron absorbing materials, heat transfer disks, etc.) are also presented in the SAR. This general information can usually be found in Chapters 1 (General Description), 2 (Principal Design Criteria), 8 (Operating Procedures), or 12 (Technical Specifications). However, the reviewer should review the SAR to assess all aspects pertinent to the DCSS at an ISFSI.

In considering the suitability of components, consider the various environmental conditions and length of time that the component will encounter each condition during the licensed storage period, as in-service environmental conditions may affect material properties over time. Note that the magnitudes of radiation and temperature decrease over the ISFSI service period. Other environmental and operating conditions that may be encountered in loading, transport (on-site), storage, unloading, and transfer to another storage or transport system may degrade performance of the materials.

X.5.1.2 Engineering Drawings

Review the engineering drawings of the SAR to understand how the cask components are assembled. The reviewer should verify that the SAR drawings contain a bill of materials, including appropriate consensus code information [e.g., American Welding Society (AWS), American Society of Mechanical Engineers (ASME), American Society for Testing and Materials (ASTM), or American Concrete Institute (ACI) specification number, type, class, and/or grade of material) or other similar specification documents for fabrication, examination, assembly, and testing control. Further, verify that the drawings identify all cask components to be coated (if applicable).

X.5.2 Materials Selection

X.5.2.1 Applicable Codes and Standards

The reviewer should verify that the identified codes and standards are appropriate for the material control of the component. Verify that materials selections are appropriate for the environmental conditions to be encountered during loading, unloading, transfer and storage

operations. The suitability of materials and fabrication of major structural components (e.g., shell, bottom plate, shield lid, structural lid, basket fuel tube) may be assessed using the applicable construction code of record.

X.5.2.2 Material Properties

The material properties provided for the major structural components (including stainless steel, precipitation-hardened steels, carbon steel bolting materials, aluminum alloys, concrete, neutron and gamma shielding materials, and neutron absorbing materials, etc.) can usually be ascertained from applicable codes and standards, such as the ASTM Standards. However, other references (e.g., Military Handbook Specifications or International Standards) may be used to obtain the values of mechanical properties specified in the SAR. The reviewer should obtain reasonable assurance that the particular class and grade of structural material are acceptable under the applicable construction code of record. Proposed alternative materials should be justified so that the reviewer can assess their acceptability for the given component under the intended service conditions.

In conjunction with the other technical disciplines (i.e., structural, confinement, thermal, shielding and criticality), verify, as needed, that selected parameters have been appropriately defined (e.g., the temperature dependent values for the stress allowables, modulus of elasticity, Poisson's ratio, weight density, thermal conductivity, and coefficient of thermal expansion).

The reviewer may find it useful to tabulate the major structural materials to facilitate the review. The following information could be tabulated: specification number; grade, type, and class of the material; nominal composition; product form; yield and tensile strength level; notes about the materials; etc.

X.5.2.3 Weld Design and Specifications

General

There are two nationally recognized codes that address welding, ASME[2] and AWS D1.1[3]. The ASME Code governs welded pressure vessels, from domestic water heaters to nuclear reactors. The AWS D1.1 "Structural Welding Code" is the applicable code for welding structural steel, such as the steel used for bridges and steel-framed skyscrapers. The NRC staff recommends the use of the ASME welding code as the preferred code for storage casks. However, the ASME Code is a voluntary consensus standard which has been adopted by most vendors. Some older cask designs used the AWS Code. Note that the various construction codes differ from one another in their requirements for materials and welding procedures because each code is specialized with a particular application in mind.

Standard weld and nondestructive examination (NDE) symbols may be found in AWS A2.4, "Symbols for Welding and Nondestructive Testing," to interpret such symbols found on the drawings submitted with the SAR.

Weld Design and Materials

Except for welded closure lids, discussed later, all welds of the confinement shell should be full penetration welds. Verify that the NDE for these confinement welds is volumetric.

All weld filler metals should be specified by ASME Section II, Part C, and an associated AWS classification.

Weld metals for austenitic stainless steels and nickel-based alloys are specified according to base material chemistry. For these materials, a slight degree of overmatching (i.e., more alloy content than the base material) is normal practice (e.g., type 308 filler is commonly used for type 304 base metals).

For any weld, the specified weld metal strength must equal or exceed the specified base metal strength. Consult ASME Section II, Part C, for weld metal properties. A weld schedule, showing the base and weld metal combinations to be used in the cask, should have been provided as an aid in comparing base and weld metal properties.

Fracture Control

For designs that use carbon or alloy steels, dynamic fracture toughness and nil-ductility or fracture appearance transition temperature test data should have been submitted for samples of weld metal, heat affected zone (HAZ) metal, and base materials that have been taken from weldments that use the same materials of construction and welding procedures as used for construction.

The air hardening propensity of such materials during welding may have a significant adverse influence on the fracture toughness of the weld zone. (Air hardening refers to a steel with sufficient carbon or other alloying elements which causes the steel to harden significantly during cooldown in air, resulting in hard, brittle weld deposits and HAZs.) Consequently, the importance of preheat and post-weld heat treatment (PWHT) is paramount. Adherence to PWHT Table WB-4622.1-1 of Section III, Division 3 (1998) is recommended. Staff experience has shown that the Code option of a lower temperature PWHT for a longer time is generally undesirable. It is especially detrimental when fracture toughness is important to the design. Therefore, Table WB-4622.4(c)-1 of Section III, Division 3 (1998), or similar, is generally unacceptable.

The reviewer should note that a full temperature PWHT of a closure lid may not be feasible due to the potential for overheating of the fuel cladding, thereby precluding welded closures for materials requiring PWHT.

Welded Lids

Most cask designs use two lids, an inner shield lid and an outer structural lid. The structural lid weld joint may be either a full-penetration weld or a partial-penetration groove weld.

Carbon and Alloy Steel Cask Designs

The reviewer should verify that the applicant has considered all the closure lid weld material and technique improvements that accrued from previous DCSS design and fabrication experience. For example, refer to the technical evaluation in NRC Confirmatory Action Letter 97-7-001, dated July 22, 1998. Some of the DCSS improvements resulting from that action include:

- shell plates made from low sulfur, calcium-treated, vacuum-degassed steel;

- application of minimum 200° F preheat;
- use of low-hydrogen electrodes;
- low carbon equivalent base metals and weld metals;
- magnetic particle (MT) examination of the root pass;
- maintenance of preheat as a postheat treatment for a minimum of one hour; and
- minimum of two-hour delay after postheat before performing final volumetric NDE.

The structural lid weld should be examined by ultrasonic testing (UT) or other volumetric methods. Review the applicant's evaluation of the critical flaw size using the linear-elastic fracture mechanics methodology based on service temperature, dynamic fracture toughness, and critical design stress parameters, as specified in Section XI of the ASME Code.

Progressive surface examinations, utilizing dye penetrant testing (PT) or MT, are permitted only if unusual design and loading conditions exist. In addition, a stress-reduction-factor of 0.8 is imposed on the weld strength of the closure joint to account for imperfections or flaws that may have been missed by progressive surface examinations. The weld design should be approved by the NRC on a case-by-case basis.

Austenitic Stainless and Nickel-Base Alloy Steels Cask Design

For designs employing austenitic lid materials and welds, either volumetric or multi-pass PT inspection methods are acceptable.

For either UT or PT examination, the minimum detectable flaw size must be demonstrated to be less than the critical flaw size. The critical flaw size should be calculated in accordance with ASME Section XI methodology; however, net section stress may be governing for austenitic stainless steels, and must not violate ASME Section III requirements. Flaws in austenitic stainless steels are not expected to exceed the thickness of one weld bead.

If using UT, the UT acceptance criteria are the same as those of NB-5332 for pre-service examination. In accordance with Code practice for supplementing volumetric examinations with a surface examination, UT examination must be performed in conjunction with a root pass and cover pass PT examination.

If PT is specified (i.e., no volumetric inspection), a stress reduction factor of 0.8 must be applied to the weld design.

X.5.2.4 Bolt Applications

The reviewer should verify that all bolts have the required tensile strength, resistance to corrosion and brittle fracture, and a coefficient of thermal expansion that is similar to the materials being bolted together. Confirm that the bolting materials are not sensitive to stress corrosion cracking under anticipated operating conditions.

X.5.2.5 Coatings

Coatings in DCSSs are used primarily as corrosion barriers or to facilitate decontamination. They may have additional roles, such as improving the heat rejection capability by increasing the emmisivity of cask internal components.

The reviewer should determine the appropriateness of the coating(s) for the intended application by reviewing the coating specification for each protective coating that is applied to an important to safety component. A specification that describes the scope of the work, required materials, the coating's purpose, and key coating procedures, should assure that the appropriate and compatible coatings have been selected by the DCSS designers. A coating specification should include the following:

- scope of coating application;
- type of coating system;
- surface preparation methods;
- applicable coating repair techniques; and
- coatings qualification testing, as applicable.

Additional guidance regarding coating specification details are described below.

Scope of Coating Application

The coating specification should identify the purpose of the coating, a list of the components to be coated, and a description of the expected environmental conditions (e.g., expected conditions during loading, unloading, and dry storage).

The reviewer should verify that the coatings will not react with the cask internal components and contents, and will remain adherent and inert when exposed to the various environments of a spent fuel cask. The most prevalent, potentially degrading environments include the immersion in borated spent fuel pool water during loading and unloading operations, and high temperature and high radiation (including neutrons) environments encountered during vacuum drying evolutions and long-term storage.

Coating Selection

The reviewer should verify that the coating specification identifies the manufacturer's name, the type of primers and topcoat(s) comprising the coating system, and the minimum and maximum dry coating thickness(es). The coating manufacturer's technical literature for all coatings specified for cask interiors must be submitted in the SAR for staff review.

The reviewer should verify that the coating selected for cask components is capable of withstanding the intended service conditions over the design service life. Failures can be prevented by ensuring that the selection and the application of the coating is controlled by adhering to the coating manufacturer's recommendations.

Surface Preparation

The reviewer should verify that the coating specification identifies whether solvent or abrasive cleaning methods should be used to prepare surfaces prior to coating application. This information should ensure that proper surface preparation techniques could be implemented during cask fabrication.

The reviewer should confirm that the specified type and degree of surface cleaning and the required surface profile meet the coating manufacturer's specification. Any deviations from the

manufacturer's standards for surface preparation must be supported by appropriate tests that demonstrate acceptable coating performance under all design conditions.

Coating Repairs

The reviewer should verify that the coating specification identifies the general requirements for repairing damage to the coating. This information will assist the reviewer(s) in evaluating the effects of repairs on the integrity of the coating and whether the designated repair methods could be implemented during or after cask fabrication.

The reviewer should examine the design to determine whether the structure is assembled before or after its various parts are coated. If a complex structure is to be coated after assembly, it is very important that the consequences of a potential coating failure be analyzed to determine whether other cask functions or component features could be compromised by the failure.

The consequences of coating failure depend on the type of coating and service environment, and may include the following:

- Partial and/or complete coating failure that alters the corrosion resistance of DCSS structural and shielding components (primarily during loading/unloading operations);
- Partial and/or complete coating failure that alters the emmisivity and heat transfer of basket components;
- Particulates (cloudiness) that form in spent fuel pool water or cask during loading or unloading that may affect such operations; and/or
- Aggressive or reactive chemical species that form and consequently impact the performance of other cask components during long-term exposure to radiation (e.g., gamma and neutron).

Coating Qualification Testing

Coatings used on cask external surfaces may have been selected upon the basis of their performance requirements and exposure conditions. The applicant may have used related industrial conditions as a documented guide or basis for coating selection without performing further laboratory tests.

Any coating used inside a DCSS must have been tested to demonstrate the coatings performance under all conditions of loading and storage. The conditions evaluated should include exposure to radiation, high temperature during vacuum drying and storage, and immersion during loading, unloading and transfer operations. The coating must be demonstrated to remain intact and inert for the full duration of the DCSS design life.

There are a number of standardized ASTM tests for coatings performance. In reviewing ASTM (or other) tests used to qualify coatings for service in storage casks, consideration should be given to the applicability of a test to the service conditions.

Planning, execution, and interpretation of coating qualification tests must be performed by a qualified coatings engineer (e.g., certified by the National Association of Corrosion Engineers). The reviewer should ensure that appropriate, qualified expertise has been employed by the applicant for any coatings qualification program.

The reviewer should verify that the coating specification includes a description of the coating qualifications testing program, as applicable. The following information, which is important to qualifying a coating, includes, but is not limited to:

- The size and shape of samples used for the coating tests, as well as the type of material(s), and a description and results of any tests conducted on partial or full-size production mock-ups.

- The test sample surface preparation method(s) and expected or measured surface profile. Sample surface preparation should be performed in accordance with written production procedures, using the same equipment, materials, and qualified personnel as intended for production coating. Inspection methods and acceptance criteria should be included.

- Application method(s) and measured control parameters, including records of temperature and humidity, cure cycle and times, and any other monitoring or acceptance tests such as dry film thickness, hardness, and adhesion. The methods and parameters should be employed in accordance with written production procedures using the same equipment, methods, materials, and qualified personnel.

- A test plan description which clearly describes the rationale for and the types and sequences of all coating qualification tests, lab protocols, numbers of samples, inspection methods, and acceptance criteria. Raw test results should be tabulated or otherwise presented. The test plan should include (1) laboratory coupons for demonstrating coating suitability/qualification, and (2) partial or full size production mock-up tests that demonstrate that the selected coating can be applied successfully to real production parts under production shop conditions to give reasonable assurance that field performance will meet laboratory, test-based expectations.

- An interpretation and discussion of the test program results by a certified coatings engineer. This evaluation should examine, at a minimum, the coating performance against the specific tests and the overall requirements for coating performance. The overall program must be assessed as to whether it is likely to be an effective predictor of actual performance. A recommendation for the use of the coating, with specific restrictions, if any, must be included.

The application should also include general requirements applying to all tests:

- Test durations for immersion must equal or exceed the combined maximum design (or technical specification) durations for loading and vacuum drying.

- An evaluation of any observed gasses, bubbles or other evidence that a gas was produced during the test. Coatings that produce flammable gas require a mitigation program to prevent burnable or explosive gas concentrations during all phases of cask operations.

X.5.2.6 Gamma and Neutron Shielding Materials

Concrete, steel, depleted uranium, and lead typically serve as gamma shields, while filled polymers are often used for neutron shielding materials.

The reviewer should confirm that temperature-sensitive shielding materials will not be subject to temperatures at or above their design limits during both normal and accident conditions. The reviewer should determine whether the applicant properly examined the potential for shielding material to experience changes in material densities at temperature extremes. (For example, elevated temperatures may reduce hydrogen content through loss of water in concrete or other hydrogenous shielding materials.)

With respect to external, polymer neutron shields, the reviewer should verify that the application:

- Describes the test(s) demonstrating the neutron absorbing ability of the shield material.
- Describes the testing program and provides data and evaluations that demonstrate the thermal stability of the resin over its design life while at the upper end of the design temperature range. Describes the nature of any temperature-induced degradation and its effect(s) on neutron shield performance.
- Describes what provisions exist in the neutron shield design to assure that excessive neutron streaming will not occur as a result of shrinkage under conditions of extreme cold. This description is required because polymers generally have a relatively large coefficient of thermal expansion when compared to metals.
- Describes any changes or substitutions made to the shield material formulation. For such changes, describes how they were tested and how that data correlated with the original test data regarding neutron absorption, thermal stability, and handling properties during mixing and pouring or casting.
- Describes the acceptance tests that were conducted to verify that any filled channels used on production casks did not have significant voids or defects that could lead to greater than calculated dose rates.

X.5.2.7 Neutron Absorbing/Poison Materials for Control of Criticality

Neutron absorbing materials are used in storage casks to ensure that sub-critical conditions are maintained during normal and accident conditions. Typically, these neutron absorbing materials are in the form of fixed plates or rods for which no structural credit is given.

The boron isotope (^{10}B) is the principal neutron absorbing isotope in most of the absorber plate materials used or proposed for DCSS. However, cadmium and gadolinium are also common neutron absorbing elements.

For all boron-containing materials, the reviewer should verify that the SAR and its supporting documentation describe the material's chemical composition, physical and mechanical properties, fabrication process, and minimum poison content. This description should be detailed enough to verify the adequacy and reproducibility of properties important to

performance as required in the SAR. For plates, the minimum poison content should be specified as an areal density (e.g., milligrams of ^{10}B per cm^2). For rods, the mass per unit length should be specified.

In heterogeneous absorber materials, the neutron poisons may take the form of particles dispersed or precipitated in a matrix material. Materials with large poison particles (e.g., 80-micrometer particles of unenriched boron carbide) have been shown to absorb significantly fewer neutrons than homogeneous materials with the same poison loading [Burrus[4], Wells[5]]. The reduced neutron absorption in heterogeneous materials results from particle self-shielding effects, streaming and channeling of neutrons between poison particles. Therefore, the reviewer should verify that the absorber material's heterogeneity parameters (e.g., particle composition, size, dispersion) are adequately characterized and controlled, and that the criticality calculations employ appropriate corrections (e.g., reduced poison content) when modeling the heterogeneous material as an idealized homogeneous mixture.

Qualifying the Material Fabrication Process

Qualification tests should have been conducted at least once for a given set of materials and manufacturing processes to demonstrate acceptability and durability of the resulting neutron absorber product over the licensed service life. Qualification tests are generally conducted on one or more representative samples or coupons of the fabricated material. Acceptable qualification tests may include: neutron attenuation or reactivity worth measurements to assess the required minimum absorption characteristics; neutron radiography or radioscopy to check for uniform distribution of poison material in plates; immersion of the fabricated absorber in pool water to simulate the cask environment during loading; exposure of the absorber to a radiation field to assess the effects of radiolysis; and exposure of the absorber material to the full range of service temperatures.

The qualification tests and test samples should be evaluated for the following effects: redistribution of the neutron poison; dimension and weight changes due to material instability (e.g., cracking, spalling, debonding of absorber cladding from the poison matrix material or the matrix material from the poison particles; embrittlement; galvanic reactions; hydrogen generation in spent fuel pool water; weight reduction due to outgassing; oxidation or hydriding). The reviewer should verify that the qualification testing has been completed for each neutron absorbing material. These are minimum requirements for new materials.

The effects of material heterogeneity on poison effectiveness should be tested by performing neutron attenuation and/or reactivity worth measurements on material samples or coupons. The test measurements should be calibrated against identical measurements performed on known homogeneous materials of similar composition (e.g., zirconium diboride with an appropriate thickness of aluminum for calibrating measurements of Boral or borated aluminum [Gao[6]]. The true mass of poison material in the test samples should be determined by chemical assay or other appropriate measurements. Note that the heterogeneity effects can vary significantly with poison particle composition (e.g., ^{10}B enrichment), particle size, poison areal density, and poison volumetric density in the bulk material. It is therefore important to verify that qualification testing addressed the appropriate ranges of material heterogeneity parameters.

Acceptance Testing of Fabricated Materials

For all absorber materials, the reviewer should verify that the acceptance tests in Chapter 9 of the SAR include weighing and dimensional measurements (e.g., plate thickness) and visual examination of the material for evidence of defects such as cracks, porosity, blisters, or foreign inclusions.

To the extent practical, test coupons should be removed from every other plate in a lot and at random locations on a plate. Rejection of a given test coupon shall result in rejection of the contiguous plate(s). If absorption properties are repeatable in the first 25% of the lot, reduced sampling may be performed. A rejection of a test coupon during reduced sampling should invoke a return to 100% inspection of the lot (i.e., one test coupon from every other plate).

X.5.2.8 Concrete and Reinforcing Steel

The reviewer should verify that the materials and material properties used for the design and construction of reinforced concrete components that are important to safety comply with the requirements of American Concrete Institute (ACI) 359[7]. ACI 359 is also an acceptable standard for reinforced concrete components for radioactive material containment vessels. For concrete components not covered by ACI 359, ACI 349[8] is acceptable.

The reviewer should verify that the materials and material properties used for the design and construction of reinforced concrete components that are not important to safety comply with the requirements of ACI 318[9]. The NRC also accepts the use of ACI 349 for these applications.

For some DCSS or ISFSI applications, the concrete to be used for the storage pad may have to be reviewed for suitability. The structural reviewer will have the most significant input to the review in terms of strength-related requirements, but the materials aspects, in terms of durability and temperature limits of the concrete, are the responsibility of the materials reviewer.

Reactive materials (e.g., aluminum) that tend to react chemically with wet concrete should not be used as imbeds in concrete.

X.5.2.9 Seals

The reviewer should verify that radiation to be encountered by elastomer O-ring seals in storage service will not cause polymerization to an extent that would adversely affect the safety performance of the seals. In the range of 10^7 rads, an O-ring compound must be selected with care. For higher dose rate environments, elastomer O-rings should not be specified. At lower dose rates, factors other than radiation may be more significant.

The reviewer should verify that O-ring seals do not reach their maximum operating temperature limit during normal and off-normal conditions of storage. The applicant should include the O-ring manufacturer's data sheets specifying temperature and radiation tolerances in the SAR.

Review the applicant's evaluation demonstrating that at the minimum normal operating temperature (usually -40° F), the O-ring seal will neither fail by brittle fracture nor stiffen (loose elasticity) to an extent that prevents the seal from meeting its service requirements.

The reviewer should verify that under the environmental conditions expected in storage service, O-ring seals will not chemically react or decompose in a manner that would significantly affect other components of the DCSS.

X.5.3.1 Chemical and Galvanic Reactions

Loss of Corrosion Resistance

The SAR should include an analysis of whether any chemical, galvanic, or other reactions among the materials (e.g., moderator material, sealants, steels, neutron absorbers) and environments would occur. Pursuant to NRC Bulletin 96-04[10] , confirm that the DCSS will perform adequately under the operating environments expected (e.g., short-term loading/unloading or long-term storage) during the license period such that no adverse chemical or galvanic reactions are produced. The review should also include consideration of possible reactions resulting from the interaction of DCSS components with borated water.

Flammable Gas Generation

The reviewer should evaluate the possible generation of hydrogen or other flammable gases. If appropriate, consider embrittling effects of hydrogen taking into account the metallurgical state of the DCSS components.

Verify that temperatures inside the cask do not promote the formation of vapors from a coating material (e.g., zinc). Alternatively, the applicant should demonstrate that this vapor will not interact unfavorably with the fuel or any cask component important to safety. Absent this demonstration, the materials should not be approved.

In cooperation with the containment reviewer, verify that appropriate operating procedures (SAR Chapter 8) contain adequate guidance for detecting the presence of hydrogen and preventing the ignition of combustible gases during cask loading and unloading operations.

X.5.4 Spent Fuel Cladding Integrity

X.5.4.1 Temperature Limits

The cask system must be designed to prevent degradation of fuel cladding that results in a type of cladding breach, such as axial-splits, where irradiated spent fuel particles may be released into the cask cavity. Additionally, the fuel cladding should not degrade to the point where more than one percent (1%) of the fuel rods develop pinhole or hairline crack-type failures under normal storage conditions. This criterion is consistent with the assumptions of the confinement analysis for normal conditions of storage. The 1% failure assumption is for safety analysis purposes only, and relates to assumptions for thermal analysis, containment performance, and cask unloading operations. "Damaged fuel" is defined as fuel with a breach in the cladding that is larger than a pinhole failure or hairline crack.

The reviewer should verify that cladding temperatures for each fuel assembly type proposed for storage will be below their expected damage thresholds for normal conditions of storage. Zircaloy fuel cladding temperature limits at the beginning of dry storage are typically below

380° C (716° F) for a 5-year cooled fuel assembly and 340° C (612° F) for a 10-year cooled fuel assembly for normal conditions and a minimum of 20 years cask storage (PNL-4835). Temperature limits will be lower with increased fuel assembly cooling time (or increased burnup) mainly due to lower decay heat rates of older fuel.

It should be noted that fuel cladding temperature limits are a complex function of power history (including transients), cladding thickness, pre-pressurization of fuel rods during fabrication, burnup, fission gas, and hoop stress. Substantial variation in the end-of-life internal rod pressures and fuel design characteristics may warrant temperature limits lower than those noted above for certain fuel types. Therefore, fuel cladding limits for each fuel type should be calculated and presented in the SAR.

The reviewer should evaluate the method(s) used to determine the temperature limits and associated cladding hoop stresses. Note that the storage of fuel clad in materials other than Zircaloy-4 or Zircaloy-2 (e.g., advanced alloy cladding materials like M5 or Zirlo) will be approved on a case-by-case basis. At the present time, there is limited information available to the staff relative to the expected degradation modes of advanced alloy clad fuel under storage conditions. Therefore, temperature limit calculations using methods approved for Zircaloy-4 or Zircaloy-2 may need to be modified to account for differences in the degradation processes of fuel with advanced alloys.

The temperature limits may be calculated using methodologies that are based on expected cladding behavior during storage. NUREG-1536 endorses the diffusion controlled cavity growth methodology to calculate the maximum cladding temperature limits during dry storage. The use of other methodologies that account for the full range of materials behavior under the expected storage conditions, such as the Commercial Spent Fuel Management Program (CSFM) methodology as described in PNL-6189[11] and PNL-6364[12], is acceptable to the staff for calculation of cladding temperature limits. Alternative methodologies may be approved by the staff if they are sufficiently justified. However, these alternative methodologies must be validated with experimental data, and associated modeling uncertainties must be addressed.

Hoop stress calculations should be established on the basis of fuel and cladding properties that are representative of the spent fuel to be stored (e.g., cladding dimensions, internal rod pressures). High burnup fuel (i.e., fuel with burnups exceeding 45,000 MWd/MTU) may have unusual characteristics, such as wall thinning from increased oxidation and increased internal rod pressure from fission gas buildup and changes in fuel dimensions, which must be evaluated. The SAR should use conservative values for surface oxidation thickness. Note that oxidation may not be of a uniform thickness along the axial length of the fuel rods and average values may under-predict wall thinning. Temperature limits will be more restrictive with increased fuel cooling time (and/or increased burnup), largely as a result of the slower fuel heat decay as a function of time.

For short-term off-normal and accident conditions, the staff accepts Zircaloy fuel cladding temperatures maintained typically below 570° C (1058° F). This temperature limit is a suitable criterion for short term off-normal conditions including fuel assembly transfer operations, vacuum drying and backfilling the cask with inert gas. This limit may be lowered for high burnup fuel assemblies due to increased internal rod pressure from fission gas buildup. The applicant should have verified that these cladding temperature limits are below the limit for facility specific operations (e.g., fuel assembly transfer) and the worst case credible accident.

X.5.4.2 High Burnup Fuel

The staff may approve the storage of fuel assemblies having burnups greater than 45,000 MWd/MTU, provided that the applicant can demonstrate that the cladding will be protected from degradation which could lead to gross rupture and that the storage system is designed to allow ready retrieval of the spent fuel from the storage system. If such a demonstration cannot be performed, high burnup fuel assemblies could be enclosed by approved baskets to confine the fuel so that potential degradation of the fuel during storage will not pose problems with respect to redistribution of material during storage or subsequent transportation. Such an enclosure would also maintain subcriticality based on optimum moderation conditions and no potential for buckling and failure of fuel rods, grid spacers, and end fittings under accident conditions.

The staff believes that the Zircaloy cladding of a fuel rod can, in general, withstand uniform creep strains (i.e., creep prior to tertiary or accelerating creep strain rates) of about 1% before the cladding can become perforated, if the average hydrogen concentration in the cladding is less than about 400 to 500 parts per million (ppm)[13]. This amount of hydrogen corresponds to an oxide thickness of approximately 70-80 micrometers using the recommended hydrogen pickup fraction of 0.15 from Lanning, et al[14], and Garde[15]. The staff also believes that the strength and ductility of irradiated Zircaloy do not appear to be significantly affected by corrosion-induced hydrides at hydrogen concentrations up to approximately 400 ppm. Therefore, the staff has reasonable assurance that fuels having average assembly burnups exceeding 45,000 MWd/MTU can be safely stored if the following acceptance criteria are met:

I. A high burnup fuel assembly containing Zircaloy clad fuel may be treated as intact if both of the following conditions are met:

   A1. No more than 1% of the rods in an assembly have peak cladding oxide thicknesses greater than 80 micrometers; and

   A2. No more than 3% of the rods in an assembly have peak cladding oxide thicknesses greater than 70 micrometers.

II. A high burnup fuel assembly should be treated as potentially damaged fuel if either of the following conditions is met:

   B1. The fuel assembly does not meet both criteria A1 and A2; or

   B2. The fuel assembly contains fuel rods with oxide that has become detached or spalled from the cladding.

The administrative controls section of the SAR Technical Specifications should specify a program to be implemented by the cask licensee to assure the criteria described above are met prior to loading the cask with high burnup fuel. As part of this program, the applicant may use cladding oxidation thickness measurements or predictions based on consideration of reactor operation variables affecting peak cladding oxidation (e.g., in-core flux, length of a cycle, number of cycles, power excursions, coolant temperature and amount of time at that temperature, the coolant water chemistry, and the cladding material). In cases where there are no previously documented measurements of the oxide thickness to validate cladding oxidation predictions, the program may have to incorporate peak cladding oxide thickness measurements.

For the storage of Zircaloy-clad fuel assemblies meeting criteria A1 and A2, the reviewer should coordinate with the criticality, thermal, shielding, and confinement reviewers, as appropriate, to ensure the following assumptions are made in the applicant's analyses. For the confinement analysis, the applicant should assume that the source term of 50% of the rods with peak cladding oxide thicknesses greater than 70 micrometers are available for release from the cask unless justification for a different fraction is presented. This source term should be added to the source term for the assumed rod breakage fraction for normal and off-normal conditions. For the criticality, thermal, and shielding analyses, the applicant should demonstrate that 10 CFR Part 72 requirements are met assuming that the rods with oxide thickness greater than 80 micrometers in a high burnup fuel assembly are failed (e.g., the fuel is allowed to redistribute in a cask) under normal, off-normal, and accident conditions.

For Zircaloy-clad fuel with average assembly burnups greater than 45,000 MWd/MTU meeting criteria A1 and A2, the applicant should employ an acceptable methodology (e.g., CSFM) for calculating cladding temperature limits using a 1% creep strain limit. Further, the analysis should demonstrate that the reduced cladding thickness due to oxidation does not compromise the structural ability of the cladding to withstand the expected loads encountered under normal, off-normal, and accident conditions.

Zircaloy-clad fuel assemblies that meet criterion B1 or B2 should be treated as damaged fuel. Alternatively, these fuel assemblies may be treated as intact fuel provided the appropriate demonstration of cladding integrity for these assemblies under normal, off-normal, and accident conditions is included in the SAR. Acceptable data and analyses to support the demonstration of cladding integrity may include, but are not limited to, the following:

- An estimation of the peak cladding oxide thickness and amount of hydrogen absorbed by the cladding during reactor operation. This information will ensure that the oxide thickness and hydrogen concentration associated with hydride-embrittled zirconium alloys are below those that could significantly reduce the ductility or overall integrity of the cladding.

- A calculation of the cladding hoop stress to establish both the parameters of the accelerated creep tests and the accuracy of the cladding life prediction. The stress calculation should account for the effects of (1) a reduction of thickness due to cladding oxidation, and (2) the fuel rod internal pressure considering the initial fill gas, the release of fission gases to the rod-free volume, the generation of any other gases (e.g., helium) due to effects caused by the irradiation of any internal cladding coatings, and the gas temperature.

- Experimentally derived data and analyses to identify the cladding failure mechanism(s) under expected storage conditions.

X.5.4.3 Cask Reflooding

For cask unloading operations, cladding integrity should be maintained during reflooding so as not to interfere with fuel handling and retrieval. The SAR should include a quench analysis supporting specified minimum quench fluid temperature and maximum fluid flow rate during reflood. This analysis should also be referenced in Chapter 11 of the SAR as having been considered in the development of thermal models for the unloading procedures, and be included, as appropriate, in the Technical Specifications. The NRC accepts the fact that the

total stress on the cladding must be maintained below the material's minimum yield stress. The total stress includes the thermal stress combined with the cladding hoop stress from internal rod pressure and the rod-gas plenum temperature. The analysis should account for high burnup effects on the fuel (e.g., waterside corrosion, high internal rod pressure) and minimum manufacturing wall thickness.

X.6 Evaluation Findings

The evaluation findings are prepared by the reviewer on satisfaction of the regulatory requirements of Section X.3. Review these requirements and provide a summary statement for each. These statements should be similar to the following examples:

Section(s) _____ of the SAR adequately describe(s) the materials used for SSCs important to safety and the suitability of those materials for their intended functions in sufficient detail to evaluate their effectiveness.

The applicant has met the requirements of 10 CFR 72.122(a). The material properties of SSCs important to safety conform to quality standards commensurate with their safety function.

The applicant has met the requirements of 10 CFR 72.104(a), 106(b), 124, and 128(a)(2). Materials used for criticality control and shielding are adequately designed and specified to perform their intended function.

The applicant has met the requirements of 10 CFR 72.122(h)(1) and 236(h). The design of the DCSS and the selection of materials adequately protects the spent fuel cladding against degradation that might otherwise lead to gross rupture of the cladding.

The applicant has met the requirements of 10 CFR 72.236(h) and 236(m). The material properties of SSCs important to safety will be maintained during normal, off-normal, and accident conditions of operation so the spent fuel can be readily retrieved without posing operational safety problems.

The applicant has met the requirements of 10 CFR 72.236(g). The materials properties of SSCs important to safety will be maintained during all conditions of operation so the spent fuel can be safely stored for a minimum of 20 years and maintenance can be conducted as required.

The applicant has met the requirements of 10 CFR 72.236(h). The [cask designation] employs materials that are compatible with wet and dry spent fuel loading and unloading operations and facilities. These materials should not degrade over time or react with one another during any conditions of storage.

References

1. A. B. Johnson and E. R. Gilbert, Pacific Nuclear Laboratories, "Technical Basis for Storage of Zircalloy-Clad Spent Fuel in Inert Gases," PNL-4835, September 1983.

2. American Society of Mechanical Engineers, Boiler and Pressure Vessel Code, Section II, "Specification for Welding Rods, Electrodes and Filler Metals."

3. American Welding Society, "Structural Welding Code Steel," AWS D1.1.

4. W. R. Burns, "How Channeling Between Chunks Raises Neutron Transmission Through Boral," *Nucleonics*, 16, 1, 91, 1958.

5. A. H. Wells, D. R. Mamon, and R. A. Karam, "Criticality Effect of Neutron Channeling Between Boron Carbide Granules in Boral for a Spent-Fuel Shipping Cask," *Transactions of the American Nuclear Society*, Vol. 54, pp. 205-206, 1987.

6. J. Gao, "Modeling of Neutron Attenuation Properties of Boron-Aluminum Shielding Materials," Masters dissertation, University of Virginia, August 1997.

7. American Concrete Institute and American Society of Mechanical Engineers (Joint Committee), "Code for Concrete Reactor Vessels and Containments," ACI 359. (Also designated as ASME Boiler and Pressure Vessel Code, Section III, "Rules for Construction of Nuclear Power Plant Components," Division 2.)

8. American Concrete Institute, "Code Requirements for Nuclear Safety Related Concrete Structures," ACI 349.

9. American Concrete Institute, "Building Code Requirements for Reinforced Concrete," ACI 318.

10. NRC Bulletin 96-04, "Chemical, Galvanic, or Other Reactions in Spent Fuel Storage and Transportation Casks," July 1996.

11. I. S. Levy, et al, Pacific Northwest Laboratory, "Recommended Temperature Limits for Dry Storage of Spent Light-Water Zircalloy Clad Fuel Rods in Inert Gas," PNL6189, May 1987.

12. M. E. Cunningham, et al, "Control of Degradation of Spent LWR Fuel During Dry Storage in an Inert Atmosphere," PNL-6364, September 1987.

13. Pacific Northwest National Laboratory Technical Evaluation Report of WCAP-15168 (Dry Storage of High Burnup Spent Nuclear Fuel), February 2000.

14. D. D. Lanning, et al, Pacific Northwest National Laboratory, "FRAPCON-3: Modifications to Fuel Rod Material Properties and Performance Models for High Burnup Applications," NUREG/CR-6534, Vol. 1 (PNNL-11513, Vol. 1), 1997.

15. A. M. Garde, "Hot Cell Examination of Extended Burnup Fuel From Fort Calhoun," DOE/ET/34030-11, September 1986.

John Rash

From: John Rash
Sent: Wednesday, October 27, 2004 12:19 PM
To: Bridgette Fulton; James Williams; James Monroe; Mike Distel
Cc: Ken Pettibone; Jeff Moore
Subject: Meeting on Assembly of C-X parts

As a follow to a meeting from this morning it's been suggested that we meet to discuss assembly of the C-X parts.

Please let me know if you are available to meet tomorrow 10/28 at 10:00am in the conference room to iron out details concerning the assembly process.
Assembly of the parts is to begin November 8th.

The following are issues to be discussed:

1) Which rivets do we want to use, solid or pull?

2) Are there enough tools to install the rivets in the time required?

3) Do we want to set up a separate area just for the riveting?

4) Production schedule

Bridgette,

It would be helpful to have a person from the ballmat assembly area attend the meeting.

Thanks,
John

John Rash

From: John Rash
Sent: Wednesday, October 27, 2004 12:19 PM
To: Bridgette Fulton; James Williams; James Monroe; Mike Distel
Cc: Ken Pettibone; Jeff Moore
Subject: Meeting on Assembly of C-X parts

As a follow to a meeting from this morning it's been suggested that we meet to discuss assembly of the C-X parts.

Please let me know if you are available to meet tomorrow 10/28 at 10:00am in the conference room to iron out details concerning the assembly process.
Assembly of the parts is to begin November 8th.

The following are issues to be discussed:

1) Which rivets do we want to use, solid or pull?

2) Are there enough tools to install the rivets in the time required?

3) Do we want to set up a separate area just for the riveting?

4) Production schedule

Bridgette,

It would be helpful to have a person from the ballmat assembly area attend the meeting.

Thanks,
John

John Rash

From: John Rash
Sent: Wednesday, October 27, 2004 12:19 PM
To: Bridgette Fulton; James Williams; James Monroe; Mike Distel
Cc: Ken Pettibone; Jeff Moore
Subject: Meeting on Assembly of C-X parts

As a follow to a meeting from this morning it's been suggested that we meet to discuss assembly of the C-X parts.

Please let me know if you are available to meet tomorrow 10/28 at 10:00am in the conference room to iron out details concerning the assembly process.
Assembly of the parts is to begin November 8th.

The following are issues to be discussed:

1) Which rivets do we want to use, solid or pull?

2) Are there enough tools to install the rivets in the time required?

3) Do we want to set up a separate area just for the riveting?

4) Production schedule

Bridgette,

It would be helpful to have a person from the ballmat assembly area attend the meeting.

Thanks,
John

John Rash

From: John Rash
Sent: Wednesday, October 27, 2004 12:19 PM
To: Bridgette Fulton; James Williams; James Monroe; Mike Distel
Cc: Ken Pettibone; Jeff Moore
Subject: Meeting on Assembly of C-X parts

As a follow to a meeting from this morning it's been suggested that we meet to discuss assembly of the C-X parts.

Please let me know if you are available to meet tomorrow 10/28 at 10:00am in the conference room to iron out details concerning the assembly process.
Assembly of the parts is to begin November 8th.

The following are issues to be discussed:

1) Which rivets do we want to use, solid or pull?

2) Are there enough tools to install the rivets in the time required?

3) Do we want to set up a separate area just for the riveting?

4) Production schedule

Bridgette,

It would be helpful to have a person from the ballmat assembly area attend the meeting.

Thanks,
John

Modeling of Neutron Attenuation Properties of Boron-aluminum Shielding Materials

A Dissertation Presented to
the Faculty of the School of Engineering and Applied Science
University of Virginia

In Partial Fulfillment
of the Requirements for the Degree of
Master of Science in Nuclear Engineering

by
Jun Gao
August, 1997

APPROVAL SHEET

This dissertation is submitted in partial fulfillment
of the requirements for the degree of
Master of Science in Nuclear Engineering

Author

This dissertation has been read and approved by the examining Committee:

Dissertation advisor

Accepted for the School of Engineering and Applied Science:

Dean, School of Engineering and Applied Science
August 1997

Abstract

Various boron containing materials are used widely in nuclear industry as neutron absorbers. The neutron attenuation properties of zirconium diboride(ZrB_2), borated aluminum, and BORAL, were studied using monoenergetic and polyenergetic beams. The neutron channeling and streaming effect was investigated for BORAL and borated aluminum. At the University of Virginia Reactor (UVAR), borated aluminum sample areal densities were measured by utilizing a series of zirconium diboride standards with aluminum shims. The effectiveness of this method was verified. The energy spectrum of the UVAR transmittance beam was determined for the neutron attenuation property study.

MCNP was demonstrated to be an effective tool to model a neutron gauging system, including the source, the test object and the detector. MCNP modeling and experimental methods were used to conduct various studies of neutron attenuation of the absorbers.

For a homogeneous material, exponential attenuation was observed in a monoenergetic beam and this was confirmed by MCNP simulations. Experiments showed non-exponential attenuation in the same material for a polyenergetic beam.

Zirconium diboride is a naturally occurring chemical compound, which has a uniform distribution of ^{10}B. Its measured ^{10}B areal density is the same as its theoretical areal density. Borated aluminum is an alloy of boron and aluminum, which contains highly enriched ^{10}B. Experiments and MCNP simulations showed that borated aluminum has the same neutron attenuation properties as zirconium diboride with a proper

aluminum shim. Therefore, borated aluminum with a uniform distribution of ^{10}B can be treated as a homogeneous mixture of boron atoms and aluminum atoms. The actual ^{10}B areal density can be calculated directly from the physical loading of ^{10}B. BORAL does not have a uniform distribution of boron atoms. The boron carbide particles (~ 85 μm) in BORAL core cause neutron channeling and streaming. With the same ^{10}B loading, BORAL gives a higher transmission than a homogeneous ^{10}B containing material. Experiments showed that 22% more ^{10}B was required to get the same transmission coefficient.

The method of using zirconium diboride with a proper thickness of aluminum shim to measure the areal density of borated aluminum was verified by experimental and computational methods.

An approximation of the UVAR neutron transmittance beam spectrum was determined by using a non-linear least squares method to fit a series of measured transmission coefficients of ZrB_2 disks. Limited by the number of data points, current results may not be able to represent the real energy spectrum, but a comparison of calculated and modeled transmission coefficients indicated that it could be used effectively for the purpose of neutron attenuation studies for samples with ^{10}B areal density greater than 8 mg/cm^2.

ACKNOWLEDGMENTS

I would like to thank Dr. Jack Brenizer, my dissertation advisor. His insight into this project and guidance were invaluable. I am also very appreciative of his editorial comments during the preparation of this thesis. I would like to thank Mr. Marvin Wachs of Eagle-Picher Boron for supplying necessary information and test samples. I would also like to thank the graduate students and staff members at the Reactor Facility. Whenever I need them, they were ready to help. Special thanks goes to Dudley Raine, who helped me to get started with MCNP, to Carl Stebbings, who helped me in acquiring the radioscopic images, and to Dr. Zina En for her information on track-etch techniques.

I would also like to thank my parents and brothers, who are back in China, my motherland. It is their encouragement and support that made it possible for me to continue my academic career in this country.

Special thanks goes to Mrs. Gerda Pirsch, my international host family. She takes care of not only me, but all her students just like a mother. Her help in all areas made a newcomer's life much easier.

Jun Gao
August, 1997

TABLE OF CONTENTS

LIST OF FIGURES

LIST OF TABLES

CHAPTER 1

INTRODUCTION

1.1 Background

Today, radioactive materials produced by the nuclear industry create a variety of radiation, such as alpha particles, beta particles, gamma rays, neutrinos and neutrons. Alpha and beta particles are relatively easily shielded by thin sheets of metals. Neutrinos, although highly penetrating, show little physiological importance to human body. High energy gamma rays and neutrons need special shielding considerations. To get effective radiation protection with a minimum amount of shielding material, the materials and the corresponding thickness needs to be determined carefully. In neutron shielding problems, besides radiation protection, the issue of criticality, i.e., prevention of neutron multiplication, also needs to be considered when shielding materials are used in the storage and transportation of fresh and spent reactor fuel. Gamma radiation is most effectively absorbed by high-density materials, for example, lead, steel and concrete, because gamma photons interact mainly with the orbital electrons. The more electrons an element has, the higher the chance photons will be absorbed while penetrating. However, the interaction mechanism of neutrons with matter is totally different from photons, and often a good gamma photon shielding material provides little neutron shielding. Neutron interactions with matter may be classified into two groups: absorption and scattering. Light elements, like hydrogen and lithium, whose mass numbers are close to one, have high neutron scattering cross sections. This is why water, polyethylene and graphite are

often used as moderator in nuclear reactor designs. Only a few elements including boron, cadmium and some certain rare earth elements have relatively high neutron absorption cross sections. Table 1.1 presents a list of the physical properties and neutron capture cross sections for common neutron absorbers.

Table 1.1. Comparison of physical properties of several high neutron absorption cross section possessed materials [1].

Element	Atom-Wt.	Density (g/cm^3)	Melting point (°C)	Thermal capture cross section (barn)
Boron	10.82	2.34	2300	755
Cadmium	112.41	8.64	321	2550
Gadolinium	157.26	7.95	1350	46000
Samarium	150.35	7.52	1052	5500
Europium	152.0	5.24	826	4600
Dysprosium	162.51	8.6	2600	1100

However, the usefulness of a particular material as a neutron absorber does not depend only on the effective cross section. In most neutron absorption reactions, a considerable amount of binding energy is liberated in the form of secondary gamma radiation. The induced secondary gamma photons' energy may go as high as 5 to 10 MeV, which in turn requires additional photon shielding. Heat dissipation is also required in this process. The ideal absorber would have a high absorption cross section without emission of additional long-range secondary radiations.

Boron is a very unique element that has some outstanding properties which other high neutron-capture-cross-section materials do not have. First, the energy of the secondary gamma ray from $^{10}B(n, \alpha)^{7}Li$ reaction[1] (Eq. 1.1) is only about 0.5 MeV,

$$^{10}_{5}B + ^{1}_{0}n \rightarrow ^{7}_{3}Li + ^{4}_{2}\alpha + 0.48\ MeV\ \gamma + 2.31\ MeV. \qquad (1.1)$$

which can be easily absorbed. By contrast, cadmium shielding emits a 6 MeV gamma ray and the energies of the secondary gamma photons from the rare earth elements are even higher. Second, as shown in Eq. 1.1, there are no radioactive elements produced. On the other hand, cadmium leaves a residue of four radioactive isotopes after absorbing neutrons [1]. Thirdly, boron has a high melting point (2300°C) and good chemical and physical stability. The low melting point of cadmium (321°C) limits its use as a shielding material in a nuclear reactor. Also, a few other characteristics of boron makes it the best neutron absorber. These include a low atomic weight and thus small shielding volume, the ability to economically enrich the ^{10}B in natural boron, and a relatively low price compared to rare earth elements. In natural boron, 18.8% is boron isotope with mass 10, ^{10}B, which has a thermal neutron absorption cross section about 4000 barns.

BORAL was introduced to nuclear industry as a thermal neutron absorber by Brooks & Perkins. It is a composite material consisting of boron carbide particles evenly dispersed within a matrix of aluminum encased between two thin layers of aluminum, which gives BORAL a "sandwich" structure. The content and placement of boron

---

1 When thermal neutrons (0.025 eV) are used to induce this reaction, about 94% of all reactions lead to the ^{7}Li excited state, and 6% directly to the ground state [14].

carbide provides BORAL a very high removal cross section for thermal neutrons. Both boron carbide and aluminum are unaffected by long-term exposure to gamma radiation. Some other physical and chemical properties, such as stability, strength, durability and corrosion resistance, also make BORAL a good neutron shielding material. However, BORAL also has some big drawbacks. Boron carbide in the central layer of BORAL is in the form of fine particles, and the size of the particles averages 85 microns in diameter. The average spatial separation is 1.25 to 1.50 particle diameters [2]. The macroscopic scale distribution of boron carbide particles makes it impossible to make BORAL a homogeneous boron containing material. The spaces between the boron carbide chunks can also allow neutrons to pass through BORAL without being attenuated. This phenomenon is known as neutron channeling between grains and has been studied by Burrus [3] and Wells [4]. The intergranular streaming effect increases the transmission of neutrons through the BORAL shielding. The physical structure of BORAL also causes difficulties in fabricating BORAL plate into neutron shielding components. For example, a plasma arc method is needed to cut BORAL plate into certain shapes [5].

Eagle-Picher Boron Department is producing a different form of boron product as a new neutron absorber, namely borated aluminum. In this thesis, "borated aluminum" is used specifically to refer to this product. Borated aluminum is an alloyed metal compound of boron and aluminum, in which the boron is highly enriched in ^{10}B. Boron is dispersed in the aluminum as a second phase. Other alloying elements are added to obtain the desired chemical composition. The mixture is cast into ingots using a direct chill mold. Different profiles or thickness final products are extruded or rolled from

billets, which are prepared from an ingot. The borated aluminum is made to build shielding baskets, in which the fuel assemblies are to be placed. Since boron and aluminum are a second phase mixture, boron atoms are believed to be distributed at atomic scale, or very close to atomic scale, among aluminum atoms. Thus, there should be no apparent streaming effect while using the borated aluminum plates as neutron shields. At the University of Virginia, different profiles of borated aluminum plates were inspected for boron homogeneity by using neutron radiography techniques and the ^{10}B areal densities were measured with neutron gauging methods.

1.2 University of Virginia Facilities

The University of Virginia Reactor (UVAR) is a pool-type research reactor, which has a thermal power of two megawatts. The core consists of MTR plate-type fuel elements and is submerged in a pool of about 76,000 gallons of water. Figure 1.1 shows the configuration of the UVAR core and experimental facilities. As seen in this figure, two neutron beam ports were used as neutron sources for this work, one for neutron transmittance (gauging) measurements and one for real-time neutron radiography. The south east beam port is used for neutron transmittance measurements. The dry section of the neutron beam port that penetrates the reactor shielding wall is collimated into two neutron beams. Measurements can be made with either beam or the two beams simultaneously. Both upper and lower beams are collimated so well that the dose rate at the position 30 cm beside the sample position is less than 0.5 mR/hr. Both neutron beams are polyenergetic, but a detailed energy spectrum of these two beams was not available.

The north beam port serves as the neutron radiography beam port, and has been in operation for many projects since the early 1980's. The beam was designed to have an L/D ratio between 30 and 60, but by inserting another aperture, the L/D ratio can go up to 120. The cadmium ratio is 88 as measured by gold foils and the neutron flux at the imaging plane for borated aluminum inspection is approximately 4×10^6 n/cm^{2}s at an L/D ratio of 30.

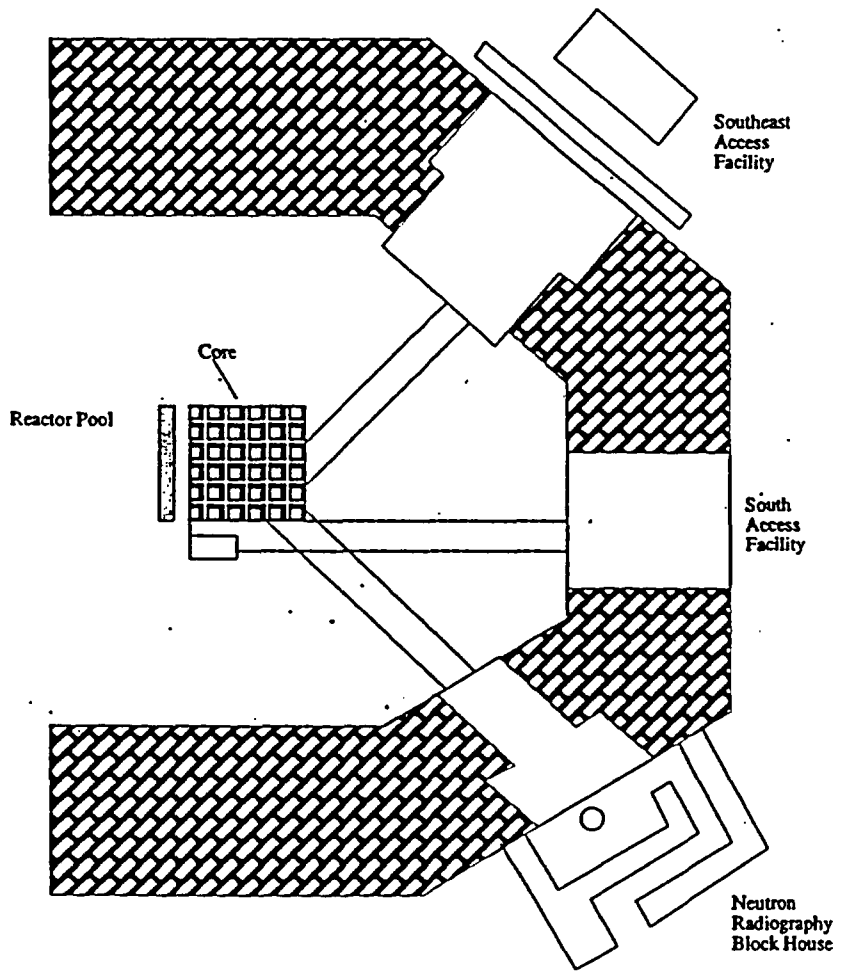

Figure 1.1. A sketch of the University of Virginia Reactor and the neutron beam ports (not to scale).

1.3 Monte Carlo Method and MCNP Code

The Monte Carlo method was initially developed as a radiation transport research tool at Los Alamos during World War II. Generally, Fermi, von Neumann, and Ulam were credited for the invention of Monte Carlo techniques as a mathematical discipline. As opposed to other computational methods, Monte Carlo methods are nondeterministic and are capable of treating very complex three-dimensional configurations. For a given set of cross section data, the errors in Monte Carlo calculations are in the form of stochastic uncertainties instead of systematic errors as in other deterministic methods [6].

A simplified procedure for a Monte Carlo simulation of nuclear particle transport is outlined as follows. A finite number of particle histories are simulated through the use of a pseudo-random number generator. Each particle's history starts by sampling the source distribution to determine the particle's initial energy, position, and direction. The particle will then travel some number of mean free paths which is also decided stochastically before colliding. After this, the material region and point of collision are given, and then the nuclide that particle has collided with and what kind of reaction, i.e., capture or scattering, are determined by randomly sampling the cross section data. If the reaction is a capture, this particle's history is terminated. If scatter occurs, then secondary particle's new energy and direction must be determined. The same procedures as above are applied repeatedly to this particle and all successive collisions until the particle gives up all its energy and is captured, or escapes from the region of interest.

MCNP4A code was used intensively in this work to model different boron shielding materials and simulate the attenuation properties of neutrons in these materials.

MCNP stands for Monte Carlo N-Particle transport code, and it has the ability of modeling neutron, photon, and electron transport problems in three-dimensional geometries. MCNP was originally developed by the Radiation Transport Group at Los Alamos National Laboratory. In the 1960's, the first version of this code, known as MCS, and then MCN, was written to solve neutron transport problems in three dimensions by using interaction data from separate libraries [7]. The photon codes MCG and MCP were then added and in 1973, MCN and MCG were merged to form MCNG [8]. The Version 1 of MCNP finally appeared in 1977, which stood for Monte Carlo Neutron Photon transport code until the electron transport code was added in 1990.

Users can define very complex objects by using some regular geometric surfaces in MCNP, and the radiation source definition parameters in MCNP are very powerful for constructing complicated source configurations. Since Version 3B, MCNP allows the user to define repeated structures and makes it possible to describe only once the cells and surfaces of any structure that appears more than once in a geometry. This feature was useful for this work in modeling the structure of BORAL.

1.4 Problem Definition

The criterion used to evaluate different boron neutron absorbers is the ^{10}B areal density of the materials. Areal density (a.d.) is defined as the amount of ^{10}B in grams per square centimeter of surface area. There are several methods developed to quantitatively determine the areal density for neutron shields. According to previous research [9], the neutron transmission measurements provide the most accurate method for determining

the ^{10}B content of manufactured parts.

At UVa, a ^{10}B areal density measurement system was built that utilizes a series of known areal density zirconium diboride (ZrB_2) disks. Because of previous experience with the material, its uniform boron content, and its ability to be accurately ground to a desired thickness, zirconium diboride was chosen as the standard test specimen material. The neutron beam can be calibrated by measuring the neutron transmission coefficient for the standard specimens, which contain an accurately known quantity of ^{10}B, and plotting the logarithm of the transmission coefficient versus the ^{10}B areal density. The measured transmission coefficient for an unknown test sample may then be converted to an areal density by use of this plot as a look-up table. The detailed neutronic inspection procedure of the borated aluminum can be found in Reference 10. For different profiles or thickness of borated aluminum products, pure aluminum shims are attached to the ZrB_2 disks to match the thickness of the borated aluminum plate. Since ZrB_2 disks and the borated aluminum products are different composites, the validity of using ZrB_2 disks with proper thickness of aluminum shims as calibration standards to measure the areal density of borated aluminum coupons needed to be verified. The advantage of using the calibration method instead of direct measurement method is that it is independent of the neutron beam characteristics and experimental setup.

The absorbing cross section of any material to a certain energy of neutrons is unique. Therefore, in a monodirectional, monoenergetic neutron beam with a point detector, the exponential attenuation property of the shielding material is assumed. However, in a polyenergetic neutron beam which may have multiple energy components,

or have a continuous neutron energy spectrum, neutron attenuation does not follow a simple exponential rule. Instead, the number of transmitted neutrons is the sum, or integral, of the transmitted neutrons corresponding to each energy component. The neutron transmittance beam at UVAR is a polyenergetic beam with a high thermalized component. The detailed energy spectrum could be measured by neutron activation analysis, but because of the low flux, this experiment was not performed. An indirect way of estimating the neutron spectrum was investigated in this thesis. The method included measuring a series of known areal density test specimens and using MCNP to fit the experimental data with multiple energy components. The neutron energy spectrum could then be unfolded and a good discretized approximation could be obtained.

BORAL, borated aluminum and zirconium diboride are three different boron containing materials. The first two are used widely in nuclear industry as neutron absorbing materials. They have different chemical and physical properties as well as different ^{10}B enrichments. Neutron attenuation properties of these materials were studied and compared with both experimental work and Monte Carlo modeling. A better understanding of the materials' physical structure was acquired by studying the significance of streaming effect in BORAL and borated aluminum.

Thus, the research goals for this thesis were: 1) to study the neutron attenuation properties of zirconium diboride, borated aluminum and BORAL and to investigate the streaming properties of BORAL and borated aluminum, 2) to verify the method of using ZrB_2 disks with aluminum shims to measure the areal densities of borated aluminum samples, and 3) to determine the energy spectrum of the UVAR polyenergetic neutron

transmittance beam.

CHAPTER 2

THEORY

This chapter provides the necessary theoretical background for the work done in this thesis. Neutron gauging techniques were used to quantitatively determine the ^{10}B concentration in different samples and the data obtained also served as an experimental base for the Monte Carlo modeling of the structure of those samples. A brief description of the neutron gauging system is presented and compared to neutron radiography system. The basic interaction mechanism of neutrons with matter is discussed. Exponential and non-exponential attenuation of neutrons is discussed with respect to monoenergetic and polyenergetic neutron beams. Special attention is paid to a few elements, ^{10}B, ^{11}B, Al, Zr, which are related to the thesis. The neutron channeling effect among granules of certain shielding materials was studied and a few mathematical models are summarized for a better understanding of later experimental and simulation results.

2.1. Neutron Gauging Techniques

Neutron gauging techniques have been used widely in many non-destructive testing applications [11][12]. A neutron gauging system, like other gauging systems, typically consists of three major components, namely source, sample, and detector. Depending on the applications, transmission or scattering geometry may be used (Figure 2.1). The three interaction phenomena of neutrons with matter (moderation, absorption and scattering) are the underlying physics principles of neutron gauging. The detector

counts primary neutrons from the source, which may have been slowed down and changed in direction by interactions in the sample. The output of the system is a scalar quantity, often the count rate or the total number of counts in a given interval. Gauging can be used to determine the relative amounts of particular elements, e.g., hydrogen and boron, provided that the constituent elements of the test sample are known beforehand. The technique is typically used to provide quantitative data such as measurements of thickness or moisture content of a material. Standard samples can be used for calibration. Since generally no effort is made to measure the energy of penetrated neutrons, gauging in this sense is not selective and cannot identify unknown materials.

The following section gives a brief discussion on the major components used in a neutron gauging system.

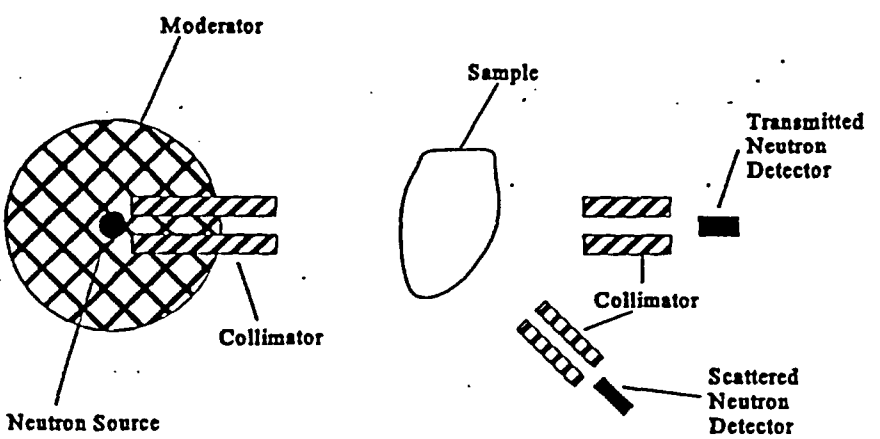

Figure 2.1. A schematic drawing of a neutron gauging system.

Source

The neutron source used in a gauging system can be selected from three source categories: reactor, radioisotope and accelerator [13]. Nuclear reactors are very prolific sources of neutrons. The flux is often very high. Most reactor beams are well moderated before they hit the targets, so the content of thermal neutrons is higher compared to other neutron sources. The major drawback of reactor sources is the lack of mobility, but many applications allow the test objects to be taken to the neutron source rather than requiring the source to be taken to the test objects. Thus, reactors continue to play a major role in neutron radiography and gauging. The fluctuations of the reactor power cause the fluctuations in the beam intensity, which would be noted as a fluctuating signal in a gauging system. In order to avoid erroneous results, some correction techniques have to be applied. For example, a dual detector setup is often used, the second detector simply being a beam monitor.

Radioisotopes are also often used as neutron sources. With sufficient energy, a gamma photon or an alpha particle can induce a (γ, n) or an (α, n) reaction. By intimately mixing certain light elements with a radioisotope that decays by the emission of high-energy photons or alpha particles, neutron sources can be fabricated. For instance, ^{124}Sb/Be source with (γ, n) reaction and ^{238}Pu/Be source with (α, n) reaction are often used in the laboratory [18]. The flux from these radioisotope sources are much lower compared to reactor sources. Spontaneous fission element ^{252}Cf can give a very high neutron flux and is used also as a neutron source, but it is extremely expensive and the shielding for a high flux ^{252}Cf source can be massive. The advantage of radioisotope

neutron sources is that they are relatively small in size and therefore semiportable. The beam is relatively stable because mainly it depends only on the reaction rate. Since the nuclear reactions are happening all the time, proper shielding around these sources is necessary, which could cause the difficulty in moving and storing them.

Accelerator sources generate neutrons by bombarding suitable target materials with energetic positive ions. The $^{2}H(d, n)^{3}He$ reaction and the $^{9}Be(d, n)^{10}B$ reaction are the two reactions widely used to produce neutrons. However, to get high neutron yield, sophisticated equipment is required and the investment is substantial.

Neutron gauging is not tied so closely to neutron source availability as radiography is, since the intensity required is much lower than for radiography.

Source moderator and collimator

A moderator is necessary only in slow neutron transmission or scattering gauging techniques. In neutron radiography a carefully designed source collimator is one of the most important parts of the system. In neutron gauging, collimators are most useful in conjunction with the thermal neutron transmission or scattering techniques, e.g., a collimated reactor beam. For many applications in gauging, source collimators are not necessary.

Neutron detector

Most gauging applications have been based on detection of thermal or epithermal neutrons [14]. The BF_3 proportional tube is a widely used slow neutron detector. Boron trifluoride gas with highly enriched ^{10}B in this device serves both as the target for slow neutron conversion into secondary charged particles as well as a proportional gas. The

detection efficiency of a BF_3 tube is a function of the neutron energy and the active length of the tube. When neutron energy goes up, the detection efficiency drops dramatically.

Detector collimator

Collimators are employed for small object gauging but not for large samples. Materials like borated polyethylene and cadmium are often used in collimators.

Neutron radiography (NR) is another technique used to obtain information about the internal structure of an object by using the penetrating nature of neutron radiation [15]. Neutron radiography is similar to X-ray radiography in the principle of their techniques and is complementary in nature. Like gauging, NR also consists of placing the object in a neutron beam, but the geometric pattern of transmitted neutron intensity is recorded, i.e., a picture is taken. Images can be recorded on films or by a real-time neutron camera. Radiography involves the recording of a spatially modulated signal on a medium which produces a visible image. Gauging, on the other hand, involves only the detection of the radiation intensity with an appropriate electronic or hard-copy display. Neutron radiography, therefore, has the advantage of a visible image while gauging offers real-time read-out with lower flux requirements. When the sample object is too thick, or the flux is not high enough, the image from neutron radiography will not have enough dynamic range to show the details of the test object's structure. In this case, gauging has to be used to acquire quantitative information.

2.2. Neutron Attenuation

The interaction mechanism of neutrons with matter is fundamentally different from that for the interactions of photons [16][17][18]. Because of the neutral charge property, neutrons essentially interact only with the atomic nucleus, whereas photons interact more often with the atomic electrons. The probability of a neutron interacting with a nucleus is described in terms of cross section (σ), which, for convenience, is often expressed in barns (1 barn = 10^{-24} cm^2). Loosely, the cross section can be considered as the target area which the particle encounters if an interaction is to occur. It can be represented graphically by drawing a region around the nucleus with the area of the region being proportional to the interaction probability as illustrated in Figure 2.2. The cross section (σ) mentioned here is also known as microscopic cross section, because it is considering the probability of a neutron interacting with only one nucleus.

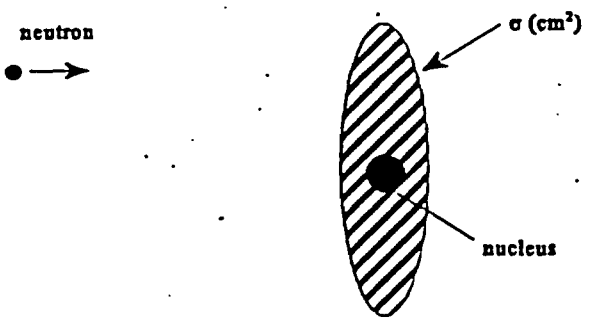

Figure 2.2. Diagrammatic representation of the neutron cross section.

Neutron interactions with matter can be classified into two categories, absorption and scattering. Scattering reactions allow the moderation or slowing down process to

occur. Elastic scatter occurs when both the kinetic energy and momentum of the incoming and emergent particles are conserved. Inelastic scatter occurs when the nucleus is raised to an excited state and emits a gamma ray in addition to a neutron. Absorption processes can be divided into three types: radioactive capture (n, γ), capture with particle emission, and fission. Some elements' total cross sections, which are of concern in this thesis work, are plotted in Figure 2.3. As can be seen here, the thermal cross section of ^{10}B drops rapidly with increasing neutron energy and is proportional to $1/v$. The thermal cross sections of ^{11}B, Al, and Zr are three orders of magnitude smaller than ^{10}B and do not vary much over a large neutron energy range.

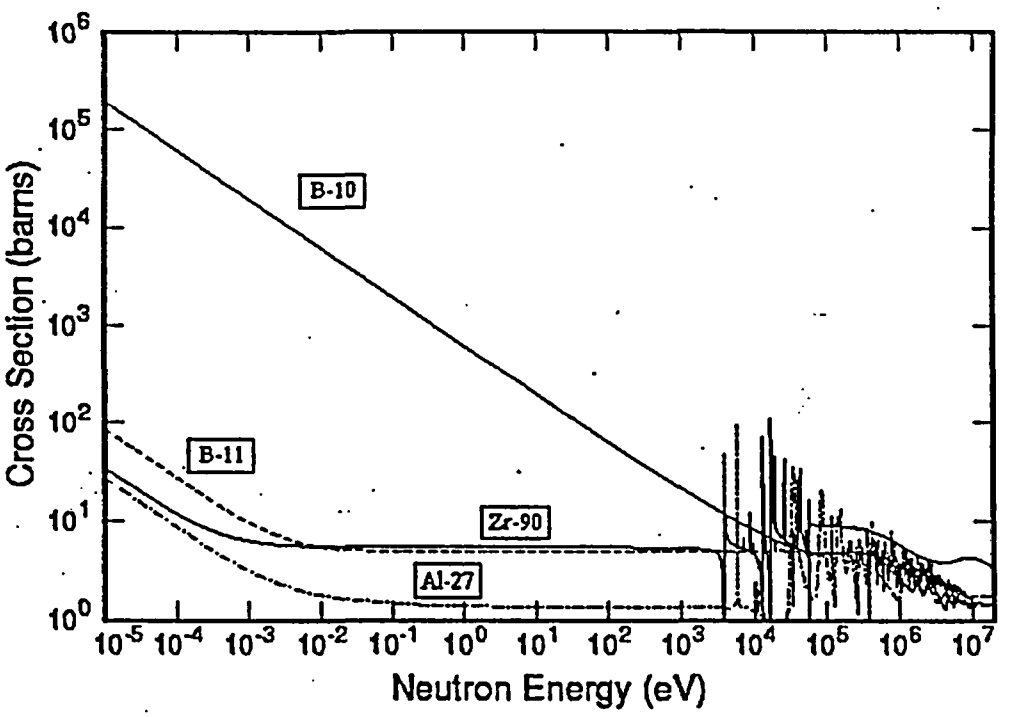

Figure 2.3. Cross section versus neutron energy for some elements of interest. (Data obtained from T-2 Nuclear Information Service using ENDF/ B-VI ACE library)

Now consider a collimated monoenergetic neutron beam impinging perpendicularly on a surface of area, as shown in Figure 2.4.

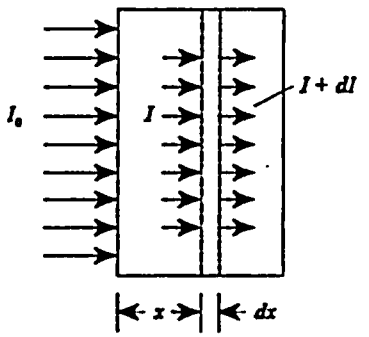

Figure 2.4. Illustration of collimated neutron beam attenuation.

Let S = surface area, cm^2,

x = distance from front surface, cm,

I_0 = initial beam intensity, n/cm^{2}s,

I = intensity at distance x, n/cm^{2}s,

σ = microscopic cross section, cm^2/nucleus,

N = density of target atoms, nuclei/cm^3.

The decrease in intensity, dI, as the neutrons pass through the differential slab, is the intensity at that point times the probability of interaction,

$$dI = -I\sigma N dx. \tag{2.1}$$

After separating variables and integrating for a thickness x, the intensity, I, at distance x is:

$$I = I_0 e^{-\sigma N x} = I_0 e^{-\Sigma x}, \tag{2.2}$$

where $\Sigma = \sigma N$ = macroscopic cross section, cm^{-1}, which represents the effective target area per unit volume of material. The neutron intensity decreases exponentially.

For any material, the microscopic cross section, $\sigma(E)$, is a function of neutron energy (E). The simple exponential attenuation is good for a monoenergetic neutron beam, because the microscopic cross section is a constant corresponding to that particular energy. When the neutron beam is a polyenergetic beam, the attenuation gets a little complex. Suppose a neutron beam has n discrete energy branches, E_1, E_2, ..., E_n. The initial flux for the energy branches are I_{01}, I_{02}, ..., and I_{0n}, respectively:

$$I_0 = I_{01} + I_{02} + \ldots + I_{0n}. \tag{2.3}$$

Consider the neutron attenuation problem with the same geometry setup used in the previous discussion. It is easy to see that each energy component can be individually treated as a monoenergetic and monodirectional neutron beam, and therefore, the exponential attenuation rule applies:

$$I_i = I_{0i} e^{-\sigma(E_i)Nx} = I_{0i} e^{-\Sigma(E_i)x}, \qquad i = 0, 1, \ldots, n \tag{2.4}$$

where, I_i is the intensity of branch i at distance x from the front surface. Notice, both the microscopic and macroscopic cross section depend on the energy. Furthermore, the total beam intensity at distance x is just the simple summation of the intensities of all branches:

$$I = I_{01}e^{-\Sigma(E_1)x} + I_{02}e^{-\Sigma(E_2)x} + \ldots + I_{0n}e^{-\Sigma(E_n)x},$$

$$= \sum_{i=1}^{n} I_{0i}e^{-\Sigma(E_i)x}. \qquad i=1, 2, \ldots, n \tag{2.5}$$

The sum of a series of exponential function is not a simple exponential function. Thus, the intensity of a polyenergetic beam decreases non-exponentially through a shielding material.

The transmission coefficient (T) of a neutron beam through a sample object is simply defined as:

$$T = \frac{I}{I_0}. \tag{2.6}$$

The transmission coefficient gives the quantitative ratio of penetrated neutrons.

2.3. Neutron Streaming and Channeling

Neutron attenuation property of a homogeneous material was discussed in last section. The picture gets much more complex when the neutron absorbers are distributed nonhomogeneously in a shielding material. BORAL is a perfect example of strongly neutron absorbing chunks, boron carbide clumps, dispersed in a weakly scattering matrix; aluminum. There are three issues in this kind of material which a uniform material does not have: spatial self-shielding, neutron channeling and streaming through the non-absorbing matrix. Figure 2.5 shows a schematic drawing of the structure of BORAL.

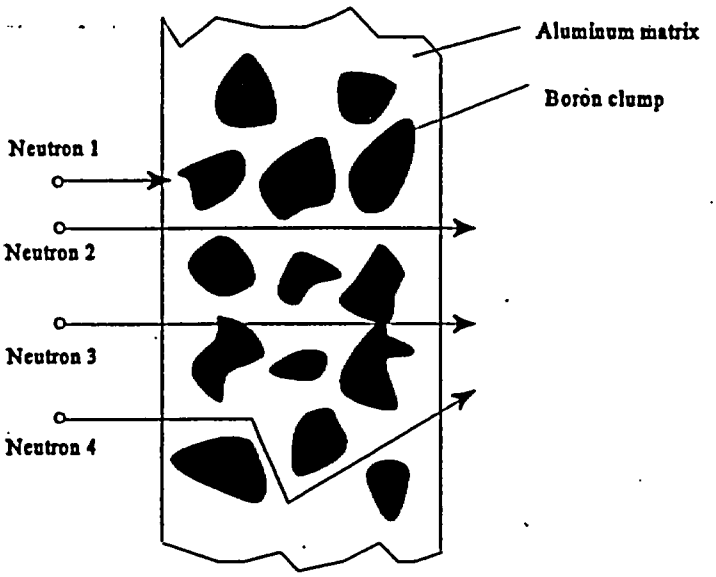

Figure 2.5. A schematic drawing of the BORAL core structure.

Consider first the case of Neutron 1. Since the size of boron carbide clump is in macro scale, this neutron will be most likely absorbed by this clump and will not be able to penetrate. As a result, the two clumps behind the first clump will not contribute to the neutron attenuation. Therefore, part of the shielding materials are wasted because of self-shielding.

Channeling is another problem which arises at nonhomogeneous materials. In the case of Neutron 2, the gap between the absorbing chunks gives neutrons a good chance to transit the shielding matrix without being attenuated because the neutron scattering cross section of aluminum is very small compared to the neutron absorbing cross section of ^{10}B. For Neutron 3, it does not see a open gap, but since on its path only a very thin layer of ^{10}B exists, the probability of penetrating is also increased.

When scattering occurs in the aluminum matrix, neutrons still have a high

probability of streaming around the boron clumps and manage through the material before giving up their energy. This is considered as neutron streaming effect as illustrated by Neutron 4.

In conclusion, neutrons have a better chance to penetrate this material without being attenuated compared to a homogeneous material. The same loading of ^{10}B, i.e., same areal density will give a higher transmission coefficient. The effective areal density will be smaller than the calculated areal density.

Several numerical models have been investigated and developed to calculate the transmission coefficient of a collimated neutron beam through BORAL plates. In Byrson, Lee and Burn's paper [19], three schemes were summarized and calculated neutron transmissions were compared to experimental results. The first model was developed by Burrus [3]. In this scheme, BORAL plate is treated as sequential layers containing purely absorbing particles. Walti used a unit-cell method to calculate the spatial self-shielding in an isotropic flux environment [20]. After the absorber-to-moderator flux ratio was calculated with this model, an effective cross section and neutron transmission coefficient was calculated for the BORAL using a volume and flux weighting. The third model was designed for collimated beam and the structure of BORAL was modeled with a unit cell which consisted of a spherical chunk centered in an aluminum cylinder. The transmission coefficient of a collimated neutron beam incident normally on the face of the cylinder was then obtained. The neutron transmission coefficients approximated with these models were fairly close to the experiments, especially for the second and third model. These results were also compared to the transmission coefficients obtained from a homogeneous

model. For same ^{10}B loading, higher transmission coefficients were observed as expected.

Another study done by Wells [4] at Georgia Tech on a spent fuel shipping cask made from BORAL showed that intergranular channeling effect is a significant phenomena for BORAL of the thickness typically used in spent fuel casks. The study showed that the granulated boron carbide areal density of 0.040 g $^{10}B/cm^2$ is equivalent to a homogeneous areal density of 0.033 g^{10}B g/cm^2. The article concluded that the channeling of neutrons between neutron absorber particles in fixed neutron poison materials can reduce the criticality control effectiveness of the material.

CHAPTER 3

EXPERIMENT SETUP AND TECHNIQUES

In order to investigate the neutron attenuation properties of boron containing materials, three series of neutron shielding materials, namely zirconium diboride disks, borated aluminum and BORAL sheets, were studied. The polyenergetic neutron transmittance beam at the UVAR and a monoenergetic neutron beam at the University of Michigan were utilized to measure the transmission coefficients of these materials. This chapter describes experimental methods for this work and in Chapter 4, the same experiments were simulated with MCNP to gain a better understanding of the physical structure of these materials and their neutron attenuation properties. Results of both experiments and simulations are presented in Chapter 5.

3.1 Material Properties

Boron, specifically the ^{10}B isotope, has long been used as a neutron absorber. Boron is naturally available in several forms: crystalline, amorphous and boron carbide. Various boron shielding products are commercially supplied to nuclear industries.

3.1.1 Zirconium Diboride

Zirconium diboride (ZrB_2) is a chemical compound of boron and zirconium, in which the content of ^{10}B could be natural or enriched. Eagle-Picher Boron provides the industry nuclear grade zirconium powder and tile. Because of its uniform boron content

and the ability to be accurately ground to certain thickness, a series of hot pressed ZrB_2 disks were used at UVAR as calibration specimens to measure the areal density of unknown boron aluminum samples. The zirconium diboride sheets are very fragile and as a result they are not used by the industry as shielding materials. In these experiments, each ZrB_2 specimen was mounted in a superpure aluminum block for the physical protection of the delicate disk. The thickness of the aluminum block was chosen to match the thickness of the thin unknown samples. The theoretical ^{10}B areal density of each zirconium diboride disk can be calculated by the following formula:

$$A = W \rho E T, \tag{3.1}$$

where A = ^{10}B areal density, mg/cm^2,

W = weight fraction of boron, wt %,

ρ = material matrix density, mg/cm^3,

E = ^{10}B enrichment, wt ^{10}B %,

T = disk thickness, cm.

3.1.2 Borated Aluminum

Borated aluminum is a neutron absorber made by Eagle-Picher Industries, Inc., which is used to build storage baskets for nuclear reactor fuel assemblies. The material is fabricated under a quality assurance program. The compound used to produce the master alloy is checked for the ^{10}B enrichment by isotopic spectrography. The master alloy contains between 4.5 wt.% and 5.2 wt.% boron. It is checked to ensure that the second

phase is aluminum diboride. The 6351 aluminum alloy is prepared by melting the master alloy, the boron content is adjusted by adding 1100 aluminum, and the other alloying elements are added to obtain the desired chemical composition. The aluminum is cast into ingots using a direct chill mold. As the ingots are poured, five samples are taken at the top, at 25%, 50%, 75% and at the bottom of the ingot in order to verify the chemistry of the aluminum and the boron content. Billets are prepared from an ingot. From a billet, different profiles of final borated aluminum products are extruded or rolled [21].

If the ^{10}B is distributed uniformly in the aluminum, its theoretical areal density can be calculated with the same formula, Eq. 3.1, used for the zirconium diboride. As an example, one borated aluminum sample used in this thesis work had a boron weight fraction of 0.5%, density of 2.7 g/cm^3, and ^{10}B enrichment of 95%.

The track-etch imaging technique was used to study the microstructure of borated aluminum. This technique is based on the exposure of the test material, placed in a close contact with a solid state nuclear track detector (SSNTD), to ionizing radiation. The reaction products, such as alpha particles, protons, and fission fragments, while passing through the detector, create local damage zones in the SSNTD surface layer with several nanometers in diameter (latent tracks). These tracks are then extended to several micrometers under specific chemical treatment. The technique is especially useful for micromapping of some doping or residual elements in the materials. The image obtained from track-etch experiments indicates the surface effects of the test sample in micro scale, whereas an neutron radiography image gives the line integral of neutrons through the test sample in a macro scale.

In order to determine the boron distribution in borated aluminum, the track-etch imaging technique was applied at UVa [22]. The experiments were based on exposing borated aluminum samples to thermal neutrons and detecting the $^{10}B(n, \alpha)^{7}Li$ reaction

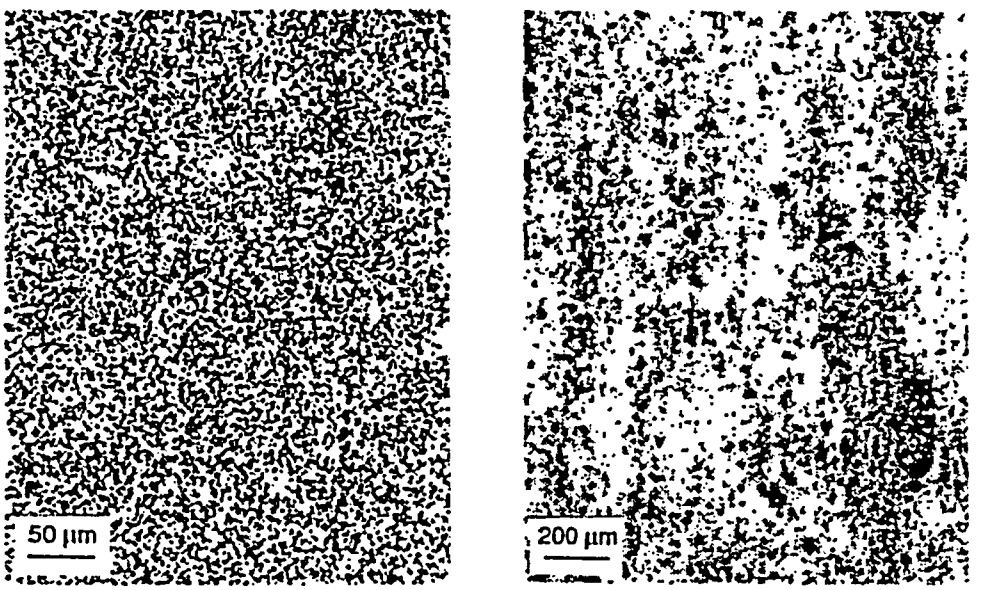

Figure 3.1. The distribution of boron in aluminum alloys: a)Al-6xxx, extruded, $C_B \approx 2.5\%$, b)Al-1100, hot-rolled, $C_B \approx 4.5\%$.

products with SSNTDs. Figure 3.1 shows the microstructure of borated aluminum. The black dots are tracks created by alpha particles from the (n, α) reaction. Therefore, each dot corresponds to a neutron-boron interaction. As seen here, the boron distribution of extruded sample a) is fairly uniform compared to sample b). Sample b) is from a hot rolled sample produced by using a different boron loading technique and shows the deformation of boron distribution caused by the rolling process. The borated aluminum samples used in later transmittance experiments were from the same process as sample a). The Monte Carlo modeling of borated aluminum was also based on the uniformly distributed sample.

3.1.3 BORAL

BORAL is a thermal neutron poison product of Brooks & Perkins, which has been used extensively in a wide range of neutron absorbing and shielding applications. Because of its good neutron shielding capabilities, BORAL is used around the world for spent fuel shipping and storage containers. It has also been used on the inner section of reactor shields, shutdown control rods, and as neutron curtains and shutters for thermal columns.

BORAL has a very unique "sandwich" structure as shown in Figure 3.2. The inner part of BORAL is a core of fine boron carbide particles, dispersed evenly throughout a matrix of aluminum. The outer cladding or "skins" of the sandwich panel is 1100 alloy aluminum. Boron carbide is a compound having a high natural boron content in a physically stable and chemically inert form. Macroscopically, the boron carbide particles may appear to be uniformly distributed in the aluminum matrix. However, the microstructure of BORAL core was revealed to be very nonhomogeneous by using optical microscopy method [23]. In Figure 3.3, boron carbide can be distinguished as dark grey particles of various sizes. Two reactive phases surrounding the boron carbide particles are identified as AlBx compounds and Al-B-C compound. The existence of gaps among the boron carbide chunks can be observed.

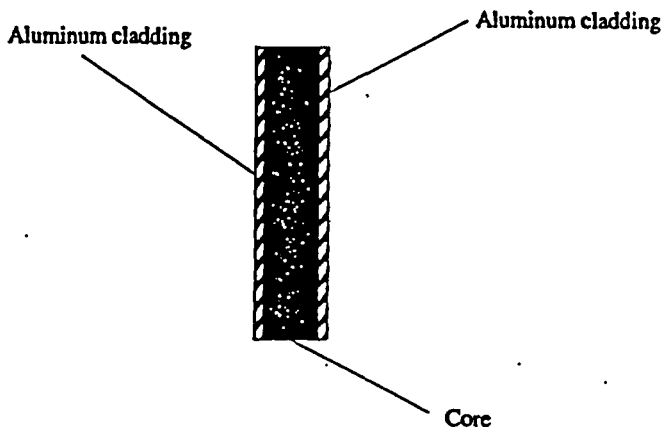

Figure 3.2. The macro structure of BORAL.

Figure 3.3. An optical micrograph of a BORAL sample with a 62% boron carbide compact [23].

BORAL panels can be furnished either in the flat panel form or fabricated into a variety of plane geometrical shapes by standard metalworking methods and techniques. The shielding capability of BORAL is assured by wet chemical analysis or neutron attenuation testing and is specified as a minimum of grams of ^{10}B per square centimeter of surface area. BORAL panels with thicknesses (including cladding) from 2.11 mm to 4.37 mm, used for high density spent fuel racks, have a constant core composition and constant cladding thickness. ^{10}B loading is from 0.025 g/cm^2 to 0.060 g/cm^2, respectively. By simple calculation, for the panels with total cladding thickness of 0.512 mm, the core ^{10}B volume concentration is 0.156 g/cm^3. According to a Brooks & Perkins report, 18 wt% ^{10}B in natural boron, 28.28 wt% boron in boron carbide, and the boron carbide density of 2.51 g/cm^3, the boron carbide's volume ratio in the core region can be calculated as 44.11% [2].

3.2 Experimental Setup

This section describes the experimental setup of the neutron gauging system used to measure the neutron transmittance through the various shielding materials. The setup described here is a typical neutron gauging system as discussed in the previous chapter, which consists of three major components: the neutron source, sample object and the detector.

3.2.1 Neutron Transmittance Beam Description

The neutron source is the University of Virginia Reactor (UVAR), a 2 MW light-

water pool reactor with partial graphite reflection. Figure 3.4 shows the detailed configuration of the neutron transmittance beam port. It consists of an in-pool beam tube, an air path in the graphite and concrete block in the access facility, which is immediately on the other side of the pool wall, a beam tube in the shielding dolly, a lead shield at beam exit and a beam stop.

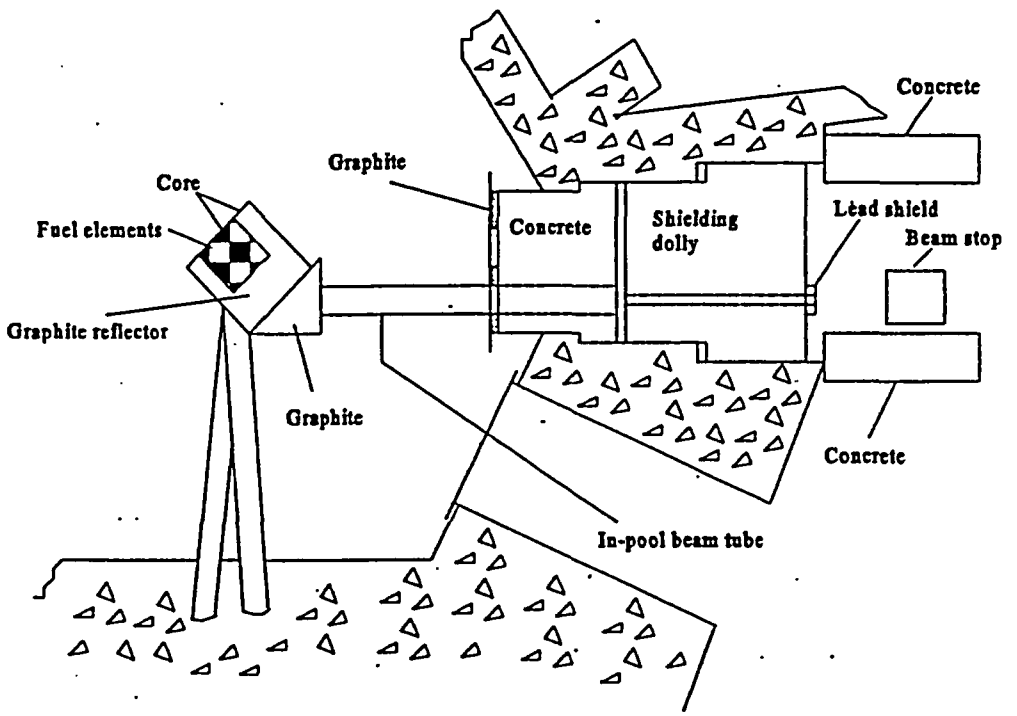

Figure 3.4. The UVAR neutron transmittance beamport facility configuration.

The in-pool beam tube starts with a triangular nosepiece made of aluminum and filled with solid graphite. The nosepiece is used to collect neutrons from a large area of the reactor core and scatter them into the beam tube. Attached to the nosepiece is an air-filled aluminum tube with an inner diameter of 12.7 cm. In order to suppress the gamma

flux, the in-pool tube is not pointing directly at the core fuel elements.

The dry section of the neutron beam port that penetrates the reactor shielding wall is then collimated into two neutron beams in the shielding dolly. Figure 3.5 shows the design of beam tube through the shielding dolly. Three steel tubes were used and the outer tube is filled with borated mortar and lead shot. The voids in the two inner tubes form two collimated neutron beams. The space in between the tubes is filled with borated mortar and lead shot to block neutrons and gamma photons. The center line distance between the two beams is 4.7 cm and the area of each beam is 1 cm^2 at the sample position. Measurements with either one or two beams can be made simultaneously. The thermal flux is about 5×10^4 n/cm^2s for the upper beam and 7×10^4 n/cm^2s for the lower beam. The cadmium ratio is measured to be approximately ten (10) measured with gold foils.

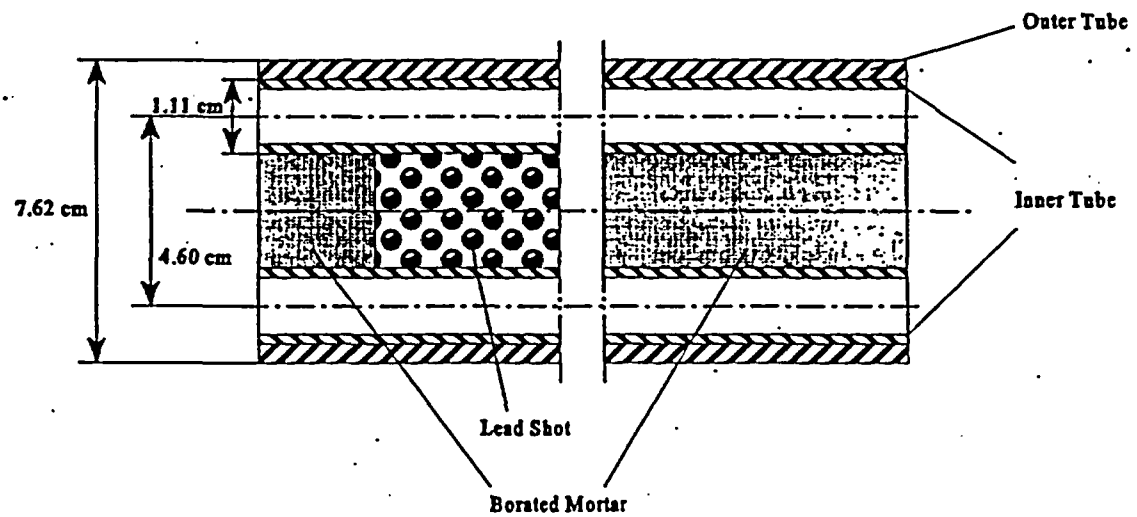

Figure 3.5. A diagram of the design in the shielding dolly which splits the neutron transmittance beam into two separate beams.

A series of zirconium diboride disks were measured for areal density at the University of Michigan's monoenergetic beam facility illustrated in Figure 3.6. Neutrons come out from the reactor and impinge upon a single crystal copper monochrometer. Because of the Bragg scattering effect, for a certain neutron incident angle, neutrons will be reflected to the same angle and the scattered neutrons along this direction have the same energy, which can be computed using de Broglie wavelength theory and Bragg's Law [24].

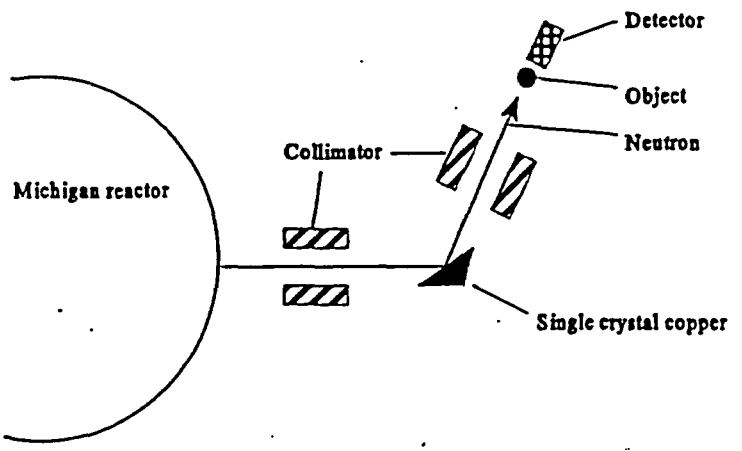

Figure 3.6. The monoenergetic neutron beam setup at the University of Michigan.

3.2.2 UVa Equipment Setup

Figure 3.7 shows the equipment setup for the attenuation measurements at UVa. The two separate beams exit the collimators, penetrate the sample and the transmitted neutrons are detected by two independent BF_3 neutron detectors. The detector tubes are shielded with borated aluminum to maintain the independence of each measurement. Additional shielding behind the detectors acts as a beam stop.

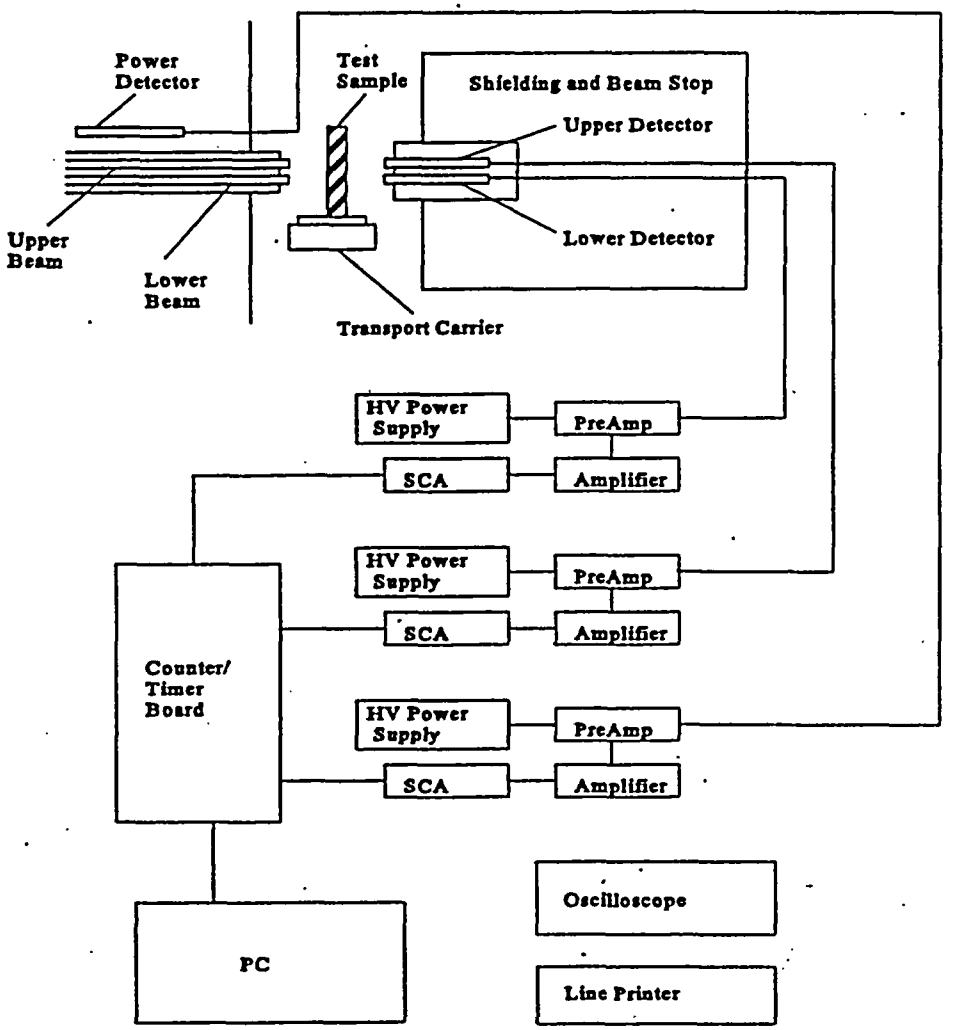

Figure 3.7. A schematic side view of equipment setup for the neutron transmission measurements at UVa.

The sample object was carried in front of the beam by a transport carrier system which consists of a roller track, plate holder, roller chain and gear drive, and a 400 step stepper motor. A top view of the carrier relative to the neutron beams and detectors is shown in Figure 3.8. Neutron transmittance data was collected using one or two

independent counting systems, each consisting of a BF_3 neutron detector, preamplifier, high voltage power supply, linear amplifier, and single channel analyzer (SCA). A third BF_3 neutron detector system was used as reference detector to monitor any changes in neutron intensity due to small fluctuations in the reactor power. The signals from each SCA were routed to a computer controlled counter-timer board.

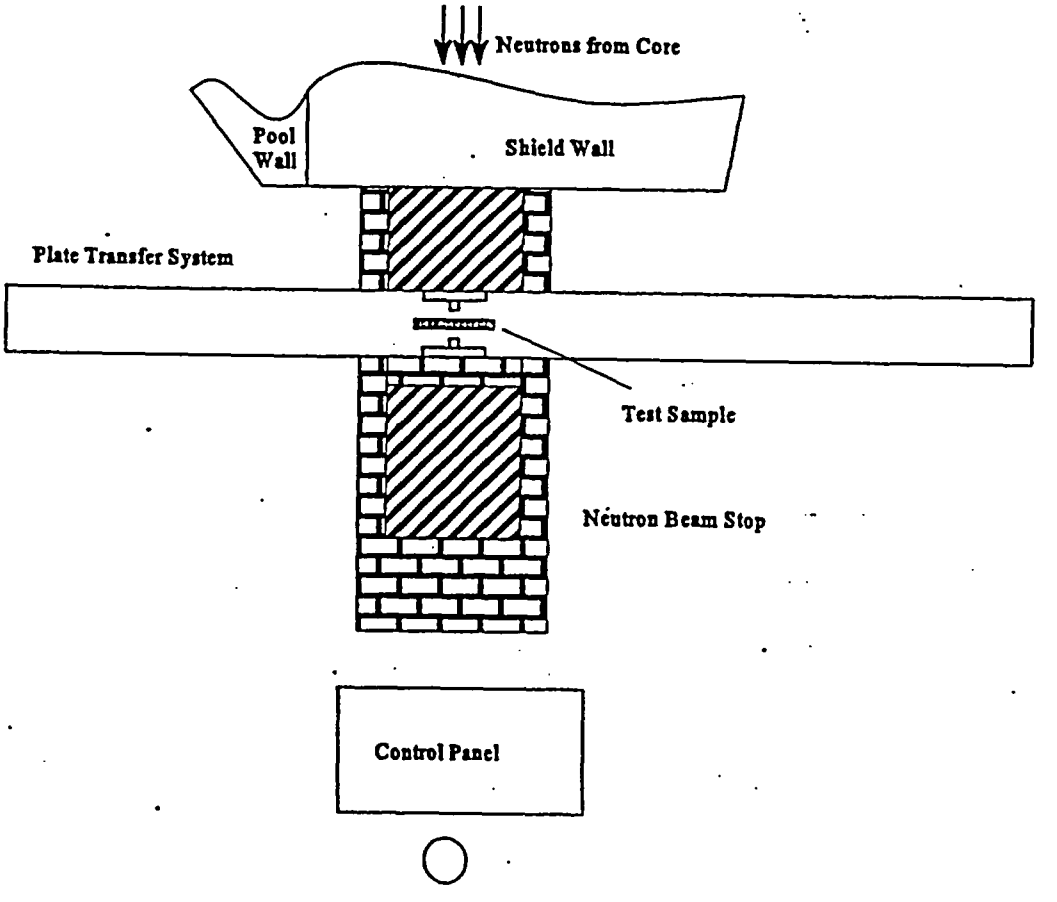

Figure 3.8. A top view of the neutron gauging system setup used at UVa.

3.2.3 Counting Techniques and Transmission Calculations

Several counting programs were developed by previous researchers to control the whole neutron gauging system and acquire the transmitted neutron counts. For most samples in this work, the counting time was 30 seconds to obtain good counting statistics. The counting time was doubled for thick samples (areal density > 40 mg $^{10}B/cm^2$). For every measurement, the counting time, raw counts and power counts were displayed on the monitor and simultaneously recorded onto the hard disk. The power counts were used to monitor the variation of reactor power and served as a correction factor in the transmission calculation. Transmission coefficients were calculated by:

$$T = \frac{I}{I_0} = \frac{\frac{C_{raw(sample)}}{t_{raw(sample)}}}{\frac{C_{raw(blank)}}{t_{raw(blank)}}} \times \frac{\frac{C_{power(blank)}}{t_{power(blank)}}}{\frac{C_{power(sample)}}{t_{power(sample)}}}, \qquad (3.2)$$

where,

$C_{raw(sample)}$ = raw counts of the tested object,

$t_{raw(sample)}$ = count time for the tested object,

$C_{raw(blank)}$ = raw counts of the neutron beam without being attenuated,

$t_{raw(blank)}$ = count time for the blank beam counts,

$C_{power(sample)}$ = power counts acquired the same time as counting the sample,

$t_{power(sample)}$ = power counts counting time when counting the sample,

$C_{power(blank)}$ = power counts acquired the same time as counting the blank beam,

$t_{power(blank)}$ = power counts counting time when counting the blank beam.

The background neutron counts in a one minute counting time interval were insignificant compared to the counts from the reactor neutron beams and therefore, were not taken into account in Eq. 3.2.

CHAPTER 4

MCNP SIMULATIONS

In a neutron gauging system, there are many different parameters that can affect the physical variable we are interested in. For example, the neutron source could be monoenergetic or polyenergetic, the test sample could vary in physical and chemical composition and different detectors could be used. In any particular experimental setup, most of the gauging system's components are fixed and therefore, it is hard to study the relationship between the variable of interest, in this case the transmission coefficient through different boron containing materials, and other parameters built in the system. In an experiment it is difficult to isolate each component's contribution. On the other hand, in a computer simulation each parameter can be controlled separately and its effect can be studied individually while other parameters are kept constant.

MCNP4A was used to model the neutron attenuation properties of the different materials studied in this work. It was installed on an IBM RS/6000 model 340 workstation running on the AIX 3.2.5 operating system that is mainly used for the computational analysis of nuclear engineering problems. In order to get good statistics, a large number of particles are used in the Monte Carlo simulations and, therefore, the computation times are significant. The UVa SP2 (Scalable POWERparallel System) was used to handle large scale problems. Currently, the SP2 consists of 16 RS/6000s, each known as a node, which can lower the computing time required to obtain the results of the programs by spreading the work over several of the processing nodes.

4.1 MCNP Basics [25]

To simulate a real world event with MCNP, some input files are needed to initiate the program and start the Monte Carlo simulation. The main input file provided by the user has all the necessary descriptions of the real transport problem, including the physical setup, sample materials, and source descriptions, etc. It has the following form:

```
Message Block
Blank Line Delimiter
Title Card
Cell Cards
      .
      .
Blank Line Delimiter
Surface Cards
      .
      .
Blank Line Delimiter
Data Cards
      .


Blank Line Terminator
Anything else
```

The message block at the beginning of an input file is optional and it can be used to avoid retyping an often-repeated message. However, the title card, which occupies columns 1 - 80 of a line, is required for every problem and it is used as a title in various places in the MCNP output. To describe the geometric setup of a problem, MCNP divides the three-dimensional region into some appropriate cells in a selected Cartesian coordinate system (right-handed system is often chosen). Using the cell specifications, MCNP is able to track particles through the geometry. The information of cells are

supplied in the cell cards block. Each cell is defined by the intersections, unions, or complements of the regions' bounding surfaces, which are predefined in the surface cards block of the input file. MCNP allows the user to define first- and second- degree surfaces and some special fourth-degree surfaces (elliptical tori). The flexibility to construct combinatorial geometry of MCNP is superior than many other Monte Carlo codes. Information about the sample materials, source definitions, tally cards and other relevant data are listed in the data cards block. More details on data collection for all these cards construction of this project are discussed in the following sections of this chapter.

The output file from MCNP contains the tally information specified by the user in the input file and standard summary information in ledger tables to give the user a better idea of how the problem ran. This information can give insight into the physics of the problem and the adequacy of the Monte Carlo simulation. The output file also keeps a log of the messages while the program is running, so if any error occurs, the user can debug the input deck by reading the information listed in this file.

MCNP also supports two plotting capabilities. PLOT is used to plot two-dimensional slices of a problem geometry specified in the input file. The MCPLOT can plot the tally results produced by MCNP to help the user understand better the results. The geometry plotter is very valuable for debugging geometries, especially complicated geometries. The user's time can be saved by visually verifying the geometry setup using the geometry plotter.

4.2 Geometry

MCNP is a very generalized-geometry Monte Carlo transport code, which treats any arbitrary three-dimensional configurations of materials in geometric cells bounded by first- and second-degree surfaces and some fourth-degree surfaces (elliptical tori), in a properly constructed Cartesian coordinate system. MCNP tracks particles through the geometry by using the cell specifications. Each cell is surrounded by one or several surfaces and by using intersections, unions and complements of the regions bound by those surfaces, the cell can be defined. To specify a surface, certain information needs to be supplied, such as the surface type, the coefficients to the analytic surface equations and maybe some known points on that surface.

The experimental setup used in our neutron gauging system has a very simple geometry. As shown in Figure 3.7, it has three distinct regions, the source, the shielding material and the detector. Since the neutron transmission coefficient is the only concern in this study, the details of the neutron beam coming out of the reactor core, which has a complex geometry, were not simulated. Instead, a simplified parallel neutron plane source with estimated energy spectrum was used to simulate the UVAR beam. For the same reason, the details of the BF_3 neutron detector used in the experimental work was not modeled. Only the number of neutrons penetrating through the sample within a certain interested area, which is the same as the area of the detector, was tallied. Three different shielding materials were modeled to study their neutron attenuation properties. The first two materials, zirconium diboride disks with aluminum shims and borated aluminum, had a relatively straightforward structure, and therefore the descriptions of the

geometry were simple. The third material, BORAL, whose core structure was a macroscopic mixture of boron carbide chunks and aluminum matrix, was extremely difficult to model. The following section provides the MCNP models of these three materials excerpted from some input files.

The plane neutron source was located on the first surface of the object. The detector was a void at the back of the objects. Without loss of reality and to simplify the problem, the objects were treated as round disks. The thickness of the disks were calculated for the different materials.

The set of cell cards for modeling of zirconium diboride disk with aluminum, shown in Figure 4.1, is given below:

```
1    1     -5.7273        1 -2 -3     $ ZrB2 disk region, density
2    2     -2.7000        3 -2 -4     $ Al shim
3    0                    4 -5 -6     $ detector
4    0                    #1:#2:#3    $ outer region
```

Each row of the cell card consists of four parts of data. The first number is the cell number. In this case, cell 1 is the ZrB_2 disk region, cell 2 stands for the aluminum shim, cell 3 is the detector region (void) used for tally the results and cell 4 is the outer region of the objects. The second number in each line is the corresponding material number in that cell and the description of that material is given in the data cards. If the material number is 0, that region is treated as a void and particles will travel through it without any interactions. Here, material number 1 is zirconium diboride and material number 2 is 1100 aluminum. The third number is the density of the material. A negative value is interpreted as the mass density in units of g/cm^3, and a positive entry is interpreted as the

atomic density in units of 10^{24}atoms/cm^3. The density number is omitted when that region is void.

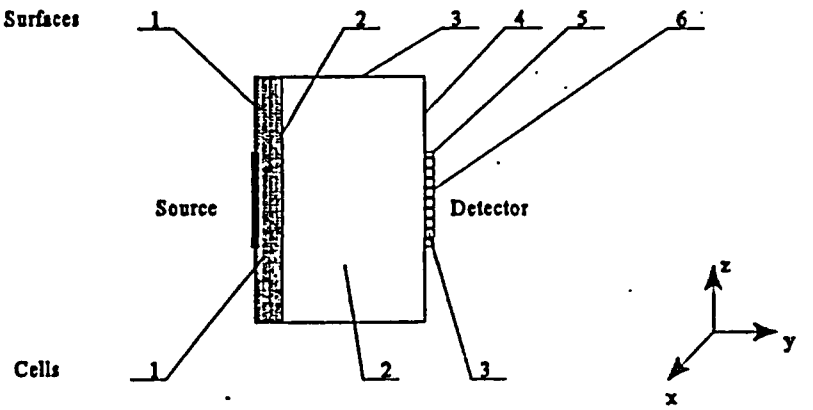

Figure 4.1. The MCNP geometry setup for zirconium diboride disk with aluminum shim.

The last series of numbers specify the spacial geometry of that cell. By using Boolean operators, intersection (no symbol - implicit), union (colon, ":") and complement (pound, "#"), on some predefined surfaces and cells, a new cell's position and shape can be defined. Each surface in Euclidean geometry divides the whole space into two separate regions. In order to differentiate one region from the other, the concept of sense was introduced. A point (x, y, z) is defined as having positive (or negative) sense with respect to a surface when the expression for that surface evaluated at (x, y, z) is positive (or negative). In the example above, cell 1 is the region that has a positive sense with respect to surface 1, AND a negative sense to surface 2 AND a negative sense to surface 3. Cell 4 is the union of regions that outside of cell 1, 2 and 3. When a neutron enters this cell, its history is ended.

MCNP provides a very convenient way to define first- and second-degree surfaces

(and some fourth-degree surfaces) for the geometry setup. There are total 26 surface types available in MCNP, and each of them has a unique mnemonic.. The following is a surface definition example used in ZrB_2 disks simulation:

```
1    py  0                    $ source plane,1st surface of disk
2    cy  2.539                $ cylindrical surface, radius
3    py  0.01981              $ 2nd surface of disk, 1st surface of Al
4    py  0.55481              $ 2nd surface of Al
5    cy  0.5642               $ 1cm2 detector
6    py  0.56481              $ detector surface
```

The surface types, equations, their mnemonics, and the order of the card entries are given in the MCNP manual [25]. The first number in each surface definition line specifies the surface number which is used in the cell definitions. The second part is the mnemonic to specify the surface type and the remaining card entries are the coefficients required by that surface type. In the example above, "`3  py  0.01981`," means surface 3 is a plane normal to Y-axis located at $y = 0.01981$ cm. Surface 2 is a cylindrical surface defining the outer surface of the objects.

The cell and surface definitions of borated aluminum is even simpler, because in this case, enriched boron and aluminum is mixed together uniformly in the second phase and is treated as an alloy. Cell 1 and cell 2 were combined for modeling the borated aluminum.

However, because of the package structure of BORAL, the modeling of boron carbide chunks randomly distributed in aluminum matrix is extremely difficult. The repeated structure feature of MCNP was utilized to try to describe the structure of

BORAL.

The primary goal of the repeated-structures capability in MCNP is to make it possible to describe only once the cells and surfaces of any structure that appears more than once in a geometry. A simple model of BORAL core with uni-sized spheres was constructed as following:

```
c cell definitions
1    2      -2.71        1 -2 -3 imp:n=1
2    0                   2 -3 -4 fill=1 (0 0.1538 0) imp:n=1
3    2      -2.71        4 -3 -5 imp:n=1
4    0                  -6 7 -8 9 -10 11 fill=2 lat=1 u=1 imp:n=1
5    1      -2.51       -12  u=2 imp:n=1
6    2      -2.71        12  u=2 imp:n=1
7    0      -1:5:3       imp:n=0

c surface definitions
1    py  0
2    py  0.0256
3    cy  2.5
4    py  0.2816
5    py  0.3072
6    px  0.0045
7    px -0.0045
8    py  0.0045
9    py -0.0045
10   pz  0.0045
11   pz -0.0045
12   so  0.00425
```

The first block defined the cells in this model and the second block gave the definitions of geometric surfaces. As discussed before, BORAL has three regions, two skins and one core. Cell 1 and 3 defined the front and back skins, and cell 7 was the outside region. Cell 2 was the core region, which was filled with boron carbide and aluminum. "`fill=1`" indicated that cell 2 was filled with `universe 1`, where `universe 1` was defined by cell 4. Cell 4 was a cube with a length of 90 μm which was filled with `universe 2`. And `universe 2` was defined by cell 5 and 6. Cell 6 is boron carbide sphere which had a diameter of 85 μm. Cell 5 was the region outside of the sphere, and the material was

aluminum. So cell 4 was just an aluminum cube but the center was occupied by boron carbide. Therefore, the core region defined by cell 2 was filled with this kind of cubes one by one. This was a very crude model of BORAL core, because the irregular-

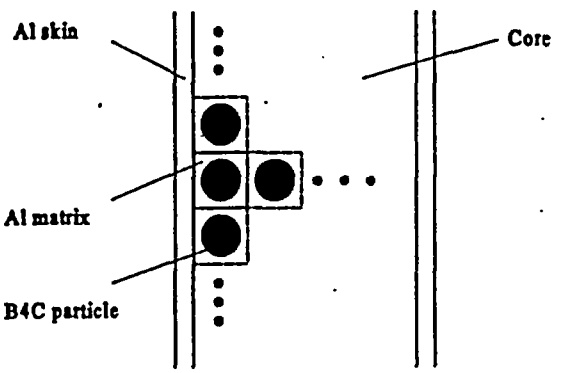

Figure 4.2. A crude model of BORAL core structure with MCNP.

shaped and various-sized B_4C particles were represented by spheres of one size and there was no randomness in the positioning of the spheres (Figure 4.2). The surfaces were defined in the second block. Surface 12 defined a sphere to represent a B_4C particle, whose diameter was 85 μm, which is the reported average size of B_4C particles in the core [23]. It was calculated that the volume ration of B_4C in the core was 44%, which was equivalent to putting a sphere of 85 μm into a box with length of 90 μm. Surfaces 6 to 11 defined the required surfaces of this box.

When the cells are defined, a problem mode (type) card and the cell importances are required in the input deck. For neutron transport study, `mode n` was used to specify this problem type. MCNP also supports photon (`mode p`) and electron (`mode e`) transport modes and the combinations of these three. An importance number was assigned to each cell as a weight value for the particles in that cell, and the higher the importance value,

the more weight fraction is given to the particles. When the importance of a cell is zero, the particle's history will be terminated if it enters the cell. The importance cards play a major role in some special Monte Carlo techniques, such as geometry splitting, Russian roulette and weight cutoff. In the modeling conducted in this work, every cell except the outer region is given equal importance, 1. Below is this part of input deck for the simulation of zirconium diboride disks:

```
c     ****** Problem run mode ******
mode  n
c     ****** Cell importances ******
imp:n 1 1 1 0
```

4.3 Materials

Material cards specify the isotopic composition of the materials in the cells and the cross section evaluations which are to be used. The following was the material definition used for zirconium diboride simulation:

```
c     ****** Material Definitions ******
m1      40000.50c  -0.81410          $ Zr
        5010.50c   -0.10232          $ B-10, enrichment 0.5504
        5011.55c   -0.08358          $ B-11,
m2      13027.50c  1                 $ Al
```

Two materials were used here. Material 1 is ZrB_2, and material 2 is aluminum. The material numbers were used in the previous cell definitions. The material number is followed by specifications of the constituents of this material, in the format of

ZAID1 fraction1 ZAID2 fraction2 ...

The *ZAIDi* is the nuclide identification number that has the form of *ZZZAAA.nnX*, where *ZZZ* is the atomic number, *AAA* is the atomic mass (for naturally occurring elements, *AAA = 000*), *nn* is the library identifier, and *X* is the class of data (*X = c* for continuous-energy neutron tables, *X = d* for discrete-reaction tables). Available cross section libraries and nuclide *ZAID* numbers can be found in Appendix G in MCNP manual. *Fractioni* is the atomic fraction (or weight fraction if entered as a negative number) of constituent *i* in the material. In this example, material 1 was the ZrB_2 compound, where Zr is natural zirconium and ^{10}B is 55.04% enriched. Weight ratios were input to model zirconium diboride.

In the borated aluminum model, since the boron and aluminum were assumed to be mixed together close to the atomic scale, a similar material definition using weight ratios of the constituent elements was used. This was also the case for the definition of boron carbide (B_4C) in BORAL core modeling.

4.4 Source Definition

To start any MCNP problem, a source definition has to be given in the source cards section. Four different sources can be specified by using four cards: general source (SDEF card), surface source (SSR card), criticality source (KCODE card), and user supplied source. Some source distribution functions, which are specified on the `SIn`, `SPn`, `SDn` and `DSn` cards, can be used for all but the criticality sources. The source geometry, the behavior of the particles emitted from the source and other source characteristics need to be further defined with some detailed variables.

In this work, neutron attenuation experimental data for different boron containing materials were obtained using both monoenergetic and polyenergetic neutron beams. Therefore, two kinds of neutron sources with different energy spectrums were constructed and used in all the simulations to permit comparison of the MCNP results with the experimental results. The monoenergetic beam at the University of Michigan was relatively easy to model since the single energy is known, whereas, the polyenergetic beam of the UVAR was very hard to simulate because the energy spectrum remains unknown, even though the beam's geometric design is clear. Both beams were well collimated and in the simulations, same geometries were used.

In the following section, a monoenergetic neutron beam setup is listed and used as an example to illustrate how to set up the source cards in the input deck for MCNP. Then, a discussion on the energy spectrum analysis of the UVAR beam is given.

The MCNP description of University of Michigan's monodirecitonal monoenergetic beam is given as follows:

```
c *** uniformly distributed monoenergetic(0.06eV) disk source  ***
sdef  pos=0 0 0 sur=1 rad=d1 dir=1 erg=6e-8 vec=0 1 0
si1 . 0.5642                    $ 1 cm2 area, radius
```

This defines a plane disk source located on surface 1, as seen in Figure 4.1. The center of the source is on the origin. Neutrons are emitted with energy of 0.06 eV, pointing on the positive Y axis direction. The required mnemonic `sdef` for the definition of general source was followed by a series of source variables. The combination of these variables described the characteristics of this source. A plane disk source was set up to represent

the parallel beams with an area of 1cm^2 (radius = 0.5642 cm). Since the only physical quantity of concern was the transmission coefficient for sample object, the source's physical location did not matter. To simplify the problem without changing the question itself, the source was put right on the front surface of the object in the center position. The `sur` value was set to a plane surface 1, which indicated the position of the particles was sampled on that plane. In some other applications, cell sources with volume distributions are needed and in those cases, the variable `sur` was set to zero. The sampled value of `pos` was set to be `0 0 0`, which was a point on plane surface 1. This is crucial because MCNP, for the sake of speed, does not check it. Erroneous results may be obtained if the point defined by `pos` is not on the source surface. The sampled position of the particle was at a distance from `pos` equal to the sampled value of `rad`. `rad` was set to `d1` here, which means the radius variable was given by a probability distribution. The corresponding information is given in the next line; `si1 0.5642`, is interpreted as `si1 0 0.5642` and provided the effect of card `sp1 -21 1`, which means the particle position was sampled uniformly within radius `0.5642` of point `0 0 0`. The combination of `dir` and `vec` defines the required monodirectional source. The `vec` value is `0 1 0`, which defines a reference vector pointing in the positive Y axis direction. The `dir` is the cosine of the angle between the sampled direction vector and the reference vector. With a value of 1, indicating the angle is 0, the sampled particle direction is parallel to the Y axis and points to the shielding objects.

To properly simulate the UVAR neutron gauging beam was rather difficult. The geometry presented in Chapter 3 is clear and the same setup was used as the

monoenergetic beam listed above. Special effort was made to analyze the beam energy spectrum. The transmission coefficients for a series zirconium diboride disks with known areal densities, ranging from 8 mg^{10}B/cm^2 to 60 mg^{10}B/cm^2, were measured using the UVAR beam. In a semi-logarithmic plot of transmission coefficient versus areal density (or thickness), a non-linear curve was seen, which means the attenuation coefficient was not unique and the beam was polyenergetic. This confirms the non-exponential attenuation theory, when multiple energies' neutrons are present. According to the discussion of neutron attenuation theory in Chapter 2, the attenuation follows the exponential rule in a monoenergetic and monodirectional neutron beam, since the cross section is unique for that particular neutron energy. The same semi-logarithmic plot will show a straight line and the absolute value of the line's slope corresponds to the macroscopic attenuation coefficient. There are several different ways to determine the neutron beam spectrum. One way to do this is to irradiate series of threshold foils and do activation analysis, but the problem with this is that this neutron beam's flux is not high enough and the irridiation has to be very long to get a statistically valid answer. An alternative way is to use MCNP to model the whole UVAR core and beam setup to obtain an accurate beam spectrum. However, this is a very complicated and time consuming job. On the other hand, since the experimental data of the transmission coefficients contains the information of the beam energy characteristics, by fitting the curve with the a series of straight lines, a quick and good decomposition of the continuous spectrum can be obtained. Initial attempts were tried using a combination of two energies, each with a Maxwellian distribution, to fit the curve. After a few rounds of iteration, an acceptable

result was achieved but it was hard to improve the accuracy in this game by just guessing. To optimize the fit, the method of non-linear least squares fitting to an arbitrary function was utilized for this purpose. As was previously discussed, the transmission coefficient for monoenergetic neutron particles can be described in a simple exponential form:

$$T = \frac{I}{I_0} = e^{-\Sigma x}. \tag{4.1}$$

After discretizing the continuous neutron energy spectrum into a series of single energy branches, the transmission coefficient takes the following form:

$$T = \frac{I}{I_0} = \sum_i (f_i \times e^{-\Sigma(E_i)x}), \tag{4.2}$$

where f_i is the amount percentage of the i^{th} branch in the neutron beam. Four energy branches were used to fit the experimental curve. Eight parameters were needed to be approximated, namely, E_1, E_2, E_3, E_4, f_1, f_2, f_3 and f_4. A detailed discussion on how to use the nonlinear least squares method to optimize the parameters can be found in Chapter 5.

The following is the final source cards used in the input deck for the UVAR polyenergetic neutron beam simulation:

```
sdef  pos=0 0 0 sur=1 rad=d1 dir=1 erg=d2 vec=0 1 0
si1   0.5642
si2   1 5.47e-8 51.2e-8 125e-8 506e-8
sp2   0.960308  0.025959  0.007882 0.005851
```

Notice here the only difference from single energy source is the addition of two lines used

to describe the energy spectrum. `erg=d2` implies that the value of the source energy was sampled from distribution number 2. Source energy information and probability were given in the `si2` and `sp2` cards. The `1` following `si2` means discrete source energies values were used, and therefore, the following four numbers after the `1` are the four energies obtained from best curve fit. Accordingly, the `sp2` card gave the probability of each of energy branch. For example, about 96 of every 100 neutron particles emitted from this source have an energy of 5.47e-8 MeV.

4.5 Tally Card

MCNP provides six standard neutron tallies that are easily modified to suit the needs of different users. All tallies are normalized on a per starting particle basis. The tally card used in the simulation of zirconium diboride disks was as follows:

```
c **Tally card, count number of neutrons at 2nd surface of detector**
f1:n  6
```

The `f1` tally was chosen, because it gives the number of particles crossing a surface. The quantity it estimates is:

$$F1 = \int_A \int_\mu \int_t \int_E J(r, E, t, \mu)\, dA dt d\mu dE, \qquad (4.3)$$

which integrates over area (A), angle (μ), time (t) and energy (E). Since the result is normalized, the transmission coefficient of the neutron shielding material can be read directly from the output file. The relative error can also be obtained from the output file.

At the beginning of this work, there was some confusion in selecting the proper

tally. In MCNP `f1` is called the surface current tally and `f2` is called the surface flux tally. The `f2` tally was used in some previous work, but actually it is a limiting case of the cell flux as it is taking the particle entry angle into account. However, in a neutron attenuation study, every particle that crosses the tally surface should be counted regardless of the entry angle. Thus, `f1`, the surface "current" tally, gives the correct quantity and therefore it was chosen in all the simulations.

CHAPTER 5

RESULTS AND ANALYSIS

This chapter presents the results of the experimental work and Monte Carlo modeling studies. Most of the experiments were done using UVAR's polyenergetic neutron transmittance beam. Some of the calibration data on the series of zirconium diboride disks was acquired from University of Michigan's monoenergetic beam. The experiments were simulated using MCNP4A on University of Virginia's SP2 computer. The experimental and modeling results and discussions are given on each problem. Exponential and non-exponential neutron attenuation properties are observed in different beam facilities through thin and thick shielding materials. The validity of using zirconium diboride disks with aluminum shims as the calibration series when measuring the areal densities of borated aluminum coupons was confirmed. The procedures used to measure the areal density of unknown borated aluminum coupons are discussed. To show the streaming factor, a series of BORAL sheets were measured.

5.1 ZrB_2 with Monoenergetic Beam

A series of zirconium diboride disks, listed in Table 5.1, were measured to determine their areal densities and transmission coefficients at University of Michigan using a 0.06 eV monoenergetic neutron beam. Each disk was mounted in a superpure aluminum block, and its thickness, diameter and density were accurately measured. Every disk was uniquely marked and its identity maintained throughout the program. The

Table 5.1. Zirconium diboride calibration specimen information.

ZrB_2 disk number	Diameter (mm)	Thickness (mm)	Density (g/cm^3)	Measured Areal Density ($mg^{10}B/cm^2$)
3	50.78	0.1448	5.7334	8.39
7	50.78	0.1702	5.7238	9.58
5	50.78	0.1981	5.7273	11.18
25	50.78	0.2083	5.6566	12.08
11	50.78	0.2565	5.6647	15.27
12	50.78	0.2743	5.6389	16.14
14	50.78	0.3480	5.7520	20.79
23	50.78	0.5004	5.7696	30.52

ZrB_2 used here was 18.59 wt% total boron enriched to 55.04 wt% ^{10}B. The background count rate was subtracted from all measured count rates prior to computation of the transmission coefficient. The standard deviation of the measured count rate was used to determine the 95 percent confidence interval for the attenuation coefficient.

The same series of disks was modeled with MCNP to study the attenuation properties and transmission coefficient. Based on the physical and chemical data of the zirconium diboride disks, an MCNP input deck was constructed for every disk of this array. Appendix I shows the input deck for disk No. 3. The input decks were almost identical except for the surface cards definition, because the thickness of zirconium diboride varied one from another, even though the aluminum holder thickness was a constant. In the material card, weight ratio of Zr, ^{10}B and ^{11}B was used for zirconium diboride. ^{10}B weight percent was 0.10232 (= 18.59 % × 55.04 %), ^{11}B weight percent was 0.08358 (= 18.59 % × (1 - 55.04 %)), and Zr weight percent was 0.81410 (= 1 -

18.59%). As stated in Chapter 4, the cell structure of each disk setup was the same and the source card defined a monoenergetic (0.06 eV) and monodirectional neutron source. The number of transmitted neutrons through the object was tallied. The transmission coefficient was obtained after each input deck was run individually on the SP2.

Figure 5.1 shows a semi-logarithmic plot of transmission coefficient versus ZrB_2 thickness. Results from experiments and modeling were plotted together. The data agreed well with each other within ±10% error.

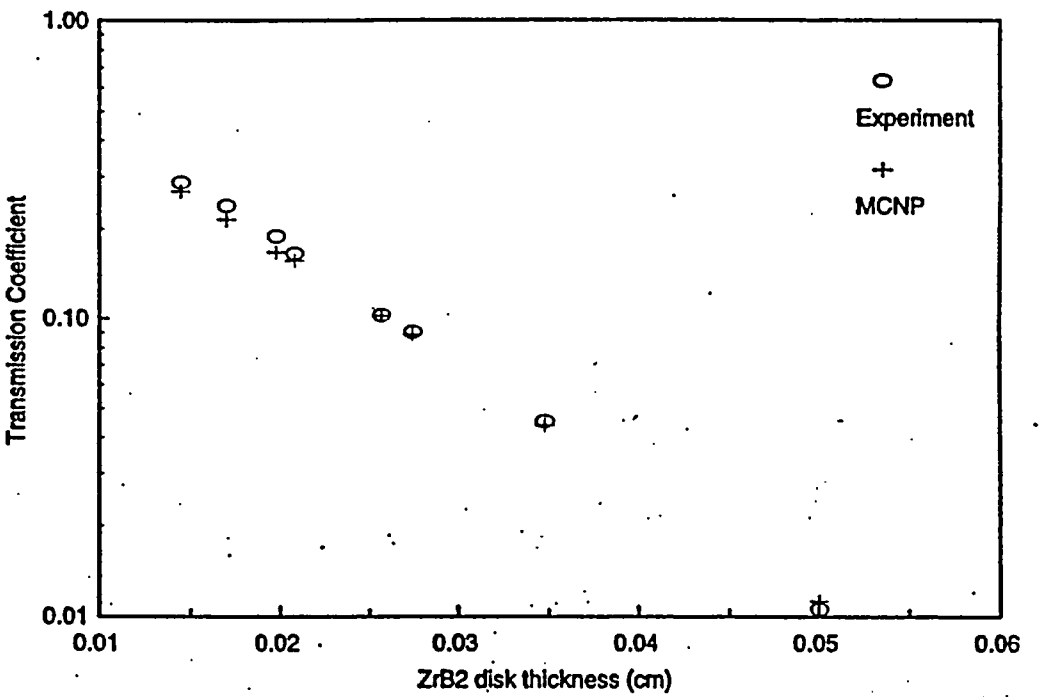

Figure 5.1. A comparison of experimental and MCNP simulation transmission coefficients of zirconium diboride disks.

The theoretical transmission coefficient of an alloy containing ^{10}B may be calculated from the equation:

$$I = I_0 e^{-\Sigma X} = I_0 e^{-N\sigma X} = I_0 e^{-\frac{N_0 \sigma}{A_0} \rho X} = I_0 e^{-\frac{N_0 \sigma}{A_0} A}, \quad (5.1)$$

and the transmission coefficient, T, is:

$$T = \frac{I}{I_0} = e^{-\Sigma X} = e^{-N\sigma X} = e^{-\frac{N_0 \sigma}{A_0} \rho X} = e^{-\frac{N_0 \sigma}{A_0} A}, \quad (5.2)$$

where I_0 is the intensity of the thermal neutron beam without alloy material present,

I is the intensity of the thermal neutron beam with alloy material present,

N is the atom density of the ^{10}B neutron absorber (atoms/cm^3),

Σ is the macroscopic absorption cross section of ^{10}B (cm^{-1}),

σ is the microscopic absorption cross section of ^{10}B (cm^2/atom or barns),

X is the material thickness (cm),

A is the areal density of the ^{10}B alloy (g ^{10}B/cm^2),

N_0 is Avogadro's Number, 6.024×10^{23} atoms/mole,

A_0 is the atomic mass of ^{10}B, 10.013 grams/mole,

ρ is the density of ^{10}B in the alloy.

For a neutron beam with an energy of 0.06 eV, σ is 2496 barns[1], and in this case, the density of ^{10}B (ρ) is 0.5841 g ^{10}B/cm^3(= 5.708 g/cm^3 × 18.59 wt.B % × 55.04 wt.^{10}B%). The theoretical calculation of the macroscopic cross section of ^{10}B, Σ, is:

---

[1] From ENDF/B-VI cross section library.

$$\Sigma = \frac{N_0 \sigma \rho}{A_0} = \frac{6.024\times10^{23}\frac{atoms}{mole}\times2496\times10^{-24}cm^2\times0.5841\frac{g}{cm^3}}{10.013\frac{g}{mole}} = 87.7cm^{-1}. \quad (5.3)$$

Both series of data were analyzed with linear regression method. The independent variable is thickness and the dependent variable is *ln*(transmission coefficient). The slope, constant and regression coefficient (R^2) are listed in Table 5.2. Both regression coefficients were close to 1, which confirmed that the exponential attenuation rule applied to the monoenergetic and monodirectional neutron beam. The physical meaning of the absolute value of slope is the macroscopic attenuation coefficient. Both were slightly greater than the theoretical value, because in the theoretical calculation, the aluminum, ^{11}B and zirconium were not taken into account. In the experiments and simulations, these elements contributed to neutron attenuation by a scattering effect. In the real disk setup, some glue was used to bind the zirconium diboride and aluminum holder together, which gave an even higher attenuation coefficient, because glue is a high hydrogen content material. The regression results of the experimental data also had a non-zero constant, which implied some experimental error in the measurements.

Table 5.2. Linear regression results of the experimental and MCNP simulated transmission coefficients of ZrB_2 using a 0.06 eV neutron beam.

	Theoretical (w/o aluminum)	MCNP	Experiment
R^2	1	0.99966	0.99943
Slope	-87.7	-89.3	-93.6
Constant	0	-0.00597	0.151

The agreement of experimental data and Monte Carlo simulations justified the usage of MCNP to study a well-defined neutron gauging system. The geometry setup and source descriptions in the MCNP input deck effectively simulated the real experimental system. The material definition of zirconium diboride with enriched ^{10}B was at an atomic scale, and the agreement of the results showed that this assumption was valid. The input deck used here also served as a template for the successive simulations. From another point of view, since MCNP is a well-known and benchmarked program, the agreement also verified the correctness of the experiments done at the University of Michigan.

5.2 UVAR Beam Energy Spectrum Determination

The UVAR neutron transmittance beam is used routinely to determine the areal density of unknown boron containing materials. The nominal value of the measured sample's areal density was obtained from a look-up table constructed using a series of ZrB_2 specimens with known areal densities. In this application, the spectrum of the neutron beam was irrelevant, because the same neutron beam was used with the calibration series and the unknown samples. For this and the reasons mentioned earlier,

this beam's spectrum was not measured. As described in Chapter 3, it was believed that this transmittance beam was a well thermalized polyenergetic beam.

To study the neutron attenuation properties of materials in polyenergetic neutron beams, the UVAR beam was used in experiments and modeled with MCNP. Therefore, a quantitative knowledge of the beam spectrum was required.

Along with the zirconium diboride series used in the previous section, seven additional zirconium diboride disks, transmission coefficients were measured with UVAR's transmittance beam. The newly formed series covered a larger areal density range with the greatest ^{10}B areal density of about 60 mg/cm^2. The physical properties of the new disks are listed in Table 5.3. The ^{10}B enrichment in these disks and the manufacturing procedure were the same as the previous series.

Table 5.3. Information on the additional zirconium diboride disks.

ZrB_2 disk number	Diameter (cm)	Thickness (cm)	Density (g/cm^3)
56	5.075	0.0254	5.7222
60	5.075	0.0356	5.8043
64	5.075	0.0424	5.7225
67	5.075	0.0533	5.7992
71	5.075	0.0605	5.7809
74	5.029	0.0686	5.8935
78	5.029	0.0864	5.8576
81	5.029	0.1041	5.8915

Figure 5.2 shows the measured transmission coefficients versus the thickness in a semi-logarithmic plot. As can be seen, the attenuation curve was not a straight line as was the case in the previous experiment. This indicated that the polyenergetic characteristic of the beam and agreed with the non-exponential attenuation theory discussed in Chapter 2.

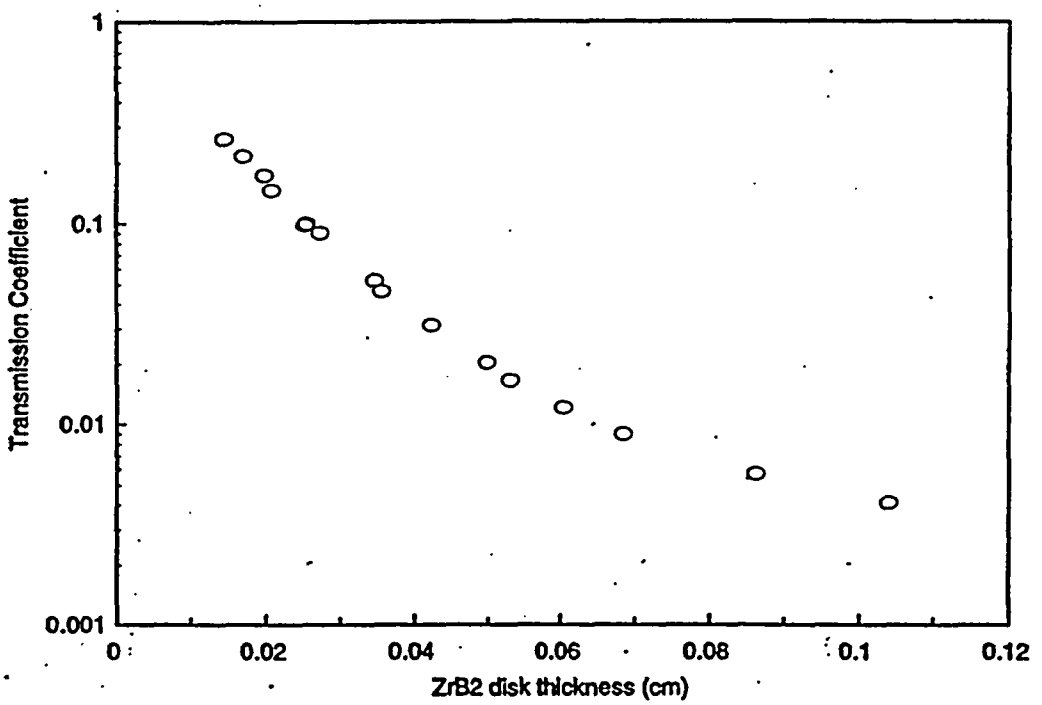

Figure 5.2. The measured transmission coefficients of ZrB_2 specimens with UVAR polyenergetic beam.

With the help of MCNP, the energy spectrum of the neutron beam can be estimated based from the experimental data. If the simulated transmission coefficients of this series of zirconium diboride disks matched their corresponding experimental data for a given source energy spectrum definition in the MCNP models, then this energy

spectrum definition is an acceptable approximation of the real spectrum. Several attempts were made to obtain a good approximation.

Since the geometry modeling of this gauging system and the material description of zirconium diboride disks with aluminum holders with MCNP have been previously shown to be effective, in the search of the energy spectrum, these parameters were kept the same as used in last section. In every iteration, the trial source energy spectrum was used throughout the whole series, and transmission coefficients were tallied and compared to experimental data.

At first, two energies, one thermal component and one epithermal component, were used to represent the spectrum. Four parameters were required, the two energies and their relative percentages. After several iterations on these four parameters, the best fit result was obtained as shown in Figure 5.3. The source definition used was:

```
sdef  pos=0 0 0 sur=1 rad=d1 dir=1 erg=d2 vec=0 1 0
si1   0.5642
si2   s 3 4
sp2   0.96 0.04
sp3   -2 4.5e-8
sp4   -2 69.0e-8
```

Both the thermal and epithermal components were modeled with a Maxwellian fission energy spectrum, and the peak energies were 0.045 eV and 0.69 eV respectively. The frequency distribution of these two energies are 96% and 4%. As seen in Figure 5.3, the first and last points matched with the experimental data, but the middle points were not in good agreement. This implied that two components were not enough to represent the polyenergetic beam spectrum and more branches had to be added. However, whenever

one energy branch was added in, two more parameters, the energy and its percentage, were introduced. For example, to estimate with four branches, four energies and four ratios need to be determined. In fact, since the sum of the four ratios is one, only three ratios left. Still, there were seven parameters remaining. To adjust all of them manually to get a best fit of the experimental data seemed to be impossible and unreasonable.

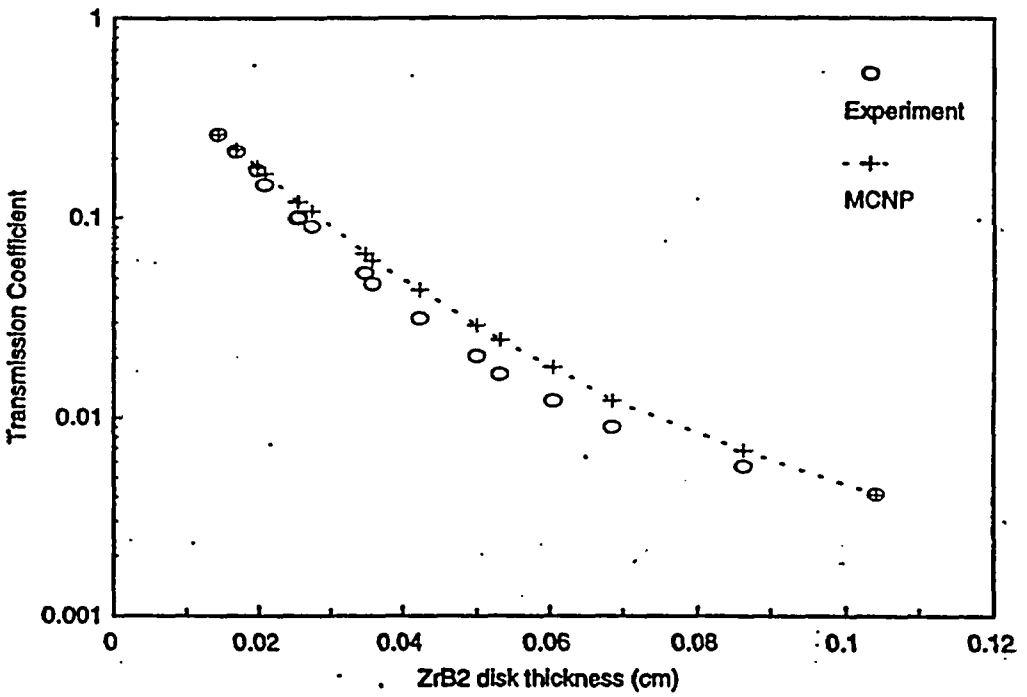

Figure 5.3. A trial of using two energies in MCNP to match the experimental data.

In the previous section, exponential attenuation was observed and successfully modeled for a monoenergetic beam. The non-exponential transmission coefficient curve was the result of polyenergetic characteristic of the beam. If the continuous spectrum was discretized into the combination of multiple single energy beams, each disk's

transmission coefficient is just the summation of the transmission coefficients for all energies. The whole curve is the summation of a family of exponential curves.

Non-linear least squares method was utilized to fit the experimental data with an arbitrary function [26]. When using a function $y = f(x)$ to fit a series of experimental data (x_i, y_i), the measure of goodness of fit χ^2 is defined as:

$$\chi^2 \equiv \sum \left\{ \frac{1}{\sigma^2} [\, y_i - y(x_i) \,]^2 \right\}, \tag{5.4}$$

where the σ_i are the uncertainties in the data points y_i.

According to the method of least squares, the optimum values of the parameters a_j are obtained by minimizing χ^2 with respect to each of the parameters simultaneously, i.e.,

$$\frac{\partial}{\partial a_j} \chi^2 = \frac{\partial}{\partial a_j} \sum \left\{ \frac{1}{\sigma_i^2} [\, y_i - y(x_i) \,]^2 \right\} = 0. \tag{5.5}$$

It is rather difficult to derive an analytical expression for calculating the parameters of a non-linear function $y(x)$. Instead, χ^2 can be considered a continuous function of the n parameters a_j describing a hypersurface in n-dimensional space, and the space can then be searched for the appropriate minimum value of χ^2. There are a number of ways of finding the minimum value. A gradient search method was used for this work. In this method, all the parameters a_j are incremented simultaneously, with the relative magnitudes adjusted so that the resultant direction of travel in parameter space is along the gradient, i.e., the direction of maximum variation, of χ^2. Reference 26 has the details of this

algorithm.

A C-language program (Appendix II) was written to use this algorithm to search for the optimum values of the fit curve. The form of the non-linear fit function is:

$$T = a_0 e^{-\mu_0 x} + a_1 e^{-\mu_1 x} + a_2 e^{-\mu_2 x} + (1-a_0-a_1-a_2) e^{-\mu_3 x}. \qquad (5.6)$$

The input of this program was the series of the experimental data, i.e., pairs of transmission coefficient and the corresponding thickness, the guessed initial values of the parameters and the step length for each parameter. Since only 16 data points were available, the program cannot accurately determine the seven unknown parameters simultaneously. Based on the trials of the two-energy approximation, the macroscopic attenuation coefficients (μ_i), were estimated first and supplied to the program. The program can then determine the optimized value of the a_i. The predicted transmission coefficients were plotted against the experimental data for comparison. After several rounds of iterations on μ_i's and a_i's, an acceptable fit function was constructed.

With the four macroscopic attenuation coefficients, next step was to find the corresponding energy. Similar to the previous section, MCNP simulations were conducted on this series of ZrB_2 disks with some selected monoenergetic neutron source. The transmission coefficients were plotted as a function of areal density and the macroscopic attenuation coefficient was obtained through exponential regression. The coefficient was then compared to a coefficient known from the fit. The energy was adjusted until these two coefficients matched. This process was repeated for all the four attenuation coefficients. Finally, four energies were determined and, with their relative

ratios obtained earlier from the curve fit, a source description (Section 4.4) for the polyenergetic beam at UVAR was constructed. Using this energy definition, the whole zirconium diboride series were again simulated with MCNP. The resulting transmission coefficients were plotted against the experimental data as presented in Figure 5.4. As expected, the two curves matched very well. This energy description of UVAR transmittance beam was also used for the later modeling of borated aluminum and BORAL for comparisons of the simulations to the experimental data obtained using this beam.

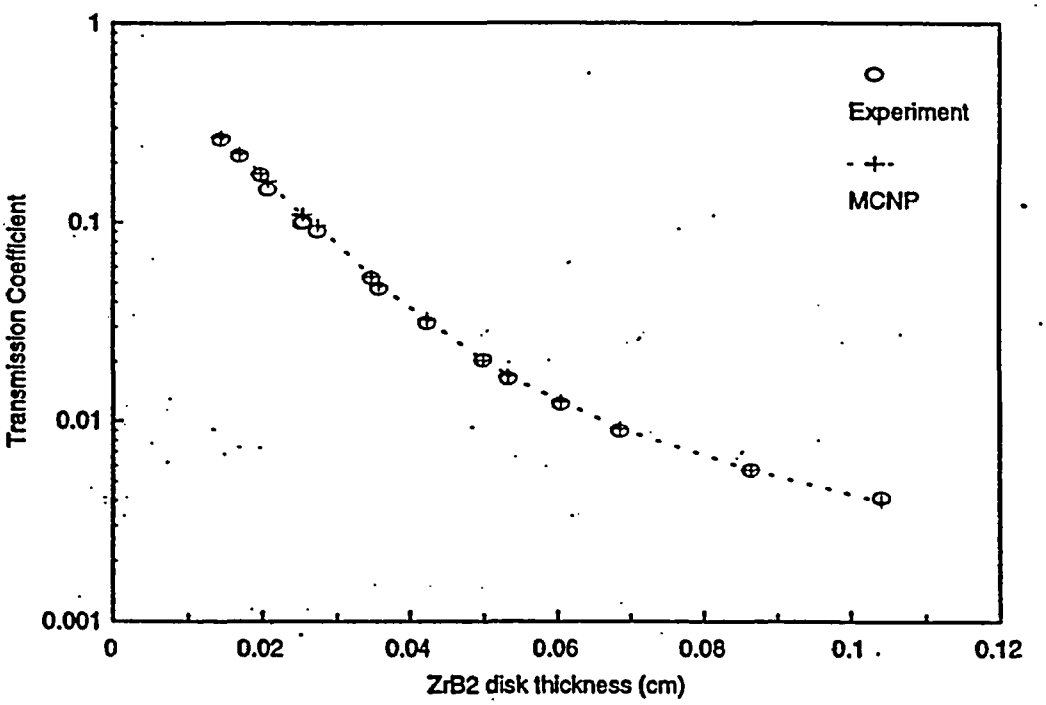

Figure 5.4. A comparison of transmission coefficients of ZrB_2 series from experiment and from MCNP simulations with a best-fit energy spectrum.

One thing noticed here is that in the four energies that derived from the non-linear least squares fit, the lowest energy is 0.0547 eV, instead of pure thermal energy 0.025 eV. It is believed that the transmittance beam should be fairly thermal. Five independent MCNP simulations with monoenergetic neutron source were conducted. Four derived energies and the ideal thermal energy were used. The transmission coefficients are plotted in Figure 5.5. Each curve showed an exponential attenuation. The lack of pure thermal branch can be explained by carefully examining this plot. When the thickness is about 0.06 cm (a.d.~30mg $^{10}B/cm^2$), the transmission ratio for 0.025 eV is less than 0.1% and this value keeps dropping dramatically when thickness goes even higher. In the experimental data; half of the points were from ZrB_2 with a thickness greater than 0.06 cm, where almost no neutrons with 0.025 eV energy can penetrate. Therefore, when fitting these numbers, there appeared to be no 0.025 eV neutrons in the spectrum. The first half of the data can fit well without 0.025 eV neutrons because the transmission coefficients are fairly close for all energy branches. The effect of the 0.025 eV neutrons can be replaced by other energies with a different weight ratio, in this case 0.0547 eV with 96%. This explains why no 0.025 eV energy neutrons were approximated although they are believed to be present in the beam. The spectrum obtained with this method may not be the real spectrum, but it can be considered as an effective one when studying the attenuation properties of shielding materials with areal densities greater than 8 mg$^{10}B/cm^2$.

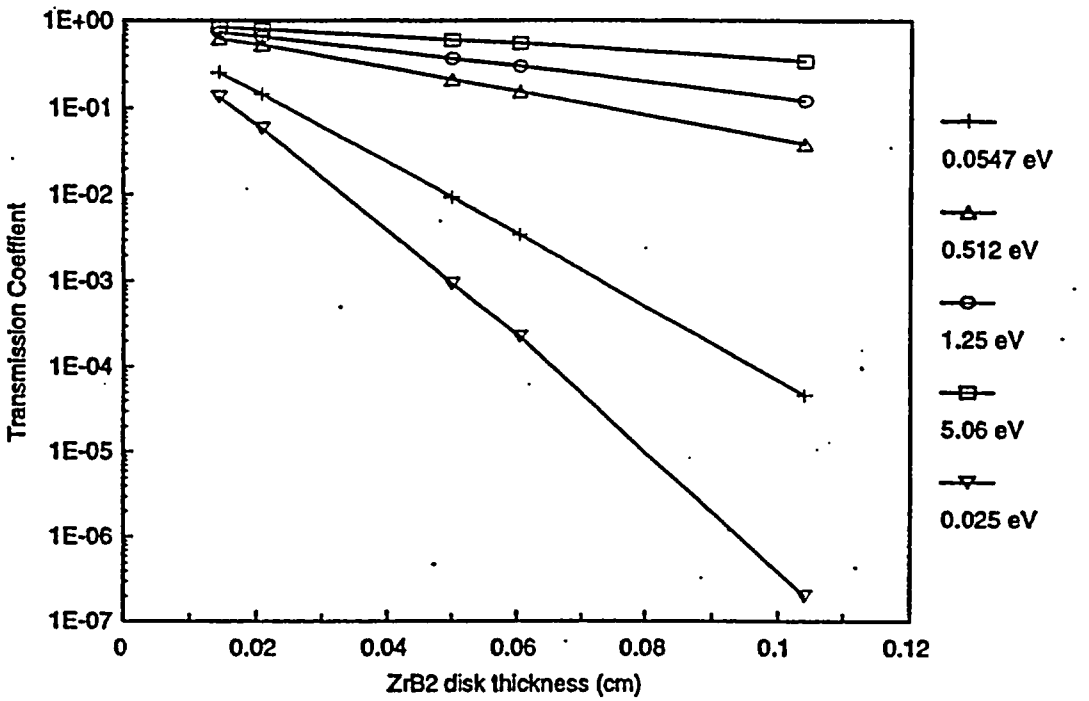

Figure 5.5. A comparison of macroscopic absorption coefficients of zirconium diboride for different neutron energies. Data was obtained from MCNP simulations.

5.3 Verification of the Effectiveness of Using Aluminum Shims

In the current borated aluminum areal density measurement procedure, the first step is to measure the transmission coefficients of the series of zirconium diboride disks with aluminum holders and construct a look-up table.

Each zirconium diboride calibration disk was glued to a corresponding aluminum holder. In the real measurement, sometimes the zirconium side faced the beam and sometimes the aluminum side faced the beam. In order to make sure the order of the two pieces in the setup did not affect the calibration curve, a verification experiment was

conducted. The disk array listed in Table 5.1 was measured twice with the UVAR's transmission beam to determine the transmission coefficients. The first series of measurements were obtained with the zirconium side facing the beam and the disk array was turned around for the second series of measurements. The transmission coefficients versus the areal density were plotted for the two experiments in Figure 5.6. Within the range of experimental error, these two curves overlapped. This is to say, the neutron attenuation properties are the same for these two setups. This result can be expected because in a material like this, ^{10}B dominates the thermal neutron attenuation and other elements' effect is insignificant. MCNP simulations were also done on the two setups and same curve overlapping was obtained.

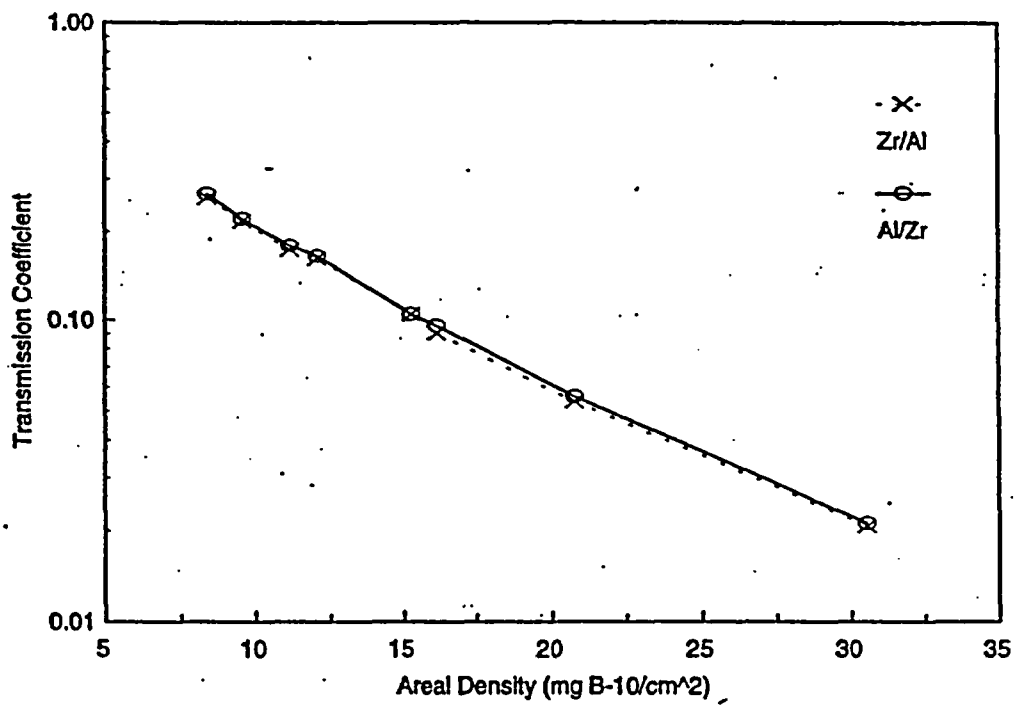

Figure 5.6. A comparison of the attenuation property for two different ZrB_2 setups.

The zirconium diboride disks were in aluminum holders for two main reasons. First, the aluminum holders were used to protect the thin and fragile ZrB_2 specimens and to make it easier to work with them. Second, the aluminum holders served as shims. The borated aluminum samples have a very high weight percent (~ 99.5%)of aluminum and are much thicker than any of the ZrB_2 disks because of the aluminum. To measure any given thickness of borated aluminum, each disk in the calibration array was shimmed to about the same thickness with pure aluminum pieces. The idea was to make the two different materials have close constituents, even though the constituents were in a different chemical form.

The No. 3 through No. 23 ZrB_2 specimens were measured to determine their transmission coefficients with three different aluminum shim thickness, and the results are shown in Figure 5.7. The first setup was the zirconium diboride disks with aluminum holders, where the holders' thickness was 0.535 cm. Shim 1 total aluminum thickness was 0.762 cm and Shim 2 total thickness was 1.905 cm. The effect of using the wrong shim thickness can be illustrated by the following example. Assume the unknown sample has the same thickness as Shim 2. If the measured transmission coefficient is 0.07 (7%), by using the look-up curve of Shim 2, an areal density of 17.25 mg $^{10}B/cm^2$ is obtained and reported as the measured result. However, assume the calibration specimens were not shimmed thick enough, e.g., Shim 1 was used, and the corresponding look-up curve was constructed. From this curve, corresponding to a transmission coefficient of 7%, the areal density would be reported as 18.12 mg $^{10}B/cm^2$. The relative error would be 5%, where the shim difference was quite big, 1.143 cm. A similar comparison can be made

between Shim 1 and just the aluminum holder, and the relative error of measured areal density would be within 2%, if an inappropriate thickness (0.227 cm thinner) of shim was used. It can be concluded that although the scattering cross section of aluminum is relatively insignificant compared to the thermal absorption cross section of ^{10}B, to have an accurate measurement of areal density, the zirconium diboride specimens need to be shimmed to the correct thickness of the unknown samples to construct a good calibration curve. On the other hand, if the total thickness of test standards and aluminum shims is off only by a couple millimeters, the result is still acceptable (the error is within 2%).

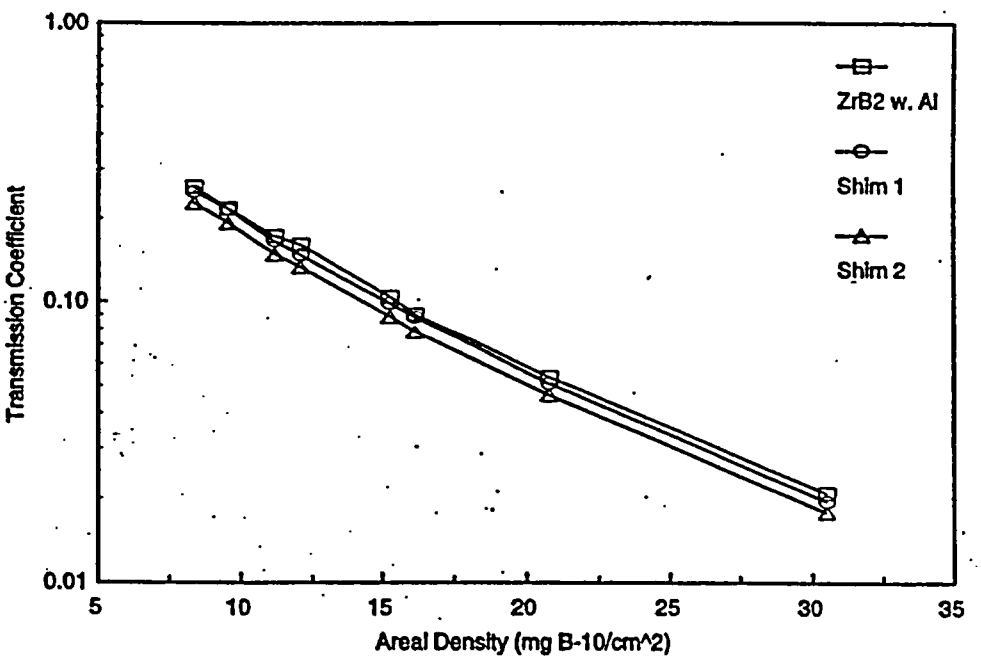

Figure 5.7. A comparison of neutron attenuation of zirconium diboride with different aluminum shims.

5.4. Comparison of Borated Aluminum and ZrB_2

The legitimate way to measure the areal density of ^{10}B in borated aluminum with the calibration method, is to construct the calibration curve using a series of known areal density of the same material, borated aluminum. However, the borated aluminum is not a naturally occurring compound and the atomic structure of the alloy remains unclear. Moreover, a truly uniform distribution of ^{10}B in aluminum is hard to manufacture and the fabricated product needs to be inspected for homogeneity. Although there is another way, wet chemical analysis, to measure the areal density different from the neutron transmittance method, it is slow and not very accurate. For these reasons, it is very difficult to have an array of borated aluminum with known areal densities to serve as calibration disks. On the contrary, zirconium diboride is a chemical compound whose formula is well-known and the uniformity of ^{10}B is guaranteed. By a transmittance measurement using a monoenergetic neutron beam, the areal density of a given piece of zirconium diboride can be measured accurately. Then, the series of zirconium diboride disks with measured known areal density can be used as calibration standards for measuring borated aluminum areal densities. The basis for this is that zirconium diboride disks with a proper thickness of aluminum holders have the same neutron attenuation property as borated aluminum.

These two materials were modeled with MCNP to compare their attenuation properties. As shown in Eq. 3.1, the theoretical areal density (A) of ^{10}B in an alloy by multiplying the weight fraction boron (W) by the matrix density (ρ), the isotopic enrichment (E) and the thickness (T).

Since the values for the four variables on the right hand side of the formula for each zirconium diboride disk were known, the ^{10}B areal density could be calculated. For example, disk No. 12:

$$A_{12} = 18.59\%\frac{g\ boron}{g} \times 5.6389\frac{g}{cm^3} \times 0.5504\frac{g\ ^{10}B}{g\ boron} \times 0.02743\ cm$$
$$= 0.01583\frac{g\ ^{10}B}{cm^2} = 15.83\frac{mg\ ^{10}B}{cm^2}. \quad (5.7)$$

To calculate the thickness of borated aluminum which has the same ^{10}B areal density, similar formula was used, but this time A is known and T is unknown.

$$T = \frac{A}{WPE} = \frac{0.01583\frac{g\ ^{10}B}{cm^2}}{0.5\%\frac{g\ boron}{g} \times 2.7\frac{g}{cm^3} \times 95\%\frac{g\ ^{10}B}{g\ boron}} = 1.2335\ cm. \quad (5.8)$$

This thickness was used in the input deck of borated aluminum model. From here, the thickness of a proper aluminum shim for ZrB_2 No. 12, whose thickness is known (0.02743 cm), can be calculated by:

$$T_{Al} = 1.2335\ cm - 0.02743\ cm = 0.9592\ cm. \quad (5.9)$$

This thickness of aluminum shim and the thickness of ZrB_2 disk were used in the model of zirconium diboride. The same calculations were done for all the other specimens and after the data were collected, MCNP simulations were run on the two series. Transmission coefficients were collected and plotted versus areal density as shown in

Figure 5.8. As can be seen, these two curves were almost identical, which means when the ^{10}B areal density was the same, borated aluminum and zirconium diboride with an aluminum shim have the same attenuation coefficient.

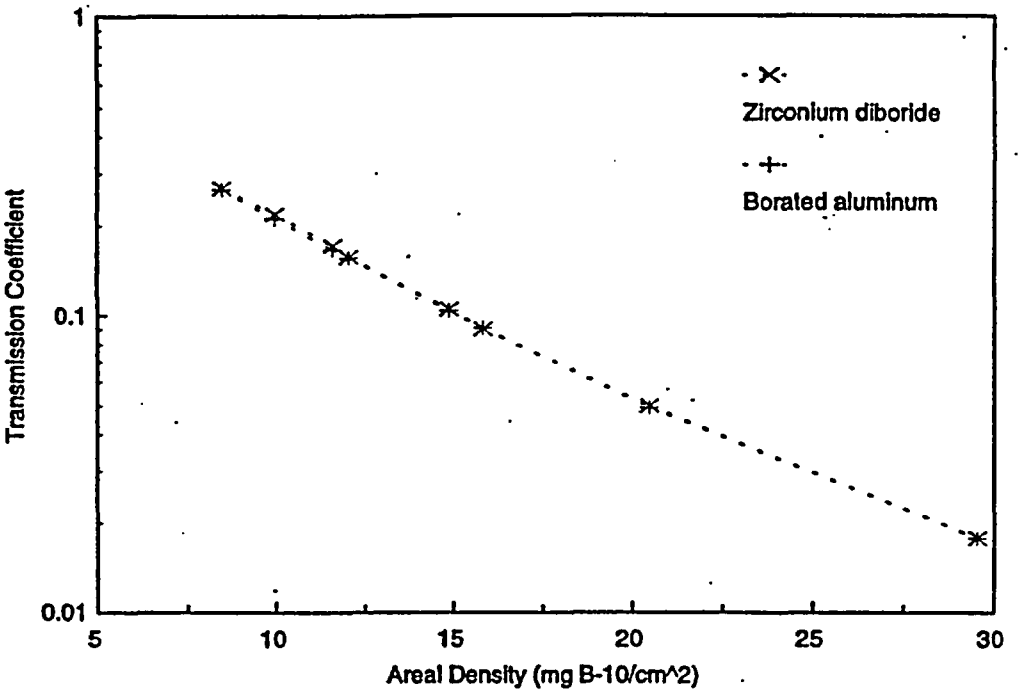

Figure 5.8. A neutron attenuation comparison of zirconium diboride with aluminum and borated aluminum. (Results from MCNP simulations)

In order to verify the MCNP simulations, transmission experiments were conducted on borated aluminum and zirconium diboride disks. Two borated aluminum step wedges, illustrated in Figure 5.9, were provided by Eagle-Picher Boron and were used to measure the transmission coefficients in borated aluminum. In order to be able to compare with zirconium diboride, aluminum shims of the proper thickness were added to match the thickness of each step of the borated aluminum wedge. The transmission

coefficient of each step of the two step wedges was measured individually. Additional measurements were made after stacking the two wedges together to cover a larger range of areal densities.

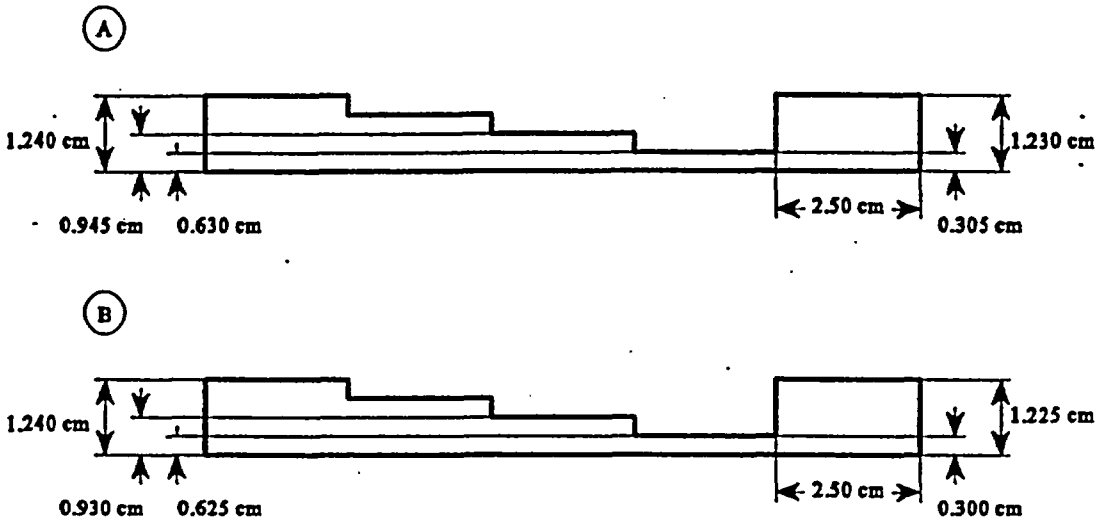

Figure 5.9. The dimensions of the two borated aluminum step wedges.

The borated aluminum pieces were checked for ^{10}B uniformity with neutron radiography technique. Figure 5.10 shows an image of piece A obtained from a CCD camera with the UVAR's neutron radiography facility. Though limited by field of view and the neutron flux, three of the four steps can be easily seen. The distribution of boron is fairly homogeneous. Additional radiography images using a real-time neutron camera confirmed the uniformity of both plates. The wet chemical analysis from Eagle-Picher Boron on this sample reported the weight ratio of boron is 0.637±0.022%. The maximum and minimum value of the weight ratio are 0.697% and 0.596%, respectively. The theoretical ^{10}B areal density of each step can be calculated by Eq. 3.1, where $W = 0.637\%$. The transmission coefficients of borated aluminum and zirconium diboride with

aluminum are plotted in Figure 5.11. As known from previous experience, the experimental error of wet chemical analysis is about ±20%. The two series matched each other well in this error range.

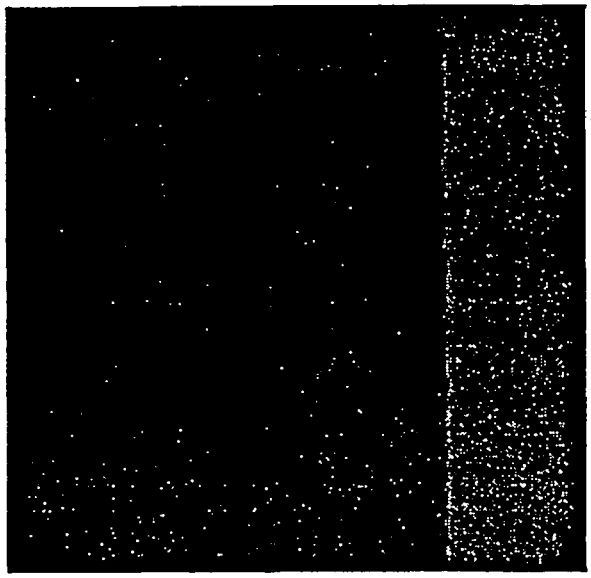

Figure 5.10. A neutron radioscopic image of the borated aluminum step wedge obtained with a CCD camera. (Integration time = 3000 s, Neutron flux = 3.6×10^6 n/cm^{2}s)

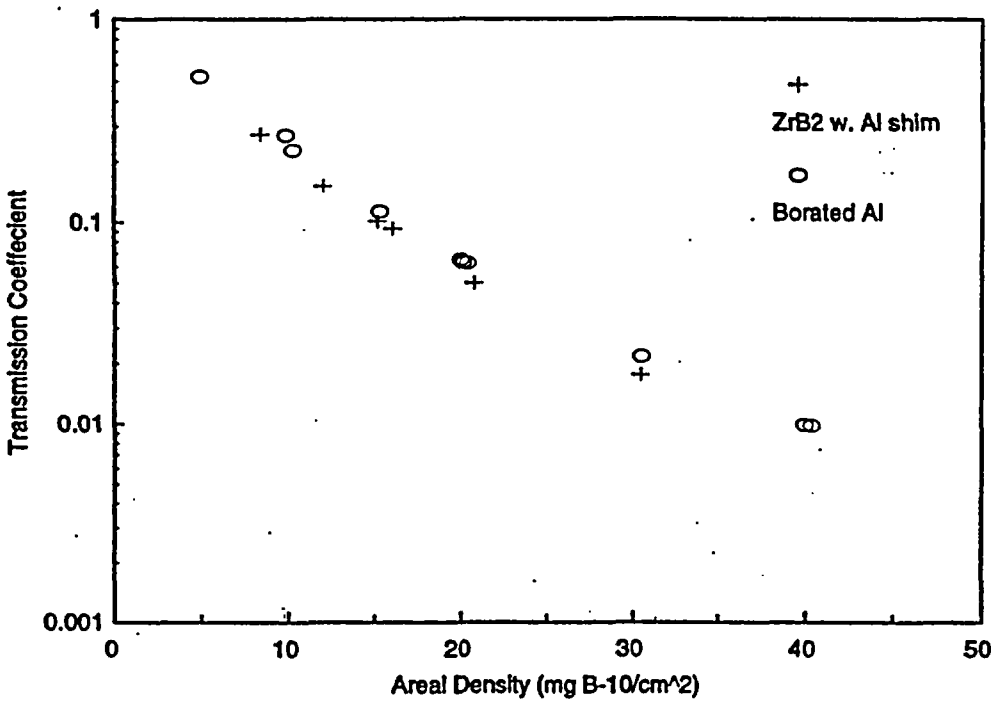

Figure 5.11. A comparison of experimental results of borated aluminum and zirconium diboride with aluminum shim.

These two materials, borated aluminum and zirconium diboride with aluminum shim, were in totally different chemical and physical form, the boron weight percent was different, the ^{10}B enrichment was different, and aluminum exists in one material as a separate block and the other as a constituent of the alloy. The only common points were the ^{10}B areal density and the total thickness. With all the differences, the same neutron attenuation property can be explained by the same amount of ^{10}B, which provides the major neutron removal by absorption. Neutrons are also attenuated by scattering by the other elements, ^{11}B, Zr and Al. Their thermal neutron scattering cross sections are very close, among them aluminum dominates the scattering because of the massive volume.

The same object thickness gave about the same neutron scattering. In conclusion, it is valid to use zirconium diboride disks with proper aluminum shims to measure the areal density of borated aluminum. Also, no neutron streaming or channeling was observed in borated aluminum, which is to say the effective or measured areal density of borated aluminum is the same as its theoretically calculated areal density.

5.5 Comparison of BORAL and ZrB_2

In order to compare the neutron attenuation of BORAL with zirconium diboride and borated aluminum, and to study the streaming effect of BORAL, several BORAL plates purchased from Brooks & Perkins were collected and transmission coefficients were measured in the UVAR's neutron transmittance beam. Information on these BORAL plates is given in Table 5.4. As seen in this table, only two plates' areal densities were certified by the producer. In order to have a relatively large range of areal density, the uncertified plates were also used in the experiments. To get more data points, some plates were stacked together to form a new thickness. Table 5.5 lists the plate combinations for the nine measurements. The effect on the neutron attenuation because of the slight increment (~1 mm) of aluminum skins, when two or three plates were stacked together, was assumed to be insignificant based on the discussion in Section 5.3.

Table 5.4. Information on the BORAL plates used in neutron attenuation study.

BORAL plate number	Areal density ($mg^{10}B/cm^2$)	Certified Number
1	>16.5	Not certified
2	>16.5	Not certified
3	>16.5	Not certified
4	>20	Not certified
5	>20	Not certified
6	32.6	S/N 6-03097-1
7	41.6	S/N 6-32244-2
8	>50	Not certified
9	>50	Not certified

Table 5.5. A series of BORAL plates formed with known areal density for transmission coefficients measurement.

Measurement number	BORAL plate combination	Areal density ($mg^{10}B/cm^2$)	Corrected areal density ($mg\ ^{10}B/cm^2$)
1	1	>16.5	18.5
2	4	>20	31
3	6	31.6	No correction
4	1+2	>33	37
5	1+4	>36.5	49.5
6	4+5	>40	62
7	7	42.6	No correction
8	1+2+3	>49.5	55.5
9	8	>50	53

Transmission coefficients are plotted in Figure 5.12 and compared to the results of the series of zirconium diboride disks which were obtained earlier in Section 5.2. As shown in Figure 5.12, the two transmission coefficients corresponding to the two known areal density BORAL plates fell on the ZrB_2 curve. However the data points from the unknown plates and their combinations were off the ZrB_2 curve, especially the measurements involving plate 4 and 5 (a.d. > 20 mg $^{10}B/cm^2$). Further inspection of these two plates showed that their physical thickness were close to that of the certified piece which has an areal density of 31.6 mg $^{10}B/cm^2$. Plate 4 and 5's core thickness were then measured and their areal densities were calculated to be 31.0 mg$^{10}B/cm^2$ by multiplying the thickness by the core density (156 mg $^{10}B/cm^3$), which is a nominal number from Brooks & Perkins. Similar corrections were done on the other uncertified plates, which showed the actual areal density of the 16.5 plates should be 18.5 and the 50 plates should be 53, all in mg $^{10}B/cm^2$. The transmission coefficients were replotted in Figure 5.13, using the corrected areal densities listed in the fourth column of Table 5.5. The good match of the transmission coefficient curves of ZrB_2 and BORAL implied that when having the same ^{10}B areal density, these two materials have the same neutron attenuation effect.

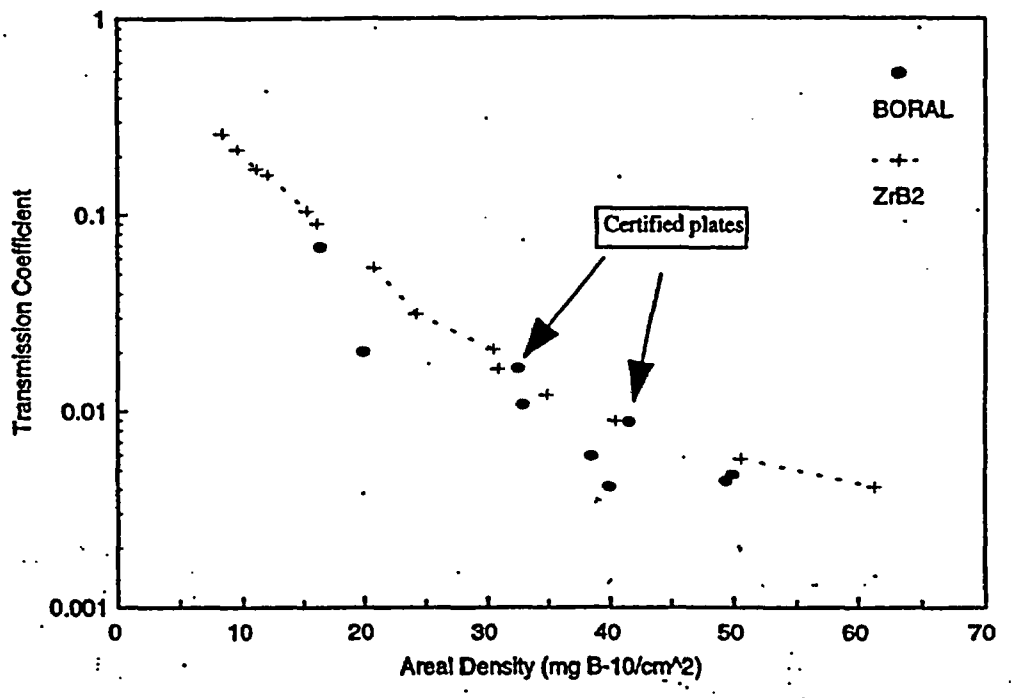

Figure 5.12. The raw experimental data of BORAL plates compared to the results of ZrB_2.

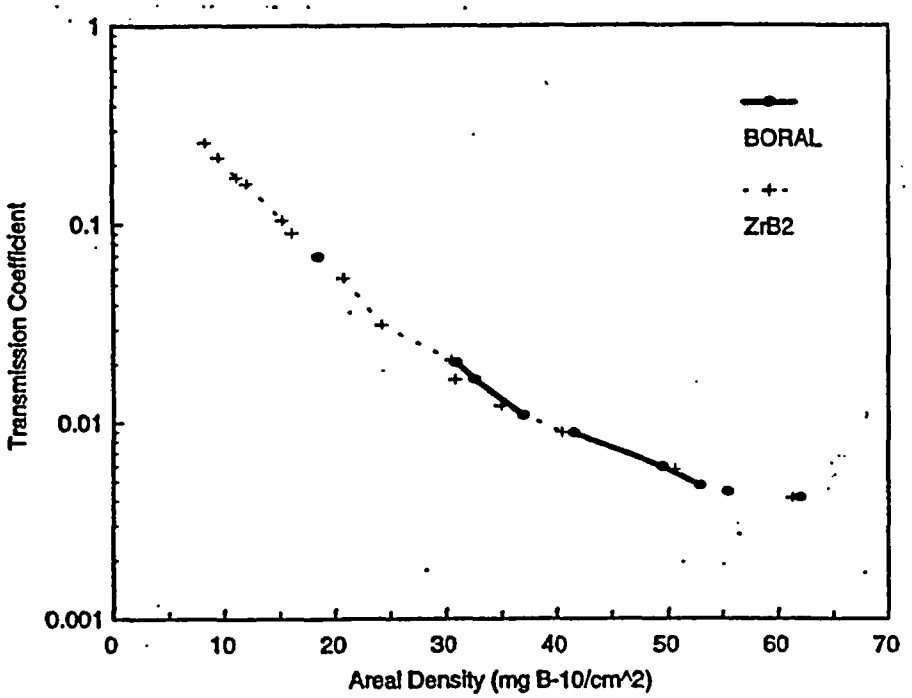

Figure 5.13. A comparison of BORAL plates with corrected areal density with ZrB_2.

However, evidence from other researchers previous research [3][4][19] showed that neutron channeling exists in BORAL and with same loading of ^{10}B, BORAL will give a higher transmission than a homogeneous material. But in the above experiments, the streaming effect was not observed. It was suspected the certified areal densities of ^{10}B from Brooks& Perkins were effective areal density and the actual loading was higher. The reported ^{10}B density in the core is a constant, which can be calculated by:

$$\frac{Nominal\ ^{10}B\ areal\ density}{core\ thickness} = 0.156\ g\ ^{10}B/cm^3. \qquad (5.10)$$

In order to determine the actual ^{10}B density, a piece of BORAL core was removed from a BORAL sample. The mass of this piece was measured with a precise digital balance and the volume was determined by measuring the displacement of water in a graduated cylinder. The results were:

$$M_{measured} = 7.0378\ g,$$

$$V_{measured} = 2.70\ cm^3.$$

Then the core density is:

$$\rho_{core} = \frac{M_{measured}}{V_{measured}} = \frac{7.0378\ g}{2.70\ cm^3} = 2.606\ g/cm^3$$

Since,

$$\rho_{Al} = 2.71\ g/cm^3\ ,\ \rho_{B_4C} = 2.51\ g/cm^3$$

Suppose the mass ratio of B_4C in core is x, then,

$$x \times \rho_{B_4C} + (1-x) \times \rho_{Al} = \rho_{core}$$

Thus,

$$x = 0.52$$

$$\rho_{^{10}B} = 2.606\frac{g\ core}{cm^3} \times 0.52\frac{B_4C}{core} \times 0.7828\frac{boron}{B_4C} \times 0.18\frac{^{10}B}{boron}$$

$$= 0.191\ \frac{g\ ^{10}B}{cm^3}$$

Compared to the effective ^{10}B loading, the actual loading is 22.3% (= 0.191- 0.156 /0.156) higher. In other words, to get an effective areal density the same as a homogenous boron absorber, 22.3% more ^{10}B has to be loaded in BORAL because of the streaming reduction among boron carbide chunks. This confirmed the experimental results of Wells [4], who indicated that a 25% boron content deduction should be taken into account for BORAL.

MCNP simulation of BORAL was also attempted. The model using the uni-sized sphere discussed in Chapter 4 gave too much transmission. This can be explained by the lack of randomness in B_4C particle size, shape and arrangement. Another model was also based on the repeated structure. The difference was multiple sizes of spheres were randomly put into one unit cubic cell. Then this cell was repeated in the BORAL core region. However, there was no dramatic improvement in the results, and the transmission ratio was still too high. The problem with this model is even though there is some randomness in the unit cell, every layer of the core still had the same structure since by repeating that cell, the adjacent layers were not statistically independent. To avoid the statistical dependence of adjacent layers, the repeated structure feature of MCNP cannot be used. Another thought of first distributing multiple sizes of micron-scale spheres randomly in a centimeter-scale region and then feeding their coordinates to MCNP was unrealistic because of the huge size of the input file. Since MCNP cannot handle random geometry, new techniques and more powerful tools need to be developed to conduct this type of simulation.

CHAPTER 6

SUMMARY, CONCLUSIONS AND FUTURE WORK

6.1. Summary and Conclusions

The initial research goals for this thesis as listed in Chapter 1 were:

1) to study the neutron attenuation properties of zirconium diboride, borated aluminum and BORAL and to investigate the streaming properties of BORAL and borated aluminum,

2) to verify the method of using ZrB_2 disks with aluminum shims to measure the areal densities of borated aluminum samples,

3) to determine the energy spectrum of UVAR polyenergetic neutron transmittance beam.

MCNP was demonstrated to be appropriate to model the neutron gauging system, which consists of the neutron beam, the test object and the detector. The neutron attenuation properties in monoenergetic beam and polyenergetic beam of three different boron containing materials, namely zirconium diboride, borated aluminum and BORAL, were studied. Data was obtained from both experiments and Monte Carlo simulations.

Zirconium diboride is an atomic scale chemical compound which has a uniform distribution of ^{10}B. Its theoretical ^{10}B areal density is the same as its measured areal density. Borated aluminum is an alloy with boron distributed in aluminum in which the boron is highly enriched in ^{10}B. Experiments and MCNP simulations showed that it has

the same neutron attenuation property as zirconium diboride with an aluminum shim. Therefore, borated aluminum with a uniform distribution of ^{10}B can be treated as an atomic scale mixture of boron atoms and aluminum atoms. The actual ^{10}B areal density can be calculated directly from the physical loading of ^{10}B. This study showed that BORAL has the same attenuation coefficient as zirconium diboride when the effective ^{10}B areal density is used for BORAL. In other words, to get the same attenuation property for BORAL plate as a homogeneous material, about 22% more ^{10}B needs to be loaded. This attenuation reduction result agreed with previous researchers' experimental results and mathematical models.

The effectiveness of using ZrB_2 disks to measure the areal density of borated aluminum samples at UVa was verified since borated aluminum and zirconium diboride with proper thickness of aluminum shim showed the same neutron attenuation properties.

Neutron attenuation for a monoenergetic and monodirectional beam follows exponential attenuation rule. In a polyenergetic beam, non-exponential attenuation was observed. By using non-linear least squares method, an approximation of the UVAR's neutron transmittance beam energy spectrum was obtained. Although the obtained spectrum is not determined as the true spectrum of neutron beam, it can be used effectively in the study of neutron attenuation properties for materials with areal densities greater than 8 mg $^{10}B/cm^2$.

6.2. Future Work

A few suggestions of future work on this topic can be made as:

• Refine the model of the BORAL core. Boron carbide particles with various size and shape distribute randomly in the aluminum matrix. New techniques need to be developed to describe this structure closely. Since MCNP cannot correctly handle random geometry problem, a more powerful Monte Carlo code is necessary for the studying of neutron attenuation property of BORAL and BORAL like materials.

• The non-linear least squares method could give a closer energy spectrum approximation, if some thinner ZrB_2 disks (a.d.< 8 mg $^{10}B/cm^2$) can be made and their transmission coefficients are added to the current experimental curve (Figure 5.2).

• To have a better picture of the energy spectrum of the neutron transmittance beam, MCNP simulations on the whole UVAR core and the beamport layout are necessary. This will be a time consuming job, but it can be done.

REFERENCES

1. Private communications from M. Wachs, Eagle-Picher Industries, Inc., Boron Dept., P.O.Box 798, Quapaw, OK 74363.

2. *BORAL the Neutron Absorber*, Brooks & Perkins, Inc.

3. W. R. Burrus, "How Channeling Between Chunks Raises Neutron Transmission Through Boral," *Nucleonics*, 16, 1, 91, 1958.

4. A. H. Wells, D. R. Marnon, and R. A. Karam, "Criticality Effect of Neutron Channeling Between Boron Carbide Granules in Boral for a Spent-Fuel Shipping Cask," *Transaction of American Nuclear Society*, Vol. 54, pp. 205-206, 1987.

5. *High Density Fuel Storage Products*, Brooks & Perkins Product Performance Report 624, Brooks & Perkins, Inc.

6. E. E. Lewis and W. F. Miller, Jr., *Computational Methods of Neutron Transport*, John Wiley & Sons, Inc., 1984.

7. E. D. Cashewell, J. R. Neergaard, W. M. Taylor, and G. D. Turner, *MCN: A Neutron Monte Carlo Code*, Los Alamos Scientific Laboratory Report, LA-4751, January, 1972.

8. E. D. Cashwell, J. R. Neergaard, C. J. Everett, R. G. Schrandt, W. M. Taylor, and G. D. Turner, *Monte Carlo Photon Codes: MCG and MCP*, Los Alamos Scientific Laboratory Report, LA-5157-MS, March, 1973.

9. M. Wachs, J. S. Brenizer, Jr., and A. Wells, *Zirconium Diborde Neutron Transmission Standards*, Final Report Job 92-168, Eagle-Picher Industries, Inc., June, 1993.

10. J. S. Brenizer, Jr. and R. O. Johnson, *Inspection Procedures For Eagle-Picher Boron-Aluminum Manufactured Parts*, UVA-EPI001:Rev. GEN.3.0, University of Virginia, January, 1995.

11. G. M. Reynolds, Neutron Gaging Systems, "Practical Applications of Neutron Radiography and Gaging," ASTM STP 586, *American Society for Testing and Materials*, pp. 58-73, 1976.

12. J. J. Haskins, "Nuclear Applications of Neutron Radiography and Gaging, Practical Applications of Neutron Radiography and Gaging," ASTM STP 586, *American Society for Testing and Materials*, pp. 235-237, 1976.

13. D. C. Cutforth, "Neutron Sources for Radiography and Gaging, Practical Applications of neutron Radiography and Gaging," ASTM STP 586, *American Society for Testing and Materials*, pp. 20-34, 1976.

14. G. F. Knoll, *Radiation Detection and Measurements*, 2nd Edition, John Wiley & Sons, Inc., 1989.

15. H. Berger, "Detection Systems for Neutron Radiography, Practical Applications of Neutron Radiography and Gaging," ASTM STP 586, *American Society for Testing and Materials*, pp. 35-57, 1976.

16. A. R. Foster and R. L. Wright, Jr., *Basic Nuclear Engineering*, 3rd Edition, Allyn and Bacon, Inc., 1977.

17. R. A. Rydin, *Nuclear Reactor Theory and Design*, University of Virginia, 1995.

18. J. K. Shultis and R. E. Faw, *Radiation Shielding*, Prentice-Hall, Inc.,1996.

19. J. W. Bryson, J. C. Lee, and R. R. Burn, "Calculation of Neutron Transmission Through Boral Shielding material," *Transaction of American Nuclear Society*, Vol. 30, pp. 596-597, 1978.

20. P. Walti, *Nuclear Science Engineering*, 45, 321, 1971.

21. R. Chiocca, D. Francois, and P. Morin, *Specification for Profiles in Enriched Borated Aluminum*, Transnucleaire 0845-A-41 Rev. 2, 1993.

22. Z. En, N. Jumaev, M. M. Usmanova, H. J. Kim, J. W. Ho, J. Jang and J. S. Brenizer, Jr., "Application of SSNTDs For Study of Boron Distribution In Alloys," *Radiation Measurements*, accepted for publication, Egypt, 1996.

23. C. J. Beidler, W. E. Hauth, III, and A. Goel, "Development of a B4C/Al Cermet for Use as an Improved Structural Neutron Absorber, Journal of Testing and Evaluation," *JTEVA*, Vol. 20, No. 1, pp. 67-70, January, 1992.

24. R. Gautreau, *Theory and Problems of Modern Physics*, McGraw-Hill, Inc., 1978.

25. J. F. Briesmeister, Ed., *MCNP - A General Monte Carlo N-Particle Transport Code*, Version 4A, LA-12625, 1993.

26. P. R. Bevington, *Data Reduction and Error Analysis for the Physical Sciences*, McGraw-Hill, Inc., 1969.

APPENDIX I

This appendix contains two sections. The first section is a complete sample input deck of MCNP. Input decks for other simulations are constructed based on this input file. Section 2 is a sample LoadLeveler script file used to submit MCNP job to SP2.

A.1.1 A Sample MCNP Input Deck for the Modeling of ZrB_2 in a Monoenergetic Beam

```
Determination of neutron transmission coefficient
c    ********************************************************************
c    ZrB2 Disk No.3, use monoenergetic neutron beam of MI(0.06eV)
c    ****** Object Cell Volume Definitions ******
1    1      -5.7334          1 -2 -3     $ ZrB2 disk region, density
2    2      -2.7000          3 -2 -4     $ Al shim
3    0      4 -5 -6
4    0      #1:#2:#3                     $ outer region

c    ****** Object Surface Definitions     ******
1    py  0                        $ source plane,1st surface of disk
2    cy  2.539                    $ cylindrical surface, radius
3    py  0.01448                  $ 2nd surface of disk, 1st surface of Al
4    py  0.54948                  $ 2nd surface of Al
5    cy  0.5642
6    py  0.55948

c    ****** Material Definitions          ******
m1     40000.50c  -0.81410              $ Zr
       5010.50c   -0.10232              $ B-10, enrichment 0.5504
       5011.55c   -0.08358              $ B-11
m2     13027.50c  1                    $ Al
c    ****** Problem run mode            ******
mode  n
c    ****** Source characteristics      ******
c    ****** uniformly distributed monoenergetic(0.06eV) disk source ****
sdef  pos=0 0 0 sur=1 rad=d1 dir=1 erg=6e-8 vec=0 1 0
si1   0.5642                    $ 1 cm2, radius
c    ****** Tally card, count number of transmitted neutrons ******
f1:n  6
c    ****** Cell importances ******
imp:n 1 1 1 0
e0    1e-11 1e-10 1e-9 1e-8 1e-7 1e-6 1e-5 1e-4 1e-3 1e-2 .1 1 2
c    ****** Number of particles ******
nps   1000000
```

A.1.2. A Sample Script Command File for Submitting Jobs to SP2

```
# @ environment = "LL_JOB=TRUE"
# @ initialdir = /home/jg6e/mcnp/samples
# @ error       =error.$(Cluster)
# @ output      =output.$(Cluster)
# @ class      = medium
# @ job_type = serial
# @ notify_user =jg6e@virginia.edu
# @ notification = always
# @ queue
# ------------------------------------------------------------------------
set echo
date
mcnp n=z03mo
echo job done
```

APPENDIX II

This appendix contains the code listing of the curve fitting program, which was written in C. It was designed to fit the experimental transmission coefficients data with multiple exponential functions. The non-linear least squares fitting algorithms were used for this purpose.

A.2.1. The Curve Fitting Program

```
#include <stdio.h>
#include <stdlib.h>
#include <math.h>
#include <malloc.h>

/*
 * Declarations of function prototype
 */
void gridls();
void gradls();
double fchisq();
double functn();

/*
 * Main function in charge of input, output and calling fitting   *
functions.
 */
main()
{

  double *X, *Y, *sigmaY;
  int nPts, nTerms, mode;
  double *A, *deltaA, *sigmaA;
  double *Yfit;
  double chiSqr;

  double chi;
  double e;
  int count;
  int i;
  FILE *inF;

  inF = fopen( "data.dat", "r");

  fscanf(inF, "%d %d %d", &nPts, &nTerms, &mode);
  X= calloc(nPts, sizeof(double));
  Y= calloc(nPts, sizeof(double));
  Yfit = calloc(nPts, sizeof(double));
  sigmaY = calloc(nPts, sizeof(double));
```

```
    A = calloc(nTerms, sizeof(double));
    deltaA =  calloc(nTerms, sizeof(double));
    sigmaA =  calloc(nTerms, sizeof(double));
    for(i=0;i<nTerms;i++)
     fscanf(inF, "%lf %lf", &A[i], &deltaA[i]);
    for(i=0;i<nPts;i++)
     fscanf(inF, "%lf %lf %lf", &X[i], &Y[i], &sigmaY[i]);
    for(i=0;i<nPts;i++)
      printf("%f %f\n", X[i],Y[i]);

    e=0.00000001;
    count=0;
    chi=100;

    while(1){
     count++;
     printf("%d ",count);
     gradls(X,Y,sigmaY, nPts, nTerms, mode, A, deltaA, sigmaA,
           Yfit, &chiSqr);
     printf("%lf %lf\n", chi, chiSqr);
     if( (fabs(chiSqr-chi)/chi < e )|| count>2500 ) break;
     chi=chiSqr;
     if(chi==0) chi=0.000001;
    }

    for(i=0;i<nTerms;i++)
      printf("%f\n", A[i]);

    for(i=0;i<nPts;i++)
     printf("%f %f\n", X[i], Yfit[i]);
    fclose(inF);

}

/*
 * Fitting routine using grid-search with modifications from Bevington
 */
void gridls( double X[], double Y[], double sigmaY[],
             int nPts, int nTerms, int mode,
             double A[], double deltaA[], double sigmaA[],
             double Yfit[], double *chiSqr)
{
  int nFree;
  int free;
  int i, j;
  double chiSq1, chiSq2, chiSq3;
  double fn,save;
  double delta;
  int flag;

  nFree = nPts - nTerms;
  free = nFree;
  *chiSqr = 0.0;
  if(nFree <= 0) return;
  for ( j=0; j<nTerms; j++) {
/*
 * Evaluate chi square at first two search points.
 */
```

```
    for ( i=0; i<nPts; i++)
      Yfit[i] = functn(X, i, A);
    chiSq1 = fchisq( Y, sigmaY, nPts, nFree, mode, Yfit);
    fn = 0.0;
    delta = deltaA[j];
    flag = 0;
    while(!flag) {
      A[j]+=delta;
      for (i=0; i<nPts; i++)
        Yfit[i] = functn(X, i, A);
      chiSq2 = fchisq( Y, sigmaY, nPts, nFree, mode, Yfit);
      if(chiSq1 < chiSq2)
        flag = -1;
      else if (chiSq1 > chiSq2)
            flag = 1;
    }
/*
 * Reverse direction of search if chi square is increasing.
 */
    if ( flag == -1) {
      delta = -delta;
      A[j]+=delta;
      for(i=0; i<nPts; i++)
        Yfit[i] = functn(X,i, A);
      save = chiSq1;
      chiSq1= chiSq2;
      chiSq2 = save;
    }
/*
 * Increment A[j] until chi square increases.
 */
    flag = 0;
    while(!flag){
      fn++;
      A[j]+=delta;
      for(i=0; i<nPts; i++)
        Yfit[i] = functn ( X, i, A);
      chiSq3 = fchisq( Y, sigmaY, nPts, nFree, mode, Yfit);
      if(chiSq3 < chiSq2){
         chiSq1= chiSq2;
         chiSq2 = chiSq3;
      }
      else flag =1;
    }
/*
 * Find minimum of parabola defined by last three points.
 */
    delta *= (1.0/ ( 1.0 + (chiSq1 - chiSq2)/(chiSq3 - chiSq2)) +0.5);
    A[j]-=delta;
    sigmaA[j] = deltaA[j]* sqrt(2.0/(free *(chiSq3- 2*chiSq2 +
      chiSq1)));
    deltaA[j] = deltaA[j]* fn/3.0;

  }

/*
 * evalute fit and chi square for final parameters.
 */
```

```
  for (i =0;i<nPts;i++)
    Yfit[i] = functn( X, i, A);
  *chiSqr = fchisq( Y, sigmaY, nPts, nFree, mode, Yfit);
  return;
}

/*
 * Fitting routine using gradient-search with modifications from
 * Bevington.
 */
void gradls( double X[], double Y[], double sigmaY[],
             int nPts, int nTerms, int mode,
             double A[], double deltaA[], double sigmaA[],
             double Yfit[], double *chiSqr)
{
  int nFree;
  int free;
  int i, j;
  double chiSq1, chiSq2, chiSq3;
  double fn,save;
  double delta;
  double sum;
  int flag;
  double *grad;

  grad= calloc(nTerms, sizeof(double));

  nFree = nPts - nTerms;
  free = nFree;
  *chiSqr = 0.0;
  if(nFree <= 0) return;
  for(i=0;i<nPts;i++)
    Yfit[i] = functn (X, i, A);
  chiSq1  = fchisq( Y, sigmaY, nPts, nFree, mode, Yfit);
/*
 * Evaluate gradient of chi square
 */
  sum = 0;
  for (j =0; j<nTerms; j++) {
    delta = 0.1 * deltaA[j];
    A[j] += delta;
    for(i = 0; i<nPts; i++)
      Yfit[i] = functn(X, i, A);
    A[j] -= delta;
    grad[j] = chiSq1 -  fchisq( Y, sigmaY, nPts, nFree, mode, Yfit);
    sum+= grad[j]*grad[j];
  }
  for (j=0;j<nTerms;j++)
    grad[j] = deltaA[j]* grad[j]/sqrt(sum);
/*
 * Evaluate chi square at new point.
 */
  flag=0;
  while(!flag){
    for(j=0;j<nTerms; j++)
      A[j]+=grad[j];
    for(i=0;i<nPts; i++)
      Yfit[i]= functn(X, i, A);
```

```
    chiSq2 =  fchisq( Y, sigmaY, nPts, nFree, mode, Yfit);
/*
 * Make sure chi square decreases.
 */
    if(chiSq1<=chiSq2) {
      for(j=0;j<nTerms;j++){
        A[j]-=grad[j];
        grad[j]/=2.0;
      }
    }
    else flag=1;
  }
/*
 * Increment parameters until chi square starts to increase.
 */
  flag =0;
  while(!flag){
    for(j=0;j<nTerms;j++)
      A[j]+=grad[j];
    for(i=0;i<nPts;i++)
      Yfit[i] = functn(X, i, A);
    chiSq3 = fchisq( Y, sigmaY, nPts, nFree, mode, Yfit);
    if(chiSq3<chiSq2){
      chiSq1=chiSq2;
      chiSq2=chiSq3;
    }
    else flag =1;
  }


/*
 * Find minimum of parabola defined by last three points.
 */
    delta = 1.0/ ( 1.0 + (chiSq1 - chiSq2)/(chiSq3 - chiSq2)) +0.5;
    for(j=0;j<nTerms;j++)
      A[j] -= delta*grad[j];
    for(i=0;i<nPts;i++)
      Yfit[i] = functn(X, i, A);
    *chiSqr= fchisq( Y, sigmaY, nPts, nFree, mode, Yfit);
    if(chiSq2 < *chiSqr){
     for(j=0;j<nTerms;j++)
       A[j]+= (delta-1.0)*grad[j];
     for(i=0;i<nPts;i++)
       Yfit[i] = functn(X, i, A);
     *chiSqr = chiSq2;
    }
  return;
}

/*
 * Evaluate reduced chi square for fit to data.
 */

double fchisq( double Y[], double sigmaY[],
               int nPts, int nFree, int mode,
               double Yfit[])
{
  double chiSq;
```

```
  double weight;
  int free;
  int i;

  chiSq = 0.0;
  if(nFree<=0)
    return 0;
/*
 * Accumulate chi square
 */

  for( i=0; i<nPts; i++) {
    if(mode < 0) {
     if(Y[i]<0)
      weight = 1.0 / (-Y[i]);
     else if ( Y[i] ==0)
      weight = 1.0;
     else weight = 1.0/ Y[i];
    }
    else if(mode == 0) {
     weight = 1.0;
    }
    else if(mode >0) {
     weight = 1.0 / (sigmaY[i]* sigmaY[i]);
    }
    chiSq+= weight *(Y[i] - Yfit[i]) *(Y[i] - Yfit[i]);
  }
/*
 * Divide by number of degrees of freedom
 */

  free = nFree;
  return chiSq/free;
}

/*
 * Fitting function form.
 */

double functn( double X[], int i, double A[])
{
  return A[0]*exp(-96.4*X[i])+ A[1]*exp(-31*X[i])+ A[2]*exp(-20*X[i])
         + (1 - A[0] - A[1] - A[2]) * exp(-10*X[i]);
}
```

om: K. Scot Leuenroth [SLeuenroth@netcony.com]
ent: Monday, September 13, 2004 11:55 AM
To: Jim Hobbs
Cc: Kenneth O. Lindquist
Subject: Emailing: Boral-metamic Min-Cert Chart.pdf

Boral-metamic
Min-Cert Chart.p...

Jim,

Here is the revised figure for the Boral comparison. Min-Certified values that you provided were used in the Boral fit calculations.

Scot Leuenroth
Sleuenroth@netcony.com

Neutron Attenuation Comparison: Boral vs B4C Al Composite

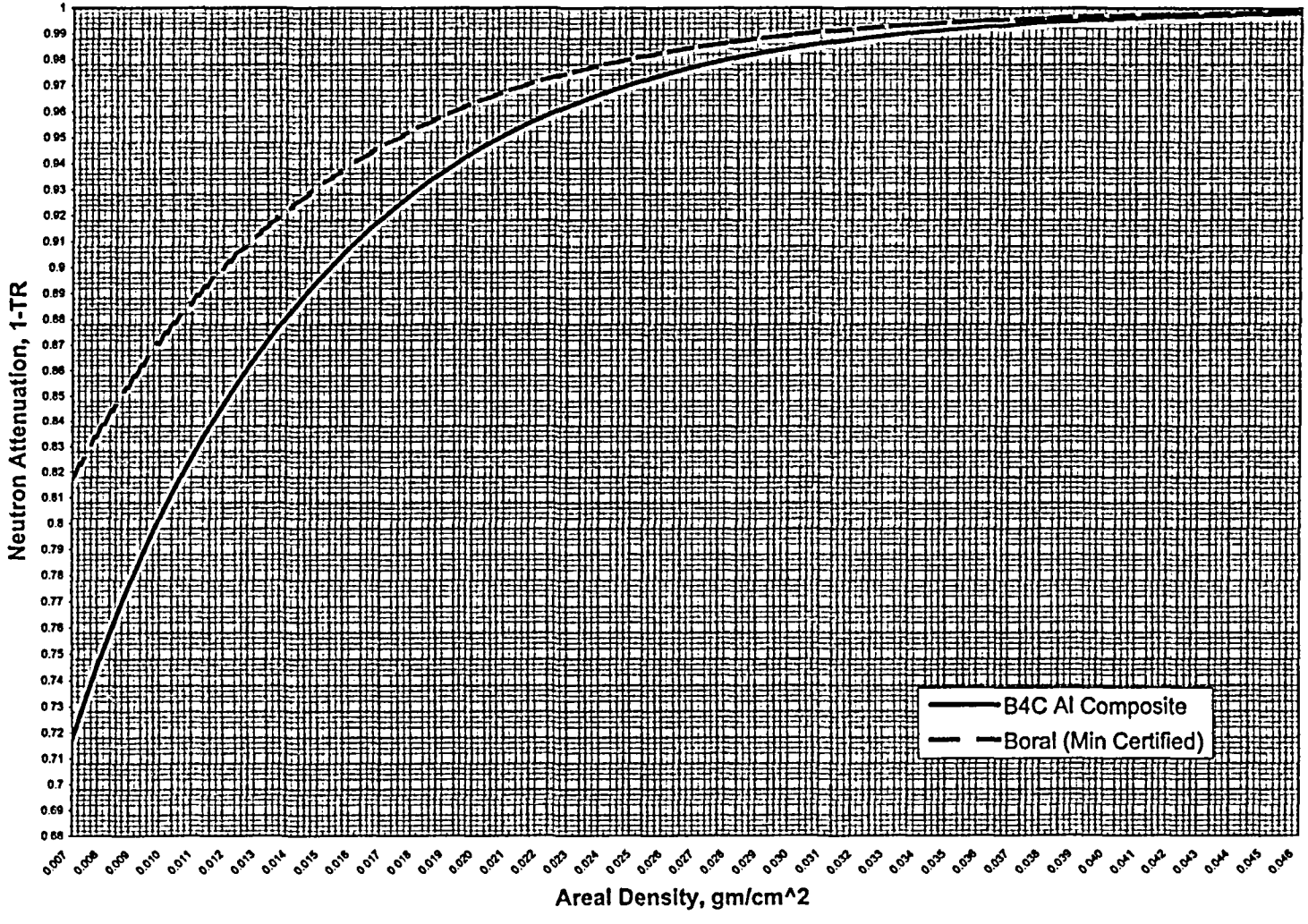

NAC INTERNATIONAL

Atlanta Corporate Headquarters
3930 East Jones Bridge Road
Norcross, GA 30092
Phone: 770-447-1144
Fax: 770-447-1797
www.nacintl.com

March 22, 2002

RHS

Ms. Rebecca Karas
Project Manager
Spent Fuel Project Office
United States Nuclear Regulatory Commission
11555 Rockville Pike
Rockville, MD 20852

Subject: Summary of NAC Boral Testing Program

Reference:
1. NAC Letter QA20010095, Smith to McGinty, February 5, 2001, re: Evaluation results for ENSA Fuel Tube Pressure Testing
2. Conference Call, Smith, Pennington & Danner to Karas. August 10, 2001, re: ENSA Fuel Tube Boral Blisters
3. NAC Letter QA20010537, Smith to Karas, September 7, 2001, re: Boral Deformation (Blistering)
4. Conference Call, Thompson to Karas, February 21, 2002, re: NAC Boral Test Program
5. Conference Call, Thompson to Karas, March 8, 2002, re: NAC Boral Testing Report

Dear Ms. Karas:

In accordance with the Reference 5 conference call discussions, NAC International (NAC) herewith submits a non-proprietary summary report, "Evaluation of the Structural Fitness of Boral for Use in NAC Spent Fuel Canisters," on the Boral testing recently completed by NAC.

Also, please note that NAC moved its corporate offices in mid-February. The new address is:

NAC International
3930 East Jones Bridge Road
Norcross, GA 30092

Please contact me if you have any questions or require any additional information.

Sincerely,

TC Thompson

Thomas C. Thompson
Director, Licensing
Engineering & Product Development

Enclosure

ED20020142

Evaluation of the Structural Fitness of Boral™ for Use in NAC Spent Fuel Canisters

March 2002

NAC INTERNATIONAL

NAC International (NAC) has recently completed a comprehensive testing program to evaluate the structural fitness of Boral™ for use in NAC's PWR spent fuel storage and transportation canisters. The testing program included nine separate tests that represented, or exceeded, the maximum design basis conditions that the Boral™ will experience during actual canister operations. Based on the test results, NAC has concluded that Boral™ is structurally stable and will perform its function as a neutron absorber under all canister operating conditions.

Boral™ is manufactured and supplied by AAR Cargo Systems of Livonia, Michigan. Boral™ is a composite laminate material that is used as a neutron absorber for criticality control in NAC's spent fuel dual-purpose canisters and spent fuel transportation casks. The outer layers (cladding) of Boral™ are series 1100 aluminum, which enclose a core mixture of series 1100 aluminum powder and B_4C powder.

The NAC Boral™ testing program was initiated as a result of "blistering" that occurred on Boral™ sheets used in the Dual-Purpose Trillo (DPT) cask fabricated by NAC's licensee in Spain, Equipos Nucleares, S.A. (ENSA), for its customer, Empresa Nacional de Residuos Radiactivos, S.A. (ENRESA). The blisters are deformations of the outer aluminum cladding. ENSA reported to NAC in August 2001 that blisters were found on several Boral™ sheets after performing acceptance tests for the first DPT cask. At a later date, ENSA disassembled all of the fuel tubes and determined that blisters were present on a total of 11 sheets, which were located in 10 different fuel tubes.

The testing sequence performed by ENSA included the following test conditions and operational steps:

Hydrostatic Tests

The cask with basket was pressurized at 18 psig for a period of 40 minutes; atmospheric pressure for 12 hours; pressurized to 131 psig for 10 minutes; then reduced to 101 psig for 30 minutes.

Drying

After the hydrostatic tests were completed, the cask was opened and the basket was taken out of the cask to dry. Accessible areas of the basket assembly were manually dried using dry cloth. The basket was exposed to natural air drying for six days prior to vacuum drying.

Vacuum Drying

The basket was replaced in the cask, and the cask was vacuum dried for 24 hours at ambient temperature. Following the 24 hours of vacuum drying, a vacuum of 11 mbar was held for 10 minutes with no pressure increase.

Thermal Test

Twenty-one heaters with a heat output of 1.285 kW each (total heat output of 27 kW) were used to heat the cask. The duration of the heat-up was 44 hours. The temperature was measured by two thermocouples located in two fuel tubes near the center of the basket, approximately halfway down the tube length. The maximum temperature, measured at the center of the basket, at completion of the thermal test was 438°F.

The blisters were the result of pressure in the Boral™ core. ENSA initially postulated that the blisters were caused by hydrogen generated by a chemical or galvanic reaction. NAC's theory was that water was forced into the relatively porous Boral™ core during the high-pressure hydrostatic tests, and the water flashed to steam during the thermal test. After conducting independent testing programs, both ENSA and NAC now believe the blisters were caused by steam pressure. The steam most likely resulted from localized high heat-up rates.

In response to the blistering occurrence at ENSA, NAC initiated a comprehensive test program to assess the structural fitness of Boral™ for its function as a neutron absorber in NAC's spent fuel storage/transportation canisters. Note that the Boral™ used in the DPT cask is thicker than the Boral™ used in the NAC-MPC and NAC-UMS® PWR canisters (0.10 inch for the DPT cask, 0.075 inch for the MPC/UMS®), and the DPT acceptance test parameters were much different from the conditions that Boral™ will be exposed to during NAC spent fuel canister operations. Since NAC was fabricating and delivering canisters to its customers, this NAC Boral™ testing program was designed specifically to evaluate and qualify Boral™ for use in the NAC-MPC and NAC-UMS® PWR canisters. The testing program simulated the operating environments, with conservative margins, that Boral™ will experience during actual canister loading and closure operations for NAC spent fuel canisters.

NAC's Project Plan for the evaluation defined the objectives for the testing program as:

- Identify any physical changes in Boral™ sheets when subjected to the conditions experienced in the operations and testing of spent fuel storage/transportation canisters.
- Determine if the conditions typically experienced in loading, pressure testing and drying a spent fuel canister could lead to blistering, deformation, delamination or other changes that could reduce the functional effectiveness of the Boral™ sheets used in the NAC-MPC or NAC-UMS® systems.
- Obtain results and backup data to support NAC's evaluation of the structural fitness of Boral™ to perform its intended function.

The NAC testing program was designed to determine if Boral™ is structurally capable of withstanding the environmental conditions inside an NAC PWR spent fuel canister. The most severe conditions occur while the fuel is being loaded in the canister in the spent fuel pool and during the canister closure, draining and drying operations. These conditions include: water pressure during fuel loading (for a 40-foot deep pool, the water pressure at the bottom is 17.3 psig); the hydrostatic pressure test of the shield lid weld of 21 psig; and the heat-up of the

Boral™ after the water is drained from the canister and the canister is vacuum dried (maximum of 30°F/hr for design basis fuel of 23 kW/canister). The tests were designed to simulate the design basis limits as described in the applicable NAC-MPC and NAC-UMS® Final Safety Analysis Reports (FSARs). Significant margins were added to the test values to assure conservatism. The conditions that occur during the fuel loading and canister closure operations were evaluated and were found to bound any other conditions during normal interim storage at the ISFSI or during normal transport conditions.

The testing program was implemented in three phases:

Phase 1 – Engineering Tests

Seven engineering tests were performed. The test samples included bare Boral™ sheet segments (approximately 8 inches x 8 inches) and Boral™ enclosed in stainless steel "panels." The panel is a mock-up of a fuel tube wall, fabricated in a manner similar to the NAC fuel tube design for Yankee Rowe and Connecticut Yankee (continuous weld around the sheath with clipped corners). These tests were performed to establish test parameters and procedures for the later Quality Assurance (QA) Program-compliant tests and to develop benchmark data to verify the reasonableness of the QA test results. The samples used in the engineering tests included Boral™ material with different characteristics, such as passivated samples and samples with different thicknesses and different boron areal densities. The tests focused on the specific Boral™ thickness that is used in NAC PWR canisters, although two of the engineering tests included samples of the thicker ENSA Boral™ sheets. The tests showed that Boral™ absorbs water when subjected to hydrostatic pressure, but all of the water escapes when the Boral™ is heated at the maximum design heat-up rate. None of the engineering tests, including tests at heat-up rates significantly higher than the maximum design basis, caused blisters or other deformation in the bare samples or enclosed Boral™ sheets.

Note that the engineering tests were considered informational and were not required to meet all NAC Quality Procedure requirements. However, each Phase 1 test was governed by an NAC prepared test procedure and was performed in accordance with the QA program of the testing organization.

Phase 2 – QA Compliant Tests of Boral™ Sheet Samples

The Phase 2 testing was the data verification step. Four Boral™ samples, approximately 8 inches x 8 inches, were used. The test parameters and sequence were similar to Phase 1 tests. The purpose of the Phase 2 tests was to verify the performance data of Boral™ in a QA compliant test. The samples were taken from the working inventory of material used in the Maine Yankee project (a standard NAC-UMS® PWR design). This material is similar to the Boral™ that will be used in the NAC-MPC canister projects (Yankee Rowe and Connecticut Yankee). The Phase 2 tests were performed at greater-than-design-basis hydrostatic pressure and heat-up rates. No blisters or other deformation occurred in the Phase 2 samples. The Phase 2 tests verified the data compiled in the engineering tests and confirmed the structural integrity of Boral™ in canister operating conditions.

Phase 3 – QA Compliant Test of an Enclosed Boral™ Sheet

The Phase 3 test was the acceptance test of the structural performance of Boral™ in the most conservative NAC PWR fuel tube design configuration. The fabricated panel represents the side of a fuel tube. The panel was made of a Boral™ sheet, approximately 42 inches long, enclosed in a stainless steel sheath. The sheath is identical to the cover sheath used in the fuel tube. The sheath is continuously welded to a backing plate (the backing plate is thicker than a fuel tube wall for stability and ease of handling) and has clipped corners, proportionately sized, that model the design of the Yankee Rowe and Connecticut Yankee NAC-MPC fuel tubes. Testing of the continuously welded sheath is considered to envelop the NAC-UMS® stitch weld design, since the continuous weld is more restrictive of water/steam flow and potentially could have a higher backpressure within the sheath.

NAC analyzed the effect of the cover sheath on the ability of water/steam to escape from the Boral™ in the fuel tube configuration in NAC Calculation EC 455-9564, "Boral Blister Investigation – Technical Justification of Scale Model Test Specimen." The calculation analyzed the pressure increase resulting from vaporization of the trapped water in the Boral™ and the stainless steel cover sheath and concluded that the cover sheath does not restrict the flow of water from the enclosed Boral™ sheet in a fuel tube. The vaporization pressure poses no threat to the integrity of the Boral™ or the fuel tube structure. The calculation also provides the justification of using a scale model section to approximate the performance of the fuel tube design.

The conclusion of Calculation EC 455-9564 was verified by the results of two separate engineering tests using enclosed Boral™ (in two different ovens, one under a vacuum), as well as the Phase 3 QA test. After the first panel engineering test, the cover sheath was removed and the Boral™ sheet was visually examined. There were no blisters or other deformation the Boral™. The second panel tested in an engineering test was kept intact to show the sheath condition after testing (no damage or deformation). The Phase 3 test, performed in accordance with the applicable provisions of NAC's QA program, was the acceptance test for the NAC-MPC/UMS® fuel tube design. The cover sheath on the Phase 3 panel was removed and the Boral™ sheet was visually examined. There were no blisters or other deformation to the Boral™.

The results of the extensive testing program performed by NAC demonstrate that Boral™ is structurally stable under the conditions that the Boral™ will experience during NAC canister operations. Tests at values well above the maximum operating values confirmed that adequate material performance margins exist.